A CONTRIBUTION TO THE CLINICAL VALIDATION OF A GENERIC METHOD FOR THE CLASSIFICATION OF OSTEOARTHRITIC AND NON-PATHOLOGICAL KNEE FUNCTION

Gemma Marie Whatling, M.Eng (Hons)

PhD Thesis

2009

Institute of Medical Engineering and Medical Physics

School of Engineering

Cardiff University

ProQuest LLC
789 East Eisenhower Parkway
P.O. Box 1346
Ann Arbor, MI 48106-1346

ABSTRACT

The Cardiff Dempster-Shafer (DS) classifier is a generic automated technique for analysing motion analysis (MA) data. It can accurately discriminate between level gait characteristics of non-pathological (NP) and osteoarthritic (OA) knee function. It can also quantify and visualise the functional outcome of a total knee replacement (TKR).

A number of studies were undertaken to explore and enhance this method. The training set for the classifier was increased by 48% by collecting additional knee function data for level gait. Knee function for nine new patients was classified pre and post-TKR surgery. At 12 months post-TKR, two patients exhibited non-dominant NP knee function. The remaining patients did not recover NP gait. This finding is similar to previous classifications of level gait.

To improve the distinction between varying degrees of knee function, stair gait was introduced into the trial. A staircase was designed and validated. Adduction and flexion moments acting about the knee joint and medial component of the ground reaction force were found to be important in the classification of OA and NP knee function from stair gait. Using a combination of these variables the DS classifier was able to characterise OA and NP function for 15 subjects correctly with 100% accuracy, determined using a leave-one-out method of cross validation. The variables were tested to assess the outcome of TKR surgery. The patient assessed recovered NP stair gait post surgery.

An image based study was undertaken to investigate the quality of the MA data used in the DS classifier. A step up/down activity for 5 NP and 5 TKR subjects was recorded using non-simultaneous MA and dynamic fluoroscopy. Accurate knee kinematics were computed from the fluoroscopy images using KneeTrack image registration software. MA measured significantly larger knee joint translations and non-sagittal plane rotations. The largest errors in MA derived kinematics were 9.53° for adduction-abduction range of motion (ROM) measured from the NP cohort and 2.63cm compression-distraction ROM of the tibio-femoral joint, measured from the TKR cohort.

The generic nature of the DS classifier was tested by its application to distinguish hip function following a lateral (LA) and posterior (PA) approach to total hip arthroplasty. The use of different variables was investigated with the classifier. The best classifier was able to distinguish between NP and LA function with 96.7% accuracy, LA and NP with 86.2% accuracy and between LA and PA with 81.5% accuracy. The PA approach was found to lead to more characteristic NP hip function than LA.

These studies show that variables from stair gait should be included in addition to level gait in the classifier. Due to errors when measuring non-sagittal plane rotations using MA, these should be interpreted with caution. The generic nature of the classifier has been proven by its application to another joint, thus answering another orthopaedic question.

ACKNOWLEDGEMENTS

I would like to express my thanks to those people who have contributed to making my research an invaluable experience over the past three years.

Firstly I would like to thank my supervisor Dr Cathy Holt whose drive and passion for biomechanics has been inspirational. I will always be grateful for the patience she has shown and the knowledge she has shared. Her trust in my abilities has given me the confidence to embrace all the opportunities available. She has made my PhD an enjoyable experience, always encouraging me to present my work at every opportunity. I also wish to express my sincere gratitude to my second supervisor Dr Sam Evans for his technical support and valuable advice.

It was a pleasure to work with Dr Lianne Jones, Barry Lovern and June Madete whilst conducting the clinical trials. I also wish to thank colleagues, family and patients who volunteered their time to take part in the trials. Special thanks is given to my Dad for helping me to design and construct the staircase.

My appreciation is given to the orthopaedic surgeons, Mr Chris Wilson and Mr Rhys Williams from the University Hospital of Wales Cardiff and Mr Alderman, Mr Philips and Mr Dabke from the Royal Gwent Hospital, for assisting with patient recruitment and their clinical support.

Special thanks is given to Dr Scott Banks for his software, training and always being available to answer my queries. My time spent at the University of Florida with Dr Banks and Dr Benjamin Fregly proved to be invaluable.

I give thanks to Dr John Evans and Professor Derek Jones at CUBRIC for their technical support in the acquisition of MRI scan data. Also, my appreciation is given to Rebecca Vaughan-Roberts and Lynda Muir of the University Hospital of Wales Cardiff for the acquisition of fluoroscopy images.

Special recognition to Dr Philippe Young from Exeter University for the use of Simpleware software and for the upgrades to the software to help with my research. Also thanks to the staff at Simpleware for their invaluable technical support, with special thanks to Florian Pierron, Matthias Larcher and Hatice Ozturk.

Many thanks to my sponsor DePuy Ltd. who made this work possible through their generous funding. Also, to Depuy Ltd. and Wright Medical Technology, Inc. for access to 3D CAD TKR implant models.

Finally, I would like to pay a special thanks to my friends and family for their continual support. Most importantly to my parents Lynne and John Whatling, my Grandad George Sawyer and Nick Patterson, for their continuous love, patience and encouragement. Their humour and positivity helped lift my spirits through some trying times whilst aiming to reach my final goal.

CONTENTS

CHAPTER 4: METHODOLOGIES TO ASSESS STAIR ASCENT AND DESCENT

ABBREVIATIONS

2D/3D	2 dimensional/ 3 dimensional
AAR	Adduction-abduction rotation
ACL	Anterior cruciate ligament
ALCS	Anatomical local coordinate system
AMA	Adduction moment measured during stair ascent
ANN	Artificial Neural Network
ANOVA	Analysis of Variance
AP	Anterior-posterior
APF	Anterior-posterior force
BM	Body mass
BMI	Body mass index
BOE	Body of evidence
BOE_c	Combined body of evidence
CAD	Computer aided design
COM	Centre of mass
COP	Centre of pressure
CT	Computed Tomography
DICOM	Digital Imaging and Communications in Medicine
DOF	Degrees of freedom
DS	Dempster-Shafer
DST	Dempster-Shafer theory
EMG	Electromyography
FE	Finite element
FER	Flexion-extension rotation
FHM	Frontal hip moment

FHP	Frontal hip power
FMA	Flexion moment measured during stair ascent
FMD	Flexion moment measured during stair descent
FP	Force plate
FTKR	Fixed platform total knee replacement
GCS	Global co-ordinate system
GRF/GRFs	Ground reaction force/forces
HTO	High Tibial Osteotomy
IDA	Inverse dynamic analysis
IER	Internal-external rotation
JCS	Joint co-ordinate system
KJC	Knee joint centre
KOS	Knee outcome survey
LA	Lateral approach to THA
LCS	Local coordinate system
LDA	Linear Discriminant Analysis
LOO	Leave-one-out
MA	Motion analysis
MC	Moment calculation
MDF	Medium-density fibreboard
ML	Medial-lateral
MLCS	Marker cluster local coordinate system
MLF	Medial-lateral force
MLFA	Medial-lateral force measured during stair ascent
MRI	Magnetic resonance imaging
NP	Non-pathological
OA	Osteoarthritis

OB	Objective Function
OKS	Oxford knee score
PA	Posterior approach to THA
PC	Principal Component
PCA	Principal Component Analysis
PLCS	Pointer local coordinate system
PO	Pelvic obliquity
QTM	Qualisys Track Manager
ROM	Range of motion
RTKR	Rotating platform total knee replacement
SGC	Stair gait cycle
STA	Soft tissue artefact
T1-T4	Transducers 1-4
THA	Total hip arthroplasty
TKR	Total knee replacement
VF	Vertical force
VFD	Vertical ground reaction force measured during stair descent

NOTATION

P_m	The MLCS coordinates of the pointer's point
P_p	The PLCS coordinates of the pointer's point
$\mathbf{T}_{pg}$	Transformation matrix relating orientation of the PLCS in the GCS
$\mathbf{T}_{mg}$	Transformation matrix relating orientation of the MLCS in the GCS
$\mathbf{T}_{gm}$	Inverse of the matrix $\mathbf{T}_{mg}$
$\mathbf{T}_{ma}$	Transformation matrix relating orientation of the MLCS in the ALCS
$\mathbf{T}_{am}$	Inverse of the matrix $\mathbf{T}_{ma}$
$\mathbf{T}_{tf}$	Transformation matrix relating orientation of the tibia relative to the femur
L	Component loadings matrix
R	Rotation matrix
θ_{FE}	Flexion-extension angle
θ_{AA}	Adduction-abduction angle
θ_{IE}	Internal-external rotation angle
λ_{ML}	Medial/Lateral Shift
λ_{AP}	Anterior/Posterior Drawer
λ_{CD}	Compression/Distration
F_x	Force component in the force plate coordinate system
F_y	Force component in the force plate coordinate system
F_z	Force component in the force plate coordinate system
M_x	Moment component in the force plate coordinate system
M_y	Moment component in the force plate coordinate system
M_z	Moment component in the force plate coordinate system
w	Weight
h	Height
{NP}	The hypothesis "the subject has NP knee function"

{OA}	The hypothesis "the subject has OA knee function"
$cf(v)$	Confidence factor
bpa	Basic probability assignment
$m(.)$	Probability mass function (*bpa*)
$m_c(.)$	Combined probability mass function (*bpa*)
v	Input variable
k	DS control parameter
θ	DS control parameter
A	DS control parameter
B	DS control parameter
Θ	Frame of discernment
Θ_L	Lower uncertainty boundary
Θ_U	Upper uncertainty boundary
COP_x	X coordinate position measured in the force plate coordinate system
COP_y	Y coordinate position measured in the force plate coordinate system
M	Net muscle moment
M_{KJC}	Moment acting about the KJC
r_{KJC}	Position vector of the KJC relative to the origin of the GCS
r	Position vector of COP relative to GCS
F	GRF vector
Rz, Ry	Reaction force acting at the KJC
at	Tangential acceleration of the shank COM
ar	Radial acceleration of the shank COM
$\boldsymbol{\alpha}$	Angular acceleration of the segment in the plane of movement
K	Mass radius of gyration of the shank about the COM
I_o	Moment of inertia

CHAPTER 1
INTRODUCTION AND LITERATURE REVIEW

1.1 INTRODUCTION

Human motion analysis (MA) is routinely used in both the clinical and research sectors to provide time dependent quantitative biomechanical information of the musculo-skeletal system during the execution of a motor task.

Originating in the research environment, MA has now become a widely utilised non-invasive investigative and diagnostic clinical tool. It is used for the assessment of neuromuscular disorders such as cerebral palsy and spina bifida, assessing joint injury and degeneration, postoperative testing of joint prosthetic designs and for surgical decision making. MA plays an important role in clinical assessments. Simultaneous movements of multiple body segments can be recorded in three-dimensions for particular tasks and subtle deviations in movement can be captured that cannot be perceived by the human eye. It also aids the physician to distinguish between primary movement abnormalities and any secondary compensatory mechanisms that may overshadow the cause of the problem.

During a data collection session, a wealth of biomechanical data regarding joint and segment kinematics and kinetics is collected from the patient who performs specific daily activities. The greatest challenge is how to use this information for clinical benefit (Whittle, 1996). A common problem is the difficulty in objectively analysing and thus gaining meaningful conclusions from such a wealth of data.

In clinical motion analysis, quantitative motion data is expressed in a concise format as a clinical report and a team of experts interpret the kinetic, kinematic and electromyographic (EMG) graphical outputs and video analysis. This procedure is subjective, relying entirely on expert knowledge and opinion which in itself can be contradictory.

The main concerns with subjectively analysing motion data is firstly the vast amount of data collected and secondly, the relevance of each functional variable in discriminating pathological joint function is unknown. No individual variable is capable of providing a complete description of a subject's gait (Jacobs *et al.*, 1972) and the variable may support or offer no support to a subject's correct classification.

The ultimate goal of MA is to communicate reliable, objective information on which to base clinical decisions, quantify outcomes and ultimately predict the outcomes of various interventions. It would be advantageous in many cases to remove the reliance on subjective expert opinion in the interpretation of motion data in favour of an automated generic diagnostic procedure. It may also be advantageous to be able to combine objective and subjective measures, such as level of pain, when making clinical decisions.

In response to the challenges associated with interpreting motion analysis data, Jones, (2004) developed an objective classification tool to automate a diagnosis from the MA data. This tool was developed to aid orthopaedic surgeons and therapists in making clinical diagnostics and monitoring decisions. It was originally developed to characterise knee function, provide a visual output of a patient's knee pathology and quantify the level of benefit achieved by a total knee replacement (TKR). The classifier can be used as a fully or partially automated tool, allowing the input variables to be chosen either manually through expert opinion or using a feature selection algorithm. The control parameters can also be selected by expert opinion or by and optimisation approach.

The work described in this thesis contributes towards the clinical validation of this classification tool in determining knee osteoarthritis and monitoring recovery after TKR. The tool itself has been reported to have a high accuracy of 97.62% (Jones, 2004). The current study concentrates on the quality of the inputs to the classifier. To date, variables from level gait have been considered. As a continuation to this approach, knee function data during level gait was collected and processed for additional subjects to increase the training cohort for the classifier. The classifier was then used to assess the outcome of TKR surgery for an additional nine patients. For the assessment of TKR function, stair gait is an important daily activity for

consideration and was thus introduced as an assessment activity. This required the design and validation of a staircase and the development of in-house software to include knee moment calculations. A study was performed to compare stair gait computed using different data collection and analysis methods. The use of stair gait variables as inputs to the classifier was investigated.

Errors associated with the current data collection protocol were investigated through an imaging study. This involved establishing a method that uses dynamic fluoroscopy and image registration using KneeTrack software (S.A Banks, USA). Furthermore, the classifier is generic, and this was demonstrated by its application to a new clinical problem, to characterise total hip replacement function following lateral and posterior surgical approaches.

This work stems from the development of a classification method to analyse gait data collected during a clinical trial at Cardiff University.

1.1.1 Background to clinical trial

Knee Osteoarthritis (OA) is a degenerative disease where the protective articular cartilage lining the ends of the tibia and femur gradually roughen and become thin. In severe cases this leads to extremely painful bone on bone contact and wear. As a reaction to this, the surrounding bone thickens due to the formation of osteophytes and the synovium swells. The shape of the joint changes and it can become painful and stiff, with a subsequent reduced range of motion (Arthritis Research Campaign, 1998). Furthermore, the muscles surrounding the joint begin to atrophy. As a joint degenerates, its functional ability is therefore altered. It is thus important to have robust methods that quantify the changes that occur due to the disease process. For reference, the anatomy and function of a healthy knee joint it described in Appendix A.

There are two main treatments for knee OA depending on its severity. High Tibial Osteotomy (HTO) is performed for early stage OA where the medial compartment of the knee is affected by OA. This procedure realigns the joint space to redistribute the loads acting through the knee, delaying the need to replace the joint. For severe cases

of knee OA, surgery is performed to replace the worn components of the joint with prosthetic articulating surfaces. In cases where the arthritis is confined to one side of the knee, a partial knee replacement, also called unicompartmental knee replacement may be performed, (Figure 1.1a). This procedure preserves as much of the healthy bone as possible and replaces the opposing surfaces only on the side of the knee joint that is damaged. If the arthritis is widespread then TKR surgery is the preferred option where the entire joint surface is replaced. There are two types of total knee replacements. These are a traditional fixed-bearing knee (Figure 1.1b) and a mobile bearing (rotating platform) knee (Figure 1.1c). The main difference is in the design of the tibial component of the implant. In fixed bearing designs, the plastic bearing is securely attached to the top surface of the tibial tray. In mobile bearing designs, the plastic bearing can rotate to imitate natural knee motion. The goals for a TKR are to reduce pain associated with OA and restore a degree of non-pathological (NP) joint function (Andriacchi, 1993; Myles *et. al.*, 2002). The functional demands can vary depending on the patient.

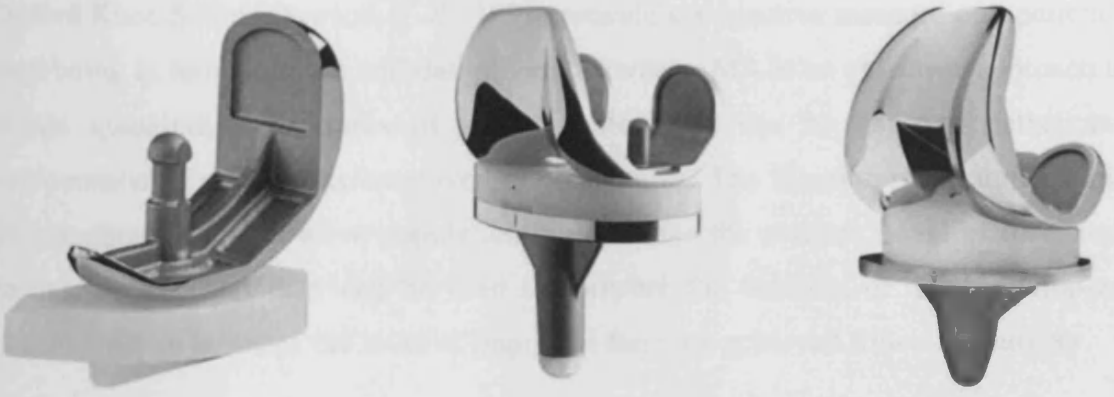

(a) (b) (c)

Figure 1.1 Examples of knee replacement options. (a) Preservation® Uni-compartmental Knee System, (b) Sigma® Fixed Bearing Knee System, (c) Sigma® RP-F Knee System (mobile bearing). Images from DePuy Orthopaedics, Inc.

As the evolution and development of TKR implants and surgical methods has increased the longevity of the implant, surgeons are beginning to describe a new generation of patient. These patients are requesting a TKR at a younger age, lead an active lifestyle and request an implant that would enable them not only to lead an

active lifestyle but one where they would be able to continue playing a range of sports.

The increasing demand from patients drives the orthopaedic market to continually develop and improve implant designs to accommodate the patients' needs. Pre clinical testing of implants involves in-silico and in-vitro studies. In-silico techniques are used heavily in the design and development stages of implants as they do not require physical components. Finite element modelling is used to simulate the effects of various loading conditions on the implants. In-vitro studies test the performance of an implant according to ISO standards. Simulators are used to measure implant wear, fatigue and micromotion between implant and bone. Useful feedback for implant designs can be obtained from post surgery testing, in-vivo to measure the performance of the implant in the patient for a range of activities, during and beyond the recovery period. The two systems in place to assess knee function before and after TKR surgery are patient-reported scoring systems and MA studies. The scoring systems such as the Knee Outcome Survey (KOS) (Irrgang *et al.*, 1998), WOMAC and the Oxford Knee Score (Dawson *et al.*, 1998) provide a subjective measure of a patient's well being in terms of pain and daily living activities. MA is an objective approach to obtain quantitative measures of knee function and can be used to detect any compensatory mechanisms employed at other joints. The function of an implant can be compared to a normative population to determine the patients' level of functional recovery. The MA data can be used to compare the function of different implant design types in terms of the level of improved function achieved following surgery.

The clinical trial at Cardiff was established to examine knee function of patients who are suffering from OA, before and after TKR surgery. The ultimate goal of the trial is to characterise the differences between two different DePuy TKR designs. The two designs are the P.F.C. Sigma (fixed bearing knee system, (FTKR)) and the DePuy P.F.C. Sigma R.P. (rotating platform knee system (RTKR)). It was hypothesised that the RTKR would produce knee biomechanics more characteristic of non-pathological (NP) function compared with the FTKR. However, comparing the data from the two designs was initially a challenge in a number of ways:

1. A vast amount of data is collected during a data collection session. This includes anthropometrical measurements, kinetic and kinematic waveforms, temporal-distance parameters and patient related information.

2. An initial study compared the designs in terms of one discrete variable (transverse plane range of motion (ROM)) (Holt *et al.*, 2002). Using one variable to compare function of a 6 degree of freedom (DOF) joint meant that potentially important information lies redundant. This study also used parameterised waveforms for the analysis. This introduces the danger of discarding valuable temporal information; also, gait parameters defined using NP waveforms are not always identifiable in pathological waveforms.

This motivated the development of the Dempster-Shafer (DS) classification method to analyse MA data.

1.1.2 The DS classification method

In response to the data analysis requirements for the clinical trial, the DS classification method was developed to produce an automated analysis from MA data to differentiate the characteristics of OA (pre-operative TKR) and NP knee function. It can diagnose the extent to which a patient has developed OA and recovered after subsequent TKR surgery. A detailed explanation of the method is provided in Chapter 2. The following is a brief summary of the method.

The DS classification method exploits the Dempster-Shafer (DS) theory of evidence to allow for a degree of ignorance in a subjects classification. This allows for a level of uncertainty as to whether a gait variable indicates OA or not. Due to the nature of MA data the ability to make decisions in the presence of uncertain, inadequate and conflicting evidence is an important feature of the DS classification method.

The method transforms each input variable obtained from a gait analysis into a set of three exact belief values. These are a level of belief that the subject has OA knee function, a belief that a subject has characteristics of NP function and an associated level of uncertainty. Together these form a characteristic body of evidence (BOE)

that offers either positive or negative support to a particular classification hypothesis. As previously mentioned, using one variable to assess joint function is not ideal. It would be of far greater value to determine how the alteration of multiple variables has combined to produce an overall transformation in a subjects' gait pattern. As part of this method, the BOEs associated with each variable are combined using the Dempster's rule of combination. The final combined BOE indices are represented as a unique point on a simplex plot. Simplex plots are used to visualise the final classification of subjects knee function as either OA or NP, based on the final combined BOE indices. Simplex plots are also used to provide a visual representation of the contribution of each input variable to the final classification. The visual outputs provide a simple means for a clinical interpretation of the results from MA and can be used to monitor periodic changes in a subject's knee function due to TKR surgery and subsequent recovery, as illustrated in Figure 1.2. The simplex plot is divided into four regions of knee function classification: (A) Dominant NP (B) Non-dominant NP (C) Non-dominant OA (D) Dominant OA. It is expected that a subject with NP knee function would lie to the left of the decision boundary and a subject with OA function to the right. A subject situated in region D has a stronger OA classification than one situated in region C.

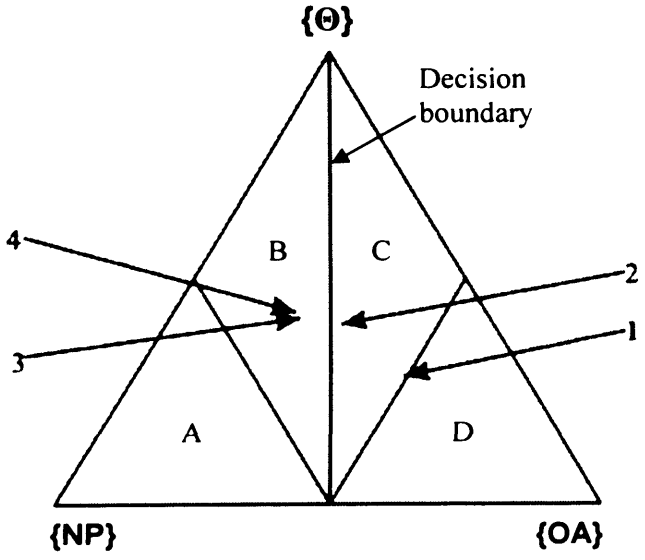

Figure 1.2 Simplex plot showing knee function of a patient (1) with advanced knee OA, (2) 3 months post TKR surgery, (3), 6 months post TKR surgery and (4), 12 months post TKR surgery. Region A indicates the region of dominant NP knee function, B indicates the region of non-dominant NP knee function, C indicates the region of non-dominant knee OA and D indicates the region of dominant OA knee function. Figure adapted from Jones and Holt, (2008).

The DS method was compared with two other well established methods, (Jones, 2004), namely the Artificial Neural Network (ANN) and Linear Discriminate Analysis (LDA). The DS method proved to be highly accurate, classifying subjects with an out-of-sample accuracy of 97.62%, calculated using a Leave-One-Out (LOO) cross validation approach, compared with 63.89% using ANN and 95.24% using LDA. Using a sample of n subjects, the LOO approach trains the classifier on (n-1) training cases to determine the control variables used in the classification. It then tests the classifier on the remaining case. This process is repeated n times and the LOO error accuracy is calculated as the average test case error rate. The out-of-sample accuracy is defined as 100 minus the LOO error. This method provides nearly an unbiased estimate of the true error rate, even for small sample sizes (Weiss and Kulikowski, 1991).

A need for a universal tool to assess outcome following TKR surgery is widely recognised. Davies, (2002) outlined requirements that must be fulfilled by any method employed to assess TKR outcome. How the classifier addresses the main recommendations is briefly discussed below:

1. **The level of benefit achieved by surgery should be established:** The BOE indices generated using this method quantify knee function pre and post surgery. The benefit achieved by surgery is visualised using simplex plots.

2. **The method should enable the direct comparison between subjects:** This also is made possible using the BOE indices and simplex plot.

3. **The outcome should be related to the clinical results:** There has been no significant correlation between classification output and a subjective clinical score, namely the KOS. This is due to the different perspectives on the assessment of knee function provided by the scores and MA.

4. **It should be simple:** The method consists of five steps which are simple and logical to follow. The visual representations of the final classification and of the influence each input variable has on the final classification, make the interpretation of MA data straightforward.

5. **Important measurable characteristics of the knee that are clinical variables and are easily quantified should be used:** input variables can be selected manually or using a feature selection algorithm.

6. **It should enable a direct comparison between different surgical techniques or implants to be made:** It is anticipated that the tool can be used to compare outcomes of different surgical techniques or implants. Although this requires further investigation.

Following the establishment of this reliable, accurate method of analysing MA data to characterise joint function, there are a number of investigations that would aid its validation and to explore its capabilities.

1. The success of classification methods is highly dependent on the appropriate selection of the input variables. An amount of uncertainty exists as to which variables are the most relevant for solving a clinical problem. To date, MA data from level gait has been analysed. However, it is possible that MA data from other dynamic tasks have different influences on the final subject classification.

2. The final classification will be affected by the accuracy in the measured MA data. Large errors can exist in non-sagittal knee rotations measured using MA. The errors associated with the current measurement protocol should be investigated.

3. The DS classifier is a generic method. However, its merits to other clinical applications have not yet been investigated. It is proposed that it is applied to an alternative clinical application.

The next section of this chapter provides an overview of the use of the classifier to date, outlines other studies that have assessed knee function and highlights the range of errors associated with motion analysis. The review is intentionally brief as each subsequent chapter contains an associated theoretical background.

1.2 LITERATURE REVIEW

1.2.1 The DS Classifier

The DS classifier is a visual tool that can be used to support orthopaedic decisions (Jones, 2004; Beynon *et al.*, 2006; Jones *et al.*, 2006; Jones and Holt, 2008). In a study of nine TKR subjects (Jones and Holt, 2008) assessed pre-operatively and 3, 6, and 12 months post-operatively, the tool successfully identified the extent to which a subject had recovered after TKR surgery. However it must be noted that none of the subjects displayed dominant normal knee characteristics following TKR surgery using level walking as the motor task under investigation. Two of the subjects showed an improvement such that they moved into a non dominant NP region on the simplex plot. This implies that the prosthetic knee does not function in the same way as the normal knee and is in agreement with other studies (Myles *et al.*, 2002; Irrgang *et al.*, 1998; Benedetti *et al.*, 2003; Fuchs *et al.*, 2002; Whittle and Jefferson, 1989).

The findings of this study raise the question; how much influence does the dynamic motor task under investigation have on the final classification? Clinically relevant variables from level gait have been used with the DS classifier, selected from the literature. However, the BOE indices and thus position of the subject on the simplex plot does not alter to a large extent post-surgery. A more biomechanically demanding task may therefore help distinguish functional characteristics to a greater degree. For example, stair gait which provides an approximation to other daily actives involving the flexed knee during high load (Garling *et al.*, 2007). It is accepted that completely normal function is not achieved post TKR but it would be good practice to test the classifier using a further motor task to determine whether levels of improvement post surgery remain small. For clinical applications, it would be desirable for the DS classifier to segregate subject function to a greater degree so that different levels of joint degeneration/improvement can be mapped on the simplex plot. If the changes in joint function remain small, the simplex plot representation may need to be redesigned. This may be achieved by identifying the range of improvement achievable following a TKR and segregating this into regions to define a scale of improvement.

1.2.2 Measuring knee function – Stair ascent/descent

Studies of level gait to assess knee function are common. However, it has been recognised that knee characteristics can be difficult to distinguish due to the limited range of motion involved, which results in small kinematic and kinetic changes between subject groups (Andriacchi *et al.*, 1982). This may explain the small changes in knee function measured using the DS classification method. Stair ascent and descent presents itself as a potentially valuable activity for investigation. It has been used successfully by a number of studies to differentiate knee function characteristics. The activity involves greater ranges of motion of the lower limbs and larger moments acting at the knee than level gait (Kaufman *et al.*, 2001) and 12-25% increase in knee loading compared to level gait (Morrison, 1969). Previous studies have used stair climbing data to assess lower limb function of able-bodied subjects (Andriacchi *et al.*, 1980; McFadyen and Winter, 1988; Kowalk *et al.*, 1996); Yu *et al.*, 1996) and to differentiate the functional characteristics of the different types of TKR replacement designs (Andriacchi *et al.*, 1982; Catani *et al.*, 2003). Knee mechanics for patients with knee OA have not been studied as extensively during stair climbing (Kaufman *et al.*, 2001). These studies also assess moments acting about the knee joint during stair gait. The joint moments have not been considered in the previous studies at Cardiff using the classifier and thus would merit investigation.

1.2.3 Accuracy studies for motion analysis systems

There are three main sources of error associated with MA. Instrumental errors can cause inaccuracies in marker coordinate data and force plate measurements. Anatomical calibration errors can be generated by the misplacement of landmark positions used to establish joint axes. This also means that inaccuracies in the reconstruction of bony landmarks positions from plate mounted markers can also occur. The largest errors in measurements of human movement are soft tissue artefact (STA), (Andriacchi and Alexander, 2000). The reader is directed to Della Croce, (1996) for a comprehensive overview of the literature related to STA.

Using a link model to compute kinematics from MA data, each segment is incorrectly assumed to be rigidly associated with the cluster of markers attached to it. STA arises

from the relative movement between skin mounted markers and the underlying bone due to the interposition of soft tissue, inertial effects, skin deformation, gravity, muscle contractions and sliding. The amount of STA will alter depending on the subject, the motor task under investigation, the marker positions and experimental protocol.

A range of assessments have been carried out to quantify the magnitude of STA during a range of activities. Studies have used intracortical pins (Cole *et al.*, 1993; Fuller *et al.*, 1997; Karlsson and Lundberg, 1994; Lafortune and Lake, 1991; Lafortune *et al.*, 1992; Yack *et al.*, 2000), external fixation devices (Angeloni *et al.*, 1992; Cappozzo *et al.*, 1996) and percutaneous trackers (Holden *et al.*, 1997; Manal *et al.*, 2000; Manal *et al.*, 2002) to quantify the motion of skin markers with respect to underlying bony segments. These methods are reliable but limit the natural motion of the skin and underlying tissues.

The amplitude of STA can be overwhelming and has been observed to be in the order of 10-20mm during active movements (Sati *et al.*, 1996). The range of errors reported in the literature is due to the different experimental methods and motor tasks analysed. STA introduces errors in the determination of instantaneous positions and orientations of bones (Benedetti *et al.*, 1998) and this propagates to the computation of knee kinematics with the greatest effect on non-sagittal plane joint movements. This can nullify the usefulness of these variables in the clinical interpretation of gait analysis (Stagni *et al.*, 2005). It also has an effect on the computation of joint moments. Murphy (1990) found that measuring knee kinematics through skin mounted markers could underestimate actual rotations by 50%, make the underlying kinematics look noisy and degrade the repeatability of results.

The frequency content of STA is similar to that of bone movement and thus it is not possible to distinguish between them by means of filtering techniques. Due to high subject variability of the STA, subject specific models are preferable. Two main approaches are used to reduce the effects of STA on joint kinematics; those using models operating at a body segment level and those making use of multi-link body models (Della Croce, 2006). Numerous approaches are limited due to task and inter-

subject variability of STA. Models that compensate for STA using subject specific models are favoured.

Roentgen photogrammetry has also been used (Sati *et al.*, 1996; Imai *et al.*, 2003; Nilsson *et al.*, 1991; Papaioannou *et al.*, 2008). This involves the use of x-rays or fluoroscopy images and steel or tantalum markers attached to the skin or implanted in bone. It does not limit skin motion but does not usually allow for a full 3D tracking of skin markers and can only be used to study the joint in a static condition.

For the current Cardiff protocol, the knowledge of how STA propagates to knee kinematics is necessary to improve methods to clinically interpret gait analysis data. Only once the magnitude of this error is accurately quantified can steps be taken towards accounting for the errors in the classification procedure.

1.2.4 Background Discussion

The DS classifier is potentially an extremely useful and practical tool for many clinical applications. It has high classification accuracy with a superior performance as compared with the ANN and LDA methods to analyse MA gait data.

It has been observed that, despite the high classification accuracy, when using the DS method to monitor recovery post TKR, the position of the patients on the simplex plot does not move considerably. This indicates poor recovery of patients and is in agreement with other studies that TKR function does not reach a level that is considered to be normal (Benedetti *et al.*, 2003; Andriacchi, 1993; Myles *et al.*, 2002; Fuchs *et al.*, 2002; Whittle and Jefferson, 1989). It would be useful in a clinical situation to be able to monitor more defined changes on the simplex plot for comparative and diagnostic purposes. It can be questioned how much of the patient outcome is related to the implant, patient factors, (i.e. Body Mass Index (BMI) or level of physiotherapy post surgery), and the input variables used. Also, the classifier currently characterises OA and TKR function relative to a normative function measured from a younger population with no pathology. It may be more beneficial and realistic to characterise function against the non-operative leg or an age matched population. This would remove a region of functional ability on the classification

simplex plot that the patient would never be expected to achieve. However, choosing a suitable comparison would be difficult as it is common for patients with a TKR to have developed a level of OA of the contralateral knee joint due to compensatory mechanisms.

The current variables used are selected based on published studies, and agree with factors that surgeons suggest being useful indicators of knee function. It would be useful to investigate the effect of using variables from other dynamic activities on a subject's classification. The inclusion of variables from a more demanding activity may help produce a greater distinction between patient groups. Previously only gait data has been considered. It is clear that a range of daily activities should be included to investigate the effect on the classification output. It would also be useful to compare the classification output with the more traditional diagnostic method of analysing kinematic and kinetic waveforms.

This work introduces kinematic and kinetic measures from stair ascent and descent. This involves the design of a suitable staircase and joint moment calculations to be included in the current analysis software. The efficacy of using stair gait variables with the DS classifier is investigated.

The DS classifier was developed to accommodate a level of uncertainty associated with characterising MA data. Uncertainty is one form of ignorance inherent with MA data, the other forms are imprecision and incompleteness. In this work, the initial stages of assessing the imprecision of the input variables to the classifier are addressed. A method is developed using dynamic fluoroscopy and image registration (Banks and Hodge, 1996) to obtain an appreciation of the kinematic errors associated with the Cardiff MA protocol.

1.3 AIM AND OBJECTIVES OF THE STUDY

The aim of this study was to contribute to the clinical validation of the DS classification method.

In order to address the aim, the studies described in this thesis were undertaken to explore the following 5 key objectives:

1. Use the current data collection and DS classification method to assess TKR outcome of new patients visiting the laboratory.

On starting this study, TKR outcome had been assessed for nine subjects using the DS classification method. Increasing this number would assist in determining the clinical merits of the analysis method. This involved increasing the training set for the classifier and using it to assess NP, OA and TKR knee function from level gait. It was expected that patients gait would improve post TKR surgery. However, due to previous findings, it was unlikely that subjects would be characterised in the dominant NP region of the classification output.

2. Introduce stair ascent and descent into the protocol.

Functional measures from stair gait have been used successfully in other studies to understand NP knee function, assess lower limb pathologies and compare treatment options. Thus it was hypothesised that it should be able to improve the differentiation between various knee function characteristics as compared to level walking. To enable this activity to be included into the data collection protocol, a staircase was designed to interface with force plates and be suitable for use by patients with a range of movement abilities. The accuracy of measuring forces and centre of pressure from the staircase was tested. It was important that the staircase did not adversely effect measurements from the force plate.

The measurement of knee joint moments may be important in the assessment of stair gait and thus the calculations should be included in the in house analysis software. There are a range of methods to assess stair gait reported in the literature. For this reason, a study using subjects with non-pathological knee function was performed to compare common data collection and analysis methods. It was explored whether the use of different methodologies to assess stair gait would affect the resulting kinetic and kinematic waveforms and it was important to determine to what extent the results may differ.

3. Utilise the DS method to distinguish OA and NP knee function based on the measurements taken during stair gait.

Are variables from stair gait useful indicators of knee OA and should they be considered with the classification method? These questions were investigated by determining functional variables from stair climbing that are able to distinguish between OA and NP knee function. As a preliminary study, these variables from stair gait were used with the DS classifier to quantify changes in knee function following TKR. Following a clinical gait course, the classification output was compared to a traditional waveform analysis. The outputs were used to explore the hypothesis that stair gait variables are useful in the classification process due to the high biomechanical demands of the activity on the knee joint.

4. Develop an image based method to quantify the errors in the knee kinematics associated with the current method where markers are attached to the skin.

The accuracy of MA data will affect the clinical relevance of classifications. An imaging study was undertaken to gain an appreciation of the errors associated with MA data. Image registration techniques were established, involving dynamic fluoroscopy and the shape matching technique of Banks and Hodge, (1996). Knee kinematics from a step up/down activity measured using non-simultaneous MA and fluoroscopy were compared. The MA method was expected to produce significantly larger out of plane rotations and significantly larger joint translations than the image registration method. This is because these movements in the knee will be most affected by STA.

For the assessment of NP subjects the question was raised as to whether MRI data can be used to develop subject specific bone models of selected subjects for use with image registration? It was hypothesised that this should be possible and a proof of concept study was performed using Simpleware segmentation software (Simpleware Ltd.).

5. Demonstrate the generic nature of the DS classifier by applying it to another study.

The method is generic and thus should be applicable to other MA studies. The generic nature of the DS method was explored by using it to characterise and compare hip function following two surgical approaches to total hip arthroplasty. The DS method should be applicable to the assessment of other joints and it was expected to determine useful functional differences in postoperative outcome following the two surgical approaches.

1.4 THESIS SUMMARY

The following chapters address the 5 key objectives as follows:

Chapter 2 provides a detailed description of the data collection and classification protocol currently employed at Cardiff University to assess knee function of NP, OA and TKR subjects.

Chapter 3 presents the outcome of TKR surgery for nine new patients. The DS classifier is used to assess patient knee function prior to surgery and throughout a 12 month recovery period. The DS classifier is trained using knee function data from level walking using the method of Jones, (2004) and Jones and Holt, (2008). As an improvement to the analysis procedure, the training cohort for the DS classifier is increased by 48% to enhance classifier performance.

Chapter 4 proposes stair gait as important measures for inclusion to the Cardiff assessment protocol. A new staircase design that interfaces with force plates is described along with its validation. Current methodologies for assessing stair gait kinematics and kinetics are compared. A method to assess stair gait is recommended for use with the Cardiff protocol.

Chapter 5 presents a study which explores the use of stair gait with the DS classifier. Stair gait variables are used to characterise osteoarthritic knee function and quantify the level of improved knee function for one subject following TKR. This study was

presented at five conferences, the 16th annual meeting of ESMAC, (Whatling *et al.*, 2007a), 6th Combined Meeting of the Orthopaedic Research Societies, (Holt *et al.*, 2007), 8th International Symposium on Computer Methods in Biomechanics and Biomedical Engineering, (Whatling *et al.*, 2008a) 16th Congress of the European Society of Biomechanics, (Whatling *et al.*, 2008b) and the 10th International Symposium on 3D analysis of human movement of the International Society of Biomechanics, (Whatling *et al.*, 2008c).

Chapter 6 presents a study to examine the errors in knee kinematics associated with the passive marker motion analysis method employed at Cardiff. An image registration protocol to assess knee kinematics is developed for this study. The work from this chapter was presented in two conference papers. The first paper was presented at the 8th International Symposium on Computer Methods in Biomechanics and Biomedical Engineering, (Whatling *et al.*, 2008d). The second paper was delivered as a podium presentation at the 10th International Symposium on 3D analysis of human movement of the International Society of Biomechanics, (Whatling *et al.*, 2008e).

Chapter 7 demonstrates the generic nature of the DS classifier by applying it to a new clinical application. The DS classifier is used to compare hip function following a posterior and direct lateral approach to total hip arthroplasty. This work produced a journal publication (Whatling *et al.*, 2008f) and conference papers presented at the 7th International Symposium on Computer Methods in Biomechanics and Biomedical Engineering, (Whatling *et al.*, 2006a), 9th Symposium on 3D analysis of Human Movement, (Whatling *et al.*, 2006b), 5th World Congress of Biomechanics, (Whatling *et al.*, 2006c), The Institution of Mechanical Engineers Meeting Engineers & Surgeons: Joined at the hip, (Whatling *et al.*, 2007b), 16th annual meeting of ESMAC, (Whatling *et al.*, 2007c), 8th International Symposium on Computer Methods in Biomechanics and Biomedical Engineering, (Whatling *et al.*, 2008g) and 10th International Symposium on 3D analysis of human movement of the International Society of Biomechanics, (Whatling *et al.*, 2008h).

Chapter 8 provides a set of conclusions drawn from this work and provides directions for future studies.

CHAPTER 2
THE CARDIFF PROTOCOL FOR MEASURING KNEE FUNCTION

Cardiff University has a state of the art data collection and analysis procedure to assess knee function of non-pathological (NP), osteoarthritic (OA) and total knee replacement (TKR) subjects. This chapter provides a detailed summary of the patient recruitment, data collection, data handling and classification procedures that are currently in place as part of an on-going clinical trial conducted in the motion analysis (MA) laboratory in the School of Engineering, Cardiff University. The data collection and handling protocol was established by Holt *et al.*, (2000) and the classification method by Jones, (2004). This chapter provides a basis of the protocol which is expanded in subsequent chapters.

2.1 PATIENT RECRUITMENT

Ethical approval for the clinical trial was granted by the Bro Taf Health Authority Local Research Ethics Committee (reference number 98/2610). Patients suitable for the trial were selected by two orthopaedic consultants from the University Hospital of Wales. They were given an information sheet, informed consent was obtained and they were referred to the clinical trial for four MA sessions. A copy of the information sheet and consent form is given in Appendix B. A patient's first visit was typically one week prior to TKR surgery. Subsequent visits were at three, six and 12 months after their operation date. A cohort of subjects without lower limb pathology was recruited following emails and posters circulated throughout Cardiff University.

2.2 DATA COLLECTION

2.2.1 Equipment set up and calibration

The laboratory is equipped with an opto-electonic measurement system (Proreflex, Qualisys, Sweden) run using Qualisys Track Manager (QTM) software. The laboratory system comprises eight 120Hz infra-red motion capture units (Figure 2.1a), capturing at 60 Hz, two force platforms (Bertec Corporation, Numbers N60202 and

N60203, Type 4060H) embedded in the laboratory floor (Figure 2.1b) and capturing with a sample rate of 1080Hz, two Panasonic NV-GS27 digital video cameras (© Panasonic UK Ltd.) and a computer.

A map of the infra-red camera layout is shown in Figure 2.2. The cameras were modified to this position at the start of the current work to create a large measurement volume. This allows the cameras to detect the movement of retro-reflective markers attached to the lower limbs during a variety of daily tasks. The video cameras were positioned to record fontal and lateral viewpoints of a subject's gait and were synchronised with the motion and force data collection.

(a) (b)

Figure 2.1 (a) An infra-red MCU digital camera and (b) the force platforms (FP) embedded in the floor of the laboratory.

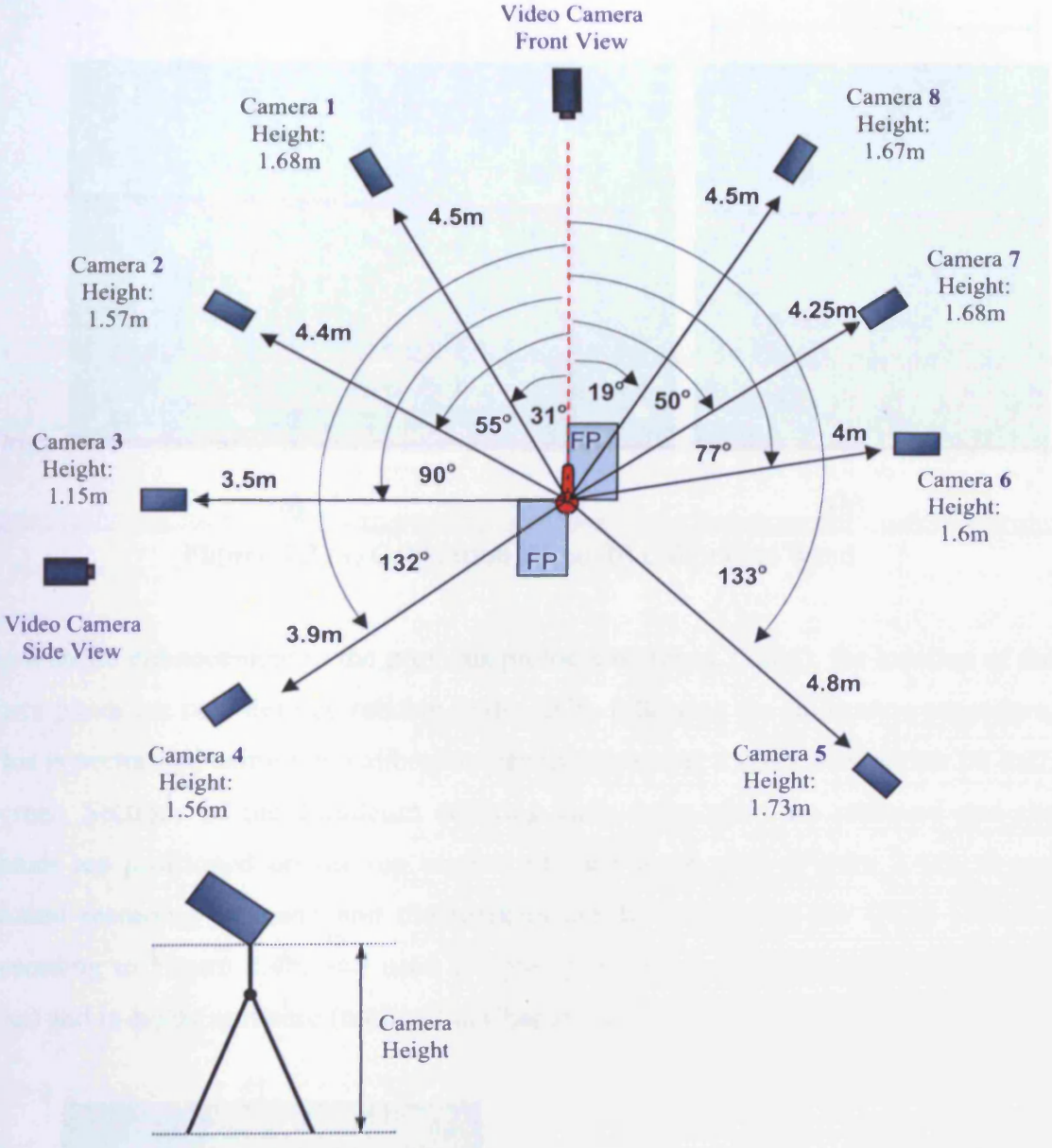

Figure 2.2 Camera Set up for the clinical trial to assess knee function.

Prior to data collection, the laboratory is calibrated to define a global coordinate system (GCS). The calibration is performed using a 750mm wand kit (Qualisys, Sweden). An L shaped calibration frame (Figure 2.3a) is placed on the floor of the laboratory. This defines the x-axis of the GCS along the long arm of the frame, the y-axis along the short arm of the frame and the z-axis vertically upwards. The origin of the GCS is defined as the location of the marker in the corner of the L frame during the calibration. A marked wand (Figure 2.3b) is moved over the frame to calibrate a bounding volume large enough to capture the movement of a subject's lower limbs during one complete level and stair gait cycle.

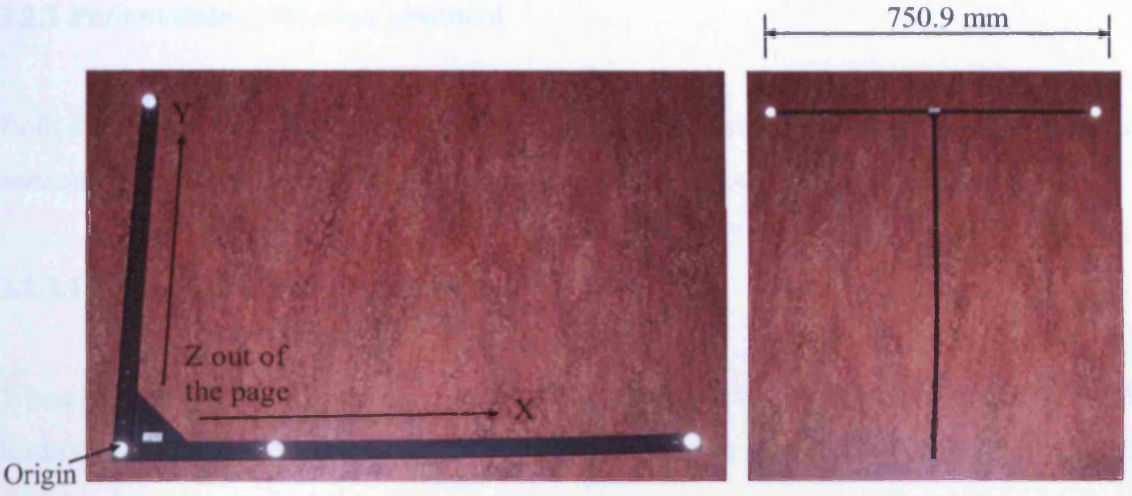

(a) (b)

Figure 2.3 (a) Calibration frame (b) Calibration wand

As a useful enhancement to the previous protocol of Jones, (2004), the location of the force plates are now defined relative to the GCS, following the calibration procedure. This is performed using two calibration panels containing a reflective marker on each corner. Sections of the Linoleum covering each force plate are removed and the panels are positioned on the top surface of each force plate (Figure 2.4a). A one second recording is made and the markers are labelled using the QTM software according to Figure 2.4b, and used for post processing using Visual3D (C-motion, Inc.) and in-house software (outlined in Chapter 4).

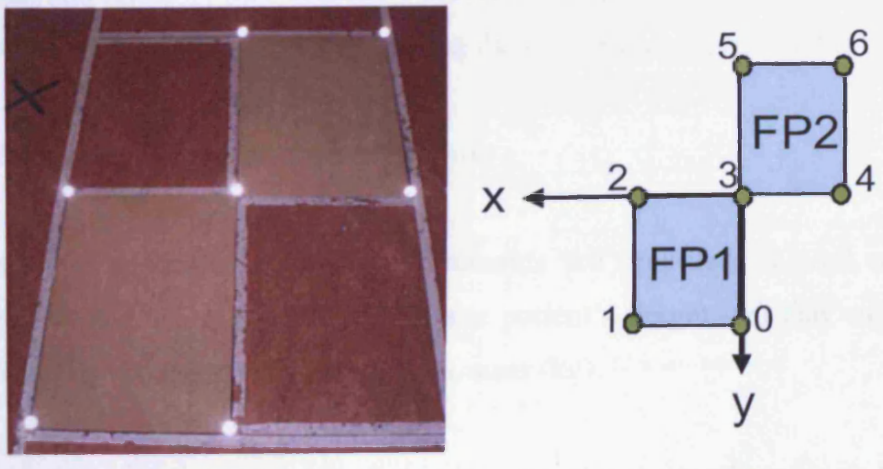

(a) (b)

Figure 2.4 (a) Calibration panels positioned on top of each force plate (b) Numbering protocol for the corners of each force plate. X and Y indicate the direction of the GCS

2.2.2 Patient data collection protocol

Both knees are tested, regardless of the knee under investigation. A data collection session consists of a number of stages. These will now be described in detail.

2.2.2.1 Collection of subject details

When the patients are referred to the trial, there is no prior knowledge of their clinical history or clinical scores relating to their knee function that were measured in clinic. For this reason, during the first assessment session a patient information sheet is completed during a discussion with the patient. This provides a summary of the patient's relevant personal details and their account of their medical history. The information gathered includes the subject's date of birth, the date they first approached a doctor due to problems with their knee and their operation date. We also establish if the knee problems have been gradual or caused by an accident, if the pain is constant or triggered during specific movements and if the subject has any other medical complaints. It is important to gain a picture of the patient's health and determine if there are any factors other than knee problems that may affect the data collection session.

For patient visits after the operation, an account of their recovery, function of their new joint and levels of physiotherapy received is recorded on the information sheet. A copy of the information sheet used during data collection is provided in Appendix C.

2.2.2.2 Anthropometrical measurements

A number of anthropometrical measurements are recorded. A wall mounted tape measure (Seca Ltd.) is used to record the patient's height (m) and weighing scales (Seca Ltd.) used to measure the subject's mass (kg).

Thigh girth (cm) is measured to determine quadriceps muscle mass and provides an indication of muscle wastage in the affected knee. This is measured using a measuring tape positioned behind the knee with the subject sitting with their feet flat on the floor and knees flexed to 90^{o}. An average of three measurements is recorded.

Medial–lateral and anterior-posterior knee widths are measured using callipers to provide information on knee swelling. With the subject remaining in a seated position, callipers are used to measure the medial-lateral knee width between the epicondylar gaps. With the subject standing, the callipers are used to measure the anterior-posterior knee width. This is measured between the crease at the back of the knee and the most protruding part of the kneecap.

2.2.2.3 Marker placement

Marker clusters are used as technical markers to track the thigh segment and shank segment during dynamic movements. Each cluster consists of copolymer polypropylene with a non-slip backing and four passive retro reflective markers. Each cluster was previously moulded for comfort and to fit the curvatures of various segment sizes. A marker cluster is attached laterally on the thighs and shanks of each subject in positions where skin movement it known to be minimised (Cappello *et al.*, 1997) and secured in place using self adhesive Coban™ tape, (Figure 2.5).

Figure 2.5 Marker clusters positioned laterally on the shank and thigh and secured using Coban™ tape

2.2.2.4 Anatomical calibration

This anatomical calibration is performed to identify the position coordinates of three anatomical landmarks per segment (thigh and shank). These are used in post processing to determine orthogonal anatomical joint axes attached to the thigh and shank.

With the subject standing in a neutral position, manual palpation is used to identify each anatomical landmark in turn for the shank (medial epicondylar gap, lateral epicondylar gap and medial malleolus) and thigh (medial epicondylar gap, lateral epicondylar gap and upper border if the trochanter). The locations of the anatomical landmarks are shown in Figure 2.6. The point of an aluminium pointer containing four retro-reflective markers is used to manually digitise each anatomical landmark in 3D space, during a one second recording, Figure 2.7. Each measurement records the position of the maker clusters attached to the segments and the markers attached to the pointer, in terms of the GCS of the laboratory. A pointer is used as it is able to locate positions closer to the bone as compared with surface mounted markers. The location of the point relative to the markers on the pointer were previously determined, allowing accurate identification of each landmark using marker coordinate data.

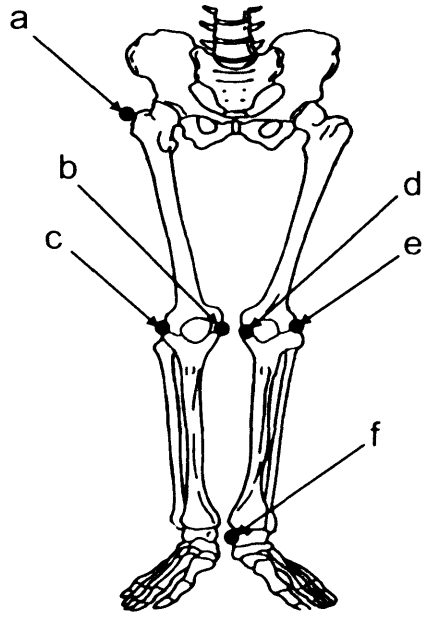

Figure 2.6 Location of anatomical landmarks for the femur: a) upper border of the trochanter, b) medial epicondylar gap, c) lateral epicondylar gap; and tibia: d) medial epicondylar gap, e) lateral epicondylar gap, f) medial malleolus.

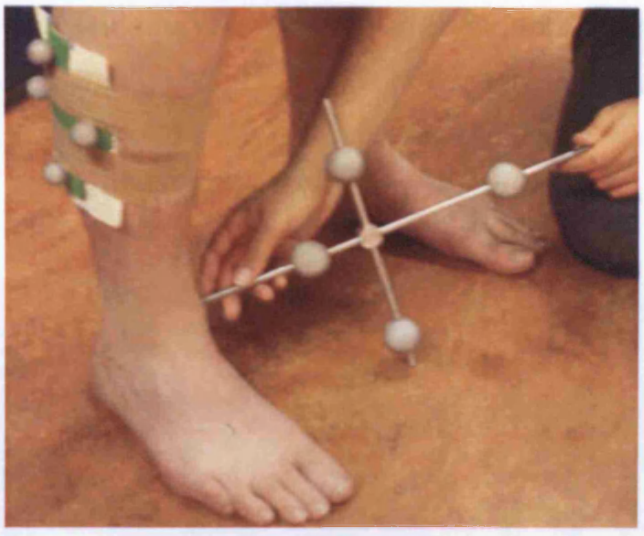

Figure 2.7 Identification of an anatomical landmark using the point of a marked aluminium pointer containing retro-reflective markers

2.2.2.5 Neutral position measurement

With the subject standing in a neutral position, a one second recording of the coordinate position data of the marker clusters is measured in terms of the GCS. This is performed to determine a constant relationship between anatomical axes established for the femur and tibia and the thigh and shank marker cluster axes. The movement of the marker clusters alone are then used to measure all subsequent articulations at the knee.

2.2.2.6 Walking trials

The subject is positioned behind a marked line in the laboratory and is instructed to walk at a self selected speed to a second line at the far side of the laboratory (Figure 2.8). A marking system on the walkway disguises the force plates embedded in the floor. During each measurement the coordinate data for each marker is recorded and each force plate records the ground reaction forces (GRFs). The two video cameras are synchronised with the recordings to provide a visual recording.

The aim of these measurements is to obtain 6 gait cycles (heal strike of one foot to the next heal strike of the same foot) for each leg where the foot has contacted the force plate cleanly (i.e. contacted within the bounds of the force plate). The subjects are unaware of the force plates and so they are lined up before each trial to maximise their potential of hitting a force plate without them targeting it.

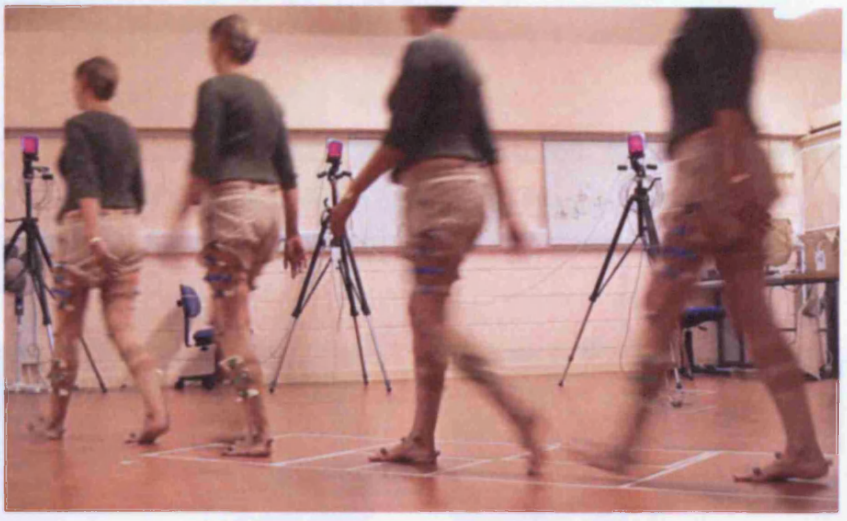

Figure 2.8 A walking trial showing markings to disguise the force plates.

2.2.2.7 Assistive range of movement trials

In these tests the knee joint is moved passively to measure its full range of motion. When a joint is passively moved, it is expected to produce a greater range of motion (ROM) than during active movements, where the subjects move their own joint. Two types of passive movements are performed with the subject sitting. The first test is assisted flexion-extension, where the shank is moved to flex and extend the knee repeatedly for a ten second duration, (Figure 2.9). The second test measures internal-external rotation, (Figure 2.10). For this test the subjects heel remains on the ground and their foot is rotated internally and externally to produce rotation about the long axis of the shank. This test is also performed for ten seconds. The data from these measurements have never been considered in the Cardiff analysis protocol and warrant investigation in future work.

(a) (b)

Figure 2.9 Assistive knee (a) flexion and (b) extension. Stills taken from a Panasonic NV-GS27 digital video camera (© Panasonic UK Ltd.)

(a) (b)

Figure 2.10 Assistive knee (a) internal rotation and (b) external rotation. Stills taken from a Panasonic NV-GS27 digital video camera (© Panasonic UK Ltd.)

2.2.2.8 Sit-to-stand tests

The subjects are initially sitting in a chair without arms with one foot contacting the floor within the bounds of a force plate. Force and marker position data are measured as the subject stands from a seated position. The data from these measurements are also redundant and warrant study in future work.

2.2.2.9 Knee Outcome Questionnaires

Each subject is asked to independently complete two knee outcome questionnaires to rate the function of both their knees. The questionnaires used are the activities of daily living scale of the knee outcome survey (KOS) (Irrgang *et al.*, 1998) and a new addition to the trial for the current study is the Oxford Knee Score (Dawson *et al.*, 1998). Both scores allow the patients to subjectively measure their symptoms and functional limitations to daily activities imposed by their knee pathology or surgery. A copy of the KOS and Oxford Knee Score is given in Appendix D.

KOS consists of 17 questions; seven relating to symptoms and ten relating to functional disability. The subject must select one from a number of associated statements which best describes their recent experience. A scoring system is used to rate knee function and display it as a percentage. A high final score is associated with a high level of knee function and vice-versa.

The Oxford Knee Score is intended specifically for use with knee surgery and asks the patients to assess their knee function by looking back over the last 4 weeks. It consists of 12 questions. There are 5 categories of response, each scored from 1 to 5, from least to most difficulty or severity. The scores are combined to produce a single score with a range from 12 for least difficulties to 60 for most difficulties. The final score is represented as a percentage.

2.3 DATA HANDLING

Raw data is processed to produce a dataset of information relating to a subjects knee function. Patient information and the variables produced during the data processing stage are stored in a database. The process for computing knee joint kinematics and kinetics from the raw data will now be discussed.

2.3.1 Computing knee joint kinematics

The infra-red cameras reconstruct the three dimensional coordinates of each marker in terms of the GCS of the laboratory. Sixty frames of coordinate data are measured each second. QTM is used to track the markers for the duration of each measurement. This process enables the labelling of each marker for post processing, the quality of the marker trajectories is verified and gaps in the data are filled. Data corresponding to one gait cycle is selected for the walking trials. This requires the trajectory of the markers to be cropped to remove superfluous data.

Previously developed Matlab software (Holt *et al.*, 2000) is used to determine knee rotations and translations from the marker coordinate data. This method establishes local coordinate systems on the pointer, each marker cluster and an anatomical coordinate system attached to the femur and tibia. The software uses the method of Söderkvist and Wedin, (1993) to calculate a series of transformation matrices to ultimately relate the position of the coordinate systems in the tibia and femur.

The approach of Söderkvist and Wedin, (1993) was used to define the transformation matrices describing the relative position of two coordinate systems. This method accounts for errors in the reconstruction of the marker coordinates due skin movement artefact, muscle contraction and sterophotogrammetric noise (Cappello *et al.*, 1997). The measurement errors are minimised by determining an optimal solution for the rotation matrix and translational vector by solving a least squares problem using singular value decomposition.

Using matrix decompositions, the joint coordinate system approach of Grood and Suntay, (1983) is applied to the final transformation matrix to describe the three dimensional rotational and translational motion of knee joint.

A flow diagram of the method used to calculate the six degrees of freedom at the knee is given in Figure 2.11.

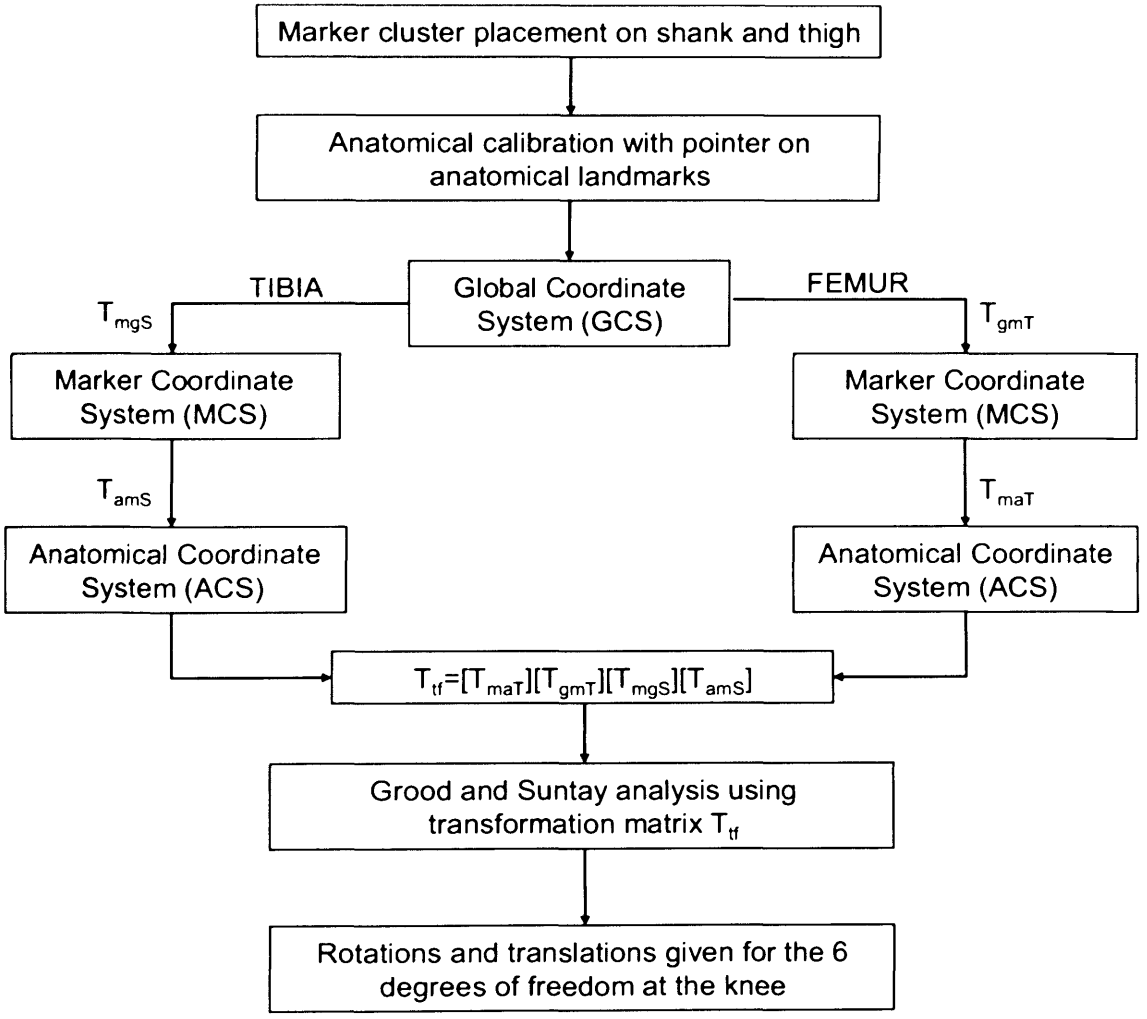

Figure 2.11 Flow diagram of the method to calculate knee rotations and translations. Adapted from Holt *et al.*, (2000).

T_{am} relates the location and orientation of the ACS to the MCS;
T_{mg} relates the location and orientation of the MCS to the GCS;
T_{gm} relates the location and orientation of the GCS to the MCS;
T_{ma} relates the location and orientation of the MCS to the ACS;
Subscripts T and S refer to the thigh and shank segments

The method will now be discussed. Each step is repeated for each frame of a measurement.

2.3.1.1 Anatomical landmark calibrations

Initial calculations are performed to establish local coordinate systems (LCS) within the pointer, marker clusters, tibia and femur. To establish a LCS on a rigid body, the coordinates of at least three non-collinear positions on that body must be known (Zatsiorsky, 1998). These are used to create three mutually orthogonal vectors forming the LCS. The following procedure is followed for each anatomical calibration measurements to define the position of three anatomical landmarks per segment (thigh and shank).

For each anatomical landmark calibration, the GCS coordinates of the pointer markers are used to establish a pointer local coordinate system (PLCS). This is achieved by defining mutually orthogonal vectors using the four markers and the vector method. The origin of the PLCS was defined as the centre of marker P_2 and the orientation of the axis system was defined as in Figure 2.12. The transformation matrix $\mathbf{T}_{pg}$ was then computed to relate the orientation of the PLCS in the GCS of the laboratory.

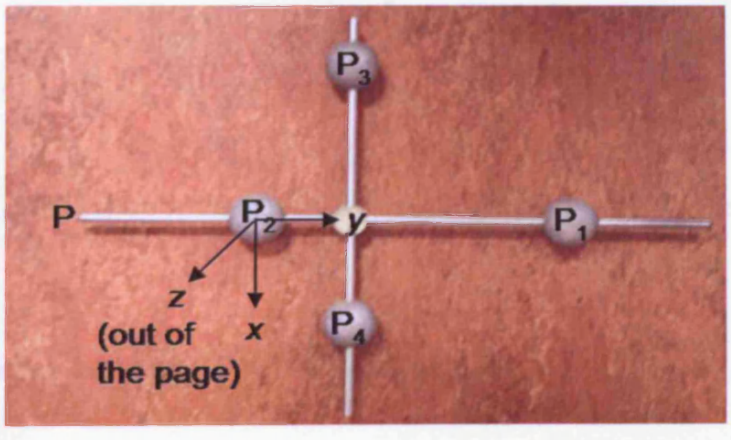

Figure 2.12 Pointer local coordinate system (PLCS) established using the four pointer markers P_1, P_2, P_3 and P_4. P denotes the point of the pointer.

For each anatomical landmark calibration, the GCS coordinates of the marker cluster markers are used to establish a marker cluster local coordinate system (MLCS). This was achieved by defining mutually orthogonal vectors using the four markers and the vector method. The origin of the MLCS was defined as the centre of marker M_2 and the orientation of the axis system was defined as in Figure 2.13. The transformation

matrix $\mathbf{T}_{mg}$ was then computed to relate the orientation of the MLCS in the GCS of the laboratory.

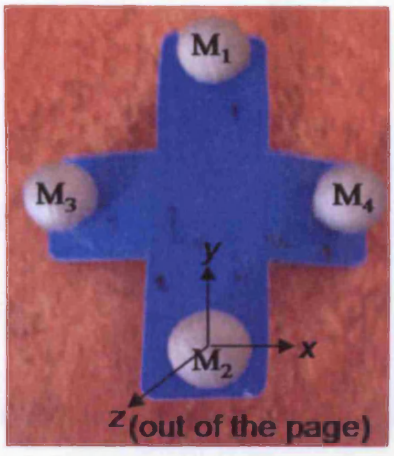

Figure 2.13 Marker cluster local coordinate system (MLCS) established using the four markers M_1, M_2, M_3 and M_4.

The MLCS coordinates of the pointer's point (P_m) are computed using (2.1) to establish the location of the anatomical landmark in the MLCS.

$$\mathbf{P}_m = [\mathbf{T}_{gm}][\mathbf{T}_{pg}][\mathbf{P}_p] \tag{2.1}$$

where P_p are the PLCS coordinates of the pointer's point and $\mathbf{T}_{gm}$ is the inverse of $\mathbf{T}_{mg}$.

2.3.1.2 Anatomical calibration for the femur and tibia

An anatomical local coordinate system (ALCS) is a fixed body axis system on the bone. These were established on the tibia and femur using the MLCS coordinates of the three anatomical landmarks (P_m) on that segment. Three mutually orthogonal vectors were defined to establish the femoral ALCS (Figure 2.14a) and tibial ALCS (Figure 2.14b) using the vector method. The origin of each system was positioned midway between the medial and lateral epicondylar gaps. The transformation matrix $\mathbf{T}_{ma}$ was then computed to relate the orientation of the MLCS in the ALCS.

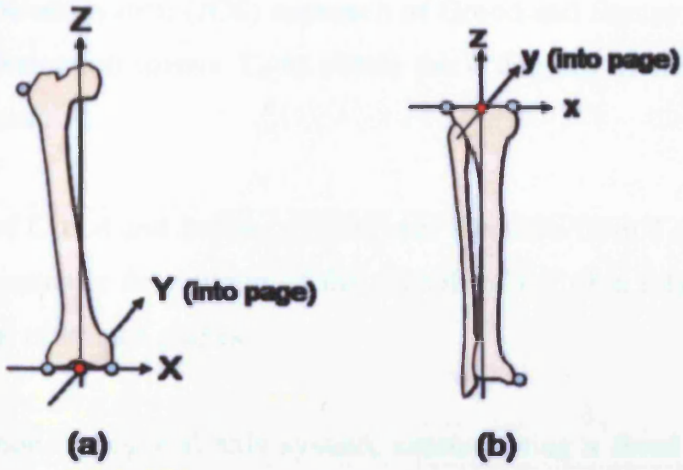

Figure 2.14 The ALCS Cartesian coordinate systems defined in (a) the femur and (b) the tibia. Capitalised letters X, Y Z denote the femoral system axes while lower case letters x, y, z denote the tibial system axes. Blue circles identify anatomical landmarks. Red circles denote origins of coordinate systems

2.3.1.3 Calculations of knee rotations and translations

The fixed body axes in the tibia and femur have been developed in relation to the marker clusters. Rigid body analysis is assumed which allows the rigid marker clusters to be used to track the position and pose of the shank and femur segments. For subsequent measurements including the neutral position and dynamic activities, $\mathbf{T}_{mg}$ is recalculated for the shank and thigh. This relates the orientation of the MLCS in the GCS of the laboratory.

The transformation matrix $\mathbf{T}_{tf}$ is calculated using 2.2. This relates the orientation of the tibial ALCS to the femoral ALCS.

$$\mathbf{T}_{tf} = [\mathbf{T}_{ma,T}][\mathbf{T}_{gm,T}][\mathbf{T}_{mg,S}][\mathbf{T}_{am,S}] \qquad (2.2)$$

where the subscripts T and S refer to the thigh and shank segments respectively, and $\mathbf{T}_{gm}$ and $\mathbf{T}_{am}$ are the inverses of $\mathbf{T}_{mg}$ and $\mathbf{T}_{ma}$ respectively.

The joint coordinate system (JCS) approach of Grood and Suntay (1983) is applied to the final transformation matrix $\mathbf{T}_{tf}$ to obtain the 6 degrees of freedom (DOF) of the tibio-femoral joint.

The approach of Grood and Suntay, (1983) uses elements from $\mathbf{T}_{tf}$ in a set of equations to provide a geometric description of the 6 DOF of the tibia relative to the femur in terms of clinical reference planes.

The JCS is a non-orthogonal axis system, created using a fixed body axis from the femur and tibia and a floating axis which is not fixed to either body, (Figure 2.15). The x-axis of the femur is taken as the flexion-extension axis of the joint rotation, the z-axis of the tibia is the internal-external rotation axis and the axis orthogonal to the previous two at any instant in time (floating axis) is the abduction-adduction axis. Three linear motions are used to describe the translational behaviour of the tibia with respect to the femur along the axes of the joint coordinate system. These are medial-lateral tibial shift along the femoral fixed axis, anterior-posterior tibial drawer along the floating axis and joint compression-distraction along the tibial fixed axis.

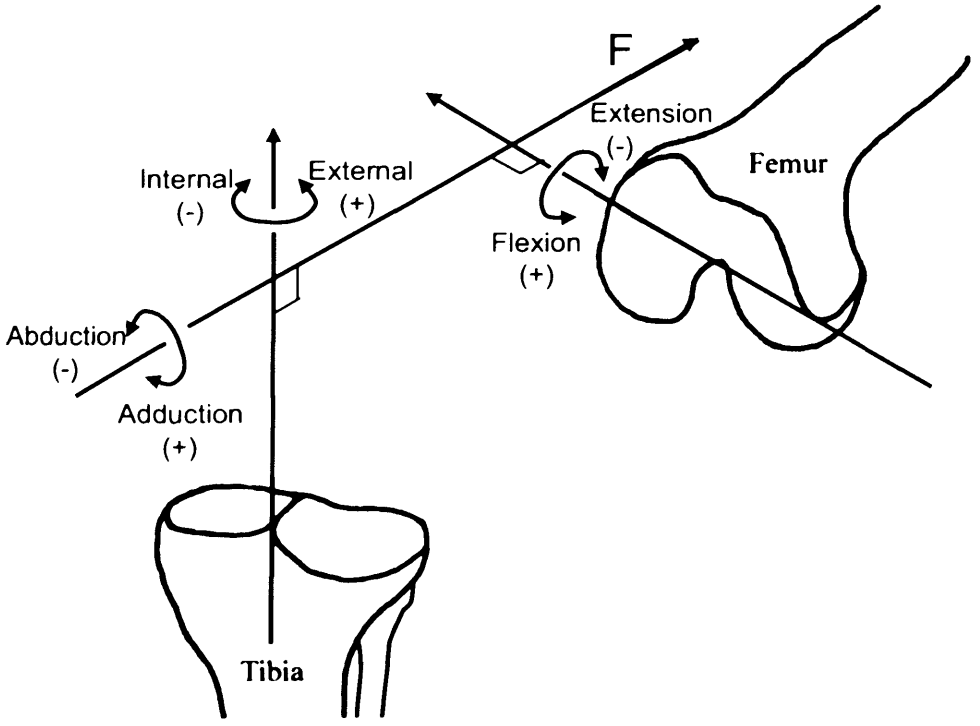

Figure 2.15 The joint coordinate system for the knee consists of two fixed body axes and a floating axis. The joint rotations occur about these three axes. Flexion-extension is about the femoral body axes, external-internal tibial rotation is about the tibial fixed axis and adduction-abduction us about the floating axis (F).

The knee joint rotations and translations can be determined from the transformation matrix T_{tf}. This is a 4 x 4 matrix consisting of a 3 x 1 translation vector [L], a 3 x 3 rotation matrix of direction cosines [R], and a 1 x 4 vector [0 0 0 1].

$$T_{tf} = \left[\begin{array}{cccc} & [R] & & [L] \\ \hline 0 & 0 & 0 & 1 \end{array}\right] = \begin{bmatrix} T_{11} & T_{12} & T_{13} & T_{14} \\ T_{21} & T_{22} & T_{23} & T_{24} \\ T_{31} & T_{32} & T_{33} & T_{34} \\ 0 & 0 & 0 & 1 \end{bmatrix} \qquad (2.3)$$

This contains the kinematics of the tibiofemoral joint. These were resolved according to the conventions of Grood and Suntay, (1983). The equations used to compute the knee joint rotations will now be listed, along with an explanation to its exact interpretation based of the matrix decomposition for each calculation. The sign convention used to define clinical rotations is used.

Flexion-extension angle (θ_{FE})

Flexion is defined as a positive angle and is the angle formed between the floating y-axis and the z-axis of the JCS according to 2.4.

$$\theta_{FE} = \tan^{-1}\left(\frac{T_{3,2}}{T_{3,3}}\right) \qquad (2.4)$$

Where $T_{3,2}$ is the projection of the y-axis of the tibia LCS onto the Z-axis of the femur LCS, indicated by Zy in Figure 2.16. $T_{3,3}$ is the projection of the z-axis of the tibia LCS onto the Z-axis of the femur LCS indicated by Zz in figure 2.16. When the tibial system axes is rotated by angle 0 to represent knee flexion, it can be seen that Figure 2.16 a and b are equivalent and θ_{FE} can be interpreted as indicated in Figure 2.16b.

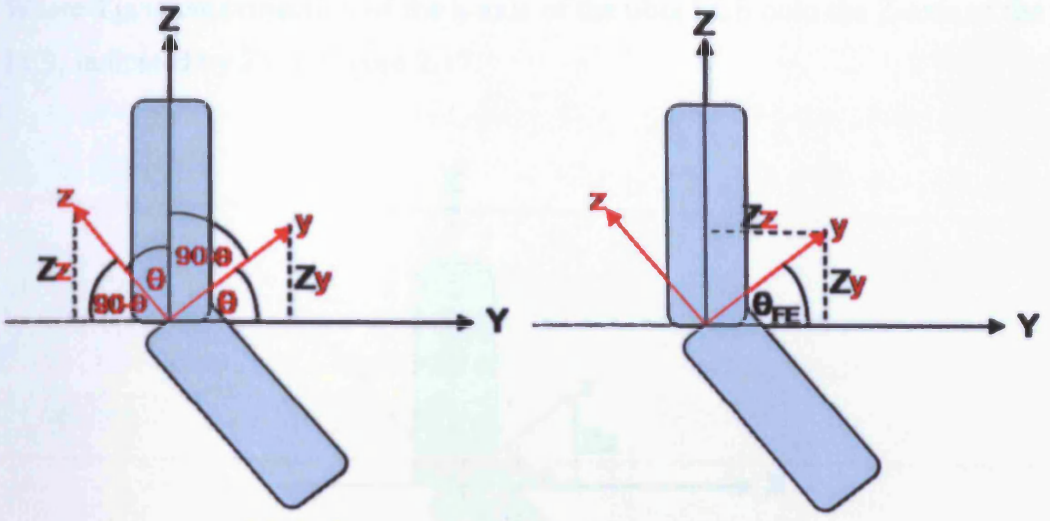

(a) (b)

Figure 2.16 Two-dimensional illustration of knee flexion in the sagittal plane. Capitalised letters X, Y Z denote the femoral system axes while lower case letters x, y, z denote the tibial system axes. The tibial system axes have been rotated about the x axis by angle θ. The resulting flexion angle θ_{FE} is shown in (b).

Adduction-abduction angle (θ_{AA})

Adduction is defined as a positive angle. It is the rotation of the tibia about the floating Y-axis of the JCS and is defined as the angle is between the X fixed body axes of the femur and z body axes of the tibia.

For the right knee it is defined by the following equation:

$$\theta_{AA} = \frac{\pi}{2} - \cos^{-1}\left(T_{3,1}\right) \qquad (2.5)$$

For the left knee it is defined by the following equation:

$$\theta_{AA} = \cos^{-1}\left(T_{3,1}\right) - \frac{\pi}{2} \qquad (2.6)$$

Where $T_{3,1}$ is the projection of the x-axis of the tibia LCS onto the Z-axis of the femur LCS, indicated by Zx in Figure 2.17.

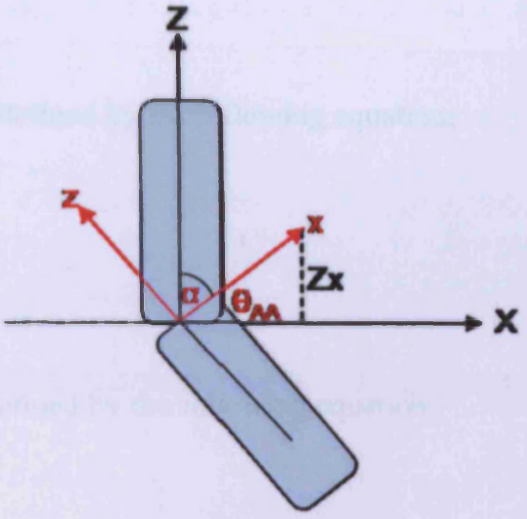

Figure 2.17 Illustration of θ_{AA} movement of the tibia in the frontal plane. Capitalised letters X, Y Z denote the femoral system axes while lower case letters x, y, z denote the tibial system axes.

Using equation 2.5 and 2.6 examples of the calculation of θ_{AA} will now be given. $T_{3,1}$ is illustrated as Zx in Figure 2.17 and is equivalent to xcosα

If $\alpha = 20^{\circ}$,

For the right leg $\theta_{AA} = 70^{\circ}$ (adducted to 70°)

For the left leg $\theta_{AA} = -70^{\circ}$ (abducted to 70°)

If $\alpha = 120^{\circ}$,

For the right leg $\theta_{AA} = -30^{\circ}$ (abducted to 30°)

For the left leg $\theta_{AA} = 30^{\circ}$ (adducted to 30°)

Internal-external rotation angle (θ_{IE})

External rotation is defined as a positive angle. It is the rotation of the tibia about the z-axis of the JCS.

For the right leg it is defined by the following equation;

$$\theta_{IE} = -\tan^{-1}\left(\frac{T_{2,1}}{T_{1,1}}\right) \qquad (2.7)$$

For the left leg it is defined by the following equation;

$$\theta_{IE} = \tan^{-1}\left(\frac{T_{2,1}}{T_{1,1}}\right) \qquad (2.8)$$

Where $T_{2,1}$ is the projection of the tibial x-axis onto the femoral Y-axis, represented by Yx in Figure 2.18. $T_{1,1}$ is the projection of the tibial x-axis onto the femoral X-axis, indicated by Xx in Figure 2.18. Figure 2.18 shows the direction of θ_{IE} indicating external tibial rotation according to the left and right leg conventions from equations 2.7 and 2.8.

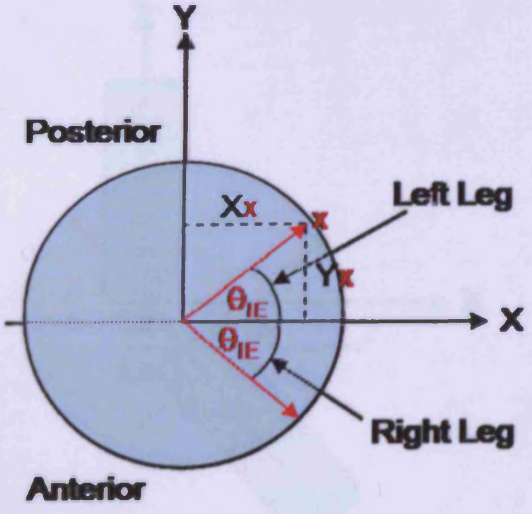

Figure 2.18 Illustration of the tibial rotation θ_{IE} in the transverse plane. Capitalised letters X, Y Z denote the femoral system axes while lower case letters x, y, z denote the tibial system axes.

The software also computes joint translations following Lafortune *et al.*, (1992). Previously, only joint rotations have been considered in analyses. Joint translations are affected by angular displacements about the floating Y-axis in the JCS. All three translations are independent of flexion-extension and internal-external rotation. Drawer translation is also independent of abduction-adduction, but shift and distraction are affected by angular displacements around the floating axis and thus use θ_{AA} in their calculations.

Medial/Lateral Shift

$$\lambda_{ML} = -\left(T_{1,4} + T_{3,4} \sin \theta_{AA}\right) \tag{2.9}$$

Where $T_{1,4}$ is the displacement of the tibia along the x-axis of the JCS (equivalent to the x-axis established in the femur). $T_{3,4}$ is the displacement of the tibia along the z axis of the JCS (equivalent to z axis of the tibia). According to the JCS, λ_{ML} is measured along the X femoral anatomical-body fixed axis. It is the summation of the pure translation of the tibia along the x-axis and the component of Lz acting along the x-axis created by the angle θ_{AA}.

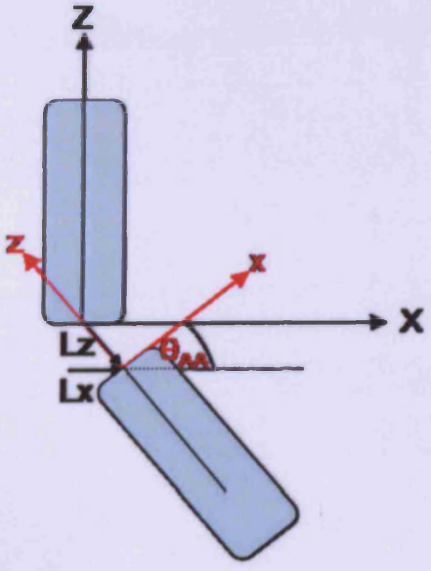

Figure 2.19 Illustration of the knee joint in the frontal plane and the elements used to compute tibial medial/lateral shift

Anterior/Posterior Drawer

$$\lambda_{AP} = -T_{2,4} \tag{2.10}$$

where $-T_{2,4}$ is the linear anterior translation of the tibia relative to the femur, measured along the floating axis of the JCS.

Compression/Distraction

$$\lambda_{CD} = T_{3,4} + T_{1,4} \sin \theta_{AA} \tag{2.11}$$

Where $T_{1,4}$ is the displacement of the tibia along the x-axis of the JCS and $T_{3,4}$ is the displacement of the tibia along the z-axis of the JCS. Figure 2.19 can be used to visually illustrate the components used in the calculation. According to the JCS, λ_{CD} is measured along the z tibial-body fixed axis. It is the summation of the pure translation of the tibia along the z-axis and the component of Lx acting along the z-axis created by the angle θ_{AA}.

For measurements of walking, the resulting rotation and translation waveforms are re-sampled over 100 points and an average of the six walking trials for each waveform is computed.

2.3.2 Computing kinetics

Three dimensional ground reaction forces (GRF's) were computed from the signals generated from the force plates using previously developed Matlab software (Holt *et al.*, 2000).

There are two force platforms in the laboratory. The coordinate system for each force plate is shown in Figure 2.20. (This differs to the Bertec manual). The origin of each force plate is located on the top surface and at the centre of the top plate.

Each force plate has been calibrated separately for an amplifier gain of unity for all channels. Therefore, each raw signal is divided by the amplifier gain before further processing. The amplifier gain is set to 20 for all channels in the current measurement protocol. The amplifier has an output range of ± 10VDC and this was the optimum gain for collecting MA data.

The force and moment components are calculated by multiplying the signals with the calibration matrix for each plate. To obtain three dimensional forces (F_x, F_y and F_z) and moment components (M_x, M_y and M_z) in the force plate coordinate system.

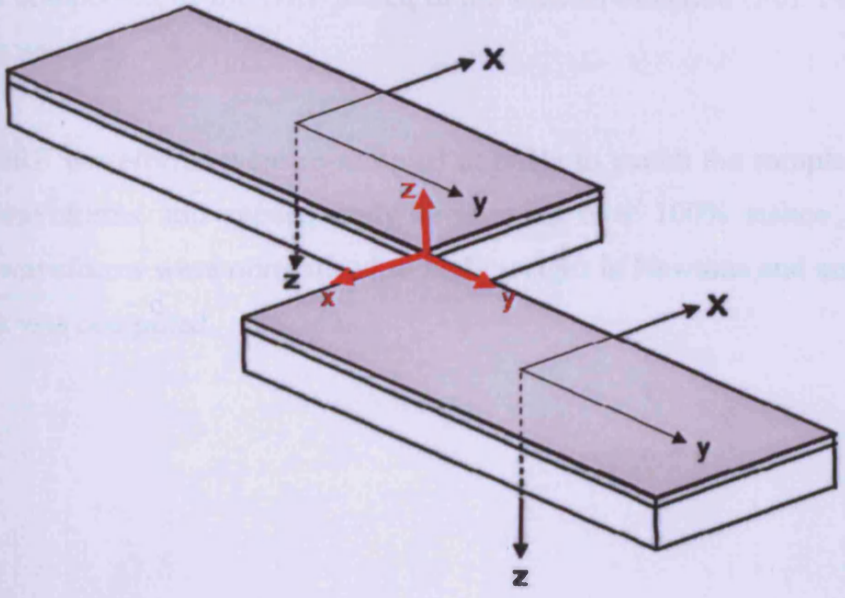

Figure 2.20 Force plate coordinate systems. The red axes illustrate the direction and origin of the GCS in the laboratory.

The component of force acting in the x direction of the force plate is multiplied by -1 to allow the direction of the force measurements to be interpreted in terms of the GCS of the laboratory.

For walking trials, subjects are asked to walk over the plates in the negative y direction. Therefore, the forces produced can be described as follows:

F_x gives the component of the force acting in the medial-lateral direction (F_{ML}). F_{ML} acting in the lateral direction is defined positive. Therefore, a correction is made for the right leg where

$$F_{ML} = -F_x \tag{2.12}$$

F_y gives the component of the force acting in the anterior-posterior direction (F_{AP}) F_{AP} acting in the anterior direction is defined positive. Therefore, a correction is made for both legs where

$$F_{AP} = -F_y \tag{2.13}$$

F_z gives the component of the GRF acting in the vertical direction (F_V). F_V is positive when acting upwards.

The three GRF waveforms were re-sampled at 60Hz to match the sample rate of the kinematic waveforms and subsequently re-sampled over 100% stance phase. The three GRF waveforms were normalised to body weight in Newtons and an average of the six trials was computed.

2.3.3 Representation of temporal waveforms using principal component analysis

Kinematic and kinetic waveforms are further processed using Principal Component Analysis (PCA). PCA is used as a data reduction method to represent each waveform in a discrete form whist retaining temporal information. This removes the danger of discarding valuable temporal information which can occur when waveforms are parameterised.

Previously developed Matlab software, (Jones, 2004) is used to obtain PC representation of the kinetic and kinematic waveforms. A summary of each stage in the procedure will now be given.

2.3.3.1 Standardisation of data

The dataset used for this method contains data for the kinetic and kinematic waveforms from each subject being analysed. Each waveform contains 100 points as they were previously sampled at each 1% from 0 to 100% of the gait cycle. Each 1% of the waveform is referred to a variable. The first stage is to standardise the entire dataset so that each variable has zero mean and unit standardization (Chau, 2001).

2.3.3.2 Calculation of the correlation matrix

The next stage is to calculate a correlation matrix for the entire set of standardised variables (Chau, 2001).

2.3.3.3 Eigendecomposition of the correlation matrix

An eigen-decomposition of the correlation matrix is derived. (Daultrey, 1976; Tabachnick and Fidell, 1989; Chau, 2001). From this, 100 eigenvalues and eigenvectors are obtained. The eigenvalues give the variance of each Principal Component (PC). The first PC has the largest associated variance whilst the last PC has the smallest variance.

2.3.3.4 Retention of PCs

Although PCA produces the same number of PCs as there are original variables, not all the PCs will be retained. The variances of the majority of PCs will be negligible so that the original data can be described by a smaller number of PCs. The Cardiff protocol currently uses the Kaiser's rule to select PCs. This rule is widely used in gait analysis and selects PCs by examining the size of their individual variances. Kaiser's rule states that any PC with a variance less than one contains less information than the original variables (which have unit variance) and are therefore not worth retaining.

2.3.3.5 Calculation of the component loadings matrix

The resulting PCs are interpreted and assigned a meaningful label. A matrix of component loadings is calculated to give a weighted relationship between the PCs and the original variables (Tabachnick and Fidell, 1989; Daultrey, 1976). A threshold value is selected and the variables with loadings above this threshold are collated. This study uses a threshold of 0.71 as suggested by Comrey, (1973). This threshold is used to ensure that each PC has a different interpretation, as above this threshold a variable can only load against one component.

2.3.3.6 Calculation of the PC scores

PC scores are calculated for each individual in the sample (Daultrey, 1976; Tabachnick and Fidell, 1989. The final PC scores are linear combinations of the original variables.

2.3.3.7 Interpretation of PCs (in terms of a gait cycle)

The PCs can be interpreted by determining the periods of the gait cycle they represent. The events of a gait cycle are depicted in Figure 2.21 and the timings of each event are recorded in Table 2.1.

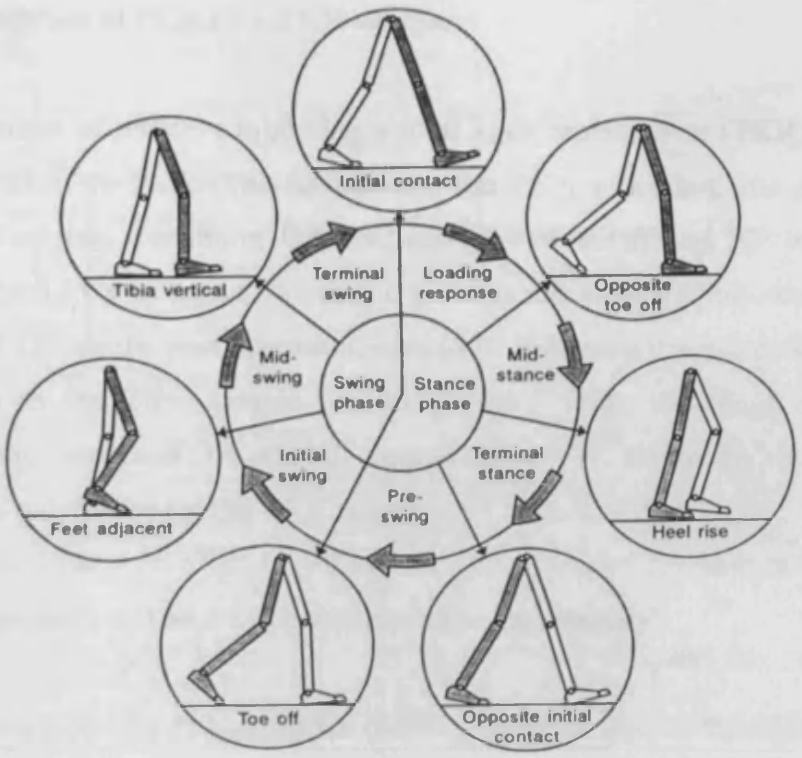

Figure 2.21 Phases and events of a single gait cycle of the right leg

(taken from Whittle, 1996, *pp.*59)

Table 2.1 Timing of gait events (taken from Jones, 2004)

Gait cycle event	Timing of event (% gait cycle)	Timing of event (% stance phase)
Initial contact	Instantaneous	Instantaneous
Loading response	0 – 12	0 – 16
Mid-stance	12 – 30	16 – 48
Terminal stance	30 – 50	48 – 81
Pre-swing	50 – 62	81 – 100
Initial swing	62 – 75	–
Mid-swing	75 – 85	–
Terminal swing	85 – 100	–

2.3.3.8 Application of PCA to a TKR sample

In the assessment of patients following a total knee replacement (TKR), a modified approach is taken to PCA. This is because the PCA procedure has already been applied to a sample containing OA (patient pre-operative) and NP waveforms to determine which PCs to retain. When the patients are assessed following a TKR at three, six and 12 months post operation, instead of following the full procedure again, the variables in the TKR sample are standardised using the mean and standard deviation of the combined OA and NL sample and the PC scores for each previously selected PC is calculated for the TKR sample.

2.3.4 Anthropometrical and temporal distance parameters

Previously developed Matlab software (Jones, 2004) is used to calculate a subject's body mass index, cadence and percentage stance phase.

BMI is defined as

$$\text{BMI} = \frac{w}{h^2} \quad (\text{kgm}^{-2}) \tag{2.14}$$

where w and h are the subject's mass and height respectively.

In this software, cadence is defined as the number of strides per minute, where a stride length is measured between successive placements of the same foot (Whittle, 1996).

Percentage stance phase computes the duration of the stance phase as a percentage of the gait cycle.

2.4 FUNCTIONAL CLASSIFICATION

Data collected from the clinical trial is interpreted using a classification method to objectively differentiate between the characteristics of non-pathological (NP) and osteoarthritic (OA) knee function.

The classification method developed and currently employed at Cardiff University (Jones, 2004) is based around the Dempster-Shafer theory of evidence (DST) and builds on the work of Safranek *et al.*, (1990) and Gerig *et al.*, (2000). The DST is founded on the work of Dempster (1968) and Shafer (1976) to provide a non-Bayesian way of using mathematical probability to quantify subjective judgements. It allows for a degree of uncertainty in the decision making process to deal with the conflicting and corroborating nature of the MA data as to whether or not a gait variable indicates normality. It achieves this by assigning levels of support to each measurement variable and subsequently combines these individual pieces of evidence to classify a subject's knee function as either NP or OA.

The DST-based classifier transforms a subject's knee function data into a set of exact belief values. These are a level of belief that a subject has OA knee function, a level of belief that a subject has NP knee function and an associated level of uncertainty. The belief values are represented as a unique point on a simplex plot to represent the final classification of a subjects knee function visually. It also provides a means of interpreting several sets of MA data simultaneously. The influence that each input variable has on the final classification is also represented on a simplex plot.

The ability to visualise patient outcomes enhances the clinical relevance and appeal of the method. It provides an indication of the severity of knee OA and has been shown to provide useful information on the effectiveness of total knee replacement surgery (Jones, 2004).

The classifier is accurate. The performance of the DS classifier was compared with two well established classification methods, the Artificial Neural Network (ANN) and Linear Discriminant Analysis (LDA). After training the DS classifier, it was able to

classify new subjects with a superior accuracy of 97.62%, compared with 63.89% using ANN and 95.24% using LDA.

The classifier can be used as a fully or partially automated tool. There are four DS control parameters which are an intrinsic part of the tool. Values can be assigned to these by expert opinion or by an optimisation approach. In a study of knee function by Jones, (2004), a superior classifier in terms of in-sample and out-of-sample accuracy was achieved using non-optimisation compared to the optimisation method using a simulated annealing algorithm.

Input variables can also be chosen manually or in cases where it is not obvious as to which variables are most useful in determining a subject's class, the input variables can be selected using a feature selection algorithm. Jones, (2004) compared the performance of the classifier using non-optimisation, Stepwise Linear Discriminant analysis, Sequential Selection Methods (SSM) and Generic Algorithms (GA). The feature selection algorithms increased the classification accuracy but also increased the level of associated uncertainty deeming the classifications clinically irrelevant.

Consequently, the non-optimisation DS classifier is used to interpret knee function. Only the non-optimisation classification procedure will be discussed further. The reader is directed to Jones, (2004) for further information on the optimisation options for the DS classifier.

2.4.1 The DS classification method

The classification method consists of five stages:

1. Conversion of input variables into confidence factors
2. Conversion of confidence factors to BOE
3. Combination of individual BOE
4. Visualisation of BOE using simplex plots
5. Classification based on the final combined BOE, BOE_c

Each stage will now be discussed in turn. The interconnections of the individual stages are illustrated in Figure 2.22.

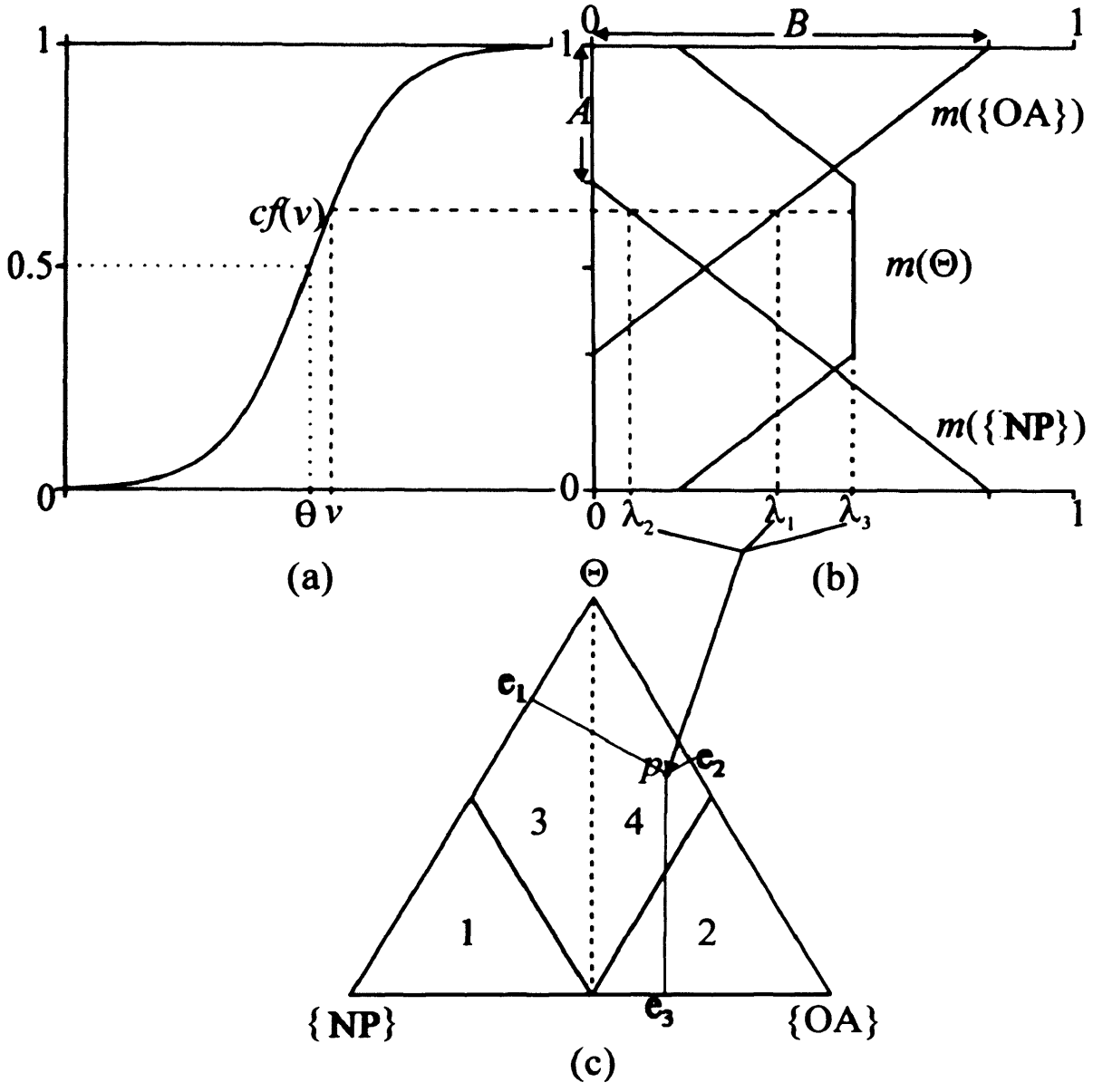

Figure 2.22 The classification method showing the interaction of its three main stages. (adapted from Jones, 2004). (a) Conversion of input variable, v, into confidence factor $cf(v)$ using the sigmoid function. θ is the value of v for which $cf(v) = 0.5$. (b) Conversion of confidence factor into body of evidence (BOE) comprising the bpa $m(\{OA\}) = \lambda_1$, $m(\{NP\}) = \lambda_2$ and $m(\Theta) = \lambda_3$. A and B are the DS control parameters. (c) Conversion of the BOE into its simplex coordinate, denoted by the point p. The simplex plot is divided into four regions denoting: 1) dominant NP classification; 2) dominant OA classification; 3) non-dominant NP classification and 4) non-dominant OA classification. The dotted vertical line is the decision boundary.

2.4.1.1 Conversion of input variables into confidence factors

The first stage of the classification procedure is to standardise each input or characteristic measurement, v, to a value on a scale of 0-1. The transformed variable is defined as a confidence factor $cf(v)$ and represents a level of confidence in (or not in) the variable's support to a subject's knee function being OA (or a given hypothesis) and satisfies the following criteria:

i. $cf(v)$ is a monotonic function
ii. $cf(v) = 1$ if the measurement implies certainty in {OA}
iii. $cf(v) = 0$ if the measurement implies certainty in {NP}
iv. $cf(v) = 0.5$ if the measurement favours neither {OA} nor {NP}

The input variable is transformed into a confidence factor using the sigmoid function. This follows the suggestion by Gerig *et al.*, (2000), and is commonly used as an activation function within Artificial Neural Networks including applications to gait analysis studies (e.g. Holzreiter and Köhle, 1993).

$$cf(v) = \frac{1}{1 + e^{-k(\bar{v} - \theta)}} \tag{2.15}$$

Where θ is the value of v for which cf(v)=0.5. i.e it is the value of the input variable for which the evidence supporting a subject's knee function being OA is equal to the evidence supporting their knee function being NP. The mean value, $\bar{v}$ is used so that θ is not biased towards {OA} or {NP}, (Beynon, 2005).

A sigmoid function with a positive gradient (positive association) implies that a characteristic measurement greater than the θ value offers more support to a subjects knee function being OA, while a characteristic measurement less than the θ value offers a more support to their knee function being NP (Figure 2.23a) and vice versa for a sigmoid function with a negative gradient (negative association), (Figure 2.23b).

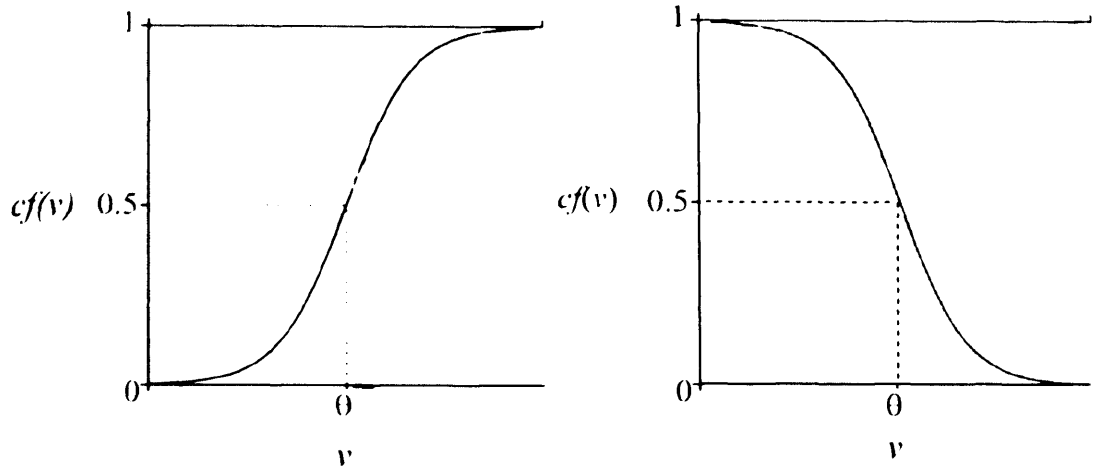

Figure 2.23 Sigmoid function with (a) positive gradient implying that a large v measurement offers more support to OA and (b) negative gradient implying that a large v measurement offers more support to NP

The k parameter adjusts the steepness of the sigmoid function to reflect the nature of the spread of the data. The absolute value of k dictates the range of measurement values that lie around the middle confidence value $cf(v) = 0.5$. Small values of k increase the range of v for which $cf(v)$ is near 0.5, which implies that the majority of v are assigned a $cf(v)$ value near 0.5. Greater values of k decrease the range of v for which $cf(v)$ is near 0.5 which implies that the majority of v are assigned $cf(v)$ values near 0 or 1.

In the software there are two options for calculating the value of k. The first approach relates k to the spread of the data as in 2.16, (Beynon, 2005).

$$k = \pm\frac{1}{\sigma} \tag{2.16}$$

where the sign depends on the nature of association deduced from knowledge of each input variable v and a large spread present in v produces a small value of k.

Alternatively k can be calculated as the Pearson's correlation coefficient for that characteristic with the subject's category label where (0 => NP and 1 => OA). The sign of the correlation coefficient gives the sign of the k value and direction of the association of v with the hypothesis. The value of the correlation coefficient indicates the degree to which v can differentiate between OA and NP.

2.4.1.2 Conversion of confidence factors to BOE

A confidence factor representing each input variables is transformed into a characteristic body of evidence (BOE). In the assessment of knee function there are two exhaustive outcomes, the subject's knee function is either OA or NP. The BOE is a set of three belief values, which express the degree to which the evidence confirms each hypothesis. These are:

i. $m(\{OA\})$ – the degree of belief in the subjects knee function being {OA}
ii. $m(\{NP\})$ – the degree of belief in the subjects knee function being {NP}
iii. $m(\{OA, NP\}) = m(\Theta)$ – the degree of belief in either the subjects knee function being OA or NP

The value $m(\{OA, NP\})$ is the associated uncertainty and represents the value which cannot be assigned to {OA} or {NP}.

One condition of the belief values in a BOE is that they sum to 1. i.e.

$$m(\{OA\}) + m(\{NP\}) + m(\{OA, NP\}) = 1 \tag{2.17}$$

the belief values are defined as follows: (Safranek *et al.*, 1990)

$$m(\{OA\}) = \frac{B}{1-A} cf(v) - \frac{AB}{1-A} \tag{2.18}$$

$$m(\{NP\}) = \frac{-B}{1-A} cf(v) + B \tag{2.19}$$

and

$$m(\Theta) = 1 - m(\{OA\}) - m(\{NP\}) = \frac{1-A-B}{1-A} \tag{2.20}$$

where A depicts the dependence of $m(\{OA\})$ on the confidence factor and B the maximal support that can be assigned to $m(\{OA\})$ or $m(\{NP\})$. If either $m(\{OA\})$ or $m(\{NP\})$ are negative, their values are set to zero prior to the calculation of $m(\Theta)$.

The A and B control variables relate directly to the values of exact belief in {OA} and {NP} as well as the level of associated uncertainty. The assignment of values to A and B is dependent on the general limits of uncertainty $[\Theta_L, \Theta_U]$ allowed for the individual input variables. Different limits can be assigned to each of the individual variables; however, to date, the classifier has been used where the same limits have been assigned to each variable (following Beynon *et al.*, 2002). The assignment of values to A and B in this way works best with an appreciable level of uncertainty is allowed in the classification, (Safranek *et al.*, 1990).

The values of A and B are expressed as:

$$A = \frac{\Theta_U - \Theta_L}{1 + \Theta_U - 2\Theta_L} \tag{2.21}$$

$$B = 1 - \Theta_L \tag{2.22}$$

2.4.1.3 Combination of individual BOE

A BOE would have been constructed for each input variable used in the classification. Each BOE offers evidence to support their classification to the OA or NP knee function group. The Dempster's rule of combination is used to combine individual independent BOEs to a final combined BOE (BOE_c).

In the case where only two exhaustive outcomes exist, OA and NP, the combination of two independent BOE $m_i(.)$ and $m_j(.)$ is given by the following three formulaic expressions.

$$(m_i \oplus m_j)(\{OA\}) = m_c(\{OA\}) = \frac{m_i(\{OA\})m_j(\{OA\}) + m_j(\{OA\})m_i(\Theta) + m_i(\{OA\})m_j(\Theta)}{1 - (m_i(\{NP\})m_j(\{OA\}) + m_i(\{OA\})m_j(\{NP\}))} \quad (2.23)$$

$$(m_i \oplus m_j)(\{NP\}) = m_c(\{NP\}) = \frac{m_i(\{NP\})m_j(\{NP\}) + m_j(\Theta)m_i(\{NP\}) + m_j(\{NP\})m_i(\Theta)}{1 - (m_i(\{NP\})m_j(\{OA\}) + m_i(\{OA\})m_j(\{NP\}))} \quad (2.24)$$

$$(m_i \oplus m_j)(\Theta) = m_c(\Theta) = 1 - m_c(\{OA\}) - m_c(\{NP\}) \quad (2.25)$$

The combined BOE (BOE_c) comprises the same three focal elements as present in the individual BOE namely {OA}, {NP} and Θ. BOE_c can be combined with another BOE and applied iteratively, this allows the combination of all characteristic BOEs. Dempster's rule is commutative and associative and hence it does not matter on the order in which the evidence is combined (Gerig *et al.*, 2000).

2.4.1.4 Visualisation of BOE using simplex plots

The final BOE_c comprises the same three focal elements as present in the individual BOE. Given the three expressions $m(\{OA\})=\lambda_1$, $m(\{NP\})=\lambda_2$ and $m(\{\Theta\})=\lambda_3$, a simplex coordinate is used to represent this set of belief values as a single point on a simplex plot.

In the simplex plot, (Figure 2.22c), a point p exists within an equilateral triangle such that the least distance from p to each of the sides of the equilateral triangle are in the same proportion as the ratios of the values λ_1, λ_2 and λ_3. The distance from p to e_i is equal to $\lambda_i h$, where h is the height of the triangle.

A central decision boundary illustrated by a dashed line is created within the simplex plot where $m(\{NP\}) = m(\{OA\})$. To the left of the decision boundary, the belief that

the subject has NP knee function is greater than the belief they have OA knee function (i.e. $m(\{NP\}) > m(\{OA\})$). To the right of the boundary, the belief the subject has OA knee function is greater than the belief they have NP knee function (i.e. $m(\{OA\}) > m(\{NP\})$).

The simplex plot is divided further to generate four classification regions as in Figure 2.22c. Region 1 highlights the area of dominant NP function in which ($m(\{NP\})>0.5$). Region 2 highlights the area of dominant OA function where ($m(\{OA\})>0.5$). Region 3 highlights the area of non-dominant NP function where ($m(\{OA\})<m(\{NP\})<0.5$) and region 4 shows non-dominant OA function where ($m(\{NP\})<m(\{OA\})<0.5$). A point situated in region 1 indicates knee function more characteristic of NP than a point situated in region 3 and thus the BOE_c for this subject has more association to {NP}.

Each individual BOE and the BOE_c is visualised using this method. Visualisation of the BOE_c is useful when tracking a patient's progress following a TKR and for comparing groups of patients. A plot of individual BOEs provides a visual representation of the influence of each input variable on the final classification.

2.4.1.5 Classification based on the final combined BOE, BOE_c

Using the combined BOE_c, the following decision rule is used (following the work of Safranek *et al.*, 1990).

1. If $m_c(\{OA\}) > m_c(\{NP\})$ then a subject is considered to have OA knee function.

2. If $m_c(\{NP\}) > m_c(\{OA\})$ then a subject is considered to have NP knee function.

2.4.2 Evaluating Classification Accuracy

The software has two methods of calculating classification accuracy by examining its misclassification rate. The first is a re-substitution approach (in-sample classification). This is where the classifier is trained using a set of n subjects and the classification accuracy is calculated using the same n subjects that were used to design the classifier (Weiss and Kulikowski, 1991). This method is a biased estimate of the true error rate (Raudys and Jain, 1991; Toussaint, 1974) and should only be used when the number of training cases is large.

The second is the leave-one-out (LOO) method of cross-validation (out-of-sample classification). This trains the classifier using (n-1) training cases (to calculate the control variables k, θ, A and B). These control variables are then used to classify the remaining subject's knee function. This process is repeated n times and the LOO error is calculated as the average error rate of all the left out subjects. The out-of-sample accuracy is then defined as 100 minus the LOO error. The LOO method is a more efficient use of a data set (Weiss and Kulikowski, 1991) and is nearly an unbiased estimate of the true error rate for small sample sizes, (Raudys and Jain, 1991; Weiss and Kulikowski, 1991).

2.4.3 Ranking Input Variables

An objective function (OB) is used to quantitatively represent a measure of classification performance and the uncertainty that each input variable offers to the classification. In terms of the simplex plot, it is a measure of the difference between the actual position of the subject and the desired optimum position at either the {OA} or {NP} vertex, depending on their actual category. OB is calculated as the Euclidean distance of the mean coordinates of the two groups of subjects to their correct vertex (Beynon *et al.*, 2002). A value of OB close to zero implies a robust classification where the subject is positioned at the correct vertex.

Variables are ranked according to their OB in order of the variable with the lowest associated OB to the variable with the highest associated OB. Using a LOO approach to the classification, for each variable the OB is calculated from the in-sample

population (n-1), repeated n times. The final ranking of the input variables is then based on the average ranking from n runs.

2.4.4 Effect of changing the control variables

Jones, (2004) investigated the effect of changing the values of the control variables for the classification of OA and NP knee function. It was found that training k using the Pearson's correlation coefficient produced a higher classification accuracy and lower OB than when it is trained using equation 2.16. It was also found that the classifier is very sensitive to the choice of the uncertainty limits, $[\Theta_L, \Theta_U]$. As Θ_L is increased, the distance of the simplex coordinates of all subjects from the Θ vertex decreased. This increased the level of uncertainty in the final classification and moved subjects into the non-dominant regions of the simplex plot. Due to the high level of variability in MA data, it is therefore important that the values of Θ_L, and Θ_U are selected to produce a classifier that is accurate but also of practical clinical use where the majority of subjects lie within the dominant regions and any misclassified subject's lies within non-dominant regions of the simplex plot.

2.4.5 Classifying new subject data

The classifier is trained using a sample containing subjects with NP and OA knee function to determine values for the control variables k, θ, A and B. For the assessment of new subjects or for assessing subsequent patient visits (e.g. for assessing the outcome of TKR surgery), these pre-determined control variables are used to transform the input variables of the new sample into a BOE_c to classify the new subject data.

This chapter has described the existing data collection and analysis protocol to quantify knee function, employed on a clinical trial at Cardiff University. Chapter 4 outlines the development of this protocol to include a staircase and the computation of knee joint moments. The use of a full lower limb marker set and commercial software is introduced to perform comparison of current data collection and processing methods. The application of the classifier to assess TKR outcome is demonstrated in Chapter 3.

CHAPTER 3
ASSESSING THE OUTCOME OF TOTAL KNEE REPLACEMENT SURGERY FROM LEVEL GAIT VARIABLES

The DS classifier enables the level of benefit achieved by total knee replacement (TKR) surgery to be established and visualised. As a continuation from previous investigations (Jones, 2004; Jones and Holt, 2008), the outcome of TKR surgery was assessed for a further nine patients. For this study, the training set for the classifier was increased by 48% to enhance its performance.

Using the protocol outlined in Chapter 2, knee function during level gait was assessed for a further 20 subjects (10 with knee osteoarthritis (OA) and 10 with no pathology (NP)). The analysis programs were updated to accommodate for changes in the motion analysis procedure since the initial investigations were undertaken. Nine of the OA patients (TKR sample) were also assessed at approximately 3, 6 and 12 months after TKR surgery. Following the work of Jones, (2004), the variables listed in Table 3.1 were computed and used to represent a subject's knee function. The DS classifier was used to assess the outcome of TKR surgery for the TKR sample. By combining the new and existing datasets, the control parameters of the DS classifier k, θ, A and B, were calculated using the non-optimisation method, from the variables of 30 OA and 32 NP subjects. k was calculated using the correlation coefficient method and A and B from the limits $[\Theta_L, \Theta_U] = [0.8, 1]$. The control parameters were then used to transform the input variables of the TKR sample into a combined body of evidence (BOE_c) for each patient assessment. These were used to monitor changes in knee function post surgery.

The oxford knee score (OKS) and knee outcome survey (KOS) were completed by each patient at their assessments to provide a subjective measure of how they perceive their knee function. The questionnaires assess knee function from a different perspective to the DS classifier. Whereas the classifier assesses knee function during level gait, the questionnaires measure knee function during a variety of daily activities, also considering clinical parameters such as buckling, instability and pain. A high score using the KOS and a low score using the OKS corresponds to a high

level of NP knee function. The results of this study will be now be presented and discussed for each patient in turn.

Table 3.1 Summary of the variables used in the classification

(adapted from Jones and Holt, 2007)

Variable	Variable Description	Variable Interpretation
v_1	Body mass index (BMI) (kg/m2)	Indicator of loading through the knee
v_2	Cadence (min^{-1})	Indicator of ability to walk with a normal gait
v_3	Stance phase (per cent of the gait cycle)	Indicator of ability to load knee during gait
v_4	APFPC1 Score	Difference between the peak anterior GRF and the peak posterior GRF
v_5	APFPC2 Score	Magnitude of the anterior–posterior GRF during the period from late mid stance to mid terminal stance
v_6	APFPC3 Score	Magnitude of the anterior–posterior GRF during late pre-swing
v_7	VFPC1 Score	Magnitude of the vertical GRF during a portion of mid-stance and the period from heel rise to opposite initial contact
v_8	VFPC2 Score	Magnitude of the vertical GRF from loading response to mid-stance
v_9	VFPC3 Score	Magnitude of the vertical GRF during the phase from heel strike transient to the first peak vertical GRF
v_{10}	FERPC1 Score	Magnitude of knee flexion from initial contact to opposite initial contact
v_{11}	FERPC2 Score	Magnitude of knee flexion during the phase from 58% to 76% of the gait cycle
v_{12}	AARPC1 Score	Magnitude of knee abduction–adduction during the stance phase
v_{13}	AARPC2 Score	Magnitude of knee abduction–adduction during the initial swing
v_{14}	AARPC3 Score	Magnitude of knee abduction–adduction during the terminal swing
v_{15}	IERPC1 Score	Magnitude of internal–external rotation from the loading response to the mid swing
v_{16}	Mediolateral (ML) knee width (mm)	Indicator of knee swelling
v_{17}	Anterior–posterior (AP) knee width (mm)	Indicator of knee swelling
v_{18}	Thigh girth (mm)	Indicator of muscle mass

3.1 PATIENT 1 (P1)

P1 was followed before and at three stages after TKR surgery. The timing of these visits is given in Table 3.2.

Table 3.2 Visit summary for P1

Visit	Visit type
1	1 week preoperative
2	4 months postoperative
3	8 months postoperative
4	12 months postoperative

3.1.1 Knee outcome scores

The scores from the questionnaires completed by P1 at each of the four visits are tabulated in Table 3.3.

Table 3.3 KOS and Oxford knee scores for the four visits for P1

Visit	KOS score (%)	Oxford knee score (%)
1	75	-
2	87.5	33.33
3	93.75	28.33
4	88.75	28.33

3.1.2. DS classifier results

The BOE_c values for the four visits of P1 are recorded in Table 3.4. The corresponding simplex representations of the BOE_c are depicted in Figure 3.1.

Table 3.4 BOE_c values for the four visits of P1.

BOE_c	Visit			
	1	2	3	4
$m_c(\{OA\})$	0.6036	0.3822	0.4171	0.2848
$m_c(\{NP\})$	0.1570	0.3645	0.3274	0.4381
$m_c(\Theta)$	0.2395	0.2533	0.2555	0.2771

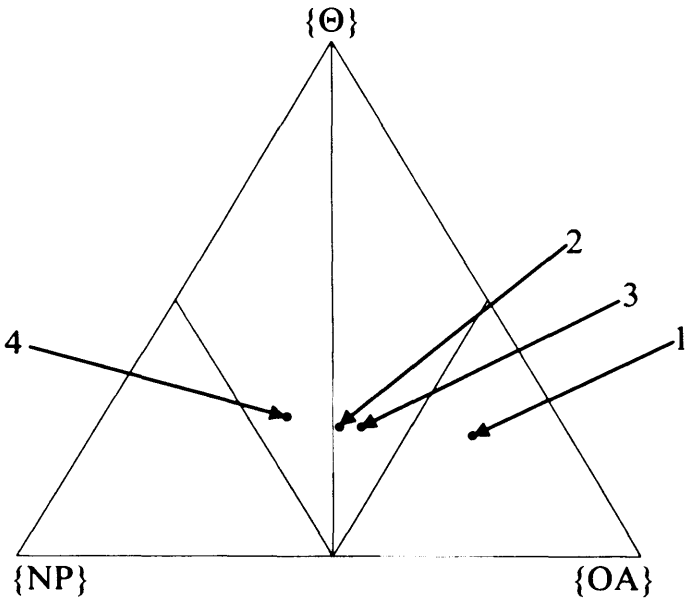

Figure 3.1 Simplex plot showing the simplex coordinate representations of the BOE_c for the four visits of P1

The most influential BOE_c in the classification are highlighted in Table 3.4. The OA belief value, $m_c(\{OA\})$ is the most influential in the classification of P1 at visit 1. Since $m_c(\{OA\})>[\ m_c(\{NP\})+\ m_c(\Theta)]$, P1 is classified in the dominant OA region of the simplex plot. The value of $m_c(\{OA\})$ decreased at visit 2 and the level of NP function, indicated by $m_c(\{NP\})$ increased. For this visit, $m_c(\{OA\})$ and $m_c(\{NP\})$ are almost equal resulting in the classification of P1 on the decision boundary. At visit 3, P1 exhibits greater OA functional characteristics indicated by the reduction in $m_c(\{NP\})$ and increase in $m_c(\{OA\})$. At visit 4 $m_c(\{OA\})$ is the smallest from all the visits and $m_c(\{NP\})$ is the largest from all the visits. Since $m_c(\{NP\})> m_c(\{OA\})$, P1 is classified in the NP side of the simplex plot. Throughout all 4 visits, the level of uncertainty in the classification, indicated by $m_c(\Theta)$, remained almost constant.

3.1.3 Discussion of results

The KOS results indicated an increase in knee function for the first 3 visits. The highest score was obtained at visit 3 and this reduced by 5% at visit 4. The OKS results indicated an increase in knee function from visit 2 to 3 and then remained constant. The classifier also identified an increase in NP knee function between visit 1 and 2 as P1 moved into the non-dominant OA region. At visit 3 knee function worsens slightly. At visit 4, it improves and P1 exhibits non-dominant NP function.

3.2 PATIENT 2 (P2)

P2 was followed before and at three stages after TKR surgery. The timing of these visits is given in Table 3.5.

Table 3.5 Visit summary for P2

Visit	Visit type
1	1 week preoperative
2	3 months postoperative
3	7 months postoperative
4	13 months postoperative

3.2.1 Knee outcome scores

The scores from the questionnaires completed by P2 at each of the four visits are tabulated in Table 3.6.

Table 3.6 KOS and Oxford knee scores for the four visits for P2

Visit	KOS score (%)	Oxford knee score (%)
1	52.5	-
2	70	45
3	83.75	36.67
4	85	35

3.2.2 DS classifier results

The BOE_c values for the four visits of P2 are recorded in Table 3.7. The corresponding simplex representations of the BOE_c are depicted in Figure 3.2.

Table 3.7 BOE_c values for the four visits of P2.

BOE_c	Visit			
	1	2	3	4
$m_c(\{OA\})$	0.7917	0.5386	0.4240	0.4893
$m_c(\{NP\})$	0.0103	0.2448	0.2997	0.3006
$m_c(\Theta)$	0.1981	0.2166	0.2763	0.2102

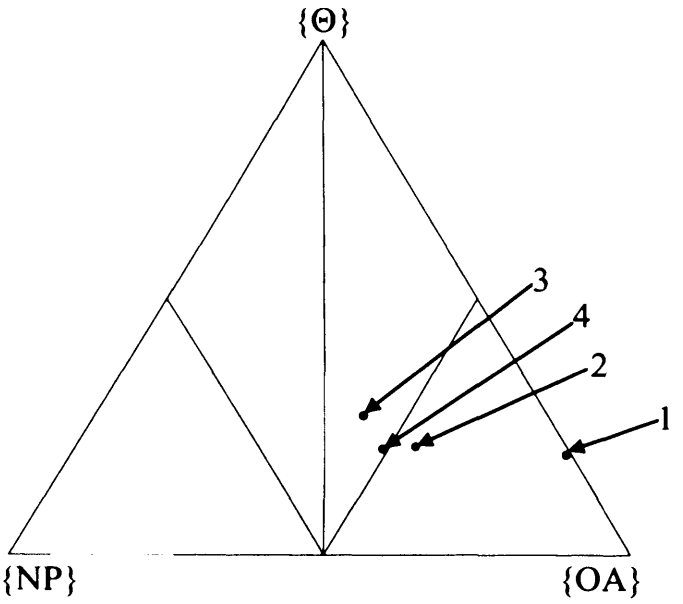

Figure 3.2 Simplex plot showing the simplex coordinate representations of the BOE_c for the four visits of P2

The most influential BOE_c in the classification are highlighted in Table 3.7. The OA belief value, $m_c(\{OA\})$ is the most influential in the classification of P2 for all 4 visits. At visits 1 and 2, $m_c(\{OA\})>[\, m_c(\{NP\})+ m_c(\Theta)]$, resulting in the classification of P2 in the dominant OA region of the simplex plot. The OA characteristics decrease from visit 1 to 3 indicated by a decrease in $m_c(\{OA\})$. The NP characteristics steadily increase from visit 1 to 4. At visit 4, $m_c(\{OA\})$ increases to a similar value to visit 2, although $m_c(\{NP\})$ is higher than in visit 2 which moves the final classification closer to the NP side of the simplex plot. The uncertainty in the classification increases from visit 1 to 3. At visit 4, the value of $m_c(\Theta)$ is similar to visit 2.

3.2.3 Discussion of results

The KOS results indicate an increase in knee function at each visit. This is in agreement with the OKS results. The DS classifier identifies an improvement in NP knee function between each visit. This suggests P2 has experienced some relief from OA. However, the final classification for visit 4 indicates similar function as visit 2 due to an increase in OA gait characteristics. This may be due to P2 maintaining old habits to compensate for symptoms associated with knee OA.

3.3 PATIENT 3 (P3)

P3 was followed before and at three stages after TKR surgery. The timing of these visits is given in Table 3.8.

Table 3.8 Visit summary for P3

Visit	Visit type
1	2 weeks preoperative
2	3 months postoperative
3	6 months postoperative
4	12 months postoperative

3.3.1 Knee outcome scores

The scores from the questionnaires completed by P3 at each of the four visits are tabulated in Table 3.9.

Table 3.9 KOS and Oxford knee scores for the four visits for P3

Visit	KOS score (%)	Oxford knee score (%)
1	46.25	63.33
2	83.75	33.33
3	73.75	41.67
4	86.25	31.67

3.3.2 DS classifier results

The BOE_c values for the four visits of P3 are recorded in Table 3.10. The corresponding simplex representations of the BOE_c are depicted in Figure 3.3.

Table 3.10 BOE_c values for the four visits of P3.

BOE_c	Visit			
	1	2	3	4
$m_c(\{OA\})$	0.6752	0.2855	0.3791	0.2697
$m_c(\{NP\})$	0.1086	0.4530	0.2914	0.4682
$m_c(\Theta)$	0.2162	0.2616	0.3295	0.2622

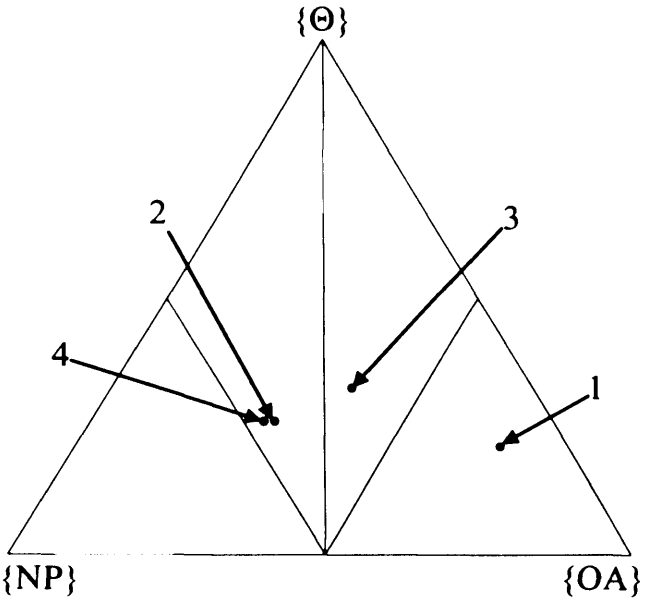

Figure 3.3 Simplex plot showing the simplex coordinate representations of the BOE_c for the four visits of P3

The most influential BOE_c in the classification are highlighted in Table 3.10. The OA belief value, $m_c(\{OA\})$ is the most influential in the classification of P3 for visit 1. $m_c(\{OA\})>[\ m_c(\{NP\})+\ m_c(\Theta)]$, resulting in the classification of P3 in the dominant OA region of the simplex plot. At visit 2, a high level of NP knee function is restored moving P3 to the non-dominant NP region of the simplex plot where $m_c(\{NP\})>$ $m_c(\{OA\})$. At visit 3, $m_c(\{NP\})$ decreases and $m_c(\{OA\})$ increases resulting in knee function classified in the non-dominant OA region of the simplex plot. The classification of P3 at visit 4 is similar to visit 2. The level of uncertainty in the classification is similar for visits 1, 2 and 4. It is slightly higher for visit 3 which moves the classification point higher in the simplex plot (towards the $\{\Theta\}$ vertex).

3.3.3 Discussion of results

The results from the KOS and OKS questionnaires indicate an increase in knee function from visit 1 to 2, followed by a decrease in knee function at visit 3. The score indicating the highest level of knee function was obtained for visit 4 using both the KOS and OKS. The changes in knee function observed from the results of the questionnaires are in agreement with the DS classification output and $m_c(\{NP\})$ values.

3.4 PATIENT 4 (P4)

P4 was followed before and at three stages after TKR surgery. The timing of these visits is given in Table 3.11.

Table 3.11 Visit summary for P4

Visit	Visit type
1	10 days preoperative
2	3 months postoperative
3	6 months postoperative
4	12 months postoperative

3.4.1 Knee outcome scores

The scores from the questionnaires completed by P4 at each of the four visits are tabulated in Table 3.12.

Table 3.12 KOS and Oxford knee scores for the four visits for P4

Visit	KOS score (%)	Oxford knee score (%)
1	26.25	86.67
2	61.25	50
3	70	51.67
4	81.25	43.33

3.4.2 DS classifier results

The BOE_c values for the four visits of P4 are recorded in Table 3.13. The corresponding simplex representations of the BOE_c are depicted in Figure 3.4.

Table 3.13 BOE_c values for the four visits of P4.

BOE_c	Visit			
	1	2	3	4
$m_c(\{OA\})$	0.8277	0.7489	0.7425	0.6949
$m_c(\{NP\})$	0.0504	0.0881	0.0804	0.1266
$m_c(\Theta)$	0.1219	0.1630	0.1772	0.1785

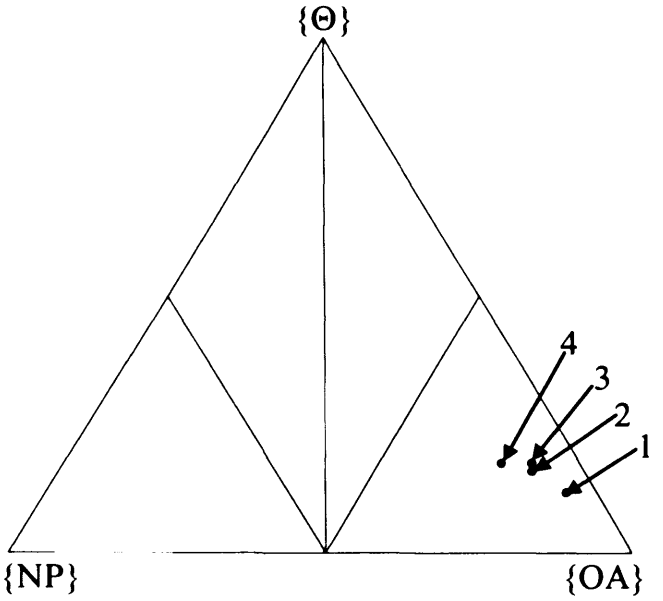

Figure 3.4 Simplex plot showing the simplex coordinate representations of the BOE_c for the four visits of P4

The most influential BOE_c in the classification are highlighted in Table 3.13. The value of $m_c(\{OA\})$ is consistently more influential in the classification of P4 throughout the 4 assessments. At all stages of recovery, P4 has dominant OA classification since $m_c(\{OA\})>[\ m_c(\{NP\})+\ m_c(\Theta)]$. This is reflected in the positioning of the simplex coordinates within the dominant OA classification region. From visit 1 to visit 2, there is an increase in $m_c(\{NP\})$ and decrease in $m_c(\{OA\})$. The BOE_c are similar for visits 2 and 3, reflected by the position of the simplex coordinates. There is an increase in $m_c(\{NP\})$ and decrease in $m_c(\{OA\})$ from visit 3 to 4. This resulted in a simplex coordinate position closer to the {NP} vertex for visit 4.

3.4.3 Discussion of results

The KOS results for P4 indicate an increase in knee function between each of the four visits. The OKS indicate an improvement between visit 1 and 2, a slight set back in knee function at visit 3, followed by an improved knee function at visit 4. The BOE_c values from the classification suggest there has been limited recovery in NP knee function. The changes in the OKS scores reflect the changes observed through examination of $m_c(\{NP\})$.

3.5 PATIENT 5 (P5)

P5 was followed before and at three stages after TKR surgery. The timing of these visits is given in Table 3.14.

Table 3.14 Visit summary for P5

Visit	Visit type
1	1 week preoperative
2	3 months postoperative
3	7months postoperative
4	12 months postoperative

3.5.1 Knee outcome scores

The scores from the questionnaires completed by P5 at each of the four visits are tabulated in Table 3.15.

Table 3.15 KOS and Oxford knee scores for the four visits for P5

Visit	KOS score (%)	Oxford knee score (%)
1	48.75	60
2	57.5	58.33
3	62.5	43.33
4	78.75	36.66

3.5.2 DS classifier results

The BOE_c values for the four visits of P5 are recorded in Table 3.16. The corresponding simplex representations of the BOE_c are depicted in Figure 3.5.

Table 3.16 BOE_c values for the four visits of P5.

BOE_c	Visit			
	1	2	3	4
$m_c(\{OA\})$	0.6705	0.8129	0.7161	0.6180
$m_c(\{NP\})$	0.1137	0.0503	0.0916	0.1427
$m_c(\Theta)$	0.2158	0.1368	0.1923	0.2392

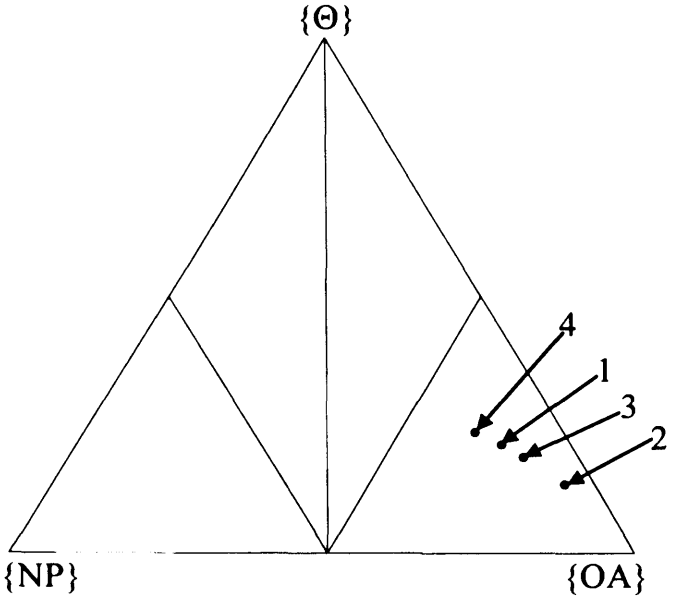

Figure 3.5 Simplex plot showing the simplex coordinate representations of the BOE_c for the four visits of P5

$m_c(\{OA\})$ is the most influential BOE_c in each of the four classifications. The $m_c(\{OA\})$ values are highlighted in Table 3.16. At all stages of recovery, P5 has dominant OA classification since $m_c(\{OA\}) > [m_c(\{NP\}) + m_c(\Theta)]$. This is reflected by each simplex coordinate positioned within the dominant OA classification region. From visit 1 to visit 2, there is a decrease in $m_c(\{NL\})$ and increase in $m_c(\{OA\})$, reflected by the simplex coordinate moving closer to the {OA} vertex. From visit 2 to visit 3, $m_c(\{OA\})$ decreases and $m_c(\{NP\})$ increases. This trend is also evident between visit 3 and visit 4. This is illustrated on the simplex plot by the simplex coordinates moving closer to the {NP} vertex.

3.5.3 Discussion of results

The results from the KOS and OKS questionnaires indicate an increase in knee function between each assessment. The BOE_c values indicate increased function associated with OA at visit 2 which is not reflected in the results from the clinical questionnaires. P5 then begins to recover a degree of NP function indicated by the increased value of $m_c(\{NP\})$ at visits 3 and 4. This result is in agreement with the results from both clinical questionnaires.

3.6 PATIENT 6 (P6)

P6 was followed before and at three stages after TKR surgery. The timing of these visits is given in Table 3.17.

Table 3.17 Visit summary for P6

Visit	Visit type
1	1 week preoperative
2	3 months postoperative
3	-
4	13 months postoperative

3.6.1 Knee outcome scores

The scores from the questionnaires completed by P6 at each of the four visits are tabulated in Table 3.18.

Table 3.18 KOS and Oxford knee scores for the four visits for P6

Visit	KOS score (%)	Oxford knee score (%)
1	21.25	76.67
2	50	56.67
3	-	-
4	42.5	66.67

3.6.2 DS classifier results

The BOE_c values for the four visits of P6 are recorded in Table 3.19. The corresponding simplex representations of the BOE_c are depicted in Figure 3.6.

Table 3.19 BOE_c values for the four visits of P6.

BOE_c	Visit			
	1	2	3	4
$m_c(\{OA\})$	0.6000	0.6244	-	0.6029
$m_c(\{NP\})$	0.2121	0.1741	-	0.1964
$m_c(\Theta)$	0.1879	0.2014	-	0.2007

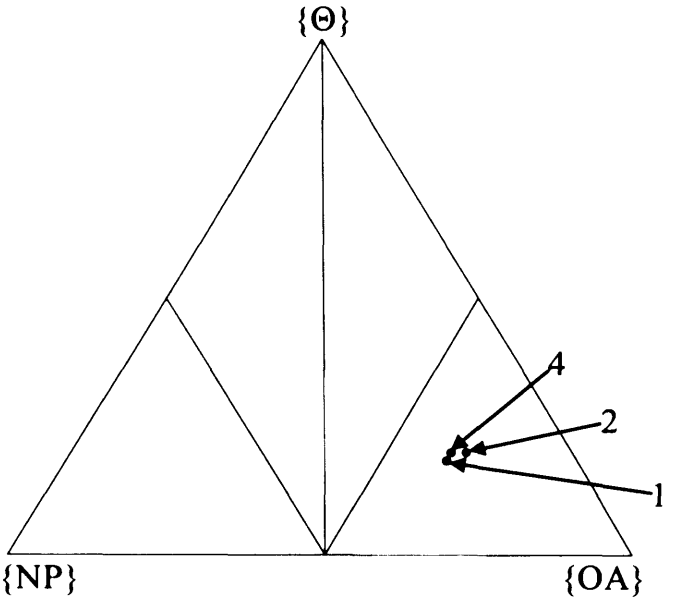

Figure 3.6 Simplex plot showing the simplex coordinate representations of the BOE_c for the three visits of P6

The most influential BOE_c in the classification are highlighted in Table 3.19. $m_c(\{OA\})$ is consistently more influential in the classification of P6 for each assessment. At all stages of recovery, P6 has dominant OA classification since $m_c(\{OA\})>[\ m_c(\{NP\})+\ m_c(\Theta)]$. This is reflected in the positioning of the simplex coordinates within the dominant OA classification region. Small changes exist between each visit. From visit 1 to visit 2, $m_c(\{OA\})$ increases and $m_c(\{NP\})$ decreases representing a slight increase in function associated with OA. From visit 2 to 4, $m_c(\{OA\})$ decreases and $m_c(\{NP\})$ increases representing a degree of recovery of NP function. However, the degree of NP function measured at visit 4 is less than that measured pre-operatively at visit 1.

3.6.3 Discussion of results

P6 shows very little recovery of NP function throughout the 13 month assessment duration. This is reflected by the consistently large $m_c(\{OA\})$ from the classifications and of the small improvements measured using the knee outcome scores, (28.75% change in the KOS results and 20% change in the OKS).

3.7 PATIENT 7 (P7)

P7 was followed before and at three stages after TKR surgery. The timing of these visits is given in Table 3.20.

Table 3.20 Visit summary for P7

Visit	Visit type
1	2 weeks preoperative
2	4 months postoperative
3	7 months postoperative
4	13 months postoperative

3.7.1 Knee outcome scores

The scores from the questionnaires completed by P7 at each of the four visits are tabulated in Table 3.21.

Table 3.21 KOS and Oxford knee scores for the four visits for P7

Visit	KOS score (%)	Oxford knee score (%)
1	36.25	70
2	41.25	60
3	50	61.67
4	43.75	61.67

3.7.2 DS classifier results

The BOE_c values for the four visits of P7 are recorded in Table 3.22. The corresponding simplex representations of the BOE_c are depicted in Figure 3.7.

Table 3.22 BOE_c values for the four visits of P7.

BOE_c	Visit			
	1	2	3	4
$m_c(\{OA\})$	0.7952	0.7453	0.7678	0.7550
$m_c(\{NP\})$	0.0596	0.0953	0.0883	0.0867
$m_c(\Theta)$	0.1452	0.1594	0.1439	0.1583

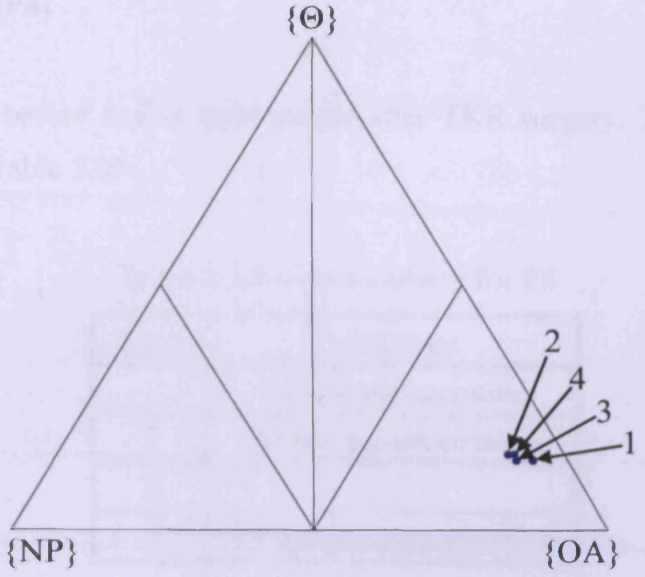

Figure 3.7 Simplex plot showing the simplex coordinate representations of the BOE_c for the four visits of P7

$m_c(\{OA\})$ is the most influential BOE_c in each classification and their values for each assessment are highlighted in Table 3.22. At all stages of recovery, P7 has dominant OA classification since $m_c(\{OA\})>[\ m_c(\{NP\})+\ m_c(\Theta)]$. This is reflected in the positioning of the simplex coordinates within the dominant OA classification region. Minimal changes occur between visits. From visit 1 to visit 2, $m_c(\{OA\})$ decreases and $m_c(\{NP\})$ increases representing a slight recovery of NP function. From visit 2 to 3, there is an increase in function associated with OA indicated by an increase in $m_c(\{OA\})$ and decrease in $m_c(\{NP\})$. From visit 3 to visit 4, $m_c(\{OA\})$ decreases and $m_c(\{NP\})$ increases representing a slight recovery of NP function.

3.7.3 Discussion of results

The KOS results indicate an improvement in knee function between visits 1 to 3, then a slight decrease in function exhibited at visit 4. The OKS results indicate an improvement in function from visit 1 to visit 3, after which knee function remains constant. Considering all the results, P7 displays very little recovery of NP function throughout the 4 visits. This is reflected by the consistently large $m_c(\{OA\})$ from the classifications and by the small improvements measured using the knee outcome scores, (13.75% change in the KOS results and 8.33% change in the OKS).

3.8 PATIENT 8 (P8)

P8 was followed before and at three stages after TKR surgery. The timing of these visits is given in Table 3.23.

Table 3.23 Visit summary for P8

Visit	Visit type
1	1 week preoperative
2	3 months postoperative
3	-
4	13 months postoperative

3.8.1 Knee outcome scores

The scores from the questionnaires completed by P8 at each of the four visits are tabulated in Table 3.24.

Table 3.24 KOS and Oxford knee scores for the four visits for P8

Visit	KOS score (%)	Oxford knee score (%)
1	38.75	80
2	78.75	45
3	-	-
4	92.5	26.67

3.8.2 DS classifier results

The BOE_c values for the four visits of P8 are recorded in Table 3.25. The corresponding simplex representations of the BOE_c are depicted in Figure 3.8.

Table 3.25 BOE_c values for the four visits of P8.

BOE_c	Visit			
	1	2	3	4
$m_c(\{OA\})$	0.6253	0.5150	-	0.3728
$m_c(\{NP\})$	0.1433	0.2404	-	0.3225
$m_c(\Theta)$	0.2314	0.2446	-	0.3046

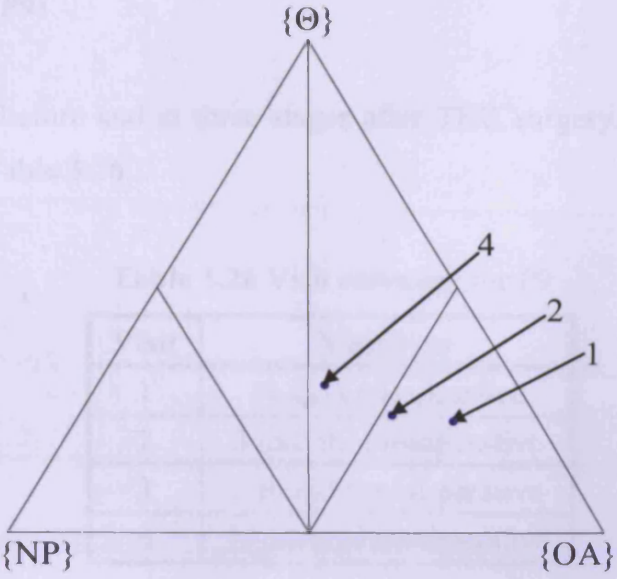

Figure 3.8 Simplex plot showing the simplex coordinate representations of the BOE_c for the three visits of P8

The most influential BOE_c in the classification are highlighted in Table 3.25. The OA belief value, $m_c(\{OA\})$ is the most influential in the classification of P8 at visit 1 and visit 2. Since $m_c(\{OA\})>[\ m_c(\{NP\})+\ m_c(\Theta)]$, P8 is classified in the dominant OA region of the simplex plot. The value of $m_c(\{OA\})$ decreased at visit 2 and the level of $m_c(\{NP\})$ increased, indicating a degree of improved NP gait characteristics. At visit 4, P8 exhibits further improved characteristics of NP gait indicated by a further reduction in $m_c(\{OA\})$ and increase in $m_c(\{NP\})$.

3.8.3 Discussion of results

The KOS and OKS results indicate large improvements in knee function between visits 1 to 4. This is in agreement with the $m_c(\{NP\})$ values which also indicate an increase in NP gait characteristics at each subsequent visit. Despite improvements in knee function, P8 was never classified as demonstrating NP function.

3.9 PATIENT 9 (P9)

P9 was followed before and at three stages after TKR surgery. The timing of these visits is given in Table 3.26.

Table 3.26 Visit summary for P9

Visit	Visit type
1	11 days preoperative
2	3 months postoperative
3	6 months postoperative
4	12 months postoperative

3.9.1 Knee outcome scores

The scores from the questionnaires completed by P9 at each of the four visits are tabulated in Table 3.27.

Table 3.27 KOS and Oxford knee scores for the four visits for P9

Visit	KOS score (%)	Oxford knee score (%)
1	45	56.67
2	65	43.33
3	81.25	38.33
4	83.75	36.67

3.9.2 DS classifier results

The BOE_c values for the four visits of P9 are recorded in Table 3.28. The corresponding simplex representations of the BOE_c are depicted in Figure 3.9.

Table 3.28 BOE_c values for the four visits of P9.

BOE_c	Visit			
	1	2	3	4
$m_c(\{OA\})$	0.4780	0.6127	0.5680	0.5144
$m_c(\{NP\})$	0.2593	0.1754	0.2239	0.2527
$m_c(\Theta)$	0.2627	0.2119	0.2081	0.2329

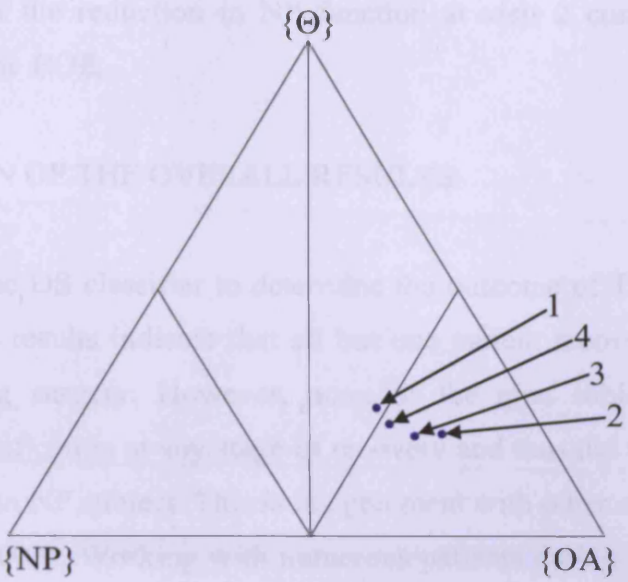

Figure 3.9 Simplex plot showing the simplex coordinate representations of the BOE_c for the four visits of P9

The most influential BOE_c in the classification are highlighted in Table 3.28. $m_c(\{OA\})$ is consistently more influential in the classification of P9 at each assessment. Small changes exist between each visit. At visit 1, the simplex coordinates for P9 are situated in the non dominant OA region of the simplex plot. From visit 1 to visit 2, $m_c(\{OA\})$ increases and $m_c(\{NP\})$ decreases representing a slight increase in function associated with OA. From visit 2 to 3, $m_c(\{OA\})$ decreases and $m_c(\{NP\})$ increases representing a degree of recovery of NP function. From visit 3 to 4, $m_c(\{OA\})$ decreases and $m_c(\{NP\})$ increases representing a further degree of recovery of NP function. However, the degree of NP function measured at visit 4 is less than that measured pre-operatively at visit 1 and the degree of OA function measured at visit 4 is greater than that measured at visit 1. For visits 2 to 4, P9 has dominant OA classification since $m_c(\{OA\}) > [m_c(\{NP\}) + m_c(\Theta)]$. This is reflected in the positioning of the simplex coordinates within the dominant OA classification region.

3.9.3 Discussion of results

The KOS and OKS indicate an improvement in knee function at each subsequent visit. This agrees with the improvement in $m_c(\{NP\})$ between visit 2 to 4. However,

it does not reflect the reduction in NP function at visit 2 compared with visit 1, demonstrated by the BOE_c.

3.10 DISCUSSION OF THE OVERALL RESULTS

This study used the DS classifier to determine the outcome of TKR surgery for nine new subjects. The results indicate that all but one patient recovered a degree of NP function following surgery. However, none of the nine subjects recovered to a dominant NP classification at any stage of recovery and thus did not exhibit level gait characteristics of an NP subject. This is in agreement with other studies, (Jones, 2004; Benedetti *et al.*, 2003). Working with numerous patients during the clinical trial, the lack of NP function is not surprising considering the deterioration of soft tissue and altered joint structure of the patients. Also, post surgery, the patient may maintain compensatory mechanisms that were originally developed to reduce the pain during level gait. Common compensatory mechanisms include off loading the affected joint and using a reduced range of motion.

The outputs from the classifier were similar to those from the study by Jones, (2004) where 9 subjects were also assessed for level gait. Interestingly, for this study, P1 and P3 achieve a classification near the dominant NP region of the simplex plot. Both subjects achieve $m_c(\{NP\}) > 0.4$ which has never been achieved from previous patients. This indicates a marked improvement in their knee function. It may also demonstrate that by training the classifier using a larger cohort and thus a greater range of knee function, it is able to better distinguish between varying levels of knee function. However, additional subjects are needed still to increase the training cohort to investigate this.

It was observed that not all subjects demonstrated a consistent recovery of NP function. From the current study and from the outputs in the study by Jones, (2004), it appears to be fairly common for a patients' knee function to exhibit greater characteristics of OA following a visit where they exhibit improved NP function. This may be due to comorbidities, which are common with patients with OA or the result of the termination of any physiotherapy sessions the patients may have been

receiving. It may also be affected by the patients becoming accustomed to an artificial joint.

The changes in the BOE_c were not always in agreement with the KOS and OKS scores. This is likely to be because the questionnaires are subjective and record the patients observed improvement in their knee function, whereas the classifier is a quantitative objective approach to assess their knee function. It would be useful in future analyses to investigate why some questionnaires agree and others do not.

This chapter has demonstrated the use of the DS classifier to assess the outcome of TKR function. It would be useful to investigate the use of knee function variables from alternative dynamic tasks such as stair gait to determine whether this enhances the classifier. The next chapter introduces stair gait into the clinical trial and variables from stair gait are investigated with the DS classifier in Chapter 5.

CHAPTER 4
METHODOLOGIES TO ASSESS STAIR GAIT

In the assessment of knee function, valuable biomechanical data can be obtained from a range of daily activities. To date, level gait has been considered in isolation to characterise knee function using the DS classification method. This chapter introduces stair gait as a proposed activity of daily living for inclusion into the existing protocol. A new staircase design is described along with accuracy tests for its validation. In response to the range of reported methodologies for assessing stair gait, a study was undertaken to compare methods of data collection, choice of stair gait sequence and methods of analysis. The results from this study are discussed and a stair gait assessment methodology is recommended for use with the current Cardiff protocol.

4.1 LITERATURE REVIEW

Stairs are frequently encountered in daily living making stair ascent and descent an important activity when assessing lower limb function. The action of ascending and descending a staircase is biomechanically more demanding on lower limbs compared with level gait. This is due to the requirement of the knee joint and lower limb muscles to support and either 'pull up' or 'lower' the body to progress to the next step, whilst providing clearance for the swinging leg to avoid the intermediate step. The activity demands a greater range of lower limb motion, larger moments acting at the knee (Kaufman *et al.*, 2001) with 12-25% increase in knee loading compared to level walking (Morrison, 1969). With these attributes, it is proposed that measurement of stair gait can be used to improve the differentiation between various knee function characteristics as compared to level walking, where the range of motion (ROM) is limited, resulting in small kinematic and kinetic changes (Andriacchi *et al.*, 1982). Further, due to the higher level of muscle motor activity, it has the advantage of significantly lower intra-subject variability, as compared with level gait (McFadyen and Winter, 1988). This is an important advantage when assessing pathology and monitoring treatments where variability due to the condition may be reduced, making deviations from normal function more noticeable.

Understanding stair gait has implications for treatment planning, implant design, rehabilitation planning and for design within public environments. Data from stair ascent and descent has been used to assess lower limb function of able-bodied subjects (Andriacchi *et al.*, 1980; Kowalk *et al.*, 1996; McFadyen and Winter, 1988; Nadeau *et al.*, 2003; Yu *et al.*, 1997), to differentiate different types of Total Knee Replacement (TKR) designs (Andriacchi *et al.*, 1982; Andriacchi *et al.*, 1993; Catani *et al.*, 2003) to functionally assess ACL deficiency (Thambyah *et al.*, 2004) and ACL reconstruction (Andriacchi *et al.*, 1993) and to assess knee mechanics of patients with early stage Osteoarthritis (Kaufman *et al.*, 2001). These studies highlight the merits of using functional measures from stair gait to understand non-pathological knee function, assess lower limb pathologies and compare treatment options.

Although several studies of stair gait have been reported, there is currently no standard method of data collection, step height or description of moments, making it difficult to compare results. Methodologies used by selected studies are summarised in Table 4.1.

The literature has demonstrated stair gait to be a valuable measure when assessing knee function and this provided the motivation to explore whether incorporating stair gait into the current protocol would enhance clinical assessment and knee function classification.

In response to the inconsistency in measurement protocols described in the literature, the remainder of this chapter introduces a new staircase design that interfaces with force plates; and compares common data collection and analysis methods to measure knee function during stair ascent/descent. Based on this work, recommendations are made for the inclusion of stair gait assessment into the Cardiff protocol.

Table 4.1 Description of methodologies used by selected studies

	Step height/tread (m)	Method of interfacing step with force plate	Moment calculation
Della Croce and Bonato, (2007)	0.178/0.28	This interlaced stairway is secured to two force plates using tap bolts. It is composed of two rigid metal frames covered with wooden steps and rises, allowing GRF and COP measurement from 4 foot contacts	Not in the scope of this paper
Protopapadaki *et al.*, (2007)	0.18/0.285	Force plate embedded into the top surface of the second step	Link segment method using Vicon Polygon software. Expressed as external moments
Thambyah *et al.*, (2004)	0.155/0.40	Calibrated force plate embedded into the top surface of the second step	Inverse Dynamic Analysis (IDA) using VICON Clinical Manager Software (Oxford Metrics Limited)
Catani *et al.*, (2003)	0.16/0.28	Steps positioned onto force plates	Moments determined according to the Calibrated Anatomical System Technique (CAST) (Benedetti *et al.*, 1998; Cappozzo *et al.*, 1995) and resolved into the JCS (Grood and Suntay, 1983)
Nadeau *et al.*, (2003)	0.17/0.26	Force plate embedded in the floor in front of the staircase, a second positioned under step 1 and a third mounted on a solid frame serves as step 2	IDA (Bresler and Frankel, 1950) performed with Kingait3 software (Mishac Kinetics)
Costigan *et al.*, (2002)	0.2/0.3	Portion of walkway is removed to create a step with a force plate as the top surface	IDA ignoring the movement of the ankle joint. The shanks mass includes the mass of the foot and shoe. The shanks mass moment of inertia is modified using the principal axis theorem
Kaufman *et al.*, (2001)	0.18/0.25	Steps independently mounted onto force plates	IDA using Orthotrack 4.0 (Motion Analysis Corp.)
Kowalk *et al.*, (1996)	0.203/0.254	Steps mounted onto force plates and pre-loaded prior to testing	IDA using Gait lab software (Vaughan *et al.*, 1992). Moments defined in reference to the JCS
Yu *et al.*, (1996)	0.18/0.25	Steps independently mounted onto force plates	IDA using Orthotrak II (Motion Analysis Corp.). Moments expressed in the tibia reference frame
McFadyen *et al.*, (1988)	0.22/0.28	Force plate bolted to two steel risers become part of second step	Uses 'BIOMECH' package (Winter *et al.*, 1980) and calculations from (Bresler and Frankel, 1950)
Andriacchi *et al.*, (1980 & 1982)	0.21/0.255	Independent section of the first step rests on a force plate	Cross product of a vector defining the position of the joint centre and of the vector defining the GRF. Moments are resolved into the JCS

4.2 THE NEW STAIRCASE DESIGN

During clinical trials to assess lower limb function, data is generally collected for a number of daily activities. When including a staircase, it is important to set up and remove it from the measurement volume efficiently and expediently. The main challenges of designing a staircase for clinical assessments are firstly, ensuring it is safe for patient use and secondly, designing a method of interfacing it with force plates for the measurement of GRFs and computation of joint moments. Existing staircase designs fall into three categories depending on their method of interfacing with a force plate (Andriacchi *et al*, 1980; Catani *et al.*, 2003; Della Croce and Bonato, 2007; Kowalk *et al.*, 1996; Protopapadaki *et al.*, 2007; Thambyah *et al.*, 2004). These are to (i) bolt a step onto a force plate; (ii) embed a force plate into the top surface of a step and; (iii) position the steps onto a force plate. Each has advantages and disadvantages. Mounting a staircase onto a force plate can limit the range of activities tested and incorporating a force plate into a step is costly. The third approach either limits the size of the step to fit within the dimensions of the force plate rendering it unsafe for patient use, or a section of the step is independent to the staircase and contacts the force plate. This requires the subject to step within the confines of the 'independent' section of the step.

A staircase based on the third method of interfacing with a force plate was designed and custom built specifically for the clinical trial, where it would be used by patients with late stage osteoarthritis and TKR. To ensure its suitability for the clinical trial, it was designed according to the design specifications listed in section 4.2.1.

4.2.1 Staircase design specifications

1. Safety of the staircase is paramount, both for the staff running the data collection session and the patients. The staircase must be safe for subjects with varying ability to use and for staff to set up and move into storage.

2. The staircase must be easily moved to and from the storage area to the set up point during a data collection session.

3. It must interface with a force plate to measure 3D forces. The force plates cannot be moved during a patient measurement session. Equipment cannot be bolted to the force plates, not only due to time constraints but also it could affect the accuracy of the force plate.

4. It must be of low cost and easy to manufacture.

5. It must be robust and durable.

6. It must measure forces to the same degree of accuracy as the force plates.

4.2.2 Design and construction

The new staircase (Figure 4.1) interfaces with force plates to directly measure 3D forces as a subject ascends and descends the staircase, whilst providing flexibility and rapid assembly during data collection.

Figure 4.1 The new staircase

The staircase consists of four independent steps constructed from 0.02m medium-density fibreboard (MDF). MDF was chosen as it is less expensive than natural wood; it has a high strength and lends itself to manufacturing flexibility as it is available in

large sheet sizes. Step dimensions (height 0.16m, tread 0.28m) comply with building regulations for stairs. The angle of pitch is 30° ensuring suitability for the disabled and elderly. The method of interfacing a step with a force plate is as follows. A 0.3m x 0.26m x 0.003m section was removed from the underside of each of the first three steps and a 0.006m MDF panel of similar dimensions was manufactured. This was positioned between the force plate and a step. As the force plates are embedded 0.002m below floor level, this raises the step 0.001m from the ground ensuring direct measurements from the force plate, (Figure 4.2). A 6lb counterbalance maintains this position. Each of the first three steps has the facility to interface with a force plate.

Figure 4.2 MDF Panel providing Interface between step 1 and a force plate

Each step is strengthened internally at the base where the material has been removed to accommodate the MDF panel. The step is also strengthened vertically to prevent deformation (Figure 4.3) as subjects' ascend and descend the staircase. This will ensure 3D forces applied though the steps are measured directly and accurately from the force plate beneath the step.

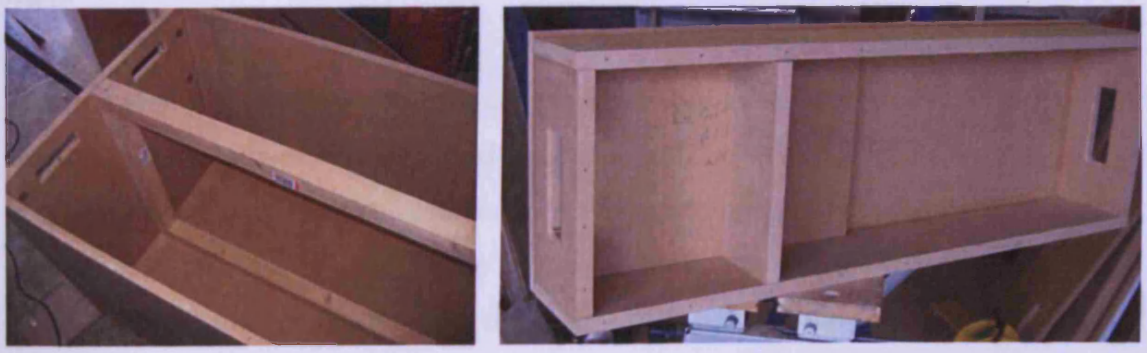

Figure 4.3 Horizontal and vertical reinforcements used to strengthen and prevent deformation.

Each step contains 0.03m x 0.11m handholds (Figure 4.4) on either side to assist staff when moving the staircase. The handholds were routered to remove sharp edges and provide a smooth contact area.

Figure 4.4 Handholds used for carrying the steps

A detachable handrail can be positioned on either side of the staircase to increase safety. The top (fourth) step is surrounded by a handrail for added safety and is moved using portable rollers.

The staircase was home produced and manufactured using DIY tools. This reinforces the ease of manufacture and by removing the need to contract it out, cost was minimised. Due to the nature of MDF, safety during the manufacturing process was paramount. Glasses and masks were worn at all times and the dust produced was removed from the work space regularly. The MDF was sealed and stained before the staircase was assembled. This stops the release of urea formaldehyde from the cut surfaces and prevents moisture being absorbed by the MDF which could cause it to warp.

The four step design allows the staircase to be moved as separate units and stacked for storage. It also provides flexibility during data collection sessions. In the simplest of tests, the patient may only be required to perform a step up/down activity. In this case, only the first step needs to be set up in the measurement volume. Alternatively, for a full assessment the design provides the ability of the first three steps to interface with a force plate and measure GRFs. The steps can be positioned so that the GRF is measured from either the right or left hand side of the staircase. The set up of the

staircase is dependent on the location and number of the force plates. In the following study, the GRFs were measured from the first and second steps, (Figure 4.5).

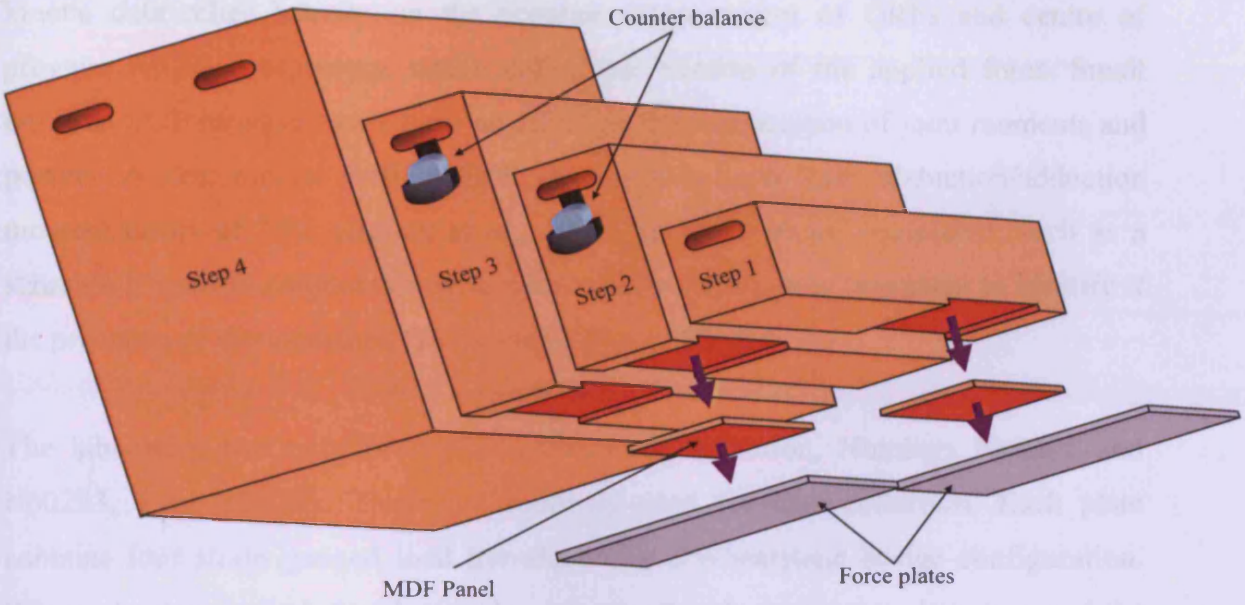

Figure 4.5 A graphical projection from beneath the staircase illustrating the separate steps and method of force plate contact.

4.3. FORCE PLATE ACCURACY TESTS AND STAIRCASE VALIDATION

Force plates are an integral part of clinical motion analysis. The true estimation of kinetic data relies heavily on the accurate measurement of GRFs and centre of pressure (COP) coordinates, which define the location of the applied force. Small errors in COP measurements have an effect on the computation of joint moments and powers. A 2cm medial shift in COP can result in peak knee abduction/adduction moment errors of 35% (Besser *et al.*, 1993). In cases where equipment, such as a staircase is used in conjunction with a force plate system, it is important to identify if the precision of the measured GRFs and COP are affected.

The laboratory has two force plates, (Bertec Corporation, Numbers N60202 and N60203, Type 4060H). These are routinely used for data collection. Each plate contains four strain gauged load transducers in a Wheatstone bridge configuration. When a load is applied, the electrical resistance of each strain gauge increases and the strain caused by the deformation is converted into electrical signals and subsequently amplified using an instrumentation amplifier. The signals from the force plate are multiplied with a calibration matrix to determine three orthogonal forces and the moments about each axis of the force plate coordinate system, shown in Figure 4.6. These are subsequently used to compute the centre of pressure (COP) of the applied force and the free moment acting between a subject's foot and the plate.

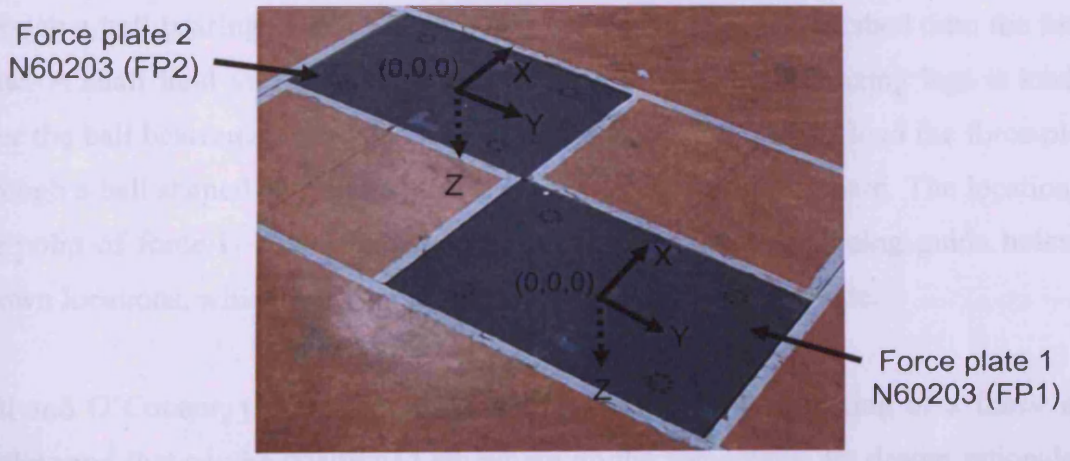

Figure 4.6 Force plates and their coordinate system. The origin of the force plate system is at the centre of the plate on the top surface. Patients walk over the plates and ascend the stairs in the negative y direction, with the positive x direction to their right.

Through contact with the technical support team at Bertec, it was revealed that the manufacturer's factory settings are 0.5% error for forces and moments and ± 2mm for COP. For the calibration procedure of the force plates, known weights are applied at known locations and the measured signals are then used to compute the elements of the calibration matrix using a matrix inversion method.

Tests were carried out firstly to determine the accuracy of the two force plates in the laboratory. Then, the accuracy of force and COP measurements when Step 1 and Step 2 independently interface with each of the force plates was evaluated. These tests were performed to verify whether or not reliable kinetic data can be derived when the staircase interfaces with each of the force plates.

Various methods have been reported for the quality assessment and calibration of force plates. For force assessments, custom apparatus are used to apply a known force at a known point. The measured force and COP are compared to the known values to determine their accuracy. For static tests the test loads are applied to the force platform at a large number of known locations over the platform and the applied loads should cover the operational range of the measurement device. The required testing load is suggested as 900N to equal average adult body weight (Gill and O'Connor, 1997).

Vertical forces can be applied in a number of ways. Hall *et al.*, (1996) transmits force through a ball bearing. The ball bearing is positioned on a grid scribed onto the force plate. A shaft held vertically with an external housing and stabilizing legs is loaded over the ball bearing. Similarly, Bobbert and Schamhardt, (1990) load the force plate through a ball shaped stylus attached to the corner of a wooden board. The location of the point of force is controlled using an aluminium sheet containing guide holes at known locations, which is bolted to the top surface of the force plate.

Gill and O'Connor, (1997) describe a prototype for a rig consisting of a frame and loading rod that can be positioned anywhere on the force plate. Its design rationale is to apply loads safely, test the vertical force and COP accurately and without a lengthy testing time.

Shear forces can be applied in isolation using a rig containing a system of pulleys (Hall *et al.*, 1996) or they can be applied in combination with vertical loads. Besser *et al.*, (1993) uses a calibration procedure for force plates with stairs bolted to them. A jig was used to apply vertical loads of 180N alone and in combination with 45N shear loads. The location of the test points were identified at 5cm intervals using graph paper.

Holden *et al.*, (2003) describes a method involving the use of a rigid rod containing retro-reflective markers and a pointed tip at each end. A hand held loading bar and a base plate with machined conical depressions seat both rod extremities. The base plate is placed onto the platform while the loading bar is handled by the operator. Forces are applied manually through a broad range of angles, with negligible applied moment of a force couple. Marker and force plate signals are generated simultaneously to allow the working status of the force plate to be determined in terms of the orientation and tip position of the rod by comparing estimates from kinematic and kinetic information. A similar method used for 'spot checking' COP location estimates is proposed by Rabuffetti *et al.*, (2001), except this method requires the rod to be kept almost vertical during data collection so that shear components of the force are minimised.

Middleton *et al.*, (1999) evaluated the accuracy of COP measurements for use with stabilometry research. This requires the COP to be accurately located when force is distributed across two feet and the centre of pressure it located between the feet. Two rectangular model feet made of steel were filled with lead to approximately 300N used to simulate standing COP.

For the current investigation, a method was required to evaluate the accuracy of the force plate system to measure three force components, COP and to test the linearity of each transducer. The method was also required to be suitable to also test the three force components and COP applied to the top surface of the first and second steps of the staircase. The procedure was required to be straightforward to perform, provide information on the accuracy of each force plate and identify any affects in accuracy due to the staircase interfacing with each force plate.

Initial testing of the vertical force and COP measurements were completed using a pointed chisel piece and 5Kg weight, (Figure 4.7). The chisel was inserted into a cut out section of the weight. The weight was applied vertically at 77 known locations on FP1 and 45 locations on step 1 and step 2. These tests were repeated 5 times and an average of the three force and COP data from the 5 trials were computed. The maximum average difference between the applied force (combined weight of the chisel and metal weight) and that of the vertical force measurement by FP1 was 6.4N or 12.5% of the applied force. Although efforts were made not to apply additional weight to the chisel, this could not be guaranteed. Also, a vertical force could not be applied in isolation as shear forces of up to up to 2.54N in the x direction and 2.74N in the y direction were also measured during these measurements.

The difference between the actual and recorded COP measurements ranged from 0.10 mm to 10.85 mm (x-direction) and from 0.03 mm to 7.24 mm (y-direction) for FP1. There was a gradual increase in error towards the negative x direction on the plate. The difference between the actual and recorded COP for step 1 ranged from 0.02 mm to 13.39 mm (x-direction) and from 0.05 mm to 4.26 mm (y-direction). For step 2 they ranged from 0.08 mm to 10.27 mm (x-direction) and from 0.00 mm to 5.34 mm (y-direction).

Figure 4.7 Initial method of performing accuracy tests. Step 1 is positioned on the panel on FP1. A weight is applied to a chisel pointing at a known location

Due to the limitations experienced by this method, testing equipment was designed to allow each force to be tested in isolation and allow larger forces to be used in the procedure. The final methodology used to assess the accuracy of each force plate and

of the first two steps independently mounted onto each of the force plates will now be discussed.

4.3.1 Methodology

Static tests were performed with the plates *in situ*. This allowed the evaluation of the system as it would be used during a clinical trial. The force plates were switched on and allowed to warm-up for at least half an hour before collecting data as recommended in the Bertec user manual, (Bertec Corporation). This allowed for the force plate system to reach thermal stability. All force plate measurements were sampled at 1080Hz. Two sets of equipment were designed for the experimentation to ensure loads were applied to the force plate at precise locations and orientation.

4.3.1.1 Equipment designs

The following piece of equipment, (Figure 4.8) was designed to hold a stack of cylindrical weights to vertically load the force plate. It was manufactured from solid stainless steel at the Cardiff Engineering Workshop. A metal ring is used to position the pole at precise locations on a force plate or step. A stainless steel handle can be inserted into a hole towards the top of the pole if required. A groove is cut into the base of the pole to locate the flexible wire used in the shear force tests. This design avoids the need for large framework, which is often necessary in designs where a stylus is loaded at specific positions on the plate and is small for storage.

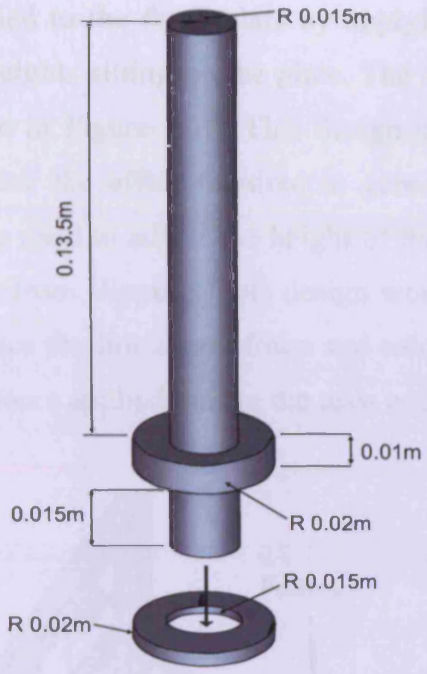

Figure 4.8 Stainless steel pole used to stack cylindrical weights

The weights used for the accuracy tests were calibrated using a load cell, (Figure 4.9). A hole of same dimensions as the pole was drilled from the centre of each weight so that they are aligned centrally when stacked to prevent them from tipping during the tests.

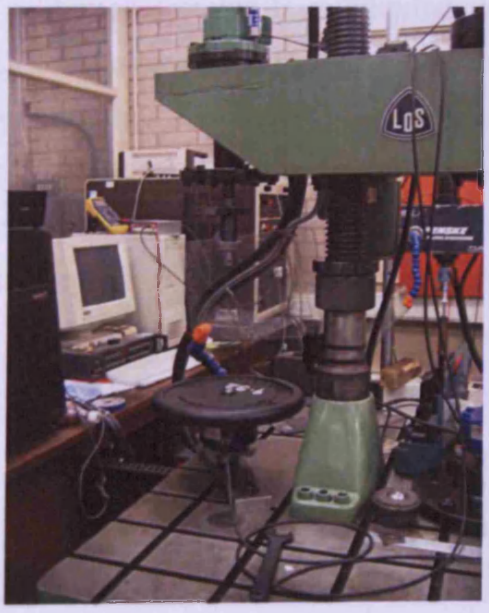

Figure 4.9 Calibration of a cylindrical weight using a load cell

Shear forces can be applied to the force plate by applying a horizontal force to the stainless steel pole and weights sitting on the plate. The initial design of apparatus to test shear forces is shown in Figure 4.10. This design uses pulleys, flexible fishing wire and weights to reduce the effort required to generate large horizontal forces. Screws at the front can be used to adjust the height of the wire connected to the pole and rubber feet prevent it from slipping. This design would require the calibration of the weights used to produce the horizontal force and calculation of the friction in the system so that the actual force applied during the tests could be determined.

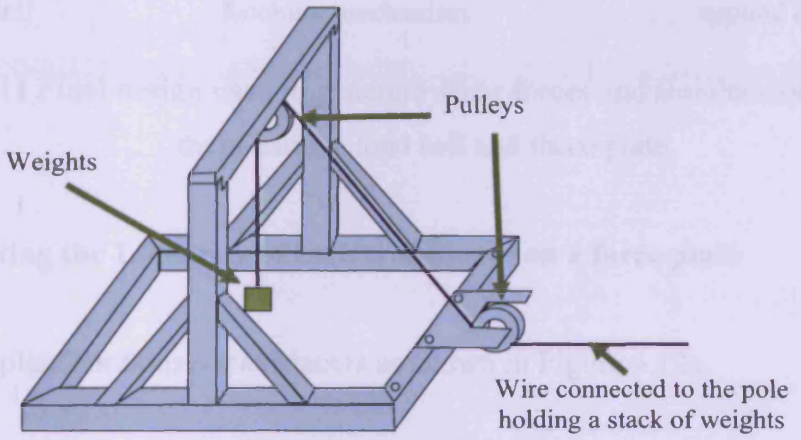

Figure 4.10 Initial design of a rig for testing the accuracy of horizontal (shear) forces

An alternative to using calibrated weights is to simultaneously measure horizontal forces using the force plates and a load cell. This inspired the final design used for the testing of horizontal forces (Figure 4.11). A flexible wire is looped around the base of the pole containing a stack of weights. The other end of the wire is secured to one end of a load cell (Nene Instruments Ltd). A wire is attached to the other end of the load cell, through a locking device, under a guide and into a raised handle. The handle is turned until the required load is registered on the load cell and the wire is secured in place by tightening two screws on the locking device.

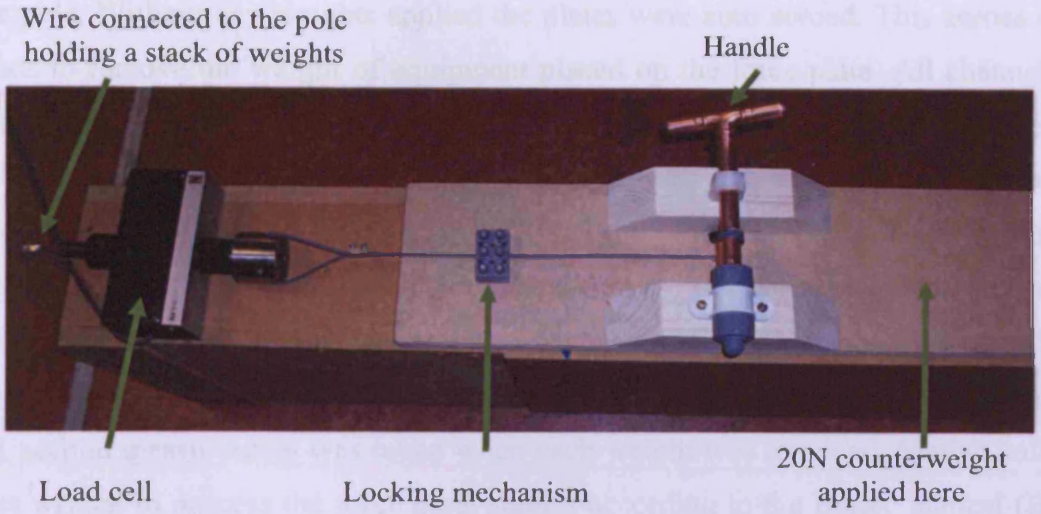

Figure 4.11 Final design used to generate shear forces and simultaneously measure them using a load cell and force plate

4.3.1.2 Testing the Linearity of each transducer on a force plate

Each force plate contains 4 transducers as shown in Figure 4.12a.

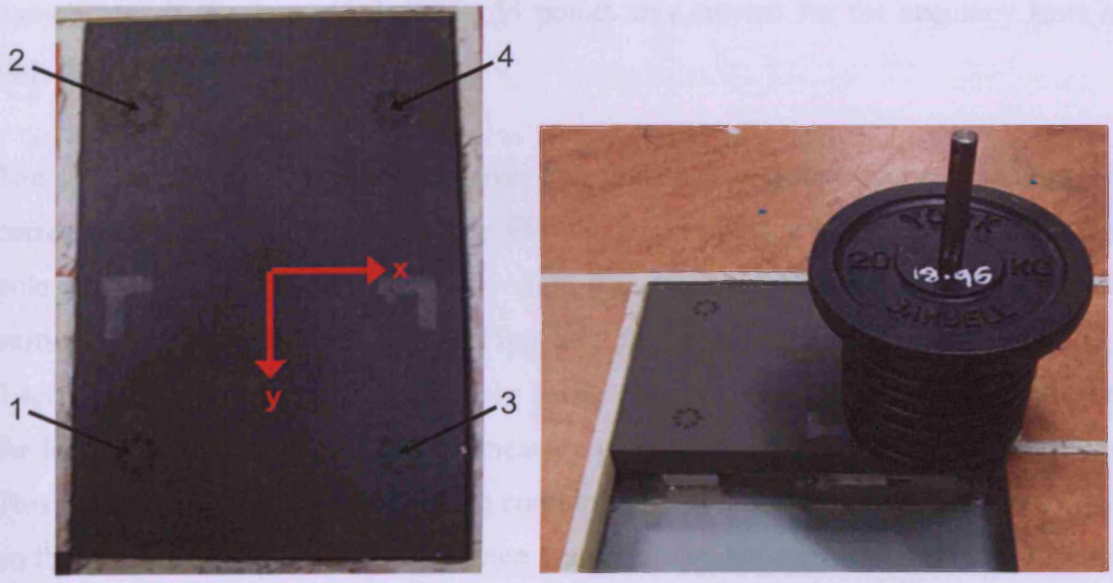

Figure 4.12 (a) the location of the force transducers on the force plate (b) Full load applied to force transducer 1 on a force plate

The linearity of each transducer was determined by incrementally loading and unloading it at its centre through a force range of approximately 1000N. The alignment ring was used to identify the centre of a transducer and to correctly position

the pole. Without any weights applied the plates were auto zeroed. This zeroes offset loads to remove the weight of equipment placed on the force plate. All channels are set to near zero (less than ±3mV at unity gain). True zeroing is performed by subtracting the baseline reading from the collected data. A 1 second measurement was taken without any load applied so that an average of the force plate signals could be applied as an offset for all subsequent measurements. The pole was loaded one weight at a time and a 1 second recording taken for each additional weight. Once loaded to approximately 1000N, (Figure 4.12b) the pole was unloaded one weight at a time and a 1 second measurement was taken when each weight was removed. Matlab software was written to process the force plate signals according to the Bertec manual (Bertec Corporation). An offset computed from the initial measurement was applied to each of the subsequent measurements in the series. An average of the signals from each 1 second recording was computed.

4.3.1.3 Testing vertical force and COP (applied to either a force plate or step)

Graph paper was used to define 77 points over the surface of the force plate, at 5cm increments. A similar grid defining 54 points was created for the accuracy tests on step 1 and step 2.

The alignment ring was positioned over a defined point so that the centre of the ring corresponds with the test point. The FP was zeroed before each measurement. The pole containing a single cylindrical weight was positioned in the ring so that is sits vertically with the handle in place, (Figure 4.13a). A measurement was recorded for a 3 second duration. After approximately 1.5 seconds the pole was lifted. An average of the last 100 frames of data from the measurement was used to provide a zero baseline. This was subtracted from data before computing the vertical force and COP. For tests on the steps, a height of 0.163m for step 1 and 0.323m for step 2 was accounted for in the calculations. The vertical force applied at each location was 130.48N. This was calculated as the combined weight of the pole, handle and cylindrical weight. This test was repeated for each point on the grid. Both force plates were tested. Also, step 1 (Figure 4.13b) and step 2 were tested on each of the force plates. The steps are positioned at pre-defined locations of the force plate during the clinical trial. For consistency, the accuracy tests for the steps were performed with the steps mounted

on the MDF panel in the same location of the force plate used in the clinical trial, where the front of the step is in line with the front of the force plate.

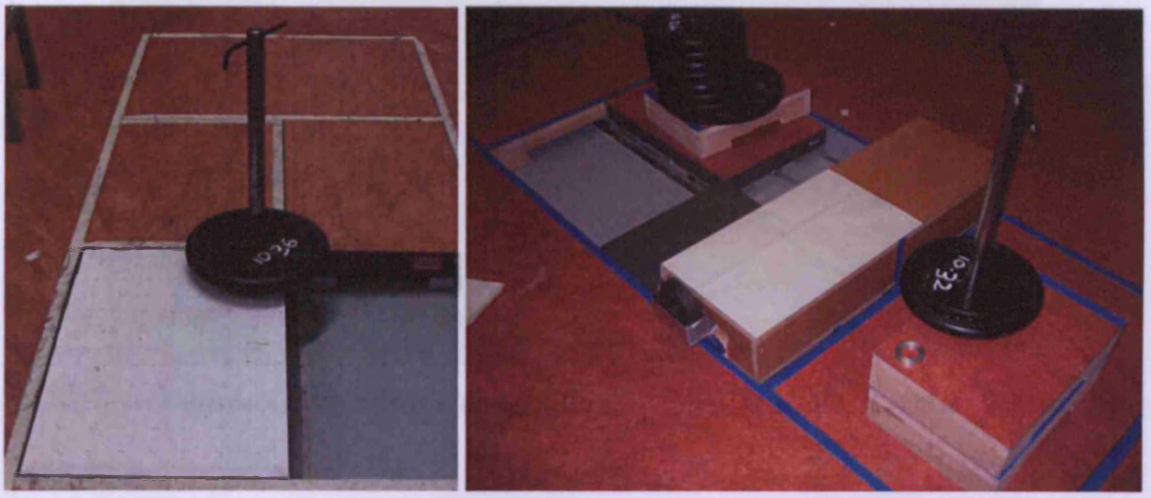

Figure 4.13 (a) pole and weight used for the COP and vertical force tests (b) step 1 situated in position on FP1 for testing

4.3.1.4 Testing shear forces (applied to either a force plate or step)

Prior to measurement, the force plate was zeroed and a 1 second measurement was taken to provide a zero baseline. The pole holding 488.6N was positioned at a specific location using the alignment ring. Shear loads of approximately 160N were applied to the pole along the positive x-axis and y-axis of the force plate coordinate system separately, (Figure 4.14). The load cell (Nene Instruments Ltd.) was synchronised with the force plate system. A measurement was taken for 1 second. The weights and pole were removed and another 1 second baseline reading was taken. The two baseline readings were used to compute an offset which was applied to the raw signals from the force plate. 8 positions on each force plate were tested along each of the horizontal force plate axes. A single point was tested on step 1 and step 2. The location of the testing point was approximately x=0, y=16cm in relation to the force plate coordinate system. This location was chosen as this is the centre of the location where subjects contact the step. Step height was accounted for in the calculations.

Figure 4.14 Experimental set up for shear force measurements

The load cell was calibrated by measuring a 0N, 20N weight (Figure 4.15) and 40N weight for 1 second. An average of the voltages generated during each measurement was computed. A calibration factor of 48.673 was determined to convert the voltage signal to the applied force in Newtons. The measurement from the force plate was compared with the measurement from the load cell.

Figure 4.15 Calibrating the Load cell (Nene Instruments Ltd.)

4.3.2 Results for force plate 1 (FP1)

Figure 4.16 illustrates the force plate and the location at which each test is measured. The transducers are labelled T1 to T4. Points 1 to 77 are the locations of each COP and vertical force test. The numbers highlighted in bold red are the locations used to test the horizontal components of force in the positive x and y directions of the force plate.

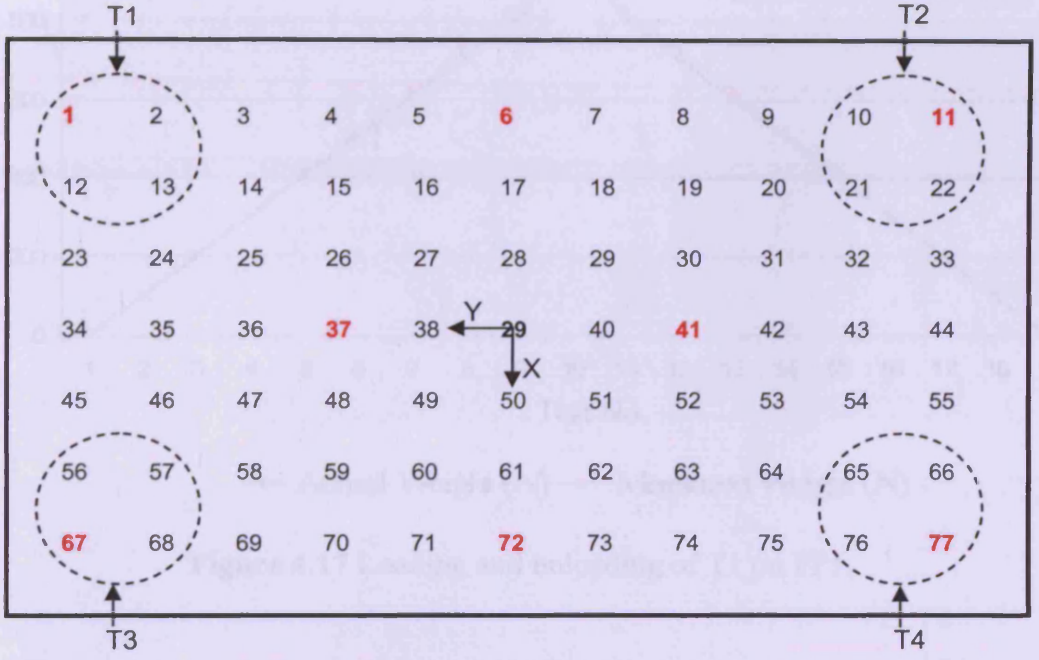

Figure 4.16 The naming protocol for the tests on FP1. T1 to T4 indicate the location of each transducer. Test points 1 to 77 are indicated; those in bold red are also used as locations for the shear force tests.

4.3.2.1 Linearity of transducers (FP1)

The results from the loading and unloading of each transducer for FP1 are summarised in Table 4.2. The error is expressed as the measured vertical force component (Fz) minus the known weight being applied. This difference is also expressed as a percentage of the known weight for each measurement.

Figure 4.17 displays the actual and measured weight for each measurement during loading and unloading of transducer 1 (T1). Figure 4.18 displays the measured force plotted against the actual force for the loading and unloading of T1. A Pearson's

correlation revealed coefficient of 0.9999 for all four force transducers for FP1, indicating a significant correlation between the measurements. The graphs for the other three transducers follow the same pattern and thus are not shown.

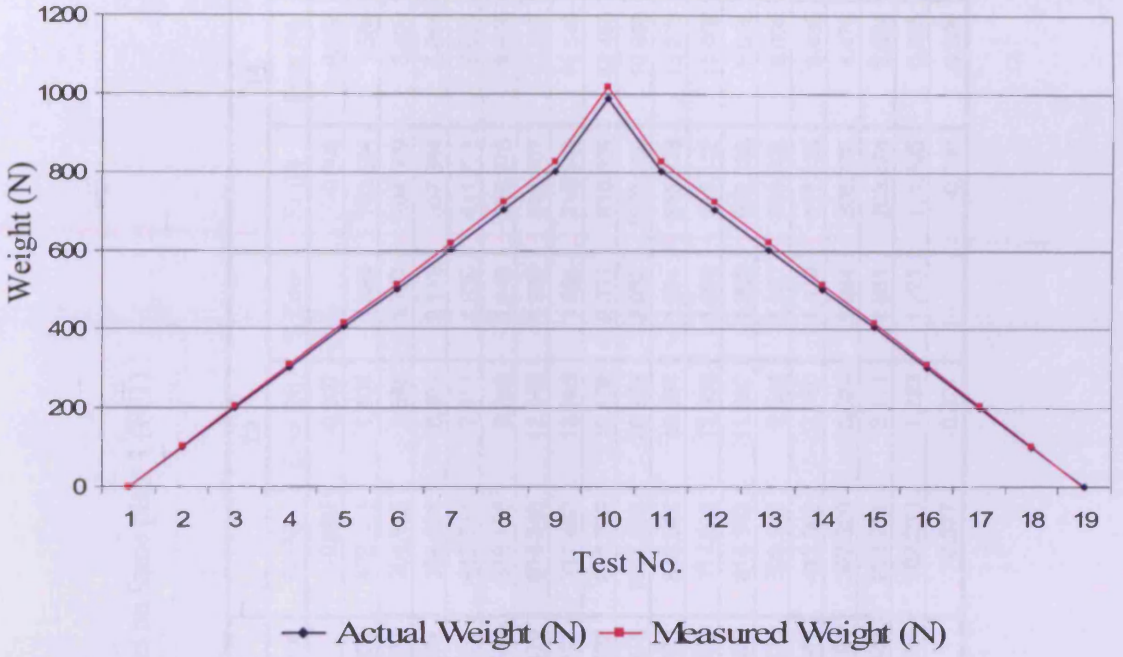

Figure 4.17 Loading and unloading of T1 on FP1.

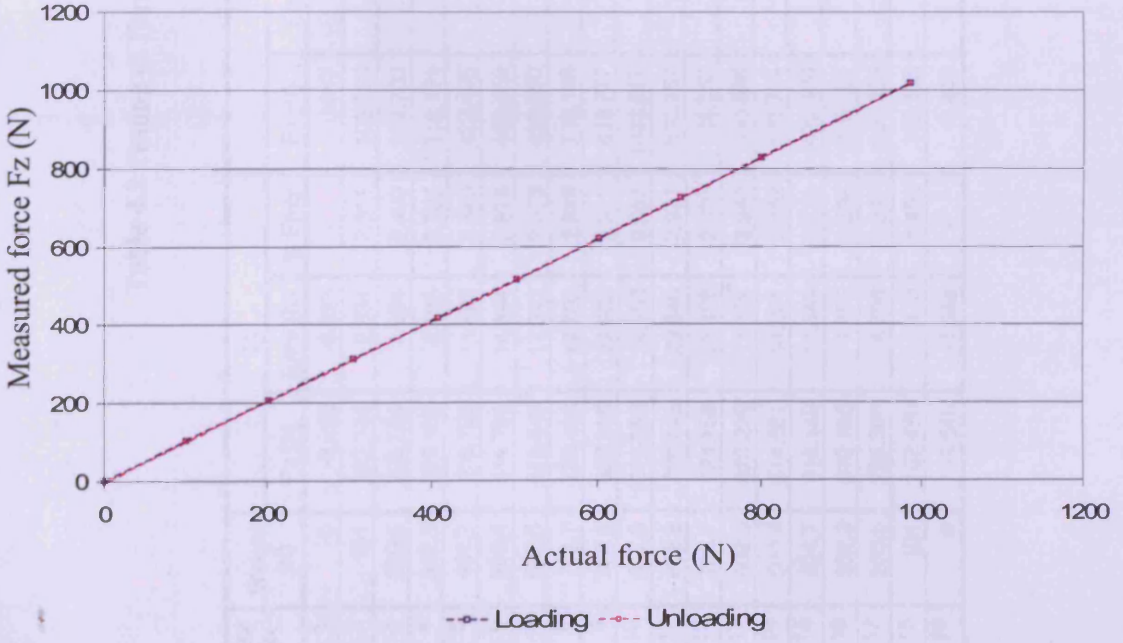

Figure 4.18 Linearity of T1 on FP1

Table 4.2 Testing of Force transducers on force plate 1 (FP1)

Test No.	Weight (N)	T1			T2			T3			T4		
		Fz (N)	Error (N)	% Error	Fz (N)	Error (N)	% Error	Fz (N)	Error (N)	% Error	Fz (N)	Error (N)	%Error
1	0	-0.023	-0.023	-	0.017	0.017	-	-0.007	-0.007	-	-0.006	-0.006	-
2	101	103.334	2.334	2.311	105.378	4.378	4.335	102.408	1.408	1.394	102.584	1.584	1.568
3	200.6	205.594	4.994	2.490	209.700	9.100	4.537	204.165	3.565	1.777	204.009	3.409	1.699
4	302.3	310.485	8.185	2.707	316.121	13.821	4.572	308.694	6.394	2.115	307.384	5.084	1.682
5	404.7	416.195	11.495	2.840	423.425	18.725	4.627	412.511	7.811	1.930	411.731	7.031	1.737
6	500.4	514.794	14.394	2.876	523.658	23.258	4.648	510.136	9.736	1.946	508.976	8.576	1.714
7	602.5	619.843	17.343	2.879	630.690	28.190	4.679	614.546	12.046	1.999	612.707	10.207	1.694
8	703.7	723.493	19.793	2.813	736.188	32.488	4.617	717.463	13.763	1.956	715.249	11.549	1.641
9	802.6	825.965	23.365	2.911	839.777	37.177	4.632	818.738	16.138	2.011	816.065	13.465	1.678
10	987.3	1016.553	29.253	2.963	1032.867	45.567	4.615	1007.558	20.258	2.052	1003.995	16.695	1.691
11	802.6	826.446	23.846	2.971	840.157	37.557	4.679	818.581	15.981	1.991	815.878	13.278	1.654
12	703.7	724.158	20.458	2.907	736.562	32.862	4.670	717.536	13.836	1.966	715.102	11.402	1.620
13	602.5	620.229	17.729	2.943	630.808	28.308	4.698	614.362	11.862	1.969	612.398	9.898	1.643
14	500.4	514.621	14.221	2.842	523.794	23.394	4.675	509.944	9.544	1.907	508.408	8.008	1.600
15	404.7	416.149	11.449	2.829	423.506	18.806	4.647	412.060	7.360	1.819	411.135	6.435	1.590
16	302.3	310.155	7.855	2.598	316.187	13.887	4.594	307.329	5.029	1.664	306.778	4.478	1.481
17	200.6	205.308	4.708	2.347	209.493	8.893	4.433	203.711	3.111	1.551	203.474	2.874	1.433
18	101	102.470	1.470	1.456	105.135	4.135	4.094	102.233	1.233	1.221	101.895	0.895	0.887
19	0	-1.548	-1.548	-	-0.446	-0.446	-	-0.327	-0.327	-	-0.509	-0.509	-

4.3.2.2 Testing vertical force and COP (FP1)

The actual and measured COP results for each test point are tabulated in Appendix E and represented in Figure 4.19. The error in COP measurement is computed as the difference between the actual and measured COP x and y coordinates. The average errors in the COP measurements recorded for 77 points on the force plate were 3.94 ± 3.25mm for the x coordinate and 3.37 ± 2.56mm for the y coordinate. From Figure 4.19, it can be seen that the COP measurements are more accurate at the centre of the force plate.

The maximum error in the measured x-coordinates was 11.17mm. This occurred at test point 59 and is indicated in Figure 4.19. The smallest error was 0.07mm and this occurred at point 45. The maximum error in the measured y-coordinate was 10.29mm. This occurred at test point 34. The smallest error was 0.02mm and occurred at position 27. These points are also indicated in Figure 4.19.

The actual and measured vertical forces for each test point are tabulated in Appendix E. The vertical force (F_z) measured by the force plate was consistently larger than the applied force, (Figure 4.20). F_z was over estimated to a greater extent in the negative x region of the force plate. In the measurements along the long axis of the plate, F_z was also overestimated to a greater extent towards the centre of the plate. The percentage error in the F_z measurement was calculated. The greatest error occurred at point 10 where F_z overestimated the known force by 4.64%. The smallest error was 0.61% and this occurred at point 66.

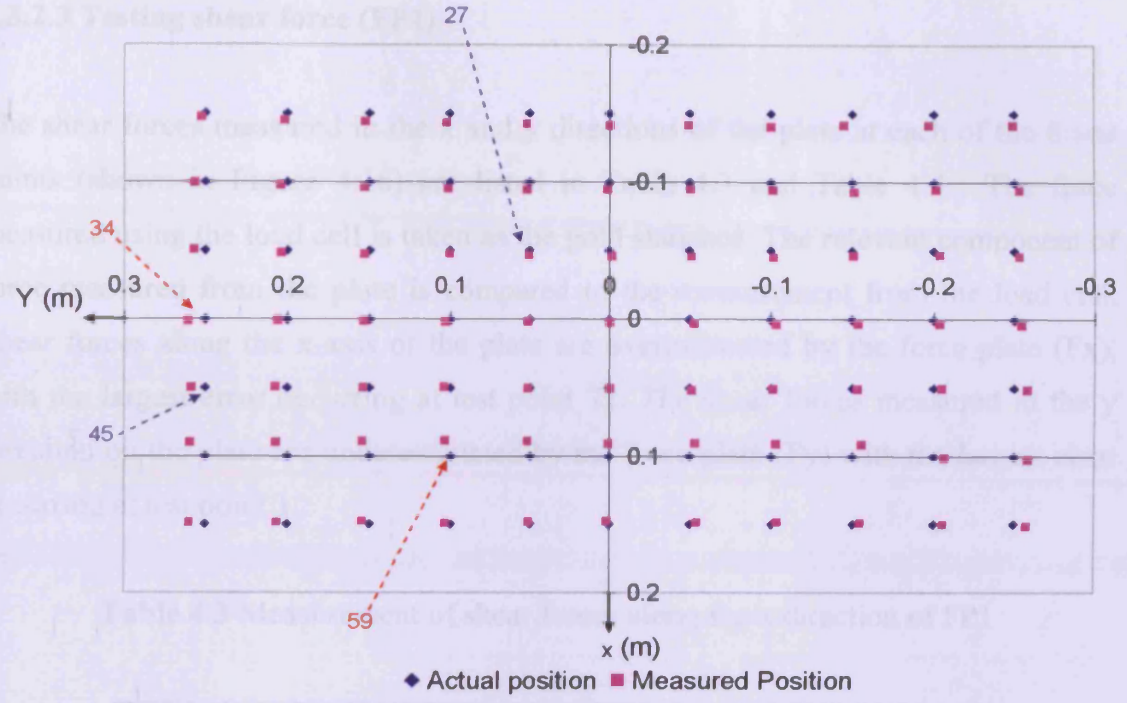

Figure 4.19 COP measurements at each test point on FP1. Position 27 is where the smallest error in the y-coordinate was measured. Position 34 is where the greatest error in y-coordinate was measured. Position 45 is where the smallest error in the x-coordinate was measured. Position 59 is where the greatest error in x-coordinate was measured.

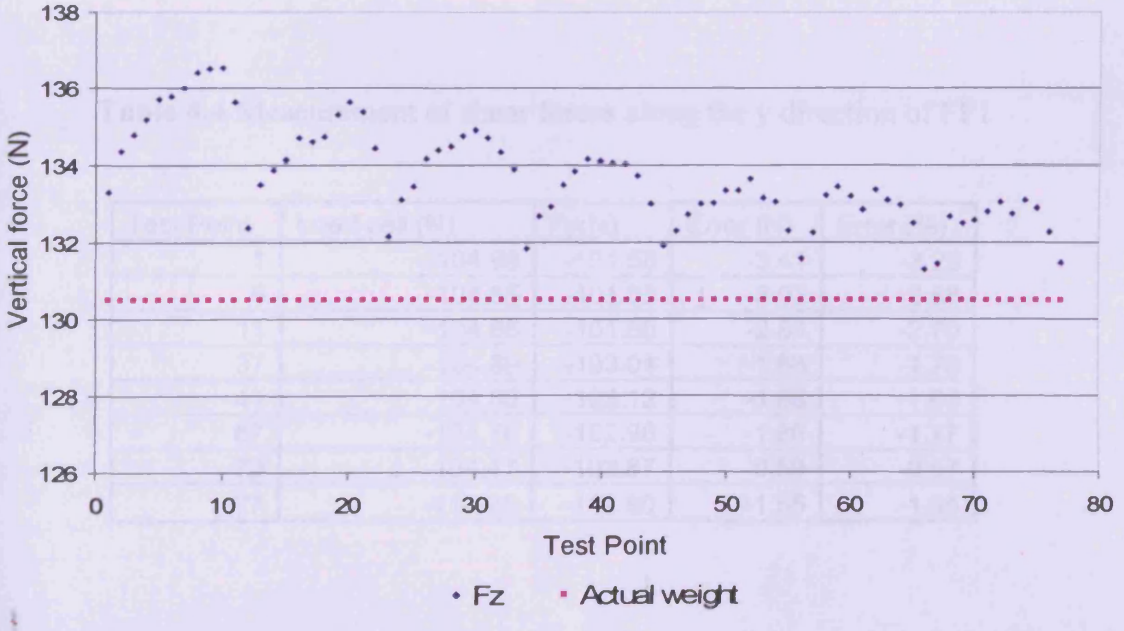

Figure 4.20 Vertical force measurements at each test point on FP1

4.3.2.3 Testing shear force (FP1)

The shear forces measured in the x and y directions of the plate at each of the 8 test points (shown in Figure 4.16) are listed in Table 4.3 and Table 4.4. The force measured using the load cell is taken as the gold standard. The relevant component of force measured from the plate is compared to the measurement from the load cell. Shear forces along the x-axis of the plate are overestimated by the force plate (Fx), with the largest error occurring at test point 72. The shear forces measured in the y direction on the plate are underestimated by the force plate (Fy) with the largest error occurring at test point 1.

Table 4.3 Measurement of shear forces along the x direction of FP1

Test Point	Load cell (N)	Fx (N)	Error (N)	Error (%)
1	-106.01	-107.98	1.97	1.86
6	-104.46	-106.00	1.54	1.48
11	-105.04	-106.15	1.11	1.06
37	-105.01	-108.01	3.00	2.86
41	-105.30	-107.54	2.24	2.13
67	-104.66	-107.85	3.20	3.06
72	-104.64	-109.85	5.21	4.98
77	-104.61	-105.90	1.29	1.23

Table 4.4 Measurement of shear forces along the y direction of FP1

Test Point	Load cell (N)	Fy(N)	Error (N)	Error (%)
1	-104.98	-101.58	-3.41	-3.25
6	-104.85	-101.83	-3.02	-2.88
11	-104.68	-101.86	-2.83	-2.70
37	-104.89	-103.01	-1.88	-1.79
41	-104.80	-103.12	-1.68	-1.60
67	-104.76	-102.90	-1.86	-1.77
72	-104.47	-103.87	-0.59	-0.57
77	-114.35	-112.80	-1.55	-1.35

4.3.2.4 Measures from Step 1 interfaced with FP1

The step is positioned with the front edge in line with the front edge of the force plate as shown in Figure 4.21a. The numbering protocol for COP and vertical force tests are shown in figure 4.21b.

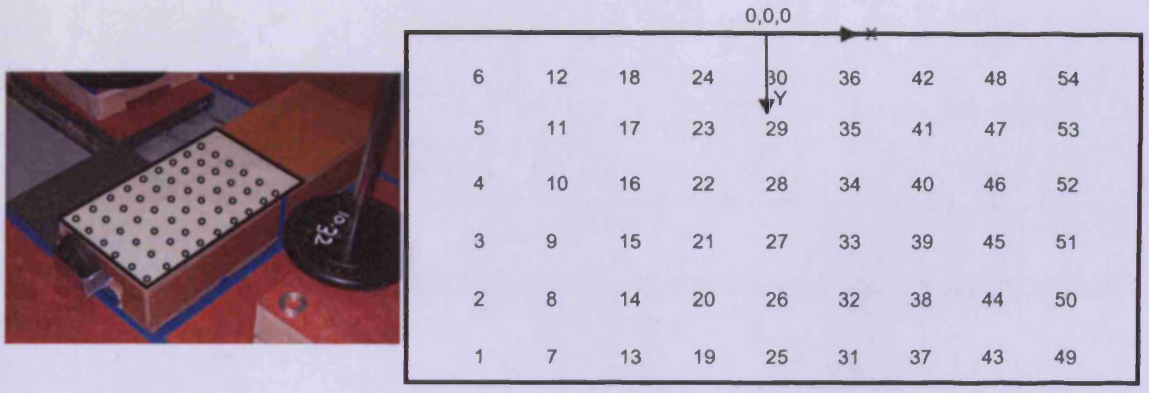

(a) (b)

Figure 4.21 (a) Positioning of step 1 on FP1 (b) numbering protocol for the test points

The actual and measured COP results for each test point are presented in Appendix E and represented in Figure 4.22. The error in COP measurement is computed as the difference between the actual and measured COP x and y coordinates. The average errors in the COP measurements recorded for 54 points on step 1 were 3.36 ± 3.46 mm for the x coordinate and 3.38 ± 2.59mm for the y coordinate. From Figure 4.22, it can be seen that the COP measurements are more accurate towards the centre and right hand side of the measurement grid.

The maximum error in the measured x-coordinates was 11.84mm. This occurred at test point 40 and is indicated in Figure 4.21. The smallest error was 0.03mm and this occurred at points 35 and 36. The maximum error in the measured y-coordinate was 9.37mm. This occurred at test point 43. The smallest error was 0.04mm and occurred at position 36. These points are indicated in Figure 4.22.

The actual and measured vertical forces for each test point are presented in Appendix E. The vertical force (F_z) measured by the force plate was consistently larger than the applied force, (Figure 4.23). F_z was over estimated to a greater extent in the negative x

region of the force plate. In the measurements along the long axis of the plate, F_z was also overestimated to a greater extent towards the centre of the plate. The percentage error in the F_z measurement was calculated. The greatest error occurred at point 6 where F_z overestimated the known force by 4.06%. The smallest error was 0.33% and this occurred at point 43.

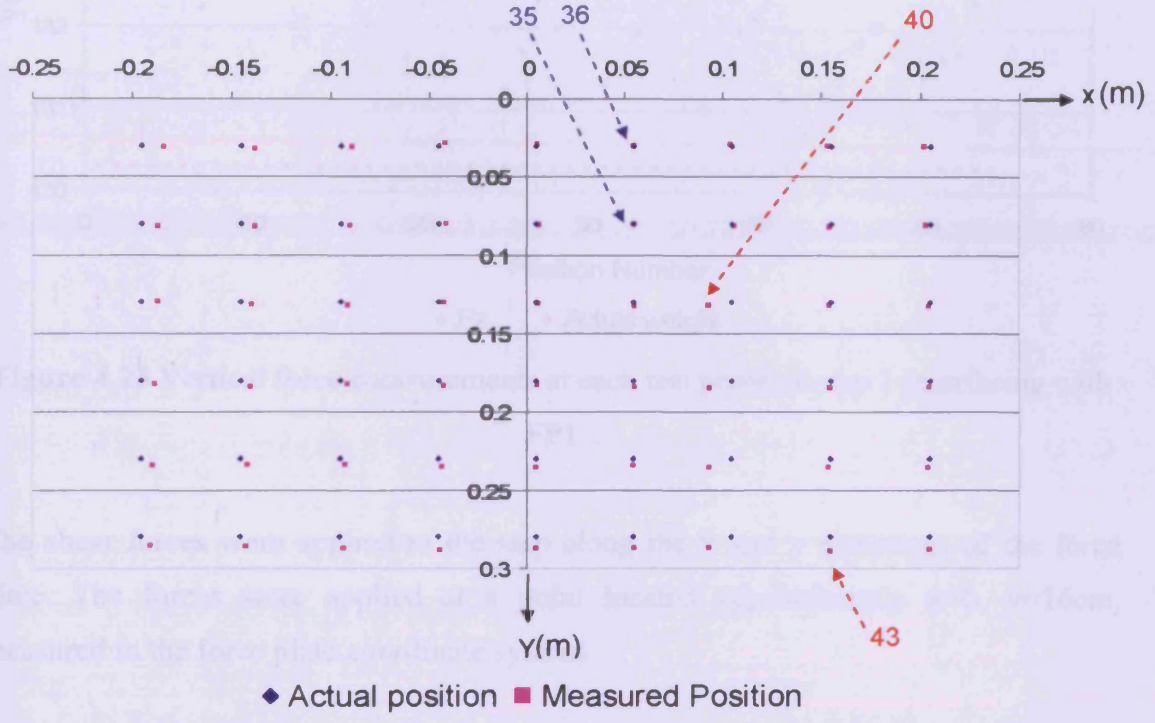

Figure 4.22 COP measurements at each test point on step 1 interfacing with FP1. Positions 35 and 36 are where the smallest error in the x-coordinate was measured. Position 40 is also where the greatest error in x-coordinate was measured. Position 36 is where the smallest error in the y-coordinate was measured. Position 43 is where the greatest error in y-coordinate was measured.

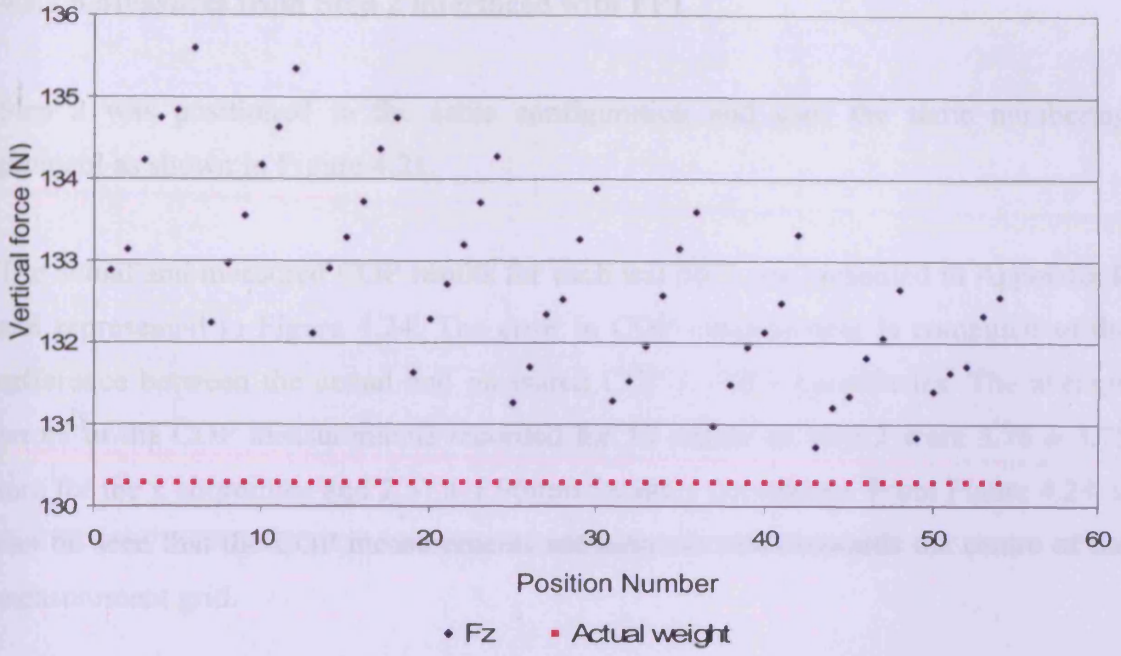

Figure 4.23 Vertical force measurements at each test point on step 1 interfacing with FP1

The shear forces were applied to the step along the x and y directions of the force plate. The forces were applied at a point located approximately x=0, y=16cm, measured in the force plate coordinate system.

Shear forces measured using the load cell and force plate are displayed in Tables 4.5 and 4.6. The relevant component of force measured from the plate is compared to the measurement from the load cell to determine the measurement error. Shear forces applied to the step in both the x and y directions of the force plate coordinate system are overestimated by the force plate.

Table 4.5 Measurement of shear forces along the x direction of FP1 for step 1

Load Cell (N)	Fx (N)	Error (N)	Error (%)
-104.82	-111.48	6.67	6.36

Table 4.6 Measurement of shear forces along the y direction of FP1for step 1

Load Cell (N)	Fy (N)	Error (N)	Error (%)
-104.59	-105.59	1.00	0.96

4.3.2.5 Measures from Step 2 interfaced with FP1

Step 2 was positioned in the same configuration and uses the same numbering protocol as shown in Figure 4.21.

The actual and measured COP results for each test point are presented in Appendix E and represented in Figure 4.24. The error in COP measurement is computed as the difference between the actual and measured COP x and y coordinates. The average errors in the COP measurements recorded for 54 points on step 2 were 3.76 ± 3.75 mm for the x coordinate and 2.51 ± 1.96mm for the y coordinate. From Figure 4.24, it can be seen that the COP measurements are more accurate towards the centre of the measurement grid.

The maximum error in the measured x-coordinates was 13.06mm. This occurred at test point 40 and is indicated in Figure 4.24. The smallest error was 0.10mm and this occurred at point 25. The maximum error in the measured y-coordinate was 6.68mm. This occurred at test point 13. The smallest error was 0.03mm and occurred at position 3. These points are indicated in Figure 4.24.

The actual and measured vertical forces for each test point are presented in Appendix E. The vertical force (F_z) measured by the force plate was consistently larger that the applied force, (Figure 4.25). F_z was over estimated to a greater extent in the negative x region of the force plate. In the measurements along the long axis of the plate, F_z was also overestimated to a greater extent towards the centre of the plate. The percentage error in the F_z measurement was calculated. The greatest error occurred at point 5 where F_z overestimated the known force by 3.69%. The smallest error was 0.60% and this occurred at point 43.

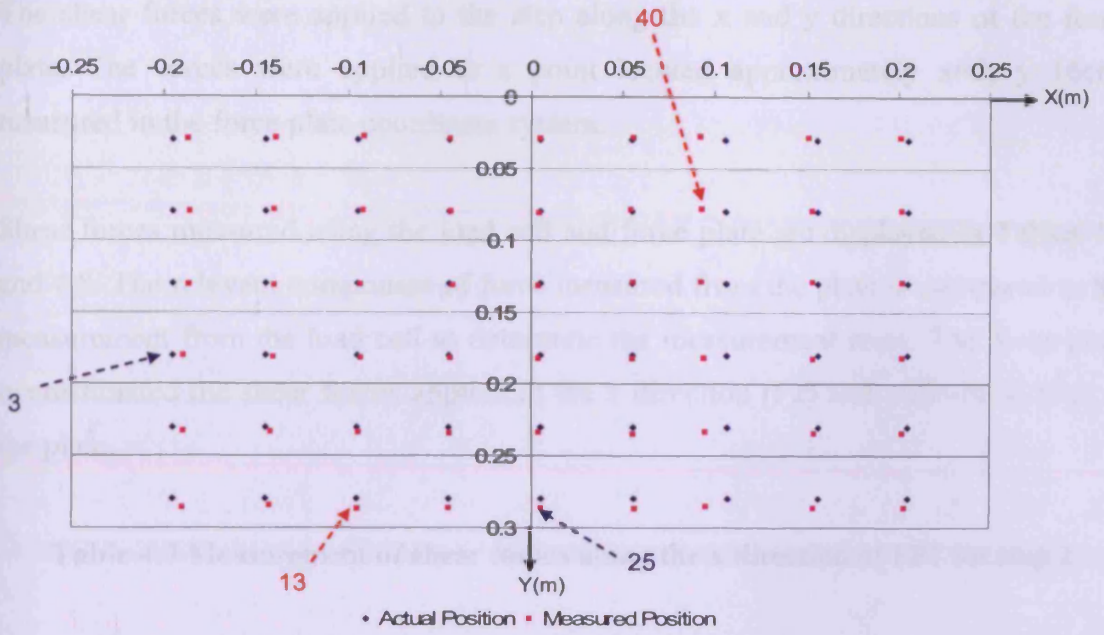

Figure 4.24 COP measurements at each test point on step 2 interfacing with FP1. Position 3 is where the smallest error in the y-coordinate was measured. Position 13 is where the greatest error in y-coordinate was measured. Position 25 is where the smallest error in the x-coordinate was measured. Position 40 is where the greatest error in the x-coordinate was measured.

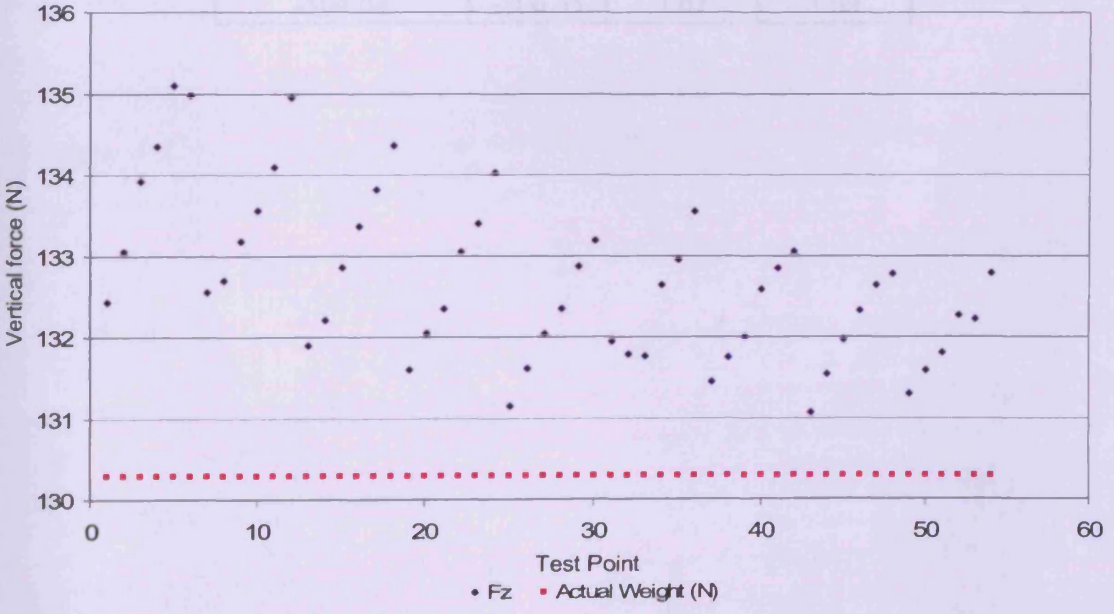

Figure 4.25 Vertical force measurements at each test point on step 2 interfacing with FP1

The shear forces were applied to the step along the x and y directions of the force plate. The forces were applied at a point located approximately x=0, y=16cm, measured in the force plate coordinate system.

Shear forces measured using the load cell and force plate are displayed in Tables 4.7 and 4.8. The relevant component of force measured from the plate is compared to the measurement from the load cell to determine the measurement error. The force plate overestimated the shear forces applied in the x direction (Fx) and y direction (Fy) of the plate.

Table 4.7 Measurement of shear forces along the x direction of FP1 for step 2

Applied force (N)	Fx (N)	Error (N)	Error (%)
-104.61	-111.83	7.21	6.90

Table 4.8 Measurement of shear forces along the y direction of FP1 for step 2

Applied force (N)	Fy (N)	Error (N)	Error (%)
-104.84	-106.51	1.67	1.59

4.3.3 Results for force plate 2 (FP2)

The tests performed on FP2 use the same naming protocol for the tests carried out on FP1 as shown in Figure 4.16.

4.3.3.1 Linearity of transducers (FP2)

The results from the loading and unloading of each transducer for FP2 are summarised in Table 4.9. The error is expressed as the measured vertical force component (Fz) minus the known weight being applied. This difference is also expressed as a percentage of the known weight for each measurement.

Figure 4.26 displays the actual and measured weight for each measurement during loading and unloading of transducer 1. Figure 4.27 displays the measured force plotted against the actual force for the loading and unloading of transducer 1. A Pearsons correlation revealed coefficient of 0.9999 for all four force transducers for FP2, indicating a significant correlation between the measurements. The graphs for the other three transducers follow the same pattern and thus are not shown.

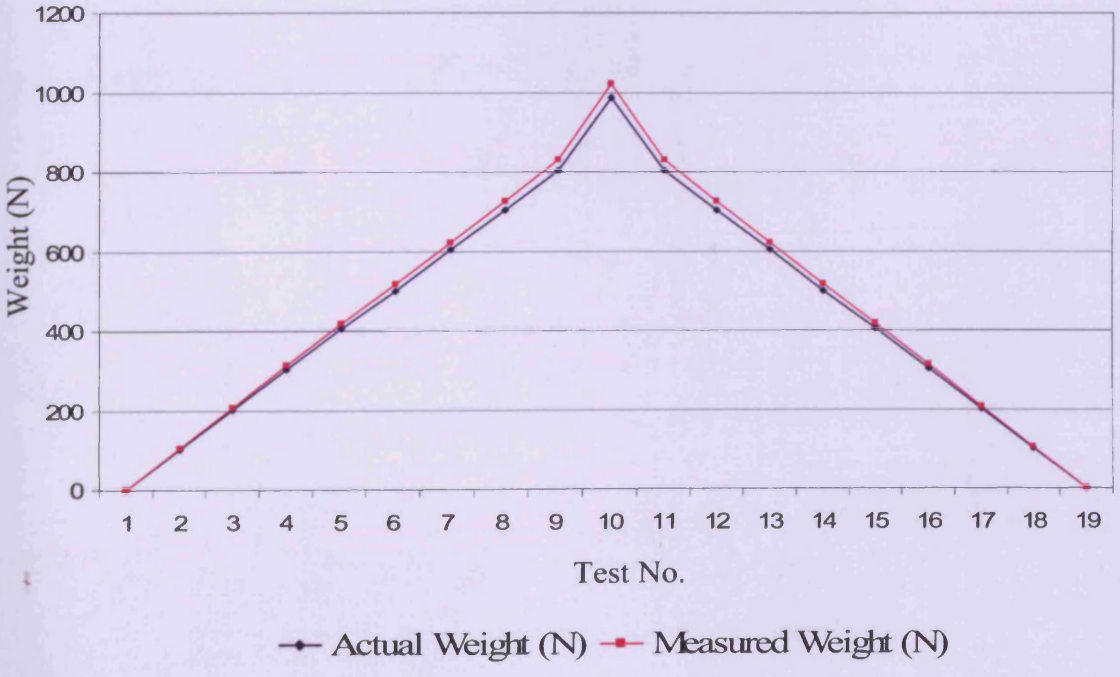

Figure 4.26 Loading and unloading of transducer 1 on FP2.

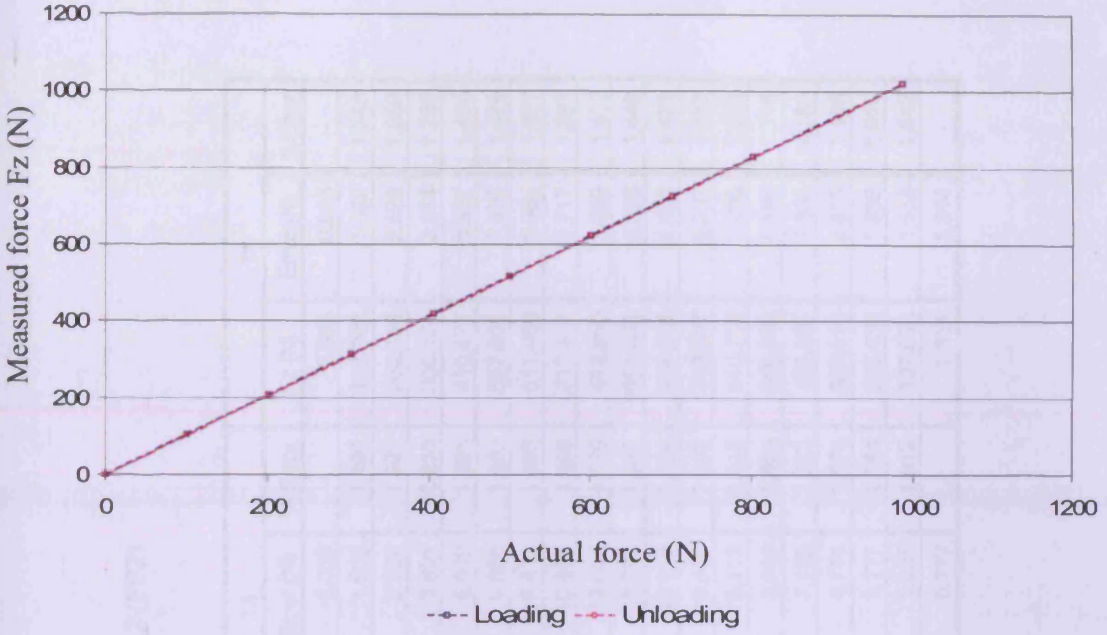

Figure 4.27 Linearity of transducer 1 on FP2

Table 4.9 Testing of Force transducers on force plate 2 (FP2)

Test No.	Weight (N)	T1			T2			T3			T4		
		Fz (N)	Error (N)	% Error	Fz (N)	Error (N)	% Error	Fz (N)	Error (N)	% Error	Fz (N)	Error (N)	%Error
1	0	-0.003	-0.003	-	-0.003	-0.003	-	-0.009	-0.009	-	0.003	0.003	-
2	101	103.538	2.538	2.513	103.992	2.992	2.963	102.505	1.505	1.490	102.362	1.362	1.348
3	200.6	206.920	6.320	3.151	206.145	5.545	2.764	203.392	2.792	1.392	203.126	2.526	1.259
4	302.3	312.021	9.721	3.216	310.078	7.778	2.573	306.104	3.804	1.258	306.174	3.874	1.282
5	404.7	417.807	13.107	3.239	415.784	11.084	2.739	410.349	5.649	1.396	410.627	5.927	1.464
6	500.4	516.545	16.145	3.226	513.787	13.387	2.675	507.250	6.850	1.369	507.800	7.400	1.479
7	602.5	622.044	19.544	3.244	619.243	16.743	2.779	611.312	8.812	1.463	611.460	8.960	1.487
8	703.7	726.449	22.749	3.233	723.731	20.031	2.846	714.225	10.525	1.496	713.417	9.717	1.381
9	802.6	829.661	27.061	3.372	826.696	24.096	3.002	815.204	12.604	1.570	813.850	11.250	1.402
10	987.3	1020.658	33.358	3.379	1018.775	31.475	3.188	1003.565	16.265	1.647	1001.603	14.303	1.449
11	802.6	828.893	26.293	3.276	827.634	25.034	3.119	815.715	13.115	1.634	814.008	11.408	1.421
12	703.7	726.324	22.624	3.215	725.064	21.364	3.036	714.550	10.850	1.542	713.207	9.507	1.351
13	602.5	621.818	19.318	3.206	620.675	18.175	3.017	611.613	9.113	1.512	610.755	8.255	1.370
14	500.4	516.229	15.829	3.163	514.980	14.580	2.914	508.446	8.046	1.608	506.986	6.586	1.316
15	404.7	417.881	13.181	3.257	416.732	12.032	2.973	411.822	7.122	1.760	409.506	4.806	1.188
16	302.3	312.001	9.701	3.209	311.230	8.930	2.954	307.071	4.771	1.578	305.915	3.615	1.196
17	200.6	207.067	6.467	3.224	206.406	5.806	2.895	203.777	3.177	1.584	202.438	1.838	0.916
18	101	104.333	3.333	3.300	104.238	3.238	3.206	102.931	1.931	1.912	102.658	1.658	1.642
19	0	0.410	0.410	-	1.022	1.022	-	0.777	0.777	-	1.314	1.314	-

4.3.3.2 Testing vertical force and COP (FP2)

The actual and measured COP results for each test point are presented in Appendix E and represented in Figure 4.28. The error in COP measurement is computed as the difference between the actual and measured COP x and y coordinates. The average errors in the COP measurements recorded for 77 points on the force plate were 2.95 ± 2.36 mm for the x coordinate and 1.51 ± 1.20mm for the y coordinate. From Figure 4.28, it can be seen that the COP measurements are more accurate at the centre of the force plate.

The maximum error in the measured x-coordinates was 10.49mm. This occurred at test point 61 and is indicated in Figure 4.28. The smallest error was 0.12mm and this occurred at point 52. The maximum error in the measured y-coordinate was 5.49mm. This occurred at test point 10. The smallest error was 0.01mm and occurred at position 14. These points are indicated in Figure 4.28.

The actual and measured vertical forces for each test point are presented in Appendix E. The vertical force (F_z) measured by the force plate was consistently larger than the applied force, (Figure 4.29). F_z was over estimated to a greater extent in the negative x region of the force plate. In the measurements along the long axis of the plate, F_z was also overestimated to a greater extent towards the centre of the plate. The percentage error in the F_z measurement was calculated. The greatest error occurred at point 4 where F_z overestimated the known force by 3.45%. The smallest error was 0.05% and this occurred at point 56.

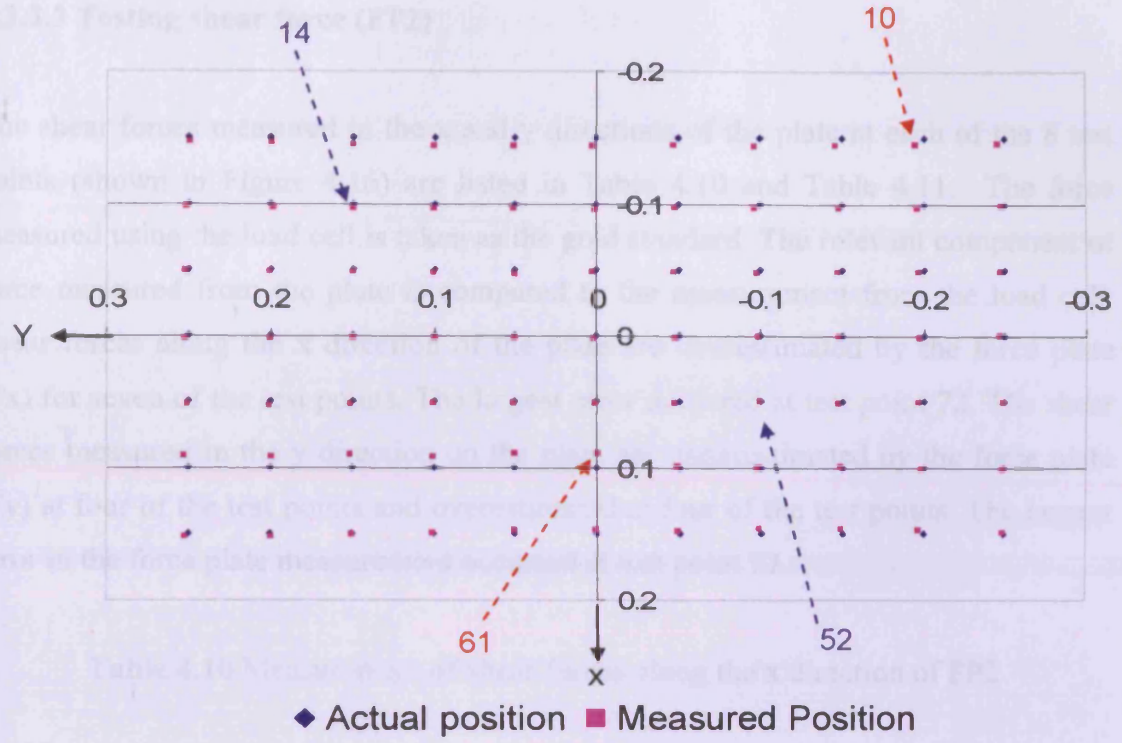

Figure 4.28 COP measurements at each test point on FP1. Position 10 is where the greatest error in the y-coordinate was measured. Position 14 is where the smallest error in y-coordinate was measured. Position 52 is where the smallest error in the x-coordinate was measured. Position 61 is where the greatest error in x-coordinate was measured.

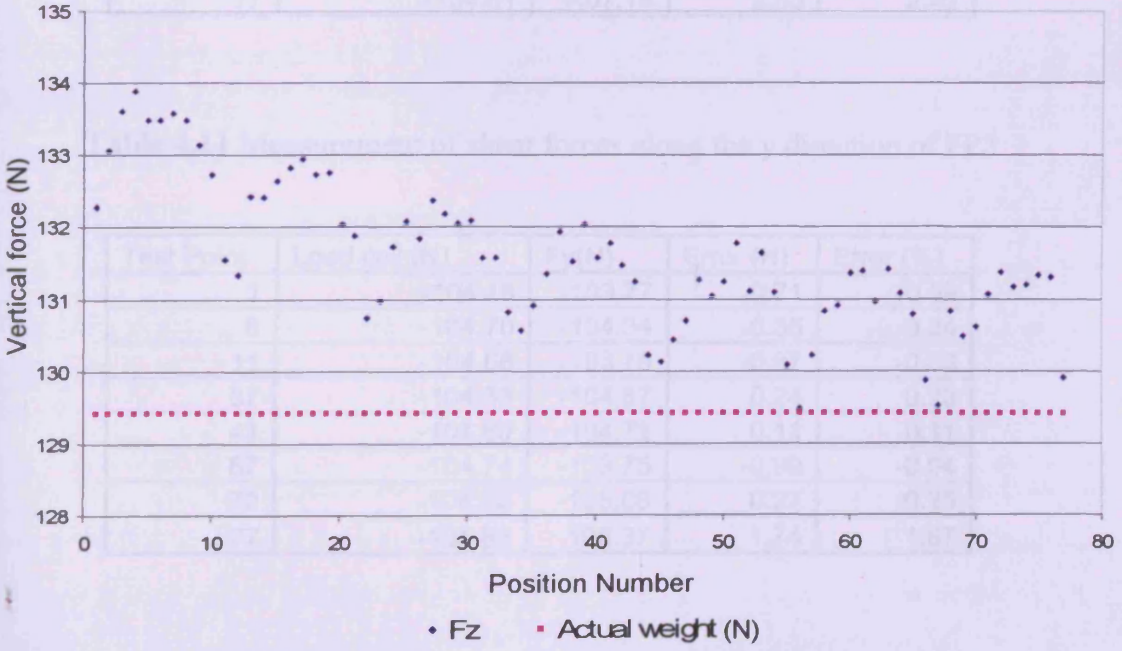

Figure 4.29 Vertical force measurements at each test point on FP2

4.3.3.3 Testing shear force (FP2)

The shear forces measured in the x and y directions of the plate at each of the 8 test points (shown in Figure 4.16) are listed in Table 4.10 and Table 4.11. The force measured using the load cell is taken as the gold standard. The relevant component of force measured from the plate is compared to the measurement from the load cell. Shear forces along the x direction of the plate are overestimated by the force plate (Fx) for seven of the test points. The largest error occurred at test point 72. The shear forces measured in the y direction on the plate are underestimated by the force plate (Fy) at four of the test points and overestimated at four of the test points. The largest error in the force plate measurement occurred at test point 77.

Table 4.10 Measurement of shear forces along the x direction of FP2

Test Point	Load cell (N)	Fx (N)	Error (N)	Error (%)
1	-104.56	-105.86	1.30	1.24
6	-104.71	-105.00	0.29	0.27
11	-104.50	-106.09	1.59	1.52
37	-104.60	-104.81	0.21	0.20
41	-104.56	-105.26	0.70	0.67
67	-104.69	-103.22	-1.48	-1.41
72	-104.48	-107.06	2.58	2.47
77	-104.61	-107.14	2.53	2.42

Table 4.11 Measurement of shear forces along the y direction of FP2

Test Point	Load cell (N)	Fy(N)	Error (N)	Error (%)
1	-104.48	-103.77	-0.71	-0.68
6	-104.70	-104.34	-0.36	-0.34
11	-104.66	-103.78	-0.87	-0.83
37	-104.33	-104.57	0.24	0.23
41	-104.60	-104.71	0.11	0.11
67	-104.74	-103.75	-0.99	-0.94
72	-104.82	-105.08	0.27	0.25
77	-104.63	-106.37	1.74	1.67

4.3.3.4 Measures from Step 1 interfaced with FP2

The step is positioned with the front edge in line with the front edge of the force plate as shown in Figure 4.30a. The numbering protocol for COP and vertical force tests are shown in figure 4.30b. In the tests carried out on the steps interfacing with FP1, the test points 49 to 54 were located towards the midpoint of the step. For the testing carried out on the steps interfacing with FP2, test points 49 to 54 are located at the outer edge of the step. This is because the steps were tested in the configuration used for the clinical trial.

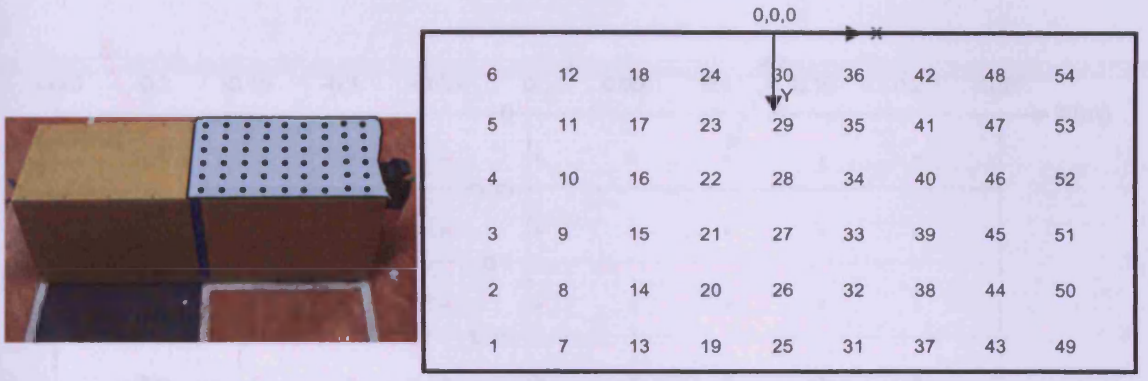

Figure 4.30 (a) Positioning of a step on FP2 (b) numbering protocol for the test points

The actual and measured COP results for each test point are presented in Appendix E and represented in Figure 4.31. The error in COP measurement is computed as the difference between the actual and measured COP x and y coordinates. The average errors in the COP measurements recorded for 54 points on step 1 were 2.30 ± 1.48 mm for the x coordinate and 1.09 ± 0.88mm for the y coordinate. From Figure 4.31, it can be seen that the COP measurements are more accurate towards the right hand side of the testing grid.

The maximum error in the measured x-coordinates was 6.06mm. This occurred at test point 6 and is indicated in Figure 4.31. The smallest error was 0.04mm and this occurred at test point 42. The maximum error in the measured y-coordinate was 3.98mm. This occurred at test point 37. The smallest error was 0.03mm and occurred at position 3. These points are indicated in Figure 4.31.

The actual and measured vertical forces for each test point are presented in Appendix E. The Vertical force (F_z) measured by the force plate was larger than the applied force in all but four test points as shown in Figure 4.32. F_z was over estimated to a greater extent in the negative x region of the force plate. In the measurements along the long axis of the plate, F_z was also overestimated to a greater extent towards the centre of the plate. The percentage error in the F_z measurement was calculated. The greatest error occurred at point 6 where F_z overestimated the known force by 3.57%. The smallest error was 0.01% and this occurred at point 31.

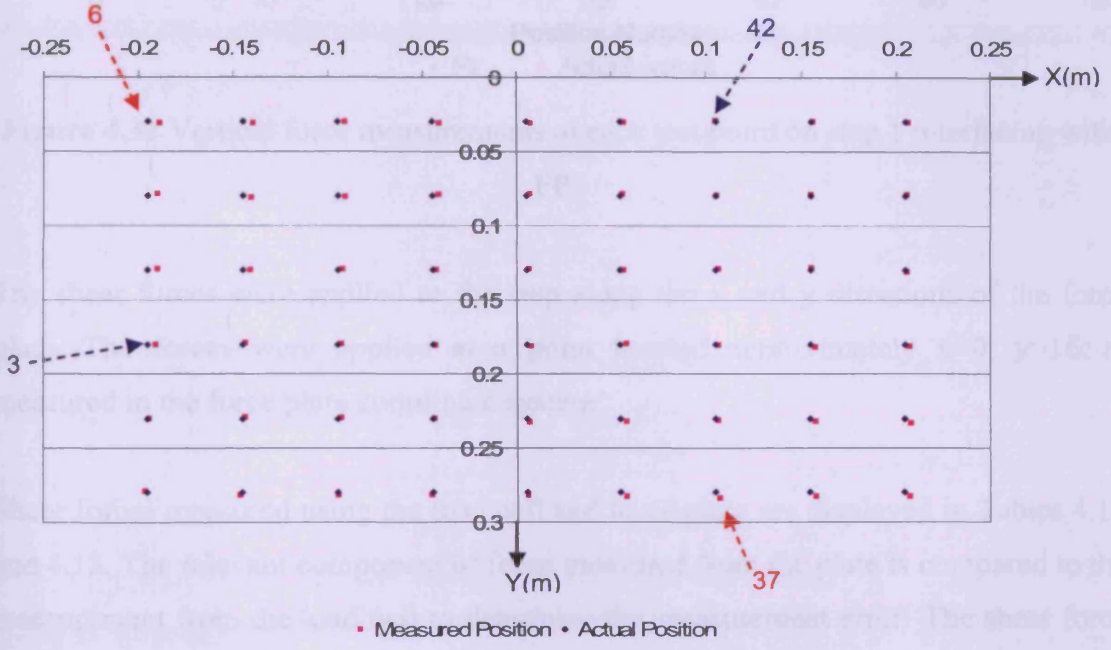

Figure 4.31 COP measurements at each test point on step 1 interfacing with FP2. Position 3 is where the smallest error in the y-coordinate was measured. Position 6 is also where the greatest error in x-coordinate was measured. Position 37 is where the greatest error in the y-coordinate was measured. Position 42 is where the smallest error in x-coordinate was measured.

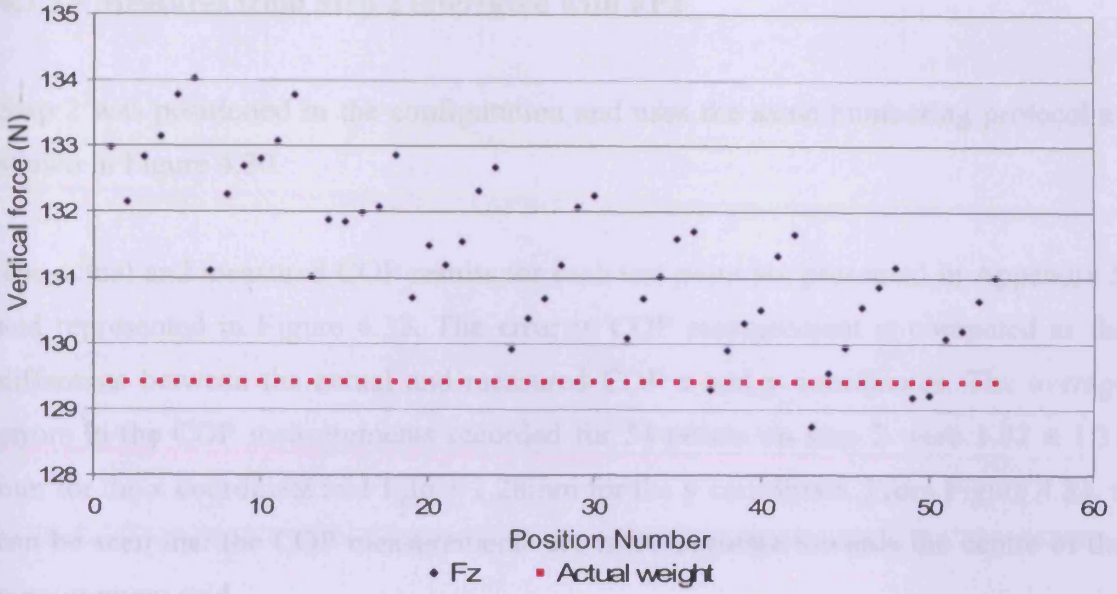

Figure 4.32 Vertical force measurements at each test point on step 1 interfacing with FP2

The shear forces were applied to the step along the x and y directions of the force plate. The forces were applied at a point located approximately x=0, y=16cm, measured in the force plate coordinate system.

Shear forces measured using the load cell and force plate are displayed in Tables 4.12 and 4.13. The relevant component of force measured from the plate is compared to the measurement from the load cell to determine the measurement error. The shear force applied to the step in the x direction of the force plate was overestimated by the force plate. The shear force measured in the y direction of the force plate was underestimated by the force plate.

Table 4.12 Measurement of shear force along the x direction of FP2 for step 1

Load Cell (N)	Fx (N)	Error (N)	Error (%)
-103.56	-104.55	0.99	0.96

Table 4.13 Measurement of shear force along the y direction of FP2 for step 1

Load Cell (N)	Fy (N)	Error (N)	Error (%)
-104.45	-103.76	-0.69	-0.66

4.3.3.5 Measures from Step 2 interfaced with FP2

Step 2 was positioned in the configuration and uses the same numbering protocol as shown in Figure 4.30.

The actual and measured COP results for each test point are presented in Appendix E and represented in Figure 4.33. The error in COP measurement is computed as the difference between the actual and measured COP x and y coordinates. The average errors in the COP measurements recorded for 54 points on step 2 were 1.82 ± 1.31 mm for the x coordinate and 1.36 ± 1.28mm for the y coordinate. From Figure 4.33, it can be seen that the COP measurements are more accurate towards the centre of the measurement grid.

The maximum error in the measured x-coordinates was 5.39mm. This occurred at test point 43 and is indicated in Figure 4.33. The smallest error was 0.03mm and this occurred at point 2. The maximum error in the measured y-coordinate was 5.60mm. This occurred at test point 19. The smallest error was 0.14mm and occurred at position 34. These points are indicated in Figure 4.33.

The actual and measured vertical forces for each test point are presented in Appendix E. The Vertical force (F_z) measured by the force plate was larger than the applied force in all but three test points, (Figure 4.34). F_z was overestimated to a greater extent in the negative x region of the force plate. In the measurements along the long axis of the plate, F_z was also overestimated to a greater extent towards the centre of the plate. The percentage error in the F_z measurement was calculated. The greatest error occurred at point 6 where F_z overestimated the known force by 3.60%. The smallest error was 0.14% and this occurred at point 51.

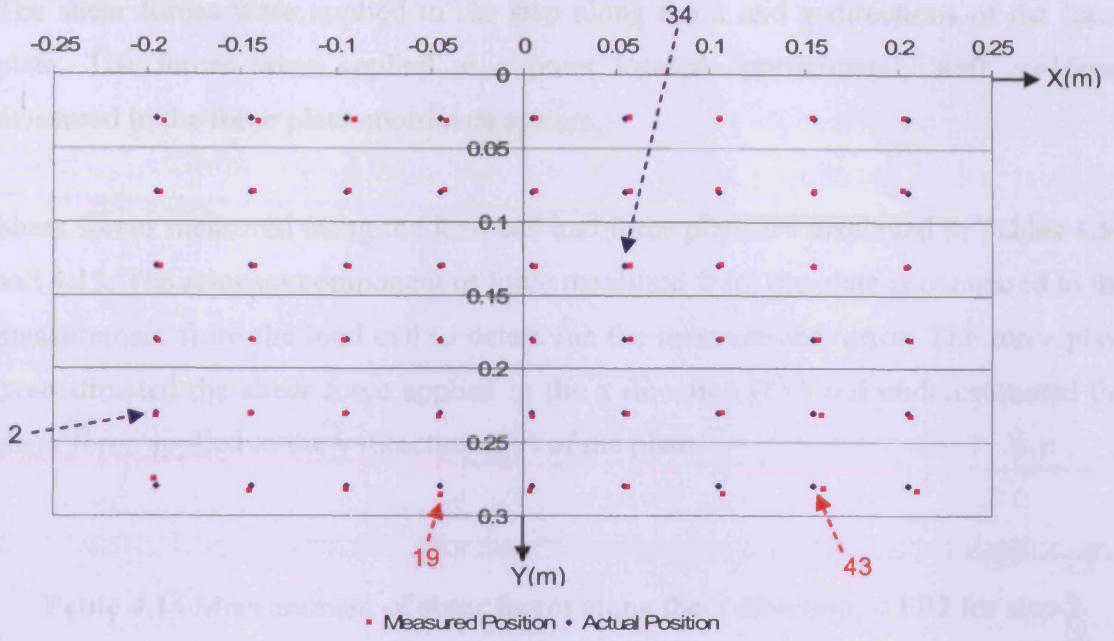

Figure 4.33 COP measurements at each test point on step 2 interfacing with FP2. Position 2 is where the smallest error in the x-coordinate was measured. Position 19 is where the greatest error in y-coordinate was measured. Position 34 is where the smallest error in the y-coordinate was measured. Position 43 is where the greatest error in the x-coordinate was measured.

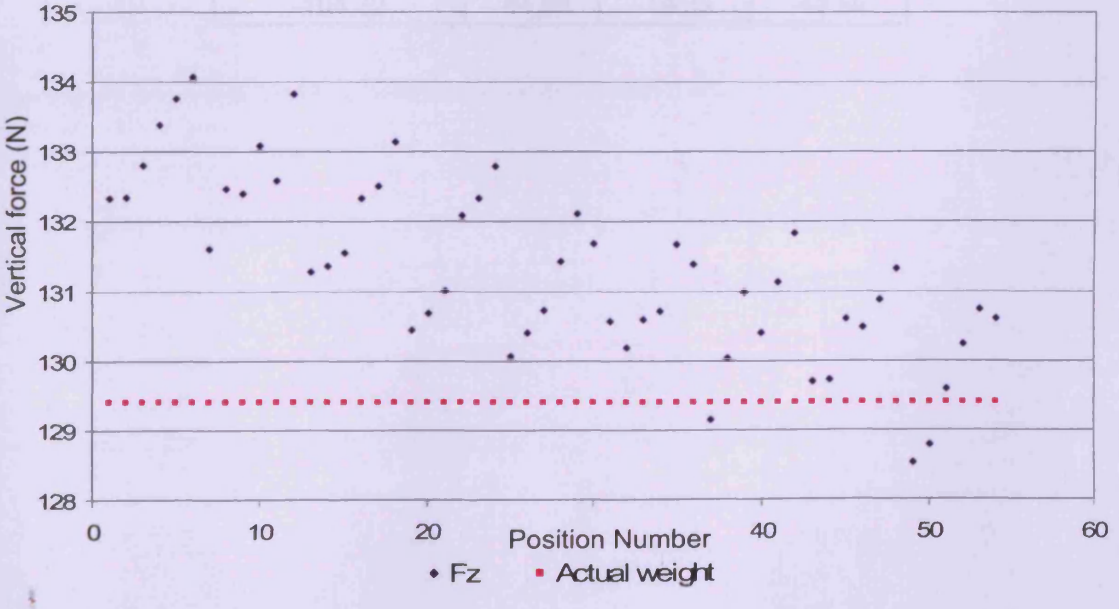

Figure 4.34 Vertical force measurements at each test point on step 2 interfacing with FP2

The shear forces were applied to the step along the x and y directions of the force plate. The forces were applied at a point located approximately x=0, y=16cm, measured in the force plate coordinate system.

Shear forces measured using the load cell and force plate are displayed in Tables 4.14 and 4.15. The relevant component of force measured from the plate is compared to the measurement from the load cell to determine the measurement error. The force plate overestimated the shear force applied in the x direction (Fx) and underestimated the shear force applied in the y direction (Fy) of the plate.

Table 4.14 Measurement of shear forces along the x direction of FP2 for step 2

Applied force (N)	Fx (N)	Error (N)	Error (%)
-104.64	-108.75	4.11	3.92

Table 4.15 Measurement of shear forces along the y direction of FP2 for step 2

Applied force (N)	Fy (N)	Error (N)	Error (%)
-104.32	-84.93	-19.39	-18.59

4.3.4 Discussion

Tests were carried out to quantify the errors associated with the measurement of 3D forces and COP from each force plate. Tests were also completed to determine the accuracy of COP and force measurements when step 1 and step 2 from the staircase interface with each force plate. For reference a summary of selected results from the accuracy tests are presented in Table 4.16.

Table 4.16 Summary of the accuracy for COP and force measurements from each force plate and step configuration

Error	FP1			FP2		
	FP	Step1	Step2	FP	Step1	Step2
Mean COPx (mm)	3.94	3.36	3.76	2.95	2.30	1.82
Max COPx (mm)	11.17	11.84	13.06	10.49	6.06	5.39
Mean COPy (mm)	3.37	3.38	2.51	1.51	1.09	1.36
Max COPy (mm)	10.29	9.37	6.68	5.49	3.98	5.60
Max Fz (% applied force)	4.64	4.06	3.69	3.45	3.57	3.60
Max Fx (% applied force)	4.98	6.36	6.90	2.47	0.96	3.92
Max Fy (% applied force)	3.25	0.96	1.59	1.67	0.66	18.59

The tests carried out on FP1 revealed that each transducer loaded and unloaded in a linear nature. However, the accuracy in the magnitude of the measured force varied between the four transducers. T2 measured Fz with the biggest error of approximately 4% of the actual load.

The plate is more accurate at measuring COP towards its origin. The errors in COP increase towards the outside of the plates. At the edges, the plate acts as a cantilever beam, which may explain this change.

Forces are overestimated on the side of the plate closest to T1 and T2. They are also overestimated towards the centre of the plate. The greatest error in measuring Fz

occurred at point 10 which is closest to T2, which has proved to be inaccurate in measuring Fz. The smallest Fz error was measured at point 66. This is located near T4 which proved to be accurate in measuring Fz in the linearity tests.

Shear forces are overestimated in the x direction up to 4.98% of the applied force and underestimated in the y direction up to 3.25% of the applied force. This may be due to the component of force acting in the other direction. (i.e. not isolating the force along one axis of the plate), also due to stretching that may be occurring in the cable used to transfer the force. The tests from step 1 and step 2 showed that the step did not adversely affect the accuracy of the measurements from the force plate.

The tests carried out on FP2 revealed that T1 and T2 were less accurate than T3 an T4 in measuring Fz. As with FP1 the measurements of COP at the centre of the plate were more accurate than the outer edges of the plate. Fz was overestimated at all test points, more so at the centre of the plate. The errors obtained from FP2 were less than those from FP1 from each test. The tests from step 1 and step 2 showed that the step did not adversely affect the accuracy of the measurements from the force plate. The average errors measured from step 1 and step 2 were less than the error determined from FP2. The maximum Fy error from step 2 was 18.59% of the applied load. This may be due to the force not being applied purely along the y axis of the plate, or from stretching of the wire used to transmit the force.

The accuracy tests have shown that the maximum errors in force plate measurements are greater than the factory calibration settings of 0.5% error for forces and ± 2mm for COP. The mean COP errors for FP2 are within the allowable factory calibration error range. The mean COP errors for FP1 are marginally outside the allowable error range. However, the accuracy of measuring forces is outside the allowable factory calibration error range for both force plates and the transducers in the plates are not functioning to the same accuracy as each other. The source of the errors may be due to the force plates moving location when the laboratory was re housed. During reassembly of the force plates, the surface that the plates are mounted on may not be flat causing deformation of the force plate base, the plates may not be level or the bolts may be over tightened.

It is recommended that the plates are calibrated to factory settings on a routine basis to ensure the signals from the force plates comply with the manufacturers' recommendations.

Limitations to these experiments are that they are static and the force plates are used to measure dynamic movements. It would therefore be useful to test the accuracy of dynamic forces measured from the force plates and stairs. The testing equipment was manufactured to apply forces in specific locations on the force plate and stair. However there may be errors introduced in using the equipment, particularly when testing the shear forces where they are applied along the axis of the force plate. Any flexibility in the wire used to transmit the forces to the plate may also introduce an error. It would be prudent to perform controlled tests on the equipment to check they are functioning as expected.

Also, the errors may be due to the use of low magnitude forces for the accuracy tests, as the forces obtained from patients during level and stair gait were within the expected range.

The stairs do not appear to adversely affect the measurements from either of the force plates and thus will be used in subsequent studies to collect kinetic data from stair ascent and descent.

4.4 A COMPARISON OF METHODOLOGIES FOR ASSESSING STAIR ASCENT AND DESCENT

This study uses motion analysis and a new staircase design to measure non-pathological knee function during stair ascent/descent and compares common data collection and analysis methods.

Motion capture synchronised with ground reaction force (GRF) measurement can quantify the kinematics and kinetics involved in daily activities. However, it is only useful as a clinical tool if accurate and practical assessments can be made using valid calculations and if similar outputs can be compared across a range of studies. During data collection using motion analysis, static calibrations are routinely performed prior to the measurement of dynamic movements to determine three landmarks per segment. These define segmental anatomical axes for the femur and tibia and their relationship with the thigh and shank external technical axes respectively. All subsequent articulations at the knee are measured using the technical axes.

This study compares two methods of anatomical calibration: (i) the traditional method of placing markers on bony landmarks using a standard marker set; (ii) palpating bony landmarks and using a marked pointer to more accurately identify and record the bony prominences. Pointer calibration data is processed using in- house software [Matlab (Version 7.1, The Mathworks, Inc)]. Marker based calibration data is processed using commercial software, Visual3D (C-motion, Inc.), with a linked model. Tibiofemoral kinematics resulting from the two approaches are compared.

Knee joint moments are an important measure for stair gait and give an indication of how the muscles are functioning to control and stabilise the knee joint during the activity. The current Cardiff protocol does not consider moments and if these are to be included in the analysis of stair gait, current methods of computing moments must be explored.

Joint moments can be computed using different mathematical methods and expressed as internal or external. This leads to confusion when attempting to validate a new set of measurements and prevents comparisons between studies. This study compares

joint moments calculated using a vector cross product approach and two inverse dynamics methods; one that ignores the foot and ankle effects and another that involves full inverse dynamics.

Two Stair Gait Cycles (SGCs) are defined for stair ascent/descent allowing for different inertial effects when raising and lowering the body's centre of mass (COM) to a greater or lesser extent. This could determine whether choice of SGC and step measuring GRFs are important factors for consideration.

Thus the studies objectives were to (i) compare two methods of computing knee joint kinematics; (ii) compare three approaches to computing moments acting about the knee joint; (iii) investigate the choice of SGC and discern which step should be used to measure the GRFs.

4.4.1 Equipment Calibration

3D Motion capture was performed using 8 Qualisys ProReflex MCU 120Hz digital cameras, capturing at 60 Hz (Qualisys, Sweden). Force data was captured at 1080Hz using 2 Bertec force plates (Bertec Corporation). Prior to the subjects assessment the laboratory was calibrated to define a global coordinate system (GCS) and the position of the force plates were defined relative to the GCS using a calibration panel positioned on top of each force plate, (Figure 4.35).

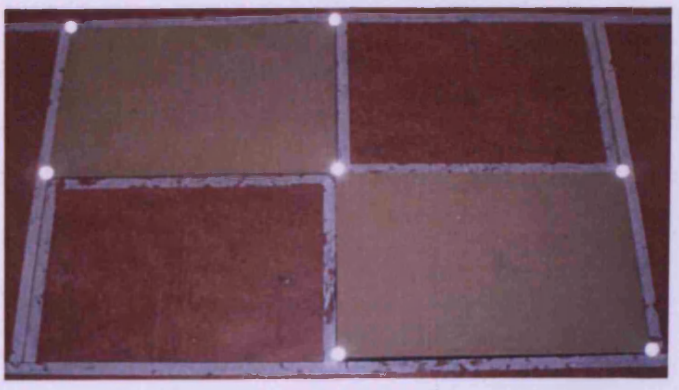

Figure 4.35 Calibration panels positioned on top of each force plate

The calibration panels were machined from MDF to match the dimensions of the force plates (0.6m x 0.4m). A passive marker was fixed to each corner of the panel so that the centre of the marker was in line with corner of the underlying force plate, (Figure 4.36).

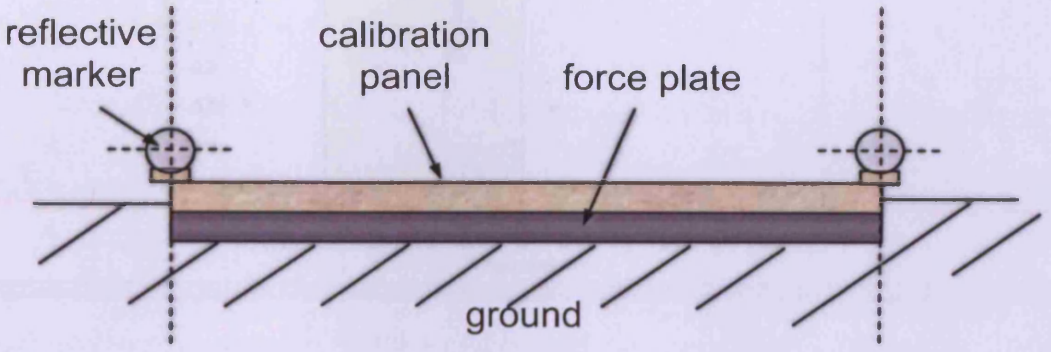

Figure 4.36 Schematic of calibration panel and force plate illustrating the alignment of the markers and the corners of the force plate

The coordinate positions of the markers on the calibration panels were recorded during a one second measurement. Customised software was written in Matlab (Version 7.1, The Mathworks, Inc.) to define the local coordinate system (LCS) for each force plate using the coordinate positions of each markers on the calibration panel. The origin of the local coordinate system was defined to coincide with the origin of the force plate. This is stated in the Bertec User's Manual (Bertec Corporation) as the top surface of the force platform and at the centre of the top plate. A transformation matrix was computed which defined the location and pose of each force plate LCS within the CGS using the method of Söderkvist and Wedin (1993). All subsequent COP coordinates were multiplied by this transformation matrix to obtain the COP coordinates expressed in the laboratory GCS, (Figure 4.37).

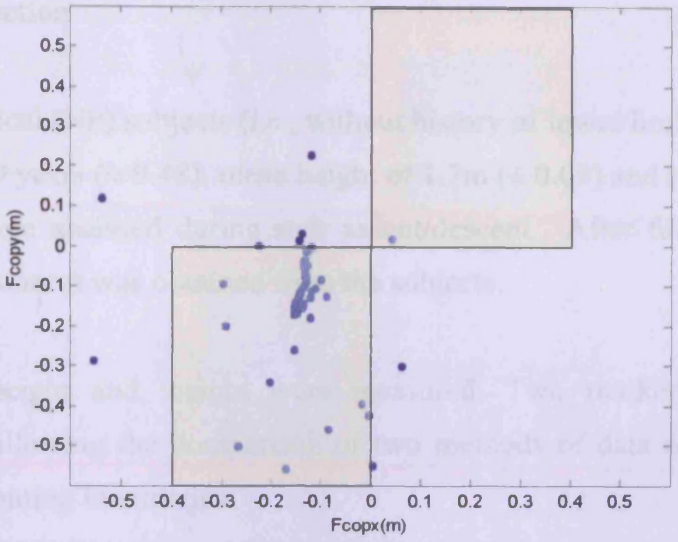

Figure 4.37 Example of COP positions measured relative to the GCS during the stance phase of a stair gait cycle. The location of the force plates are superimposed on the Figure

It is necessary to define the force plates within the GCS so that the coordinates for the point of application of the GRF, known as the centre of pressure (COP) can be expressed relative to the GCS. This was previously not an issue with the Cardiff protocol as joint moments were not considered.

Accurate information on the COP is required to calculate joint moments. The x and y coordinate positions are initially calculated within the force plate coordinate system using the following equations, where y is positive along the long axis of the plate towards the connector end and x is positive to the right when looking in the y-axis.

$$x = (-h.Fx - My)/Fz \tag{4.1}$$

$$y = (-h.Fy - Mx)/Fz \tag{4.2}$$

h is the distance between the force plate top surface and top surface of any covering material. Fx, Fy and Fz are the GRF components calculated by multiplying the force plate signal with the corresponding calibration matrix. Mx and My are moment components calculated by multiplying the signals with the corresponding force plate calibration matrix.

4.4.2 Data Collection

10 non-pathological (NP) subjects (i.e., without history of lower limb disorder), with a mean age of 44.9 years (± 9.48), mean height of 1.7m (± 0.09) and mean weight of 76 Kg (± 18.02) were assessed during stair ascent/descent. After fully explaining the tests, informed consent was obtained from the subjects.

The subjects' height and weight were measured. Two marker sets were used simultaneously allowing the comparison of two methods of data collection and two methods of computing kinematics.

Method 1 uses the approach of Holt *et al.*, (2000), as detailed in Chapter 2. Figure 4.38 shows plate-mounted passive retro reflective markers (a non-slip backing reduces slippage of the marker clusters over the skin) attached laterally to the thigh and shank. An anatomical calibration was performed with the subject in quiet standing for one second each using an aluminium pointer containing four retro-reflective markers to identify three bony landmarks per segment. A one second static measurement with the subject in quiet standing was recorded prior to dynamic trials.

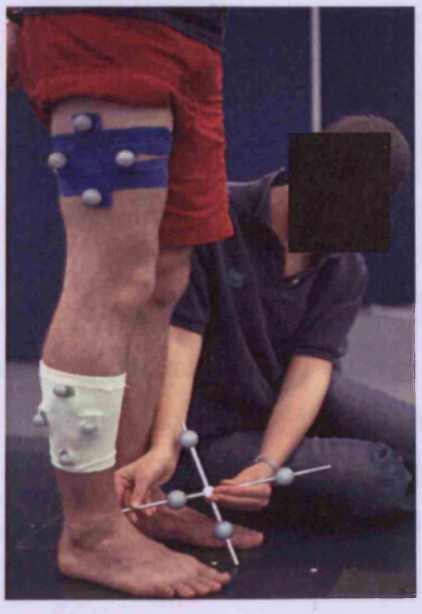

Figure 4.38 The identification of a bony landmark (medial malleolus) using the pointer. Other bony landmarks identified during the calibration include the medial and lateral epicondylar gaps and the upper border of the greater trochanter.

Method 2 uses commercial software, Visual3D (C-motion, Inc.). The landmarks from Method 1 were identified using passive markers attached to the skin. Additional markers were positioned in a modified Helen Hayes configuration, (Figure 4.39). A quiet standing measurement was recorded with the subjects feet shoulder width apart, for one second.

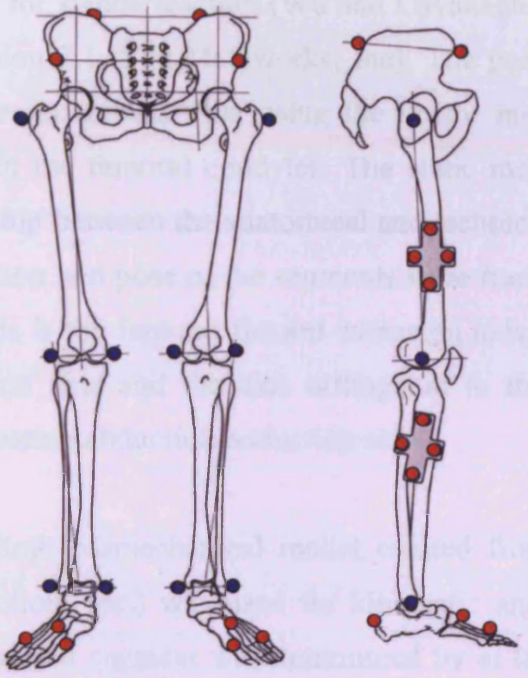

Figure 4.39 Marker set showing the modified Helen Hayes configuration as in Whatling *et al.*, (2008f). A detailed description of the marker positions is provided in Appendix F

The stairs were constructed with step 1 and 2 individually in contact with a force plate. The subjects performed stair ascent/descent without the use of a handrail. The following Stair Gait Cycles (SGCs) were recorded for ascent and descent:

(SGC1) Ascent - right foot strike on step 1 through to right foot strike on step 3;
(SGC2) Ascent - right foot strike on step 2 to right foot strike on step 4;
(SGC3) Descent - right foot off step 3 to right foot off step 1;
(SGC4) Descent - right foot off step 4 to right foot off step 2.

Three trials of each SGC were recorded for each subject.

4.4.3 Data Analysis

4.4.3.1 Knee kinematics

Method 1: The method of Holt *et al.*, (2000) was used to determine joint axes and rotations according to the Joint Coordinate System (JCS) (Grood and Suntay,1983) (suggested by the ISB for standardisation (Wu and Cavanagh, 1995)) using in house software Matlab (Version 7.1, The Mathworks, Inc). The pointer calibration defines orthogonal axes in the femur and tibia using the vector method, positioning their origin midway between the femoral condyles. The static measurement was used to determine the relationship between the anatomical and technical axes. Assuming rigid body analysis the position and pose of the segments were tracked using rigid clusters of markers. The X-axis is the femoral flexion-extension axis, the Z axis is the tibial internal-external rotation axis and the axis orthogonal to the previous two at any instant in time is the floating abduction-adduction axis.

Method 2: A lower limb biomechanical model created from static measurements using Visual3D (C-Motion, Inc.) was used for kinematic and kinetic analysis. The pose of each rigidly defined segment was determined by at least three non-collinear points using the vector method. The shank was defined using the position of the epicondyles and malleoli, the thigh was defined using hip joint centre regression (Bell *et al.*, 1989), and the epicondyles. The femoral axis system differs to that defined in Method 1 since the plane of the femur corresponds to the hip joint centre rather than the upper trochanter. Joint rotations were described by a Cardan-Euler sequence where the Z is the positive upwards vertical axis and Y is positive acting anteriorly.

For both methods all rotation angles were defined by the orientation of the distal with respect to the proximal segment. An average of three trials for each SGC was computed for each subject. An unpaired independent *t*-test (SPSS 12.0.2) was performed to compare the kinematic measures from Methods 1 and 2. A summary of the two kinematic calculations is provided in Table 4.17.

Table 4.17 Summary of the approaches used to compute knee kinematics

Kinematic Calculation	Identification of anatomical landmarks	Computation method
Method 1	Pointer calibration	Method of Holt *et al.*, (2000) where joint rotations are defined according to JCS, (Grood and Suntay, 1983)
Method 2	Passive markers attached to the skin	Biomechanical model and commercial software, Visual3D, (C-motion, Inc). Joint rotations are described by a Cardan-Euler sequence

4.4.3.2 Knee Kinetics

Moments are described for the right leg relative to the laboratory GCS. The axes of the GCS are aligned such that the contributions of the moment acting along the x-axis corresponds to the frontal plane moment, y-axis corresponds to the sagittal plane moment and z-axis corresponds to the transverse plane moment. They are expressed as the contribution of the forces to rotate the shank about the knee joint centre, or 'external moments' and normalised to body mass. The outputs from three moment calculations are compared:-

Moment Calculation 1 (MC1): This method has been used in a study of stair climbing (Andriacchi *et al.*, 1980). The moment of force is computed as the vector cross product of a radius vector (position vector of the knee joint centre (KJC) relative to the Centre of Pressure (COP)) and GRF vector using Matlab (Version 7.1, The Mathworks, Inc). The vectors used to compute the moment are illustrated in Figure 4.40.

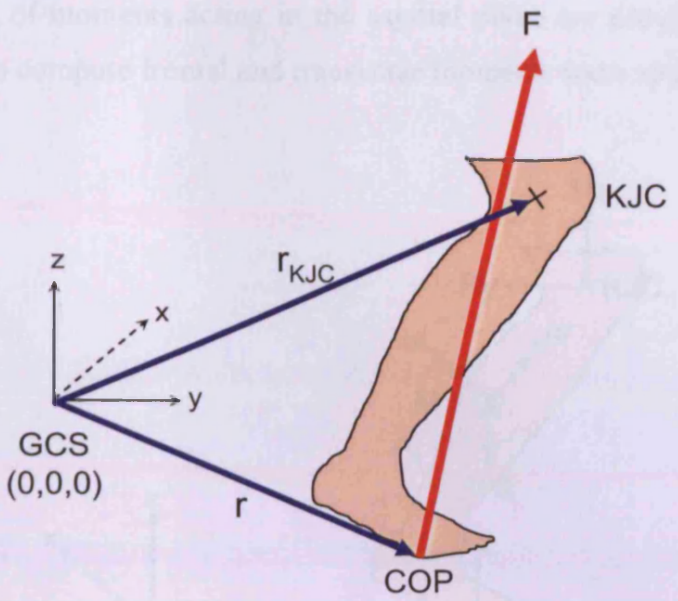

Figure 4.40 Illustration of vectors used to compute moment using the vector cross product method

$$M_{KJC} = (r - r_{KJC}) \times F \quad (4.3)$$

$$\text{Radius vector} = (r - r_{KJC}) \quad (4.4)$$

F is the GRF vector, r is the position vector (relative to the origin of the GCS) of the point where the force is acting and r_{KJC} is the position vector of the KJC (relative to the origin of the GCS). The direction of the resultant moment is perpendicular to the position vector and F. The direction the moment about each axis of rotation follows the right-hand rule. (i.e. Point thumb in the direction of an axis of the GCS and your fingers curl in the direction of positive moment).

The knee joint centre is computed from the position data collected using Method 1. Inertial effects were ignored as they are assumed to be small in low-velocity activities (Davis *et al.*,1994).

Moment Calculation 2 (MC2): An inverse dynamics approach (IDA) was used to compute knee joint moments. The effect of the foot was ignored as no pointer position data was recorded for the foot segment. An example of the free body diagram

and calculation of moments acting in the sagittal plane are provided below. Similar methods used to compute frontal and transverse moments were applied.

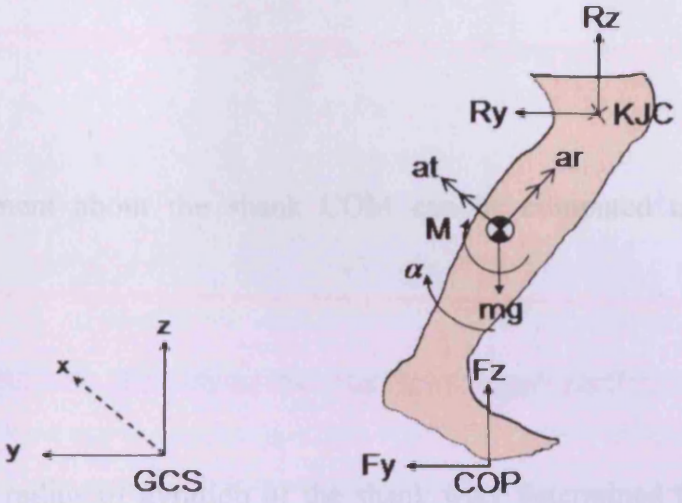

Figure 4.41 Free-body diagram for the right shank, showing reaction and gravitational forces, net moments of force and all linear and angular accelerations

Fz, Fy = GRFs acting at the distal end of the segment

Rz, Ry = reaction forces acting at the KJC

at =is the tangential acceleration of the shank COM

ar = the radial acceleration of the shank COM

α =angular acceleration of the segment in the plane of movement.

M= net muscle moment acting about the shank COM

The accelerations and forces are resolved vertically and horizontally to compute the unknown proximal reaction forces Rz and Ry using the following equations:

$$\sum F_z = ma_z \qquad (4.5)$$

$$R_z = ma_z - F_z + mg \quad (4.6)$$

$$\sum F_y = ma_y \quad (4.7)$$

$$R_y = ma_y - F_y \quad (4.8)$$

The new moment about the shank COM can be computed using the following equation

$$\sum M = I_o \alpha \quad (4.9)$$

The mass and radius of gyration of the shank were determined from Zatsiorsky and Seluyanov, (1983), where:

Shank mass = 0.0433 x subject Mass (4.10)

Centre of mass position from the distal end of the shank (COM) = 0.4047 x shank length (4.11)

Mass radius of gyration of the shank about the COM (K) was determined for the three planes of movement using the following equations

Ks (sagittal plane) = 0.114 x shank length (4.12)

Kf (frontal plane) = 0.281 x shank length (4.13)

Kt (transverse plane) = 0.275 x shank length (4.14)

The moment of inertia (I_o) for the shank for the three planes of movement was determined from Winter, (1990).

I_o (sagittal plane) = Shank mass x Ks^2 (4.15)

I_o (frontal plane) = Shank mass x Kf^2 (4.16)

I_o (transverse plane) = Shank mass x Kt^2 (4.17)

Segment accelerations were calculated using the kinematic data from Method 1.

Moment Calculation 3 (MC3): Visual3D (C-Motion, Inc.) was used to create a biomechanical model of the lower limbs for each subject. This was subsequently used to compute moments using a full IDA. The reader is referred to the C-Motion website, (C-motion, Inc, 2001) for further information on the creation of the biomechanical model and IDA calculations used. This defines internal joint moments as the net internal moments generated by muscles crossing a joint. Mathematically, external moments created by the GRFs are equal and opposite the internal moment. For consistency, the moments computed from this method were negated, converting them to external joint moments and normalised to body mass.

An average of the kinetic waveforms for 3 GCSs was computed for each subject. Discrete parameters were extracted from the joint moment profiles for statistical analysis. One-way repeated measures of ANOVA were used to determine whether significant differences in the dependent variables occurred between the computational approaches. For significant *F*-ratios, a post hoc pairwise multiple comparisons Tukey test (SPSS 12.0.2) was performed. A summary of the methods used to compute moments acting about the knee are summarised in Table 4.18.

Table 4.18 Summary of the methods used to compute moments acting about the knee joint

Moment calculation	Description
MC1	Vector cross product (Andriacchi *et al.*, 1980)
MC2	IDA approach, ignoring the effect of the foot segment
MC3	Full IDA approach using Visual3D (C-motion, Inc)

4.4.3.3 Stair Gait Cycles

Paired-samples *t*-tests (SPSS 12.0.2) were applied to the kinematic measures computed from Methods 1 and 2, and to the kinetic measures computed from MC1, MC2 and MC3, to compare SGC1 and SGC2 for stair ascent initiated by the stance phase and SGC3 and SGC4 for stair descent ending in the stance phase.

4.4.4 RESULTS

4.4.4.1 Kinematics

The ROM of the kinematic waveforms computed from Method1 and Method 2 for each gait sequence is displayed in Table 4.19. Significant results were determined between the two computational methods for frontal ROM for SGC2, SGC3 and SGC4. Examples of the joint kinematic waveforms and the discrete peak values used for comparison in Table 4.19 are displayed in Figure 4.42.

Table 4.19 Kinematic measures used to compare Method 1 and Method 2

	Variables (°)	Method 1 (n=10)	Method 2 (n=10)
Ascent step 1 to step 3 (SGC1)	Sagittal ROM	$^{\Delta}$76.82 ± 3.19	77.75 ± 4.30
	Peak flexion angle	$^{\Delta}$85.47 ± 5.89	87.67 ± 5.06
	Frontal ROM	16.41 ± 8.18	10.89 ± 2.92
	Transverse ROM	14.70 ± 4.05	12.73 ± 3.51
Ascent step 2 to step 4 (SGC2)	Sagittal ROM	$^{\Delta}$80.27 ± 6.33	80.79 ± 7.97
	Peak flexion angle	$^{\Delta}$87.73 ± 7.20	89.73 ± 6.59
	Frontal ROM	17.50 ± 8.07	*11.25 ± 2.82
	Transverse ROM	15.78 ± 3.62	13.68 ± 4.21
Descent step 3 to step 1 (SGC3)	Sagittal ROM	81.16 ± 6.63	80.26 ± 5.61
	Peak flexion angle	88.58 ± 8.31	88.09 ± 6.56
	Frontal ROM	19.45 ± 7.84	*8.87 ± 1.96
	Transverse ROM	15.02 ± 5.93	11.97 ± 3.72
Descent step 4 to step 2 (SGC4)	Sagittal ROM	81.40 ± 6.86	80.11 ± 6.52
	Peak flexion angle	89.49 ± 9.13	89.14 ± 7.87
	Frontal ROM	19.57 ± 7.20	*9.89 ± 1.20
	Transverse ROM	15.65 ± 5.37	13.94 ± 6.70

Mean ± Standard deviation; * indicates a statistical significance between the data collection methods ($P < 0.05$)
$^{\Delta}$indicates a statistical significance ($P<0.05$) between SGC1 and SGC2 computed using Method 1

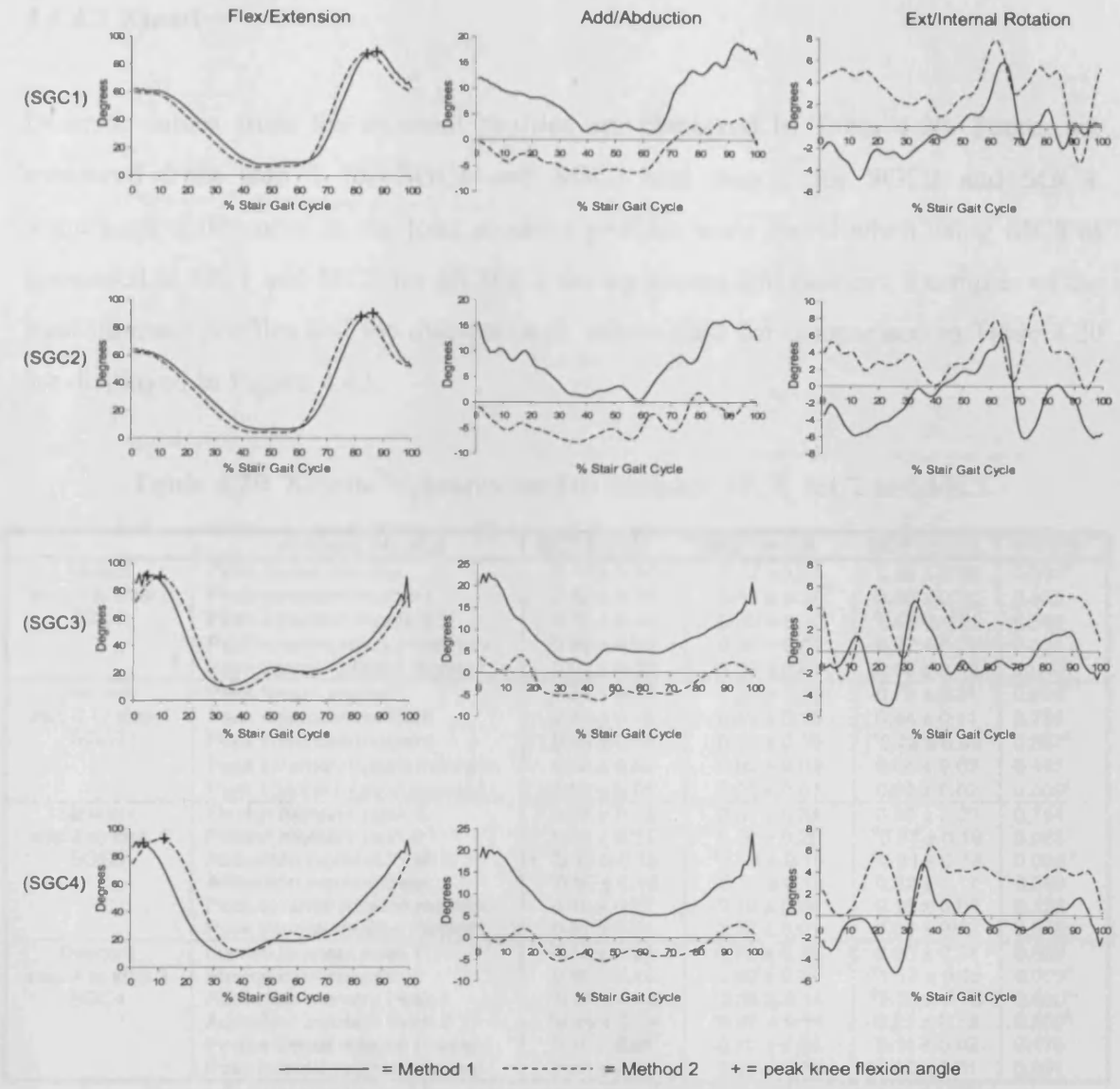

Figure 4.42 Examples of knee kinematic waveforms for (SGC1) stair ascent from step 1 to step 3, (SGC2) stair ascent from step 2 to step 4, (SGC3) stair descent from step 3 to step 1 and (SGC4) stair descent from step 4 to step 2. Each waveform represents a mean of 3 trials from a single subject.

4.4.4.2 Kinetics

Discrete values from the moment profiles are displayed in Table 4.20. Forces are measured from step 1 for SGC1 and SGC3 and step 2 for SGC2 and SGC4. Significant differences in the joint moment profiles were found when using MC3 as compared to MC1 and MC2 for all SGCs during ascent and descent. Examples of the joint moment profiles and the discrete peak values used for comparison in Table 4.20 are displayed in Figure 4.43.

Table 4.20 Kinetic measures used to compare MC1, MC2 and MC3.

	Variables (Nm/Kg)	MC1 (n=10)	MC2 (n=10)	MC3 (n=10)	p-Value
Ascent step 1 to step 3 SGC1	Peak flexion moment	1.19 ± 0.24	1.17 ±0.23	0.86 ± 0.18	0.003[a]
	Peak extension moment	0.42 ± 0.18	0.45 ± 0.19	0.46 ± 0.17	0.859
	Peak adduction moment	0.32 ± 0.10	0.30 ± 0.10	[d]0.30 ± 0.08	0.845
	Peak external rotation moment	0.06 ± 0.02	0.06 ± 0.02	0.07 ± 0.02	0.304
	Peak internal rotation moment	0.02 ± 0.12	0.02 ± 0.01	0.05 ± 0.02	0.000[a]
Ascent step 2 to step 4 SGC2	Peak flexion moment	1.21 ± 0.26	1.20 ± 0.26	0.79 ± 0.21	0.001[a]
	Peak extension moment	0.47 ± 0.15	0.49 ± 0.16	0.44 ± 0.11	0.754
	Peak adduction moment	0.36 ± 0.10	0.34 ± 0.10	[d]0.23 ± 0.09	0.007[a]
	Peak external rotation moment	0.05 ± 0.02	0.05 ± 0.02	0.06 ± 0.02	0.403
	Peak internal rotation moment	0.01 ± 0.01	0.02 ± 0.01	0.05 ± 0.02	0.000[a]
Descent step 3 to step 1 SGC3	Flexion moment peak 1	0.66 ± 0.33	0.67 ± 0.34	0.57 ± 0.29	0.754
	Flexion moment peak 2	0.83 ± 0.21	0.78 ± 0.20	[e]0.97 ± 0.19	0.088
	Adduction moment Peak 1	[b]0.40 ± 0.15	[c]0.38 ± 0.15	[e]0.21 ± 0.18	0.026[a]
	Adduction moment Peak 2	[b]0.39 ± 0.18	[c]0.37 ± 0.18	0.22 ± 0.17	0.060
	Peak external rotation moment	0.10 ± 0.27	0.10 ± 0.03	0.13 ± 0.04	0.123
	Peak internal rotation moment	0.02 ± 0.01	0.02 ± 0.01	0.02 ± 0.02	0.546
Descent step 4 to step 2 SGC4	Flexion moment peak 1	0.74 ± 0.36	0.73 ± 0.36	0.60 ± 0.34	0.633
	Flexion moment peak 2	0.86 ± 0.21	0.82 ± 0.21	[e]1.17 ± 0.25	0.003[a]
	Adduction moment Peak 1	[b]0.57 ± 0.14	[c]0.55 ± 0.14	[e]0.28 ± 0.15	0.000[a]
	Adduction moment Peak 2	[b]0.48 ± 0.14	[c]0.45 ± 0.14	0.21 ± 0.13	0.000[a]
	Peak external rotation moment	0.10 ± 0.01	0.10 ± 0.02	0.11 ± 0.02	0.178
	Peak internal rotation moment	0.02 ± 0.01	0.02 ± 0.01	0.02 ± 0.01	0.391

Mean ± Standard deviation; [a] Significant comparisons (P<0.05) for MC3 vs. MC1 and MC2
[b]indicates a statistical significance (P<0.05) between SGC3 and SGC4 computed using MC1
[c]indicates a statistical significance (P<0.05) between SGC3 and SGC4 computed using MC2
[d]indicates a statistical significance (P<0.05) between SGC1 and SGC2 computed using MC3
[e]indicates a statistical significance (P<0.05) between SGC3 and SGC4 computed using MC3

4.4.4.3 Stair Gait Cycles

Using Method 1 a significantly lower sagittal ROM and peak flexion angle was measured for SGC1 compared to SGC2. Using methods MC1 and MC2, significantly lower adduction moment peaks 1 and 2 were measured for SGC3 compared with SGC4. Using MC3, significant differences were determined between the SGCs of stair ascent for peak adduction moment and stair descent for adduction moment peak 1 and flexion moment peak 2.

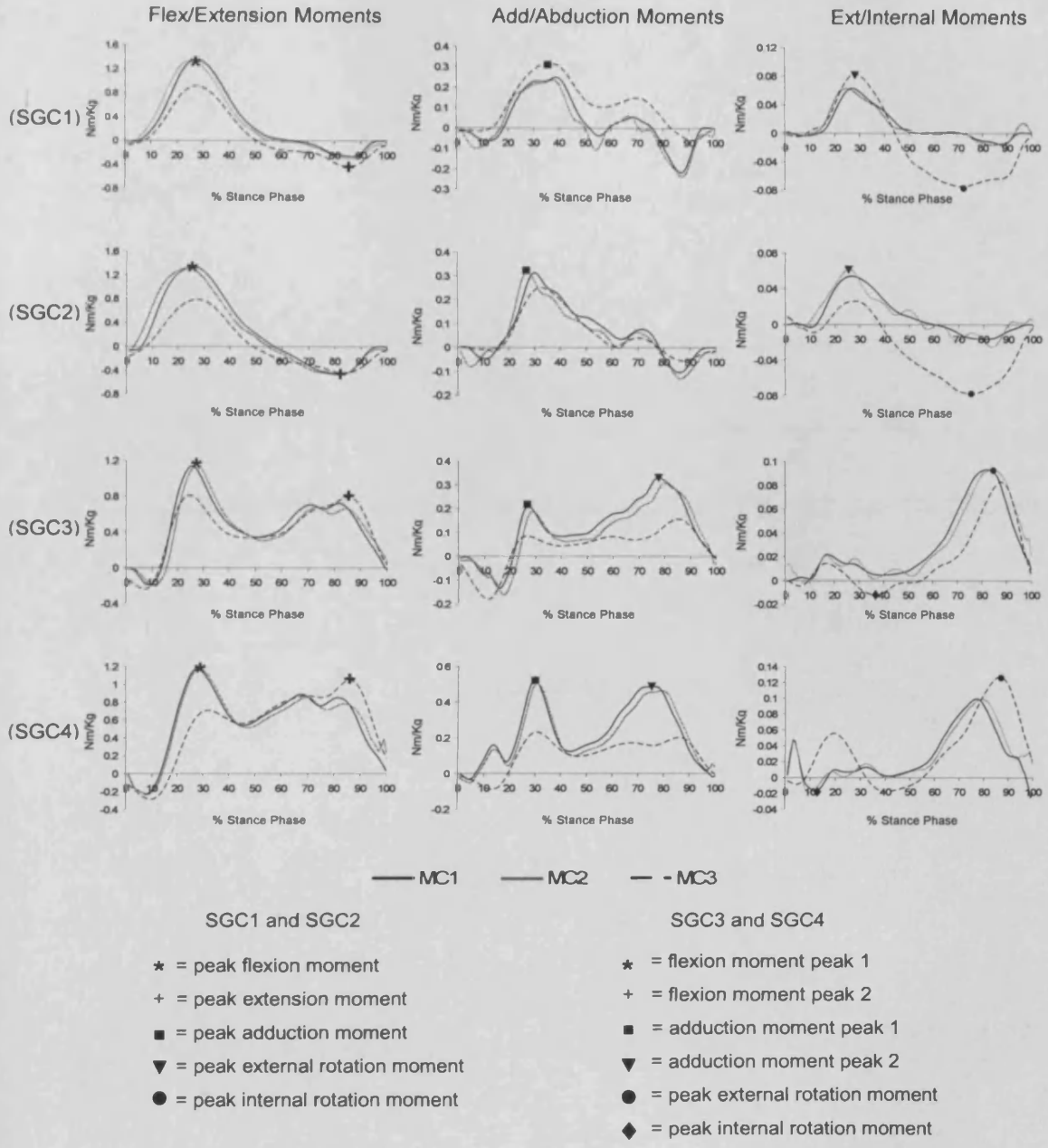

Figure 4.43 Examples of knee moment profiles for a single trial of (SGC1) stair ascent from step1 to step 3, (SGC2) stair ascent from step 2 to step 4, (SGC3) stair descent from step 3 to step 1 and (SGC4) stair descent from step 4 to step 2. For clarity, each discrete peak value is indicated for an individual waveform as an example.

4.4.5 DISCUSSION

Different SGCs were investigated to assess knee function during initial pull up phase, controlled lowering from step 1 to floor, and a cycle collected mid ascent/descent to determine differences in knee joint kinematics and moments.

The kinematic and joint moment profiles are consistent with previous studies (Andriacchi *et al.*, 1980; Costigan *et al.*, 2002; Kaufman *et al.*, 2001; Kowalk *et al.*, 1996; McFadyen and Winter, 1988; Yu *et al.*, 1997). The kinematic waveforms follow the same patterns for Methods 1 and 2, however, a significantly larger frontal ROM was calculated using Method 1 for three of the SGCs. The floating axis used to compute rotations in the frontal plane is determined as a cross product of the two vectors defined by the anatomical landmarks. A difference in the position of these landmarks affects the anatomical coordinate system in the femur, which may have an effect on small rotations in the frontal plane. The thigh segment is defined differently for Method 1 and 2. Method 1 uses the greater trochanter for the proximal landmark, whereas Method 2 uses the hip joint centre, producing different alignments in thigh segment axis.

Three methods for computing knee joint moments were explored. MC1 is a robust method of computing net moments about a joint without requiring knowledge of individual moments acting about the joint. Including inertial effects of the shank in calculation MC2 did not have any significant effects. MC2 could have been adapted to the method of Costigan *et al.*, (2002) where the moment of inertia is modified to account for foot mass, however, considering the similarity of the results from MC1 and MC2 it is unlikely to have a large effect. The only significant differences were found between the IDA approach (MC3) compared with MC1 and MC2. The movement of the foot appears to have a greater effect on the resulting moments as compared to including the inertia of the shank alone. This could be attributable to different methods of data collection but also appears to be affected by the choice of gait sequence as can be seen in Table 4.20 and Figure 4.43. Also, inertial effects modify the acceleration and deceleration of the whole body COM producing different GRF curves and thus influencing the full IDA method MC3.

Studies do not widely use the transverse moment and it is questioned whether this should be considered in future studies since only one significant difference was found between the collection methods.

Larger rotations and moments are involved during the SGC2 and SGC4 because they are collected mid ascent/descent. These are biomechanically more demanding and more sensitive to the choice of data collection and moment calculation than SGC1 and SGC3. The stair ascent/descent SGCs involve differing mechanisms to raise and lower the body COM to a greater or lesser extent, with varying inertial effects. Inertial effects on the rigid clusters of markers attached to the skin are greater for cycles collected mid ascent/descent and are more prevalent during stair descent. Significant differences in the biomechanical measures computed for different SGCs were determined. The choice of SGC appears to be more important when using Method 1 to compute the kinematics (using a pointer for the anatomical calibration and rigid marker clusters to track the movement) or MC3 for the moment calculations (using Visual3D, (C-motion, Inc) to compute an IDA) for assessing stair ascent, or when computing moments for stair descent, using either of the three moment calculation methods.

These differences in the measures from different SGCs are small and may be due to the small step height and the choice of SGC under consideration. Andriacchi *et al.*, (1980) found a large difference in flexion-extension moments during stair descent when comparing a SGC from step 3 to step 1 (where the moments were computed from the stance phase on step 1) and a SGC from step 2 to floor (where the moments were computed from the stance phase on the floor). A stair gait cycle where the GRFs were measured from floor level was not included in the current study to reduce the number of stair gait cycles required by each subject.

This study highlights the implications of comparing data from different analysis methods. Clearly describing data collection and analysis methods will enable educated judgements to be made when interpreting and comparing results from different studies. A wide range of limb configurations are mechanically feasible during stair ascent/descent (Townsend and Tsai, 1976). Moment profiles from previous studies display different patterns due to methodology, even though the magnitudes are

comparable (Kowalk *et al.*, 1996). This can be seen for the adduction and external moment profiles in Figure 4.43.

This work recognises the benefits of developing standards for the assessment of activities where methodology has a significant effect on biomechanical outcomes. It is important when comparing outcomes from a range of studies to identify the differences that exist solely due to the varying strategies adopted for stair gait for healthy, pathology related or rehabilitation regimes. This would remove the need to discern differences that are clouded by the disparity that arises when employing varying measurement and computational methods.

In future work, beyond the scope of this thesis, consideration should also be made to the reference frames for the expression of moments. For this study the orthogonal laboratory GCS was used. Alternative orthogonal frames are the proximal segment coordinate system and distal segment coordinate system. Another possibility is the non-orthogonal joint coordinate system (JCS). There is no consensus regarding an accepted standard and this contributes to the difficulties in comparing joint moment data across studies.

It is an accepted standard to define lower limb rotations according to the non-orthogonal JCS. There has been a claim in the literature (Schache and Baker, 2007) that it would be beneficial for the clinical interpretation of joint moments if they were represented in the non –orthogonal JCS. It is suggested that all calculations should be conducted in an orthogonal reference frame and then converted to the non-orthogonal frame for interpretation. In a future study it would be beneficial to identify the influence of the reference frame used for the computation of knee joint moments during stair gait. In the study by Schache and Baker, (2007), significant differences in the joint moment profiles during level gait were found with alternative reference frames and it is hypothesised that these differences would be amplified when considering stair gait.

To investigate the effect of alternative reference frames, the net moment vector could be projected along alternative reference axes using a dot product to determine the scalar components along each axis.

4.4.6 Recommendations

From this investigation, although the full IDA approach MC3 utilises information on lower limb segment properties which leads to a more informative solution for joint moment calculations, this requires information in the foot segment properties which is not available using the current Cardiff protocol. For this reason, the full lower limb marker set has been incorporated into the protocol for the clinical trial to allow the computation of full IDA using commercial software. For the remainder of the studies in this thesis, Method 1 to compute kinematics will be used with moment calculation M1. This has been used successfully in previous studies and although the computation is basic compared with the IDA approach, it can be utilised with the pointer method of computing kinematics. It is a method where the directions of individual forces do not need to be known as with the IDA method. It simplifies the calculations of moments in activities such as stair gait where the subjects' position relative to the GCS changes as they ascend and descend the stairs. Also, all moment data, regardless of computation method is interpreted using a form of pattern recognition based on deviations of signals from a normative equivalent. For this reason, as long as the limitations of this approach to computing moments is recognised and results are interpreted accordingly, meaningful data can be obtained for investigation with the classifier.

From the results of this study it is not apparent whether the choice of SGCs investigated in this study is an important consideration in the methodology. Although significantly larger adduction and flexion moments were found for stair descent using SGC4, it is unknown if this would influence the classification method and would need investigation in the future. For initial investigations into the influence of stair gait variables as inputs to the DS classifier, variables from SGC1 and SGC3 will be used. These were chosen to measure knee function from the first step to the third step during ascent and from the third step to the first step on descent. This investigates the knee during the initial pull up phase where the centre of mass is being raised against gravity (for SGC1) and during controlled lowering before stepping down to floor level (for SGC3).

This chapter provides an appreciation of the effect of methodology used to compute functional variables from stair gait. The next chapter investigates whether functional variables from stair gait can be used to classify knee joint function.

CHAPTER 5
CLASSIFYING KNEE FUNCTION USING STAIR GAIT VARIABLES

This chapter investigates the use of functional characteristics of the knee joint measured during stair gait to differentiate between non-pathological (NP) and osteoarthritic (OA) knees and assess the outcome of total knee replacement (TKR). The Cardiff protocol and new staircase described in Chapters 2 and 4 are used to quantify OA knee function during stair ascent and descent. The results are compared with NP knee function to identify stair gait adaptations associated with OA pathology. The suitability of using functional variables from stair gait to characterise NP and OA function is investigated using the Dempster-Shafer (DS) classifier. This takes a statistical approach to the signals that are found to be significant in determining the differences between the two cohorts. This work was presented at conferences (Whatling *et al.*, 2007a; Holt *et al.*, 2007; Whatling *et al.*, 2008b) and is extended to use stair gait characteristics to assess the outcome of TKR surgery, (Whatling *et al.*, 2008a; Whatling *et al.*, 2008c).

5.1 INTRODUCTION

Osteoarthritis (OA) is the most common joint disease and is a degenerative condition. Knee joint OA is more common than hip OA, but taken together they affect 10–20% of people aged over 65, becoming a major cause of pain and disability in the elderly (Arthritis Research Campaign, 2008). Knee joint OA develops when the articular cartilage lining the ends of the tibia and femur wear away resulting in painful, stiff joints with a reduced range of motion. For cases of advanced stage OA, total knee replacement (TKR) surgery is performed to replace the worn components of the joint with prosthetic articulating surfaces to remove pain and restore normal joint function.

A degeneration results in abnormal loading at the knee due to the altered quality of the contacting joint surfaces. Changes in the contours of the surfaces results in modified contact surface area and location of the load transmission across the joint. This in turn results in modified joint function and gait patterns, (Goldflies *et al.*, 1981). Quantifying the functional adaptations associated with the pathology would provide

useful information for implant designers, surgeons, clinicians and engineers to improve assessment and monitoring procedures.

It is important to study knee mechanics during activities of daily living and in particular during weight bearing activities where the biomechanical demands on the knee are high. Knee mechanics during stair ascent and descent is of particular interest as it demands greater range of motion, moments (Kaufman *et al.*, 2001; Andriacchi *et al.*, 1980) and 12-25% increase in knee loading (Morrison, 1969) compared to level walking.

The ability to climb stairs is important to one's quality of life and is often taken for granted by able bodied people. However, for individuals with knee OA, the activity can be challenging. The biomechanical requirements of stair climbing are more demanding than for level walking. This is due to the biomechanical demands on the knee joint and lower limb muscles to support, raise and propel the body against gravity to progress the body forward to the next step, and provide clearance of the swinging leg to avoid the intermediate step during stair ascent. Whilst during stair descent, the body must be continuously decelerated in a controlled manner with each descending step. Patients with OA generally have stiff joints resulting in a reduced range of motion and reduced muscle mass of their lower limbs due to their reduced mobility. This can lead to them adopting new mechanisms for ascending and descending stairs to accommodate the high demands of the activity. OA knee mechanics during stair gait have not been studied extensively. However, evaluating stair gait may provide more meaningful information on knee OA than during level walking because of its stressful nature. Kaufman *et al.*, (2001) studied patients with early stage knee OA and reports a reduced knee extensor moment and knee joint loading as stair gait adaptations used by patients.

To date, the DS classifier has been used to characterise knee joint function using input variables from level gait (Jones, 2004; Beynon *et al.*, 2006; Jones *et al.*, 2006; Jones and Holt, 2008). The DS classifier takes clinically relevant measurements to make a decision whether knee function is OA or non-pathological (NP), whilst accounting for a level of uncertainty in the decision. Once the classifier is trained using variables from a combined cohort of OA and NP subjects, it can be used to monitor the level of

recovery after TKR surgery. The level of recovery is quantified by the changes in the level of NP function and OA function exhibited by the patient. It is expected that as the patient recovers, they will display greater characteristics of NP gait and less characteristics of OA gait. Thus the patient's classification output will move from the OA region to the NP region on the simplex plot as shown in Figure 5.1.

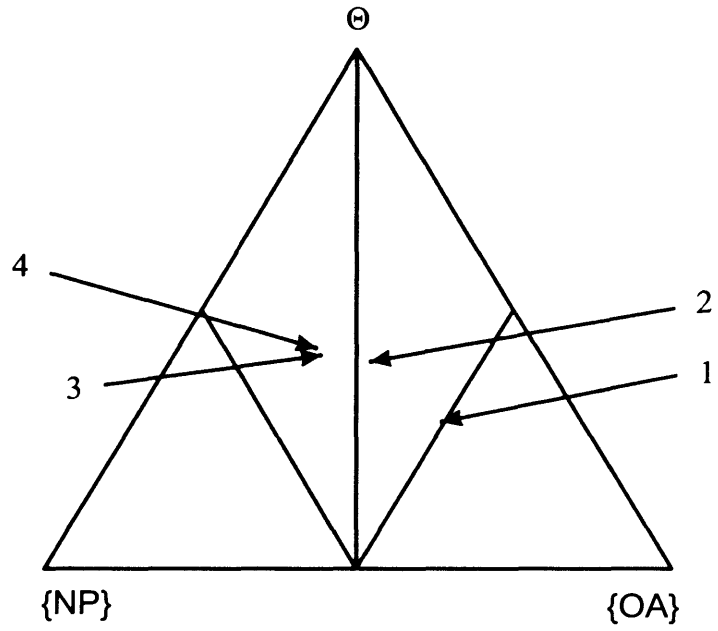

Figure 5.1 Simplex plot showing the final classification for four assessments of a patient undergoing TKR surgery. Point 1 indicates their OA knee function, point 2 indicates their 7 weeks post-operative TKR function, point 3 represents their 7 months post-operative TKR function and point 4 indicates their 15 months post-operative TKR function. (Adapted from Jones, 2004).

Individuals with knee OA adopt compensatory mechanisms to reduce the pain experienced when walking. Over time these adaptations can become habitual. Although their knee function improves following TKR, small kinematic and kinetic changes in level gait are measured following surgical intervention (Andriacchi *et al.*, 1982). This could be due to limited range of motion at the knee in all three clinical planes during this activity and also the fact that patients can maintain the old walking style that they developed prior to surgery.

In a study of asymptomatic patients to differentiate between TKR designs, Andriacchi *et al.*, (1982) concluded that stair gait produced more clearly differentiated function among the different designs than level gait. The kinematic and anatomical differences among the designs did not have as great an influence on function during level walking as they did during stair-climbing. Andriacchi *et al.*, (1982) also found that patients who appear to be clinically asymptomatic after TKR can maintain abnormal gait patterns (Andriacchi *et al.*, 1982), which can be due to the subjects maintaining old habits so that they continue to walk with the altered gait used to compensate for the pain prior to surgery, or the interaction of kinematics and the surrounding soft tissues.

More pronounced changes in knee mechanics for stair gait are expected after TKR surgery. Studies have shown the ability of variables from stair gait to differentiate the functional characteristics of the different types of TKR replacement designs (Andriacchi *et al.*, 1982; Dorr *et al.*, 1988; Kelman *et al.*, 1989; Berchuck *et al.*, 1990; Catani *et al.*, 2003).

This aim of this study is to determine functional variables from stair gait that can be used to differentiate characteristics of NP and OA knee function and investigate their ability to monitor TKR recovery.

5.2 EXPERIMENTAL METHODS

Knee mechanics during stair ascent and descent was evaluated for 6 subjects with advanced stage knee OA (4 females, 2 males, 68 ± 10.2 years, BMI 29.9 ± 2.7 Kg/m^2) and 9 NP subjects (5 females, 4 males, 52 ± 10.6 years, BMI 26.3 ± 4.45 Kg/m^2). The OA sample was assessed approximately 1 week prior to TKR surgery. Each OA subject was reassessed at approximately 3, 6 and 12 months post TKR surgery. The complete data set from one patient containing knee function data for all four visits was used as a TKR sample in this investigation. This data was collected as part of the ongoing clinical knee trial undertaken at Cardiff University and followed the protocol outlined in Chapter 2. The study was limited to this sample size because not all subjects were able to perform stair ascent and descent in a reciprocal manner at their pre-operative assessment (i.e. at no time both their feet were in contact with the same step). Also, all subjects used in this analysis did not use the handrail to assist them with the activity.

3D motion capture was performed using 8 Qualisys Proreflex MCU 120Hz digital cameras (Qualisys, Sweden), capturing at 60 Hz. Force data was collected using two Bertec force platforms (Bertec Corporation) with a sample rate of 1080Hz. Prior to data collection, the laboratory was calibrated to define a global coordinate system (GCS) and the position of the force plates were defined relative to the GCS.

Informed consent was obtained from the subjects after the tests had been fully explained. Anthropometric measurements were taken and a marker cluster containing four retro reflective markers was attached laterally on the thigh and shank of each subject. These were technical markers used to track the thigh segment and shank segment during stair climbing. An anatomical calibration was undertaken using a marked pointer to identify 3 anatomical landmarks per segment.

The stairs were constructed with the first step in contact with the force plate to measure ground reaction forces (GRFs) from the affected leg. The handrail was attached to the staircase for safety. Through experience it was found that some patients with knee OA take longer to perform stair gait. This led to issues of the handrail masking the markers from the infra-red cameras. Therefore, two positions of

the staircase were used during data collection, as shown in Figure 5.2. The subject walked on the side of the staircase next to the handrail. This allowed the leg on the side without a handrail to be recorded without marker occlusion. The movement of both limbs was recorded. Only the data from the affected knee from the OA subjects and one knee from the NP subjects are used in this study.

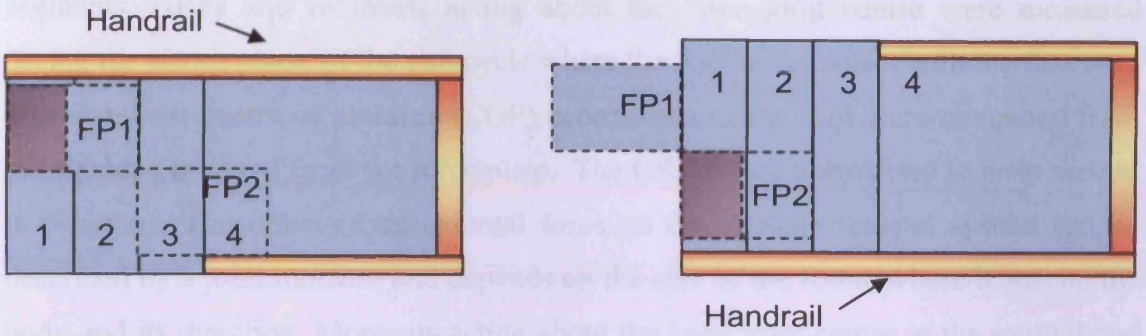

Figure 5.2 Stair positions for measuring forces from step 1 of the staircase. Position (a) is used to record right knee data during stair ascent and left knee data during stair descent, (b) is used to record left knee data during stair ascent and right knee data during stair descent. The two force plates are labeled FP1 and FP2 and the steps are labelled 1 to 4.

Each subject performed three trials of stair ascent and descent. The gait cycle for stair ascent was defined as foot strike on the first step through to foot strike of the same foot on the third step, as illustrated in Figure 5.3a. The cycle for stair descent was toe off the third step through to toe off the first step, as illustrated in Figure 5.3b.

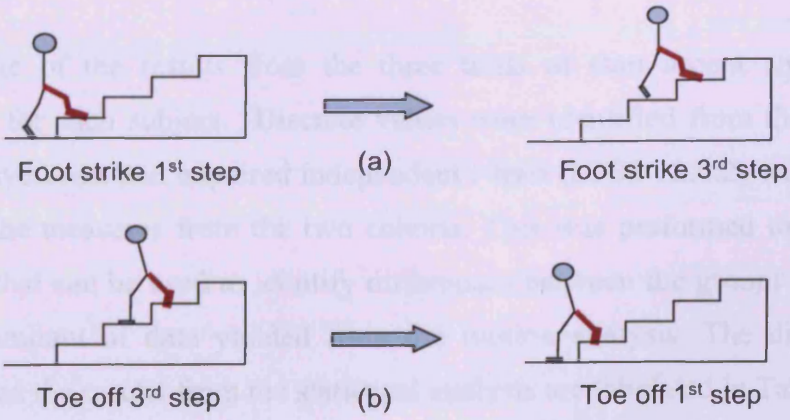

Figure 5.3 Gait cycle for (a) stair ascent and (b) stair descent

5.3 DATA PROCESSING

The method of Holt *et al.*, (2000) was used to determine joint axes and rotations according to the Grood and Suntay, (1983) Joint Coordinate System. This calculates the six degrees of freedom (three rotations and three translations) between two segments. GRFs and moments acting about the knee joint centre were measured during the stance phase of the gait cycle where the foot is in contact with the first step. GRFs and the centre of pressure (COP) coordinates of the foot were computed from the signals generated from the force plate. The GRFs were normalised to body weight in Newtons. The effect of an external force on the musculoskeletal system can be described by a joint moment and depends on the size of the force, where it acts on the body and its direction. Moments acting about the knee joint centre in the sagittal and frontal plane were computed throughout the stair gait cycles using Moment Calculation 1 from Chapter 4. This calculates the moment of force as the vector cross product of a vector defining the position of the knee joint centre relative to the COP and the relevant component of the GRF vector, (Andriacchi *et al.*, 1980). The moments were normalised to body weight and height, and expressed as a percentage. Inertial effects were ignored as they have been shown to be small in low-velocity activities (Davis *et al.*, 1994).

Data analysis was conducted in the following five stages to explore the use of stair gait variables with the DS classifier.

1. Identify salient variables for characterising NP and OA knee function

An average of the results from the three trials of stair ascent and descent were computed for each subject. Discrete values were identified from the kinematic and kinetic waveforms and unpaired independent *t*-tests (SPSS 12.0.2) were performed to compare the measures from the two cohorts. This was performed to identify salient variables that can be used to identify differences between the groups and thus reduce the vast amount of data yielded from the motion analysis. The discrete variables selected and the results from the statistical analysis are tabulated in Table 5.1.

2. Principle component analysis of selected waveforms

The variables with a statistical difference between the groups ($p<0.05$) were retained and principle component analysis (PCA) was performed on their waveforms (Jones, 2004; Deluzio *et al.*, 1997). This procedure (outlined in Chapter 2) computes and selects the principle components (PCs) that adequately describe the waveforms whilst retaining their temporal information. Kaiser's rule is used to select PCs with a variance greater than 1. These are subsequently interpreted by assessing the associated component loadings. PCs with component loadings equal to or greater than 0.71 (Comrey, 1973) are retained and interpreted in relation to the phase of the stair gait cycle they represent.

3. Use stair gait variables to classify OA and NP subjects

The PCs retained were used as inputs to the DS classifier (Jones, 2004) to characterise each subject's knee function as either NP or OA. The DS control variables k, θ, A and B, were calculated from the combined OA and NP sample using the non-optimisation method. k was calculated using the correlation coefficient method and A and B from the limits of uncertainty $[\Theta_L, \Theta_U] = [0.6, 1]$ allowed for the individual input variables. All PCs retained were used in an initial classification. Then, due to the large number of inputs, the five variables with the highest ranking and thus the greatest influence in an accurate classification were retained and used in a subsequent classification of the same subjects. This step was taken to reduce the number of variables used in the final classification because of the small sample size.

4. Use stair gait variables to monitor TKR recovery

The TKR sample consists of the data collected from four visits for one of the subjects. This data was used to investigate whether the variables selected have the potential to assess the outcome of TKR surgery. In the previous step the DS classifier was trained using the variables of the combined OA and NP sample to determine the optimum control variables for the classification. These were then used to transform the input variables of the TKR sample into a combined body of evidence, BOE_c. The BOE_c is a set of three indices defining the level of OA and NP function exhibited by the patient

and a level of uncertainty in the analysis. The three indices of the BOE_c are used as coordinates to define the patient's final classification on a simplex plot. For comparative purposes, the BOE_c of each patient visit is compared with the knee outcome survey (KOS) and oxford knee score (OKS).

5. Compare classification output of TKR recovery to the original waveforms

In this step, the classification output for the four visits in the TKR sample are described in terms of the original input variables used to make the decision. The changes in the waveforms for each of the input variables are described and compared to the changes in classification output for each visit.

5.4. RESULTS

5.4.1 Identify salient variables for characterising NP and OA knee function

The kinematic and kinetic variables selected to compare the OA and NP groups are listed in Table 5.1. A * indicates the statistically significant ($p<0.05$) difference in the measures between the OA and NP groups. For stair ascent, peak medially directed GRF, peak flexion moment and peak adduction moment were significantly different between the cohorts. For stair descent, peak vertical GRF and peak flexion moment were significantly different between the cohorts. No significant differences between the cohorts were found for the kinematic measures.

Table 5.1 Kinematic and kinetic measures for OA and NP groups

	Variables	NP Group (n= 9)	OA Group (n = 6)
Stair ascent step 1 to step 3	Sagittal ROM (°)	77.58 ± 3.51	73.41 ± 13.60
	Peak flexion angle(°)	85.84 ± 6.08	86.38 ± 13.45
	Frontal ROM(°)	14.65 ± 7.47	11.23 ± 2.77
	Transverse ROM(°)	15.65 ± 4.99	14.18 ± 3.36
	Peak flexion moment (%BW*h)	6.77 ± 1.53*	2.95 ±1.03
	Peak extension moment (%BW*h)	2.46 ± 1.25	2.79 ± 1.03
	Peak adduction moment (%BW*h)	1.86 ± 0.56 *	6.92 ± 6.02
	Peak Medial-Lateral GRF	0.06 ± 0.01*	0.04 ± 0.01
	Peak Anterior-Posterior GRF	0.07 ± 0.03	0.06 ±0.03
	Peak Vertical GRF	1.12 ± 0.08	1.08 ± 0.09
Stair descent step 3 to step 1	Sagittal ROM (°)	79.59 ± 6.78	77.73 ± 11.22
	Frontal ROM(°)	20.14 ± 6.81	16.58 ± 7.61
	Transverse ROM(°)	13.99 ± 5.14	15.79 ± 8.93
	Peak flexion angle(°)	85.03 ± 9.07	89.03 ± 11.55
	Peak flexion moment (%BW*h)	5.36 ± 1.04 *	3.53 ± 0.73
	Peak adduction moment (%BW*h)	3.42 ± 1.47	2.85 ± 1.49
	Peak Medial-Lateral GRF	0.07 ± 0.02	0.05 ± 0.02
	Peak Anterior-Posterior GRF	0.13 ± 0.04	0.13 ± 0.02
	Peak Vertical GRF	1.31 ± 0.24 *	1.05 ± 0.11
	BMI	26.29 ± 4.45	29.87 ±2.73

Mean ± Standard deviation; * Statistical significance from NP control group $P < 0.05$

5.4.2 Principle component analysis of selected waveforms

Although discrete values such as peak flexion angle are regularly used in clinical gait analysis studies, the waveforms from which the salient variables from Table 5.1 were identified were further processed using Principal Component Analysis (PCA) before being used as inputs to the classifier. Pre-processing of waveforms using PCA means that important temporal information is retained, because the parametric representations relate to specific and unique portions of the cycle. PCA was performed on the following five kinetic waveforms to compute principal components (PCs) representing each waveform for use in the classifier.

- Knee flexion moment measured during stair ascent
- Knee adduction moment measured during stair ascent
- Medial-Lateral component of the GRF measured during stair ascent
- Knee flexion moment measured during stair descent
- Vertical component of the GRF measured during stair descent

The timing of stair gait events is different to events in level gait. Stair gait has a longer stance duration than level gait. Table 5.2 was created to allow the interpretation of each PC in terms of the portion of the stair gait cycle it represents. The swing phase is not included because all salient kinetic waveforms, although represented for the duration of the stair gait cycle, only have readings during the stance phase. The timings are based on the waveforms from the subjects used in this analysis.

Table 5.2 timing of stance phase events as a percentage of the stair gait cycle

Stair cycle event	Timing of event (% gait cycle) Stair ascent	Timing of event (% gait cycle) Stair descent
Initial contact	Instantaneous	30
Loading response	0-12	30-42
Mid-stance	12-36	42-64
Terminal stance	36-61	64-87
Pre-swing	61-75	87-100

The selection of PCs to represent each waveform will now be discussed.

5.4.2.1 Flexion moment measured during stair ascent (FMA)

One hundred PCs were produced relating to the FMA waveform. The PCs and their associated eigenvalues are depicted below in Figure 5.4.

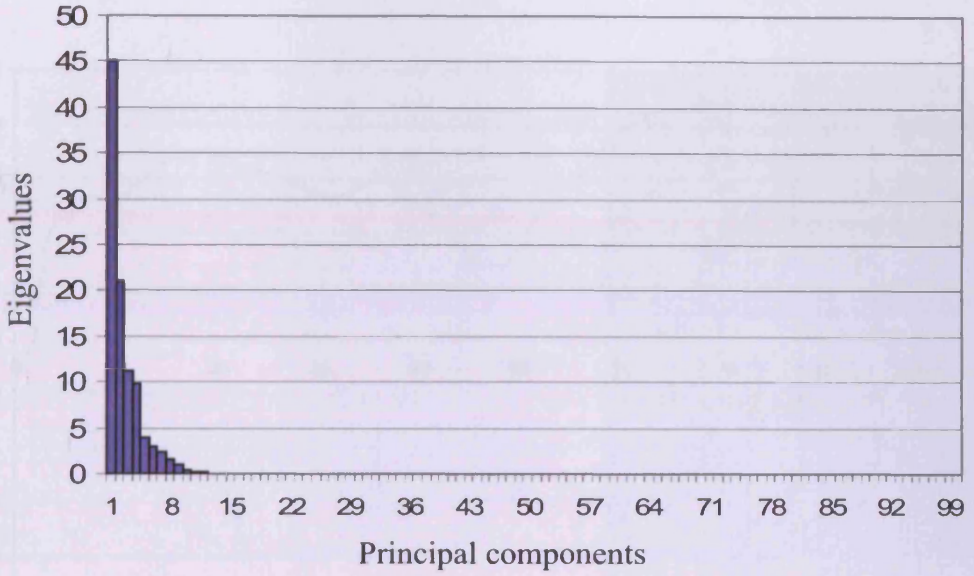

Figure 5.4 The eigenvalues of the 100 PCs for the FMA waveform

The first 8 PCs explain most of the variation in the original data. After the first few PCs the values of the associated eigenvalues rapidly approach zero. Using Kaiser's rule, eight PCs have eigenvalues greater than 1 and are retained. The eigenvalues of these eight PCs are recorded in Table 5.3.

Table 5.3 Eigenvalues of the eight Flexion Moment Ascent Principal Components (FMAPCs) retained using the Kaiser's rule

Flexion moment Ascent Principal Component	Eigenvalue
FMAPC1	45.15999
FMAPC2	21.0138
FMAPC3	11.30266
FMAPC4	9.837809
FMAPC5	3.848172
FMAPC6	2.968202
FMAPC7	2.385685
FMAPC8	1.560809

These eight PC's account for a combined variance of 98.08%. The PCs are interpreted by identifying the portions of the cycle with component loadings of 0.71 and above, following Comrey, (1973).

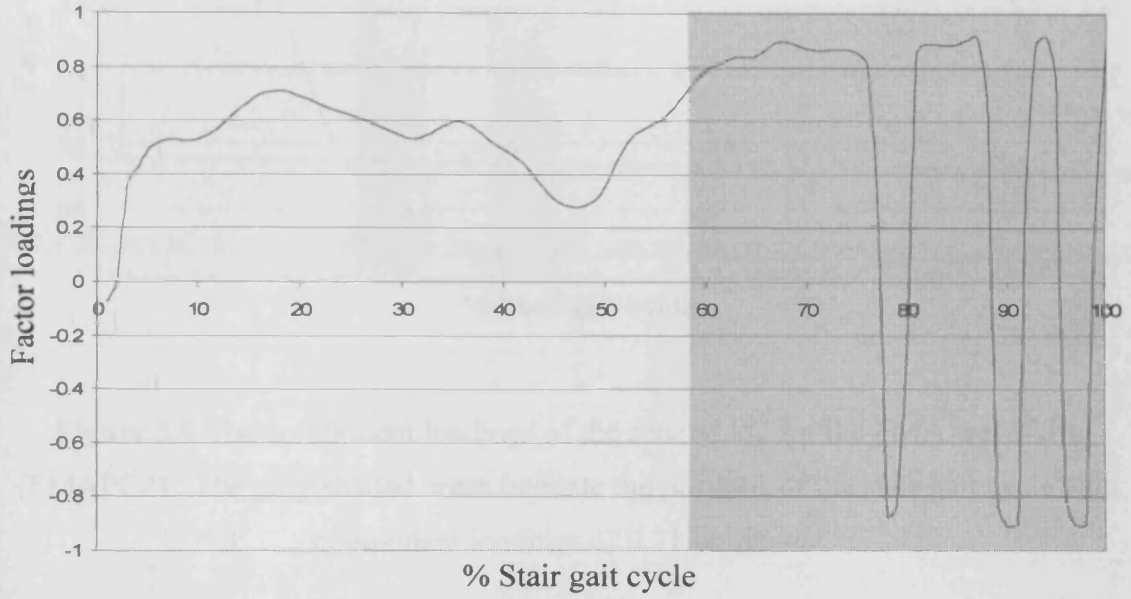

Figure 5.5 The component loadings of the first PC for the FMA waveform (FMAPC1). The grey shaded areas indicate the portions of the stair gait cycle with component loadings of 0.71 or greater.

In Figure 5.5 there is one period within the stair gait cycle where the component loading is 0.71 or above. This occurs from 59% to 100 % of the gait cycle. Thus FMAPC1 represents the flexion moment measured from mid terminal stance to the end of pre-swing during stair ascent. The factor loading from 75% to 100% occurs during the swing phase and does not represent the flexion moment. Instead it contains temporal information.

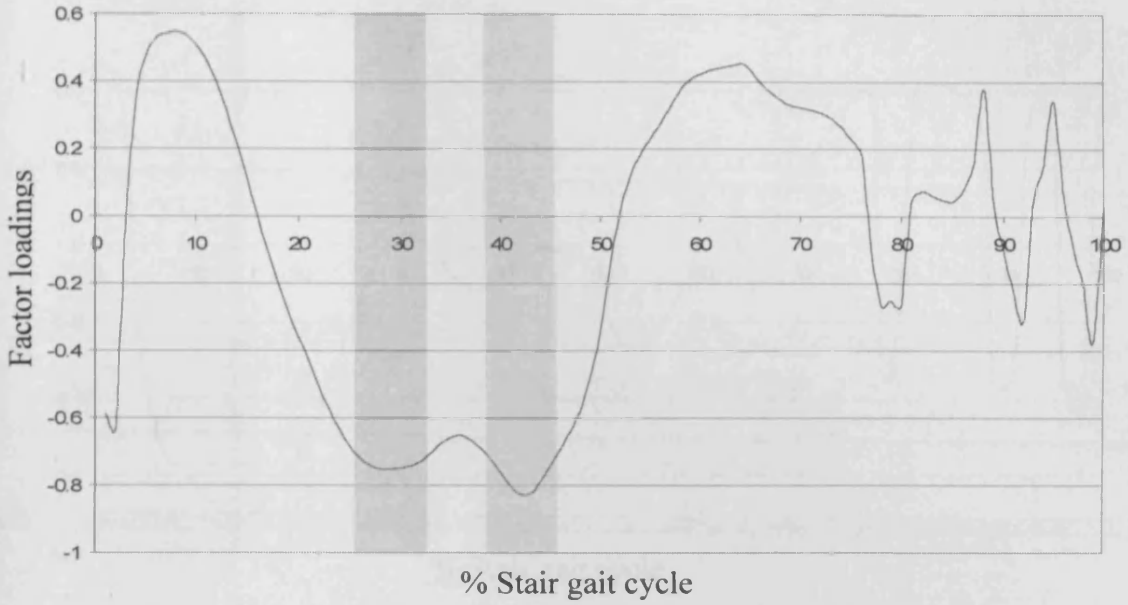

Figure 5.6 The component loadings of the second PC for the FMA waveform (FMAPC2). The grey shaded areas indicate the portions of the stair gait cycle with component loadings of 0.71 or greater.

In Figure 5.6 there are two periods within the stair gait cycle where the component loadings are 0.71 or above. The first period occurs from 26% to 32 % of the gait cycle and the second is from 39% to 45 %. Thus FMAPC2 represents the flexion moment acting from mid to late mid-stance phase and for early mid terminal stance phase.

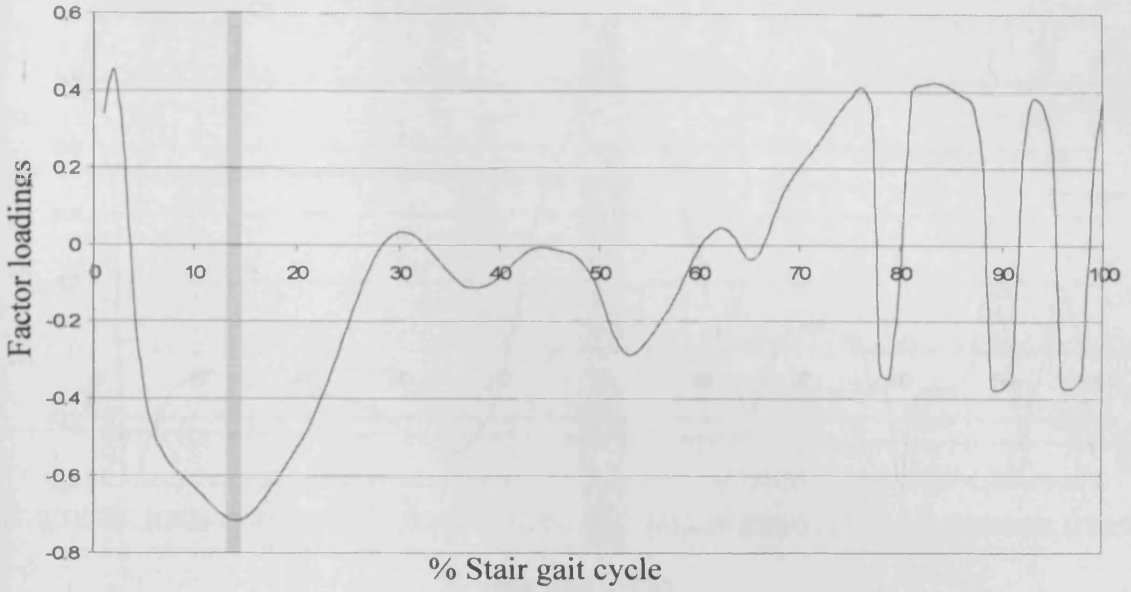

Figure 5.7 The component loadings of the third PC for the FMA waveform (FMAPC3). The grey shaded areas indicate the portions of the stair gait cycle with component loadings of 0.71 or greater.

In Figure 5.7 there is one period within the stair gait cycle where the component loadings are 0.71 or above. This occurs from 14% to 15 % of the gait cycle. Thus FMAPC3 represents the flexion moment acting briefly at early mid-stance.

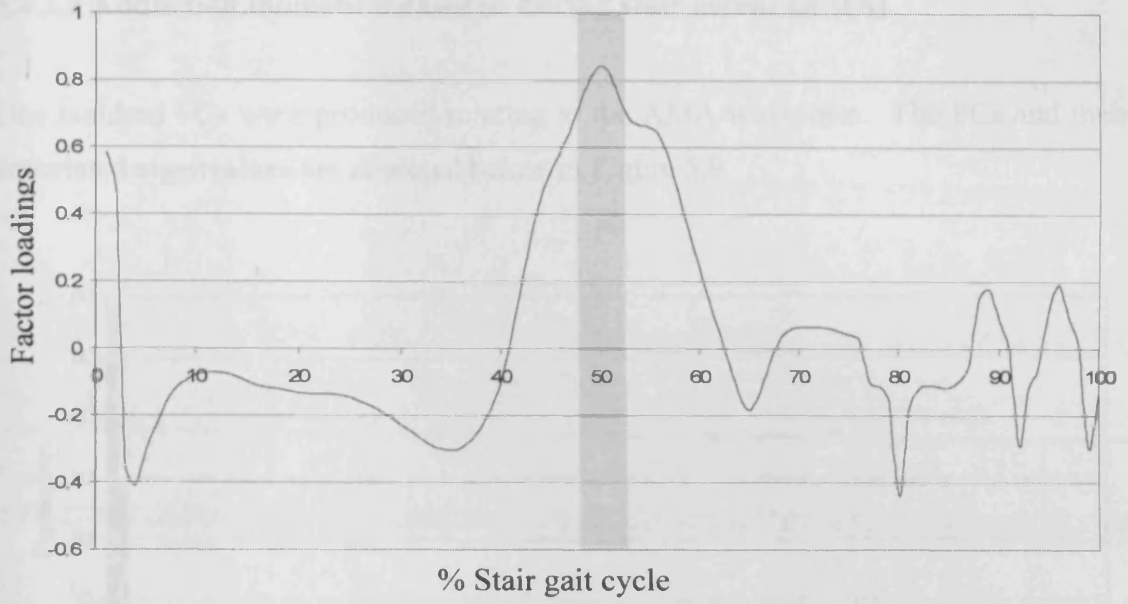

Figure 5.8 The component loadings of the fourth PC for the FMA waveform (FMAPC4). The grey shaded areas indicate the portions of the stair gait cycle with component loadings of 0.71 or greater.

In Figure 5.8 there is one period within the stair gait cycle where the component loadings are 0.71 or above. This occurs from 48% to 52% of the gait cycle. Thus FMAPC4 represents the flexion moment during the late mid-terminal stance phase.

The component loading of the remaining 4 PCs are non-interpretable since no individual portion of the stance phase in the stair gait cycle has loadings equal to or above the required threshold of 0.71. The first four PCs account for a combined variance of 87.31%.

PC scores were calculated for the OA and NP samples for FMAPC1, FMAPC2, FMAPC3 and FMAPC4.

5.4.2.2 Adduction moment measured during stair ascent (AMA)

One hundred PCs were produced relating to the AMA waveform. The PCs and their associated eigenvalues are depicted below in Figure 5.9.

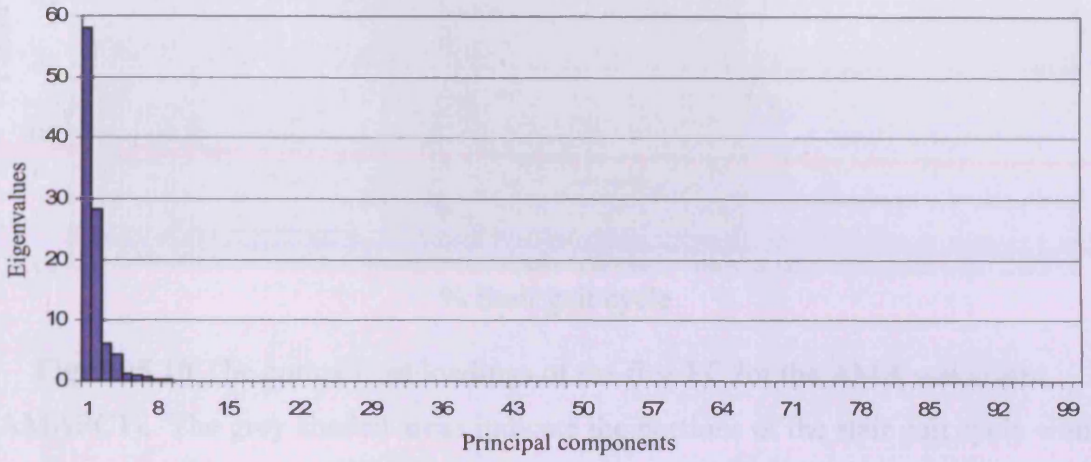

Figure 5.9 The eigenvalues of the 100 PCs for the AMA waveform

The first 5 PCs explain most of the variation in the original data. After the first few PCs the values of the associated eigenvalues rapidly approach zero. Using Kaiser's rule, five PCs are retained. The eigenvalues of these five PCs are recorded in Table 5.4.

Table 5.4 Eigenvalues of the five Adduction Moment Ascent Principal Components (AMAPCs) retained using the Kaiser's rule

Adduction Moment Ascent Principal Component	Eigenvalue
AMAPC1	58.04047
AMAPC2	28.28061
AMAPC3	6.045661
AMAPC4	4.405561
AMAPC5	1.13014

These five PC's account for a combined variance of 97.90%. The PCs are interpreted by identifying the portions of the cycle with component loadings of 0.71 and above, following Comrey, (1973).

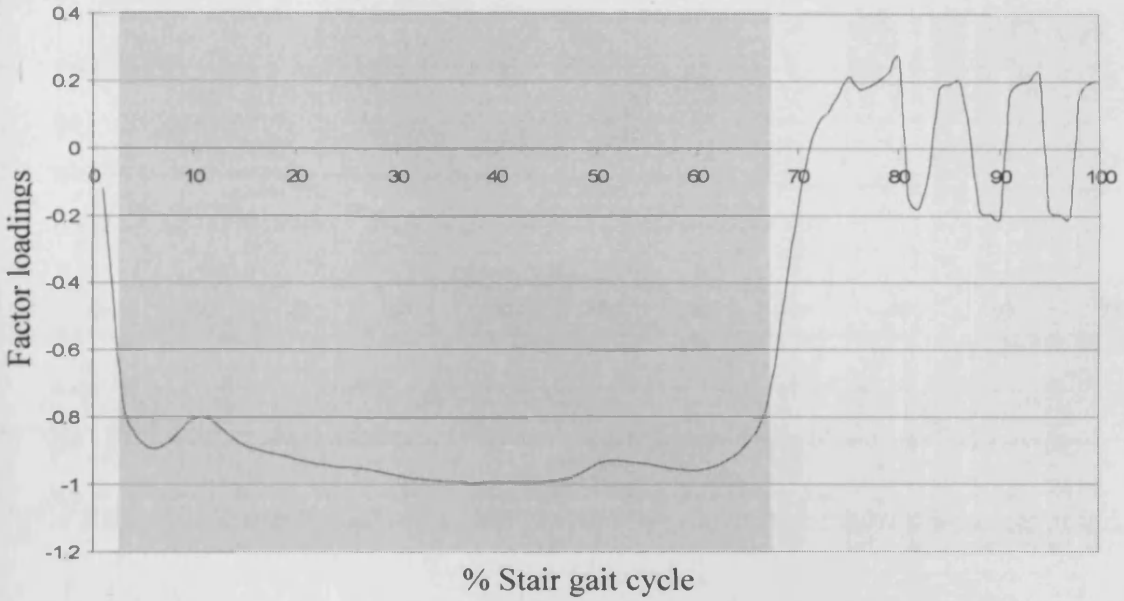

Figure 5.10 The component loadings of the first PC for the AMA waveform (AMAPC1). The grey shaded areas indicate the portions of the stair gait cycle with component loadings of 0.71 or greater.

In Figure 5.10 there is one period within the stair gait cycle where the component loadings are 0.71 or above. This occurs from 3% to 67% of the gait cycle. Thus AMAPC1 represents the adduction moment acting during early to late mid-terminal stance phase.

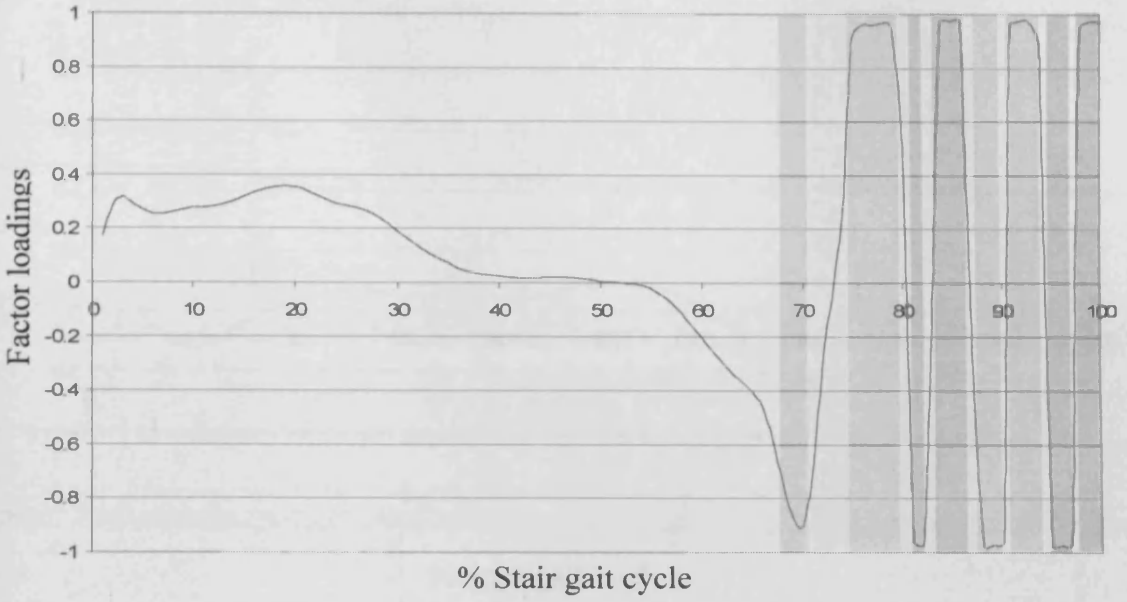

Figure 5.11 The component loadings of the second PC for the AMA waveform (AMAPC2). The grey shaded areas indicate the portions of the stair gait cycle with component loadings of 0.71 or greater.

In Figure 5.11 there are several periods of the gait cycle where the component loadings are 0.71 or above. These occur from 67% to 70% and from 75% to 100% of the gait cycle. Thus AMAPC2 represents the early to late mid-terminal stance phase and provides temporal information for the swing phase of the cycle.

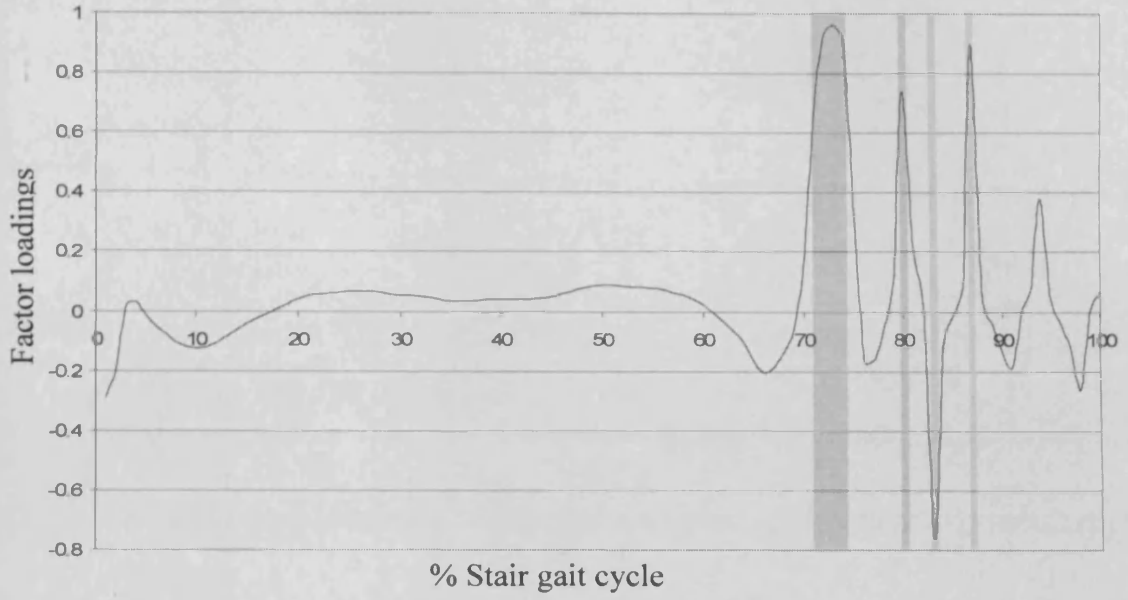

Figure 5.12 The component loadings of the third PC for the AMA waveform (AMAPC3). The grey shaded areas indicate the portions of the stair gait cycle with component loadings of 0.71 or greater.

In Figure 5.12 the component loadings are above 0.71 from 72% to 74%. Thus AMAPC3 represents adduction moment at the end of pre-swing. The loadings are also above the threshold at 80%, 83% and 87% of the stair gait cycle. These are in the swing phase of the cycle where no moments are computed.

The component loading of the remaining 2 PCs were discarded as non-interpretable since no individual portion of the stance phase in the stair gait cycle had loadings equal to or above the required threshold of 0.71. The first three PCs account for a combined variance of 92.37%.

PC scores were calculated for the OA and NP samples for AMAPC1, AMAPC2 and AMAPC3.

5.4.2.3 Medial-Lateral Force measured during stair ascent (MLFA)

One hundred PCs were produced relating to the MLFA waveform. The PCs and their associated eigenvalues are depicted below in Figure 5.13.

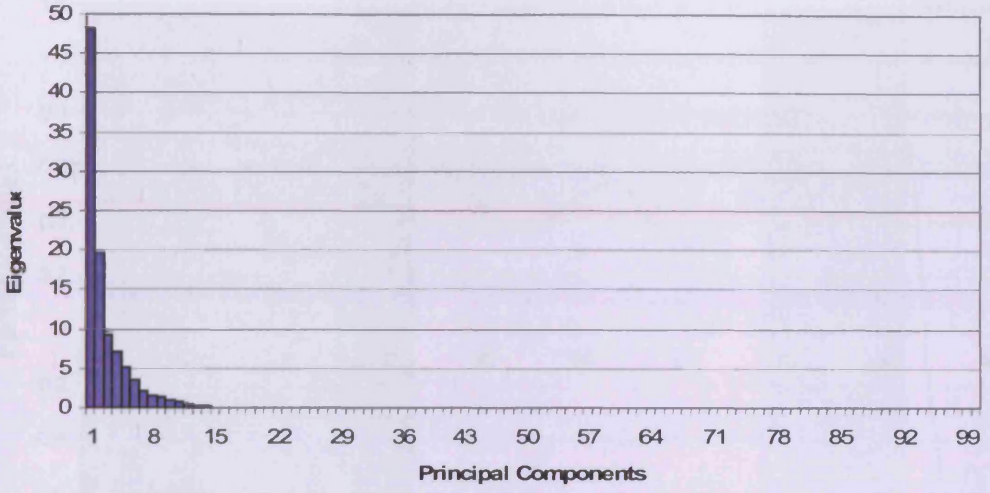

Figure 5.13 The eigenvalues of the 100 PCs for the MLFA waveform

The first nine PCs explain most of the variations in the original data as their associated eigenvalues are above 1. After the first few PCs the values of the associated eigenvalues rapidly approach zero. Using Kaiser's rule, nine PCs are retained. The eigenvalues of these nine PCs are recorded in Table 5.5.

Table 5.5 Eigenvalues of the nine Medial-Lateral Force Ascent Principal Components (MLFAPCs) retained using the Kaiser's rule

Medial-Lateral Force Ascent Principal Component	Eigenvalue
MLFAPC1	48.15196
MLFAPC1	19.5735
MLFAPC1	9.238171
MLFAPC1	7.055775
MLFAPC1	5.071686
MLFAPC1	3.578416
MLFAPC1	2.149636
MLFAPC1	1.609485
MLFAPC1	1.292975

These nine PC's account for a combined variance of 97.72%. The PCs are interpreted by identifying the portions of the cycle with component loadings of 0.71 and above, following Comrey, (1973).

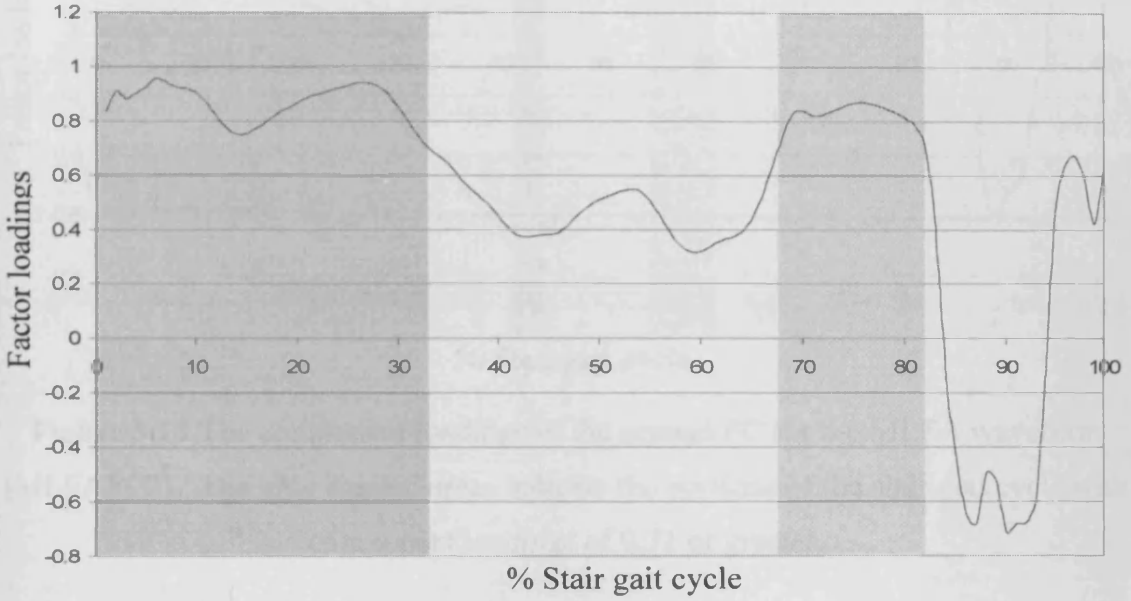

Figure 5.14 The component loadings of the first PC for the MLFA waveform (MLFAPC1). The grey shaded areas indicate the portions of the stair gait cycle with component loadings of 0.71 or greater.

In Figure 5.14 there are two periods within the stair gait cycle where the component loadings are 0.71 or above. The first period occurs from 0% to 32 % of the gait cycle and the second is from 68% to 82 %. Thus MLFAPC1 represents the medial-lateral force acting from initial contact to late mid stance and from mid pre-swing until just after the end of the stance phase. The factor loading from 75% onwards is meaningless as this is the swing phase where no forces are being measured.

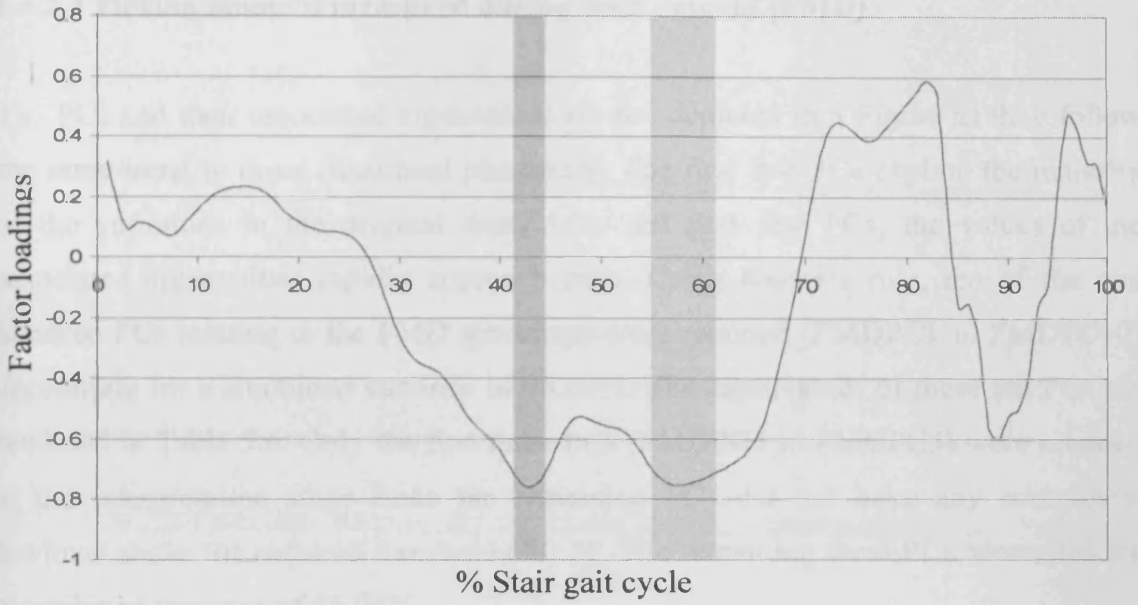

Figure 5.15 The component loadings of the second PC for the MLFA waveform (MLFAPC2). The grey shaded areas indicate the portions of the stair gait cycle with component loadings of 0.71 or greater.

In Figure 5.15 there are two periods within the stair gait cycle where the component loadings are 0.71 or above. The first period occurs from 42% to 44 % of the gait cycle and the second is from 56% to 61%. Thus MLFAPC2 represents the medial-lateral force acting during mid to late terminal stance phase.

The component loading of the remaining 7 PCs are non-interpretable since no individual portion of the stair gait cycle has loadings equal to or above the required threshold of 0.71. The first two PCs account for a combined variance of 67.72%.

PC scores were calculated for the OA and NP samples for MLFAPC1 and MLFAPC2.

5.4.2.4 Flexion moment measured during stair descent (FMD)

The PCs and their associated eigenvalues are not depicted in a Figure as they follow the same trend to those illustrated previously. The first few PCs explain the majority of the variations in the original data. After the first few PCs, the values of the associated eigenvalues rapidly approach zero. Using Kaiser's rule, ten of the one hundred PCs relating to the FMD waveform were retained (FMDPC1 to FMDPC10) accounting for a combined variance of 98.64%. The eigenvalues of these ten PCs are recorded in Table 5.6. Only the first three PCs (FMDPC1 to FMDPC3) were retained at the interpretation stage since the remaining PCs did not have any component loadings above the required threshold of 0.71. The remaining three PCs accounted for a combined variance of 66.94%.

Table 5.6 Eigenvalues of the ten Flexion Moment Descent Principal Components (FMDPCs) retained using the Kaiser's rule

Flexion Moment Descent Principal Component	Eigenvalue
FMDPC1	28.11898
FMDPC2	26.43473
FMDPC3	12.38405
FMDPC4	10.31284
FMDPC5	7.834661
FMDPC6	5.849741
FMDPC7	3.808006
FMDPC8	1.546368
FMDPC9	1.302249
FMDPC10	1.045487

The first PC is depicted in Figure 5.16. The grey areas indicate the portion of the stair gait cycle with component loadings greater or equal to 0.71. There are two periods within the stair gait cycle where the component loadings are 0.71 or above. The first period occurs from 50% to 55% and the second is from 67% to 86%. Thus the FMDPC1 represents the flexion moment during the central portion of mid-stance and for the majority of the terminal stance phase.

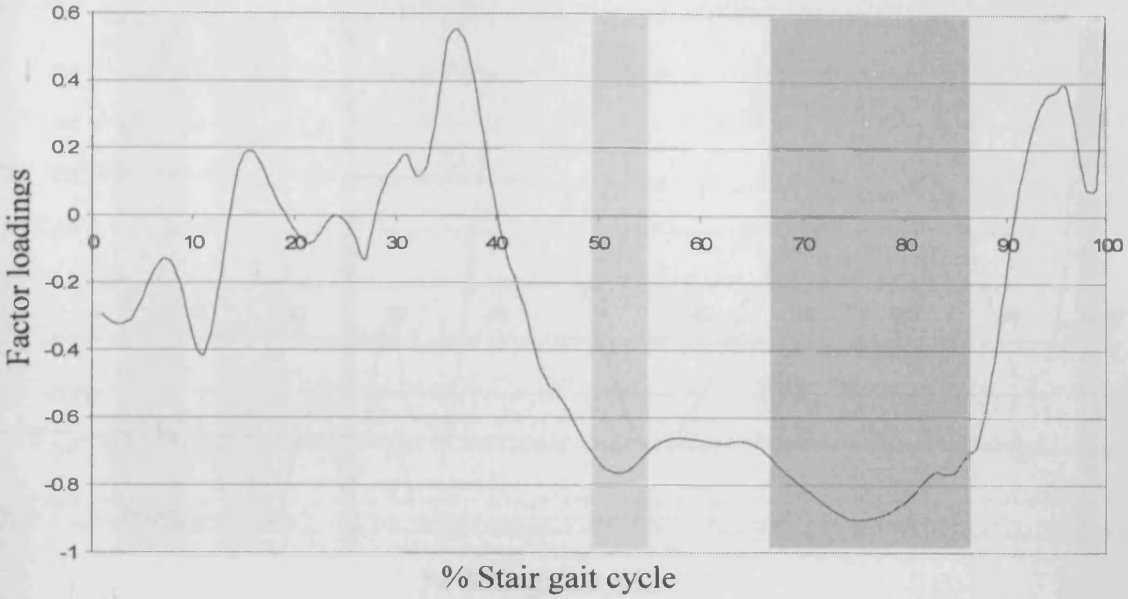

Figure 5.16 The component loadings of the first PC for the FMD waveform (FMDPC1). The grey shaded areas indicate the portions of the stair gait cycle with component loadings of 0.71 or greater.

The second PC is depicted in Figure 5.17. There are four periods within the stair gait cycle where the component loadings are 0.71 or above. The first three occur at initial toe off and during the swing phase between 3% to 9%, 13% to 19% and 25% to 26%. The final period occurs at 98% to 99%. FMDPC2 represents the flexion moment acting during the swing phase which is undesirable since no moments are measured during the swing phase of the stair gait cycle. However the temporal information retained at this portion of the measurement may be important in future interpretations. FMDPC2 also represents the late stage of pre-swing.

The third PC is depicted in Figure 5.18. There is one period within the stair gait cycle where the component loading is above 0.71. This occurs between 88% and 93% of the cycle. Thus FMDPC3 represents the flexion moment acting during the majority of the pre-swing phase.

PC scores were calculated for the OA and NP samples for FMDPC1, FMDPC2 and FMDPC3.

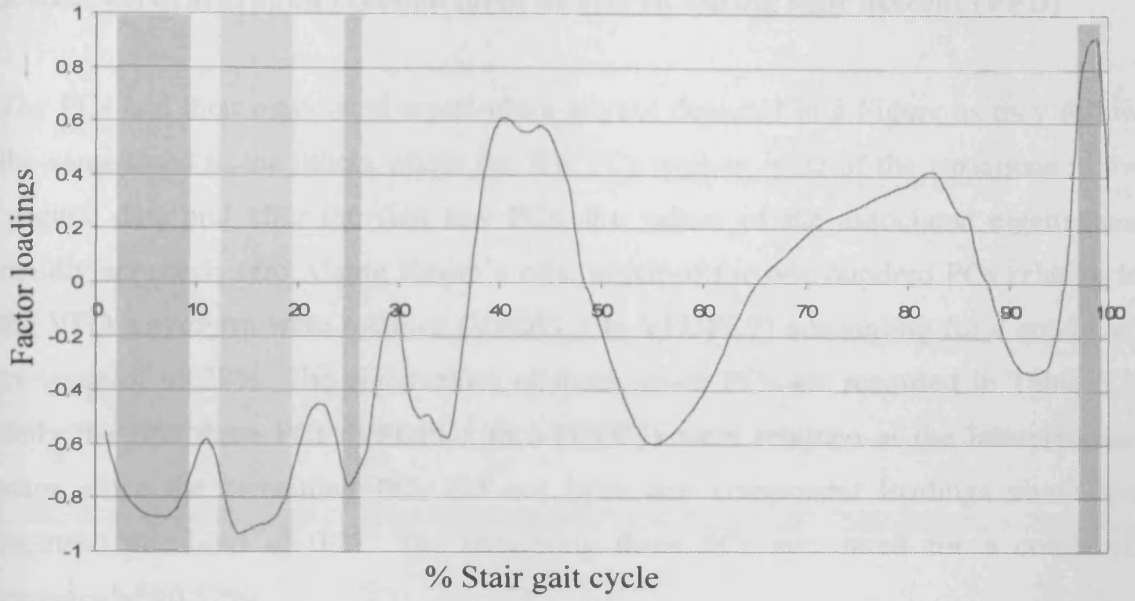

Figure 5.17 The component loadings of the second PC for the FMD waveform (FMDPC2). The grey shaded areas indicate the portions of the stair gait cycle with component loadings of 0.71 or greater.

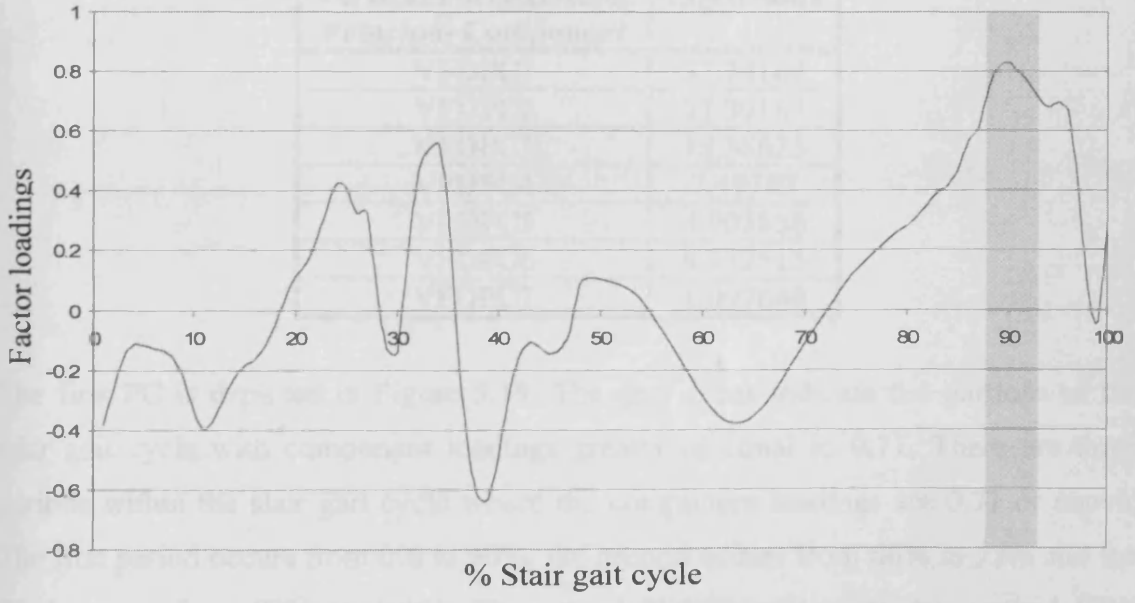

Figure 5.18 The component loadings of the third PC for the FMD waveform (FMDPC3). The grey shaded areas indicate the portions of the stair gait cycle with component loadings of 0.71 or greater.

5.4.2.5 Vertical ground reaction force measured during stair descent (VFD)

The PCs and their associated eigenvalues are not depicted in a Figure as they follow the same trend to the others where the few PCs explain most of the variations in the original data and after the first few PCs, the values of the associated eigenvalues rapidly approach zero. Using Kaiser's rule, seven of the one hundred PCs relating to the VFD waveform were retained (VFDPC1 to VFDPC7) accounting for a combined variance of 98.28%. The eigenvalues of these seven PCs are recorded in Table 5.7. Only the first three PCs (VFDPC1 to VFDPC3) were retained at the interpretation stage since the remaining PCs did not have any component loadings above the required threshold of 0.71. The remaining three PCs accounted for a combined variance of 80.52%.

Table 5.7 Eigenvalues of the seven Vertical Force Descent Principal Components (VFDPCs) retained using the Kaiser's rule

Vertical Force Descent Principal Component	Eigenvalue
VFDPC1	37.74162
VFDPC2	27.39163
VFDPC3	15.38625
VFDPC4	7.49107
VFDPC5	4.903856
VFDPC6	4.272513
VFDPC7	1.097668

The first PC is depicted in Figure 5.19. The grey areas indicate the portions of the stair gait cycle with component loadings greater or equal to 0.71. There are three periods within the stair gait cycle where the component loadings are 0.71 or above. The first period occurs from 0% to 30%, the second occurs from 66% to 73% and the third occurs from 99% to 100%. Thus the VFDPC1 represents the vertical GRF during swing phase, where although no GRFs are recorded during this phase of the cycle, important temporal information is retained in this PC. VFDPC1 also represents the vertical GRF from early to mid terminal stance and late stage pre-swing.

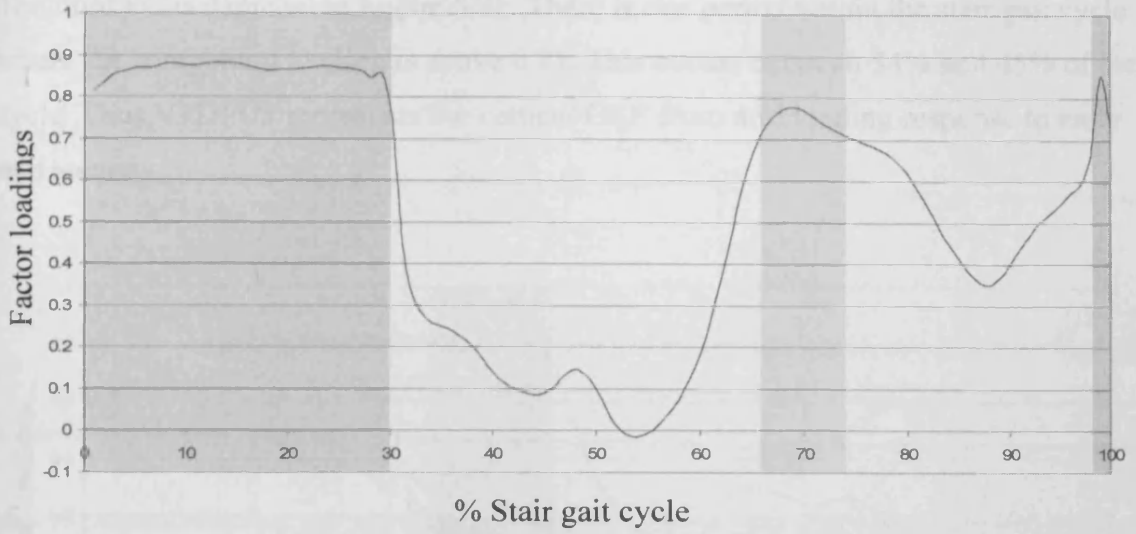

Figure 5.19 The component loadings of the first PC for the VFD waveform (VFDPC1). The grey shaded areas indicate the portions of the stair gait cycle with component loadings of 0.71 or greater.

The second PC is depicted in Figure 5.20. There are two periods within the stair gait cycle where the component loadings are above 0.71. This occurs between 50% to 61% and 81% to 88%. Thus VFDPC2 represents the vertical GRF acting from mid to late mid-stance and mid to late terminal stance.

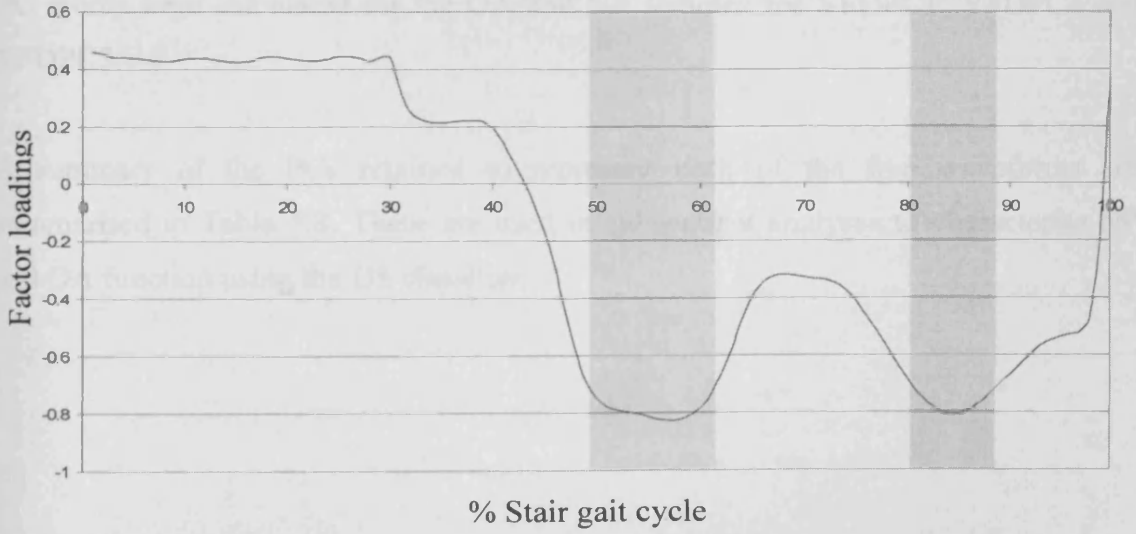

Figure 5.20 The component loadings of the second PC for the VFD waveform (VFDPC2). The grey shaded areas indicate the portions of the stair gait cycle with component loadings of 0.71 or greater.

The third PC is depicted in Figure 5.21. There is one period within the stair gait cycle where the component loading is above 0.71. This occurs between 34% and 45% of the cycle. Thus VFDPC3 represents the vertical GRF from mid loading response to early mid stance.

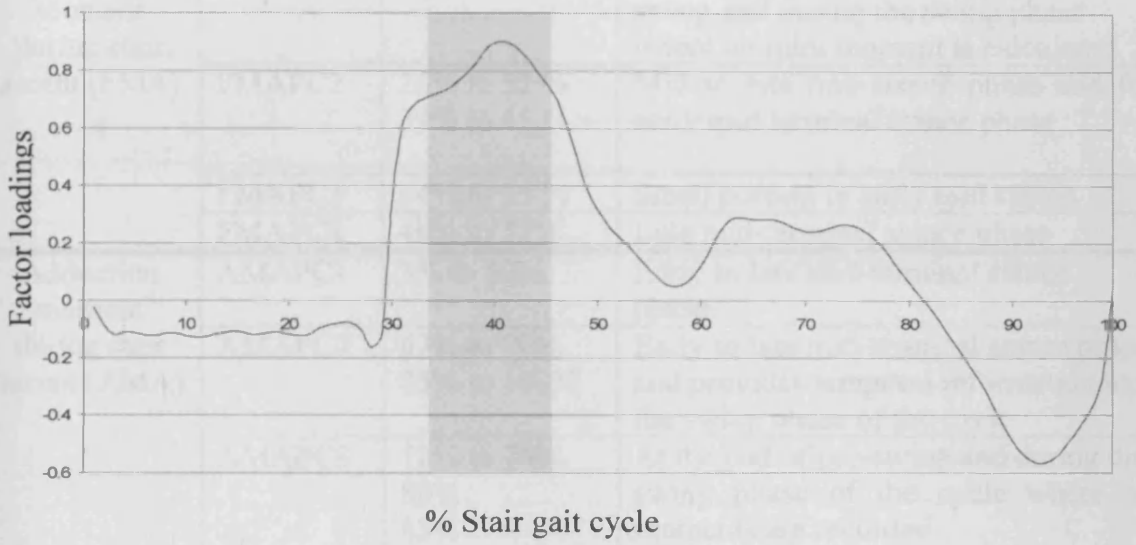

Figure 5.21 The component loadings of the third PC for the VFD waveform (VFDPC3). The grey shaded areas indicate the portions of the stair gait cycle with component loadings of 0.71 or greater.

PC scores were calculated for the OA and NP samples for VFDPC1, VFDPC2 and VFDPC3.

A summary of the PCs retained to represent each of the five waveforms are summarised in Table 5.8. These are used in subsequent analyses to characterise NP and OA function using the DS classifier.

Table 5.8 Summary of the retained PCs and the stages of the stair gait cycle that they represent

Variable	PC	% Stair Gait Cycle	Portion of the stair gait cycle the PC represents
Flexion moment during stair ascent (FMA)	FMAPC1	59% to 100 %	Mid-terminal stance to the end of pre-swing and during the swing phase where no joint moment is calculated
	FMAPC2	26% to 32 % 39% to 45 %.	Mid to late mid-stance phase and for early mid terminal stance phase
	FMAPC3	14% to 15 %	Small portion in early mid stance
	FMAPC4	48% to 52%	Late mid-terminal stance phase
Adduction moment during stair ascent (AMA)	AMAPC1	3% to 67%	Early to late mid-terminal stance phase.
	AMAPC2	67% to 70% 75% to 100%	Early to late mid-terminal stance phase and provides temporal information for the swing phase of the cycle
	AMAPC3	72% to 74%. 80% 83% 87%	At the end of pre-swing and during the swing phase of the cycle where no moments are recorded
Medial-lateral force during stair ascent (MLFA)	MLFAPC1	0% to 32 % 68% to 82 %.	Initial contact to late mid-stance and mid pre-swing until just after the end of the stance phase
	MLFAPC2	42% to 44 % 56% to 61%.	Mid to late terminal stance phase
Flexion moment during stair descent (FMD)	FMDPC1	50% to 55% 67% to 86%	Central portion of mid-stance and the majority of the terminal stance phase
	FMDPC2	3% to 9% 13% to 19% 25% to 26%. 98% to 99%.	Late stage of pre-swing and represents temporal information during swing phase of the stair gait cycle
	FMDPC3	88% to 93%	The majority of the pre-swing phase
Vertical force during stair descent (VFD)	VFDPC1	0% to 30%, 66% to 73% 99% to 100%	Swing phase, early to mid terminal stance and late stage pre-swing
	VFDPC2	50% to 61% 81% to 88%.	Mid to late mid-stance and mid to late terminal stance
	VFDPC3	34% and 45%	Mid loading response to early mid stance

5.4.3 Use stair gait variables to classify OA and NP subjects

The suitability of using functional variables from stair climbing to objectively characterise NP and OA function was investigated using the DS classifier. This procedure takes a statistical approach to the signals that are found to be significant in determining the differences between the two cohorts. The output for the classification using all the PCs listed in Table 5.8 is given in Figure 5.22.

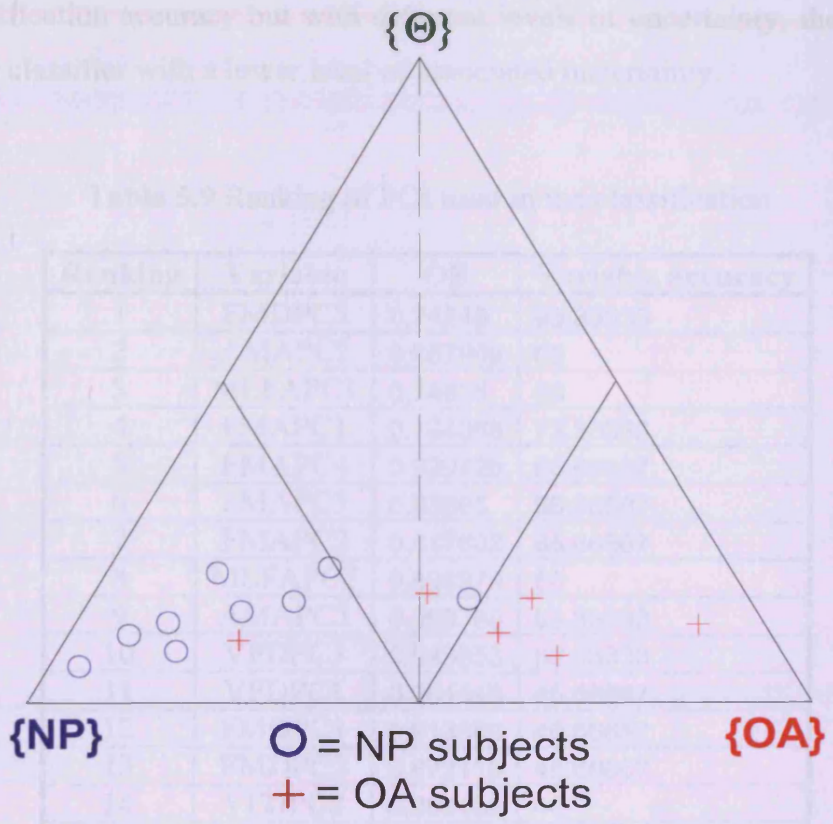

Figure 5.22 Simplex plot classifying the subjects knee function as NP or OA.

The out-of-sample classification accuracy is 86.67% determined by a Leave-one-out cross-validation. This means the classifier using these variables was able to classify new subjects with an accuracy of 86.67%. The in-sample-accuracy was 99.05%. An OA subject is misclassified in the dominant NP region of the simplex plot and there is one misclassified NP subject situated in the non-dominant OA region of the simplex plot.

The DS classifier provides a ranking of the variables used as inputs to the classifier, listed in Table 5.9. The variables are ranked according to the average accuracy in which each variable classifies new subjects (leave-one-out classification error rate) and the average OB measure, which is the Euclidean distance measure of the level of uncertainty in the classification. Variables that produce high classification accuracy are ranked higher than those with a low accuracy. In cases where the accuracy is the same, the variables are ranked according to their OB. A DS classifier with high classification accuracy will have a lower associated OB. For two classifiers with the same classification accuracy but with different levels of uncertainty, the OB will be less for the classifier with a lower level of associated uncertainty.

Table 5.9 Ranking of PCs used in the classification

Ranking	Variable	OB	Variable accuracy
1	FMDPC3	0.74248	93.33333
2	AMAPC2	0.857999	80
3	MLFAPC1	0.74835	80
4	FMAPC1	0.784365	73.33333
5	FMAPC4	0.929729	66.66667
6	FMAPC3	0.83895	66.66667
7	FMAPC2	0.817602	66.66667
8	MLFAPC2	0.838379	60
9	AMAPC3	0.958366	53.33333
10	VFDPC3	0.943853	53.33333
11	VFDPC1	0.964446	46.66667
12	FMDPC1	0.913569	46.66667
13	FMDPC2	0.872118	46.66667
14	VFDPC2	0.908439	40
15	AMAPC1	0.958081	33.33333

Because there was 1 misclassified subject from each group and an additional subject classified in a non-dominant region, the top 5 ranked variables were selected for the classification and used in a subsequent classification shown in Figure 5.23

Using the top 5 ranked variables, the classifier was able to differentiate between the characteristics of NP and OA knee function with 100% out-of-sample-accuracy and in-sample-accuracy of 99.52 %. Thus, the subset of variables used, improved the classification accuracy.

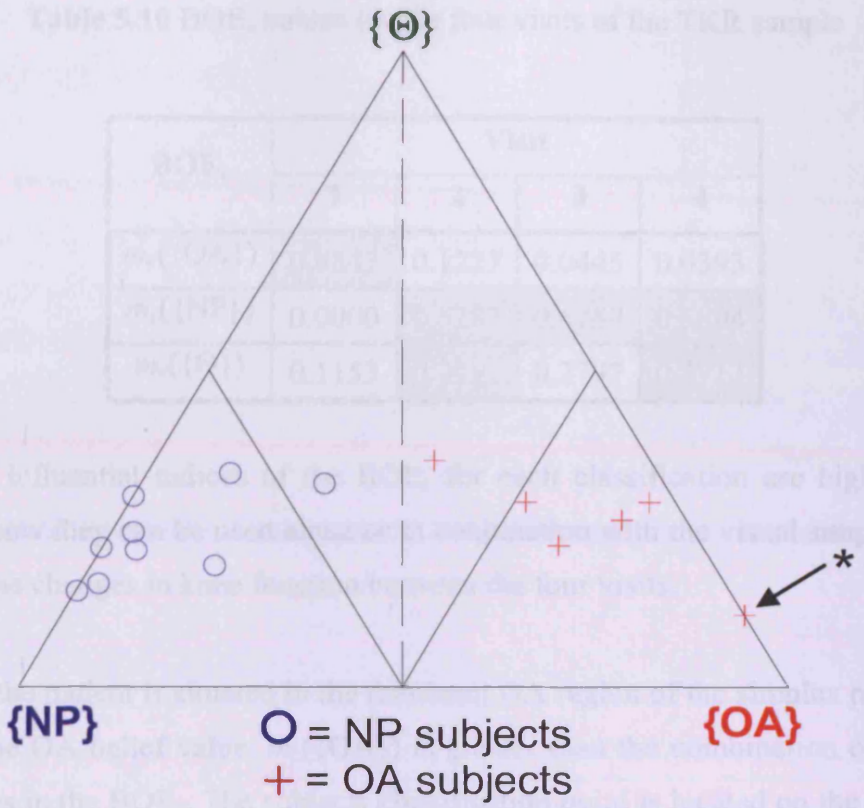

Figure 5.23 Simplex plot classifying the subjects knee function as NP or OA.
* indicates the patient with the highest level of knee OA defined by the classifier

The patient experiencing the most arthritic knee OA during their first assessment (i.e. highest value of $m_c(\{OA\})$) was selected for the investigation of TKR monitoring in section 5.4.4.

5.4.4 Use stair gait variables to monitor TKR recovery

The 5 top ranked variables identified in the previous section were collated for the TKR sample and applied to the DS classifier to test their ability to assess the level of benefit achieved by TKR surgery. The TKR sample consisted of the functional data from one patient for four assessments. The timings of the four assessments of the patient were 1 week prior to TKR replacement, 4 months post-operation, 8 months post-operation and 12 months post-operation. The BOE_c for the four visits are recorded in Table 5.10. The corresponding simplex coordinates are depicted in Figure 5.24.

Table 5.10 BOE_c values for the four visits of the TKR sample

BOE_c	Visit			
	1	2	3	4
$m_c(\{OA\})$	0.8847	0.1227	0.0445	0.0393
$m_c(\{NP\})$	0.0000	0.5282	0.6758	0.5894
$m_c(\{\Theta\})$	0.1153	0.3491	0.2797	0.3713

The most influential indices of the BOE_c for each classification are highlighted to illustrate how they can be used alone or in conjunction with the visual simplex plot to interpret the changes in knee function between the four visits.

At visit 1 the patient is situated in the dominant OA region of the simplex plot. This is because the OA belief value, $m_c(\{OA\})$ is greater than the combination of the other two indices in the BOE_c. The subjects classification point is located on the side of the triangle opposite the NP vertex because the value of $m_c(\{NP\})$ is zero. It is situated towards the bottom of the triangle because of the small value for Θ.

At visit two there is an increase in $m_c(\{NP\})$ and decrease in $m_c(\{OA\})$ so that $m_c(\{NP\})>[\ m_c(\{OA\})+\ m_c(\Theta)]$. The simplex coordinate is now situated in the dominant NP region of the simplex plot indicating a large increase in functional ability of the patient to perform stair gait. The increase in Θ From visit 1 to visit 2 moves the final classification point higher up the simplex plot.

At visit three there is a further increase in $m_c(\{NP\})$ and decrease in $m_c(\{OA\})$. This moves the simplex coordinate closer to the {NP} vertex indicating a further increase in NP characteristics. The value of $m_c(\{\Theta\})$ also decreases which moves the classification closer to the base of the triangle.

At visit 4, the BOEc indices are very similar to visit 2. The value of $m_c(\{OA\})$ is slightly smaller which moves the classification point closer to the side of the triangle opposite the OA vertex. $m_c(\{NP\})$ is slightly higher than in visit 2 which moves the classification further towards the NP vertex. However, the value of $m_c(\{\Theta\})$ increased

moving the simplex coordinate upwards in the triangle to represent the increase in uncertainty in the classification.

There is a change in function across the 4 visits, visit 1 showed the highest belief in OA function whereas for visits 2 to 4 the highest belief value was in NP function. The patient exhibited very similar knee function during visits 2 and 4.

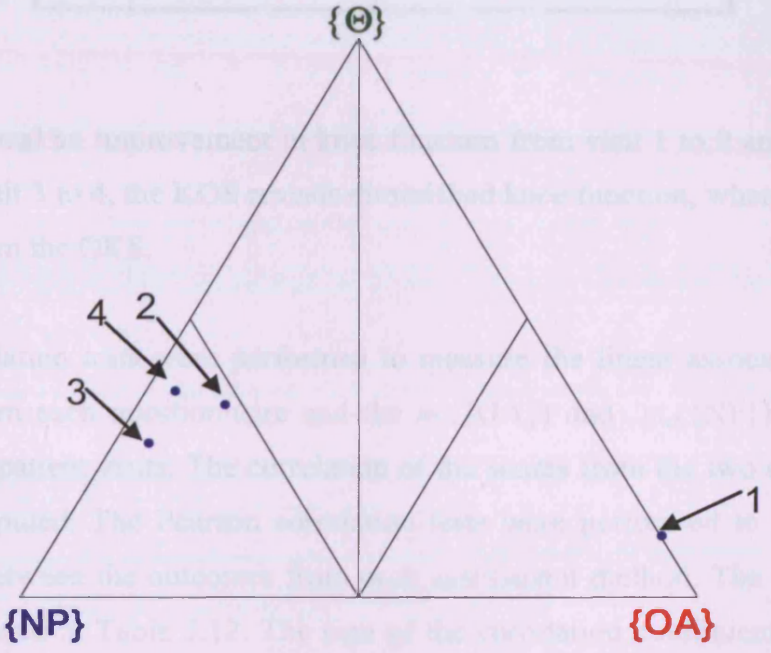

Figure 5.24 Simplex plot showing the simplex coordinate representation of the BOE_c for the four visits for the TKR sample.

5.4.4.1 Comparing objective TKR recovery with subjective measures

The oxford knee score (OKS) and knee outcome survey (KOS) was completed by the patient at each assessment visit. This provided a subjective measure of how the patient perceives their knee function. The results for the KOS and OKS for each of the four assessments are recorded in Table 5.11. A high score corresponds to a high level of knee function using the KOS questionnaire and a low level of knee function using the OKS questionnaire. The patient did not complete the OKS during their first assessment visit.

Table 5.11 KOS and Oxford knee scores for the four visits of the TKR sample

Visit	KOS score (%)	Oxford knee score (%)
1	75	-
2	87.5	33.33
3	93.75	28.33
4	88.75	28.33

The scores reveal an improvement in knee function from visit 1 to 2 and from visit 2 to 3. From visit 3 to 4, the KOS reveals diminished knee function, whereas no change is reported from the OKS.

Pearson correlation tests were performed to measure the linear association between the scores from each questionnaire and the $m_c(\{OA\})$ and $m_c(\{NP\})$ of the BOE_c from the four patient visits. The correlation of the scores from the two questionnaires was also computed. The Pearson correlation tests were performed to determine the relationship between the outcomes from each assessment method. The results of this analysis are listed in Table 5.12. The sign of the correlation coefficient indicates the direction of the relationship between the two variables. The absolute value of the correlation coefficient indicates the strength of the relationship between the variables, with larger absolute values indicating stronger relationships.

Table 5.12 Pearson correlation between BOE_c, OKS and KOS scores from four patient visits

Variables	Pearson Correlation	Correlation (p=0.05)
KOS and $m_c(\{OA\})$	-0.956	significant
KOS and $m_c(\{NP\})$	0.988	significant
OKS and $m_c(\{OA\})$	0.998	significant
OKS and $m_c(\{NP\})$	-0.813	not significant
KOS and OKS	-0.655	not significant

5.4.5 Comparing classification results with original waveforms using a clinical gait analysis approach

Clinical gait analysis is as objective method of interpreting gait data. Using a systematic approach, the clinician works backwards from observed abnormalities and critiques the gait data to determine the underlying causes. Following from a course in clinical gait analysis (ESMAC Gait course, 2007), this approach is used to provide a comparison of the inputs with the classification output for the TKR sample. An overview of the method used for clinical diagnostics is detailed below to provide a background to the procedure.

This method of interpreting gait data involves recording any deviations in the gait data from a normal range. This is usually achieved by first assessing the temporal and spatial data such as cadence, step lengths and step widths. The clinician identifies any asymmetries between the limbs and any abnormal timing for the stance and swing phases.

The joint kinematic waveforms are then considered in terms of the range of movement and timing of events. Any deviations of the waveform from a normal pattern or magnitude are considered as well as the phase of the gait cycle that it occurs. Assessing the movement in all the planes allow suggestions to be made as to what is causing any abnormal joint patterns and to discover any compensatory mechanisms.

Any deviations of the kinetic waveforms from the normal pattern or magnitude and the phase of the cycle that it takes place is also noted and used as evidence towards a diagnosis. Joint moments provide an indication of the muscles and ligaments under tension at different phases of the gait cycle. This is important for understanding what internal structures are creating the effect that is observed and whether they are supposed to be having an effect at that particular point in the gait cycle.

The information gathered is used to relate the movement to the moments that are occurring. Graphs of joint power are also considered to determine if the joint is generating or absorbing power as this indicates if the muscles are contracting concentrically or eccentrically (storage and release of energy by stretching elastic

tissues). If Electromyography is recorded, this is used to confirm a diagnosis. It allows the observation of if the muscle is firing or not at the expected phase of the cycle and observe if the activity patterns are phasic or constant.

The results can be tabulated and a joint will rarely be considered in isolation. This is because with a primary pathology, there will likely be coping or compensatory mechanisms that relate to it. A sequence of hypotheses is formed as to the detailed cause of gait abnormality that is present and their agreement with visual observations.

For the purpose of this study the waveforms from the four visits forming the TKR sample are plotted along with the mean and standard deviation of the NP cohort for each functional variable. An observational analysis of the MLFA, FMD, FMA and AMA waveforms are made and compared to classification output in Figure 5.24.

5.4.5.1 Medial-lateral force waveforms (stair ascent)

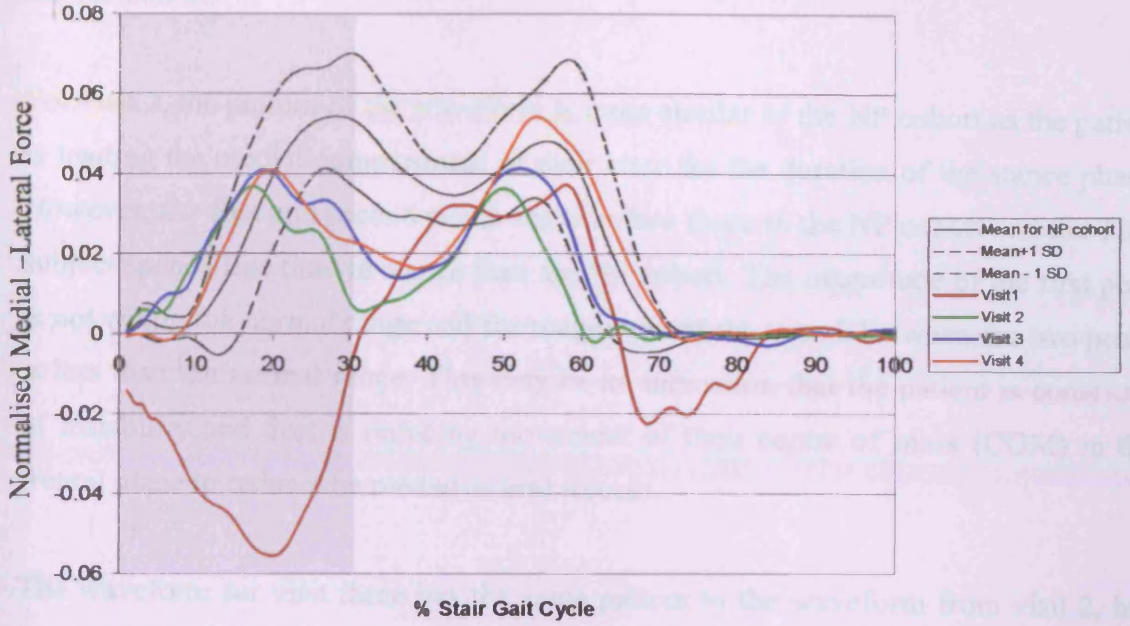

Figure 5.25 Medial-lateral force waveforms during stair ascent for four visits for the TKR subject. The mean of the NP sample is indicated by a solid black line where the dashed line indicates ± one standard deviation. The MLFAPC1 is highlighted by the grey shaded area.

During the stance phase the medial-lateral component of the ground reaction force accelerates the centre of gravity towards the unsupported side, thus a medially directed force is expected throughout most of the stance phase as shown by the NP cohort in Figure 5.25.

For visit 1, the waveform by the TKR subject deviates from the expected pattern. From loading response to late mid stance, the lateral GRF has greater magnitude than the normal range expected which may be attributed to a compensation mechanism causing the patient to move their centre of mass laterally, increasing the component of their GRF in the frontal plane. The force does not become directed medially until midway through the stance phase indicating possible loading on the lateral side of the knee joint. The characteristic double peak of the waveform takes place in half the expected duration period. This may be a result of a compensatory mechanism to reduce the duration of medial compartment loading in the knee, where OA is often more prevalent. The magnitudes of the peaks are within the lower limits of the normal

range. The magnitude of the lateral force acting just before toe off is larger than for the NP cohort.

For visit 2, the pattern of the waveform is more similar to the NP cohort as the patient is loading the medial compartment of their knee for the duration of the stance phase. However, the first and second peaks occur before those in the NP cohort and the TKR subject spends less time in stance than the NP cohort. The magnitude of the first peak is not within the normal range and the magnitude of the trough between the two peaks is less than the normal range. This may be an indication that the patient is conscious of instability and thus is reducing movement of their centre of mass (COM) in the frontal plane to reduce the medial-lateral forces.

The waveform for visit three has the same pattern to the waveform from visit 2, but the magnitude of the force has increased. The first peak force is still below the normal range. The duration of the stance phase has increased and is now within the normal range.

The pattern of the waveform for visit 4 is similar to visit three but the magnitude has increased so that both peaks are within the normal range. The force measured in the trough between the two peaks has increased further but it is still below the normal range. This is the main distinguishing difference between the TKR subject and NP cohort. At this point in the stance phase the COM is moving over the supporting leg. The TKR subject is medially loading their knee to a lesser extent than the NP cohorts at this time. This may be due to the TKR subject maintaining old habits or due to the geometry of the TKR modifying the patient's knee posture.

The principal component (MLFAPC1) used in the classification represents the first medial-lateral peak of the waveform. This would detect the large difference in visit 1 to the subsequent visits. However, it does not describe the trough between the two peaks or the magnitude of the second peak which may be important factors for consideration.

5.4.5.2 Flexion moment waveforms (stair descent)

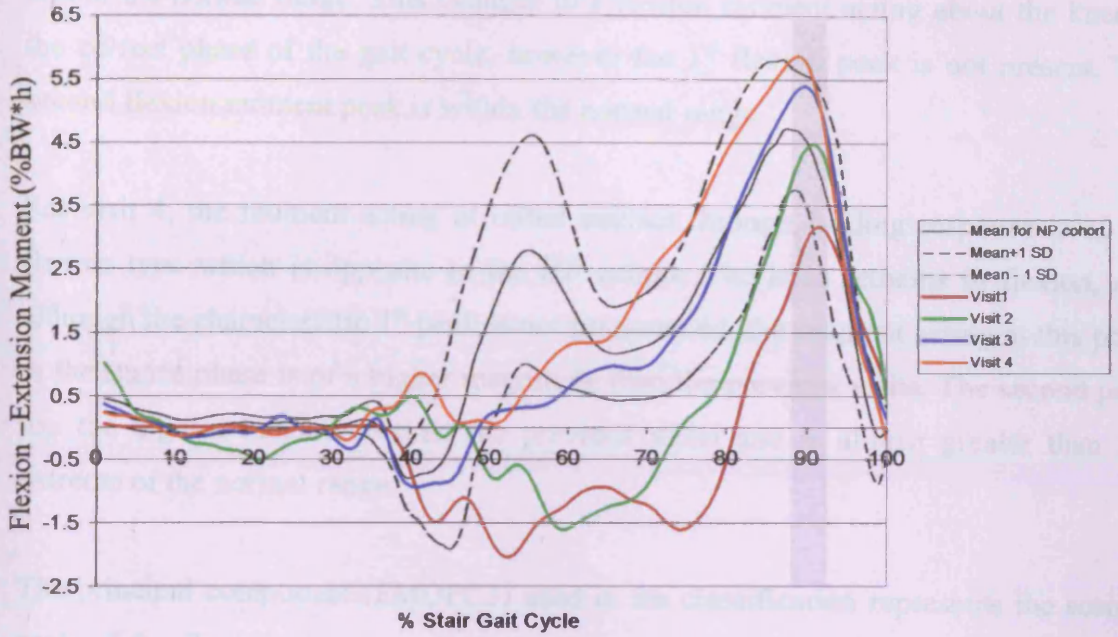

Figure 5.26 Flexion moment waveforms during stair descent for the four visits from the TKR subject. The mean of the NP sample is indicated by a solid black line where the dashed line indicates ± one standard deviation. The FMDPC3 is highlighted by the grey shaded area.

The sagittal plane moment acting about the knee joint centre during stair descent initially acts to extend the knee during loading response and progresses to flex the knee indicated by a positive double peak. The first flexion moment peak has a smaller magnitude than the second.

For visit 1, the TKR subject exhibits an uncharacteristic extension moment acting about the knee until late terminal stance. This may reflect the patients' attempts to adjust their centre of mass and is also an indication that their muscles are functioning abnormally. The magnitude of the flexion moment peak acting at 90% stair gait cycle is below the normal range.

For visit 2, the first flexion moment peak is non-existent. Instead, an extension moment acts until terminal stance. The magnitude of the second peak is within the normal range.

For visit 3, the TKR subject initially experiences an external moment of magnitude within the normal range. This changes to a flexion moment acting about the knee at the correct phase of the gait cycle, however the 1st flexion peak is not present. The second flexion moment peak is within the normal range.

For visit 4, the moment acting at initial contact through loading response is of the flexion type which is opposite to the NP cohort. The knee remains in flexion, and although the characteristic 1st peak is not pronounced, the moment acting at this point in the stance phase is of a higher magnitude than the previous visits. The second peak has the highest magnitude than the previous visits and is almost greater than the extreme of the normal range.

The principal component (FMDPC3) used in the classification represents the second peak of the flexion moment waveform. With each visit the magnitude of this peak progressively increases. There are also notable differences between the visits for the initial external moment and first flexion moment peak which are not represented in the classification. These may also be important considerations for the classification of TKR function.

5.4.5.3 Flexion moment waveforms (stair ascent)

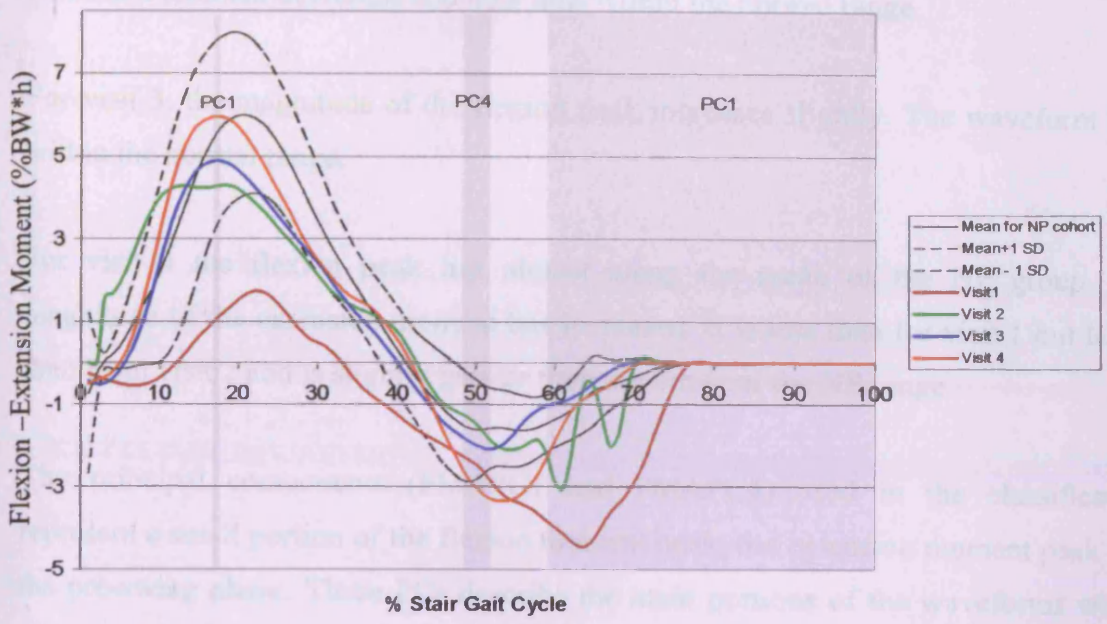

Figure 5.27 Flexion moment waveforms during stair ascent for the four visits from the TKR subject. The mean of the NP sample is indicated by a solid black line where the dashed line indicates ± one standard deviation. FMAPC1and 4 are labelled and highlighted by the grey shaded area.

The sagittal plane moments acting about the knee during stair ascent act to flex the knee from initial contact until mid stance and then acts to extend the knee until the end of terminal stance.

For visit 1, the waveform from the TKR patient follows the correct pattern, however the magnitude of the flexion peak is below the normal range and the extension moment is larger than the normal range. The extension moment begins earlier and peaks later than the NP cohort. This indicates that at the start of stance phase the subject may be leaning forward. Moving the COM in front of the supporting leg, moves the GRF vector closer to the knee joint, thus reducing flexion moment. At the end of the stance phase the GRF is acting posterior to the knee joint to produce an extension moment about the knee. The TKR subject may be flexing their knee to a larger extent than the NP group or moving their COM to produce a larger moment arm resulting in a larger extension moment.

For visit 2 the magnitude of the flexion peak increases to within the NP range. The extension moment decreases and now falls within the normal range.

For visit 3, the magnitude of the flexion peak increases slightly. The waveform falls within the normal range.

For visit 4 the flexion peak lies almost along the mean of the NP group. The magnitude of the extension moment has increased. It is less than for visit 1 but larger than from visit 2 and is slightly greater than the limits of the NP range.

The principal components (FMAPC1 and FMAPC4) used in the classification represent a small portion of the flexion moment peak, the extension moment peak and the pre-swing phase. These PCs describe the main portions of the waveforms where the main differences between the visits occur. However it may be useful to represent a larger portion of the flexion moment in future investigations.

5.4.5.4 Adduction moment waveforms (stair ascent)

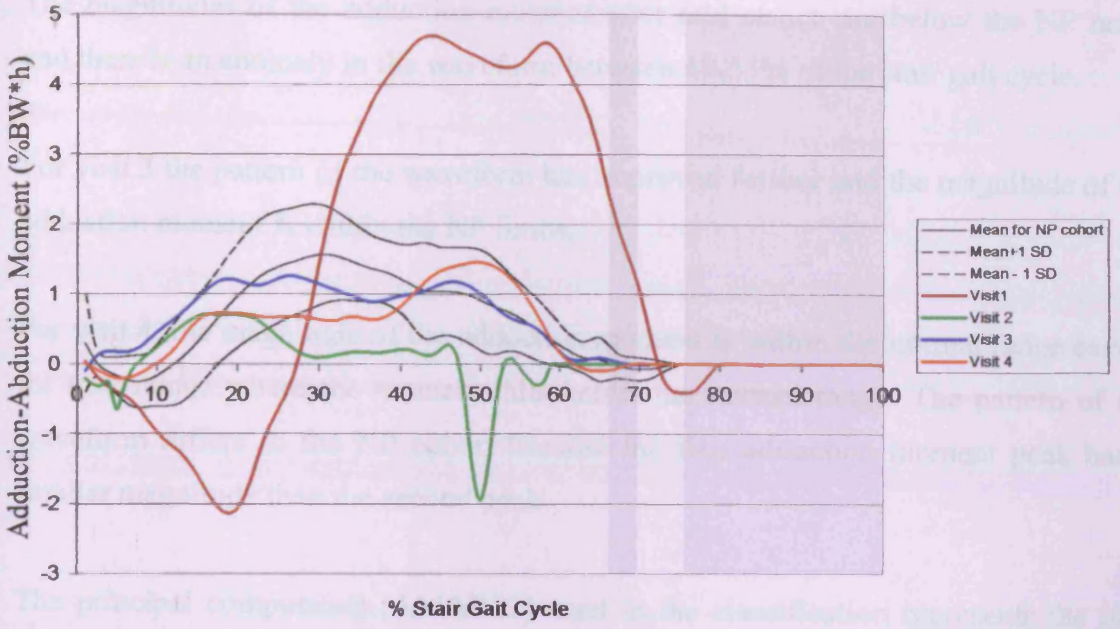

Figure 5.28 Adduction moment waveforms during stair ascent for the four visits from the TKR subject. The mean of the NP sample is indicated by a solid black line where the dashed line indicates ± one standard deviation. The AMAPC2 is highlighted by the grey shaded areas.

For the NP cohort, the frontal plane moment acting about the knee during stair ascent initially acts to abduct the knee during loading response phase as the medial-lateral GRF acts laterally to the knee joint centre. As the GRF moves medial to the knee joint centre, the moment then acts to adduct the knee for the majority of the stance phase.

For visit 1, there is a large abduction moment acting until mid stance as a result of the large lateral force exhibited in the Medial-Lateral force waveform. A large adduction moment acts for the remainder of the stance phase. The medial force acting is smaller than the NP group, thus the adduction moment must be a result of a mechanism which increases the moment arm (perpendicular distance between the medial-lateral force vector and knee joint centre). This could be attributed to the geometry of the knee joint affecting the knee alignment, or from the patient leaning their trunk to move their centre of mass in the frontal plane. The magnitudes of the moments are far greater than the limits of the NP cohort and the duration of the stance phase is longer.

For visit 2, the pattern of the waveform looks more characteristic of the NP group. The magnitudes of the adduction moment after mid stance are below the NP range and there is an anomaly in the waveform between 48-55% of the stair gait cycle.

For visit 3 the pattern of the waveform has improved further and the magnitude of the adduction moment is within the NP limits.

For visit 4, the magnitude of the adduction moment is within the normal range except for mid stance where the moment falls below the normal range. The pattern of the waveform differs to the NP cohort because the first adduction moment peak has a smaller magnitude than the second peak.

The principal components (AMAPC2) used in the classification represents the pre-swing and swing phase of the gait cycle. This appears to only highlight the differences between the TKR waveform for visit 1 and the NP waveforms. In future it is suggested that for the analysis of TKR recovery, PCs representing more characteristic portions of the cycle should be used, e.g. peak adduction moment where differences between all visits are evident.

5.4.5.5 Summary of waveform analysis

Through the waveform analysis it has become evident that a large improvement was made following visit 1 in terms of the pattern and magnitude of the waveforms. There are small differences between the waveforms for visits 2-4. To allow a comparison with the classification output, the portions of the waveform represented by the PCs used as input variables should be considered. For MLFAPC1, a large improvement in the direction and magnitude of the MLF was made after visit 1. The magnitude increased by small amounts for each of the remaining 3 visits. For FMDPC3, the magnitude of the flexion moment increases with each visit. Visit 2 and 3 are within the NP range. For visit 4, the magnitude is slightly greater than the normal range. For FMAPC1 and FMAPC4, the magnitude of the flexion moment increases with each visit. The magnitude of the extension magnitude improves for visit 2 and 3 and increases just beyond the NP range for visit 4. The AMAPC2 input distinguishes between visit 1, (where the stance phase is extended and the magnitude of the

adduction moment is higher than the NP range) and the other three visits. However, although this PC was determined to be important form the cohort of OA and NP subjects, the ability to distinguish between the 4 visits is questionable as it does not describe a large portion of the stance phase where the adduction moment is computed.

From the waveform analysis, it can be seen that as with the DS classification output there is a large increase in ability following visit 1. This is when all the waveforms begin to replicate the normal patterns. The waveforms show progressive improvements for visits 2 and 3. They improve yet again at visit 4, however there are some regions where the magnitudes of the waveforms described by FMDPC3, FMAPC1 and FMAPC4, lie outside of the NP range.

Thus the waveform analysis aids the explanation of the classification output. The patient's function improves greatly from visit 1 to 2. From visit 2 to 3, the function increases further by a small amount. From visit 3 to 4, the function improves for two of the waveforms but there are portions of the remaining two waveforms which lie outside the NP limits. This introduces a level of uncertainty to the final diagnosis and thus is given a slightly worse classification than from visit 3, as demonstrated by the classification output.

5.5 DISCUSSION

From this investigation, it is evident that functional variables from stair gait can be used to characterise OA knee function and are worth further investigation.

People with knee OA have pain, joint stiffness, decreased ROM, muscle strength, endurance and poor general mobility. The patients with knee OA adapted their stair gait to produce pain relief from dynamic joint loading. Five potentially important indicators of knee OA were identified through unpaired independent *t*-tests of discrete kinematic and kinetic measures from the NP and OA cohorts. For stair ascent, peak medial GRF, peak flexion and adduction moment were important indicators. For stair descent, peak vertical GRF and peak flexion moment were important.

For stair ascent, the difference in peak medial-lateral GRF between the OA and NP cohorts was statistically significant. During the stance phase the GRF accelerates the centre of gravity medially and the joint reaction force shifts from the medial to the lateral tibial plateau. When the force reaches its peak value, it is sustained mainly by the medial plateau. The OA group adapted their gait to reduce the GRF in the frontal plane, providing pain relief from the dynamic joint loading.

Adduction moments are produced when the GRF vector passes medial to the knee joint centre. The abduction-adduction moments play an important role at the knee, providing propulsion and mediolateral stability, (Kowalk *et al.*, 1996). Kaufman *et al.*, (2001) measured a lower adduction moment for a OA cohort compared to a NP cohort, though the results were not statistically significant. In this study a statistically larger adduction moment was produced by the OA group and there was a large variability within the group indicated by a large standard deviation. One OA subject exhibited a large adduction moment compared to the other patients. The affected knee for this patient is highly adducted as shown in Figure 5.29. During stair ascent this individual moves their trunk from side to side, inclining laterally over the supporting leg during the stance phase of stair ascent. The movement of the trunk increases the forces measured. The knee is adducted which means the resultant GRF vector acting from the centre of pressure (COP) passes medial to the knee joint centre (KJC) resulting in a large fontal plane moment.

Figure 5.29 Video camera image of patient producing large adduction moment. The estimated KJC and COP are identified.

Subjects with OA exhibited significantly lower peak external flexor moments during stair ascent. External flexor moments acting at the knee are counteracted by internal extensor moments. Thus, this result represents the contribution of knee extensor muscles. From single leg support to mid swing of the contra-lateral leg, extensor muscle activity at the knee generates the majority of the energy required to progress the subject from one step to the next (McFadyen *et al.*, 1988). The pull-up phase of stair gait is due to knee extensor activity about the knee and unlike level gait (Winter, 1983) here it is the knee which generated most of the energy. The greatest point of instability is at toe-off when the total body weight is given to the opposite limb while all three joints are flexed (McFadyen *et al.*, 1988).

Walking down stairs is achieved through eccentric contractions to control the force due to gravity (McFadyen *et al.*, 1988). The body has to be arrested from what may be considered as a 'free fall' after leaving one step and before landing on the next. The knee extensors and ankle plantar flexors are involved in significant energy absorption. During stair descent the OA cohort had a significantly lower peak flexion moment and significantly lower vertical GRF component.

The extensors are important during stair gait, and they act at the stage of the cycle where significant progression occurs (i.e. during pull up and controlled lowering). A large patellar reaction force is produced at points of maximum knee flexion during stair negotiation. This gives rise to pain on stair gait in many patients with OA.

Patients compensate for pain by altering their gait pattern using a compensation strategy such as adopting a different trunk attitude to adjust the position of their centre of mass, to reduce knee flexion moments and using quadriceps avoidance mechanisms. This explains the significantly lower result for the flexion moment during stair ascent and descent for the OA cohort.

The OA group use compensatory mechanisms to reduce the moments about the knee joint. This may be indicative of muscle weakness due to their condition. The action of reducing moments acting about the joint minimises knee joint loading. This in agreement with the reduced internal knee extensor moment reported by Kaufman *et al.*, (2001) reflecting the patients compensation to reduce the knee joint loading.

Instead of using the discrete values used in the *t*-tests in the DS classifier, principal component analysis (PCA) was performed on each of the significant waveforms to represent the waveform whilst retaining temporal information. One disadvantage to this is that the moment and GRF waveforms were represented over the gait cycle so that any differences in timing of the events of the cycle could be compared in the waveform analysis. However some PCs represent the swing phase where no moments or forces can be computed using the current protocol. In future study, it may be beneficial to represent the stance phase only.

Using all the retained PC's of the waveforms for these functional variables, the classifier was able to classify OA and NP knee function of 15 subjects with 86.67% out-of sample accuracy. Selecting the top 5 ranked PCs from this classification, the DS classifier was able to correctly classify subjects with 100% out-of-sample-accuracy determined by a Leave-one-out cross-validation.

Three of these PCs were related to the Flexion moment during ascent and descent. The remaining two are related to the adduction moment and GRF acting in the frontal plane during ascent. These variables were able to quantify TKR recovery in agreement with the waveform analysis. The correlation with the indices from the classification with two quality of life scores was tested. A significant correlation was found between the $m_c(\{OA\})$ and KOS score, $m_c(\{OA\})$ and OKS outcome and the $m_c(\{NP\})$ and KOS. No significant correlation was determined between KOS and

OKS or between $m_c(\{NP\})$ and OKS. The classification output for the TKR sample (Figure 5.24) shows a large improvement between their assessment visits 1 and 2. The patients' knee function continues to improve slightly between visits 2 and 3. Between visits 3 and 4, the patients' knee function appears to diminish by a small amount due to a higher level of uncertainty in the classification.

Determining optimum functional parameters for use in the comparison of NP and OA knee function is important for monitoring OA progression, selecting the most appropriate treatment method and for monitoring recovery following surgical intervention. The variables identified through these analyses are potentially important in the assessment of OA knee function and their use with the DS classifier is worth further investigation. It is suggested that further work should be undertaken to investigate a DS classifier that uses data collected from both level gait and stair gait.

5.5.1 Difficulties of assessing OA stair gait:

It appeared that descending stairs was a more difficult activity for the OA patients. The variation in stair climbing techniques limited the numbers in our cohorts. This study was restricted to subjects who could perform stair ascent and descent in a reciprocating manner (i.e. where both feet are never in contact with the same step). Also, patients who relied heavily on the handrail were discounted as this affects the GRF readings and moment calculations.

It is important to investigate the different climbing techniques before recommending variables to strengthen the existing classifier. Common alternative stair gait styles included stepping onto one step at a time, descending the stairs backwards, always beginning the cycle on the same foot. Some patients avoided the stairs at home due to the high step rise, although felt more comfortable using the staircase in the laboratory. Some patients had handrails installed both sides of their home stairs so they could pull themselves up the stairs. One patient reported descending the stairs on their posterior. With these differences in stair gait patterns, future work must be driven to determine a common factor that can be used in the classifier. This will involve characterising stair gait into their various approaches. For example, Lark *et al.*, (2003) found that older people have a characteristically different approach to stepping down and spend a

longer time with their supporting foot flat on the step and the knee flexed before rising onto their toes prior to the free falling downward movement. If the approaches to stair gait can be characterised then the various groups can be compared to determine the reason for them using a particular stair gait pattern.

A new test was introduced to the protocol for patients who could not progress with the standard stair gait tests. This involved stepping up onto the first step of the staircase, turning and stepping back onto the floor. This would allow important force and moment information to be computed during loading response and at terminal stance. This requires further analysis and from the findings from this initial investigation, it is suggested that flexion moment and frontal plane kinetic measures are considered as important indicators of knee OA.

Even for the subjects performing stair gait in the same manner, there is still the potential for several variations in the way that each individual ascends stairs due to them compensating for a reduced ROM of the affected joint. For this reason, the quantification of hip and ankle joint ROM would also be beneficial.

It may also be important in future studies to determine whether there is a link between BMI and the ability to perform stair gait. Kaufman *et al.*, (2001) reported that level gait patterns of subjects with OA knee function and a high BMI, deviated further from normal than those with a low BMI. This may be due to a worse level of OA than those with a lower BMI, or there may be other related compensatory factors. An increase in BMI leads to an increase in knee joint loading and so it can be hypothesised that the activity would be more difficult for those with a high BMI. If this is the case, it is important to determine variables that can be achieved by all patients that replicate a stair gait activity and perhaps include BMI as a variable in the classification of stair gait.

This preliminary study could have looked at lots of areas. In future studies this work could be expanded to investigate different stair climbing strategies and the effect of additional variables such as BMI and velocity in the classification of stair climbing. It would be desirable to incorporate salient variables from stair gait and level gait in the classification of knee function.

CHAPTER 6
KINEMATIC ERROR ASSESSMENT USING FLUOROSCOPIC ANALYSIS

The DS classification method uses motion analysis (MA) data to characterise a subject's joint function. The method has a superior accuracy to Artificial Neural Networks and Linear Discriminant Analysis when characterising knee function during level gait, (Jones, 2004). As with all methods of interpreting MA data, its ability to characterise function in a clinically useful way is dependent on the quality of the MA input data. It is important that the input variables accurately describe the joint biomechanics for it to be useful in a clinical setting to monitor joint degeneration and evaluate treatment methods. For further development of the classifier, the errors in MA data specific to the Cardiff protocol need to be quantified. This chapter outlines the development of a protocol to assess the kinematic errors associated with using passive marker motion analysis as a data collection method for the assessment of non-pathological (NP) knee and total knee replacement (TKR) function. Preliminary results of the kinematic errors for 5 NP knees and 5 knees with TKR recorded during a step up/down activity are presented and discussed. This work was presented at two conferences, Whatling *et al.*, (2008d) and Whatling *et al.*, (2008e).

Errors in kinematic data are inherent with motion analysis. Imprecision in kinematic data is caused by soft tissue artefacts (STA) which is the relative movement between markers and bone. Inaccuracies in the rotational measurement of the knee joint can be in the order of 10 to 100% (Cappozzo *et al.*, 1996). The DS classifier deals with ignorance inherent with the decision making process in terms of uncertainty. However it does not currently account for errors in the input data. This could be achieved by applying a weighting to each of the input variables so that those with a high level of inaccuracy are relied on less than those with high accuracy during the decision making process. If the classifier is to be developed in this way, an appreciation of the errors due to skin movement artefacts and the reconstruction of marker coordinates must be quantified and subsequently integrated into the classifier.

6.1 LITERATURE REVIEW

6.1.1 Inaccuracies in motion analysis data

It is a great challenge to obtain accurate movement data non-invasively. The Cardiff protocol employs the most widely accepted non-invasive method to generate in-vivo knee kinematic data. This uses infra-red cameras (optoelectronic stereo-photogrammetry), skin mounted markers and a pointer. Despite its wide usage, in clinical research this method of motion analysis (MA) is limited by experimental errors, (Della Croce, 2006).

Chapter 1 introduced three main sources of error in the procedure for collecting MA data. These are instrumental errors (Chiari *et al.*, 2005) which represent the errors with which marker coordinates are reconstructed in a global frame, errors in determining bony landmarks during the anatomical calibration (Della Croce *et al.*, 2005) and errors due to soft tissue artefact (STA). STA is the largest and most critical source of error in human movement analysis using optoelectronic stereo-photogrammetry (Andriacchi and Alexander, 2000; Leardini *et al.*, 2005a). During MA, markers attached to the skin are assumed to be rigidly associated with the underlying bone and are used to define segmental axis systems and track the movement of each segment. This assumption is incorrect as they do not have a rigid association and the position and orientation of the marker clusters are not the same as the underlying bone. STA results from the movement of skin mounted markers relative to the underlying bone and is associated with the interposition of both passive and active soft tissues. Inertial effects, skin deformation, sliding, gravity and muscle contraction all independently contribute to STA. For these reasons, STA is subject, task and marker set specific (Stagni *et al.*, 2005).

Knee kinematics obtained via surface mounted markers have a large error component due to skin movement relative to the underlying bone, especially in the out of plane directions (knee adduction-abduction and internal-external rotation). These make the estimation of small but clinically relevant angular and linear joint movements critical and prevent the use of MA to reliably assess innovative prosthesis features and clinical outcome.

The Cardiff protocol limits STA errors by using plate mounted markers to define individual body segments. This method of marker placement has a smaller STA than individual unconstrained markers mounted directly onto the skin (Angeloni *et al.*, 1992; Cappello *et al.*, 1997; Manal *et al.*, 2000). The markers are positioned on the mid portion of the thigh and shank and far from joint axes. These positions minimise movement artefacts (Cappozzo *et al.*, 1996). The largest errors occur when markers are attached to the skin in the vicinity of joints and it is recommended not to position markers in the top portion of the thigh where a thick layer of less tonic soft tissue is present which is more prone to inertial and gravitational effects than surrounding areas (Stagni *et al.*, 2005).

Research is required to understand and quantify skin movement so that the error due to the acquisition methods in measuring real bone movement can be assessed. Only once this error is accurately quantified can steps be taken towards correcting the data and acquisition methods. Quantification of STA is necessary in order to improve the reliability of MA results, improve clinical decision processes and to develop methods for STA compensation to improve bone pose accuracy. Several methods of assessment, minimisation and compensation have been reported and are summarised in Leardini *et al.*, (2005a).

Methods of assessing STA include tracking the bone using markers attached to external fracture fixation devices (Angeloni *et al.*, 1992; Cappozzo *et al.*, 1996), intra cortical pins (Cole *et al.*, 1993; Fuller *et al.*, 1997; Karlsson and Lundberg, 1994; Lafortune and Lake, 1991; Lafortune et al., 1992; Yack *et al.*, 2000) or percutaneous trackers (Holden *et al.*, 1997; Manal *et al.*, 2000; Manal *et al.*, 2002).

Techniques based on Roentgen photogrammetry are also used, where small tantalum markers attached to the skin (Sati *et al.*, 1996) or implanted in bone (Imai *et al.*, 2003; Nilsson *et al.*, 1991; Papaioannou *et al.*, 2008) are tracked radiographically.

Each of these methods can be used to directly track the movement of the underlying bone, allowing for the measurement of skin movement. These methods can also be used as a gold standard from which to compare measurements computed using MA. It is important to recognise the limitations of each method. Intracortical pins, external

fixatators and percutaneous trackers provide a reliable measurement of bony segment motion but they limit and alter skin motion. Methods exploiting Roentgen photogrammetry such as X-ray fluoroscopy do not limit skin motion but have a limited field of view and do not usually allow full 3D tracking of markers. The wide range of techniques, their limitations and the different motor tasks analysed lead to discrepancies in the magnitude of STA reported in the literature.

Studies assessing the effect of STA on knee rotations have found that estimating knee joint kinematics during walking using clusters of markers made of skin markers may be affected by inaccuracies of 10% flexion-extension, 50% adduction-abduction and 100% internal-external movement range angles. Also, markers located directly on the skin above anatomical landmarks at positions where they experience lowest joint angular displacement experience movement in the range of 10-30mm during gait and are thus unsuitable positions for marker placement (Cappozzo *et al.*, 1996).

In a study of simultaneous fluoroscopy and sterophotogrammetry, Stagni *et al.*, (2005) quantified STA artefact for a grid of retro-reflective markers attached to the thigh and shank and determined how STA propagates to knee joint angles during a selection of daily living activities. The measurement of flexion-extension at the knee by means of external markers was considered acceptably reliable. The adduction-abduction and internal-external rotations angles were the most affected by soft tissue artefact propagation, with root mean square errors (between knee rotations evaluated from skin markers and 3D fluoroscopy) of up to 192% and 117% of the corresponding range. These errors can nullify the usefulness of these variables in the clinical interpretation of gait analysis.

Large STA does not necessarily produce large propagated error on knee rotations, and the error in the kinematics is dependent on the marker set used, the patient and motor task under investigation. This aim of this study is not to measure the movement of the skin relative to the underlying bone but to determine the effect of the propagation of the STA and other sources of error associated with the Cardiff protocol in the measurement of knee rotations. This is required to determine the reliability of the MA data used with the DS classifier. The clinical trial at Cardiff monitors patient knee OA and TKR function over time and in the future aims to compare outcomes from

rotating and fixed TKR designs. It is therefore important that small changes in kinematic data can be identified and not concealed due to a large range of error in the measurements. It is important that the errors associated with the protocol are quantified for the assessment of natural knee and TKR kinematics. This will determine whether the error is different for the two main cohorts investigated in the clinical knee trial. Once the range of error currently associated with the Cardiff protocol is quantified, either a patient specific compensatory technique can be implemented during the computation of knee kinematics (Leardini *et al.*, 2005a), or alternatively, the classifier can be further developed to apply less weighting on unreliable data when characterising a patients knee function.

6.1.2 Fluoroscopy studies to assess knee function

The approach used to quantify the kinematic errors associated with the Cardiff protocol was to compare knee kinematics computed using the Cardiff protocol to those computed using a more accurate method which measures kinematics directly from the movement of the tibia and femur. The current study developed a fluoroscopy based image registration method to accurately measure knee kinematics. Image registration techniques have been used extensively to more accurately measure knee joint kinematics (Banks and Hodge., 1996; Fantozzi *et al.*, 2003; Komistek *et al.*, 2003; Stiehl *et al.*, 2001). The process involves registering three-dimensional (3D) bone models or 3D computer-aided design (CAD) implant models to a series of 2D fluoroscopic images.

This is used as a gold standard to which kinematics computed using the Cardiff protocol is compared. The alternative invasive approaches used for comparison involve direct attachment to the bone and could not be considered with patients with TKR due to the risk of infection and due to ethical approval. Dynamic fluoroscopy was chosen for its accessibility and relatively low dose compared with normal X-rays.

X-ray fluoroscopy and shape matching techniques have been successfully used to assess TKR kinematics during a range of daily activities including knee flexion, stair climbing and level gait. It is becoming a widely used diagnostic technique used to compare kinematics and perform contact analyses on different TKR options.

Recently, these techniques have been applied to measure motion in joints without metallic implants. Table 6.1 summarises selected studies to show a range of applications employing X-ray fluoroscopy and image registration techniques.

Fluoroscopy uses low dose X-rays and produces a live image feed which is displayed on a screen. A sequence of X-ray images can be collected during the execution of a specific dynamic task. High-density metallic TKR components appear very dark on fluoroscopic image, providing a clear outline of the implant features. Fluoroscopic images of natural knees have been used for image registration, though cortical bone edges are less well defined than are metallic implant edges (You *et al.*, 2001) and it is important to use optimum image settings to obtain clear images for the matching process.

The method of Banks and Hodge, (1996) is used in this study. This is an established method for computing 3D kinematics of a known object from a single view. A series of fluoroscopy images are imported into the software called KneeTrack (S. A. Banks, USA), as well as 3D models of the surface geometry of either bone or prosthesis components. A canny edge detector identifies contours of the artificial or bony edges of the joint on the fluoroscopic image. The position and orientation of the models are aligned manually to the fluoroscopic images and then an automated matching algorithm is used to align the model to each of the images. The software computes the joint rotations as the movement of the tibia relative to the femur and translations of the femur along its embedded axis. It also computes the tibiofemoral contact positions for each pose and the location of the joints centre of rotation.

The method of banks has been reported to measure TKR rotations accurately to approximately $\pm$ 1° and sagittal plane translations within approximately $\pm$ 0.5mm, determined using controlled mechanical tests. Accuracy tests were replicated by Stagni *et al.*, (2005). The relative pose of femoral and tibial components fixed in bone cement was estimated using the method of Banks and Hodge, (1996). This was compared to the pose determined using a 3D digitizer (MicroScribe 3D x 3D Digitizer, Immersion, San Jose, CA, USE), with nominal accuracy of 0.2mm. 30000 coordinates of the femoral and 23000 points of the tibial component surfaces were collected. Using the Iterative closest point technique (Besl and McKay, 1992) the

digitized points and prosthesis component CAD model was registered. The relative pose between the two registered CAD models was calculated. The accuracy with which the relative orientation and position of the components can be estimated using the KneeTrack software was computed as better than 1.5° and 1.5mm respectively.

The registration process requires 3D models of the healthy knee or TKR components. CAD models of the TKR components can be obtained from the implant manufacturer. However for knees without metallic implants 3D surface models of the bones must be created from image data. The models can be derived from Computed tomography (CT) or Magnetic resonance imaging (MRI). CT scan data is routinely used to create geometric bone models due to its high quality bone contrast and grey scale usage to give material properties.

Shape matching of bone models derived from CT data has been found to be highly accurate to within 1° rotation and 1mm in-plane translations (Rahman *et al.*, 2003). Although the exterior borders of the bones are less well defined than those of metallic implants, the bones possess interior contours that show up well on fluoroscopic images. However, the high dose of ionising radiation makes an alternative imaging modality highly desirable. The use of non-invasive MRI would be favorable and more widely used if high quality bone models could be produced. MRI is non-invasive and, although geometric field distortion and poor bone contrast degrades model fidelity compared to CT, the models can be used to provide sufficient accuracy in the assessment of knee motions from single plane X-ray (Moro-oka *et al.*, 2007).

Generating models derived from MRI rather than CT scan data would improve shape matching protocols by reducing total radiation exposure of the subject. Another benefit to using MRI is the ability to include cartilage to the models which is useful for contact and stress analysis studies. DeFrate *et al.*, (2004) demonstrates the inclusion of articular cartilage geometry to MRI-based bone models to quantify tibiofemoral contact. MRI scans were acquired using a fast image employing steady-state acquisition (FIESTA) sequence. The MRI scans had a resolution of 512 x 512 pixels and the images were spaced 0.7mm apart.

Table 6.1 A summary of the applications of fluoroscopic analysis used by selected studies

Application	Studies
Investigations of TKR kinematics during knee bends and squatting to standing position	Stiehl *et al.*, 1995; Dennis *et al.*, 1996; Stiehl *et al.*, 1997; Dennis *et al.*, 1998a; Dennis *et al.*, 1998b; Hoff *et al.*, 1998; Komistek *et al.*, 1998; Komistek *et al.*, 2000; Oakeshott *et al.*, 2003; Kanekasu *et al.*, 2004; Watanabe *et al.*, 2004; Argenson *et al.*, 2005; Yamazaki *et al.*, 2005; Yoshiya *et al.*, 2005; Delport *et al.*, 2006; van Duren *et al.*, 2007; Cates *et al.*, 2008; Chouteau *et al.*, 2008; Tamaki *et al.*, 2008; Liu *et al.*, 2009;
Investigations of TKR kinematics during normal/treadmill gait	Banks *et al.*, 1997a; Stiehl *et al.*, 1999; Schmidt *et al.*, 2003; Banks and Hodge, 2004; Sugita *et al.*, 2005; Zihlmann *et al.*, 2006; Hamai *et al.*, 2008
Investigations of TKR kinematics during stair gait or step up/down activity	Banks *et al.*, 1997b; Fantozzi *et al.*, 2003; Banks and Hodge, 2004
Investigations of non-pathological/ACL deficient and reconstructed knees/ natural knees with medial unicompartmental OA	Komistek *et al.*, 1999; Komistek *et al.*, 2003; Dennis *et al.*, 2005; Fregly *et al.*, 2005; Isaac *et al.*, 2005; Dennis *et al.*, 2006; Moro-oka *et al.*, 2008
Investigations of the inaccuracies associated with movement between markers and underlying bone for shank and thigh	Cappozzo *et al.*, 1996; Sati *et al.*, 1996; Stagni *et al.*, 2005
Investigations of unicompartmental replacement kinematics	Robinson *et al.*, 2002; Price *et al.*, 2004; Pandit *et al.*, 2008
Patellar tracking	Tang *et al.*, 2004
Investigations of TKR active and passive range of motion	Zuffi *et al.*, 1999
Investigation of contact kinematics and contact forces using TKR implants with instrumented tibial components.	Varadarajan *et al.*, 2008
Investigations of natural knee tibiofemoral contact analysis using MRI / TKR contact pressures	DeFrate *et al.*, 2004; Sharma *et al.*, 2007

6.2 A COMPARISION OF KNEE KINEMATICS COMPUTED USING NON-SIMULTANEOUS MARKER BASED MOTION ANALYSIS AND FLUOROSCOPIC ANALYSIS

The aim of this study was to quantify the errors in non-pathological (NP) knee and TKR kinematic measurements generated using the current Cardiff data collection method. This was achieved by comparing in-vivo knee kinematics of a dynamic weight bearing task computed using non-simultaneous passive marker- based motion analysis (the Cardiff protocol) and the more accurate fluoroscopic analysis and image registration method of Banks and Hodge, (1996). This study investigates the use of Simpleware software (Simpleware Ltd.) to produce high quality MRI derived bone models for use in the image registration procedure.

The objectives of the study were to:

(i) Gain expertise in quantifying natural knee and TKR kinematics using fluoroscopic analysis and the shape registration method of Banks and Hodge, (1996). This involves developing a data acquisition and analysis protocol at Cardiff University.

(ii) Investigate the use of magnetic resonance imaging (MRI) to produce subject-specific bone models of the knee joint for use with image registration. This involves a proof of concept study on the use of Simpleware software (Simpleware Ltd) to create effective 3D bone models for the matching procedure.

(iii) Gain an appreciation of the errors associated with measuring tibio-femoral kinematics using the Cardiff protocol. This will be achieved by comparing NP and TKR kinematics computed from the Cardiff protocol to those computed using image registration.

The steps required to compare the two methods of computing kinematics are illustrated in the flow-diagram in Figure 6.1.

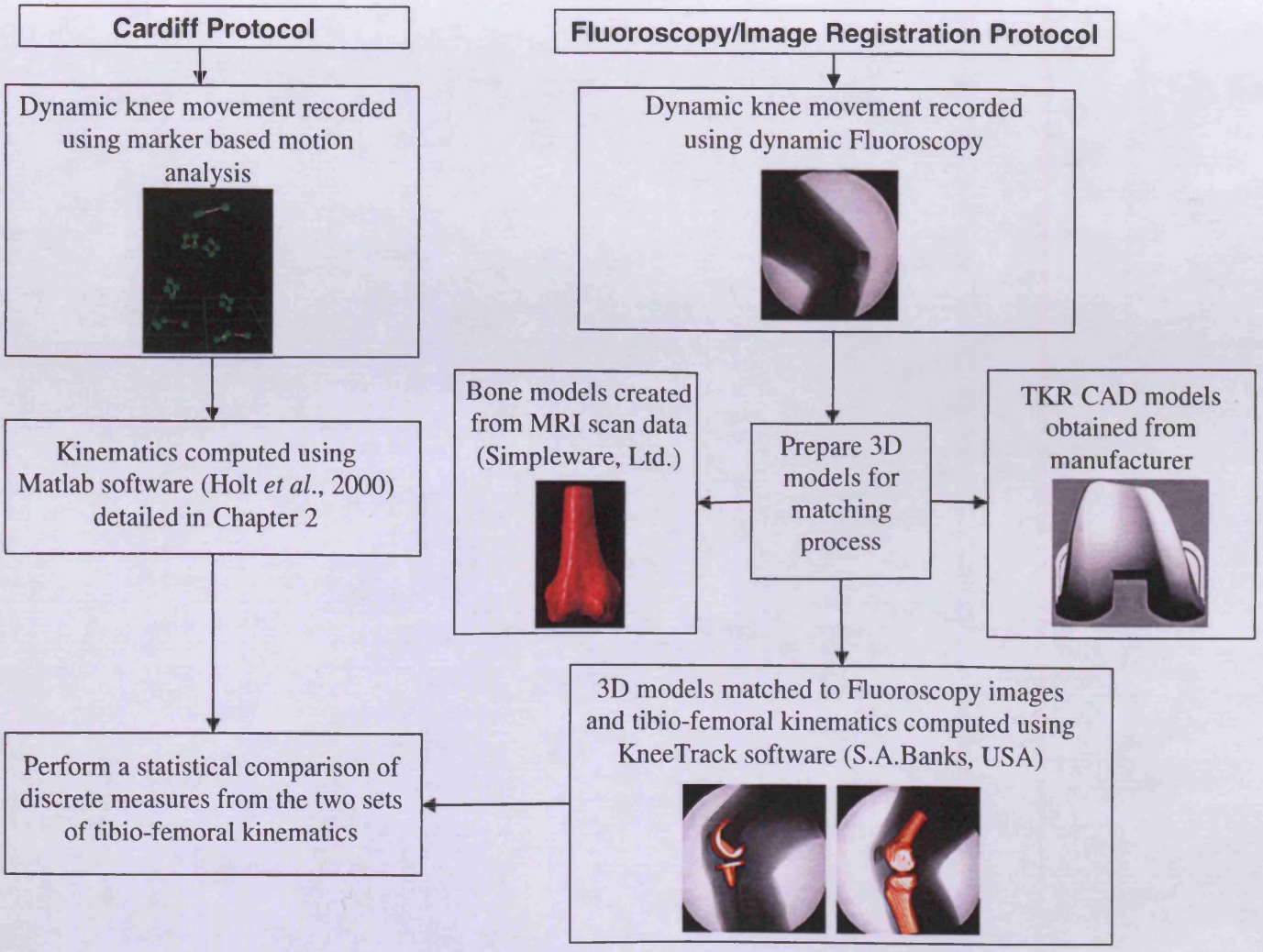

Figure 6.1 Flow diagram outlining the studies objectives

6.2.1 Subject recruitment

Five non-pathological (NP) volunteers (i.e., without history of lower limb disorder) and five subjects with a total knee replacement (TKR) were recruited for this study. The subjects with a TKR were recruited from the clinical knee trial and were tested approximately 12 months after their TKR operation. The NP cohort consisted of 1 female and 4 males with a mean age of 34.8 (± 10.28) years and mean BMI of 25.59 (± 3.35) Kg/m^2. The TKR cohort consisted of 3 females and 2 males with a mean age of 68 (± 9.86) years and mean BMI of 30 (± 3) Kg/m^2. After fully explaining the tests, informed consent was taken. Ethical approval was obtained from the South East Wales Local Research Ethics Committees. Each subject attended a session in the motion analysis laboratory and at the Radiography department at the University Hospital of Wales, to record their knee movement during a step up/down activity. A limitation to this study is the non-simultaneous measurements but this could not be overcome at the time of testing and it is something that will be rectified for future experimentation.

6.2.2 Data collection and processing using the Cardiff Protocol

Knee mechanics during activities of daily living and weight bearing are of particular interest due to their high demands on the knee. Step up/down tasks were used as the dynamic activity for this study. The Cardiff protocol was used to record six trials of the subject completing three repetitions of a step up/down task using motion analysis techniques (Figure 6.2).

Marker clusters containing four retro reflective markers were attached laterally on the thigh and shank of each subject and an anatomical calibration was undertaken using a marked pointer. 3D Motion capture was performed using 8 ProReflex MCUs (Qualisys, Sweden), capturing at 60 Hz. The step used in this study has a 16cm rise and is constructed from medium-density fibreboard (MDF). A handrail consisting of Perspex and wood is attached to the side of the step.

The same protocol was used for each measurement to maintain similar movement patterns in both the motion analysis and fluoroscopy recordings. The subject's foot

was positioned in the centre of the step and their other foot on the floor with toes touching the step as shown in Figure 6.2a. Each subject was instructed to straighten their leg to full knee extension on the step, not swinging through with the opposite leg, (Figure 6.2b), then return to the initial position. This was performed three times in a cyclic fashion to reduce the measurement duration. This was important for the fluoroscopy measurements to reduce the total radiation exposure of the volunteer.

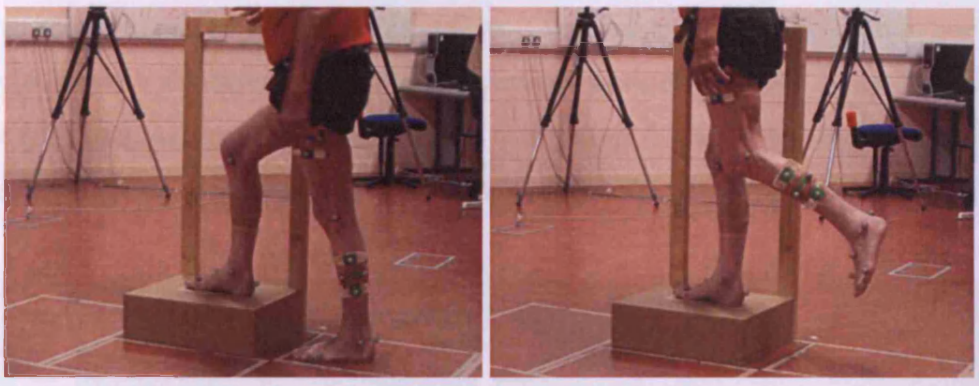

(a) (b)

Figure 6.2 Step up/down task recorded using motion analysis (Qualisys, Sweden)

Ground reaction forces (GRFs) were not considered in this study, however six additional recordings of each step up/down task was recorded with the step mounted on an MDF panel to measure simultaneous motion data and GRFs, which can be used in future analysis to investigate joint contact forces and perform stress analyses.

Kinematics from the motion analysis data were computed according to the Grood and Suntay Joint Coordinate system using in house software (Matlab Version 7.1, Mathworks, Inc) developed by Holt *et al.*, (2000). This procedure is as outlined in Chapter 2.

6.2.3 Data collection using dynamic fluoroscopy

The same tests were repeated using the same step to record knee movement using dynamic fluoroscopy (Philips).

6.2.3.1 Calibration

Prior to recording knee movement, the C-arm was moved into the position shown in Figure 6.3a with the X-ray couch in the vertical position and the table height at its lowest position. An image was taken of a calibration frame and this is used for post processing to correct all subsequent images for geometrical distortion.

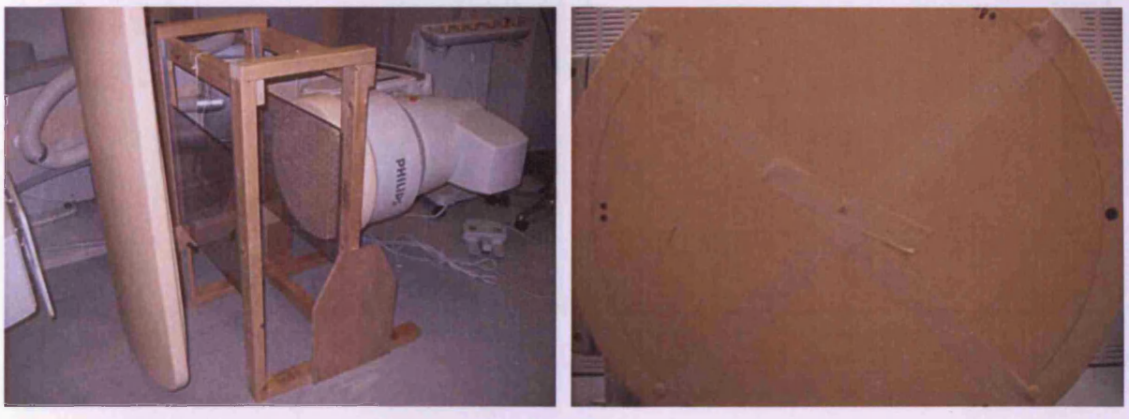

(a) (b)

Figure 6.3 (a) C-arm position and calibration frame; (b) Defining the centre of the intensifier

The calibration frame consists of two Perspex panels of dimensions (450mm x 450mm) positioned precisely 30cm apart. Each panel has a specific purpose in determining the optical geometry of the fluoroscopy system. The panel positioned closest to the image intensifier consists of a square array containing 17 x 17, 2mm diameter steel ball bearings spaced 25mm apart, (Figure 6.4a). The centre of the grid is easily identified by an additional four ball bearings forming a square around the central ball bearing. This grid is used for correcting image distortion. The second panel consists of a star array of ball bearings 25mm apart in a stair configuration, (Figure 6.4b). This is used to determine the position of the camera focus.

For the calibration image, the square array was positioned 4cm from the image intensifier. Both panels are free to move on metal sliders, allowing the height of the grids to be changed. The central markers on both grids were aligned with the centre of the image intensifier, marked by a stainless steel ball bearing fixed to the intensifier (Figure 6.3b). An additional marker can be positioned on the calibration cube to label the orientation of the resulting image. The image of the grid is used in post-processing.

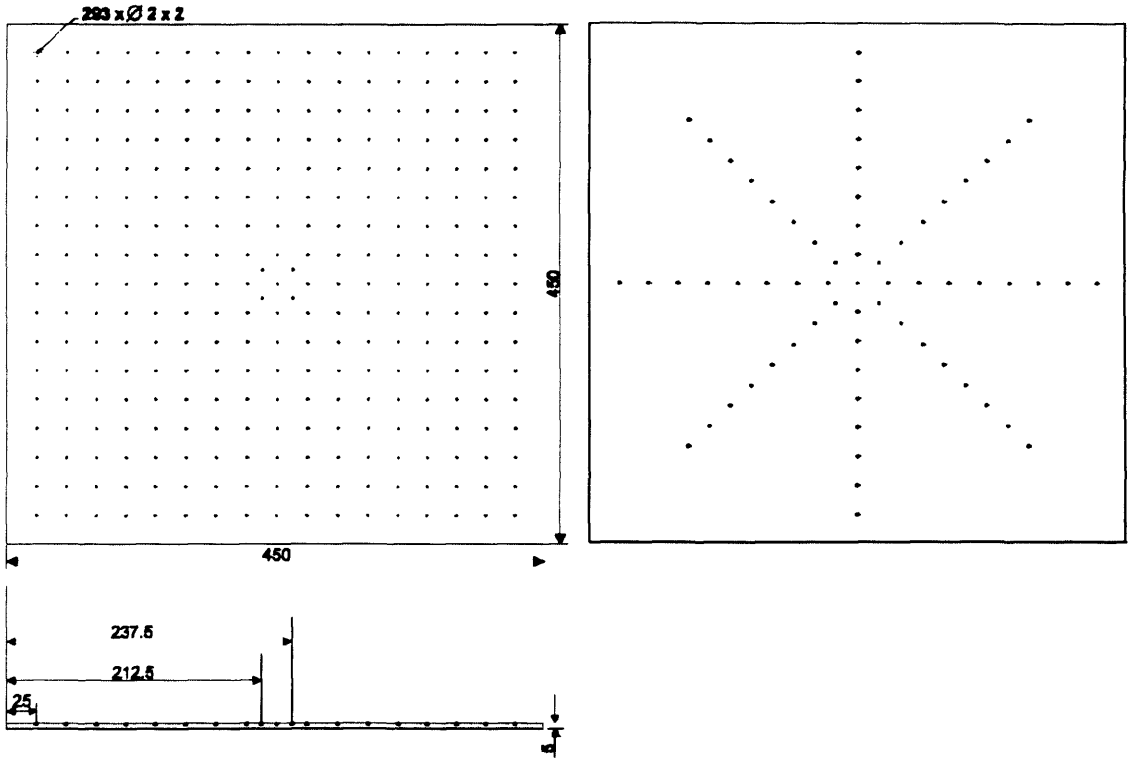

(a) (b)

Figure 6.4 Panels from the calibration frame with (a) Square array and (b) Star array. Dimensions are in mm.

The Matlab program used to determine distortion parameters assumes that the centre of the intensifier, the centre of the square grid and centre of star are aligned. Also, the markers from the square and star grid create a 3D volume, it is therefore important that the grids are aligned parallel to the image intensifier, otherwise further distortion will be introduced into the images.

It is important to note that although a calibration is preferred, for any prospective studies where no calibration has taken place, it has shown that variations in X-ray

projection parameters have a small effect on TKR kinematics computed from model-image registration with high-quality clinical radiographs (Chouteau *et al.*, 2007). In fact a misplacement of the principal point by ± 5cm and principal distance by ±15cm resulted in kinematic errors of less than 1° and 1mm. Thus it is possible to derive useful information from previously collected clinical radiographic films where the projection parameters are unknown.

6.2.3.2 Dynamic data collection

The step was centred between the image intensifier and the focus of the fluoroscope. As the subject stood with their foot centred on the step, the height of the C-arm was adjusted to centre the field of view at the lateral side of the joint cavity of their knee. It is important to centre the knee with the image intensifier because the intensifier autocorrects the contrast of the image according to the centre of the image. If the knee is not centred, the image will be dark. The contrast of the images varies from person to person depending on their mass. The fluoroscopy unit calculates the lowest dose possible to give the optimum density. This can be altered depending on the patient size and is subjective depending on the radiographer's opinion. In accordance with the ethical approval, the subjects wore a long lead rubber apron (3.5mm Pb) and the fluoroscopic procedure was limited to 15 seconds. The maximum surface dose rate for NP knees was 0.5 mGy/minute and for artificial knees it was 0.75 mGy/minute. Under these constraints, the expected dose to the surface of a normal and artificial knee was of the order of 0.08,mGy and 0.13 mGy.

The fluoroscope was used to continuously record each subject performing three repetitions of stepping up and down from the 16cm high step, (Figure 6.5). The convention used was to image the knee of interest from medial to lateral. The screening/fluoroscopy time was a maximum of 15 seconds as agreed by the radiation protection service. The images were saved in Digital Imaging and Communications in Medicine (DICOM) standard and the dimensions were 1024 x 1024 square pixels.

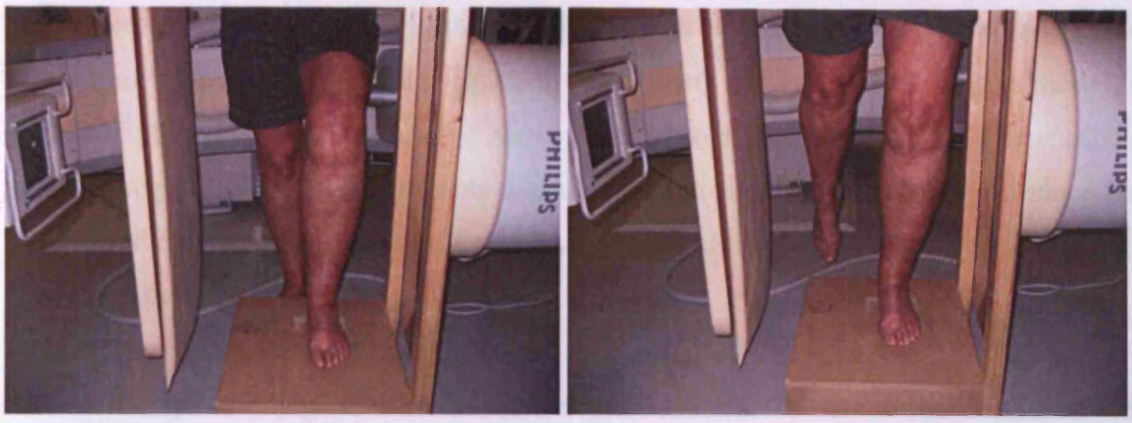

Figure 6.5 Step up/down task recorded using dynamic fluoroscopy

6.2.4 Creating Magnetic Resonance Imaging derived bone models

6.2.4.1 Magnetic resonance imaging protocol

MRI was the imaging modality of choice for this study. Scan data from the five NP subjects was obtained using a 3T GE scanner (General Electric Company) at the Cardiff University Brain Research Imaging Centre (CUBRIC).

Two sets of scans were taken, one set of whole-leg scans, followed by a higher resolution scan of the knee only. High resolution scans of the knee were required to create high resolution models of the distal femur and proximal tibia for the matching process. The whole- leg scans were required to identify landmarks such as the centre of the hip and ankle joint to generate embedded axis systems within the high resolution bone models.

Whole-leg scans with a slice thickness of 4.5mm were acquired using a body radio frequency (RF) coil for transmit/receive. To cover the length of the leg, the scans were performed in three sections, top (centred on the hip), mid (centred on knee) and bottom (centred at the mid point of tibia and fibula). The scans taken at the top and bottom of the leg (Figure 6.6a) were used to create the femoral and tibial models. Coarse scan data was sufficient to create these models because they are used to identify the anatomical landmarks used to establish anatomical axes in the high resolution bone models and are not used in the image registration process. High

resolution targeted knee scans with a slice thickness of 1mm were acquired around the knee joint with a knee RF coil, (Figure 6.6b). During the creation of a bone model, a series of closely spaced 2D image slices is used to make a virtual 3D view of the scanned region. High resolution data was obtained around the knee joint to reduce the amount of data missing between each slice and to allow for the creation of accurate models with smooth surfaces.

The challenge of using MRI is to achieve good contrast between the bone and soft tissues. The settings used for the scans are listed in Table 6.2.

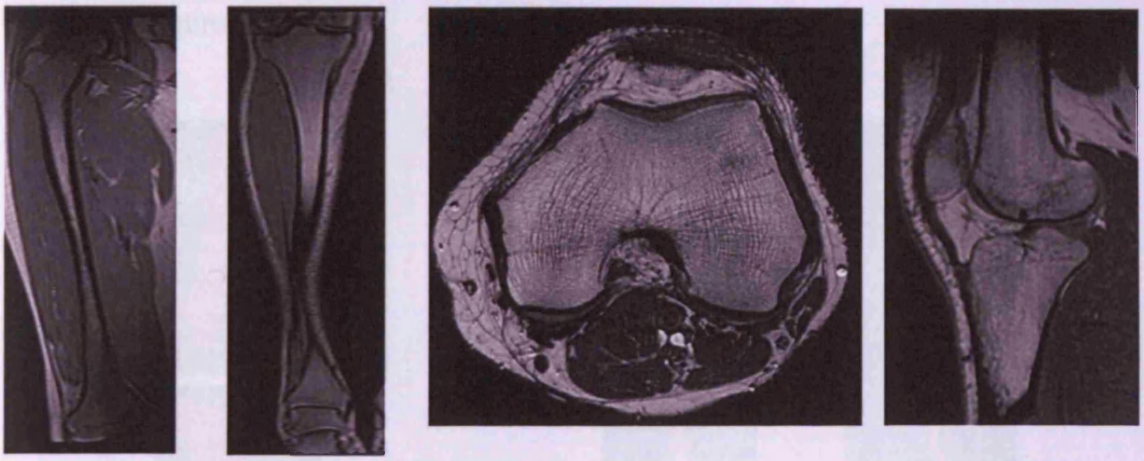

(a) (b)

Figure 6.6 Examples of (a) coarse scan MRI data of the femur and tibia and (b) high resolution MRI scan data of the knee

Table 6.2 MRI Scanner Settings

Scan Type	**Whole-leg**	**Targeted knee**
Sequence	Fast Spin Echo	3D Fast Spoiled Gradient Echo (FSPGR)
Repetition time (TR)	1140 ms	5.4 ms
Echo Time (TE)	8 ms	2.0 ms
Echo Train length	3	1
Acquisition Matrix	384 x 224	256 x 256
No. of averages	3	2
Orientation	Oblique-coronal	Oblique- sagittal
Field of view	48 cm	24 x 24 x 12.8cm
Slice thickness (gap)	3 (1.5) mm	1 (1) mm
Acquisition time	4.22 min	5.57 min

6.2.4.2 Protocol for creating geometric bone models of the femur and tibia

The image registration process requires 3D models to shape match to the fluoroscopic images. This protocol was developed to investigate the use of Simpleware software (Simpleware Ltd.) in producing high quality effective bone models of the knee from MRI scan data for use with image based registration.

Two sets of 3D bone models were created from the MRI scans. Bone models of the distal end of the femur and proximal end of the tibia were created at Simpleware, from the high resolution scan data (Figure 6.7a) using ScanIP (Simpleware Ltd). Bone models of the tibia and femur were created from the coarse (lower resolution) scan data (Figure 6.7b).

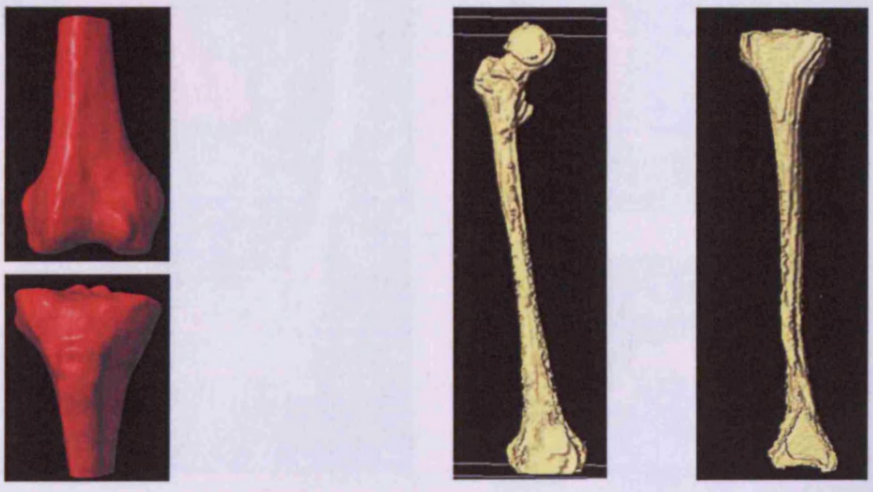

(a) (b)

Figure 6.7 Example of (a) bone models created from high resolution scans, (b) bone models created from coarse scans

The first step was to segment the bone from each image slice. The external cortical edges of the bones were segmented from each image slice using ScanIP (Simpleware Ltd), (Figure 6.8). The software offers several tools for automatic segmentation including thresholding to define the contour of the bone and floodfilling to fill inside the bone. For some slices, where the bone edges were not clearly defined, e.g. close to the centre of the knee joint, manual segmentation using the paint tool was performed.

Due to the scanning direction the stacking of the 2D MRI images in the dataset was reversed, otherwise the right knee would be representative of a left knee model. Smoothing algorithms were applied to each model to remove surface discrepancies between image slices caused by manual segmentation. A binarisation filter was applied to the models created using the high resolution scans. This improves the quality of mask smoothing. Smoothing was achieved using a recursive Gaussian filter with X, Y and Z Gaussian sigma's set to 1 mm x 1 mm x 1 mm. A Gaussian filter was also used to smooth the models created from the coarse scans. The Gaussian sigma was set to the spacing of the data which in this case was 0.9375mm x 0.9375mm x 4.5mm. The models were rendered and exported in Binary STL format.

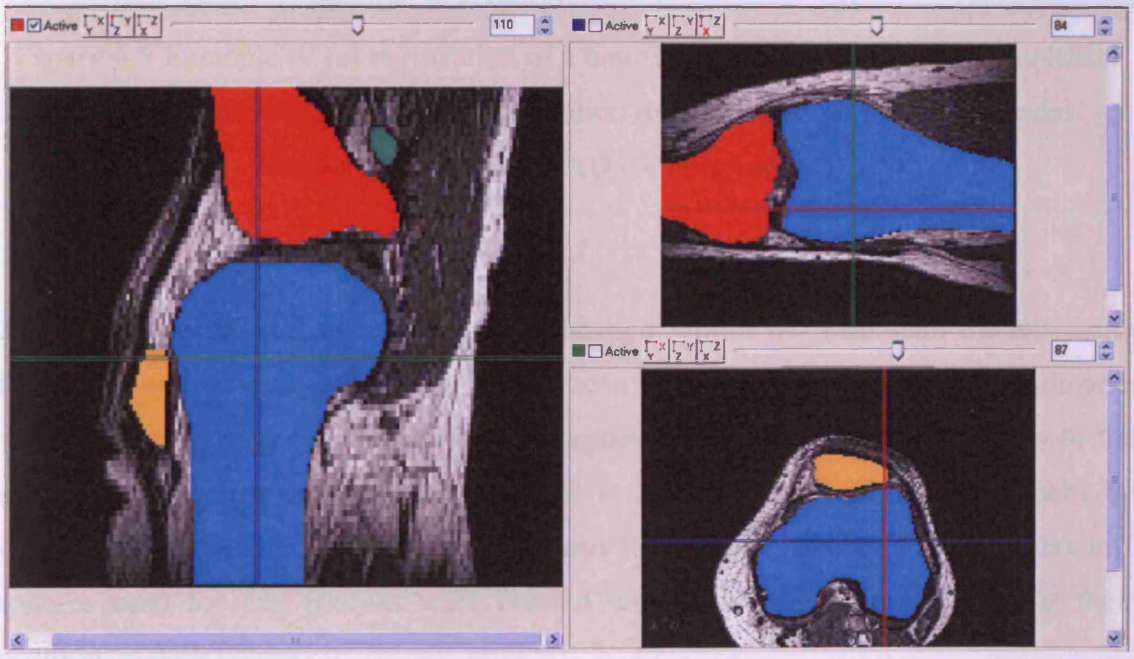

Figure 6.8 Segmentation of the bones using ScanIP (Simpleware Ltd.)

Each high resolution bone model requires an embedded coordinate system for use with the KneeTrack software (S. A. Banks, USA). This is determined using anatomical landmarks on the femur and tibia. For this reason, the models created from the coarse scans were registered with models created from the fine scans (Figure 6.9a) using +ScanCAD (Simpleware Ltd). Registration of the high resolution and coarse scan models was achieved manually using a new manipulation tool to control the rotation and translation of the models, (Figure 6.9b). The models were then converted to masks for use in the ScanIP software (Simpleware, Ltd).

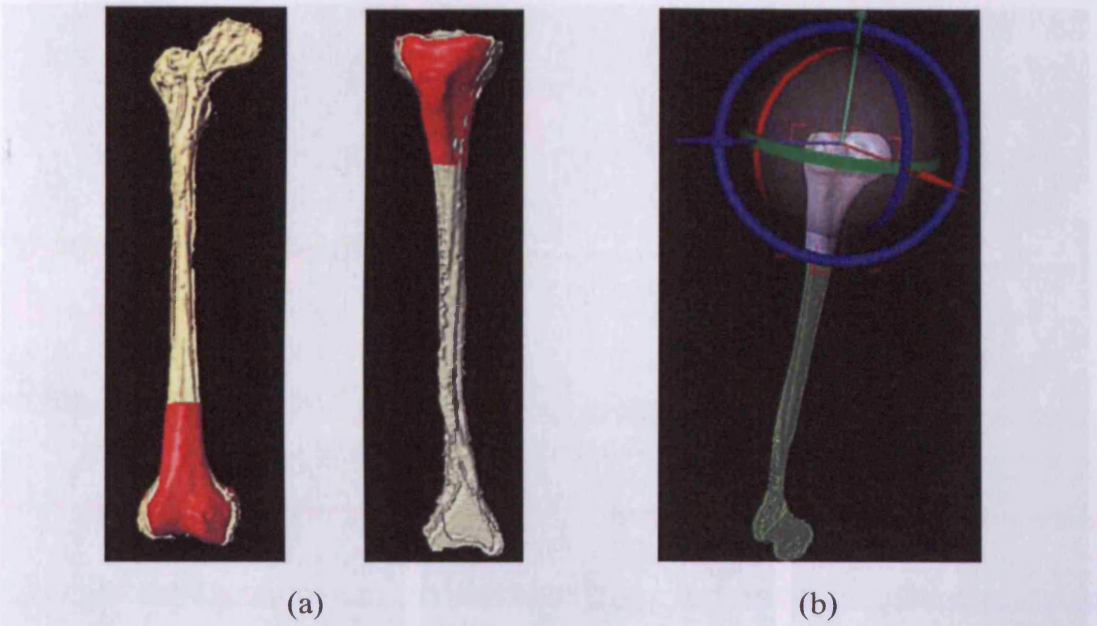

(a) (b)

Figure 6.9 Example of (a) registration of a bone model created from high resolution and coarse scan data. (b) The manipulation tool used for manual bone model registration in +ScanCAD (Simpleware Ltd.)

Anatomical coordinate systems were established within the fine scan models using three landmarks from each of the coarse scan models. The anatomical landmarks were defined by registering cylinders and spheres to models as an adaptation to the approach of Moro-oka *et al.*, 2008, which is a combination of the approaches by Asano *et al.*, 2001, Eckhoff *et al.*, 2005 and Roos *et al.*, 2005. The cylinders and spheres used for this process were created with their origin, used to define their position, at their centre.

The mediolateral x-axes (positive in the medial direction) of the femur and tibia were defined by fitting a cylinder to each posterior condyles of the femur, (Figure 6.10a). This was achieved by elongating each cylinder along it axis until only the most prominent single point of the lateral and medial aspect of the femoral condyle remain visible, as in Eckhoff *et al.*, (2005). The line connecting the centre of each cylinder was taken to be the cylindrical axis. The origin was defined at the midpoint of the cylindrical axis.

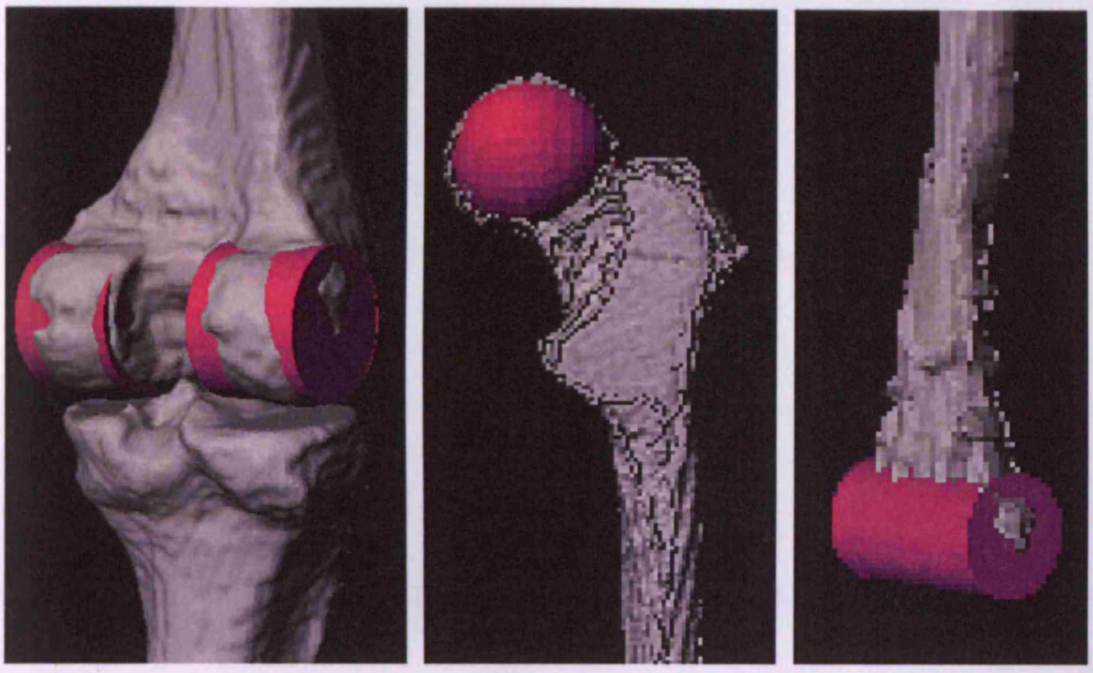

Figure 6.10 Fitting cylinders to the (a) femoral condyles, (b) malleoli and (c) fitting a sphere to the femoral head. The position of the centroid of each cylinder and sphere is known.

The proximal-distal y-axis (positive upwards) for the femur was defined by a line perpendicular to the cylindrical axis in the plane intersecting the femoral head centre. The centre of the femoral head was defined by a sphere registered to the largest cross section of the femoral head, (Figure 6.10b). The proximal/distal y-axis (positive upwards) for the shank was perpendicular to the cylindrical axis in the plane intersecting the ankle centre. The ankle centre was defined as the centre of a cylinder registered to both malleoli, (Figure 6.10c). This was essentially the midpoint in the transverse plane between the two malleoli.

The anterior-posterior (x) axis was formed from the cross product of the first two where the positive x-axis points anterior for a left knee and posterior for a right knee.

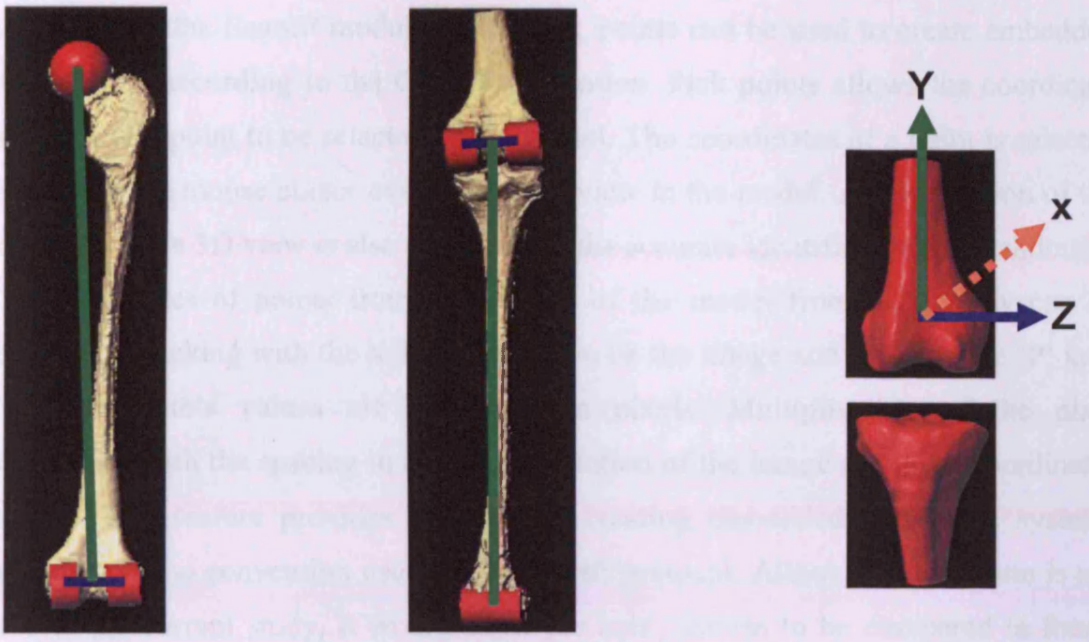

(a) (b) (c)

Figure 6.11 Defining anatomical coordinate systems in (a) the femur and (b) the tibia. (c) shows the location of the origin of the embedded coordinate system and axis convention for a right knee.

The location of the origin of each cylinder and spheres was obtained from ScanIP and used to compute vectors that define the new orthogonal coordinate systems, (Figures 6.11 a-c). An align filter was developed within the ScanIP software that aligns the high resolution bone model with the new coordinate system. Two of the orthogonal vectors and the coordinates of the origin (in pixels) are entered into the filter interface. After applying the filter the object is rotated to the required orientation for the embedded coordinate system and the software displays how much the model needs to be translated in a third party software. The high resolution bone model in the new coordinate system is exported as an STL file and the final translation is applied using Rhinoceros version 4.0.

The axis defined in this study follow the convention used in the KneeTrack software (Banks and Hodge, 1996). The axis system differs from the Grood and Suntay convention used to process kinematic data using the marker- based motion analysis coordinate data.

A function in the ScanIP module called Pick points can be used to create embedded axis systems according to the Cardiff convention. Pick points allows the coordinate positions of a point to be selected on the model. The coordinates of a point is selected by moving the mouse cursor over a 2D slice view in the model. A visualisation of the active slice in a 3D view is also provided for the accurate identification of a landmark. The coordinates of points from the surface of the model from a 3D view can be selected by clicking with the left mouse button on the image and pressing the 'P' key. The coordinate's values are expressed in pixels. Multiplication of the pixel coordinates with the spacing in the given direction of the image produces coordinates in mm. This feature provides a means of creating embedded coordinate systems according to the convention used in the Cardiff protocol. Although this system is not used in the current study, it would allow the axis systems to be compared in future work by identifying the landmarks used in the Cardiff protocol as in Figure 6.12.

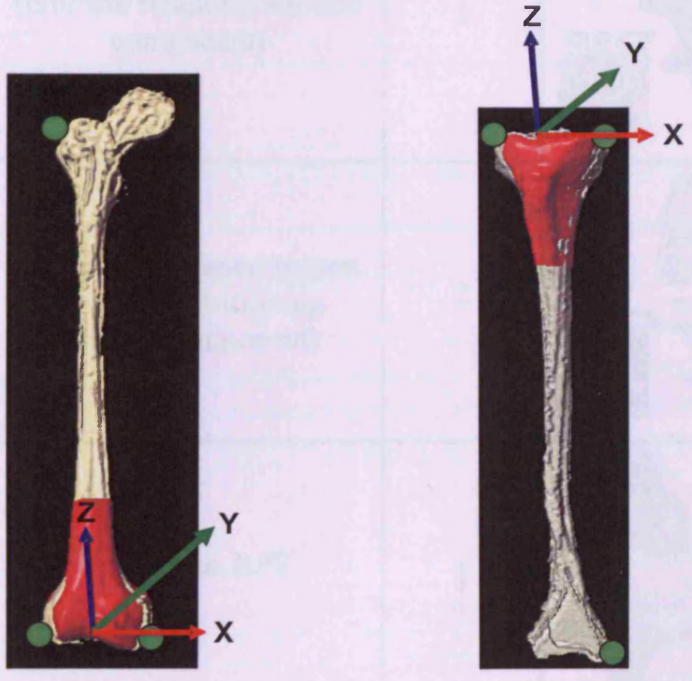

(a) (b)

Figure 6.12 Examples of axis systems defined according to the Cardiff protocol using three anatomical landmarks for a (a) right femur and (b) right tibia.

6.2.5 Protocol for preparing 3D CAD implant models for use in Image Registration

Tibial and femoral component 3D CAD models were obtained from the implant manufacturers for the 5 TKR patients. Until this point in the study, it was unknown as to what implants the patients had received. The implant codes for the TKR components were acquired for each patient and these were used to obtain the 3D CAD models from the implant manufacturer. The implant types used in this study are listed in Table 6.3.

Table 6.3 Implant types used in this study

Manufacturer	TKR Type	Quantity	Image of each implant
DePuy Orthopaedics, Inc.	PFC modular knee system (cruciate retaining femoral component)	1	
DePuy Orthopaedics, Inc.	PFC modular knee system (cruciate substituting femoral component)	2	
DePuy Orthopaedics, Inc.	PFC sigma RPF	1	
Wright Medical Technology, Inc.	ADVANCE® Medial-Pivot Knee	1	

The TKR images were obtained from *www.wmt.com* and *www.depuy.com*

A procedure to prepare the TKR implant models for use with the KneeTrack software (Banks and Hodge, 1996) will now be summarised.

The first stage was to convert the 3D CAD files into a suitable format. The implant models were converted from Binary to Ascii format in Rhinoceros version 4.0. A program was written in DOS command prompt to extract all the lines containing vertices. Files containing just the coordinates of the vertices making up each implant model were created for each component.

PV-Wave scripts provided by S. A. Banks (University of Florida) were adapted and used to reposition each component with respect to its coordinate system and generate the files required for the KneeTrack software. The implant was centred in the transverse plane and rotated to produce embedded coordinate systems with the correct sign convention for used in the shape matching process of Banks and Hodge, (1996). This requires, for the y-axis to point upwards and the z-axis to point medially. The x-axis points anterior for the left knee and posterior for the right knee.

The origins of the coordinate systems are positioned according to the geometry of each implant. For the femoral components, the following steps are taken to locate the origin. First, the position of the most posterior and superior point on the bone cut surface of the implant is determined. The distance from this point to the anterior cut surface of the implant is measured as 2r. Midway between these points, the position of the distal bone cut surface (minimum y position) is determined. Sometimes blend features on the intercondylar boxes prevent the minimum y position to be located, this is avoided by determining the minimum y position at different z locations. The origin, known as the Banks point, is located at distance r upwards from the bone cut surface. The final embedded coordinate system in shown in Figure 6.13a.

The origin for each tibial component was positioned at the midpoint of the component in the anterior-posterior direction and at the backside of the polyethylene insert, (Figure 6.13b). The distance from the upper rim of the tibial tray to the level where the PE inert sits on the base plate is measured in Rhinoceros version 4.0, (Figure 6.14).

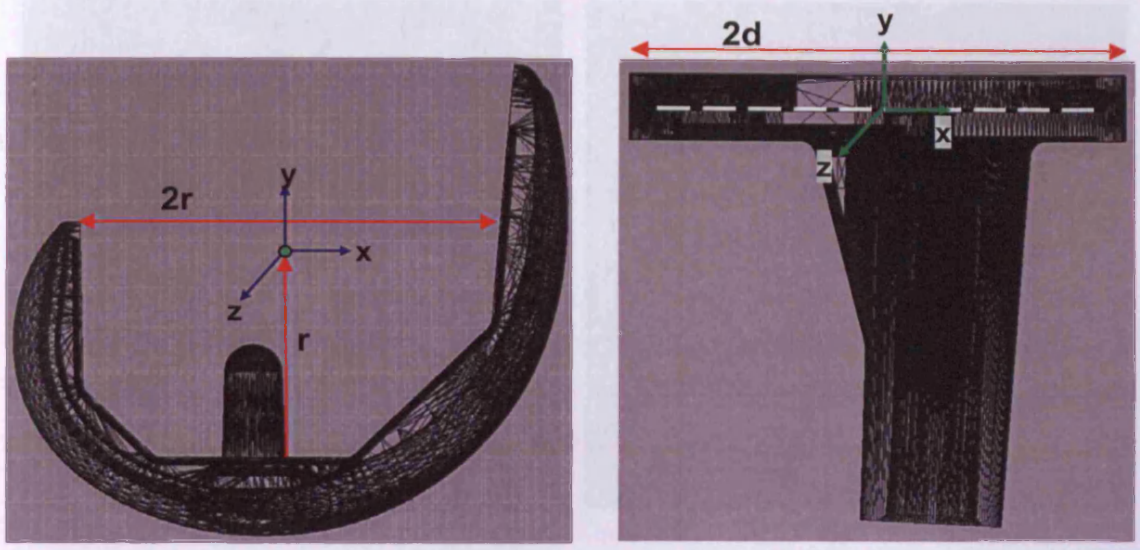

(a) (b)

Figure 6.13 Illustration of the coordinate system convention for a left TKR a) femoral component and b) tibial component

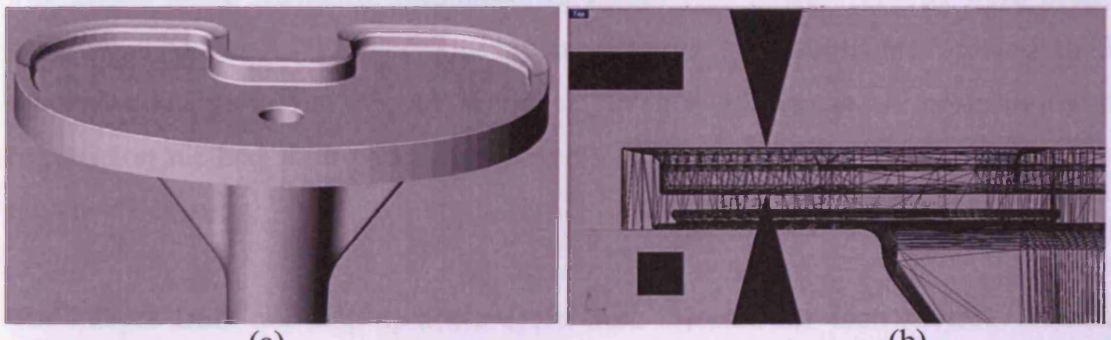

(a) (b)

Figure 6.14 Example of a (a) tibial component with a rim and (b) determining the level where the backside of the plastic bearing is located relative to the top surface

The KneeTrack software creates a plot of the contact and centre of rotation positions of the femoral condyles on the tibial plateau. An outline of the tibial plateau for each model was generated for this visualisation. Using a plot of a superior transverse region of each tibial model, points were manually selected to define an outline of the plateau. This was performed for the TKR (Figure 6.15a) and bone (Figure 6.15b) models.

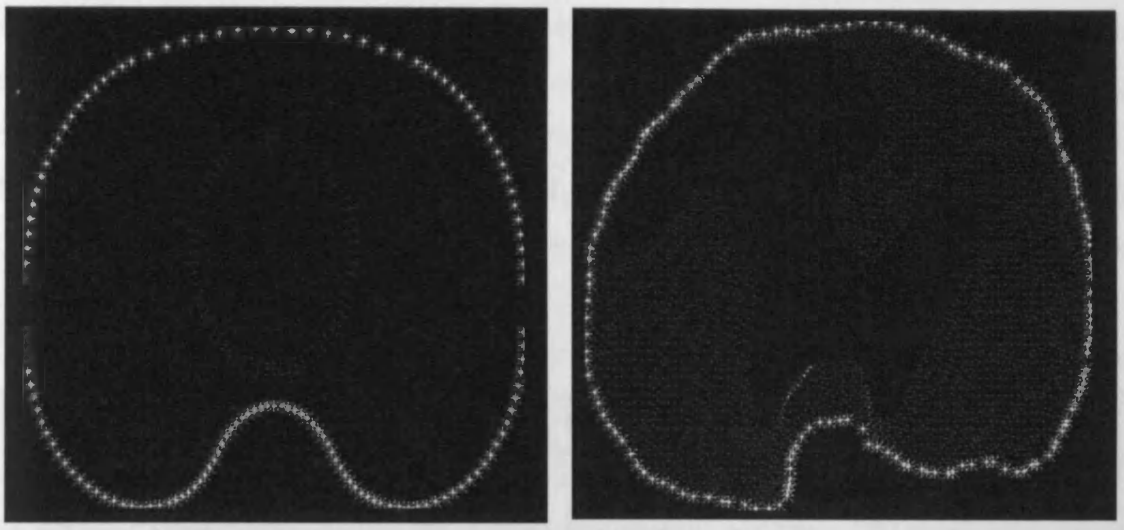

Figure 6.15 Defining the outline of the tibial plateau for a (a) prosthetic tibial component and (b) natural tibia

6.2.6 Image Registration Method

The model-based matching techniques of Banks and Hodge, (1996) were used to compute TKR and NP knee kinematics. This is an established method to 3D kinematic analysis of a known 3D object from a 2D image. A protocol for the registration method is provided in Appendix H, a summary of the main stages will now be discussed.

The images from one step up/down cycle were selected for each subject. The step up/down cycle was taken from the knee in the starting flexed position, moving into extension and returning to flexion. The fluoroscopy images were converted to uncompressed, grey, TIF files using OSIRIS (medical image manipulation and analysis software). The images were scaled to 512 x 512 square pixels for the 3D shape registration. Although images were taken from the medial side of the knee, the images had been reversed during data collection. Therefore, the original image view was obtained by flipping the images.

The images were corrected for static geometric distortion. This was achieved using Matlab calibration software provided by Scott Banks (University of Florida) and the

image of the calibration frame, containing a star and square grid of points. The software determines the transformation between known and measured coordinates on the image of the square grid. Distortion corrections are applied to the image using bilinear interpolation, so that the markers return to their known positions (Banks, 1992). The same correction was applied to all subsequent images. The internal orientation parameters of the fluoroscope (principal distance, principal point) are determined from the star grid.

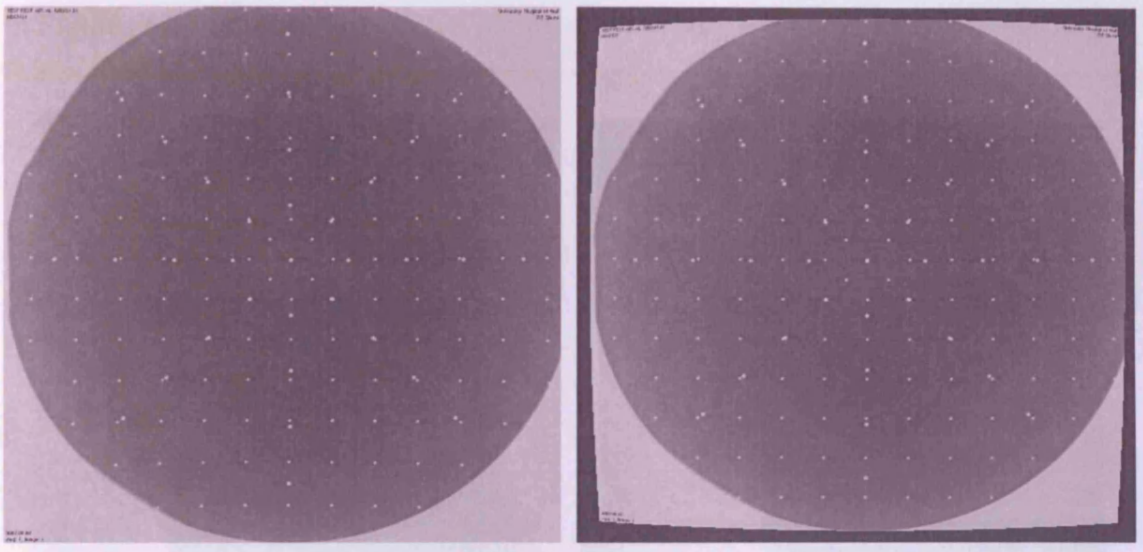

Figure 6.16 Images of the calibration target, (a) original image with geometric distortion and (b) undistorted image after correction

The 3D solid bone models and the TKR CAD models were registered to a series of frames from the 2D fluoroscopic image data for each subject. KneeTrack 0.5 software (S. A. Banks, USA) was used for the 3D shape matching process. The 3D models were projected onto each geometry-corrected image in turn. A Canny edge detector was used to identify bony and implant contours in an image. The threshold intensity for the grey scale was adjusted interactively to obtain the best fitting contour around the silhouette of each model. The 3D pose of each model was iteratively adjusted to match its silhouette to the outline of the corresponding bone or implant on the fluoroscopic image.

Initial shape matching was achieved manually. A numerical optimiser was then used to align the models to the edges in each image. The automated matching algorithm is

based on nonlinear least squares optimisation and an image edge-to-model edge distance criteria. The optimisation option for matching was not used for all images. For the matching of TKR components, the femur is matched first. The tibia is symmetric through its sagittal midline and thus two poses look reasonable during the matching process. The femur is asymmetric proximally, so by matching this first it is easier to see if the tibial matching solution is physiologically possible.

Examples of registering TKR and bone models to 2D fluoroscopic images are shown in Figures 6.17 (a to d).

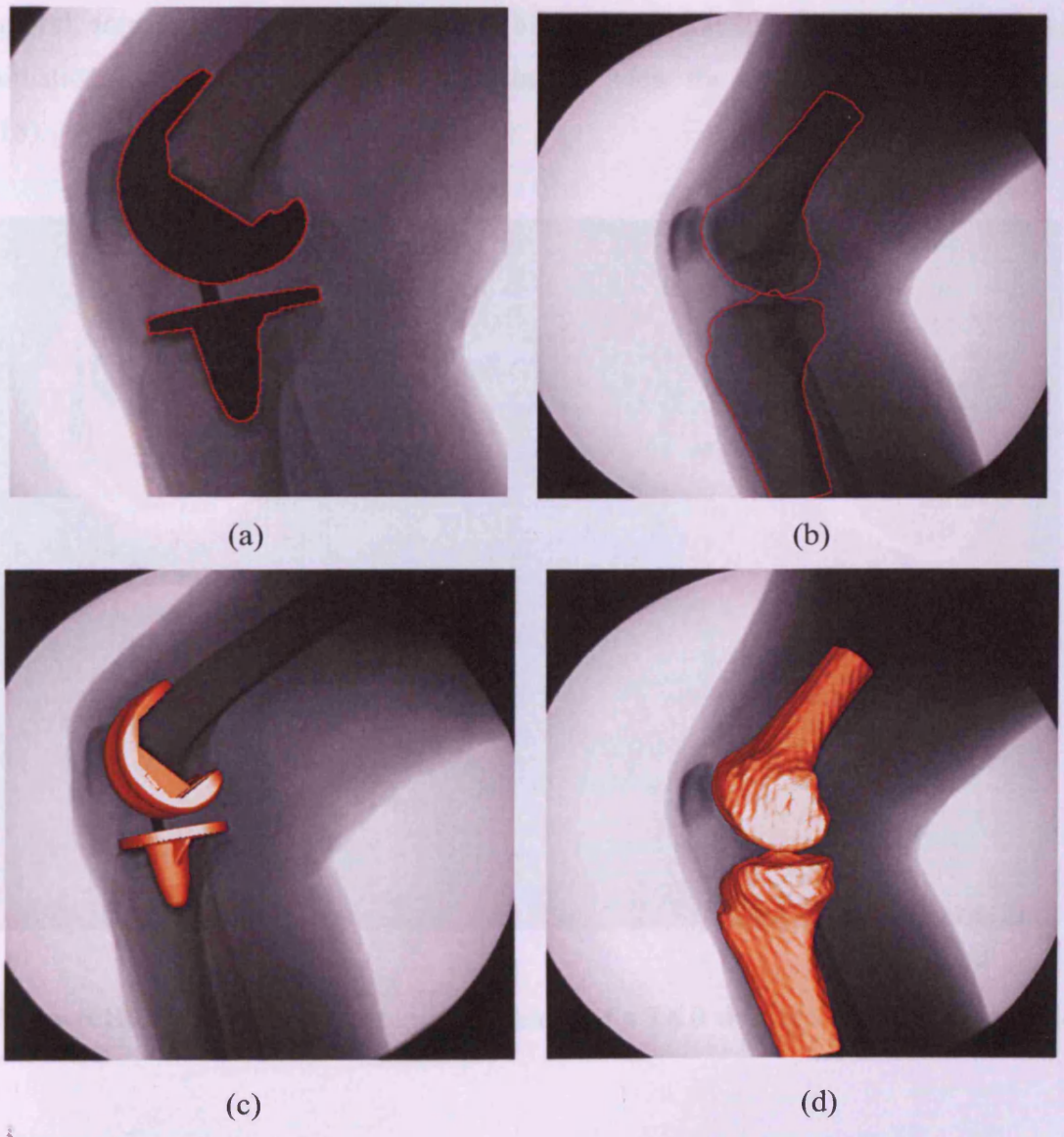

Figure 6.17 Matching the silhouette of a (a) bone model and (b) TKR components to 2D fluoroscopic images. The models can be rendered to aid visualisation shown in (a) for the TKR components and (b) for a set of bone models.

Knee joint kinematics were determined from the 3D pose of each implant component. Rotations about the appropriate clinical planes are defined by 312 Cardan/Euler angles as described by Tupling and Pierrynowski, (1987). Joint translations are computed as the movement of the femoral origin with respect to tibial coordinate system. They remain in base mathematical orientation such that superior and medial femoral translations are positive and anterior femoral translation is positive for a left knee and negative for a right knee.

The KneeTrack software provides graphs to show the pose of each component throughout the sequence of images. It also provides the knee angles and amount of femoral translation for each image. This information can be used to produce animations of the models used in matching, to view the component in 3D, (Figure 6.18).

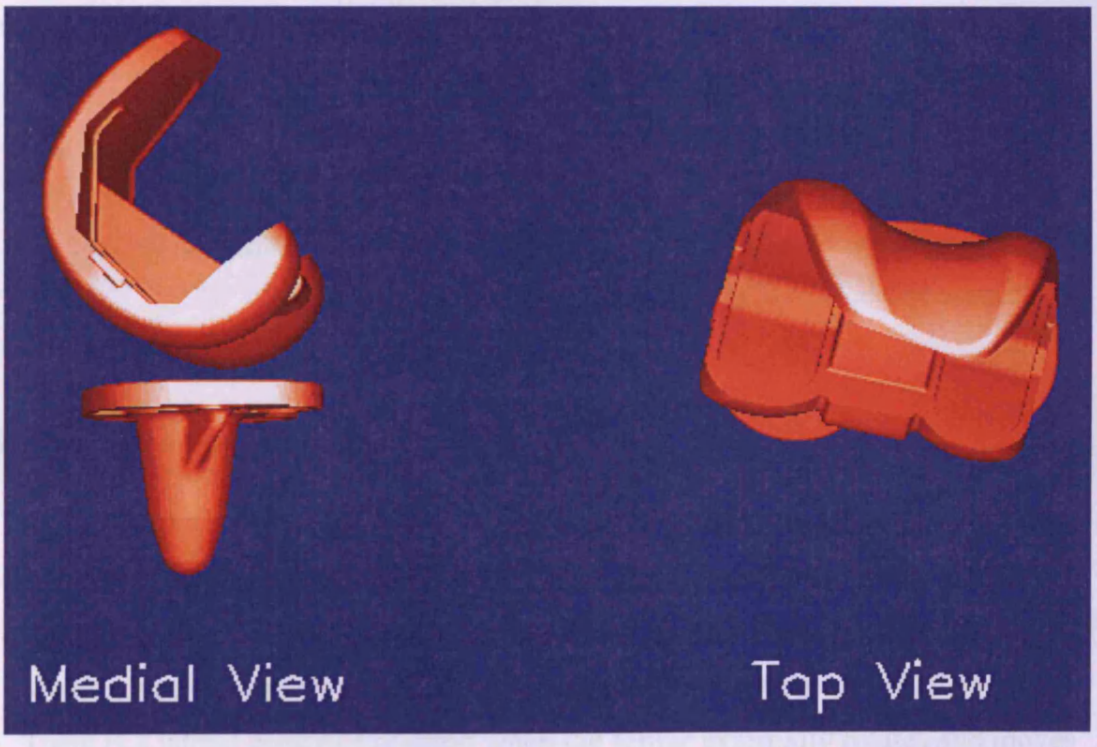

Figure 6.18 A single frame from an animation of a TKR during a step up/down cycle

There are several outputs that can be generated using KneeTrack. A useful output for the measurement of natural and TKR function is a plot of the condylar contact points and joint centre of rotation.

The contact points are expressed in the tibial reference frame and are calculated as the lowest point on each condyle with respect to the transverse plane of the tibial model. The mid point of the contacts is considered representative of antero/posterior translation of the femoral component. A line connecting these points represents the flexion-extension axis of the femur. The centre of axial rotation is calculated by solving the least-squares system of equations describing the lines connecting the medial and lateral contact points over the entire motion. The mediolateral location of the centre of rotation is normalised to the dimensions of each tibial model and expressed as a percentage of the tibial width, -50% (lateral) to +50% (medial). A negative or positive value for pivot point position implies a lateral or medial location respectively, as shown in Figure 6.19.

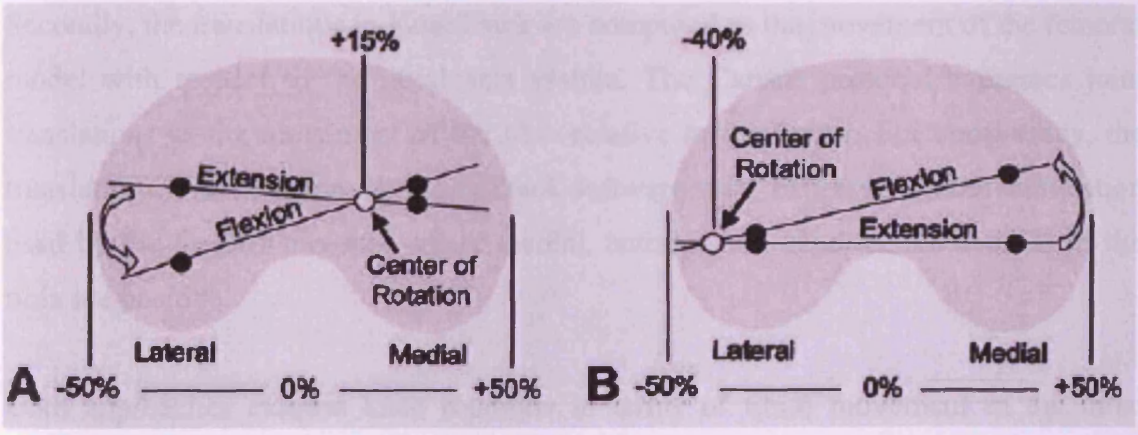

Figure 6.19 Medial and lateral condylar contact points (black circles) from each frame of data are joined to represent the flexion/extension axis. These are used to determine the centre of axial rotation (white circle). (A) There is a medial centre of rotation when the femur externally rotates and moves posterior with flexion. (B) There is a lateral centre of rotation when the femur externally rotates and moves anterior with flexion. Image reproduced from Banks and Hodge, (2004).

6.2.7 Results of comparing kinematics computed using the two methods

Joint kinematics were computed for three step up/down cycles for each subject using the Cardiff motion analysis method and for one cycle using the image registration method of Banks and Hodge, (1996).

Due to the difference in axis conventions, calculations and units used in each of the computational approaches, several amendments to the data was made before the results from the two approaches could be compared.

Firstly, the Cardiff protocol computes joint translations in metres whereas the KneeTrack software computes the translations in centimetres. Therefore the translations computed using the Cardiff protocol were expressed in centimetres for the comparison.

Secondly, the translations in KneeTrack are computed as the movement of the femoral model with respect to the tibial axis system. The Cardiff protocol expresses joint translations as the movement of the tibia relative to the femur. For consistency, the translations obtained from the KneeTrack software were expressed in the convention used by the Cardiff protocol where medial, anterior and superior movements of the tibia are positive.

Both approaches express knee rotations in terms of tibial movement in the three clinical planes (i.e. adduction-abduction, external-internal rotation and flexion-extension). The convention used in the KneeTrack calculations defines abduction angles as positive. For consistency with the Cardiff protocol, the frontal plane rotations computed from KneeTrack were negated so that adduction angles were positive in accordance with the convention used in the Cardiff protocol.

From each cycle of step up/down, the ranges of motion (ROM), peak and minimum values were selected from each kinematic waveform. As three cycles were processed from the motion analysis assessment, an average of these measures from the three cycles was computed for each subject. The average of these measures from the 5 TKR

subjects and 5 NP subjects for each measurement method were used to compare the two methods.

One way ANOVA (SPSS 12.0.2) was used to detect significant differences ($P < 0.05$) between the kinematic measurements using motion analysis and image registration. Differences between the two methods are compared separately for the 5 NP subjects and 5 TKR subjects in case the accuracy differs between the two knee types. The results from the TKR subjects are shown in Table 6.4. The results from the NP subjects are shown in Table 6.5.

Table 6.4 Kinematic measures for the TKR group computed using the Cardiff Protocol and Image registration methods

Variables		Cardiff Protocol (Marker based motion analysis)	Image Registration (Fluoroscopy and shape matching)
Flexion-Extension Rotation (°)	ROM	57.21 ± 6.62	63.74 ± 13.47
	Minimum	3.57 ± 3.56	-1.34 ± 8.30
	Maximum	60.78 ± 5.30	62.40±8.22
Adduction-Abduction Rotation (°)	ROM *	10.07 ± 1.66	2.68 ± 0.42
	Minimum	-3.69 ± 4.55	-0.76 ± 0.43
	Maximum*	6.38 ± 3.97	1.92 ± 0.65
External-Internal Rotation (°)	ROM*	9.66 ± 2.43	5.19 ± 1.94
	Minimum	-8.27 ± 8.04	-2.16 ± 6.00
	Maximum	1.39 ± 8.76	3.04 ± 5.12
Medial-Lateral Shift (cm)	ROM*	2.43 ± 0.78	0.22 ± 0.12
	Minimum	-0.78 ± 0.90	-0.02 ± 0.06
	Maximum*	1.65 ± 0.95	0.20 ± 0.13
Anterior-Posterior Drawer (cm)	ROM*	2.38 ± 0.75	0.84 ± 0.35
	Minimum*	-2.24 ± 1.15	-0.04 ± 0.22
	Maximum	0.14 ± 1.20	0.80 ± 0.19
Compression-Distraction (cm)	ROM*	3.00 ± 0.56	0.37 ± 0.17
	Minimum*	-0.08 ± 0.13	-4.52 ± 0.53
	Maximum*	2.92 ± 0.49	-4.14 ± 0.51

Mean ± Standard deviation; * indicates a statistical significance between the data collection methods ($P < 0.05$)

Table 6.5 Kinematic measures for the NP group computed using the Cardiff Protocol and Image registration methods

Variables		Cardiff Protocol (Marker based motion analysis)	Image Registration (Fluoroscopy and shape matching)
Flexion-Extension Rotation (°)	ROM	57.68 ± 7.66	60.51 ± 7.33
	Minimum	1.03 ± 10.90	-4.63 ± 10.46
	Maximum	58.70 ± 11.18	55.88 ± 6.25
Adduction-Abduction Rotation (°)	ROM*	13.26 ± 5.90	3.73 ± 1.39
	Minimum	-2.54 ± 7.23	-1.93 ± 1.63
	Maximum*	10.71 ± 7.55	1.79 ± 2.63
External-Internal Rotation (°)	ROM	11.12 ± 2.31	15.16 ± 6.67
	Minimum	-13.85 ± 8.48	-12.46 ± 7.76
	Maximum	-2.68 ± 7.41	2.71 ± 6.15
Medial-Lateral Shift (cm)	ROM*	2.27 ± 1.26	0.31 ± 0.11
	Minimum	-1.43 ± 1.56	-0.47 ± 0.13
	Maximum*	0.84 ± 0.55	-0.16 ± 0.16
Anterior-Posterior Drawer (cm)	ROM*	1.81 ± 0.70	0.55 ± 0.23
	Minimum*	-1.43 ± 0.99	0.05 ± 0.18
	Maximum	0.39 ± 0.67	0.61 ± 0.16
Compression-Distraction (cm)	ROM*	2.89 ± 1.56	0.37 ± 0.14
	Minimum*	-0.56 ± 0.32	-0.21 ± 0.18
	Maximum*	2.33 ± 1.53	0.16 ± 0.13

Mean ± Standard deviation; * indicates a statistical significance between the data collection methods ($P < 0.05$)

6.3 Comparison of bone models created using ScanIP (Simpleware, Ltd) and another commercial software

The creation of bone models was a new application for Simpleware, Ltd. For this reason, a comparison was made between a set of bone models created using Simpleware software (Simpleware Ltd.) and another commercial software.

The tibia and femur model used for the matching process for one of the NP subjects was selected for this comparative study. The original high resolution MRI scan data used to create these models were also segmented at the University of Florida using commercial software that they routinely use to create bone models for use with image registration. The external cortical bone edges were segmented using (SliceOmatic, Tomovision, Montreal, CA) and these point clouds were converted into polygonal surface models (Geomagic Studio, Raindrop Geomagic, Research Triangle Park, NC).

Initially an observational comparison of the models was performed. The surface geometry of the models appeared to be very similar with the exception of a larger medial side to the tibia model created using Simpleware software (Simpleware, Ltd.).

To provide a quantitative measure for the comparison, the volumetric difference between the models was determined as the % difference in the volumes between the two models. The two models were registered manually in +ScanCAD (Simpleware, Ltd.), Figure 6.20.

Figure 6.20 Registered bone models generated using ScanIP (green mask) and using a combination of SliceOmatic + Geomagic (blue masks)

The STL models were voxelised to 0.5^3, converted to masks and exported to ScanIP (Simpleware Ltd.) where the models were cropped along their long to make them the same length, (70mm for the femur models and 23mm from the tibia models). Boolean expressions were used to create a mask of the intersection between the two femoral models and two tibial models. Statistics tools in ScanIP were used to obtain volumes of the models. The relative volume difference was 5.12% for tibia models and 4.34% for the femoral models.

The intersection between the femur models corresponds to 94.81 % of the model created using a combination of SliceOmatic + Geomagic and 93.9% using ScanIP. The masks minus the intersection are visualized in Figure 6.21.

Figure 6.21 original masks created using (a) ScanIP and (b) a combination of SliceOmatic + Geomagic, minus the intersection between them.

The intersection between the tibia models corresponds to 90.9 % of the model created using a combination of SliceOmatic + Geomagic and 95.5%. The masks minus the intersection are visualized in Figure 6.22.

Figure 6.22 original masks created using (a) ScanIP and (b) a combination of SliceOmatic + Geomagic, minus the intersection between them.

This comparison indicates that the capabilities of ScanIP are comparable to commercial software currently used for segmenting bones for the application of image registration. The volumes of the models are similar; however, those created using Simpleware software are larger at the femoral condyles and at the lateral portion of the tibia where at the point of tibiofibular articulation, where the outline of the tibia can be less clear due to the articulation for the tibia model. These differences are due inter subject variability and the subjective nature of the segmentation process.

It would be advantageous to compute the peak and average surface discrepancies between the models. However for this to provide meaningful results, it would be important to remove any discrepancies in the surface geometries associated with inter operator variability in the segmentation process. Although for this comparison the models were created using identical MRI data, the segmentation was completed using two different people. Segmentation involves the identification of voxels in an image which is flagged as bone, resulting in a segmented mask. This is used as a basis for surface reconstruction. Any differences in the resulting geometry could be attributable to differences in the bone segmentation since this is a subjective process where the voxels belonging to bone are chosen by the operator. An example can be seen in the Figure 6.23 for three MRI slices where the outline of the lateral portion of the tibia becomes thicker. It is down to user interpretation how much of it to segment.

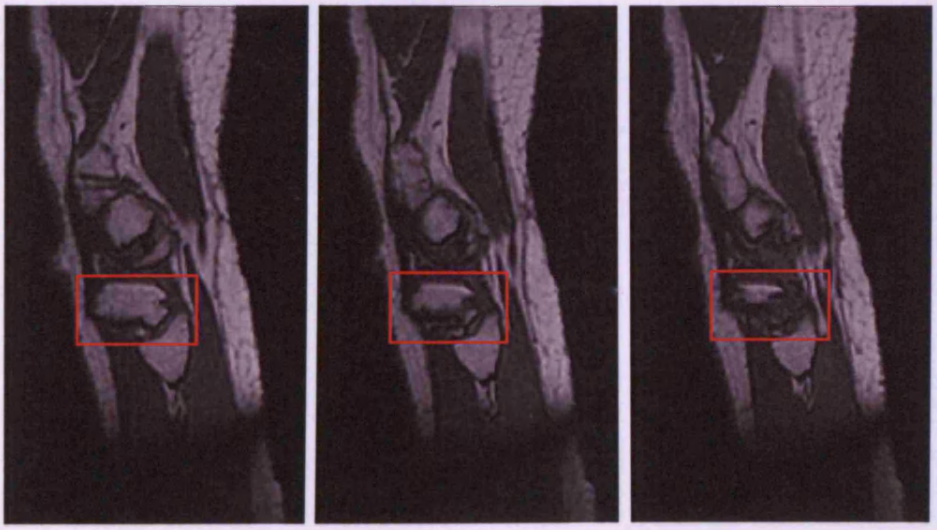

Figure 6.23 Three lateral MRI image slices of the knee. The red boxes highlight the lateral side of the knee where segmentation becomes very subjective.

In addition to the segmentation, user variability will also exist in the surface reconstruction as different smoothing algorithms may have been applied which may remove important surface details. In ScanIP, smoothing can be applied without cutting through the original segmented voxel. Thus small features which may be important in the registration procedure are not removed. The ScanIP reconstruction can be constrained to be as accurate as possible given the segmented mask. The alternative approach produces contours using SliceOmatic and Geomagic then produces Non-Uniform Rational B-Splines (NURBS) surfaces.

For an ideal surface comparison the models should be reconstructed from the same dataset. Using a virtual bone model of known dimensions and then compare the results from the two reconstruction approaches. This would also provide a useful data set that can be used to train new users in the segmentation process of bone. It would also provide a controlled means of assessing the effect of different surface reconstruction methods for the models, on the registration procedure and subsequently on the kinematic outputs.

6.4 DISCUSSION

This study investigated the errors associated with measuring knee kinematics using marker-based motion capture. Knee kinematics computed using non-simultaneous motion analysis and image registration were compared. The kinematics resulting from the image registration method were taken to be the gold standard in order to gain an appreciation of the errors associated with the Cardiff measurement protocol.

The Cardiff protocol measured significantly larger frontal and transverse rotations for the TKR cohort compared with the image registration method. Frontal plane rotations were also significantly larger using motion analysis for the NP cohort. This is in agreement with a study reporting that errors in kinematic data from motion analysis are greatest in out of plane rotations (Stagni *et al.*, 2005).

Significantly larger joint translations were measured using motion analysis for both the NP and TKR cohorts as compared to the measurements from the image registration method. The difference in translation ROM measurements from the two methods ranged from 1.26cm for the anterior-posterior drawer measured for the NP group and 2.63cm for the compression-distraction ROM for the TKR group. The motion analysis technique requires marker clusters to be attached to the lateral surface of the thigh and shank. Although the markers are positioned in locations to minimize the effect of soft tissues on marker movement, the contraction and relaxation of the quadriceps during the dynamic task introduce errors in the measurement of the underlying tibial translations. The image registration protocol is not affected by soft tissues and is a more accurate method of computing translations by directly measuring the movement of the underlying bone or implant.

The maximum and minimum values for compression-distraction of the TKR components in Table 6.4 are due to the location of the coordinate systems within the components of the implants. The distance between the origin of the tibial and femoral component coordinate systems is approximately 4 cm and varies depending on the implant design and size. This resulted in a significant difference between these measures from the Cardiff protocol and image registration methods. This has identified the need to normalise the value of compression and distraction to the

implant dimensions for each individual if these measures are required in future studies.

It is important to quantify the errors in the data collection method for future data interpretation and classification of knee function. This study has highlighted that frontal and transverse plane rotations are less reliable than sagittal plane rotations and that joint translations are overestimated using the motion analysis method.

In addition to errors associated with marker based motion analysis, there are other factors in this study which will contribute towards the differences in the kinematic measurements. The main reason is that the motion analysis and fluoroscopy measurements were taken non-simultaneously. Although the same dynamic movement was performed for each measurement, no rig was used to control movement. This meant that the same subject did not perform the activity in exactly the same fashion for both measurements. As an example, Figure 6.24a shows the flexion-extension rotation at the knee during one cycle of step up/down measured using motion analysis. Here the subject fully extends their knee to approximately 0° flexion. Figure 6.24b shows the measurement from the same person taken using fluoroscopy and image registration. For this measurement, the subject begins the activity with approximately the same degree of knee flexion, however they are measured as hyper extending their knee at full extension.

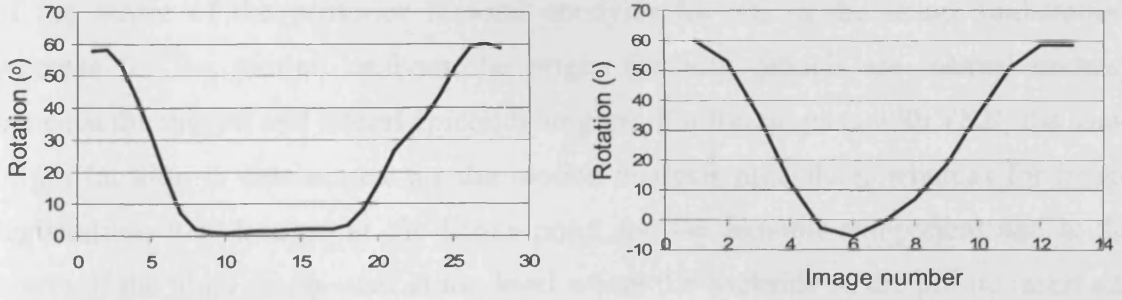

(a) (b)

Figure 6.24 Knee flexion-extension rotations measured from the same subject using (a) motion analysis and (b) fluoroscopy and image registration

Variations in knee movement in the tests would be affected by several factors including a difference in trunk movement or the speed of the tests. Also, for the

fluoroscopy measurements, the subject is in a more restricted space than in the motion analysis laboratory. This may subconsciously affect the subjects adduction-abduction and external-internal knee rotations as an avoidance mechanism in reaction to the bed attached to the fluoroscopy machine which restricts their testing volume.

A potential limitation to the study is that the kinematic differences between the two methodologies were computed from the mean kinematics of the NP and TKR group. Ideally the tests would be performed simultaneously and the differences in kinematics from the two measurement techniques would be computed for each subject separately.

The location and orientation of the embedded coordinate systems used in the Cardiff and image registration protocol are different and this may also have an effect on the resulting kinematics. The Cardiff protocol sets up coordinate systems in the bone using the medial and lateral epicondylar gaps, the upper greater trochanter and the medial malleolus as landmarks. This differs to the image registration procedure which uses the centre of the posterior condyles, hip joint centre and centre of the ankle joint as landmarks used to create embedded coordinate systems within the bone models. Depending on the choice of landmarks, the planes defined are different and the extent of the difference will depend on the subject under investigation.

The choice of landmark also affects the position of the origin of the embedded coordinate system. The origin in the femoral and tibial models is located at the level of the centre of the posterior femoral condyles for use in the image registration, whereas for the motion analysis the origin for both models are located midway between the medial and lateral epicondylar gaps. For the subjects with TKR, the same origin location is determined for the motion analysis procedure, whereas for image registration, it is located at the banks point for the femoral component and at the centre of the tibial component at the level where the backside of the plastic insert sits on the component.

The effect of the choice of landmark used to create embedded coordinate systems in the bone models can be investigated in future work by creating both axes on them in ScanIP (Simpleware, Ltd.) and computing the transformation between the two axis systems. The offset between the two axis systems can be accounted for in kinematic

calculations from the motion analysis coordinate data. This will then allow a direct comparison to be made between the kinematic outputs generated from the different axis systems.

The study demonstrated that MRI can be used as a non- invasive tool for developing segmented 3D bone models using ScanIP (Simpleware Ltd.), thus avoiding the highly invasive effects of CT scanning on healthy volunteers. It has described an application of combining fine and coarse scan models using +ScanCAD (Simpleware Ltd.) to establish anatomical or mechanical axes within the bones for use with research and commercially available kinematic modeling software.

This study has shown that using non-simultaneous methods, useful information can still be obtained. This may have implications for areas of research where simultaneous tests may not be possible.

6.4.1 Recommendations

This study has presented a method of creating bone models for use with the image registration procedure from MRI scan data. It is preferable to use MRI as there is no ionizing radiation involved. However, with this imaging modality it is difficult to distinguish the boundary of the bones at locations such as at the centre of the contacting surfaces of the knee joint. It would be important in the future to perform accuracy tests of the models used for shape matching to determine whether they provide sufficient fidelity to provide clinically relevant measurements. This can be achieved by imaging a phantom with MRI and CT. Moro-oka *et al.*, (2007) describes a method of comparing surface geometry of bone models created using MRI and CT scan data and also the accuracy of each model in computing knee kinematics using KneeTrack. CT can be taken as a gold standard for model creation because it has negligible scaling error because images are reconstructed from line-of-sight X-ray optics and provides a clear outline of cortical bone. MRI suffers from spatial distortions which vary by scanner, scan sequence and the object being scanned and provide less accurate bone definition. However, with optimum imaging settings it can be used to create superior surface models including cartilage used to compute surface interactions (DeFrate *et al.*, 2004). Using MRI, studies could be extended to assessing

knee kinematics in weight bearing positions during scanning, as in Patel *et al.*, (2004). This would also allow models to be created for use with FE modelling to assess surface pressure within the joints for healthy and OA knees.

In future work, it would be preferable to be able to obtain location coordinates for the hip joint centre and ankle centre in relation to the knee in one measurement during MRI scanning. This would remove the need to segment the coarse scan models which would reduce processing time. It would also remove the need to register fine and coarse scan models in order to determine the location of these landmarks. This process introduces errors due to the lower quality of the surface on the coarse scan models and their manual registration with the fine coarse models.

It would be preferable to remove the need to register models as previously mentioned, however, where this is not possible, it would be beneficial to have an automated procedure for the registration process. This would remove subjective error in the registration process. It would also provide a means of determining inter-person variability in the creation of the models from the same dataset.

An issue arising during the shape matching procedure was variation in the contrast of the fluoroscopy images, in particular for the NP subjects. Clear images are a function of tube voltage (kVp, gives contrast), tube current (mA, brightness or signal-to-noise ratio) and exposure time (ms, sharpness for moving objects). For the first two, the ideal situation is to take an image of the static knee in the middle of the image and then to lock these exposure parameters. For temporal resolution, a pulsed system should be used.

The development of a protocol at Cardiff for image registration could be developed for other joints. The latest version of software, called JointTrack is open source and allows for the assessment of other joints. It also provides the facility of transparent bone rendering to planar images. This allows the internal contours to be visualised, making bone registrations more accurate. For joints where ethical approval cannot be obtained for fluoroscopic imaging, e.g. the hip joint, it is possible to use these methods by creating bone models and shape matching them to X-rays taken as part of their treatment. This is possible as small errors in the principal point on the image

introduce small errors in the resulting kinematics. Thus this type of dataset would be sufficient for research purposes and for the development of new protocols.

There is an element of user training required with the use of the shape-matching procedure. Often there is more than one matching solution that appears reasonable. It is therefore essential that high quality fluoroscopy images are obtained so that the silhouette of the implant or bone can be identified accurately using the Canny edge detector in the KneeTrack software. This is used during the automatic registration procedure in the shape-matching process and thus an accurate outline is essential to result in accurate matching of the model to the image. Using automatic registration, user subjectivity is removed.

In future work, more than one trial of step up/down should be assessed for each patient. Also it could be used to compare different types of knee replacement in terms of kinematics and centre of rotation. It may also be possible to use the force data from the current motion analysis dataset, perform Inverse dynamic analysis and produce FE models to look at pressure distribution in the cartilage for the healthy volunteers.

Following from this initial study and now that the protocols are in place at Cardiff University, the investigation into simultaneous motion capture and image registration would provide further information on the errors associated with the Cardiff motion analysis protocol. Once the errors are computed, these can be accounted for in analyses of non-pathological, osteoarthritic and total knee replacement function using the current motion analysis protocol. Considerations should also be made as to how the errors should be accounted for in the assessment procedures employed at Cardiff. Also, whether the same corrections can be applied for each subject or if the corrections should be subject specific.

This study demonstrates that by fusing marker-based motion capture with image based registration techniques, errors associated with measuring knee kinematics using marker-based motion capture can be investigated. It demonstrates a method that can be used to calibrate errors associated with skin movement artefact that are produced when passive markers are attached to the skin. An appreciation of the errors associated with the Cardiff data collection technique has been determined and this is

important for future data interpretation and classification of knee function. An understanding of the level of error associated with each input variable is important when classifying knee function. Where large errors exist in a specific kinematic signal this should be relied upon less in the characterisation of knee function. The effect of errors in the signals using in the DS classifier and their effect on the classification outputs should be investigated.

It is important to combine technologies to advance the assessment of knee function. This work has the potential of leading to assessment methods using combined motion analysis and fluoroscopic information for interpretation. (Leardini *et al.*, 2005b).

6.4.2 Implications of this study to Simpleware Ltd.

This work provided a case study for Simpleware software as the creation of bone models from MRI scan data was a new application for the software. The tools created specifically for this study include a manual manipulation tool +ScanCad to rotate and translate the models. In ScanIP, an align function was created to allow the coordinate system of each model to be defined.

Suggestions for further developments include an automatic registration feature. This would remove subjectivity and manual errors on the registration of the high resolution and coarse bone models. This would also be the case when matching a sphere to the femoral head in the coarse scan model and cylinders to the malleoli and the posterior femoral condyles. Surface comparison tools would also provide a useful means of measuring inter subject variability in the creation of bone models from the same dataset. This in turn would be useful for training purposes where models produced can be compared to a model of known surface dimensions.

The ability to produce bone models using the Simpleware software and MRI data may have implications for the use in the software in subject specific surgery planning and the development of custom made implants.

This chapter has described a protocol for assessing knee function using image registration techniques. It has also shown how it can be used to gain an appreciation

of the kinematic errors associated with the current Cardiff protocol for measuring knee function. Suggestions for further work are discussed in Chapter 8. The next chapter will introduce a new application for the DS classifier other than for characterising knee function.

CHAPTER 7
NOVEL APPLICATION FOR THE DS CLASSIFIER: ASSESSING THE MERITS OF THA SURGERY

The DS classifier is a generic method to analyse motion analysis (MA) data and can be used to answer a wide range of clinical questions. To date, the classifier has been limited to characterising knee function and the changes in knee function associated with TKR. This chapter investigates the application of the DS classifier to a new clinical problem, namely to assess the relative merits of two different surgical approaches to total hip arthroplasty. The DS classifier is used to provide information on the effectiveness of two common surgical methods and to differentiate between the characteristics of hip function following the two approaches. An initial study using parameterised waveforms as inputs for the classifier is described in Whatling *et al.*, (2008f). Implications of the findings from the study for FE modelling are discussed and were presented at a conference, (Whatling *et al.*, 2008h). A further study, classifying THA function using salient principal components of kinematic and kinetic waveforms is described, (Whatling *et al.*, 2008g).

7.1 INTRODUCTION

Total hip arthroplasty (THA) is a common procedure for the treatment of hip osteoarthritis and is successful in reducing pain, improving function and patient quality of life. Gait is known to improve following THA although it does not return to what is typically quantified as normal. Numerous surgical approaches are in routine use, the most common involving either anterolateral or posterior access to the joint. Each option compromises different muscles and static constraints surrounding the hip, resulting in varying post-operative stability and control of the new joint. For this reason, surgical technique is a potential contributing factor to the level of function achieved post-operatively. Despite this, there is currently no common consensus on the best surgical approach. This study uses motion analysis techniques to obtain biomechanical data to evaluate post-operative gait and Trendelenburg tests following two principle surgical approaches: the McFarland - Osborne direct lateral approach (LA) (McFarland and Osborne, 1954) and the Moore (southern exposure) posterior approach (PA).

There are advantages and disadvantages to each procedure. The LA preserves the posterior capsule, which may reduce the rate of hip dislocation and sciatic nerve damage. The main complication to this procedure is post-operative abductor muscle dysfunction. Although the McFarland - Osborne direct LA preserves part of the insertion of gluteus medius into the greater trochanter, if migration of the abductor tendon occurs during healing, this introduces a change in the mechanical ability of the abductors, which in turn affects frontal plane stability. Abductor weakness is also reported to occur through denervation of the gluteus medius and minimus following damage to the superior gluteal nerve (Baker and Bitounis, 1989), although the role of nerve injury in the production of post-operative abductor weakness is not clear as a study found electromyographic (EMG) evidence that acute nerve injury does not correlate with clinical findings of weak abductors (Kenny *et al.*, 1999).

Advocates of the PA suggest that the main advantage in terms of function is the preservation of the abductor mechanism, resulting in a low frequency incidence of post-operative limp, (Jolles and Bogoch, 2004) and improved function (Zimmerman *et al.*, 2002). Complications associated with this approach include the potential for sciatic nerve injury and post-operative hip dislocation, (Woo and Morrey, (1982); Ritter *et al.*, 2001). The posterior joint capsule and external rotator muscle group are compromised during this procedure, affecting the posterior and lateral stability of the hip joint. The risk of hip dislocation is reported to be higher for the PA than for the LA, (Masonis and Bourne, 2002). A study using finite element modelling shows that the anterolateral approach to hip joint surgery presents a sustained risk of limp compared with a posterolateral approach (Phillips *et al.*, 2007) when the pelvic models were subjected to a loading case representative of a Trendelenburg test (Bergmann *et al.*, 2001). This was due to muscle damage following surgery. Although this result is not identified by conventional clinical assessment, it is in agreement with post-surgical gait analysis (Madsen *et al.*, 2004).

The primary cause of gait disturbances following THA is the disruption of the abductor musculature. The abductors play a crucial role during the single stance phase in gait by controlling hip abduction and pelvic obliquity. It is for this reason that a less stable gait is expected following the LA to THA.

In a previous investigation comparing an anterolateral and posterolateral approach using motion analysis, subjects following the LA exhibited a gait pattern deviating from normal in terms of increased trunk inclination, reduced sagittal plane hip range of motion (ROM), and greater loading asymmetry, whereas a normal gait pattern was exhibited for several subjects following the posterolateral approach to surgery (Madsen *et al.*, 2004). In a study of abductor strength, the PA was found to lead to a more normal hip abductor muscle strength than following an anterolateral approach (Gore *et al.*, 1982). Baker and Bitounis (1989), using a Trendelenburg test to assess abductor strength, reported abductor weakness following the LA indicated by a more positive Trendelenburg test as compared to the PA, whereas Downing *et al.*, (2001), in comparing the LA and PA, did not find significant differences in abductor strength.

The Trendelenburg test, which is a standard clinical assessment to determine the integrity of hip abductor function, is an examination of a subject's posture whilst they stand on one leg. The action of changing from a two-leg to a single-leg stance shifts the line of gravity of the superincumbent body, producing moments about the hip that must be balanced by a moment arising from the force of the abductor muscles.

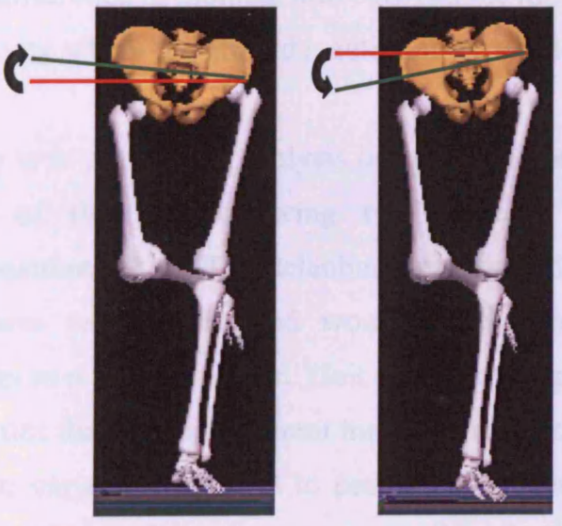

(a) (b)

Figure 7.1 (a) Positive and (b) Negative Trendelenburg tests. The red lines illustrate the horizontal position of the pelvis. The green lines illustrate the movement of the pelvis in the frontal plane.

In the case of a positive test, the pelvis on the unsupported side falls below the horizontal position, indicating abductor weakness. This action moves the line of gravity towards the supporting hip, reducing the moment lever arm and consequently the moment that must be counteracted by the abductors for stability, (Figure 7.2). The Trendelenburg test is used routinely in a clinic to assess hip stability and is included in the current study.

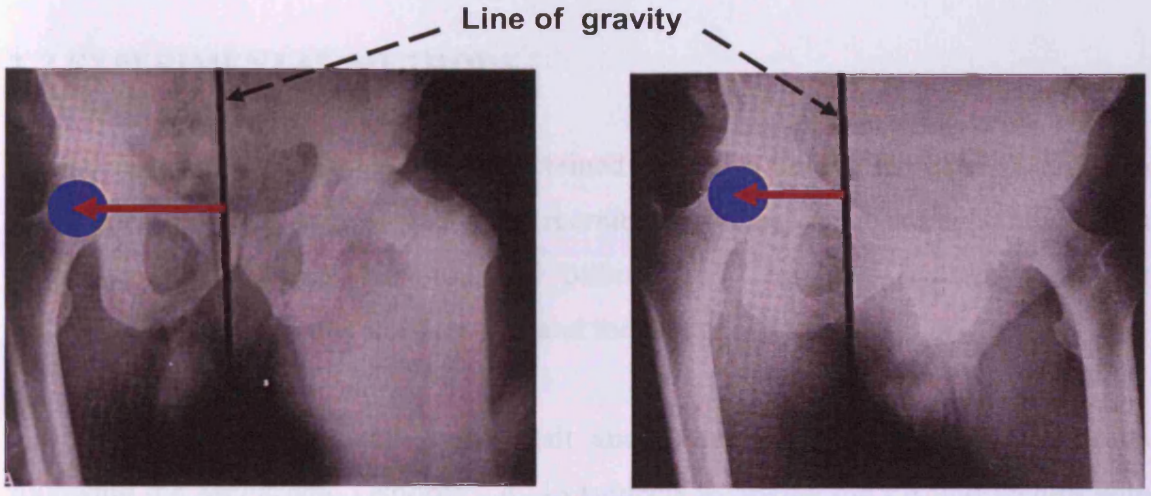

Figure 7.2 (a) Pelvis in a neutral orientation (b) Positive Trendelenburg. The red arrows illustrate the difference in moment arm between the hip joint centre and line of gravity where the ground reaction force would act.

The aim of this study is to use motion analysis techniques to perform a post-operative functional analysis of the hip following two principle surgical approaches. Quantifying pelvic position during Trendelenburg tests will allow comparison of the observational measures in a clinic and would allow subtle differences to be determined for the hip in a static situation. Gait analysis was performed to determine important characteristics that are not apparent through Trendelenburg tests alone. The kinematic and kinetic variables are used to provide an indication of post-operative recovery and surgical efficacy. Madsen *et al.*, (2004) identified the importance of quantifying gait variables to identify small differences between the groups. However, a common difficulty to this method of data collection is not only the vast amount of data yielded but its variability, which can be difficult to interpret subjectively. The current work describes a statistical analysis to determine variables that highlight significant functional differences between the two surgical approaches and also

between the operated and non-pathological hip within each surgical cohort. It then explores the use of these variables as inputs for classification using a method (Jones *et al.*, 2006) based on the Dempster-Shafer theory (DST) of evidence to characterise operated and non-pathological hip function. This method objectively analyses the mass of conflicting and corroborating data, removing the need for subjective interpretation.

7. 2 EXPERIMENTAL METHODS

Ethical approval for the study was obtained from the Gwent Research and Ethics Committee. Patients were selected and recruited by a consultant orthopaedic surgeon from the Royal Gwent Hospital. All patients were operated by two consultant orthopaedic surgeons, one used the LA and the other used the PA.

Hip function was evaluated during gait and Trendelenburg tests for 14 subjects following the McFarland Osborne LA, 13 subjects following the PA and 16 hips with no pathology (NP) forming a control group. Informed consent was obtained from the subjects after the tests had been fully explained. The LA cohort had a mean age of 64.21 (± 10.88) years, a mean height of 1.64 (± 0.08) m, and a mean mass of 82.75 (± 14.64) Kg. The PA cohort had a mean age of 60.46 (± 11.52) years, a mean height of 1.70 (± 0.07) m, and a mean mass of 90.04 (± 22.67) kg. The NP cohort had a mean age of 46.25 (± 7.42) years, a mean height of 1.72 (± 0.12) m, and a mean mass of 74.81 (± 14.34) kg. The discrepancy between the ages of the healthy and THA cohorts reflects the inherent problem encountered when obtaining data for healthy age matched cohorts that are not affected by common pathologies such as osteoarthritis and osteoporosis at the hip and other lower limb joints.

Three-dimensional (3D) motion capture was performed using QTM Software, (Qualisys, Sweden) and using eight Qualisys ProReflex MCU digital cameras, capturing at 60Hz. Force data were collected using two Bertec force platforms (Bertec Corporation) with a sample rate of 1020Hz.

During the data collection session, the subjects' height and mass were measured and 38 retro-reflective markers were positioned on their lower limbs in a modified Helen

Hayes configuration. Marker positions are shown in Figure 7.3 with the exception of a marker positioned centrally on each calcaneus. Surface markers were attached to anatomical landmarks; plate-mounted markers with a non-slip surface were used to reduce skin movement artefacts and were attached to the front of the thigh and shank.

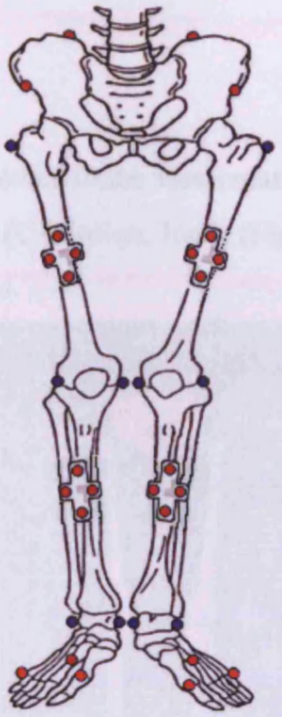

Figure 7.3 Marker Placement following a modified Helen Hayes marker set

A static measurement was taken for a quiet standing trial with the subject's feet placed approximately shoulder width apart. This data was subsequently used to define the bony segment and joint axes. Following this measurement the markers attached to the upper greater trochanter, femoral condyles and malleoli were removed. Gait trials were recorded as each subject walked the length of the laboratory in bare feet and with a self-selected speed until six trials with force plate contacts were recorded for each leg. Three Trendelenburg tests were performed on the operated and non-operated legs. As there are various ways of performing a Trendelenburg test, all subjects received the same instruction to standardise the test. Each subject was asked to step on to a force plate, to raise and flex the un-supporting leg and to return to the initial position when instructed. In cases of minimal abductor weakness, there may be a delayed positive test. For this reason, the Trendelenburg test was performed for 1 minute on each leg to introduce an element of fatigue into the abductor muscles.

Pelvic position, frontal moment and frontal power were calculated at 30 seconds into single-leg stance.

7.3 DATA PROCESSING

7.3.1 Biomechanical model

A biomechanical model of the lower limbs was created from the static measurement for each subject using Visual3D (C-Motion, Inc.), (Figure 7.4) and subsequently used for kinematic and kinetic analysis.

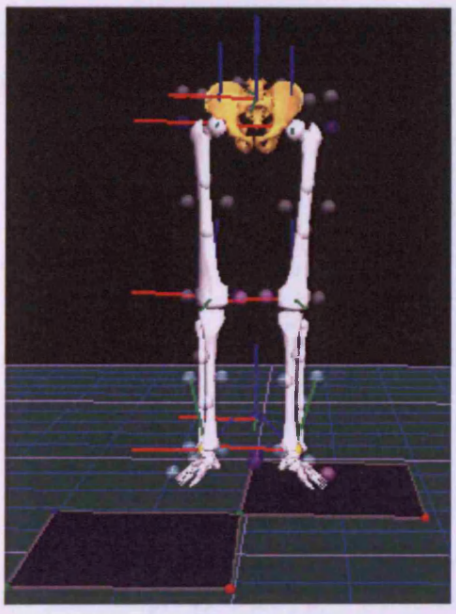

Figure 7.4 Biomechanical model created using Visual3D (C-Motion, Inc.)

The pose of each rigidly defined segment in the model was determined by at least three non-collinear points using the vector method. An axis was defined at each of the segments allowing for six degrees of freedom at each joint. Each model was assigned segment properties and patient specific information including height and mass. Movement trials were applied to the model and signal and event processing was performed. Biomechanical model-based calculations for joint angles, moments, powers and temporal parameters were defined in a pipeline. Joint rotations were described by a Cardan-Euler sequence. This describes the orientation of one segment system relative to another coordinate system as a sequence of ordered rotations about each axis of a coordinate system from its initial position. The Cardan sequence X, Y, Z was used, where Z is the positive vertical axis acting upwards and positive Y is

acting anteriorly. A segment angle was defined as the orientation of the distal segment with respect to the proximal segment. For the calculation of the segment angle of the pelvis, a virtual laboratory segment coordinate system was created and aligned to the direction of walking; the pelvic angle was computed as the orientation of the pelvis relative to the virtual laboratory. Internal joint moments, defined as the net moments generated by muscles crossing a joint, were calculated through inverse dynamic analysis and normalised to body mass (BM). Joint power, normalised to BM, was computed as the product of proximal joint moment and segmental angular velocity.

The Hip joint is a ball and socket joint with three degrees of freedom. The variables calculated were temporal parameters, hip joint ROM in three planes (Figure 7.5), pelvic tilt, obliquity and rotation (Figure 7.6).

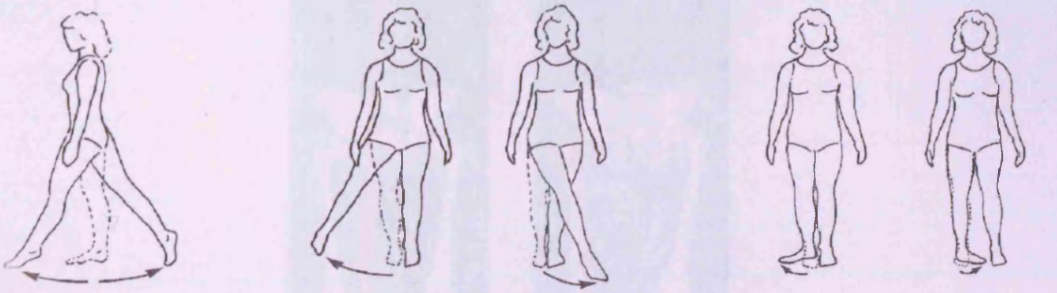

Figure 7.5 Illustration of the ROM at the hip joint, in the (a) sagittal plane, (b) frontal plane and (c) transverse plane. Image from Nordin and Frankel, (2001).

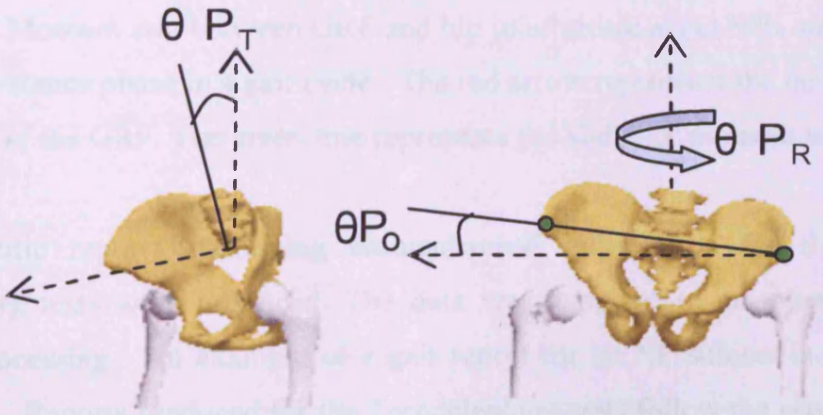

Figure 7.6 Pelvic angles: Pelvic Tilt (θP_T), Pelvic Obliquity (θP_O) and Pelvic Rotation (θP_R)

3D moments and powers acting at the hip joint were also considered to quantify the effects of muscle contractions about the joint. Abductor muscles produce torque to control abduction and pelvic obliquity, and therefore frontal moment and power are important variables to consider. The maximum value for moment and power experienced during the stance phase were determined in each plane. The moment and power at 50% stance were also calculated, as this is the point in gait when the abductor moment is at its greatest. This is due to a longer moment arm between the ground reaction force (GRF) vector and the hip joint centre (Madsen *et al.*, 2004). Figure 7.7 provides a visual representation of the change in abductor moment at 50% and 75% of the gait cycle due to the change in GRF and moment arm in the frontal plane.

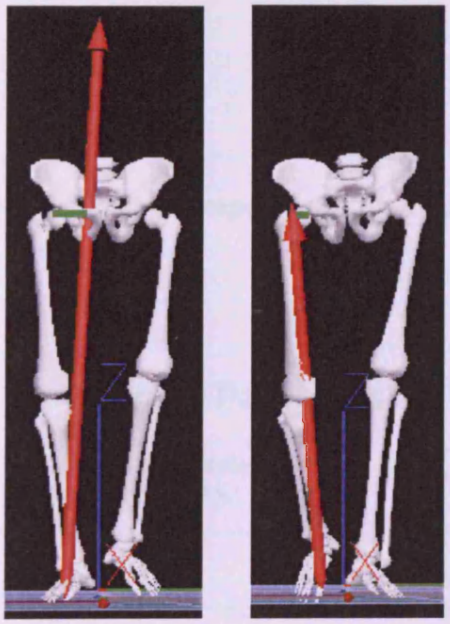

(a) (b)

Figure 7.7 Moment arm between GRF and hip joint centre at (a) 50% stance phase and (b) 75% stance phase in a gait cycle. The red arrow represents the magnitude and direction of the GRF. The green line represents the abductor moment lever arm.

Patient specific reports containing biomechanical information for the gait and Trendelenburg tests were produced. The data was exported to an external file for statistical processing. An example of a gait report for an NP subject is provided in section 7.3.2. Reports produced for the Trendelenburg tests follow the same format.

7.3.2 Example of a gait analysis report for an NP subject

Gait Analysis Report

Name : _____, _____ ___ Subject ID : _____

Height : _____ m Weight : _____ Kg Sex : Male

Date of Birth (dd/mm/yyyy) : ____/____/_____

Test Date (dd/mm/yyyy) : ____/____/_____

Diagnosis:

Test Conditions:

Cardiff University page 1

Figure 7.8 Page 1 of the gait analysis report used to collate subject information.

Temporal Parameters

Speed	1.160 m/s	0.687 Statures/s
Stride	Wid(11) 0.148±0.013m	Len(11) 1.301±0.028m
Cycle Time	Computed: 1.126 s	Actual (11) 1.121±0.013 s

Measure±StdDev (Count)		Measure±StdDev (Count)
Left : 0.654±0.019 m (6)	Step Length	Right : 0.649±0.014 m (11)
Left : 0.429±0.245 s (8)	Step Time	Right 0.562±0.011 s (11)
Left : 0.692±0.009 s (6)	Stance Time	Right : 0.700±0.000 s (5)
Left : 0.428±0.014 s (6)	Swing Time	Right : 0.423±0.009 s (5)

Double Limb Support Time (12)	0.275±0.009 s
Right Initial Double Limb Support Time (6)	0.133±0.000 s
Right Terminal Double Limb Support Time (6)	0.142±0.009 s
Flight Time (1)	1.000±0.000 s

Cardiff University page 2

Figure 7.9 Page 2 of the gait analysis report detailing temporal distance parameters.

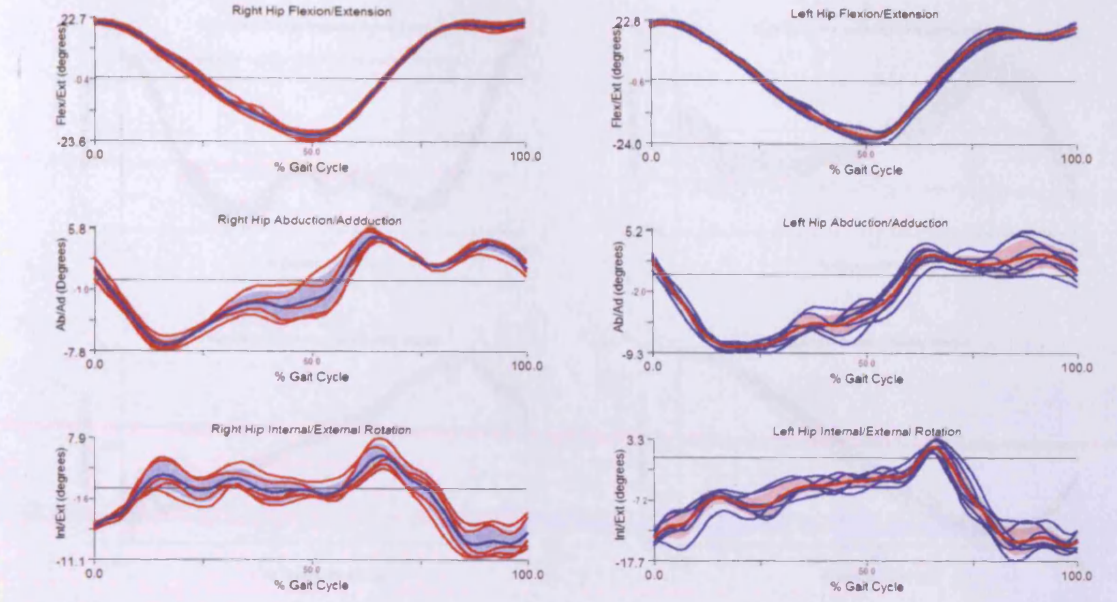

Figure 7.10 Page 3 of the gait analysis report displaying hip rotations for each gait trial, mean and standard deviation.

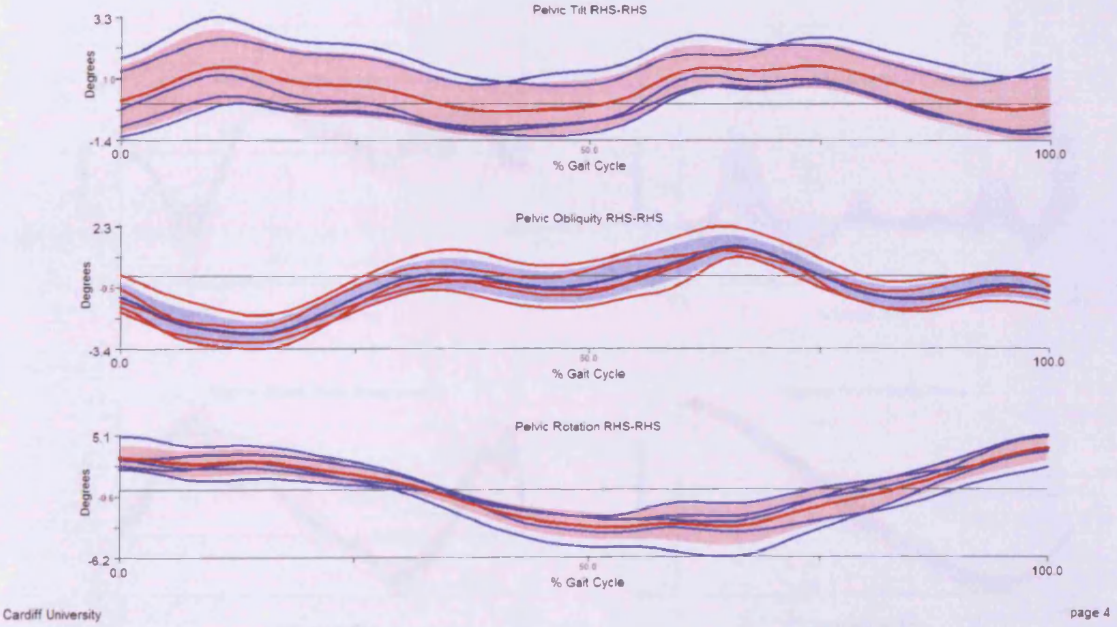

Figure 7.11 Page 4 of the gait analysis report displaying pelvic rotations for each gait trial, mean and standard deviation.

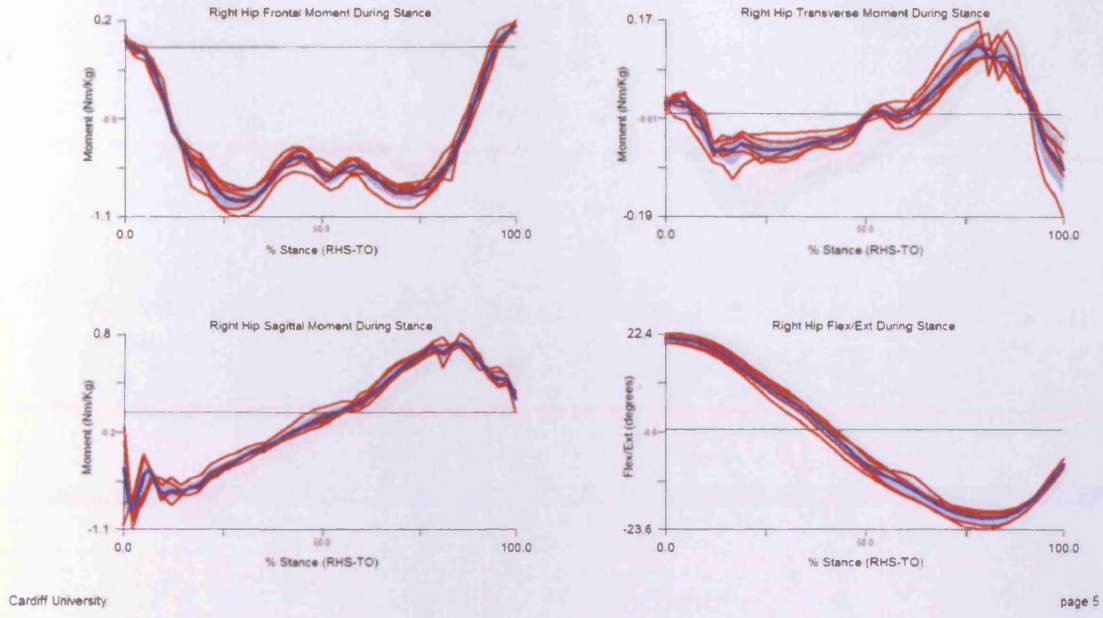

Figure 7.12 Page 5 of the gait analysis report displaying moments acting about the right hip for the stance phase in each gait trial. The mean and standard deviation for the trials are shown in blue.

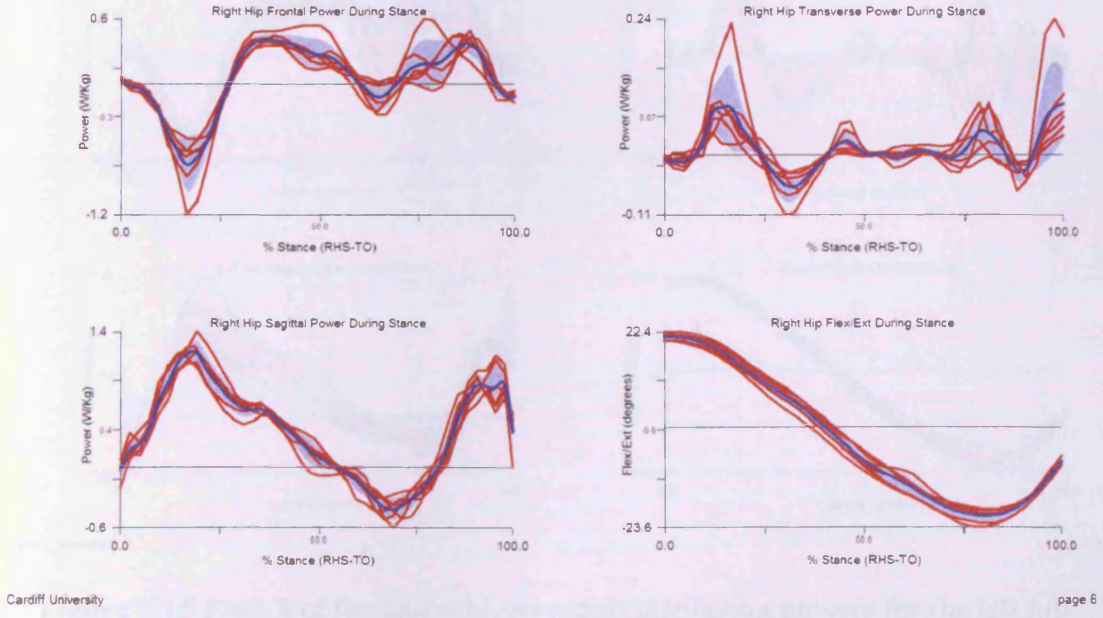

Figure 7.13 Page 6 of the gait analysis report displaying powers for the right hip calculated for the stance phase in each gait trial. The mean and standard deviation for the trials are shown in blue.

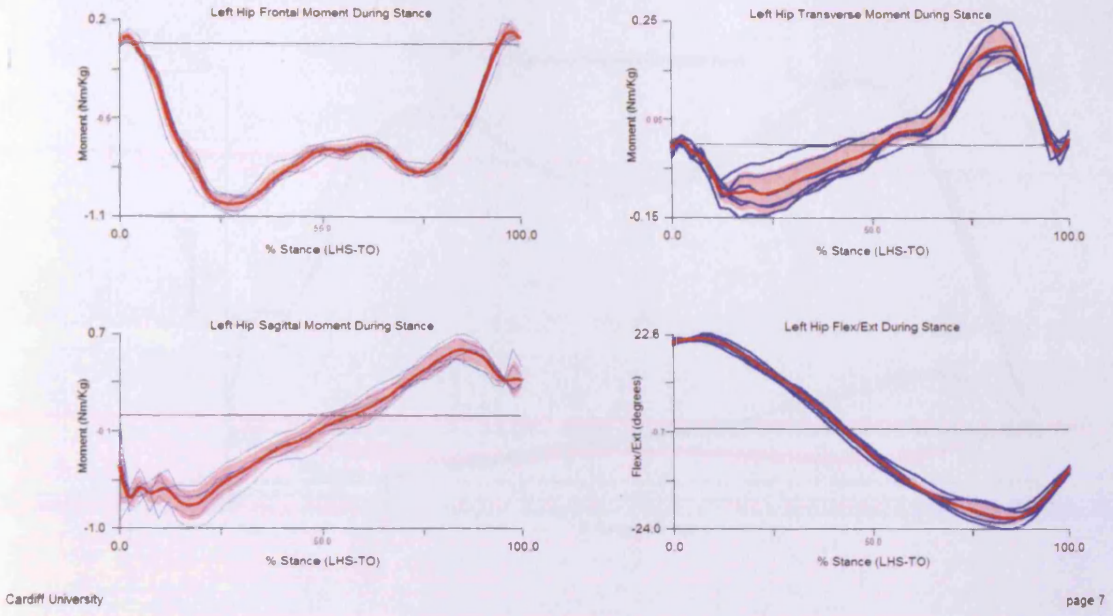

Figure 7.14 Page 7 of the gait analysis report displaying moments acting about the left hip for the stance phase in each gait trial. The mean and standard deviation for the trials are shown in red.

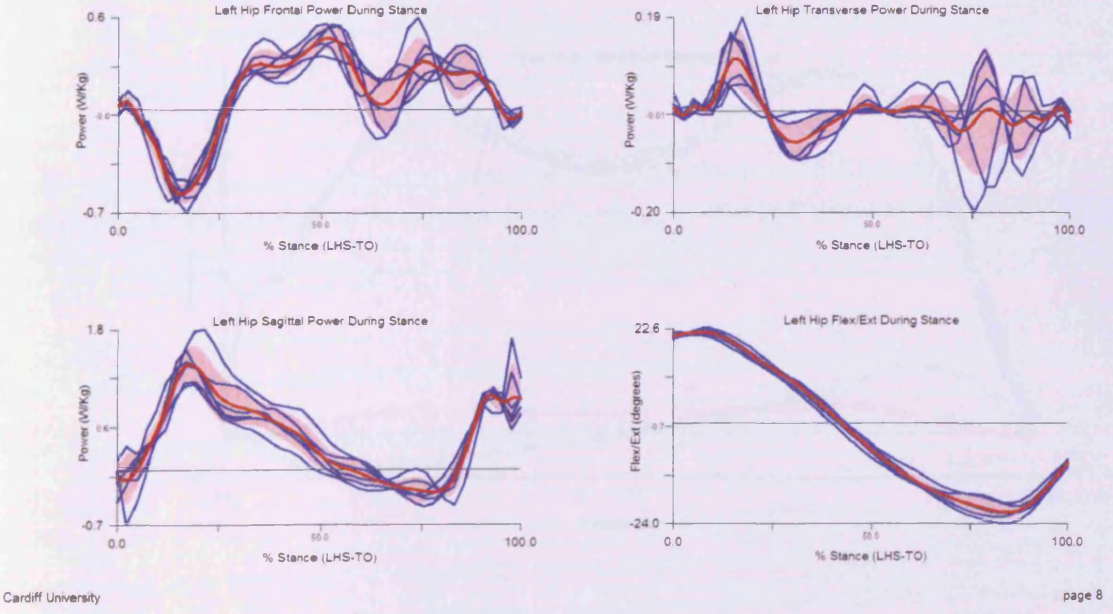

Figure 7.15 Page 8 of the gait analysis report displaying powers for the left hip calculated for the stance phase in each gait trial. The mean and standard deviation for the trials are shown in red.

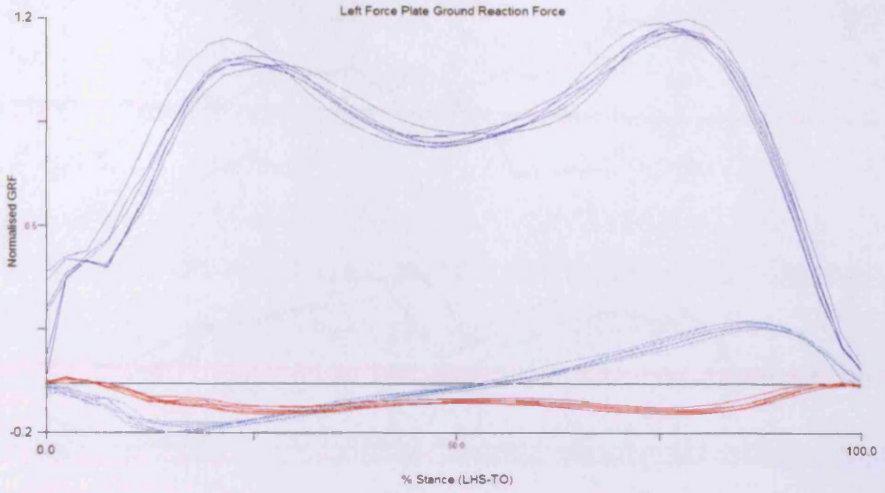

Figure 7.16 Page 9 of the gait analysis report displaying ground reaction forces for the left leg normalised by subject body weight.

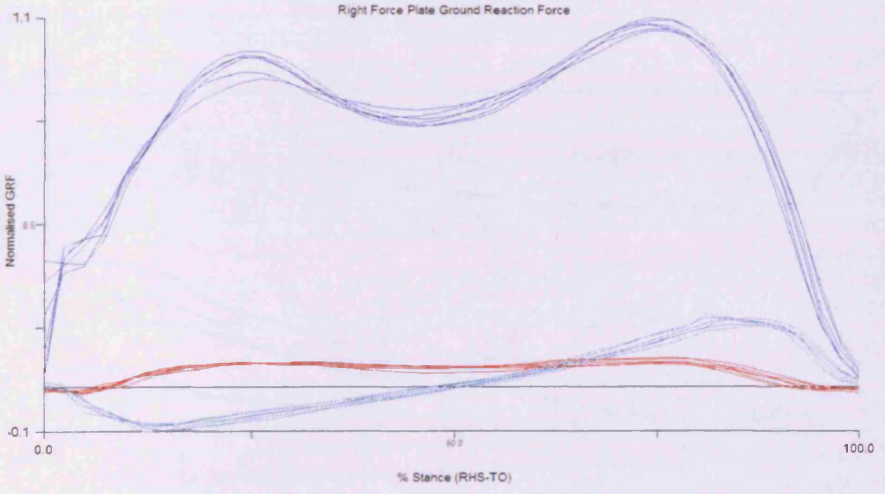

Figure 7.17 Page 10 of the gait analysis report displaying ground reaction forces for the right leg normalised by subject body weight.

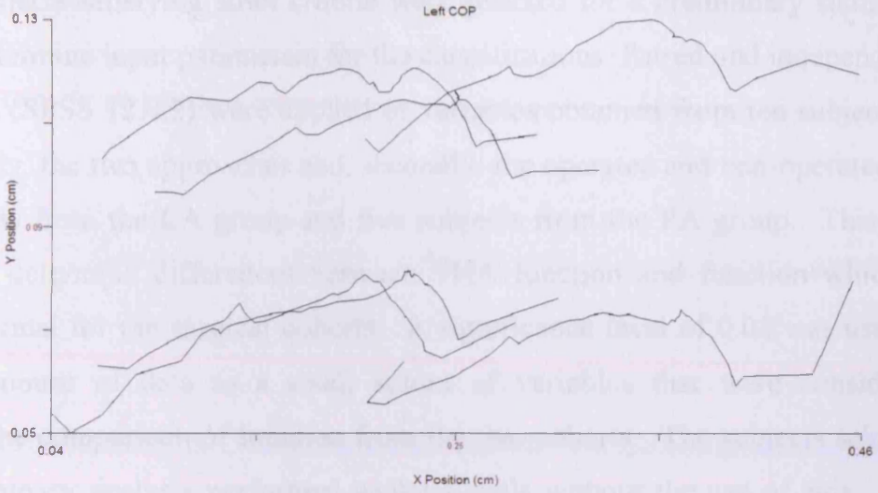

Figure 7.18 Page 11 of the gait analysis report displaying centre of pressure position (COP) of the left foot during the stance phase of each trial. The COP is expressed in the force plate coordinate system.

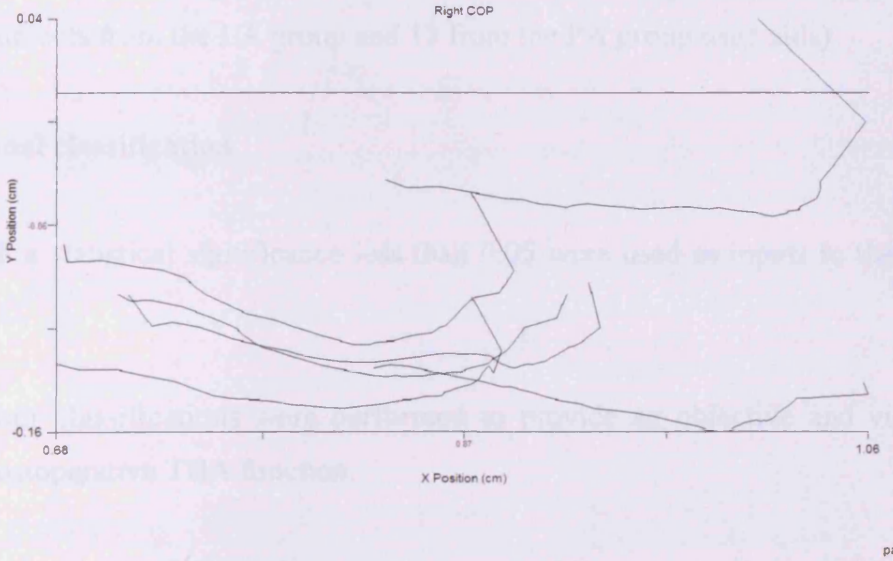

Figure 7.19 Page 12 of the gait analysis report displaying centre of pressure position (COP) of the right foot during the stance phase of each trial. The COP is expressed in the force plate coordinate system.

7.3.3 *t*-tests

Data from subjects satisfying strict criteria were selected for a preliminary statistical analysis to determine input parameters for the classifications. Paired and independent-sample *t*-tests (SPSS 12.0.2) were applied to variables obtained from ten subjects to compare, firstly, the two approaches and, secondly, the operated and non-operated leg of five subjects from the LA group and five subjects from the PA group. This was performed to determine differences between THA function and function which is considered normal for the surgical cohorts. A significance level of 0.05 was used to reduce the amount of data to a small subset of variables that were considered important in the comparison of function from the two cohorts. The subjects selected for this preliminary analysis performed walking trials without the use of aids. One subject from the LA group and five from the PA group felt unable to complete the Trendelenburg tests without an aid. These satisfied a selection criteria where 0.8 BM or greater registered on the force plate during the Trendelenburg tests to ensure that considerable effort was required from the abductors for pelvic control. The remaining subjects included when exploring the use of the classifier registered at least 0.8BM or greater on the force plate during gait trials (where five subjects from the LA group and one subject from the PA group used aids) and 0.7BM during Trendelenburg tests (where nine subjects from the LA group and 13 from the PA group used aids).

7.3.4 Functional classification

Variables with a statistical significance less than 0.05 were used as inputs to the DS classifier.

A series of four classifications were performed to provide an objective and visual indicator of postoperative THA function:

(a) NP and LA;
(b) NP and PA;
(c) PA and LA;
(d) NP and surgical group containing PA and LA.

A detailed description of the DS classification method is provided in Chapter 2. To briefly describe the method, the classification of NP and LA subjects are used as an example. The DS classifier transforms the functional hip data from each subject into a set of three belief values: a belief that the subject's hip function is non-pathological ($m(\{NP\})$); a belief that the subject has hip function characteristic of an LA to surgery ($m(\{LA\})$); an associated level of uncertainty ($m(\Theta)$). These are represented as a single point on a simplex plot to give a visual representation of hip function (Figure 7.20a). The distance of the point from each side of the equilateral triangle is in proportion to the belief values. For example, the closer the point is situated to the vertex labelled {NP}, the greater is the belief that the subject has NP hip function. The simplex plot can be split into four regions (Figure 7.20b) with a central decision boundary illustrated by the dashed line along which ($m(\{NP\})$= ($m(\{LA\})$). Region 1 highlights the area of dominant NP function in which ($m(\{NP\})>0.5$). Region 2 highlights the area of dominant LA function where ($m(\{LA\})>0.5$). Region 3 highlights the area of non-dominant NP function where ($m(\{LA\})<m(\{NP\})<0.5$) and region 4 shows non-dominant LA function where ($m(\{NP\})<m(\{LA\})<0.5$).

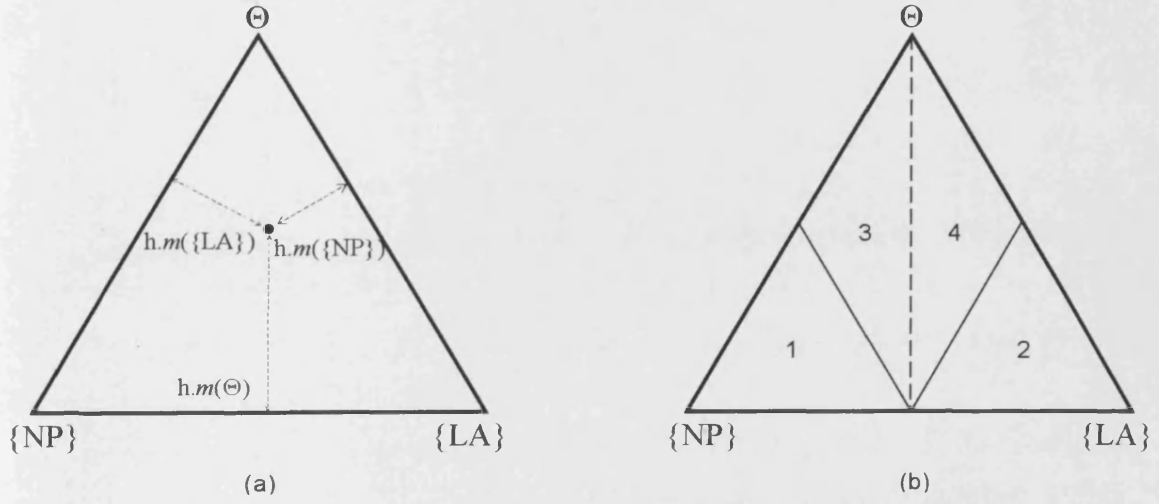

Figure 7.20 (a) Relationship between the belief values and position of the point on the simplex plot, where h is the height of the triangle. (b) Regions of dominant (1 and 2) and non-dominant (3 and 4) classification

The Dempster-Shafer control parameters k, θ, A and B, were calculated from the variables of the combined cohorts used in the classification, using the non-

optimisation approach. k was calculated using the correlation coefficient method and A and B were determined from the limits $[\Theta_L, \Theta_U] = [0.3, 0.8]$. The accuracy of the study was determined using the Leave-one-out method of cross validation, as detailed in Chapter 2.

7.4. RESULTS

Following data collection, kinematic, kinetic and temporal parameters were computed. Statistical analysis was performed on the data from five subjects from each surgical cohort to determine a subset of signals with a statistical difference, firstly, between the two cohorts and, secondly, between the operated and non-operated hip within each cohort. Variables with a statistical significance less than 0.05 were used as inputs to the DS classifier. Once the variables highlighting differences between the two surgical groups were determined, the remaining subjects were included in the analysis using the classifier.

7.4.1 Comparison between the surgical cohorts

An independent *t*-test was performed on the variables displayed in Table 7.1. Through the comparison of the two surgical cohorts, the LA group was generally found to produce lower hip and pelvic ROM during gait, with the exception of hip frontal and pelvic sagittal ROM. The difference in pelvic obliquity ROM i.e. the movement in the frontal plane for the LA group ($3.92 \pm 0.92^{\circ}$) and PA group ($6.13 \pm 1.74^{\circ}$), was found to be significant. The LA patients may compensate for this by adopting a greater pelvic ROM in the sagittal plane ($4.47 \pm 2.09^{\circ}$) as compared with the PA group ($3.08 \pm 1.11^{\circ}$).

The frontal power and moment acting about the hip are indicative of abductor muscle function. In addition to the maximum values measured during gait, values at 50% stance phase, when the abductor moment is at its greatest (Madsen *et al.*, 2004), were also considered. In comparing the surgical cohorts, lower frontal moments and powers were found for the LA group, indicating abductor muscle weakness. These differences are statistically significant, with the exception of frontal moment at 50% stance due to a large standard deviation in the LA subject group. Analysis of the measurements for the operated leg taken 30 seconds into the Trendelenburg tests indicated significantly lower frontal moments acting about the hip for the LA group as compared with the PA group. This may indicate abductor weakness or the use of compensatory mechanisms to maintain a stable pelvic position. Although no significant difference between the orientations of the pelvis (defined as the angle of

the pelvis above the horizontal in the frontal plane) was determined 30 seconds into the Trendelenburg, some variation was observed during the tests and between patients. In a normal test, the subjects' pelvis remained in a constant negative Trendelenburg position as shown in Figure 7.21a. Two patterns deviating from normal were observed, indicating abductor weakness. Firstly, although a negative test was noted initially, the pelvis then dropped towards the horizontal due to diminishing abductor strength (Figure 7.21b) and in some cases dropped below the horizontal position into a positive test (Figure 7.21c). Secondly, a subject began with a positive Trendelenburg test, and then as their abductors became more influential, they corrected their position by raising their pelvis until nearing the end of the test when their pelvis dropped below the horizontal position, as in (Figure 7.21d).

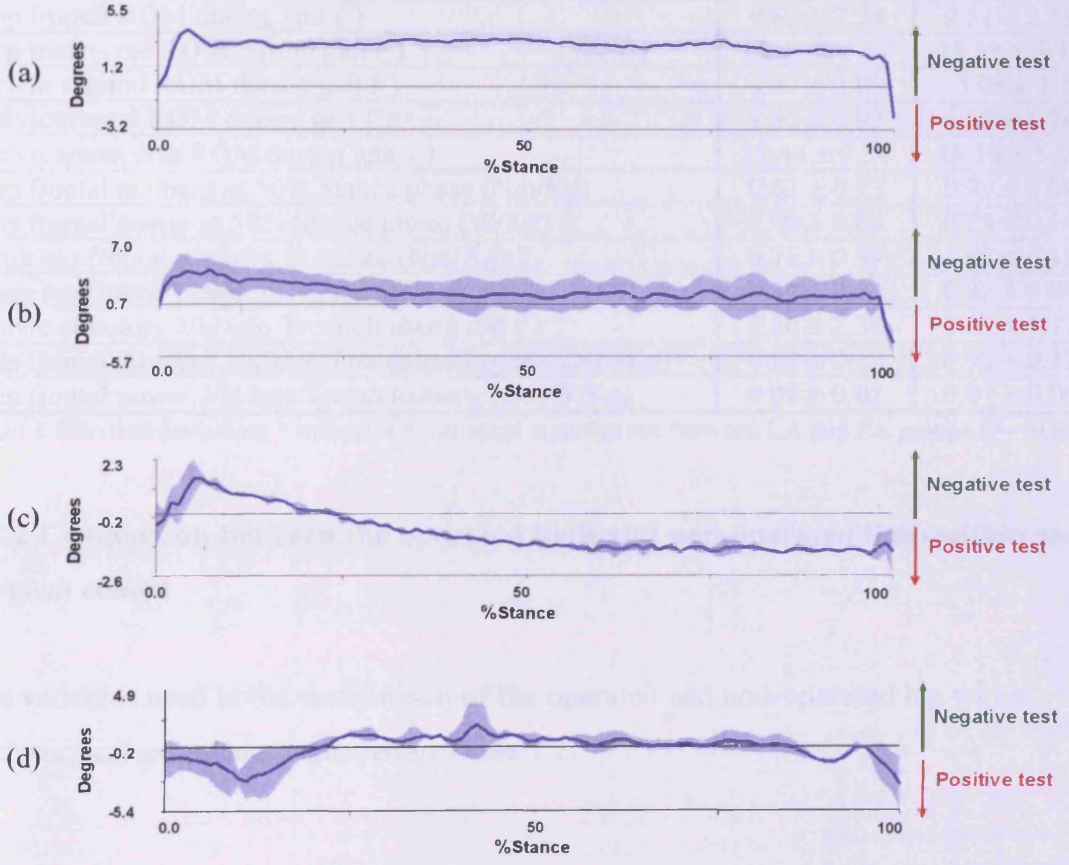

Figure 7.21 Examples of the variation in pelvic obliquity waveforms observed during the Trendelenburg tests. (a) Normal abductor function, (b) minor diminishing abductor strength, (c) significant diminishing abductor strength and (c) varying abductor control. Each graph shows the mean and standard deviation of three measurements. The subject stands on a force plate, raises and flexes their un-supporting leg, then returns to the initial position.

Table 7.1 Variables used for the independent-sample *t*-test for LA and PA groups. (Whatling *et al.*, 2008f)

Variable (unit)	LA Group (n = 5)	PA Group (n = 5)
Height (m)	1.67 ± 0.11	1.68 ± 0.07
Weight (Kg)	86.90 ± 14.66	86.5 ± 28.91
Speed (m/s)	0.98 ± 0.28	1.03 ± 0.13
Stride length (m)	1.09 ± 0.20	1.14 ± 0.14
Cycle time (s)	1.14 ± 0.15	1.10 ± 0.05
Double limb support time (s)	0.25 ± 0.08	0.23 ± 0.04
Peak GRF in stance (N)	1.11 ± 0.10	1.15 ± 0.05
Symmetry index	1.01 ± 0.02	1.04 ± 0.04
Stance time (s)	0.69 ± 0.10	0.67 ± 0.04
Hip sagittal ROM during gait (°)	29.7 ± 4.71	32.55 ± 7.82
Hip frontal ROM during gait (°)	9.62 ± 2.78	9.51 ± 2.58
Hip transverse ROM during gait (°)	11.41 ± 2.67	13.53 ± 3.79
Pelvic sagittal ROM during gait (°)	4.47 ± 2.09	3.08 ± 1.11
Pelvic frontal ROM during gait (°) *	3.92 ± 0.92	6.13 ± 1.74
Pelvic transverse ROM during gait (°)	13.44 ± 7.34	16.10 ± 5.00
Hip frontal moment at 50% Stance phase (Nm/Kg)	0.61 ± 0.22	0.79 ± 0.08
Hip frontal power at 50% Stance phase (W/Kg) *	0.08 ± 0.04	0.25 ± 0.14
Peak hip frontal moment in stance (Nm/Kg) *	0.75 ± 0.15	1.02 ± 0.13
Peak hip frontal power in stance (W/Kg) *	0.34 ± 0.10	0.82 ± 0.08
Pelvic obliquity 30s into Trendelenburg test (°)	3.86 ± 2.34	1.87 ± 1.77
Hip frontal moment 30s into Trendelenburg test (Nm/Kg)*	0.52 ± 0.19	0.95 ± 0.12
Hip frontal power 30s into Trendelenburg test (W/Kg)	0.02 ± 0.02	0.01 ± 0.00

Mean ± Standard deviation: * indicates a statistical significance between LA and PA groups ($P < 0.05$)

7.4.2 Comparison between the operated limb and non-operated limb within each surgical cohort

The variables used in the comparison of the operated and non-operated hip within each surgical group are displayed in Table 7.2.

Table 7.2 Variables used for the paired-samples *t*-test to compare operated and non-operated hip functions within the surgical groups (Whatling *et al.*, 2008f)

Variable (unit)	LA ($n = 5$)		PA ($n = 5$)	
	Operated Hip	Non-operated Hip	Operated Hip	Non-operated Hip
Hip sagittal ROM during gait (°)	29.70 ± 4.71	* 39.89 ± 3.21	32.55 ± 7.82	32.75 ± 14.14
Hip frontal ROM during gait (°)	9.62 ± 2.78	11.73 ± 0.81	9.51 ± 2.58	9.55 ± 2.91
Hip transverse ROM during gait (°)	11.41 ± 2.67	11.36 ± 3.34	13.53 ± 3.79	11.72 ± 3.15
Peak GRF in stance (N)	1.11 ± 0.10	1.10 ± 0.09	1.15 ± 0.05	1.10 ± 0.07
Stance time (s)	0.69 ± 0.10	0.71 ± 0.12	0.67 ± 0.04	0.67 ± 0.05
Hip frontal moment at 50% stance phase (Nm/Kg)	0.61 ± 0.22	0.67 ± 0.14	0.79 ± 0.08	0.82 ± 0.16
Hip frontal power at 50% stance phase (W/Kg)	0.08 ± 0.04	0.09 ± 0.13	0.25 ± 0.14	0.17 ± 0.11
Peak hip frontal moment during stance (Nm/Kg)	0.75 ± 0.15	0.85 ± 0.23	1.02 ± 0.13	1.00 ± 0.16
Peak hip frontal power during stance (W/Kg)	0.34 ± 0.09	0.60 ± 0.43	0.82 ± 0.08	0.79 ± 0.32
Pelvic Obliquity 30s through Trendelenburg test (°)	3.86 ± 2.34	4.65 ± 2.49	1.87 ± 1.77	* 5.56 ± 3.07
Hip frontal moment 30s into Trendelenburg test (Nm/Kg)	0.52 ± 0.19	0.86 ± 0.36	0.95 ± 0.12	1.00 ± 0.39
Hip frontal power 30s into Trendelenburg test (W/Kg)	0.02 ± 0.02	0.02 ± 0.02	0.01 ± 0.00	0.01 ± 0.01

Mean ± Standard deviation; * indicates a statistical significance between the operated and non-operated hip function within a surgical group ($P < 0.05$)

The ROM values for the operated and non-operated hip within the PA cohort are similar, although a large variation is evident for the operated leg sagittal ROM. A significantly lower ROM was found in the sagittal plane for the operated (29.7 ± 4.71°) compared with the non-operated (39.89 ± 3.21°) hip for the LA cohort. This suggests that, following the LA, subjects have insufficient control of the stabilising mechanisms that would normally allow them to utilise the full ROM of their operated hip during gait and a lack of confidence on their operated limb. In the comparison of the operated and non-operated leg, pelvic obliquity was significantly less for the operated hip (1.87 ± 1.77°) than the non-operated hip (5.56 ± 3.07°) for the PA group. This suggests that the abductors are weaker for the LA group as compared with the PA group and that abductor strength for the PA group has also not returned to normal.

From the statistical analysis the variables selected as inputs to the classifier were as follows: pelvic obliquity and hip sagittal ROM during gait; hip frontal power at 50% stance phase during gait; peak frontal power and moment during gait; frontal hip moment and pelvic obliquity 30 seconds into the Trendelenburg test.

7.4.3 Classification Outputs

Initial classifications were performed using the variables found to be significantly different between the two groups being classified, as in Table 7.3.

Table 7.3 Variables used in preliminary classifications

Variable	(a) {NP} {LA}	(b) {NP} {PA}	(c) {PA} {LA}	(d) {NP} {PA, LA}
Pelvic obliquity ROM during gait			✓	
Hip sagittal ROM during gait	✓			✓
Hip frontal power at 50% stance			✓	
Peak hip frontal power in stance			✓	
Peak hip frontal moment in stance			✓	
Hip frontal moment 30s into Trendelenburg test			✓	
Pelvic Obliquity 30s into Trendelenburg test		✓		

The outputs from the classification are shown in Figures 7.22a-d. With the exception of the classification in Figure 7.22a, the variables used were unable to distinguish between the subject groups or separate the subjects into their respective sides of the simplex plot. The classification accuracies were (a) 93.3%, (b) 62.1%, (c) 70.4% and (d) 60.5%. Despite using the variables identified using the *t*-test for the classification, it is clear that a combination of functional variables is required to provide a better distinction between NP and surgical groups. In classification (c), the combination of the variables used was unable to separate the functional characteristics of the two surgical groups.

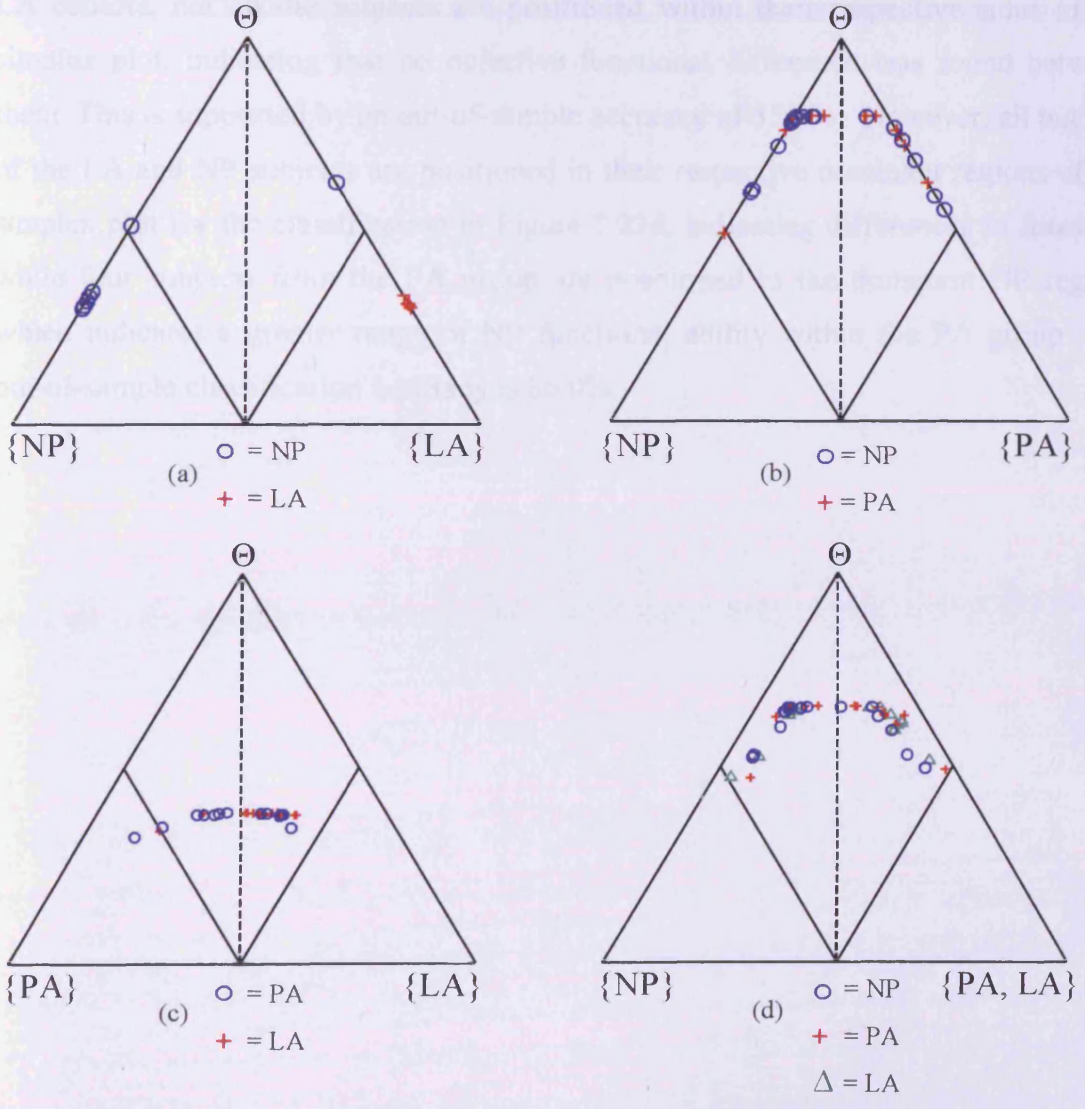

Figure 7.22 Simplex plots for the classification of (a) NP and LA, (b) NP and PA, (c) PA and LA, (d) NP and surgical group containing both PA and LA.

The following classification was performed to determine whether in combination, the variables in Table 7.3 could identify differences in function between the cohorts.

The outputs from the classifications are shown in Figures 7.23a-d. The classification in 7.23a has an out-of-sample accuracy of 93.3%. There is a distinction between the subjects exhibiting NP and LA function as the subjects are situated within their respective dominant regions of the simplex plot. A distinction between the groups is also evident for the classification in Figure 7.23b. The out-of-sample accuracy is 86.2% with four misclassified subjects; two subjects from the PA group are situated in the dominant NP region. For the classification in Figure 7.23c, between the PA and LA cohorts, not all the subjects are positioned within their respective sides of the simplex plot, indicating that no objective functional difference was found between them. This is supported by an out-of-sample accuracy of 55.6%. However, all but one of the LA and NP subjects are positioned in their respective dominant regions of the simplex plot for the classification in Figure 7.23d, indicating differences in function, while four subjects from the PA group are positioned in the dominant NP region, which indicates a greater range of NP functional ability within the PA group. The out-of-sample classification accuracy is 86.0%.

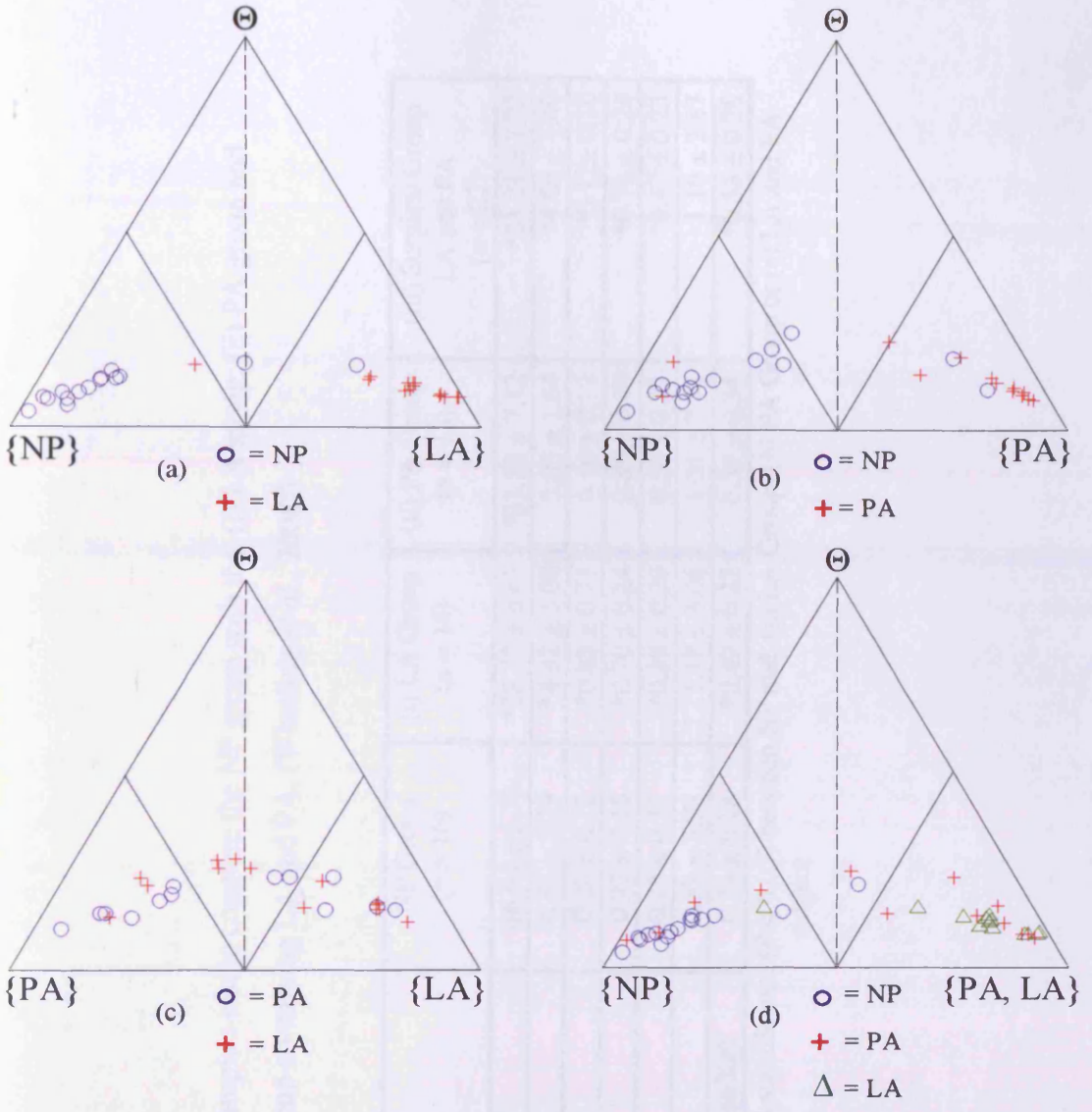

Figure 7.23 Simplex plots for the classification of (a) NP and LA, (b) NP and PA, (c) PA and LA, (d) NP and surgical group containing both PA and LA. (Whatling *et al.*, 2008f)

Independent-sample *t*-tests (SPSS 12.0.2) were applied to the variables used in the four classifications to clarify the classification outputs. The results from the *t*-tests comparing NP and surgical functions are displayed in Table 7.4. From a *t*-test on the variables to compare the LA and PA functions, a statistical difference was determined between the two approaches for peak hip frontal power in stance (LA, 0.39 ± 0.20 W/Kg, PA, 0.56 ± 0.23 W/Kg), and peak hip frontal moment in stance (LA, 0.70 ± 0.24 Nm/Kg, PA, 0.89 ± 0.20 Nm/Kg).

Table 7.4 Variables used for the independent-sample *t*-test to compare the NP group with the (i) LA group, (ii) PA group and (iii) surgical group containing LA and PA, (Whatling *et al.*, 2008f)

Variable (unit)	NP Group (n = 16)	(i) LA Group (n = 14)	(ii) PA Group (n = 13)	(iii) Surgical Group LA and PA (n = 27)
Hip sagittal ROM during gait (°)	46.94 ± 5.73	*28.72 ± 6.67	*33.88 ± 7.12	*31.21 ± 7.25
Pelvic frontal ROM during gait (°)	6.88 ± 3.29	*4.32 ± 1.08	5.03 ± 1.64	*4.66 ± 1.40
Hip frontal power at 50% Stance phase (W/Kg)	0.20 ± 0.12	*0.83 ± 0.71	0.16 ± 0.12	*0.12± 0.10
Peak hip frontal moment in stance (Nm/Kg)	0.97 ± 0.15	*0.70 ± 0.24	0.89 ± 0.20	*0.79 ± 0.24
Peak hip frontal power in stance (W/Kg)	0.75 ± 0.31	*0.39 ± 0.20	0.56 ± 0.23	*0.47 ± 0.23
Pelvic obliquity 30s into Trendelenburg test (°)	2.32 ± 3.08	1.18 ± 3.06	1.01 ± 2.78	1.10 ± 2.87
Hip frontal moment 30s into Trendelenburg test (Nm/Kg)	0.74 ± 0.18	*0.49 ± 0.22	0.59 ± 0.34	*0.53 ± 0.28

Mean ± Standard deviation; * indicates a statistical significance ($P < 0.05$) between NP and (a) LA Group, (b) PA Group or (c) LA and PA subject

7.5 DISCUSSION

From this initial study, seven clinically relevant variables have been found to be important in characterising THA function. Six out of the seven input variables relate to hip function in the frontal plane, indicating a difference between the abductor strength and stabilities of the surgical groups.

Pelvic obliquity and frontal moment acting at the hip measured 30 seconds into the Trendelenburg test were significant in the comparison of the two cohorts. This is to be expected, as it is a standard clinical test to assess pelvic position, hip stability and abductor strength. The pelvis was held at a slightly lower position when standing on the operated compared with the non-operated leg within the PA group. A difference between the abductor strengths of the operated hip and non-operated hip is expected, although a significant difference within the LA group was not found. This is due to a larger variability within the group. The angles computed for pelvic obliquity (angle of unsupported side measured above a horizontal position, as shown in Figure 7.6) are small. This highlights the benefits of the motion analysis system in detecting subtle differences but also raises the question of the reliability of using the Trendelenburg tests in a clinic for the assessment of THA patients where small differences may not be observed.

During the Trendelenburg test, hip frontal moment is significantly lower for the LA indicating a lower net torque generated by the muscles surrounding the joint. As the pelvic position is not significantly different between the two groups, this suggests that an alternative compensatory action is acting to reduce the loading on the abductor muscles. Possible mechanisms include trunk inclination over the supporting leg (Figure 7.24a-c) or the use of alternative stabilising structures surrounding the hip. Through video analysis, slight trunk inclination over the supporting leg was observed for several of the subjects. Trunk inclination occurred more frequently and was more pronounced when the subjects stood on their operated limb. For this reason, it would be beneficial to position markers on the trunk and to make EMG recordings during the tests.

Values were taken 30s into the Trendelenburg test to allow for muscle fatigue; however, it is apparent that, owing to the variability in the data, there is a danger of losing important information as the subject acts to stabilise their position. Further investigation is required to analyse these waveforms in order to produce a definitive point at which the data can be used satisfactorily for comparative studies.

(a) (b) (c)

Figure 7.24 Trendelenburg with (a) no observed trunk inclination, (b) moderate trunk inclination over the supporting leg, (c) Pronounced trunk inclination over the supporting leg, in combination with arms used for stabilisation.

During gait trials, the LA group exhibited a reduced sagittal and frontal ROM of their operated hips, compared with their non-operated hips. Lower sagittal hip ROM and pelvic obliquity ROM were measured for the LA group compared with the PA group. These subjects may have limited control or strength in the stabilising mechanisms that would allow them to use the full ROM of their operated hip. The posterior group showed a greater variation in ability and showed greater characteristics of non-pathological gait. Unfortunately, for the current study, patients were referred for post-operative gait analysis only, thus there are no comparisons with pre-operative gait analysis data. On exploring the outcomes of this study it is evident that for future similar studies, pre-operative gait should be analysed since, firstly, it would provide individual patient comparative data sets and, secondly, surgeons note that, via the LA, it is common to see chronic abductor tears at the time of surgery which obviously preceded the surgery.

Frontal moments during gait were significantly lower for the LA group compared with the NP and PA groups, owing to abductor weakness and subsequent reduced torque generation. Frontal moment measured at 50% stance was found to be an important variable. This is when the abductor moment is at its greatest because of the greatest moment arm between the GRF vector and hip joint centre. Frontal power was also found to be a salient variable in the comparison of the two surgical groups. The maximum value and value at 50% stance were considerably lower for the LA group indicating a reduced rate of change of energy.

The clinical measures determined through statistical analysis were applied to the classifier for further analysis to determine their ability to characterise NP, PA and LA functions. Using only the variables with a significant difference between the groups used in each classification, no distinction between the groups could be made, with the exception of the classification of NP and LA hip function. In this classification, hip sagittal ROM during gait was able to characterise subject function with an accuracy of 93%. However, the output from this classification showed that all but two subjects clustered in two distinct groups. Although only two subjects were misclassified, the clustering of the remaining subjects is undesirable as a range in ability between the subjects is not clear. When all seven variables were used, they were successful in classifying non-pathological and surgical function but were unable to distinguish between surgical groups.

The classification outputs display several interesting results. Firstly, from the classification of LA and NP functions (Figure 7.23a), generally all the subjects are situated within their respective dominant positions on the simplex plot, whereas the PA group displays a variation in functional ability. In the classification of NP and PA functions (Figure 7.23b), there is a less clustering of the subjects and two PA subjects exhibit characteristics of NP hip function. The spread of PA subjects across the simplex plot suggest that the difference in function is not as clearly defined as for the NP and LA classification. This is supported by the results of the independent *t*-tests displayed in Table 7.4. Six of the functional variables were significant in the comparison of the LA and NP groups, resulting in a clear divide in functional abilities, whereas only one significant result was produced in the comparison of NP and PA functions, indicating some similarities between the functions of the groups.

The variables were unable to distinguish between LA and PA subjects (Figure 7.23c). Although the *t*-tests comparing LA and PA function determined maximum frontal power and maximum frontal moment during the stance phase to be significant, the body of evidence responsible for the classification did not have sufficient positive or negative support to classify each subject correctly. Interestingly, when both surgical groups were classified against the NP function, a pattern emerged. For this classification (Figure 7.23d), the NP and LA subjects were predominantly situated within their dominant regions, whereas the PA subjects were spread across the simplex plot with several subjects situated within the NP dominant region. This confirms that a difference between the post-operative functions of the two groups existed. The PA cohort exhibits patterns more characteristic of the NP function than the LA group. Further work involving a larger cohort is required to determine whether these initial results are clinically relevant.

Initial results have determined clinically relevant measures that highlight a difference in functions following the two approaches. The PA to THA appears to lead to a more stable function and greater ROM than does the LA. A classification method has been implemented to characterise functions. A visual output allows a straightforward comparison of subject functions. With further investigation of the input variables using a larger cohort, the classifier could be used to improve patient care by predicting surgical outcomes and monitoring postoperative function.

7.6 IMPLICATIONS FOR FE PREDICTIONS OF SURGICAL OUTCOME

The outcomes reported in Table 7.1 were compared with Finite Element (FE) predictions in collaboration with Imperial College London, (Whatling *et al.*, 2008h). Hip function following LA and PA was compared using a previously published biofidelic muscular and ligamentous (free) boundary condition FE model of the pelvis. The FE model predictions were found to be in agreement with gait observations, indicating an altered function of the abductors following LA surgery.

Simulating a Trendelenburg test, the LA FE model produced a difference in the stress distribution within the cortex of the pelvis on the supporting side, predicted higher pelvic drop on the un-supporting side, lower abductor forces and higher abductor

pressures as compared with a model with intact muscles replicating NP function. These differences were not observed for the PA model.

In-vivo data can provide valuable inputs to develop and validate FE models that are accurately representative of human response to changes in muscle function. The motion analysis study demonstrates that patient's control of function varies considerably. FE models often use data obtained from a limited number of patients, as in this study where loading information was obtained from 4 patients (Bergmann, 2001). Large cohorts of more accessible marker-based gait data would provide a more robust range of kinematic and kinetic data. It would be useful in future work to use experimental biomechanical data from Trendelenburg, gait and stair climbing in conjunction with FE models. This would provide a greater understanding of muscle function involved in controlling the hip and enhance the prediction of post surgery recovery.

7.7 FURTHER ANALYSIS OF THA OUTCOMES USING PCs

The previous study used discrete measures from the kinematic and kinetic waveforms to classify THA function. Paired-sample and independent sample *t*-tests were performed on these measures to select inputs to the DS classifier. The variables were able to distinguish between NP and surgical function but were unable to characterise between LA and PA postoperative function.

The use of parameterised waveforms is common practice in gait analysis studies, however there is a danger of discarding valuable temporal information. It is possible that the information discarded by using parameterised waveforms may have been important to the classifications.

As a continuation to the previous study, additional classifications were carried out using Principle components (PCs) of the important variables, determined in section 7.4. PCA was used as a data reduction method to represent the waveforms in a discrete form whilst retaining temporal information. The most salient PCs were selected for inputs to the DS classifier.

Principle Component Analysis (PCA) was carried out on the following gait waveforms:

1. Sagittal plane hip rotation – Flexion-Extension rotation (FER)
2. Pelvic Obliquity (PO)
3. Hip frontal moment in stance phase of gait (FHM)
4. Hip frontal power in stance phase of gait (FHP)

Pelvic obliquity and hip frontal moment measured 30 seconds into the Trendelenburg test were used in the classifier as discrete values, as in the previous study.

In addition, the vertical ground reaction force (GRF), (VF), medial-lateral GRF (MLF) and the anterior-posterior force (APF) were computed to determine the effect of loading on function. Their PCs were also calculated and used as inputs for classification (c). This is because through preliminary analyses using only the kinematic variables above, a useful classification with a distinction between the LA and PA surgical groups was not achieved.

7.7.1 Summary of PCs

The procedure for calculating and selecting the PCs is given in Chapter 2. The PCA procedure was applied to the LA, PA and NP samples. The derivations of the PCs from each kinematic and kinetic gait waveforms are given in Appendix G. The PCs selected to represent each waveform are summarised in Table 7.5.

Table 7.5 Variables and their associated PCs

Variable	PC	% Gait Cycle	Portion of the stair gait cycle the PC represents
Flexion-Extension Rotation (FER)	PC1	0%to 31% 64% to 100%	Initial contact to early terminal stance and from initial swing until the end of the gait cycle
	PC2	34% to 59%	Early terminal stance to late pre-swing
Pelvic Obliquity (PO)	PC1	0% to 7% 26% to 42 % 48% to 100%	Early loading response, from mid portion of mid-stance to terminal stance and from the end of terminal stance to the end of the gait cycle
	PC2	13% to 22%	Early to mid portion of mid-stance phase
Vertical Force (VF)	PC1	2% to 38% 58% to 85%	Initial contact to mid-stance and mid terminal stance to early pre-swing
	PC2	41% to 55% 89% to 93%	Late mid-stance to early terminal-stance and late terminal stance to late pre-swing
Medial-Lateral Force (MLF)	PC1	14% to 87%	Late loading response to mid pre-swing
	PC2	89% to 100%	Mid to the end of pre-swing
Anterior-Posterior Force (APF)	PC1	4% to 49% 68% to 93%	Early loading response to the start of terminal stance and mid terminal stance to late pre-swing
	PC2	53% to 65%	Early to mid terminal stance
	PC3	94% to 100%	Late pre-swing to the end of the stance phase
Frontal Hip Moment (FHM)	PC1	12% to 88%	Late loading response to mid pre-swing
	PC2	94% to 99%	Late pre-swing phase
Frontal Hip Power (FHP)	PC1	9% to 18% 33% to 38% 52% to 60% 85% to 86%	Mid to early mid-stance, mid to late mid-stance, mid to late terminal stance and early to mid pre-swing
	PC2	24% to 27% 42% to 47%	Mid and late mid-stance

The reader is referred to page 2-28 in Chapter 2 for the events of a gait cycle (Figure 2.21) and the timings of gait events (Table 2.1).

The same four classifications as in section 7.4 were performed to provide an objective and visual indicator of postoperative THA function:

(a) NP and LA;
(b) NP and PA;
(c) PA and LA;
(d) NP and surgical group containing PA and LA.

All the PCs derived from kinematic waveforms, along with parameterised variables for pelvic obliquity and hip frontal moment measured 30 seconds into the Trendelenburg test were used for classifications (a) to (d).

In classification (d), in addition to these variables, the best classification result was achieved by including PCs from GRF waveforms. Also, not all the PCs were used in this classification. For the hip flexion-extension rotation waveform (FER), two PCs were retained using the PCA method outlined in Chapter 2. However, only the 1st PC was used in the classification. This PC represents periods of the gait cycle when the hip is in flexion and the abductor muscle groups are acting. VFPC2, MLPC1, APF1 and APF2 were used in the classification to represent GRFs during the stance phase of the cycle. Inclusion of these PCs was found to increase the accuracy of classifying the 2 surgical groups.

7.7.2 Classification outputs

The outputs from the classifications using PCs as inputs are shown in Figures 7.25a-d. The classification in 7.25a has an out- of-sample accuracy of 96.7%. There is an improved distinction between the subjects exhibiting NP and LA function than in the classification shown in Figure 7.23a, which uses the discrete input variables listed in Table 7.3. Only one NP subject is misclassified. Subjects are clustered in their respective dominant regions on the simplex plot indicating that the LA group has distinctly different function than the NP subjects.

A distinction between the groups is also evident for the classification in Figure 7.25(b), though to a lesser extent. The out-of-sample accuracy is 86.2% with four

misclassified subjects. There is less clustering of the subjects in the dominant regions indicating a range of function ability within the PA group. Two subjects from the PA group are situated in the dominant NP region and thus display NP function. This is in agreement with the previous study.

The classification of LA and PA in Figure 7.25c, has an accuracy of an 81.5%. It is evident that the introduction of kinetic variables enhanced the classification. All but one of the LA subjects are situated in the dominant LA region on the simplex plot. The majority of the PA subjects are situated in the dominant PA region. However, four subjects are classified with hip function characteristic of post LA surgical function.

The classification shown in Figure 7.25d has several misclassified subjects indicated by a 60.5% out-of-sample accuracy. However, all but three of the LA and NP subjects are positioned in their respective dominant regions of the simplex plot indicating differences in function, while three subjects from the PA group were characterised as exhibiting NP function. There is a greater range of NP functional ability within the PA group. This is in agreement with the previous classification in Figure 7.23d.

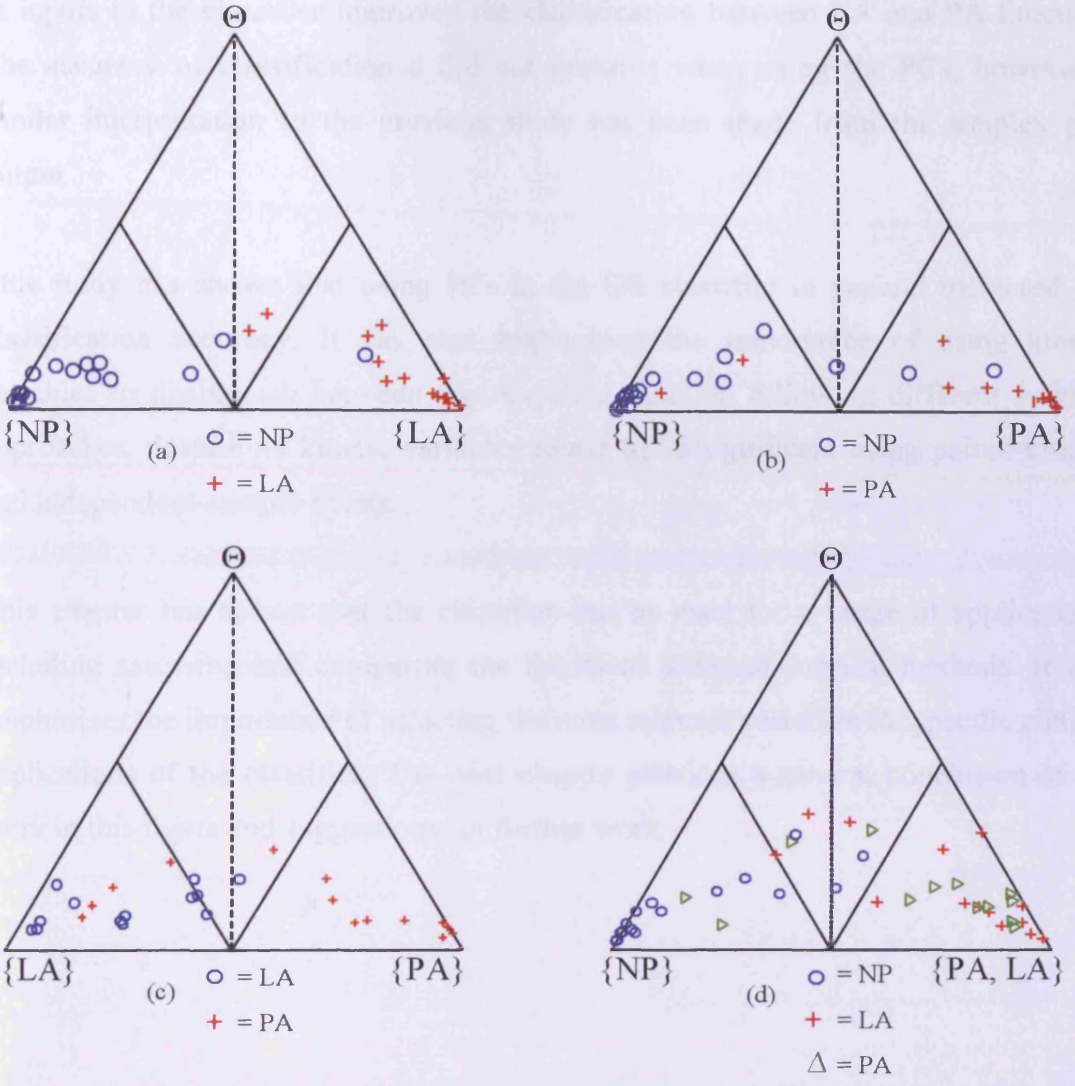

Figure 7.25 Simplex plots for the classification of (a) NP and LA, (b) NP and PA, (c) LA and PA, (d) NP and the surgical group containing both PA and LA

7.7.3 Conclusion

Principal Component Analysis was performed on the variables that highlight functional differences between the two approaches and selected PCs were used as inputs to the DS classifier. The classification outputs are similar to those from the previous study, which used discrete variables from parameterised waveforms of the same data set.

The accuracy of the classifications shown in Figures 7.25a-c was improved by using PCs of the gait kinematic waveform data. Introduction of PCs from the force datasets

as inputs to the classifier improved the classification between LA and PA function. The accuracy of classification d did not improve when using the PCs; however a similar interpretation to the previous study has been made from the simplex plot output.

This study has shown that using PCs in the DS classifier in general increased the classification accuracy. It has also highlighted the importance of using kinetic variables to distinguish between postoperative function following different surgical approaches, despite no kinetic variables found to be significant using paired-sample and independent-sample *t*-tests.

This chapter has shown that the classifier can be used for a range of applications, including assessing and comparing the merits of different surgical methods. It also emphasises the importance of selecting the most relevant variables for specific clinical applications of the classifier. The next chapter provides a general conclusion of the work in this thesis and suggestions for further work.

CHAPTER 8

CONCLUSIONS AND FURTHER WORK

8.1 CONCLUSIONS

The studies described in this thesis have contributed towards the validation of the Cardiff DS classification method.

Throughout the studies, additions to the existing motion analysis (MA) collection and analysis procedures were made. A staircase was developed and is now routinely used in assessment sessions. Moment calculations were included in the in house software for the assessment of stair gait biomechanics. Visual3D (C-motion, Inc.) was introduced as an alternative method to compute lower limb biomechanics, where biomechanical models and report templates were produced for the hip and knee assessments.

The classifier was addressed in three ways. Firstly, it was trained for the assessment of level gait using an increased cohort of NP and OA knee function. Secondly, stair gait variables were used with the DS classifier to determine their ability to characterise OA, NP and TKR function. Lastly, the DS classifier was applied to assess total hip replacement function to answer an alternative orthopaedic question as a demonstration of its generic capabilities.

Image registration techniques involving dynamic fluoroscopy were developed to assess the accuracy of the MA data used as inputs to the classifier. This technique is now available for use in the future as a stand alone method of assessing knee kinematics or for use in other accuracy studies. This method required the development of bone models. These were created successfully using Simpleware segmentation software, (Simpleware, Ltd.).

Conclusions specific to each of the objectives outlined in Chapter 1 will now be discussed in turn.

Objective 1: Use the current data collection and DS classification method to assess TKR outcome of new patients visiting the laboratory.

A study was undertaken to assess the outcome of TKR surgery for an additional 9 subjects. The cohort was limited to this sample size as only 9 patients attended three or more postoperative assessments. The DS classifier was trained using knee function data for an additional 10 NP and 10 OA knees. This increased the existing training cohort by 48%.

All but one patient recovered a degree of NP function following surgery and none recovered to a dominant non-pathological (NP) classification. The outputs were similar to those presented in Jones, (2004). However, two subjects obtained a final classification where $m_c(\{NP\}) > 0.4$. This has never been achieved for previous patients and indicates a better post-operative knee function for these two patients. It could also be a demonstration of the benefits of using an increased training set to better distinguish between varying levels of knee function. However, additional subjects are needed still to increase the training cohort to investigate this.

It was observed that not all patients display a consistent recovery of NP function at each subsequent assessment. This is also evident in the study by Jones, (2004). Changes in the BOE_c were not always in agreement with the knee outcome survey (KOS) and oxford knee score (OKS) results. This is because the KOS and OKS measure knee function in terms of the patients' judgment on how they can perform daily activities, whereas the classifier objectively analyses MA data to assess knee function.

Objective 2: Introduce stair ascent and descent into the protocol.

A staircase was designed and constructed for use in the clinical trial. Patients have revealed that the staircase was easier for them to climb compared to their staircase at home and one patient, who no longer climbs their stairs at home, would happily use the staircase in the laboratory. It was designed to allow forces to be measured from each step. Tests on the staircase revealed that it did not affect the accuracy of the forces measured from either of the force plates in the laboratory. The accuracy of

each Bertec force plate (Bertec Corporation) was also determined. The mean error in computing centre of pressure was marginally outside the factory calibration allowable error range (defined as ± 2mm by Bertec) for one of the plates. The accuracy of measuring forces is outside the factory calibration allowable error range (defined as ± 0.5% by Bertec) for both force plates. This may be due to the use of low magnitude forces for the accuracy tests, as the forces obtained from patients during level and stair gait were within the expected range.

In response to the range of reported methodologies for assessing stair gait, a study was undertaken to compare methods of data collection, choice of stair gait cycle (SGC) and methods of analysis. This study highlighted the variation in biomechanical data due to differences in methodology. It is therefore important that data collection and analysis methods are clearly defined so that educated judgements can be made when interpreting and comparing results from different studies. From the results of this study it is not apparent whether the choice of SGC investigated in this study is an important consideration in the methodology. Although significantly larger adduction and flexion moments were found for stair descent from step 3 to 1, it is unknown whether this would influence the classification method and would need investigation in the future.

Objective 3: Utilise the DS method to distinguish OA and NP knee function based on the measurements taken during stair gait.

Knee functional variables collected during stair gait were used as inputs to the DS classifier to characterise OA and NP function. Flexion moment, adduction moment and medial-lateral ground reaction forces were found to be important in distinguishing between the two groups. Principal components from these waveforms for stair ascent and descent were able to distinguish between the function of 9NP and 6OA knees with 100% accuracy. They were also used to assess the outcome of TKR surgery for one of the OA patients. At 4, 8 and 12 months post-surgery, the patient exhibited non-pathological knee function for stair gait and was classified in the dominant NP region of the simplex plot. The changes in $m_c(\{NP\})$ for each visit significantly correlated with results from a KOS (p=0.988), but not with results from an OKS (p=-0.813). Interestingly the correlation between the KOS and OKS results for each visit was not

significant (p=-0.655). The results from the classification of TKR were compared to a waveform analysis. This helped to explain the changes in classification according to the inputs used in the classification.

Variables from stair gait were demonstrated as useful variables in the classification of knee function and should be investigated in future work. A large variation in stair gait patterns existed between patients. Also, not all patients could climb stairs in a reciprocal manner. The development of simple tests that can be used to represent stair gait should be investigated for those patients who cannot perform the activity.

Objective 4: Develop an image based method to quantify the errors in the knee kinematics associated with the current method where markers are attached to the skin.

An image based method was developed at Cardiff for the assessment of NP and TKR knee function. This employed fluoroscopy and KneeTrack software (S.A Banks) to match 3D bone or TKR models to each image and subsequently compute knee kinematics. For NP subjects, models of the distal femur and proximal tibia were created using MRI scan data and Simpleware Software (Simpleware Ltd.). Image registration was used to determine errors found in marker based MA. 5 NP and 5TKR subjects were assessed non-simultaneously using MA and fluoroscopy for a step up down activity. The Cardiff MA protocol measured significantly larger frontal and transverse rotations for the TKR cohort compared with the image registration method. Frontal plane rotations were also significantly larger using motion analysis for the NP cohort. Significantly larger joint translations were measured using motion analysis for both the NP and TKR cohorts as compared to the measurements from the image registration method. The largest errors in MA derived kinematics were 9.53° for adduction-abduction range of motion (ROM) measured from the NP cohort and 2.63cm compression-distraction ROM of the tibio-femoral joint, measured from the TKR cohort.

This study demonstrated that image registration can be used to investigate errors in MA data, even if simultaneous measurements cannot be taken. Non-sagittal rotations

and all tibiofemoral translations are overestimated using MA and should be used with caution to interpret knee function.

Objective 5: Demonstrate the generic nature of the DS classifier by applying it to another study.

The DS classifier was used to provide information on the effectiveness of a lateral (LA) and posterior (PA) approach to total hip arthroplasty (THA). An initial study using parameterised waveforms as inputs for the classifier was able to characterise NP and LA subjects with 93.3% accuracy and characterise NP and PA with 86.2% accuracy. The variables used were unable to distinguish differences between postoperative function following the PA and LA to THA. The accuracy of the classifications were improved by using PCs of the gait kinematic waveform data. The distinction between the NP and LA was improved with 96.7% accuracy. With the introduction of kinetic variables, LA and PA function was classified with an accuracy of 81.5%. This study concludes that subjects following the PA approach to THA exhibit a greater range of NP functional ability compared to subjects following the LA. This is expected due to the effect of cutting through the hip abductors during the LA. The MA results were compared to Finite Element (FE) predictions in collaboration with Imperial College London. The FE model predicted a better outcome following the PA approach. It is recommended that MA data be used in conjunction with FE models in the future to assess THA.

8.2 FURTHER WORK

This study has highlighted and provoked several potential areas for improvement and investigation of the classification method:

1. Increasing the training cohort for the DS classifier for the assessment of level gait would ensure the DS control variables are trained on a dataset representative of the population. It would also be useful to train the DS classifier using age matched or data from each patient's contralateral limb to represent improvement following TKR in terms of the patients 'normal' function.

2. Stair gait variables proved to be important in the classification of NP, OA and TKR function. The choice of variables should be investigated further. This is particularly important for those patients who cannot stair climb in a reciprocal manner.
3. A classifier designed using stair gait and level gait should be investigated, as this would produce a more thorough assessment of a patient's knee function.
4. The inclusion of KOS and OKS results into the classifier would also merit investigation. The inclusion of subjective scores related to pain may enhance the classifier.
5. The inputs to the DS classifier should be investigated in light of the MA errors determined through the imaging study. Perhaps the DS classifier could be developed to rely less on the variables that were shown to be inaccurate.
6. Now that a method has been established the error in the MA data should be re-evaluated using simultaneous MA and fluoroscopy.
7. It would be good practice to assess the accuracy of the bone models created using MRI. This could be achieved using a phantom bone.
8. The use of the image registration method should be continued to assess additional patients. It would be particularly useful to use it to compare the function of different implant types.
9. The image registration method has the advantage of being highly accurate. Assessment of this technique should be adapted for other joints. This would be particularly useful to assess MA errors in other joints. For example, the shoulder.
10. It would be interesting to use the image registration procedure to assess OA knees. If cartilage could be included as part of the model, FE models could be produced and contact analyses could be performed.
11. The DS classifier is a generic method for MA data, thus its application to other MA analyses should be made to assist interpreting the data.

This thesis has described studies which explore the use of the DS classifier and contribute towards its clinical validation. This has led to several avenues of further investigation and recommendations for its development, so that in the future it may be used to directly assist medical professionals with the diagnosis of patient pathology and the assessment of various treatments.

REFERENCES

Andriacchi, T.P., Andersson, G.B., Fermier, R.W., Stern, D. and Galante, J.O. (1980). A study of lower-limb mechanics during stair-climbing. *J Bone Joint Surg Am.* 62(5), pp.749-757.

Andriacchi, T.P., Galante, J.O. and Fermier, R.W. (1982). The influence of total knee-replacement design on walking and stair-climbing. *J Bone Joint Surg Am.* 64(9), pp.1328-1335.

Andriacchi, T.P. (1993). Functional analysis of pre and post-knee surgery: total knee arthroplasty and ACL reconstruction. *J Biomech Eng.* 115, pp.575-581.

Andriacchi, T.P. and Alexander, E.J. (2000). Studies of human locomotion: past, present and future. *J Biomech.* 33(10), pp.1217-1224.

Angeloni, C., Cappozzo, A., Catani, F. and Learnidi, A. (1992). Quantification of relative displacement between bones and skin and plate-mounted markers. *Proceedings of the 8th meeting of the European Society of Biomechanics*, Rome, Italy, p.279.

Argenson, J.N.A., Scuderi, G.R., Komistek, R.D., *et al.* (2005). In vivo kinematic evaluation and design considerations related to high flexion in total knee arthroplasty. *J Biomech.* 38(2), pp.277-284.

Arthritis Research Campaign (1998). *Osteoarthritis of the knee* [Online]. Available at: http://www.arc.org.uk/arthinfo/patpubs/6027/6027.asp [Accessed: 8 Jan 2009].

Asano, T., Akagi, M., Tanaka, K., Tamura, J. and Nakamura, T. (2001). In vivo three-dimensional knee kinematics using biplanar image-matching technique. *Clin Orthop Relat Res.* 388, pp.157-166.

Baker, A.S. and Bitounis, V.C. (1989). Abductor function after total hip replacement. An electromyographic and clinical review. *J Bone Joint Surg Br.* 71(1), pp.47-50.

Banks, S.A. (1992). *Model based 3-D kinematic estimation from 2-D perspective silhouettes: application with total knee prostheses.* PhD. Massachusetts Institute of Technology, Cambridge, MA.

Banks, S.A. and Hodge, W.A. (1996). Accurate measurement of three-dimensional knee replacement kinematics using single-plane fluoroscopy. *IEEE Trans Biomed Eng.* 43(6), pp.638-649.

Banks, S.A., Markovich, G.D. and Hodge, W.A. (1997a). The mechanics of knee replacements during gait: in vivo fluoroscopic analysis of two designs. *Am J Knee Surg.* 10(4), pp.261-267.

Banks, S.A., Markovich, G.D. and Hodge, W.A. (1997b). In vivo kinematics of cruciate-retaining and –substituting knee arthroplasties. *J Arthroplasty.* 12(3), pp.297-304.

Banks, S.A. and Hodge, W.A. (2004). 2003 Hap Paul Award Paper of the International Society for Technology in Arthroplasty. Design and activity dependence of kinematics in fixed and mobile-bearing knee arthroplasties. *J Arthroplasty.* 19(7), pp.809-816.

Bell, A.L., Brand, R.A. and Pedersen, D.R. (1989). Prediction of hip joint centre location from external landmarks. *Hum Mov Sci.* 8(1), pp.3-16.

Benedetti, M.G., Catani, F., Leardini, A., Pignotti, E. and Giannini, S. (1998). Data management in gait analysis for clinical applications. *Clin Biomech.* 13(3), pp.204-215.

Benedetti, M.G., Catani, F., Bilotta, T.W., Marcacci, M., Mariani, E. and Giannini, S. (2003). Muscle activation pattern and gait biomechanics after total knee replacement. *Clin Biomech.* 18(9), pp. 871-876.

Berchuck, M., Andriacchi, T.P., Bach, B.R. and Reider, B. (1990). Gait adaptations by patients who have a deficient anterior cruciate ligament. *J Bone Joint Surg Am.* 72(6), pp.871-877.

Bergmann, G., Deuretzbacher, G., Heller, M., *et al.* (2001). Hip contact forces and gait patterns from routine activities. *J Biomech.* 34(7), pp.859-871.

Besl, P.J. and McKay, H.D. (1992). A method for registration of 3-D shapes. *IEEE Trans PAMI.* 14, pp.239–256.

Besser, M.P., Kowalk, D.L. and Vaughan, C.L. (1993). Mounting and calibration of stairs on piezoelectric platforms. *Gait Posture.* 1(4), pp.231-235.

Beynon, M.J., Jones, L. and Holt, C.A. (2002). Classification of osteoarthritic and normal knee function using three dimensional motion analysis and the Dempster-Shafer theory of evidence. *Proceedings of the International Society of Biomechanics – 7th Symposium on Human Motion Analysis, Newcastle, UK, July.* pp.85-88.

Beynon, M.J. (2005). A novel technique of object ranking and classification under ignorance: An application to the corporate failure risk problem. *European Journal of Operational Research.* 167(2), pp.493-517.

Beynon, M.J., Jones, L. and Holt, C.A. (2006). Classification of osteoarthritic and normal knee function using three-dimensional motion analysis and the Dempster-Shafer theory of evidence. *IEEE Trans Syst Man Cybern A.* 36(1), pp.173-186.

Bobbert, M.F. and Schamhardt, H.C. (1990). Accuracy of determining the point of force application with piezoelectric force plates. *J Biomech.* 23(7), pp.705-710.

Bresler, B. and Frankel, J.P. (1950). The forces and moments in the leg during level walking. *Trans Amer Soc Mech Eng.* 1, pp.27-36.

Cappello, A., Cappozzo, A., Della Croce, U. and Leardini, A. (1997). Bone position and orientation reconstruction using external markers. In: *Three-dimensional analysis*

of human locomotion. Eds. Allard, P., Cappozzo, A., Lundberg, A., Vaughan, C. Chapter 8, pp.146-171. John Wiley and Sons Ltd.

Cappozzo, A., Catani, F., Della Croce, U. and Leardini, A. (1995). Position and orientation in space of bones during movement: anatomical frame definition and determination. *Clin Biomech.* 10(4), pp.171-178.

Cappozzo, A., Catani, F., Leardini, A., Benedetti, M.G. and Della Croce, U. (1996). Position and orientation in space of bones during movement: experimental artefacts. *Clin Biomech.* 11, pp.90-100.

Catani, F., Benedetti, M.G., De Felice, R., *et al.* (2003). Mobile and fixed bearing total knee prosthesis functional comparison during stair climbing. *Clin Biomech.* 18(5), pp.410-418.

Cates, H.E., Komistek, R.D., Mahfouz, M.R., Schmidt, M.A. and Anderle, M. (2008). In vivo comparison of knee kinematics for subjects having either a posterior stabilized or cruciate retaining high-flexion total knee arthroplasty. *J Arthroplasty.* 23(7), pp.1057-1067.

Chau, T. (2001). A review of analytical techniques for gait data. Part 1: fuzzy, statistical and fractal methods. *Gait Posture.* 13(1), pp.49-66.

Chiari, L., Della Croce, U., Leardini, A. and Cappozzo, A. (2005). Human movement analysis using stereophotogrammetry. Part 2: Instrumental errors. *Gait Posture.* 21(2), pp.197-211.

Chouteau, J., Lerat, J.L., Testa, R., Moyen, B. and Banks, S.A. (2007). Effects of radiograph projection parameter uncertainty on TKA kinematics from model-image registration. *J Biomech.* 40(16), pp.3744-3747.

Chouteau, J., Lerat, J.L., Testa, R., *et al.* (2008). Kinematics of a cementless mobile bearing posterior cruciate ligament-retaining total knee arthroplasty. *Knee*, In Press.

C-Motion, Inc. (2001). *Visual3D online documentation* [Online]. Available at: http://www.c-motion.com/help/ [Accessed: 6 Mar 2009].

Cole, G.K., Nigg, B.M., Ronsky, J.L. and Yeadon, M.R. (1993). Application of the joint coordinate system to three-dimensional joint attitude and movement representation: a standardization proposal. *J Biomech Eng.* 115, pp.344-349.

Comrey, A. L. (1973). *A first course in factor analysis.* New York; London: Academic Press.

Costigan, P.A., Deluzio, K.J. and Wyss, U.P. (2002). Knee and hip kinetics during normal stair climbing. *Gait Posture.* 16(1), pp.31-37.

Daultrey, S. (1976). *Principal components analysis.* Norwich: Geo Abstracts Ltd.

Davies, A.P. (2002). Rating systems for total knee replacement. *Knee.* 9(4), pp.261-266.

Davis, R.B., Õunpuu, S. and DeLuca, P.A. (1994). Joint moments: Evaluation of ground reaction, inertial and segmental weight effects. *Gait Posture.* 2(1), p.58.

Dawson, J., Fitzpatrick, R., Murray, D. and Carr, A. (1998). Questionnaire on the perceptions of patients about total knee replacement. *Bone Joint Surg Br.* 80(1), pp.63– 69.

DeFrate, L.E., Sun, H., Gill, T.J, Rubash, H.E. and Li, G. (2004). In vivo tibiofemoral contact analysis using 3D MRI-based knee models. *J Biomech.* 37(10), pp.1499-1504.

Della Croce, U., Leardini A., Chiari, L. and Cappozzo, A. (2005). Human movement analysis using stereophotogrammetry. Part 4: assessment of anatomical landmark misplacement and its effects on joint kinematics. *Gait Posture.* 21(2), pp.226-237.

Della Croce, U. (2006). Soft tissue artifacts in human movement analysis. *Proceedings of the 9th International Symposium on the 3D analysis of human movement.* Valenciennes, France, 28-30 June.

Della Croce, U. and Bonato, P. (2007). A novel design for an instrumented stairway. *J Biomech.* 40(3), pp.702-704.

Delport, H.P., Banks, S.A., De Schepper, J. and Bellemans, J. (2006). A kinematic comparison of fixed- and mobile-bearing knee replacements. *J Bone Joint Surg Br.* 88(8), pp.1016-1021.

Deluzio, K.J., Wyss, U.P., Zee, B., Costigan, P.A. and Sorbie C. (1997). Principal component models of knee kinematics and kinetics: normal vs. pathological gait patterns. *Hum Mov Sc.* 16, pp.201-217.

Dempster, A.P. (1968). A generalization of Bayesian inference (with discussion), *J Roy Stat Soc, Series* B. 30(2), pp.205–247.

Dennis, D.A., Komistek., R.D., Hoff, W.A. and Gabriel, S.M. (1996). In vivo knee kinematics derived using an inverse perspective technique. *Clin Orthop Relat Res.* 331, pp.107-117.

Dennis, D.A., Komistek, R.D., Colwell, C.E. Jr., *et al.* (1998a). In vivo anteroposterior femorotibial translation of total knee arthroplasty: a multicenter analysis. *Clin Orthop Relat Res.* 356, pp.47-57.

Dennis, D.A., Komistek, R.D., Stiehl, J.B., Walker, S.A. and Dennis, K.N. (1998b). Range of motion after total knee arthroplasty: The effect of implant design and weight-bearing conditions. *J Arthroplasty.* 13(7), pp.748-752.

Dennis, D.A., Mahfouz, M.R., Komistek, R.D. and Hoff, W. (2005). In vivo determination of normal and anterior cruciate ligament-deficient knee kinematics. *J Biomech.* 38(2), pp.241-253.

Dennis, D.A., Komistek, R.D., Nadaud, M.C. and Mahfouz, M. (2006). Evaluation of off-loading braces for treatment of unicompartmental knee arthrosis. *J Arthroplasty.* 21(4 Suppl 1), pp.2-8.

Dorr, L.D., Ochsner, J.L., Gronley, J. and Perry, J. (1988). Functional comparison of posterior cruciate-retained versus cruciate-sacrificed total knee arthroplasty. *Clin Orthop Relat Res.* 236, pp.36-43.

Downing, N.D., Clark, D.I., Hutchinson, J.W, Colclough, K. and Howard, P.W. (2001). Hip abductor strength following total hip arthroplasty: A prospective comparison of the posterior and lateral approach in 100 patients. *Acta Orthop Scand.* 72(3), pp.215-220.

Eckhoff, D.G., Bach, J.M, Spitzer, V.M., *et al.* (2005). Three-dimensional mechanics, kinematics, and morphology of the knee viewed in virtual reality. *J Bone Joint Surg Am.* 87 (Suppl 2), pp.71-80.

Fantozzi, S., Benedetti, M.G., Learnidi, A., *et al.* (2003). Fluoroscopic and gait analysis of the functional performance in stair ascent of two knee replacement designs. *Gait Posture.* 17(3), pp.225-234.

Fregly, B.J., Rahman, H.A. and Banks, S.A. (2005). Theoretical accuracy of model-based shape matching for measuring natural knee kinematics with single-plane fluoroscopy. *J Biomech Eng.* 127(4), pp.692-699.

Fuchs, S., Flören, M., Skwara, A. and Tibesku, C.O. (2002). Quantitative gait analysis in unconstrained total knee arthroplasty patients. *Int J Rehabil Res.* 25(1), pp.65-70.

Fuller, J., Liu, L.J., Murphy, M.C. and Mann, R.W. (1997). A comparison of lower-extremity skeletal kinematics measured using skin- and pin-mounted markers. *Hum Mov Sci.* 16, pp.219-242.

Garling, E.H., Kaptein, B.L., Mertens, B., *et al.* (2007). Soft-tissue artefact assessment during step-up using fluoroscopy and skin-mounted markers. *J Biomech.* 40, pp.S18-S24.

Gerig, G., Welti, D., Guttmann, C.R.G., Colchester, A.C.F. and Szekely, G. (2000). Exploring the discrimination power of the time domain for segmentation and characterization of active lesions in serial MR data. *Medical Image Analysis.* 4(1), pp.31-42.

Gill, H.S. and O'Connor, J.J. (1997). A new testing rig for force platform calibration and accuracy tests. *Gait Posture.* 5(3), pp.228-232.

Goldflies, M.L., Andriacchi, T.P. and Galante, J.O. (1981). The relationship between varus deformity and moments at the knee during gait and the changes at the knee after high tibial osteotomy. *Trans Orthop Res Soc.* 6, p.54.

Gore, D.R., Murray, M.P., Sepic, S.B. and Gardner, G.M. (1982). Anterolateral compared to posterior approach in total hip arthroplasty: differences in component positioning, hip strength and hip motion. *Clin Orthop Relat Res.* 165, pp.180-187.

Grood, E.S. and Suntay, W.J., (1983). A joint coordinate system for the clinical description of three-dimensional motions: application to the knee. *J Biomech Eng.* 105(2), pp.136-144.

Hall, M.G., Fleming, H.E., Dolan, M.J., Millbank, S.F.D. and Paul, J.P. (1996). Static *in situ* calibration of force plates. *J Biomech.* 29(5), pp.659-665.

Hamai, S., Miura, H., Higaki, H., *et al.* (2008). Evaluation of impingement of the anterior tibial post during gait in a posteriorly-stabilised total knee replacement. *J Bone Joint Surg Br.* 90(9), pp.1180-1185.

Hoff, W.A., Komistek, R.D., Dennis, D.A., Gabriel, S.M. and Walker, S.A. (1998). Three-dimensional determination of femoral-tibial contact positions under in vivo conditions using fluoroscopy. *Clin Biomech.* 13(7), pp.455-472.

Holden, J.P., Orsini, J.A., Siegel, K.L., *et al.* (1997). Surface movement errors in shank kinematics and kinetics during gait. *Gait Posture.* 5(3), pp.217-227.

Holden, J.P., Selbie, W.S. and Stanhope, S.J. (2003). A proposed test to support the clinical movement analysis laboratory accreditation process. *Gait Posture.* 17(3), pp. 205-213.

Holt, C.A., Hayes, N.J., van Deursen R.W.M. and O'Callaghan, P.T. (2000). Three-dimensional analysis of the tibiofemoral joint using external marker clusters and the JCS approach – comparison of normal and osteoarthritic knee function. *Computer Methods in Biomechanics and Biomedical Engineering 3.* Lisbon. Gordon and Breach Science Publishers SA. pp.289-294.

Holt, C.A., Jones, L., O'Callaghan, P.O., Roy, S. and Wilson, C. (2002). Comparison of fixed and rotating bearing knee replacements in-vivo using a three-dimensional motion capture technique: preliminary results. *Proceedings of the 4th World Congress of Biomechanics.* Calgary, Canada.

Holt, C.A., Whatling. G.M., Evans. S.L. and Jones, L. (2007). The biomechanics of stair climbing for patients with advanced knee osteoarthritis. *Proceedings of the 6th Combined Meeting of the Orthopaedic Research Societies.* Honolulu, Hawaii, 20-24 October.

Holzreiter, S.H. and Köhle, M.E. (1993). Assessment of gait patterns using neural networks. *J Biomech.* 26(6), pp.645-651.

Imai, S., Higashijima, K., Ishida, A., *et al.* (2003). Determination of the position and orientation of artificial knee implants using markers embedded in a bone: preliminary in vitro experiments. *Med Eng Phys.* 25(5), pp.419-424.

Irrgang, J.J., Synder-Mackler, L., Wainner, R.S., Fu, F.H. and Harner, C.D. (1998). Development of a patient-reported measure of function of the knee. *J Bone Joint Surg Am.* 80(8), pp.1132-1145.

Isaac, D.L., Beard, D.J., Price, A.J., *et al.* (2005). In-vivo sagittal plane knee kinematics: ACL intact, deficient and reconstructed knees. *Knee*, 12(1), pp.25-31.

Jacobs, N.A., Skorecki, J. and Charnley, J. (1972). Analysis of the vertical component of force in normal and pathological gait. *J Biomech.* 5, pp.11-34.

Jolles, B.M. and Bogoch, E.R. (2004). Posterior versus lateral surgical approach for total hip arthroplasty in adults with osteoarthritis. *Cochrane Database Syst Rev,* 1: CD003828.

Jones, L. (2004). *The development of a novel method for the classification of osteoarthritic and normal knee function.* PhD Thesis, Cardiff University.

Jones, L., Beynon, M.J., Holt, C.A. and Roy, S. (2006). An application of the Dempster-Shafer theory of evidence to the classification of knee function and detection of improvement due to total knee replacement surgery. *J Biomech.* 39, pp. 2512-2520.

Jones, L. and Holt, C.A. (2008). An objective tool for assessing the outcome of total knee replacement surgery. *Proc Inst Mech Eng [H].* 222(5), pp.647-55.

Kanekasu, K., Banks, S.A., Honjo, S., Nakata, O. and Kato, H. (2004). Fluoroscopic analysis of knee arthroplasty kinematics during deep flexion kneeling. *J Arthroplasty*, 19(8), pp.998-1003.

Karlsson, D. and Lundberg, A. (1994). Accuracy estimation of kinematic data derived from bone anchored external markers. *Proceedings of the 3rd International Symposium on 3D analysis of human motion.* Stockholm, Sweden, pp.27-30.

Kaufman, K.R., Hughes, C., Morrey, B.F., Morrey, M. and An, K.N. (2001). Gait characteristics of patients with knee osteoarthritis. *J Biomech.* 34(7), pp.907-915.

Kelman G.J., Biden, E.N., Wyatt, M.P., Ritter, M.A. and Colwell, C.W. Jr. (1989). Gait laboratory analysis of a posterior cruciate-sparing total knee arthroplasty in stair ascent and descent. *Clin Orthop Relat Res.* 248, pp.21-26.

Kenny, P., O'Brien C.P, Synnott, K. and Walsh, M.G. (1999). Damage to the superior gluteal nerve after two different approaches to the hip. *J Bone Joint Surg Br.* 81(6), pp.979-981.

Komistek, R.D., Stiehl, J.B., Dennis, D.A., Paxson, R.D. and Soutas-Little, R.W. (1998). Mathematical model of the lower extremity joint reaction forces using Kane's method of dynamics. *J Biomech.* 31(2), pp.185-189.

Komistek, R.D., Dennis, D.A., Northcut, E.J., Parker, A.W. and Traina, S.M. (1999). An in vivo analysis of the effectiveness of the osteoarthritic knee brace during heel-strike of gait. *J Arthroplasty.* 14(6), pp.738-742.

Komistek, R.D., Dennis, D.A., Mabe, J.A. and Walker, S.A. (2000). An in vivo determination of patellofemoral contact positions. *Clin Biomech.* 15(1), pp.29-36.

Komistek, R.D., Dennis, D.A. and Mahfouz, M. (2003). In vivo fluoroscopic analysis of the normal human knee. *Clin Orthop Relat Res.* 410, pp.69-81.

Kowalk, D.L., Duncan, J.A. and Vaughan, C.L. (1996). Abduction-adduction moments at the knee during stair ascent and descent. *J Biomech.* 29(3), pp.383-388.

Lafortune, M.A. and Lake, M.J. (1991). Errors in 3D analysis of human movement. *Proceedings of the 1st international Symposium on 3D analysis of human movement.* Stockholm, Sweden, pp.55-56.

Lafortune, M.A., Cavanagh, P.R., Sommer H.J. and Kalenak, A. (1992). Three-dimensional kinematics of the human knee during walking. *J Biomech.* 25(4), pp.347-357.

Lark, S.D., Buckley, J.G., Bennett, S., Jones, D. and Sargeant, A.J. (2003). Joint torques and dynamic joint stiffness in elderly and young men during stepping down. *Clin Biomech.* 18(9), pp.848-855.

Leardini, A., Chiari, L., Della Croce, U. and Cappozzo, A. (2005a). Human movement analysis using stereophotogrammetry. Part 3. Soft tissue artifact assessment and compensation. *Gait Posture.* 21(2), pp.212-215.

Leardini, A., Astolfi, L., Fantozzi, S., *et al.* (2005b). Advanced multimodal visualisation of clinical gait and fluoroscopy analyses in the assessment of total knee replacement. *Comput Methods Programs Biomed.* 79(3), pp.227-240.

Liu, F., Ohdera, T., Miyamoto, H., *et al.* (2009). In vivo kinematic determination of total knee arthroplasty from squatting to standing. *Knee.* 16(2), pp.116-120.

Madsen, M.S., Ritter, M.A., Morris, H.H., *et al.* (2004). The effect of total hip arthroplasty surgical approach on gait. *J Orthop Res.* 22(1), pp.44-50.

Manal, K., McClay, I., Stanhope, S., Richards, J. and Galinat, B. (2000). Comparison of surface mounted markers and attachment methods in estimating tibial rotations during walking: an in vivo study. *Gait Posture.* 11(1), pp.38-45.

Manal, K., McClay, I., Richards, J., Galinat, B. and Stanhope, S. (2002). Knee moment profiles during walking: errors due to soft tissue movement of the shank and the influence of the reference coordinate system. *Gait Posture.* 15(1), pp.10-17.

Masonis, J.L. and Bourne, R.B. (2002). Surgical approach, abductor function, and total hip arthroplasty dislocation. *Clin Orthop Relat Res.* 405, pp.46-53.

McFadyen, B.J. and Winter, D.A. (1988). An integrated biomechanical analysis of normal stair ascent and descent. *J Biomech.* 21(9), pp.733-744.

McFarland, B. and Osborne, G. (1954). Approach to the hip: A suggested improvement on Kocher's method. *J Bone Joint Surg Br.* 36(3), 364-367.

Middleton, J., Sinclair, P. and Patton, R. (1999). Accuracy of centre of pressure measurement using a piezoelectric force platform. *Clin Biomech.* 14(5), pp.357-360.

Moro-oka, T.A., Hamai, S., Miura, H., *et al.* (2007). Can magnetic resonance imaging-derived bone models be used for accurate motion measurement with single-plane three-dimensional shape registration? *J Orthop Res.* 25(7), pp.867-72.

Moro-oka, T.A., Hamai, S., Miura, H., *et al.* (2008). Dynamic activity dependence of in vivo normal knee kinematics. *J Orthop Res.* 26(4), pp.428-434.

Morrison, J.B. (1969). Function of the knee joint in various activities. *Biomed Eng.* 4(12), pp.573-580.

Murphy, M.C. (1990). *Geomerty and kinematics of the normal human knee.* PhD Thesis, Massachusetts Institute of Technology, Cambridge, MA.

Myles, C.M., Rowe, P.J., Walker C.R.C. and Nutton R.W. (2002). Knee joint functional range of movement prior to and following total knee arthroplasty measured using flexible electrogoniometry. *Gait Posture.* 16(1), pp.46-54.

Nadeau, S., McFadyen, B.J. and Malouin, F. (2003). Frontal and sagittal plane analyses of the stair climbing task in healthy adults aged over 40 years: what are the challenges compared to level walking? *Clin Biomech.* 18(10), pp.950-959.

Nilsson, K.G., Kärrholm, J. and Gadegaard, P. (1991). Abnormal kinematics of the artificial knee. Roentgen stereophotogrammetric analysis of 10 Miller-Galante and five New Jersey LCS knees, *Acta Orthop Scand.* 62, pp. 440-446.

Nordin, M. and Frankel, V.H. (2001). *Basic Biomechainics of the Musculoskeletal System.* 3rd Edition, Lippincott Williams and Wilkins.

Oakeshott, R., Stiehl, J.B., Komistek, R.A., Anderson, D.T. and Haas, B.D. (2003). Kinematic analysis of a posterior cruciate retaining mobile-bearing total knee arthroplasty. *J Arthroplasty.* 18(8), pp.1029-1037.

Pandit, H., Van Duren, B.H., Gallagher, J.A., *et al.* (2008). Combined anterior cruciate reconstruction and Oxford unicompartmental knee arthroplasty: in vivo kinematics. *Knee.* 15(2), pp.101-106.

Papaioannou, G., Nianios, G., Mitrogiannis, C., *et al.* (2008). Patient-specific knee joint finite element model validation with high-accuracy kinematics from biplane dynamic Roentgen stereogrammetric analysis. *J Biomech.* 41(12), pp.2633-2638.

Patel, V.V., Hall, K., Ries, M., *et al.* (2004). A three-dimensional MRI analysis of knee kinematics. *J Orthop Res.* 22(2), pp.283-292.

Phillips, A.T.M., Howie, C.R. and Pankaj, P. (2007). Biomechanical evaluation of anterolateral and posterolateral approaches to hip joint arthroplasty. *J Bone Joint Surg Br.* 90 (Suppl_III), pp.*547-548.*

Price, A.J., Rees, J.L., Beard, D.J., *et al.* (2004). Sagittal plane kinematics of a mobile-bearing unicompartmental knee arthroplasty at 10 years: a comparative in vivo fluoroscopic analysis. *J Arthroplasty*, 19(5), pp.590-597.

Protopapadaki, A., Drechsler, W.I., Cramp, M.C., Coutts, F.J. and Scott, O.M. (2007). Hip, knee, ankle kinematics and kinetics during stair ascent and descent in healthy young individuals. *Clin Biomech.* 22, pp.203-210.

Rabuffetti, M., Ferrarin, M. and Benvenuti, F. (2001). Spot check of the calibrated force platform location. *Med Biol Eng Comput.* 39(6), pp.638-643.

Rahman, H., Fregly, B.J. and Banks, S.A. (2003). *Accurate measurement of three-dimensional catural knee kinematics using single-plane fluoroscopy.* Summer Bioengineering Conference. Florida, 25-29 June.

Raudys, S.J. and Jain, A.K. (1991). Small sample size effects in statistical pattern recognition: recommendations for practitioners. *IEEE Trans Pattern Analysis and Machine Intelligence.* 13(3), pp.252-264.

Ritter, M.A., Harty, L.D., Keating, M.E., Faris, P.M. and Meding, J.B. (2001). A Clinical comparison of the anterolateral and posterolateral approaches to the hip. *Clin Orthop Relat Res.* 385, pp.95-99.

Robinson, B.J., Rees, J.L., Price, A.J., *et al.* (2002). A kinematic study of lateral unicompartmental arthroplasty. *Knee.* 9(3), pp.237-240.

Roos, P.J., Neu, C.P., Hull, M.L. and Howell, S.M. (2005). A new tibial coordinate system improves the precision of anterior-posterior knee laxity measurements: a cadaveric study using Roentgen stereophotogrammetric analysis. *J Orthop Res.* 23(2), pp.327-333.

Safranek, R.J., Gottschlich, S. and Kak, A.C. (1990). Evidence accumulation using binary frames of discernment for verification vision, *IEEE Trans Robotics and Automation.* 6(4), pp.405-417.

Sati, M., de Guise, J.A., Larouche, S. and Drouin, G. (1996). Quantitative assessment of skin-bone movement at the knee. *Knee.* 3, pp.121-138.

Schache, A.G. and Baker, R. (2007). On the expression of joint moments during gait. *Gait Posture.* 25(3), pp.440-452.

Schmidt, R., Komistek, R.D., Blaha, J.D., Penenberg, B.L. and Maloney, W.J. (2003). Fluoroscopic analyses of cruciate-retaining and medial pivot knee implants. *Clin Orthop Relat Res.* 410, pp.139-147.

Shafer, G. (1976). *A Mathematical theory of Evidence*, Princeton: Princeton University Press.

Sharma, A., Komistek, R.D., Ranawat, C.S, Dennis, D.A. and Mahfouz, M.R. (2007). In vivo contact pressures in total knee arthroplasty. *J Arthroplasty.* 22(3), pp.404-416.

Söderkvist, I. and Wedin, P.A. (1993). Determining the movements of the skeleton using well configured markers, *J Biomech.* 26(12), pp.1473-1477.

Stagni, R., Fantozzi, S., Cappello, A. and Leardini, A. (2005). Quantification of soft tissue artefact in motion analysis by combining 3D fluoroscopy and stereophotogrammetry: a study on two subjects. *Clin Biomech.* 20(3), pp.320-329.

Stiehl, J.B., Komistek, R.D., Dennis, D.A., Paxson, R.D. and Hoff, W.A. (1995). Fluoroscopic analysis of kinematics after posterior-cruciate-retaining knee arthroplasty. *J Bone Joint Surg Br.* 77(6), pp.884-889.

Stiehl, J.B., Dennis, D.A., Komistek, R.D. and Keblish, P.A. (1997). In vivo kinematic analysis of a mobile bearing total knee prosthesis. *Clin Orthop Relat Res.* 345, pp.60-66.

Stiehl, J.B., Dennis, D.A., Komistek, R.D. and Crane, H.S. (1999). In vivo determination of condylar lift-off and screw-home in a mobile-bearing total knee arthroplasty. *J Arthroplasty.* 14(3), pp.293-299.

Stiehl, J.B., Komistek, R. and Dennis, D.A. (2001). A novel approach to knee kinematics. *Am J Orthop*, 30(4), pp.287-293.

Sugita, T., Sato, K., Komistek, R.D., *et al.* (2005). In vivo determination of knee kinematics for Japanese subjects having either a low contact stress rotating platform or an anteroposterior glide total knee arthroplasty. *J Arthroplasty.* 20(2), pp.154-161.

Tabachnick, B.G. and Fidell, L.S. (1989). *Using multivariate statistics.* 2nd edition. Cambridge; Philadelphia: Harper & Row.

Tamaki, M., Tomita, T., Watanabe, T., *et al.* (2008). In vivo kinematic analysis of a high-flexion, posterior-stabilized, mobile-bearing knee prosthesis in deep knee bending motion. *J Arthroplasty*, In press.

Tang, T.S., MacIntyre, N.J., Gill, H.S., *et al.* (2004). Accurate assessment of patellar tracking using fiducial and intensity-based fluoroscopic techniques. *Med Image Anal.* 8(3), pp.343-351.

Thambyah, A., Thiagarajan, P. and Goh Cho Hong, J. (2004). Knee joint moments during stair climbing of patients with anterior cruciate ligament deficiency. *Clin Biomech.* 19(5), pp.489-496.

Toussaint, G.T. (1974). Bibliography on estimation of misclassification. *IEEE Trans Information Theory.* 20(4), pp.472-479.

Townsend, M.A. and Tsai, T.C. (1976). Biomechanics and modelling of bipedal climbing and descending. *J Biomech.* 9(4), pp.227-239.

Tupling, S.J. and Pierrynowski, M.R. (1987). Use of cardan angles to locate rigid bodies in three-dimensional space. *Med Biol Eng Comput.* 25(5), pp.527-532.

van Duren, B.H., Pandit, H., Beard, D.J., *et al.*, (2007). How effective are added constraints in improving TKR kinematics? *J Biomech.* 40, pp.S31-S37.

Varadarajan, K.M., Moynihan, A.L., D'Lima, D., Colwell, C.W. and Li, G. (2008). In vivo contact kinematics and contact forces of the knee after total knee arthroplasty during dynamic weight-bearing activities. *J Biomech.* 41(10), pp.2159-2168.

Vaughan, C.L., Davis, B.L. and O'Connor, J.C. (1992). *Gait analysis Laboratory.* Champaign, Human Kinetics Publishers.

Watanabe, T., Yamazaki, T., Sugamoto, K., *et al.* (2004). In vivo kinematics of mobile-bearing knee arthroplasty in deep knee bending motion. *J Orthop Res.* 22(5), pp.1044-1049.

Weiss, S.M. and Kulikowski, C.A. (1991). *Computer systems that learn: classification and prediction methods from statistics, neural nets, machine learning, and expert systems.* San Mateo, California: M. Kaufmann.

Whatling, G.M., Holt, C.A., Madete, J.K., *et al.* (2006a). Comparison between lateral and posterior surgical approach on the outcome of Total Hip Arthroplasty.

Proceedings of the 7th International Symposium on Computer Methods in Biomechanics and Biomedical Engineering. Antibes, France, 22-25 March.

Whatling, G.M., Holt, C.A., Jones, L., *et al.* (2006b). Investigating the effects of surgical approach on total hip arthroplasty recovery using 3D gait analysis. *Proceedings of the 9th Symposium on 3D analysis of Human Movement,* Valenciennes, France, 28-30 June.

Whatling, G.M., Holt, C.A., Jones, L., *et al.* (2006c). Investigating the effect of surgical approach on the outcome of total hip arthroplasty. *Proceedings of the 5th World Congress of Biomechanics.* Munich, Germany, 29 July - 4 August. *J Biomech,* 39, (Suppl 1), p.S121.

Whatling, G.M., Jones, L., Holt, C.A. and Evans, S.L. (2007a). A study of stair climbing for patients with advanced knee osteoarthritis. *Proceedings of the 16th annual meeting of ESMAC.* Athens, Greece, 27–29 September. *Gait Posture.* 26, p. S117.

Whatling, G.M., Holt, C.A., Jones, L., *et al.* (2007b). Objective functional assessment of THA following two common surgical approaches. *Proceedings of the Institution of Mechanical Engineers Meeting Engineers & Surgeons: Joined at the hip,* One Great George Street, London, 19-21 April.

Whatling, G.M., Jones, L., Holt, C.A., *et al.* (2007c). Comparing postoperative function following two approaches to total hip arthroplasty using a novel objective analysis tool. *Proceedings of the 16th annual meeting of ESMAC.* Athens, Greece, 27–29 September. *Gait Posture,* 26, (Suppl 1), p.S70.

Whatling, G.M., Holt, C.A., Jones, L., *et al.* (2008a). Quantifying non-pathological and osteoarthritic knee function during stair walking. *Proceedings of the 8th International Symposium on Computer Methods in Biomechanics and Biomedical Engineering.* Porto, Portugal, 27 February-1 March.

Whatling, G.M., Jones, L., Holt, C.A., *et al.* (2008b). A preliminary study of stair ascent to determine indicators of advanced knee osteoarthritis. *Proceedings of the 16th congress of the European Society of Biomechanics.* Lucerne, Switzerland. 6-9 July.

Whatling, G.M., Jones, L., Evans, S.L., *et al.* (2008c). Characterising OA knee function from stair climbing. *Proceedings of the 10th International Symposium on 3D analysis of human movement.* Santpoort-Amsterdam, the Netherlands, 28-31 Oct.

Whatling, G.M., Ozturk, H., Pierron F., *et al.* (2008d). Investigating the use of MRI to produce subject-specific bone models of the knee joint. *Proceedings of the 8th International Symposium on Computer Methods in Biomechanics and Biomedical Engineering.* Porto, Portugal, 27 February-1 March.

Whatling, G.M., Ozturk, H., Pierron F., *et al.* (2008e). Fusing marker-based motion capture with image registration to study the errors associated with quantifying knee kinematics. *Proceedings of the 10th International Symposium on 3D analysis of human movement of the International Society of Biomechanics.* Santpoort-Amsterdam, the Netherlands, 28-31 October.

Whatling, G.M., Dabke, H.V., Holt, C.A., *et al.* (2008f). Objective functional assessment of total hip arthroplasty following two common surgical approaches: the posterior and direct lateral approaches. *Proc Inst Mech Eng [H].* 222(6), pp.897-905.

Whatling, G.M., Holt, C.A., Jones, L., *et al.* (2008g). Investigating the effects of surgical approach on total hip arthroplasty recovery using 3D gait analysis. *Proceedings of the 8th International Symposium on Computer Methods in Biomechanics and Biomedical Engineering.* Porto, Portugal, 27 February-1 March.

Whatling, G.M., Phillips, A.T.M., Madete, J., *et al.* (2008h). Biomechanical outcomes of total hip arthroplasty: Gait and finite element studies of lateral and posterior surgical approaches. *Proceedings of the 10th International Symposium on 3D analysis of human movement.* Santpoort-Amsterdam, the Netherlands, 28-31 October.

Whittle, M.W. and Jefferson, R.J. (1989). Functional biomechanical assessment of the Oxford Meniscal Knee. *J Arthroplasty*. 4(3), pp.231-243.

Whittle, M.W. (1996). *Gait analysis: an introduction*. 2nd Edition. Oxford: Butterworth-Heinemann.

Winter, D., Pezzack, J. and Norman, R. (1980). Waterloo Biomech-Part 1, A complete computer package for the analysis of human movement. *Proceedings of the International Conference of Rehabilitation Engineering*, Toronto.

Winter, D.A. (1983). Energy generation and absorption at the ankle and knee during fast, natural and slow cadences. *Clin Orthop Relat Res.* 175, pp.147-154.

Winter, D. (1990). *Biomechanics and motor control of human movement*. 2nd Edition. New York, A Wiley-Interscience Publication, John Wiley & Sons, Inc.

Woo, R.Y. and Morrey, B.F. (1982). Dislocations after total hip arthroplasty. *J Bone Joint Surg Am.* 64(9), pp.1295-1306.

Wu, G. and Cavanagh, P.R. (1995). ISB recommendations for standardization in the reporting of kinematic data. *J Biomech.* 28(10), pp.1257-1261.

Yack, H.J., Houck, J., Cudderford, T., Pierrynowski, M. and Ball, K. (2000). Measuring 3D knee motion with surface markers, it can be done. *Gait Posture.* 11, pp.148-149.

Yamazaki, T., Watanabe, T., Nakajima, Y., *et al.* (2005). Visualization of femorotibial contact in total knee arthroplasty using X-ray fluoroscopy. *Eur J Radiol.* 53(1), pp.84-89.

Yoshiya, S., Matsui, N., Komistek, R.D., *et al.* (2005). In vivo kinematic comparison of posterior cruciate-retaining and posterior stabilized total knee arthroplasties under passive and weight-bearing conditions. *J Arthroplasty*. 20(6), pp.777-783.

You, B.M., Siy, P., Anderst, W., *et al.* (2001). In vivo measurement of 3-D skeletal kinematics from sequences of biplane radiographs: application to knee kinematics. *IEEE Trans Med Imaging.* 20(6), pp.514-525.

Yu, B., Growney, E.S., Schultz, F.M. and An, K.N. (1996). Calibration of measured center of pressure of a new stairway design for kinetic analysis of stair climbing. *J Biomech.* 29(12), pp.1625-1628.

Yu, B., Stuart, M.J., Kienbacher, T., Growney, E.S. and An, K.N. (1997). Valgus-varus motion of the knee in normal level walking and stair climbing. *Clin Biomech.* 12(5), pp.286-293.

Zatsiorsky, V. and Seluyanov, V. (1983). The mass and inertia characteristics of the main segments of the human body. In *Biomechanics VIII-B* (Edited by Matsui, H. and Kobayashi, K.), Champaign, IL: Human Kinetics, pp. 1152-1159.

Zatsiorsky, V.M. (1998). *Kinematics of human motion.* Champaign, IL: Human Kinetics.

Zihlmann, M.S., Gerber, H., Stacoff, A., *et al.* (2006). Three-dimensional kinematics and kinetics of total knee arthroplasty during level walking using single plane video-fluoroscopy and force plates: a pilot study. *Gait Posture.* 24(4), pp.475-481.

Zimmerman, S., Hawkes, W.G., Hudson J.I, *et al.* (2002). Outcomes of surgical management of total HIP replacement in patients aged 65 years and older: cemented versus cementless femoral components and lateral or anterolateral versus posterior anatomical approach. *J Orthop Res.* 20(2), pp.182-191.

Zuffi, S., Leardini, A., Catani, F., Fantozzi, S. and Cappello, A. (1999). A model-based method for the reconstruction of total knee replacement kinematics. *IEEE Trans Med Imaging.* 18(10), pp.981-991.

APPENDIX A

Knee Anatomy and function

The knee consists of two articulations, (Figure 1.) The tibiofemoral articulation exists between the femur and tibia and the patellofemoral articulation between the patella and the femoral intercondylar groove. In this thesis, the knee joint refers to the tibiofemoral articulation.

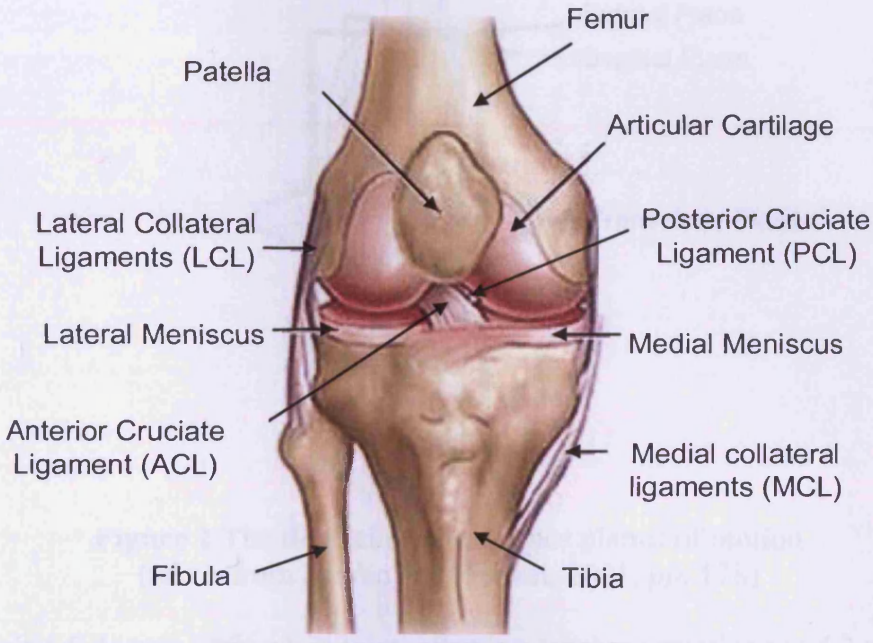

Figure 1 Anatomy of the right knee.
(Adapted from image at http://www.aclsolutions.com/anatomy.php)

Two menisci are located in the joint space between the tibia and femur. These act as shock absorbers to protect joint surfaces by increasing the contact area through which forces act. The knee joint is surrounded by a capsule lined with a synovial membrane that secretes a lubricating synovial fluid. The knee joint is nearly frictionless due to the combination of the menisci, articular cartilage coating articulating surfaces and synovial fluid.

Muscles and ligaments stabilise and control knee joint motion. They also ensure forces are transmitted centrally through the joint to minimise cartilage wear. The medial and lateral collateral ligaments stabilise the knee from side to side. The MCL resists forces acting from the outer surface of the knee (valgus forces). The LCL resists impacts from the inner surface of the knee (varus forces).

The anterior cruciate ligament (ACL) and posterior cruciate ligament (PCL) cross in the centre of the knee. In this configuration, they stabilise the knee in a rotational fashion and limit knee translations. The PCL prevents the femur from sliding anterior on the tibia and stretches from the medial condyle of the femur to the posterior intercondylar area. The ACL prevents the tibia from sliding too far anterior relative to

the femur. It stretches from the lateral condyle of the femur to the anterior intercondylar area.

Knee rotations are described in terms of the three clinical reference planes illustrated in Figure 2. The sagittal plane divides the body into right and left portions, the frontal (or coronal) plane divides the body longitudinally and the transverse plane divides a body part into upper and lower portions.

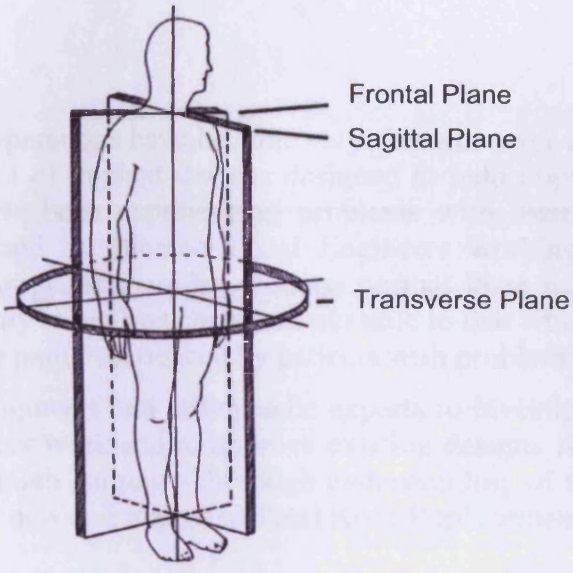

Figure 2 The three clinical reference planes of motion
(taken from Nordin and Frankel, 2001, *pp.* 178)

The knee is a 6 degree of freedom joint, allowing for three rotations and 3 translations to occur. The knee rotations are shown in Figure 3. The greatest movement in the knee occurs in the sagittal plane, where the tibiofemoral joint has approximately 140° range of motion. Movements in the frontal and transverse planes are minimal and are influenced by the position of the joint in the sagittal plane.

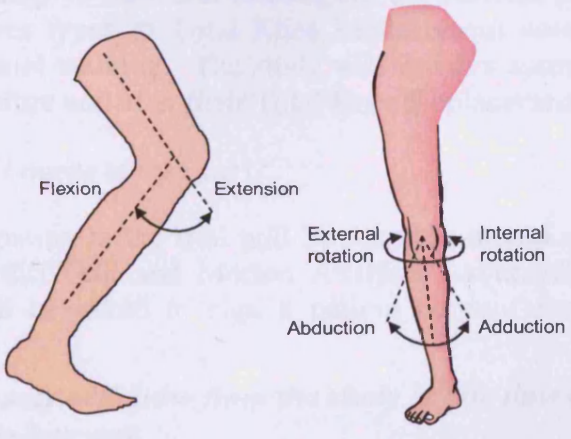

Figure 3 Movement about the knee joint

Muscles produce joint motion. The main muscles acting across the joint are the quadriceps and hamstrings. Knee extension is produced through contraction of the quadriceps. Knee flexion is produced through contraction of the hamstrings.

APPENDIX B

Patient Information Sheet

A Pre and Post Operative Study of the Functional Performance of Total Knee Replacement Patients

Total Knee Replacement

Total Knee Replacement operations have become very common over the last 10 years and there are various types of implant devices designed to help improve a patient's movement when they have been experiencing problems with their knees. These devices have been designed by Biomechanical Engineers working together with Orthopaedic Consultant Surgeons in order produce normal knee movement, hence returning the patient's ability to walk as closely as possible to that which is considered normal and eliminating the pain experienced by patients with problem knees.

It is the job of research engineers and orthopaedic experts to investigate the ways in which these types of devices work and to improve existing designs for the benefit of the patient. It is only through gaining a thorough understanding of the detailed way in which people move that new and improved Total Knee Replacement devices can be developed.

What is the purpose of this trial?

The aim of the trial is to investigate the design of Total Knee Replacement for engineering purposes. Resulting data can be used to improve design techniques in the field of Total Knee Replacement Prosthetics and to improve the measurement system for the clinical description of three dimensional motion analysis.

The study is designed to examine the effects of Total Knee Replacement on patients in terms of their ability to walk and to compare the patients ability to walk after the operation, for various types of Total Knee Replacement components, with what is measured to be normal walking. The study will involve assessment of patients who agree to take part before and after their Total Knee Replacement operation.

What will happen if I agree to take part?

The patients participating in the trial will be asked to attend at least two assessment sessions in the Cardiff Gait and Motion Analysis Laboratory. Before your first assessment you will be asked to sign a patient consent form which includes the following clause:

I understand that I may withdraw from the study at any time without it affecting my ongoing treatment in any way.

One session will be requested before the Total Knee Replacement operation and one after a period of recovery following the operation. A further request to attend a session may be made at about one year following the operation. All patients will be sent a map and directions to the place of assessment (which is five minutes walk from

the Cardiff Royal Infirmary on Newport Rd, Cardiff), and travel expenses can be reimbursed on production of a receipt for journeys to the place of assessment up to a value of £10 to cover a maximum of three assessments.

During the assessment, laboratory staff will be placing very light polystyrene or cork round markers onto the skin in various places on the legs. The markers are placed with stretchy tape and a series of recordings will be made using cameras that record the positions of the markers placed on the patient. The duration of each assessment will be a maximum of 3 hours.

The assessment will provide the staff with information that they can use to produce a representation of the movement of the patients' legs as they stand still and walk along a defined walkway in the place of assessment. From this information they can then make accurate measurements of the movements of the knee in order to assess the range of motion achieved by patients before and after their operation.

Are there any risks in participating in this trial?

The measurements taken during the trial involve the placement of very light polystyrene or cork round markers onto the skin in various places on the legs. The markers are placed with double sided sticky tape which may cause some discomfort when it is being removed.

Who is paying for the trial?

The trial is being carried out by research staff employed by the University of Wales, Cardiff School of Engineering. Principal investigators are Dr. Cathy Holt and Dr. Len Nokes of the Medical Engineering Research Unit and Mr. Chris Wilson, Senior Orthopaedic Consultant, Department of Traumatic and Orthopaedic Medicine, Cardiff Royal Infirmary. The trial is not funded by outside sources and is being run along side existing research that is taking place in the Cardiff Gait and Motion Analysis Laboratory.

Who can I contact for further information, or if I have problems related to the trial?

The trial is being run by

Dr. Cathy Holt
Senior Lecturer in Biomechanics
Cardiff School of Engineering
Cardiff University
Queen's Buildings
The Parade
Cardiff CF24 0YF
Wales
UK
Tel: 029 20874533
Fax: 029 20874939

Gemma Whatling
Research Student
Cardiff School of Engineering
Cardiff University
Queen's Buildings
The Parade
Cardiff CF24 0YF
Wales
UK
Tel: 029 20874000 ext 77900
Fax: 029 20874939

Patient Consent Form

Warning: You DO NOT have to sign this document. Please DO NOT sign this document unless you fully understand it. If there is ANYTHING which you do not understand please do not hesitate to ask for a full explanation.

I _____

of _____

_____

_____

hereby consent to participate in the pre and post-operative movement assessment of the Total Knee Replacement trial. The experimental protocol and purpose of the trial have been explained to me to my full satisfaction.

I understand that I may withdraw from this study at any time without it affecting my ongoing treatment in any way.

Signed _____ (Patient)

Witness _____

Date _____

I confirm that I have fully explained to this patient the experimental protocol which is to be used in this trial and the purpose of the trial.

Signed _____

Date _____

APPENDIX C

PATIENT TRIAL INFORMATION SHEET

DATE: _____

VISIT ID NUMBERS: _____

NAME:_____ **ID:** _____

ADDRESS: _____
_____
_____

TELEPHONE NO.: _____

AGE:_____ **DOB:** _____ **M/F:** _____

HEIGHT (m):_____

WEIGHT (kg):_____

DATE OF FIRST ASSESSMENT BY DOCTOR: _____

OPERATION DATE: _____

SURGEON/DOCTOR: _____

DATE OF 1st TRIAL: _____

		RIGHT LEG	LEFT LEG
KNEE WIDTHS:	**ML=**	_____ **cm**	_____ **cm**
	AP=	_____ **cm**	_____ **cm**
KNEE GIRTH:	**[1]**	_____ **cm**	_____ **cm**
	[2]	_____ **cm**	_____ **cm**
	[3]	_____ **cm**	_____ **cm**

PATIENT HISTORY (INJURIES/DISABILITIES):

APPENDIX D

KNEE OUTCOME SURVEY (Irrgang *et al.*, 1998)

SYMPTOMS:

1. **To what degree does pain in your knee affect your daily activity level?**

   L R
   □□ I never have pain in my knee.
   □□ I have pain in my knee, but it does not affect my daily activity.
   □□ Pain affects my activity slightly.
   □□ Pain affects my activity moderately.
   □□ Pain affects my activity severely.
   □□ Pain in my knee prevents me from performing all daily activities.

2. **To what degree does grinding or grating of your knee affect your daily activity level?**

   L R
   □□ I never have grinding or grating in my knee.
   □□ I have grinding or grating in my knee, but it does not affect my daily activity.
   □□ Grinding or grating affects my activity slightly.
   □□ Grinding or grating affects my activity moderately.
   □□ Grinding or grating affects my activity severely.
   □□ Grinding or grating in my knee prevents me from performing all daily activities.

3. **To what degree does stiffness in your knee affect your daily activity level?**

   L R
   □□ I never have stiffness in my knee.
   □□ I have stiffness in my knee, but it does not affect my daily activity.
   □□ Stiffness affects my activity slightly.
   □□ Stiffness affects my activity moderately.
   □□ Stiffness affects my activity severely.
   □□ Stiffness in my knee prevents me from performing all daily activities.

4. **To what degree does swelling in your knee affect your daily activity level?**

   L R
   □□ I never have swelling in my knee.
   □□ I have swelling in my knee, but it does not affect my daily activity.
   □□ Swelling affects my activity slightly.
   □□ Swelling affects my activity moderately.
   □□ Swelling affects my activity severely.
   □□ Swelling in my knee prevents me from performing all daily activities.

5. **To what degree does slipping of your knee affect your daily activity level?**

L R
☐☐ I never have slipping of my knee.
☐☐ I have slipping in my knee, but it does not affect my daily activity.
☐☐ Slipping affects my activity slightly.
☐☐ Slipping affects my activity moderately.
☐☐ Slipping affects my activity severely.
☐☐ Slipping of my knee prevents me from performing all daily activities.

6. **To what degree does buckling of your knee affect your daily activity level?**

L R
☐☐ I never have buckling of my knee.
☐☐ I have buckling of my knee, but it does not affect my daily activity.
☐☐ Buckling affects my activity slightly.
☐☐ Buckling affects my activity moderately.
☐☐ Buckling affects my activity severely.
☐☐ Buckling of my knee prevents me from performing all daily activities.

7. **To what degree does weakness or lack of strength of your leg affect your daily activity level?**

L R
☐☐ My leg never feels weak.
☐☐ My leg feels weak, but it does not affect my daily activity.
☐☐ Weakness affects my activity slightly.
☐☐ Weakness affects my activity moderately.
☐☐ Weakness affects my activity severely.
☐☐ Weakness of my leg prevents me from performing all daily activities.

FUNCTIONAL DISABILITY WITH ACTIVITIES OF DAILY LIVING:

8. **How does your knee affect your ability to walk?**

L R
☐☐ My knee does not affect my ability to walk.
☐☐ I have pain in my knee when walking, but it does not affect my ability to walk
☐☐ My knee prevents me from walking more than 1 mile.
☐☐ My knee prevents me from walking more than 1/2 mile.
☐☐ My knee prevents me from walking more than 1 block.
☐☐ My knee prevents me from walking.

9. Because of your knee, do you walk with crutches or a cane?

L R
☐☐ I can walk without crutches or a cane.
☐☐ My knee causes me to walk with 1 crutch or a cane.
☐☐ My knee causes me to walk with 2 crutches.
☐☐ Because of my knee, I cannot walk even with crutches.

10. Does your knee cause you to limp when you walk?

L R
☐☐ I can walk without a limp.
☐☐ Sometimes my knee causes me to walk with a limp.
☐☐ Because of my knee, I cannot walk without a limp.

11. How does your knee affect your ability to go up stairs?

L R
☐☐ My knee does not affect my ability to go up stairs.
☐☐ I have pain in my knee when going up stairs, but it does not limit my ability to go up stairs.
☐☐ I am able to go up stairs normally, but I need to rely on use of a railing.
☐☐ I am able to go up stairs one step at a time with use of a railing.
☐☐ I have to use crutches or a cane to go up stairs.
☐☐ I cannot go up stairs.

12. How does your knee affect your ability to go down stairs?

L R
☐☐ My knee does not affect my ability to go down stairs.
☐☐ I have pain in my knee when going down stairs, but it does not limit my ability to go down stairs.
☐☐ I am able to go down stairs normally, but I need to rely on use of a railing.
☐☐ I am able to go down stairs one step at a time with use of a railing.
☐☐ I have to use crutches or a cane to go down stairs.
☐☐ I cannot go down stairs.

13. How does your knee affect your ability to stand?

L R
☐☐ My knee does not affect my ability to stand, I can stand for unlimited amounts of time.
☐☐ I have pain in my knee when standing, but it does not limit my ability to stand.
☐☐ Because of my knee I cannot stand for more than 1 hour.
☐☐ Because of my knee I cannot stand for more than 1/2 hour.
☐☐ Because of my knee I cannot stand for more than 10 minutes.
☐☐ I cannot stand because of my knee.

14. How does your knee affect your ability to kneel on the front of your knee?

L R
☐☐ My knee does not affect my ability to kneel on the front of my knee. I can kneel for unlimited amounts of time.
☐☐ I have pain when kneeling on the front of my knee, but it does not limit my ability to kneel.
☐☐ I cannot kneel on the front of my knee for more than 1 hour.
☐☐ I cannot kneel on the front of my knee for more than 1/2 hour.
☐☐ I cannot kneel on the front of my knee for more than 10 minutes.
☐☐ I cannot kneel on the front of my knee.

15. How does your knee affect your ability to squat?

L R
☐☐ My knee does not affect my ability to squat, I can squat all the way down.
☐☐ I have pain in my knee when squatting, but I can still squat all the way down.
☐☐ I cannot squat more than 3/4 of the way down.
☐☐ I cannot squat more than 1/2 of the way down.
☐☐ I cannot squat more than 1/4 of the way down.
☐☐ I cannot squat because of my knee.

16. How does your knee affect your ability to sit with your knee bent?

L R
☐☐ My knee does not affect my ability to sit with my knee bent, I can sit for unlimited amounts of time.
☐☐ I have pain in my knee when sitting with my knee bent, but it does not limit my ability to sit.
☐☐ I cannot sit with my knee bent for more than 1 hour.
☐☐ I cannot sit with my knee bent for more than 1/2 hour.
☐☐ I cannot sit with my knee bent for more than 10 minutes.
☐☐ I cannot sit with my knee bent.

17. How does your knee affect your ability to rise from a chair?

L R
☐☐ My knee does not affect my ability to rise from a chair.
☐☐ I have pain when rising from a seated position, but it does not affect my ability to rise from a seated position.
☐☐ Because of my knee I can only rise from a chair if I use my hands and arms to assist.
☐☐ Because of my knee I cannot rise from a chair.

OXFORD KNEE SCORE (Dawson *et al*, 1998)

During the past four weeks:

1. **How would you describe the pain you usually have from your knee**

   L R
   ☐☐ None
   ☐☐ Very mild
   ☐☐ Mild
   ☐☐ Moderate
   ☐☐ Severe

2. **Have you had any trouble with washing and drying yourself (all over) because of your knee?**

   L R
   ☐☐ No trouble at all
   ☐☐ Very little trouble
   ☐☐ Moderate trouble
   ☐☐ Extreme difficulty
   ☐☐ Impossible to do

3. **Have you had any trouble getting in and out of a car or using public transport because of your knee? (whichever you tend to use)**

   L R
   ☐☐ No trouble at all
   ☐☐ Very little trouble
   ☐☐ Moderate trouble
   ☐☐ Impossible to do

4. **For how long have you been able to walk before the pain from your knee becomes severe? (with or without a stick)**

   L R
   ☐☐ No Pain/ > 30min
   ☐☐ 16 to 30 min
   ☐☐ 5 to 15 min
   ☐☐ Around the house only
   ☐☐ Not at all – severe on walking

5. **After a meal (sat at table), how painful has it been for you to stand up from a chair because of your knee?**

L R
☐☐ Not at all painful
☐☐ Slightly painful
☐☐ Moderately painful
☐☐ Very painful
☐☐ Unbearable

6. **Have you been limping when walking, because of your knee?**

L R
☐☐ Rarely/never
☐☐ Sometimes or just at first
☐☐ Often, not just at first
☐☐ Most of the time
☐☐ All of the time

7. **Could you kneel down and get up again afterwards?**

L R
☐☐ Yes, easily
☐☐ With a little difficulty
☐☐ With moderate difficulty
☐☐ With extreme difficulty
☐☐ No, impossible

8. **Have you been troubled by pain from your knee in bed at night?**

L R
☐☐ No nights
☐☐ Only 1 or 2 nights
☐☐ Some nights
☐☐ Most nights
☐☐ Every night

9. **How much has pain from your knee interfered with your usual work (including housework)**

L R
☐☐ Not at all
☐☐ A little bit
☐☐ Moderately
☐☐ Greatly
☐☐ Totally

10. Have you felt that your knee might suddenly "give way" or let you down?

L R
☐☐ Rarely/never
☐☐ Sometimes or just at first
☐☐ Often, not just at first
☐☐ Most of the time
☐☐ All of the time

11. Could you do the household shopping on your own?

L R
☐☐ Yes, easily
☐☐ With little difficulty
☐☐ With moderate difficulty
☐☐ With extreme difficulty
☐☐ No, impossible

12. Could you walk down a flight of stairs?

L R
☐☐ Yes, easily
☐☐ With little difficulty
☐☐ With moderate difficulty
☐☐ With extreme difficulty
☐☐ No, impossible

APPENDIX E

Results from the accuracy tests completed in Chapter 4

This appendix provides results from the vertical force and centre of pressure (COP) accuracy tests from Chapter 4. Figure 1 illustrates a force plate and the location of each COP and vertical force test in relation to the force plate coordinate system. The x and y axis of the force plate coordinate system are indicated in the diagram.

The results for the actual and measured COP coordinates for each test point on force plate 1 (FP1) are presented in Table 1. The results for the vertical force tests at each test point are tabulated in Table 2.

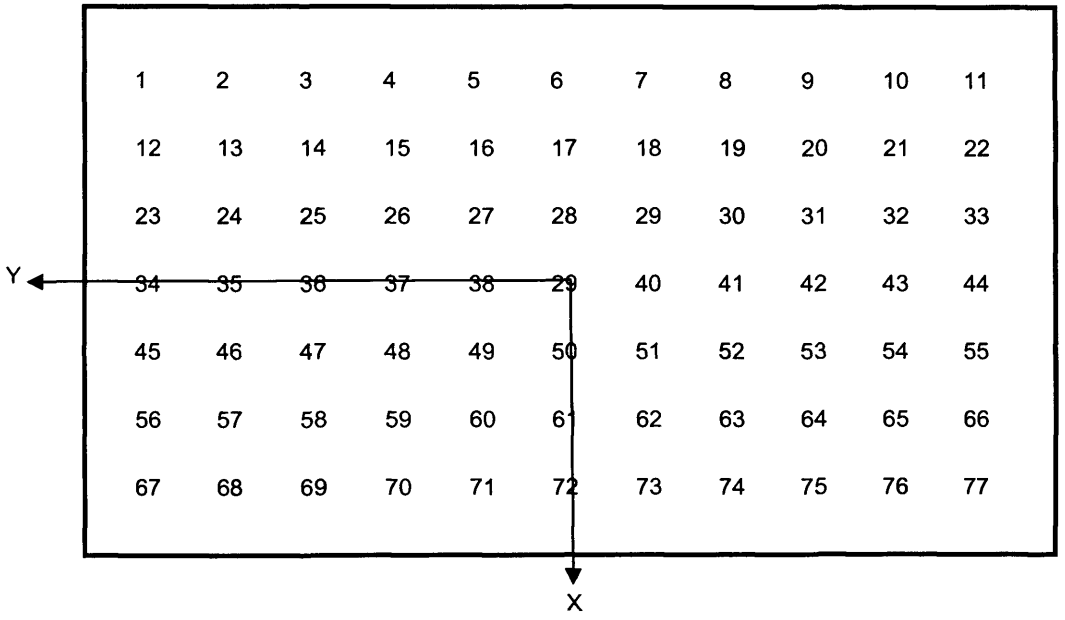

Figure 1 The naming protocol for the tests completed on both force plates

Table 1 COP measurements at each test point on FP1

Position	Actual Position		Measured Position		Difference	
	X (mm)	Y (mm)	X (mm)	Y (mm)	X (mm)	Y(mm)
1	-150	250	-146.97	252.25	3.03	2.25
2	-150	200	-144.66	201.26	5.34	1.26
3	-150	150	-143.96	152.30	6.04	2.30
4	-150	100	-143.05	101.68	6.95	1.68
5	-150	50	-141.89	51.51	8.11	1.51
6	-150	0	-141.15	-0.78	8.85	0.78
7	-150	-50	-141.16	-49.43	8.84	0.57
8	-150	-100	-140.44	-100.24	9.56	0.24
9	-150	-150	-141.55	-144.90	8.45	5.10
10	-150	-200	-141.48	-197.05	8.52	2.95
11	-150	-250	-141.67	-249.49	8.33	0.51

12	-100	250	-99.21	256.05	0.79	6.05
13	-100	200	-97.68	203.82	2.32	3.82
14	-100	150	-96.23	152.95	3.77	2.95
15	-100	100	-94.98	100.69	5.02	0.69
16	-100	50	-94.49	51.34	5.51	1.34
17	-100	0	-94.61	1.00	5.39	1.00
18	-100	-50	-94.57	-50.79	5.43	0.79
19	-100	-100	-94.23	-101.46	5.77	1.46
20	-100	-150	-93.04	-151.15	6.96	1.15
21	-100	-200	-94.68	-201.70	5.32	1.70
22	-100	-250	-94.21	-253.39	5.79	3.39
23	-50	250	-50.45	256.76	0.45	6.76
24	-50	200	-48.26	203.50	1.74	3.50
25	-50	150	-47.38	152.86	2.62	2.86
26	-50	100	-47.78	100.26	2.22	0.26
27	-50	50	-46.40	49.98	3.60	0.02
28	-50	0	-46.05	-1.82	3.95	1.82
29	-50	-50	-45.40	-51.18	4.60	1.18
30	-50	-100	-45.21	-101.59	4.79	1.59
31	-50	-150	-46.17	-150.81	3.83	0.81
32	-50	-200	-46.78	-203.91	3.22	3.91
33	-50	-250	-45.81	-253.38	4.19	3.38
34	0	250	1.10	260.29	1.10	10.29
35	0	200	0.28	205.73	0.28	5.73
36	0	150	0.77	153.21	0.77	3.21
37	0	100	1.47	102.66	1.47	2.66
38	0	50	1.43	50.83	1.43	0.83
39	0	0	1.63	-0.76	1.63	0.76
40	0	-50	2.71	-52.99	2.71	2.99
41	0	-100	3.05	-103.37	3.05	3.37
42	0	-150	2.87	-153.63	2.87	3.63
43	0	-200	2.75	-203.89	2.75	3.89
44	0	-250	3.78	-254.95	3.78	4.95
45	50	250	49.93	258.14	0.07	8.14
46	50	200	49.89	207.31	0.11	7.31
47	50	150	50.15	153.58	0.15	3.58
48	50	100	49.59	103.73	0.41	3.73
49	50	50	50.78	50.77	0.78	0.77
50	50	0	50.55	-0.58	0.55	0.58
51	50	-50	51.67	-51.21	1.67	1.21
52	50	-100	51.29	-101.37	1.29	1.37
53	50	-150	51.11	-153.41	1.11	3.41
54	50	-200	50.61	-205.34	0.61	5.34
55	50	-250	51.56	-258.53	1.56	8.53
56	100	250	90.25	258.91	9.75	8.91
57	100	200	90.39	206.69	9.61	6.69
58	100	150	89.29	154.08	10.71	4.08
59	100	100	88.83	103.33	11.17	3.33
60	100	50	89.55	51.58	10.45	1.58
61	100	0	91.24	-0.04	8.76	0.04
62	100	-50	90.65	-53.32	9.35	3.32
63	100	-100	91.12	-102.90	8.88	2.90

64	100	-150	91.42	-155.65	8.58	5.65
65	100	-200	101.36	-206.68	1.36	6.68
66	100	-250	102.66	-259.02	2.66	9.02
67	150	250	149.16	259.81	0.84	9.81
68	150	200	148.86	206.29	1.14	6.29
69	150	150	148.26	154.46	1.74	4.46
70	150	100	149.36	103.11	0.64	3.11
71	150	50	148.49	50.83	1.51	0.83
72	150	0	148.25	1.17	1.75	1.17
73	150	-50	148.96	-54.37	1.04	4.37
74	150	-100	148.44	-103.34	1.56	3.34
75	150	-150	149.34	-154.44	0.66	4.44
76	150	-200	150.39	-205.97	0.39	5.97
77	150	-250	151.66	-257.82	1.66	7.82

Table 2 Vertical force measurements at each test point on FP1

Position	Actual Weight (N)	Measured Fz (N)	% Difference
1	130.48	133.30	2.16
2	130.48	134.36	2.97
3	130.48	134.79	3.30
4	130.48	135.17	3.60
5	130.48	135.69	4.00
6	130.48	135.78	4.06
7	130.48	136.01	4.24
8	130.48	136.40	4.54
9	130.48	136.50	4.61
10	130.48	136.54	4.64
11	130.48	135.63	3.95
12	130.48	132.36	1.44
13	130.48	133.47	2.29
14	130.48	133.85	2.58
15	130.48	134.13	2.80
16	130.48	134.71	3.24
17	130.48	134.61	3.17
18	130.48	134.73	3.25
19	130.48	135.32	3.71
20	130.48	135.64	3.95
21	130.48	135.38	3.75
22	130.48	134.42	3.02
23	130.48	132.13	1.27
24	130.48	133.09	2.00
25	130.48	133.44	2.27
26	130.48	134.17	2.83
27	130.48	134.39	3.00
28	130.48	134.48	3.07
29	130.48	134.76	3.28
30	130.48	134.92	3.40

31	130.48	134.70	3.23
32	130.48	134.34	2.96
33	130.48	133.88	2.60
34	130.48	131.80	1.01
35	130.48	132.66	1.67
36	130.48	132.90	1.86
37	130.48	133.49	2.31
38	130.48	133.83	2.56
39	130.48	134.15	2.81
40	130.48	134.10	2.77
41	130.48	134.06	2.75
42	130.48	134.03	2.72
43	130.48	133.70	2.47
44	130.48	132.99	1.93
45	130.48	131.88	1.08
46	130.48	132.29	1.38
47	130.48	132.71	1.71
48	130.48	132.99	1.92
49	130.48	133.01	1.94
50	130.48	133.33	2.18
51	130.48	133.34	2.19
52	130.48	133.64	2.42
53	130.48	133.13	2.03
54	130.48	133.04	1.96
55	130.48	132.30	1.39
56	130.48	131.55	0.82
57	130.48	132.25	1.35
58	130.48	133.22	2.10
59	130.48	133.42	2.26
60	130.48	133.18	2.07
61	130.48	132.84	1.81
62	130.48	133.36	2.21
63	130.48	133.07	1.99
64	130.48	132.96	1.90
65	130.48	132.49	1.54
66	130.48	131.28	0.61
67	130.48	131.44	0.73
68	130.48	132.67	1.68
69	130.48	132.49	1.54
70	130.48	132.56	1.60
71	130.48	132.79	1.77
72	130.48	133.04	1.97
73	130.48	132.74	1.73
74	130.48	133.07	1.99
75	130.48	132.88	1.84
76	130.48	132.27	1.37
77	130.48	131.47	0.76

Figure 2 illustrates the location of each COP and vertical force test on each step in relation to the force plate coordinate system. The results for the actual and measured COP coordinates for each test point on step 1 interfacing with force plate 1 (FP1) are presented in Table 3. The results for the vertical force tests at each test point on step 1 interfacing with FP1 are tabulated in Table 4.

The results for the actual and measured COP coordinates for each test point on step 2 interfacing with force plate 1 (FP) are presented in Table 5. The results for the vertical force tests at each test point on step 2 interfacing with FP1 are tabulated in Table 6.

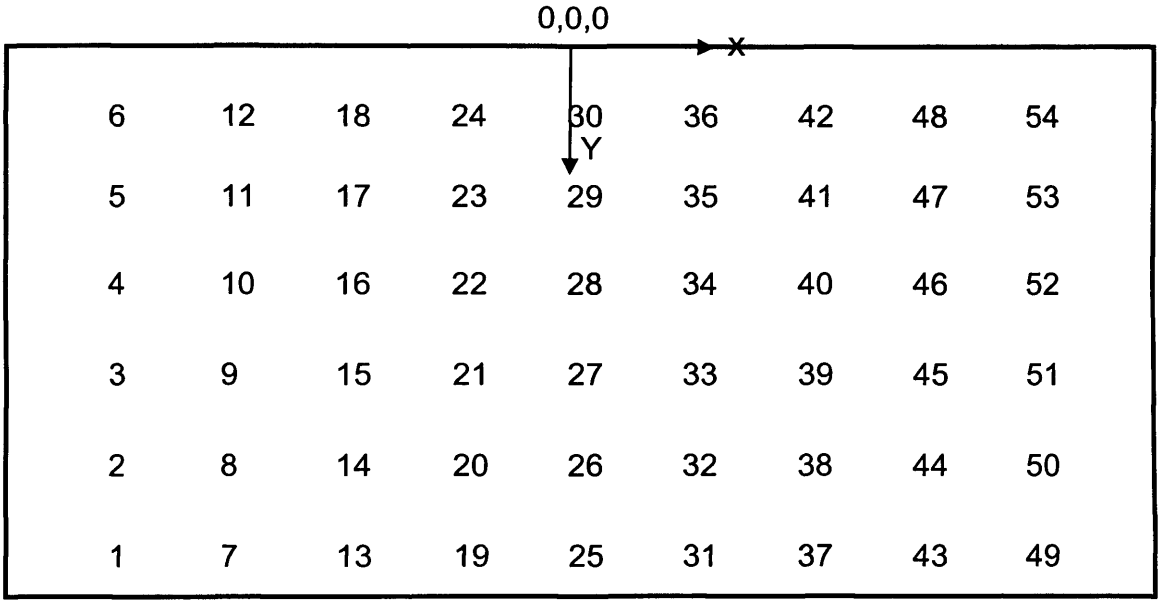

Figure 2 The naming protocol for the tests completed on each step (interfacing with a force plate).

Table 3 COP measurements at each test point on Step 1 interfacing with FP1

Position	Actual Position		Measured Position		Difference	
	X (mm)	Y (mm)	X (mm)	Y (mm)	X (mm)	Y(mm)
1	-195.00	280.00	-189.90	285.78	5.10	5.78
2	-195.00	230.00	-189.20	234.51	5.80	4.51
3	-195.00	180.00	-187.90	182.34	7.10	2.34
4	-195.00	130.00	-186.48	129.55	8.52	0.45
5	-195.00	80.00	-186.63	81.87	8.37	1.87
6	-195.00	30.00	-183.63	30.63	11.37	0.63
7	-145.00	280.00	-141.80	286.43	3.20	6.43
8	-145.00	230.00	-141.27	234.41	3.73	4.41
9	-145.00	180.00	-140.17	184.22	4.83	4.22
10	-145.00	130.00	-139.54	131.50	5.46	1.50
11	-145.00	80.00	-138.23	81.97	6.77	1.97
12	-145.00	30.00	-137.79	31.78	7.21	1.78
13	-95.00	280.00	-92.67	287.28	2.33	7.28

14	-95.00	230.00	-92.39	234.23	2.61	4.23
15	-95.00	180.00	-91.50	182.72	3.50	2.72
16	-95.00	130.00	-91.16	132.08	3.84	2.08
17	-95.00	80.00	-90.47	81.34	4.53	1.34
18	-95.00	30.00	-89.44	31.00	5.56	1.00
19	-45.00	280.00	-44.05	288.59	0.95	8.59
20	-45.00	230.00	-43.11	235.52	1.89	5.52
21	-45.00	180.00	-42.85	184.04	2.15	4.04
22	-45.00	130.00	-42.18	130.46	2.82	0.46
23	-45.00	80.00	-41.45	79.85	3.55	0.15
24	-45.00	30.00	-41.92	28.55	3.08	1.45
25	5.00	280.00	4.81	287.58	0.19	7.58
26	5.00	230.00	4.77	235.74	0.23	5.74
27	5.00	180.00	5.51	183.28	0.51	3.28
28	5.00	130.00	5.87	130.90	0.87	0.90
29	5.00	80.00	6.43	80.50	1.43	0.50
30	5.00	30.00	5.63	29.00	0.63	1.00
31	55.00	280.00	55.26	287.24	0.26	7.24
32	55.00	230.00	55.05	234.99	0.05	4.99
33	55.00	180.00	55.57	184.35	0.57	4.35
34	55.00	130.00	55.52	132.54	0.52	2.54
35	55.00	80.00	55.03	80.10	0.03	0.10
36	55.00	30.00	55.03	30.04	0.03	0.04
37	105.00	280.00	93.61	286.67	11.39	6.67
38	105.00	230.00	93.66	236.02	11.34	6.02
39	105.00	180.00	93.86	184.77	11.14	4.77
40	105.00	130.00	93.16	132.30	11.84	2.30
41	105.00	80.00	106.24	81.33	1.24	1.33
42	105.00	30.00	104.13	29.27	0.87	0.73
43	155.00	280.00	155.27	289.37	0.27	9.37
44	155.00	230.00	154.23	236.20	0.77	6.20
45	155.00	180.00	154.91	184.91	0.09	4.91
46	155.00	130.00	154.18	132.09	0.82	2.09
47	155.00	80.00	154.28	81.65	0.72	1.65
48	155.00	30.00	153.17	30.23	1.83	0.23
49	205.00	280.00	204.59	288.42	0.41	8.42
50	205.00	230.00	203.90	235.96	1.10	5.96
51	205.00	180.00	204.20	184.56	0.80	4.56
52	205.00	130.00	203.62	132.98	1.38	2.98
53	205.00	80.00	202.59	80.69	2.41	0.69
54	205.00	30.00	201.51	30.44	3.49	0.44

Table 4 Vertical force measurements at each test point on Step 1 interfacing with FP1

Position	Actual Weight (N)	Fz (N)	% Difference
1	130.28	132.88	2.00
2	130.28	133.14	2.19
3	130.28	134.23	3.03
4	130.28	134.74	3.42

5	130.28	134.84	3.50
6	130.28	135.60	4.08
7	130.28	132.24	1.50
8	130.28	132.96	2.06
9	130.28	133.56	2.51
10	130.28	134.17	2.99
11	130.28	134.63	3.34
12	130.28	135.35	3.89
13	130.28	132.11	1.40
14	130.28	132.91	2.01
15	130.28	133.28	2.30
16	130.28	133.73	2.64
17	130.28	134.36	3.13
18	130.28	134.75	3.42
19	130.28	131.64	1.04
20	130.28	132.29	1.54
21	130.28	132.72	1.87
22	130.28	133.20	2.24
23	130.28	133.71	2.63
24	130.28	134.28	3.07
25	130.28	131.26	0.75
26	130.28	131.70	1.09
27	130.28	132.34	1.58
28	130.28	132.53	1.72
29	130.28	133.27	2.29
30	130.28	133.88	2.76
31	130.28	131.29	0.77
32	130.28	131.53	0.96
33	130.28	131.95	1.28
34	130.28	132.57	1.76
35	130.28	133.15	2.20
36	130.28	133.59	2.54
37	130.28	130.97	0.53
38	130.28	131.49	0.92
39	130.28	131.94	1.27
40	130.28	132.12	1.41
41	130.28	132.49	1.69
42	130.28	133.32	2.33
43	130.28	130.72	0.33
44	130.28	131.21	0.71
45	130.28	131.35	0.82
46	130.28	131.82	1.18
47	130.28	132.06	1.36
48	130.28	132.66	1.82
49	130.28	130.84	0.43
50	130.28	131.41	0.86
51	130.28	131.63	1.03
52	130.28	131.71	1.10
53	130.28	132.34	1.58
54	130.28	132.56	1.75

Table 5 COP measurements at each test point on Step 2 interfacing with FP1

Position	Actual Position		Measured Position		Difference	
	X (mm)	Y (mm)	X (mm)	Y (mm)	X (mm)	Y(mm)
1	-195.00	280.00	-190.00	285.84	5.00	5.84
2	-195.00	230.00	-189.52	232.90	5.48	2.90
3	-195.00	180.00	-189.32	179.97	5.68	0.03
4	-195.00	130.00	-186.58	130.89	8.42	0.89
5	-195.00	80.00	-186.01	79.91	8.99	0.09
6	-195.00	30.00	-186.90	29.03	8.10	0.97
7	-145.00	280.00	-142.51	284.75	2.49	4.75
8	-145.00	230.00	-141.79	233.33	3.21	3.33
9	-145.00	180.00	-140.19	181.45	4.81	1.45
10	-145.00	130.00	-139.94	131.05	5.06	1.05
11	-145.00	80.00	-139.94	78.86	5.06	1.14
12	-145.00	30.00	-138.83	28.34	6.17	1.66
13	-95.00	280.00	-94.59	286.68	0.41	6.68
14	-95.00	230.00	-94.07	233.63	0.93	3.63
15	-95.00	180.00	-92.78	181.82	2.22	1.82
16	-95.00	130.00	-93.36	130.54	1.64	0.54
17	-95.00	80.00	-92.01	79.47	2.99	0.53
18	-95.00	30.00	-91.65	27.66	3.35	2.34
19	-45.00	280.00	-45.14	286.55	0.14	6.55
20	-45.00	230.00	-44.52	234.24	0.48	4.24
21	-45.00	180.00	-44.13	182.14	0.87	2.14
22	-45.00	130.00	-43.25	131.21	1.75	1.21
23	-45.00	80.00	-43.96	80.15	1.04	0.15
24	-45.00	30.00	-44.47	29.19	0.53	0.81
25	5.00	280.00	4.90	286.39	0.10	6.39
26	5.00	230.00	4.03	233.93	0.97	3.93
27	5.00	180.00	3.83	182.40	1.17	2.40
28	5.00	130.00	3.85	131.88	1.15	1.88
29	5.00	80.00	4.33	80.95	0.67	0.95
30	5.00	30.00	4.74	29.36	0.26	0.64
31	55.00	280.00	55.12	286.64	0.12	6.64
32	55.00	230.00	54.67	234.84	0.33	4.84
33	55.00	180.00	54.67	182.59	0.33	2.59
34	55.00	130.00	55.50	129.29	0.50	0.71
35	55.00	80.00	54.35	78.99	0.65	1.01
36	55.00	30.00	55.89	28.47	0.89	1.53
37	105.00	280.00	93.32	285.19	11.68	5.19
38	105.00	230.00	93.23	233.18	11.77	3.18
39	105.00	180.00	92.80	181.65	12.20	1.65
40	105.00	130.00	91.94	128.85	13.06	1.15
41	105.00	80.00	92.63	78.33	12.37	1.67
42	105.00	30.00	92.07	27.60	12.93	2.40
43	155.00	280.00	152.36	286.18	2.64	6.18
44	155.00	230.00	152.47	234.20	2.53	4.20
45	155.00	180.00	152.09	182.35	2.91	2.35
46	155.00	130.00	151.97	128.65	3.03	1.35
47	155.00	80.00	152.28	79.08	2.72	0.92

48	155.00	30.00	150.37	27.93	4.63	2.07
49	205.00	280.00	203.04	286.12	1.96	6.12
50	205.00	230.00	201.93	234.28	3.07	4.28
51	205.00	180.00	201.95	181.64	3.05	1.64
52	205.00	130.00	201.91	129.45	3.09	0.55
53	205.00	80.00	201.52	79.08	3.48	0.92
54	205.00	30.00	200.95	28.31	4.05	1.69

Table 6 Vertical force measurements at each test point on Step 2 interfacing with FP1

Position	Actual Weight (N)	Fz (N)	% Difference
1	130.28	132.43	1.65
2	130.28	133.05	2.13
3	130.28	133.92	2.79
4	130.28	134.35	3.12
5	130.28	135.09	3.69
6	130.28	134.98	3.60
7	130.28	132.55	1.74
8	130.28	132.69	1.85
9	130.28	133.18	2.22
10	130.28	133.56	2.52
11	130.28	134.09	2.92
12	130.28	134.95	3.58
13	130.28	131.90	1.24
14	130.28	132.21	1.48
15	130.28	132.86	1.97
16	130.28	133.36	2.36
17	130.28	133.82	2.71
18	130.28	134.36	3.13
19	130.28	131.60	1.01
20	130.28	132.04	1.35
21	130.28	132.34	1.58
22	130.28	133.05	2.13
23	130.28	133.40	2.39
24	130.28	134.02	2.87
25	130.28	131.15	0.66
26	130.28	131.61	1.02
27	130.28	132.04	1.35
28	130.28	132.35	1.58
29	130.28	132.87	1.99
30	130.28	133.19	2.23
31	130.28	131.94	1.27
32	130.28	131.78	1.15
33	130.28	131.76	1.14
34	130.28	132.64	1.81
35	130.28	132.95	2.05
36	130.28	133.54	2.50
37	130.28	131.44	0.89
38	130.28	131.75	1.12

39	130.28	132.00	1.32
40	130.28	132.57	1.76
41	130.28	132.84	1.96
42	130.28	133.05	2.13
43	130.28	131.07	0.60
44	130.28	131.54	0.96
45	130.28	131.97	1.29
46	130.28	132.32	1.56
47	130.28	132.64	1.81
48	130.28	132.78	1.91
49	130.28	131.30	0.78
50	130.28	131.58	1.00
51	130.28	131.81	1.17
52	130.28	132.26	1.52
53	130.28	132.22	1.48
54	130.28	132.78	1.92

The results for the actual and measured COP coordinates for each test point on force plate 2 (FP2) are presented in Table 7. The results for the vertical force tests at each test point are tabulated in Table 8. The test points are illustrated relative to the force plate coordinate system in Figure 1.

Table 7 COP measurements at each test point on FP2

Position	Actual Position		Measured Position		Difference	
	X (mm)	Y (mm)	X (mm)	Y (mm)	X (mm)	Y(mm)
1	-150	250	-146.78	249.41	3.22	0.59
2	-150	200	-146.04	199.27	3.96	0.73
3	-150	150	-144.15	149.85	5.85	0.15
4	-150	100	-143.56	100.46	6.44	0.46
5	-150	50	-143.93	50.99	6.07	0.99
6	-150	0	-143.67	2.02	6.33	2.02
7	-150	-50	-144.74	-47.26	5.26	2.74
8	-150	-100	-143.63	-96.42	6.37	3.58
9	-150	-150	-144.65	-145.97	5.35	4.03
10	-150	-200	-145.08	-194.51	4.92	5.49
11	-150	-250	-146.04	-245.29	3.96	4.71
12	-100	250	-98.28	251.29	1.72	1.29
13	-100	200	-97.08	198.92	2.92	1.08
14	-100	150	-96.01	149.99	3.99	0.01
15	-100	100	-96.27	100.45	3.73	0.45
16	-100	50	-96.03	50.73	3.97	0.73
17	-100	0	-95.61	0.90	4.39	0.90
18	-100	-50	-97.04	-48.41	2.96	1.59
19	-100	-100	-97.03	-96.53	2.97	3.47
20	-100	-150	-97.07	-148.08	2.93	1.92

21	-100	-200	-97.51	-195.84	2.49	4.16
22	-100	-250	-98.63	-247.83	1.37	2.17
23	-50	250	-48.57	251.58	1.43	1.58
24	-50	200	-48.21	200.78	1.79	0.78
25	-50	150	-47.98	150.04	2.02	0.04
26	-50	100	-47.00	100.28	3.00	0.28
27	-50	50	-46.77	50.48	3.23	0.48
28	-50	0	-47.74	1.86	2.26	1.86
29	-50	-50	-47.75	-47.43	2.25	2.57
30	-50	-100	-47.66	-97.45	2.34	2.55
31	-50	-150	-48.32	-147.45	1.68	2.55
32	-50	-200	-47.92	-197.06	2.08	2.94
33	-50	-250	-48.91	-246.64	1.09	3.36
34	0	250	2.68	251.69	2.68	1.69
35	0	200	2.15	200.51	2.15	0.51
36	0	150	1.99	150.10	1.99	0.10
37	0	100	1.70	99.76	1.70	0.24
38	0	50	1.69	50.58	1.69	0.58
39	0	0	2.43	1.63	2.43	1.63
40	0	-50	1.77	-48.31	1.77	1.69
41	0	-100	0.89	-98.57	0.89	1.43
42	0	-150	1.04	-148.06	1.04	1.94
43	0	-200	1.72	-197.51	1.72	2.49
44	0	-250	-0.20	-246.98	0.20	3.02
45	50	250	52.27	250.37	2.27	0.37
46	50	200	52.71	200.91	2.71	0.91
47	50	150	52.33	151.15	2.33	1.15
48	50	100	51.47	100.16	1.47	0.16
49	50	50	51.25	50.76	1.25	0.76
50	50	0	51.78	0.90	1.78	0.90
51	50	-50	51.57	-47.13	1.57	2.87
52	50	-100	50.12	-98.86	0.12	1.14
53	50	-150	51.10	-147.46	1.10	2.54
54	50	-200	51.04	-196.96	1.04	3.04
55	50	-250	50.79	-249.05	0.79	0.95
56	100	250	91.58	252.88	8.42	2.88
57	100	200	92.05	199.53	7.95	0.47
58	100	150	90.53	151.27	9.47	1.27
59	100	100	92.13	100.64	7.87	0.64
60	100	50	89.82	50.32	10.18	0.32
61	100	0	89.51	-0.53	10.49	0.53
62	100	-50	99.74	-49.11	0.26	0.89
63	100	-100	100.16	-97.74	0.16	2.26
64	100	-150	99.54	-148.36	0.46	1.64
65	100	-200	100.91	-198.98	0.91	1.02
66	100	-250	101.04	-249.27	1.04	0.73
67	150	250	152.59	251.84	2.59	1.84
68	150	200	152.44	199.50	2.44	0.50
69	150	150	150.98	149.70	0.98	0.30
70	150	100	150.34	100.54	0.34	0.54
71	150	50	147.79	49.97	2.21	0.03
72	150	0	148.02	0.61	1.98	0.61

73	150	-50	148.48	-48.83	1.52	1.17
74	150	-100	147.22	-98.65	2.78	1.35
75	150	-150	147.26	-148.71	2.74	1.29
76	150	-200	147.60	-197.03	2.40	2.97
77	150	-250	149.17	-249.18	0.83	0.82

Table 8 Vertical force measurements at each test point on FP2

Position	Actual Weight (N)	Measured Fz (N)	% Difference
1	129.41	132.28	2.22
2	129.41	133.05	2.81
3	129.41	133.60	3.24
4	129.41	133.88	3.45
5	129.41	133.48	3.15
6	129.41	133.48	3.15
7	129.41	133.58	3.22
8	129.41	133.48	3.15
9	129.41	133.14	2.88
10	129.41	132.73	2.56
11	129.41	131.54	1.65
12	129.41	131.32	1.48
13	129.41	132.42	2.32
14	129.41	132.40	2.31
15	129.41	132.64	2.49
16	129.41	132.82	2.63
17	129.41	132.93	2.72
18	129.41	132.72	2.56
19	129.41	132.75	2.58
20	129.41	132.03	2.03
21	129.41	131.88	1.91
22	129.41	130.73	1.02
23	129.41	130.97	1.20
24	129.41	131.71	1.78
25	129.41	132.07	2.05
26	129.41	131.83	1.87
27	129.41	132.36	2.28
28	129.41	132.18	2.14
29	129.41	132.04	2.03
30	129.41	132.08	2.06
31	129.41	131.56	1.66
32	129.41	131.57	1.67
33	129.41	130.81	1.08
34	129.41	130.55	0.88
35	129.41	130.90	1.15
36	129.41	131.34	1.49
37	129.41	131.93	1.95
38	129.41	131.51	1.63
39	129.41	132.03	2.02
40	129.41	131.57	1.67
41	129.41	131.77	1.82

42	129.41	131.46	1.58
43	129.41	131.23	1.41
44	129.41	130.21	0.62
45	129.41	130.12	0.55
46	129.41	130.43	0.79
47	129.41	130.68	0.99
48	129.41	131.26	1.43
49	129.41	131.04	1.26
50	129.41	131.23	1.41
51	129.41	131.77	1.82
52	129.41	131.10	1.31
53	129.41	131.64	1.72
54	129.41	131.08	1.29
55	129.41	130.07	0.51
56	129.41	129.47	0.05
57	129.41	130.20	0.61
58	129.41	130.82	1.09
59	129.41	130.90	1.16
60	129.41	131.36	1.51
61	129.41	131.38	1.52
62	129.41	130.95	1.19
63	129.41	131.41	1.54
64	129.41	131.07	1.29
65	129.41	130.78	1.06
66	129.41	129.86	0.35
67	129.41	129.51	0.08
68	129.41	130.82	1.09
69	129.41	130.47	0.82
70	129.41	130.61	0.93
71	129.41	131.06	1.27
72	129.41	131.36	1.51
73	129.41	131.17	1.36
74	129.41	131.19	1.38
75	129.41	131.33	1.48
76	129.41	131.30	1.46
77	129.41	129.91	0.39

The results for the actual and measured COP coordinates for each test point on step 1 interfacing with force plate 2 (FP2) are presented in Table 9. The results for the vertical force tests at each test point on step 1 interfacing with FP2 are tabulated in Table 10. The test points are illustrated relative to the force plate coordinate system in Figure 2.

Table 9 COP measurements at each test point on Step 1 interfacing with FP2

Position	Actual Position		Measured Position		Difference	
	X (mm)	Y (mm)	X (mm)	Y (mm)	X (mm)	Y(mm)
1	-195.00	280.00	-195.99	279.19	0.99	0.81
2	-195.00	230.00	-194.33	230.10	0.67	0.10
3	-195.00	180.00	-190.63	179.97	4.37	0.03
4	-195.00	130.00	-190.03	129.48	4.97	0.52
5	-195.00	80.00	-189.87	78.91	5.13	1.09
6	-195.00	30.00	-188.94	31.07	6.06	1.07
7	-145.00	280.00	-145.57	281.75	0.57	1.75
8	-145.00	230.00	-143.57	229.14	1.43	0.86
9	-145.00	180.00	-143.12	178.80	1.88	1.20
10	-145.00	130.00	-140.73	129.95	4.27	0.05
11	-145.00	80.00	-140.43	80.83	4.57	0.83
12	-145.00	30.00	-139.33	31.09	5.67	1.09
13	-95.00	280.00	-94.59	281.23	0.41	1.23
14	-95.00	230.00	-93.05	229.44	1.95	0.56
15	-95.00	180.00	-93.10	179.34	1.90	0.66
16	-95.00	130.00	-92.43	129.25	2.57	0.75
17	-95.00	80.00	-91.15	80.55	3.85	0.55
18	-95.00	30.00	-90.86	29.94	4.14	0.06
19	-45.00	280.00	-45.73	281.51	0.73	1.51
20	-45.00	230.00	-44.09	230.32	0.91	0.32
21	-45.00	180.00	-43.37	180.56	1.63	0.56
22	-45.00	130.00	-43.14	129.94	1.86	0.06
23	-45.00	80.00	-41.73	79.19	3.27	0.81
24	-45.00	30.00	-40.86	31.12	4.14	1.12
25	5.00	280.00	5.15	282.03	0.15	2.03
26	5.00	230.00	6.41	232.45	1.41	2.45
27	5.00	180.00	7.55	181.10	2.55	1.10
28	5.00	130.00	6.35	129.27	1.35	0.73
29	5.00	80.00	7.05	78.90	2.05	1.10
30	5.00	30.00	7.25	31.18	2.25	1.18
31	55.00	280.00	58.33	282.96	3.33	2.96
32	55.00	230.00	58.22	231.85	3.22	1.85
33	55.00	180.00	58.02	179.61	3.02	0.39
34	55.00	130.00	56.94	130.12	1.94	0.12
35	55.00	80.00	56.39	78.49	1.39	1.51
36	55.00	30.00	56.88	30.27	1.88	0.27
37	105.00	280.00	107.65	283.98	2.65	3.98
38	105.00	230.00	106.77	231.33	1.77	1.33
39	105.00	180.00	106.89	180.98	1.89	0.98
40	105.00	130.00	106.66	129.19	1.66	0.81
41	105.00	80.00	105.53	79.82	0.53	0.18
42	105.00	30.00	105.04	29.40	0.04	0.60
43	155.00	280.00	158.30	282.89	3.30	2.89
44	155.00	230.00	157.93	232.07	2.93	2.07
45	155.00	180.00	157.59	181.71	2.59	1.71
46	155.00	130.00	155.35	129.09	0.35	0.91

47	155.00	80.00	155.30	79.16	0.30	0.84
48	155.00	30.00	156.00	29.73	1.00	0.27
49	205.00	280.00	207.70	283.00	2.70	3.00
50	205.00	230.00	208.35	233.10	3.35	3.10
51	205.00	180.00	207.58	181.12	2.58	1.12
52	205.00	130.00	206.20	130.95	1.20	0.95
53	205.00	80.00	205.98	79.39	0.98	0.61
54	205.00	30.00	206.60	30.29	1.60	0.29

Table 10 Vertical force measurements at each test point on Step 1 interfacing with FP2

Position	Actual Weight (N)	Fz (N)	% Difference
1	129.41	132.98	2.76
2	129.41	132.15	2.12
3	129.41	132.84	2.65
4	129.41	133.15	2.89
5	129.41	133.77	3.37
6	129.41	134.03	3.57
7	129.41	131.11	1.32
8	129.41	132.26	2.21
9	129.41	132.68	2.53
10	129.41	132.81	2.63
11	129.41	133.07	2.83
12	129.41	133.77	3.37
13	129.41	131.01	1.24
14	129.41	131.88	1.91
15	129.41	131.85	1.89
16	129.41	131.99	2.00
17	129.41	132.08	2.07
18	129.41	132.87	2.67
19	129.41	130.69	0.99
20	129.41	131.50	1.61
21	129.41	131.20	1.38
22	129.41	131.55	1.65
23	129.41	132.32	2.25
24	129.41	132.68	2.53
25	129.41	129.90	0.38
26	129.41	130.39	0.75
27	129.41	130.68	0.98
28	129.41	131.19	1.38
29	129.41	132.07	2.06
30	129.41	132.25	2.19
31	129.41	129.42	0.01
32	129.41	130.09	0.52
33	129.41	130.69	0.99
34	129.41	131.02	1.25
35	129.41	131.59	1.68
36	129.41	131.70	1.77
37	129.41	129.30	-0.09

38	129.41	129.90	0.38
39	129.41	130.31	0.70
40	129.41	130.50	0.84
41	129.41	131.33	1.49
42	129.41	131.67	1.74
43	129.41	128.74	-0.52
44	129.41	129.55	0.11
45	129.41	129.94	0.41
46	129.41	130.55	0.88
47	129.41	130.87	1.13
48	129.41	131.17	1.36
49	129.41	129.19	-0.17
50	129.41	129.21	-0.15
51	129.41	130.08	0.52
52	129.41	130.20	0.61
53	129.41	130.65	0.96
54	129.41	131.01	1.23

The results for the actual and measured COP coordinates for each test point on step 2 interfacing with force plate 2 (FP) are presented in Table 11. The results for the vertical force tests at each test point on step 2 interfacing with FP2 are tabulated in Table 12. The test points are illustrated relative to the force plate coordinate system in Figure 2.

Table 11 COP measurements at each test point on Step 2 interfacing with FP2

Position	Actual Position		Measured Position		Difference	
	X (mm)	Y (mm)	X (mm)	Y (mm)	X (mm)	Y(mm)
1	-195.00	280.00	-196.38	274.93	1.38	5.07
2	-195.00	230.00	-195.03	231.85	0.03	1.85
3	-195.00	180.00	-194.08	181.19	0.92	1.19
4	-195.00	130.00	-192.53	130.34	2.47	0.34
5	-195.00	80.00	-192.52	80.41	2.48	0.41
6	-195.00	30.00	-190.83	32.46	4.17	2.46
7	-145.00	280.00	-145.99	283.29	0.99	3.29
8	-145.00	230.00	-144.71	230.75	0.29	0.75
9	-145.00	180.00	-143.90	180.43	1.10	0.43
10	-145.00	130.00	-142.94	130.53	2.06	0.53
11	-145.00	80.00	-143.28	80.16	1.72	0.16
12	-145.00	30.00	-140.66	32.47	4.34	2.47
13	-95.00	280.00	-95.09	281.90	0.09	1.90
14	-95.00	230.00	-95.62	231.04	0.62	1.04
15	-95.00	180.00	-95.86	180.78	0.86	0.78
16	-95.00	130.00	-93.30	130.81	1.70	0.81
17	-95.00	80.00	-93.60	79.05	1.40	0.95
18	-95.00	30.00	-90.68	30.92	4.32	0.92
19	-45.00	280.00	-44.72	285.60	0.28	5.60
20	-45.00	230.00	-45.30	232.69	0.30	2.69

21	-45.00	180.00	-44.57	181.20	0.43	1.20
22	-45.00	130.00	-43.45	129.83	1.55	0.17
23	-45.00	80.00	-42.69	78.92	2.31	1.08
24	-45.00	30.00	-41.53	31.54	3.47	1.54
25	5.00	280.00	3.79	283.05	1.21	3.05
26	5.00	230.00	5.42	232.87	0.42	2.87
27	5.00	180.00	5.94	181.59	0.94	1.59
28	5.00	130.00	7.01	130.71	2.01	0.71
29	5.00	80.00	6.98	79.13	1.98	0.87
30	5.00	30.00	6.90	29.83	1.90	0.17
31	55.00	280.00	56.69	280.58	1.69	0.58
32	55.00	230.00	56.54	230.75	1.54	0.75
33	55.00	180.00	58.07	180.26	3.07	0.26
34	55.00	130.00	57.82	129.86	2.82	0.14
35	55.00	80.00	57.93	79.11	2.93	0.89
36	55.00	30.00	57.39	29.43	2.39	0.57
37	105.00	280.00	107.42	284.90	2.42	4.90
38	105.00	230.00	107.36	230.38	2.36	0.38
39	105.00	180.00	106.68	180.24	1.68	0.24
40	105.00	130.00	106.65	129.40	1.65	0.60
41	105.00	80.00	104.87	78.40	0.13	1.60
42	105.00	30.00	105.86	29.57	0.86	0.43
43	155.00	280.00	160.39	281.35	5.39	1.35
44	155.00	230.00	159.52	231.60	4.52	1.60
45	155.00	180.00	158.06	180.23	3.06	0.23
46	155.00	130.00	155.59	130.69	0.59	0.69
47	155.00	80.00	155.49	79.32	0.49	0.68
48	155.00	30.00	154.60	29.47	0.40	0.53
49	205.00	280.00	209.68	283.36	4.68	3.36
50	205.00	230.00	206.45	232.86	1.45	2.86
51	205.00	180.00	206.26	180.77	1.26	0.77
52	205.00	130.00	204.44	130.41	0.56	0.41
53	205.00	80.00	202.55	78.19	2.45	1.81
54	205.00	30.00	202.82	29.06	2.18	0.94

Table 12 Vertical force measurements at each test point on Step 2 interfacing with FP2

Position	Actual Weight (N)	Fz (N)	% Difference
1	129.41	132.34	2.26
2	129.41	132.34	2.27
3	129.41	132.80	2.62
4	129.41	133.39	3.07
5	129.41	133.76	3.36
6	129.41	134.07	3.60
7	129.41	131.60	1.69
8	129.41	132.46	2.36
9	129.41	132.40	2.31
10	129.41	133.09	2.84

11	129.41	132.58	2.45
12	129.41	133.83	3.41
13	129.41	131.28	1.44
14	129.41	131.35	1.50
15	129.41	131.55	1.66
16	129.41	132.33	2.25
17	129.41	132.50	2.39
18	129.41	133.14	2.88
19	129.41	130.44	0.80
20	129.41	130.68	0.98
21	129.41	131.01	1.24
22	129.41	132.08	2.06
23	129.41	132.33	2.26
24	129.41	132.78	2.61
25	129.41	130.06	0.50
26	129.41	130.40	0.77
27	129.41	130.72	1.01
28	129.41	131.43	1.56
29	129.41	132.11	2.09
30	129.41	131.68	1.75
31	129.41	130.56	0.89
32	129.41	130.19	0.60
33	129.41	130.60	0.92
34	129.41	130.71	1.00
35	129.41	131.67	1.75
36	129.41	131.39	1.53
37	129.41	129.14	-0.21
38	129.41	130.03	0.48
39	129.41	130.98	1.21
40	129.41	130.40	0.76
41	129.41	131.13	1.33
42	129.41	131.83	1.87
43	129.41	129.69	0.22
44	129.41	129.72	0.24
45	129.41	130.60	0.92
46	129.41	130.48	0.83
47	129.41	130.87	1.13
48	129.41	131.32	1.48
49	129.41	128.53	-0.68
50	129.41	128.78	-0.49
51	129.41	129.60	0.14
52	129.41	130.24	0.64
53	129.41	130.74	1.03
54	129.41	130.60	0.92

APPENDIX F

MARKER POSITIONS FOR LOWER EXTREMITY ANALYSIS USING VISUAL3D (C-motion, Inc.)

The marker placement used for lower limb assessments is shown in Figure 1. An explanation of the position and role for each marker is listed below.

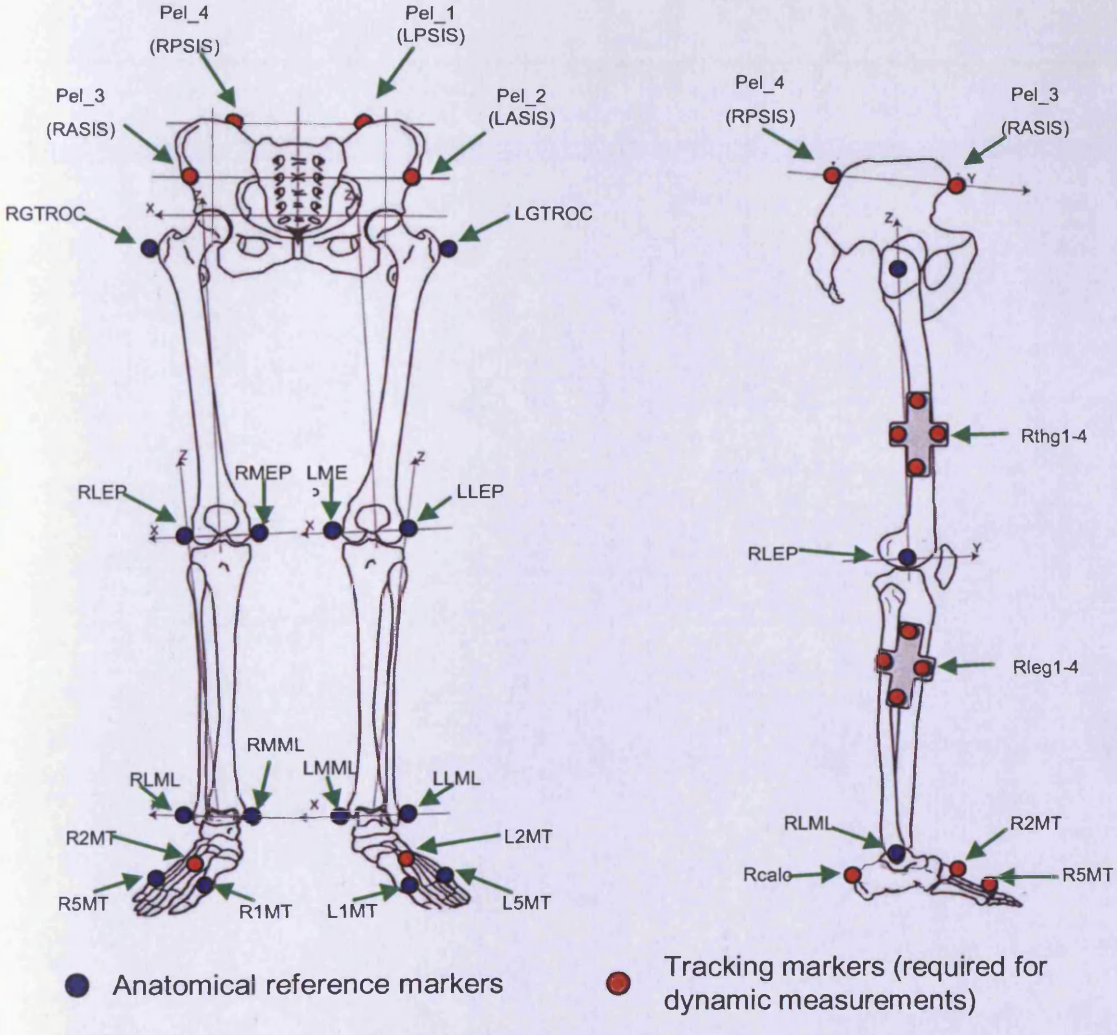

Figure 1 Marker positions for lower limb motion analysis assessment using Visual3D (C-motion, Inc).

Rcalc & Lcalc

These markers are used to track the foot. Markers are positioned centrally on the subjects heal. If they are placed too close to the floor, they will get obstructed during heal strike.

R1MT & L1MT

These markers are positioned on the medial aspect of the 1st metatarsal head. These are tracking markers and the medial distal reference points for the feet.

R 5MT & L5MT

These markers are positioned on the lateral aspect of the 5th metatarsal head. These are tracking markers and the lateral distal reference points for the feet.

R 2MT & L2MT

These are tracking markers positioned on the 2nd metatarsal in the centre of the foot.

Pel_1 & Pel_4 – PSIS markers

These are tracking markers for the pelvis and are positioned on the right and left posterior superior iliac spine (PSIS). The PSIS are located directly underneath the dimples just above the buttocks. If you put your hands on your hips you will be able to feel your PSIS with your thumbs.

Pel_2 & Pel_3 – ASIS markers

These are tracking markers for the pelvis and are positioned on the left and right anterior superior iliac spine (ASIS). To find these landmarks follow the iliac crest anteriorly to until you reach the end of the crest.

R&L GTROC

These are the reference markers for the pelvis and proximal lateral reference point for the thighs. They are also reference points from which the hip joint centres are determined.

The markers are positioned on the upper boarder of the greater trochanter of the femur. The trochanter is more prominent with hip flexion and adduction. The subject

is asked to tilt their trunk laterally towards the hip. Palpate the thigh until you reach the upper boarder of the greater trochanter. The posterior edge is relatively uncovered by muscle tissue. The subject is asked to stand in a neutral position before applying the marker.

RMEP & LMEP- medial epicondyles

This is the medial distal reference point for the thigh and the medial reference point for the shank. The markers are positioned on the medial epicondyle plateau. This is located by palpating from the base of the knee cap and around the top edge of the tibia. The subject is asked to bend their knee. As they do this, a gap between the condyles can be felt. The marker is positioned here.

R LEP & LLEP- lateral epicondyles

This is the lateral distal reference point for the thigh and the lateral proximal reference point for the shank. The marker is positioned on the lateral epicondyle plateau.

MML&LML

These are markers positioned on the medial and lateral malleolus respectively. They are used as distal reference points for the shank and proximal reference points for the foot.

Rthg1-4 & Lthg 1-4

These form a rigid cluster of markers secured laterally to each thigh to track their movement.

Rleg1-4 & Lleg 1-4

These form a rigid cluster of markers secured laterally to each shank to track their movement.

APPENDIX G

PC selection for Chapter 7

This appendix outlines the selection process of PCs for inputs to the DS classifier in section 7.7. It also provides graphs illustrating the variability of the waveforms for the LA, PA and NP cohorts.

Flexion-Extension rotation (FER) results

One hundred PCs were produced relating to the FER waveform. The PCs and their associated eigenvalues are depicted below in Figure 1.

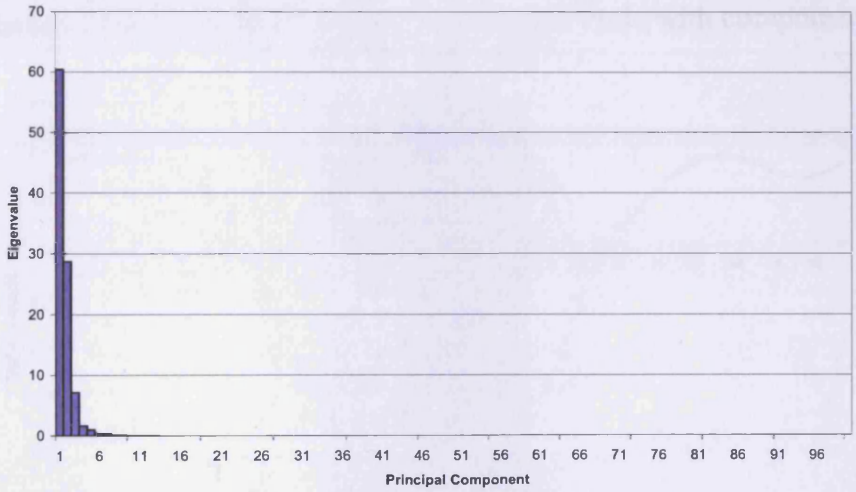

Figure 1 The eigenvalues of the 100 PCs for the FER waveform

The first 4 PCs explain most of the variation in the original data. After the first few PCs the values of the associated eigenvalues rapidly approach zero. Using Kaiser's rule, four PCs were retained. The eigenvalues of these four PCs are recorded in Table 1.

Table 1 Eigenvalues of the four Flexion-Extension Rotation Principal Components (FERPCs) retained using Kaiser's rule

Flexion-Extension Rotation Principal Component	Eigenvalue
FERPC1	60.430
FERPC2	28.681
FERPC3	7.166
FERPC4	1.639

These four PC's account for a combined variance of 87.92%. The four PCs are interpreted by identifying the portions of the cycle with component loadings of 0.71 and above, following Comrey, (1973).

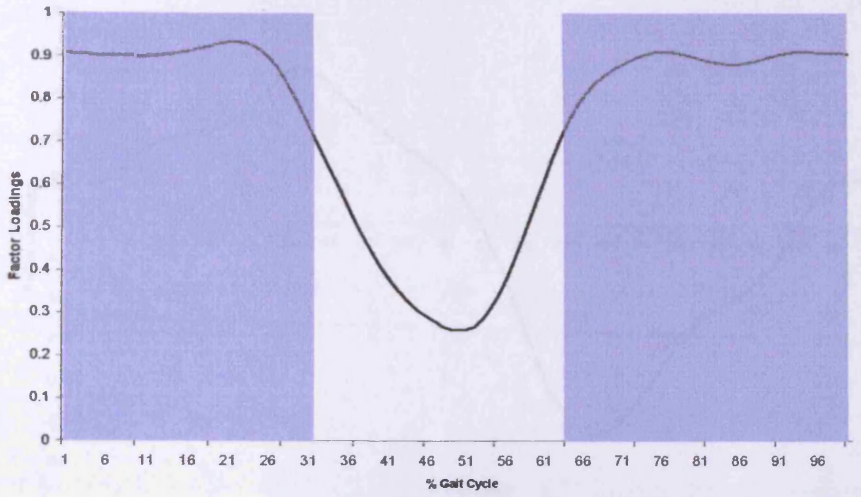

Figure 2 The component loadings of the first PC for the FER waveform (FERPC1). The blue shaded areas indicate the portions of the gait cycle with component loadings of 0.71 or greater.

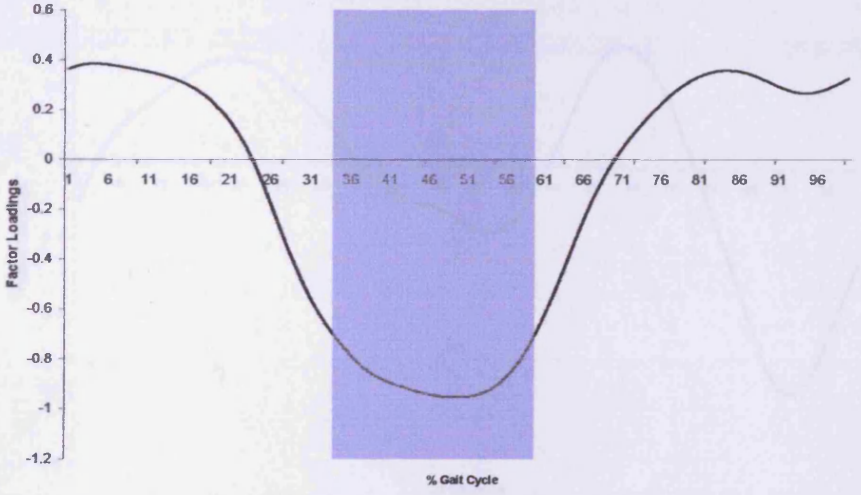

Figure 3 The component loadings of the second PC for the FER waveform (FERPC2). The blue shaded area indicates the portion of the gait cycle with component loadings of 0.71 or greater.

In Figure 2 there are two periods within the gait cycle where the component loadings are 0.71 or above. The first period occurs from 0% to 31 % of the gait cycle and the second is from 64% to 100 %. Thus FERPC1 represents FER from initial contact to early terminal stance and from initial swing until the end of the cycle.

In Figure 3, a single period is highlighted from 34% to 59% of the gait cycle where the component loading is 0.71 or greater. Thus FERPC2 represents the period from early terminal stance to late pre-swing.

The component loadings of the remaining 2 PCs are non-interpretable since no individual portion of the gait cycle had loadings equal to or above the required threshold. The first two PCs account for a combined variance of 89.11%.

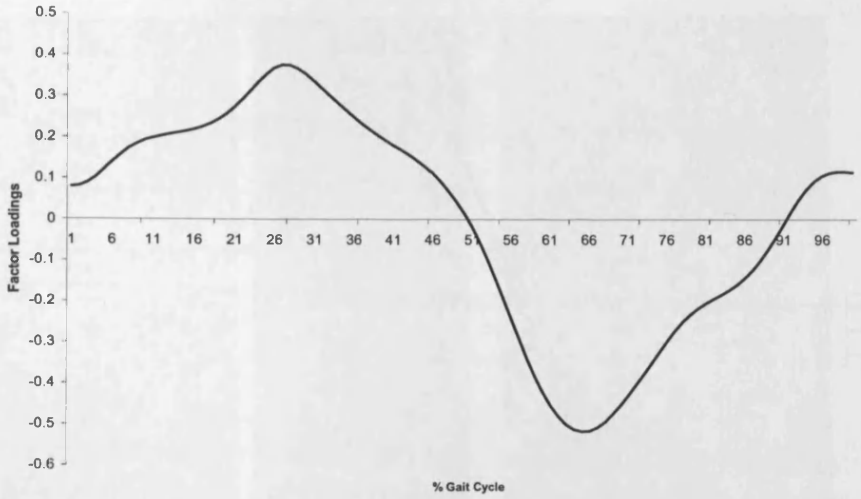

Figure 4 The component loadings of the third PC for the FER waveform (FERPC3). No portion of the gait cycle has component loadings of 0.71 or greater.

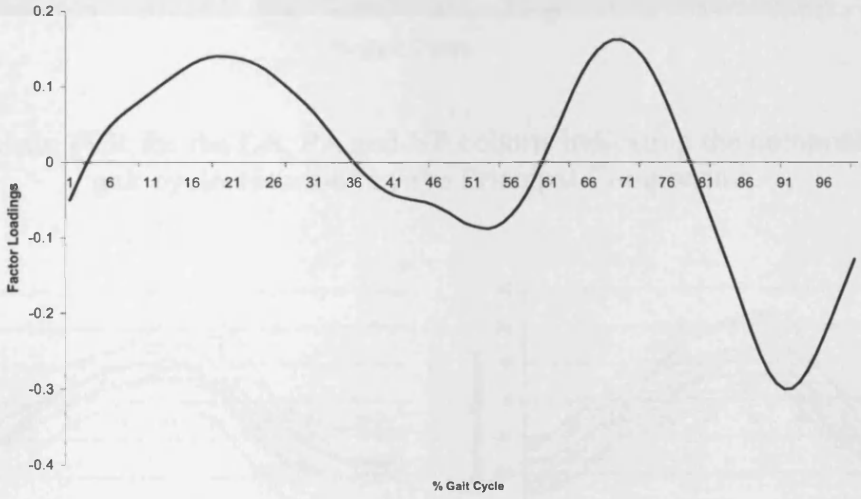

Figure 5 The component loadings of the fourth PC for the FER waveform (FERPC4). No portion of the gait cycle has component loadings of 0.71 or greater.

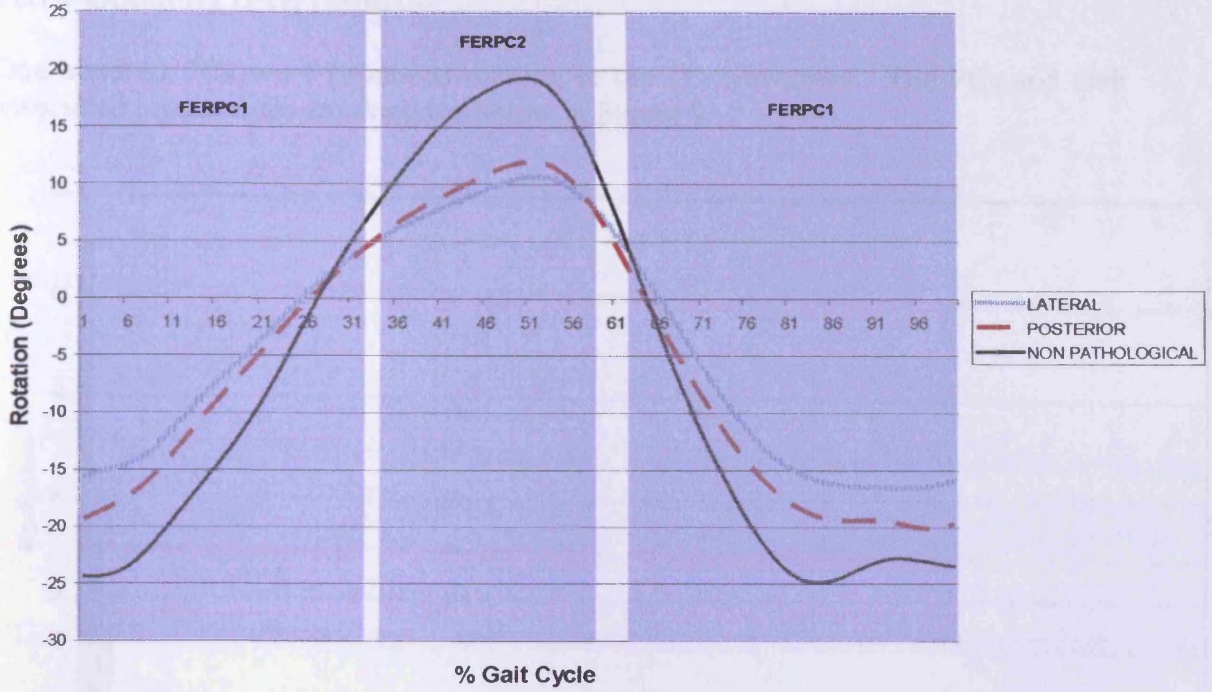

Figure 6 Mean FER for the LA, PA and NP cohorts indicating the components of the gait cycle described by the Principal Components.

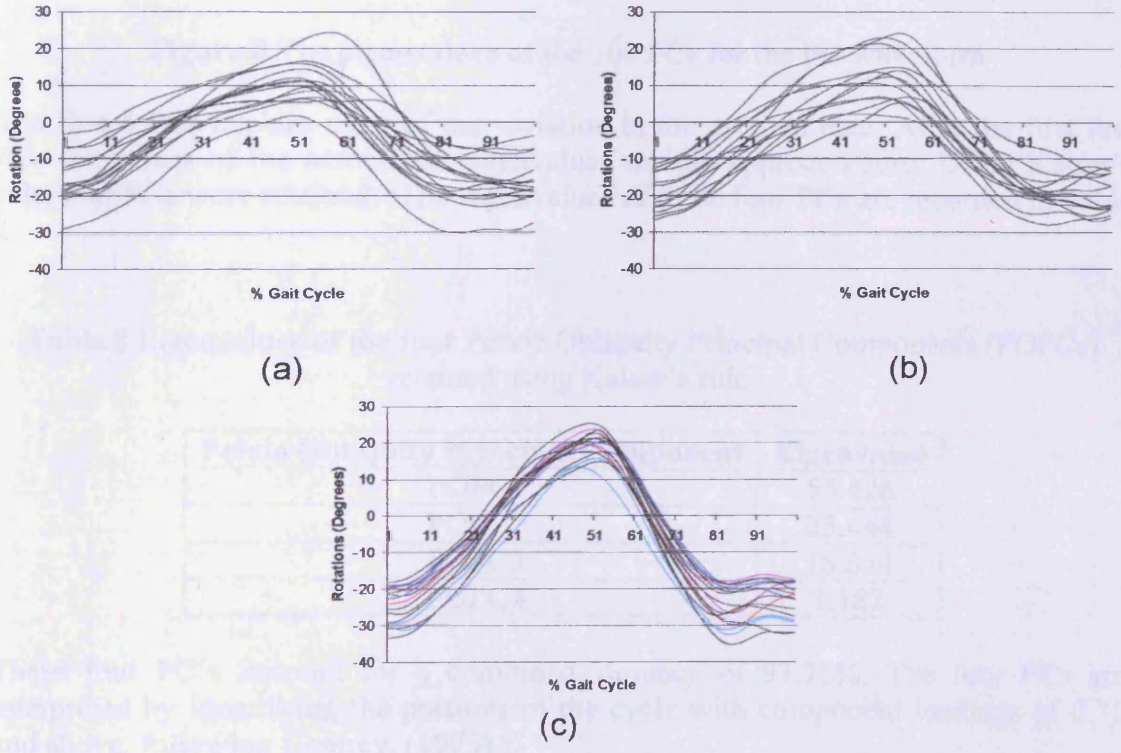

Figure 7 Variation between subjects in the (a) LA (b) PA (c) NP cohorts.

Pelvic Obliquity (PO) results

One hundred PCs were produced relating to the PO waveform. The PCs and their associated eigenvalues are depicted below in Figure 8.

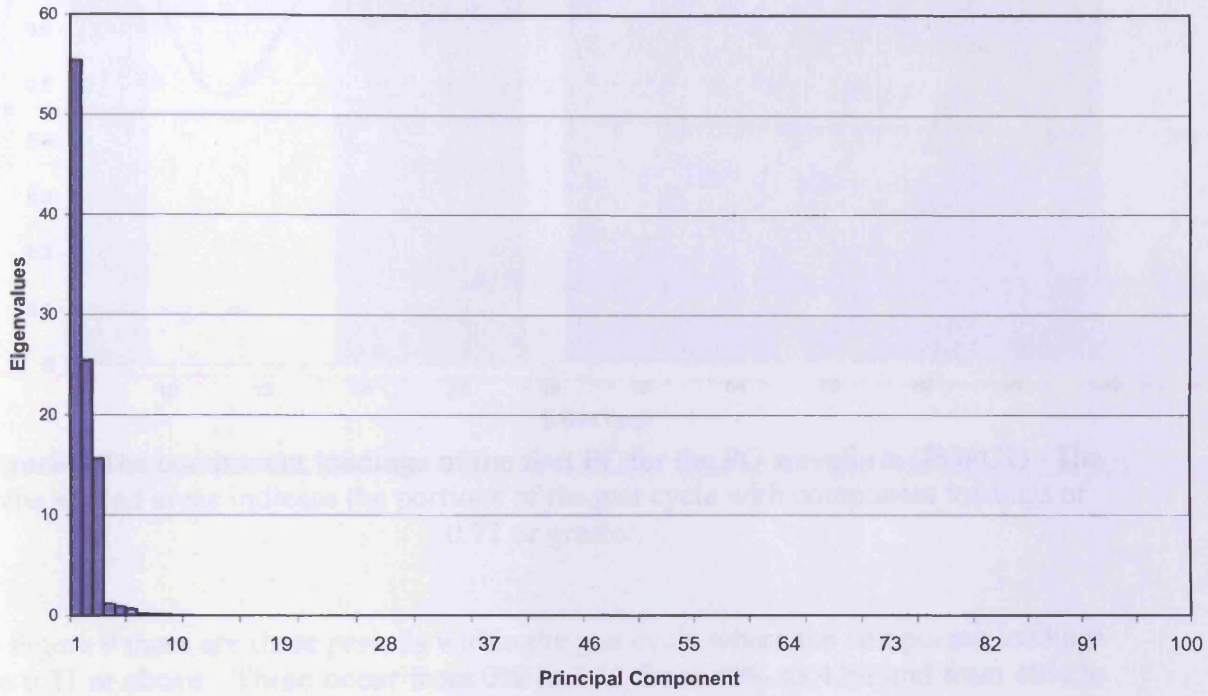

Figure 8 The eigenvalues of the 100 PCs for the PO waveform

The first 4 PCs explain most of the variation in the original data. After the first few PCs the values of the associated eigenvalues rapidly approach zero. Using Kaiser's rule, four PCs were retained. The eigenvalues of these four PCs are recorded in Table 2.

Table 2 Eigenvalues of the four Pelvic Obliquity Principal Components (POPCs) retained using Kaiser's rule

Pelvic Obliquity Principal Component	Eigenvalue
POPC1	55.426
POPC2	25.444
POPC3	15.654
POPC4	1.182

These four PC's account for a combined variance of 97.71%. The four PCs are interpreted by identifying the portions of the cycle with component loadings of 0.71 and above, following Comrey, (1973).

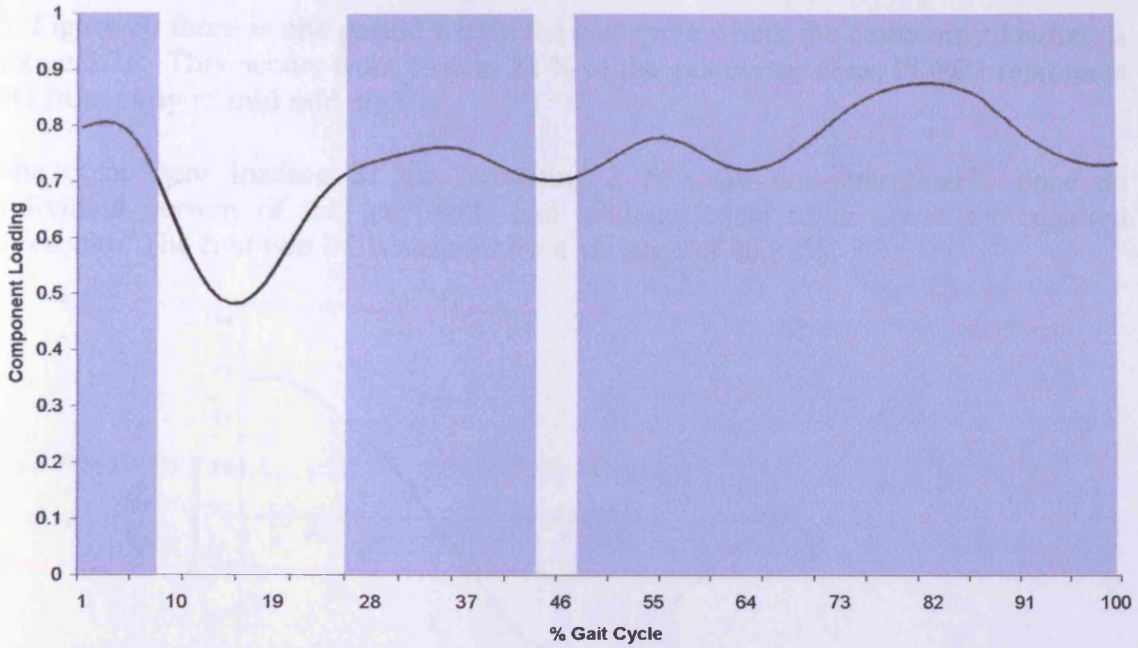

Figure 9 The component loadings of the first PC for the PO waveform (POPC1). The blue shaded areas indicate the portions of the gait cycle with component loadings of 0.71 or greater.

In Figure 9 there are three periods within the gait cycle where the component loadings are 0.71 or above. These occur from 0% to 7 %, from 26% to 42% and from 48% to 100% of the gait cycle. Thus, POPC1 represents PO during early loading response, from the mid portion of mid-stance to terminal stance and from the end of terminal stance to the end of the gait cycle.

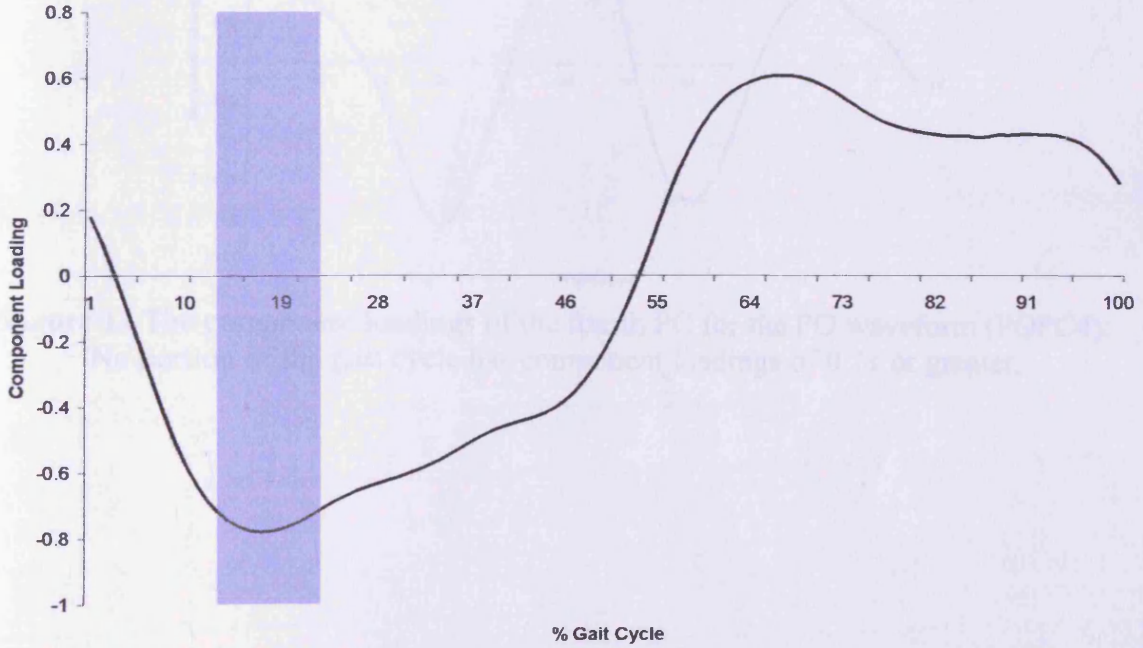

Figure 10 The component loadings of the second PC for the PO waveform (POPC2). The blue shaded area indicates the portion of the gait cycle with component loadings of 0.71 or greater.

In Figure 10 there is one period within the gait cycle where the component loading is above 0.71. This occurs from 13% to 22 % of the gait cycle. Thus, POPC2 represents PO from early to mid mid-stance.

The component loading of the remaining 2 PCs are non-interpretable since no individual portion of the gait cycle had loadings equal to or above the required threshold. The first two PC's account for a variance of 80.87%.

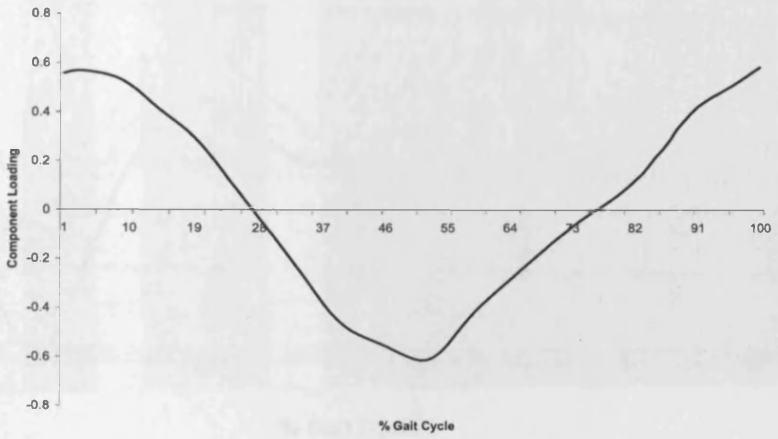

Figure 11 The component loadings of the third PC for the PO waveform (POPC3). No portion of the gait cycle has component loadings of 0.71 or greater.

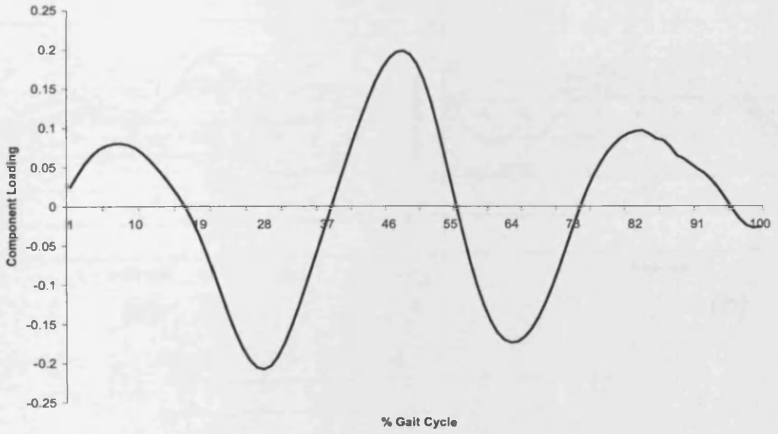

Figure 12 The component loadings of the fourth PC for the PO waveform (POPC4). No portion of the gait cycle has component loadings of 0.71 or greater.

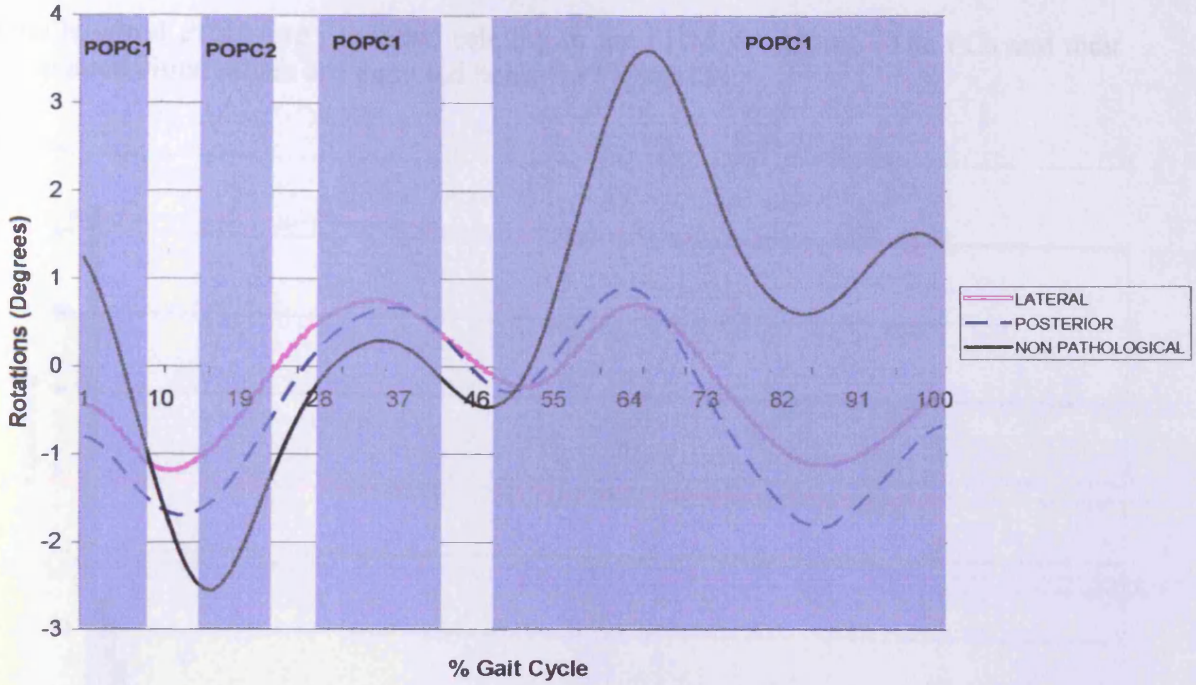

Figure 13 Mean PO for three cohorts indicating the components of the gait cycle described by the Principle Components.

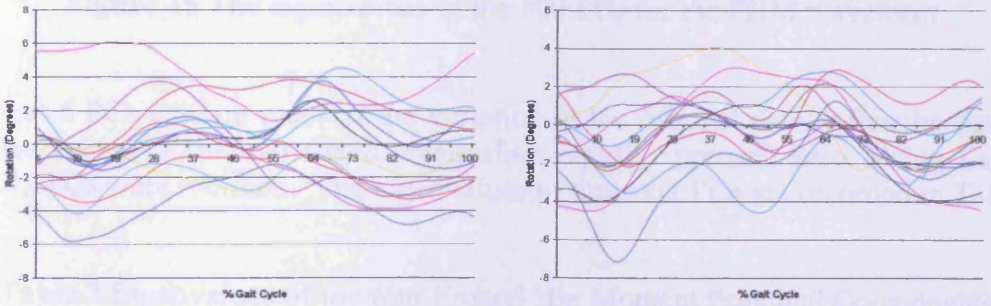

(a) (b)

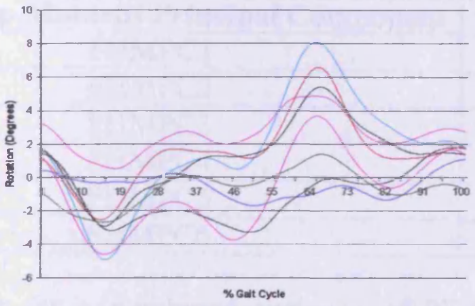

(c)

Figure 14 Variation between subjects in the (a) LA (b) PA and (c) NP cohorts.

Frontal Hip Moment (FHM) Results

One hundred PCs were produced relating to the FHM waveform. The PCs and their associated eigenvalues are depicted below in Figure 15.

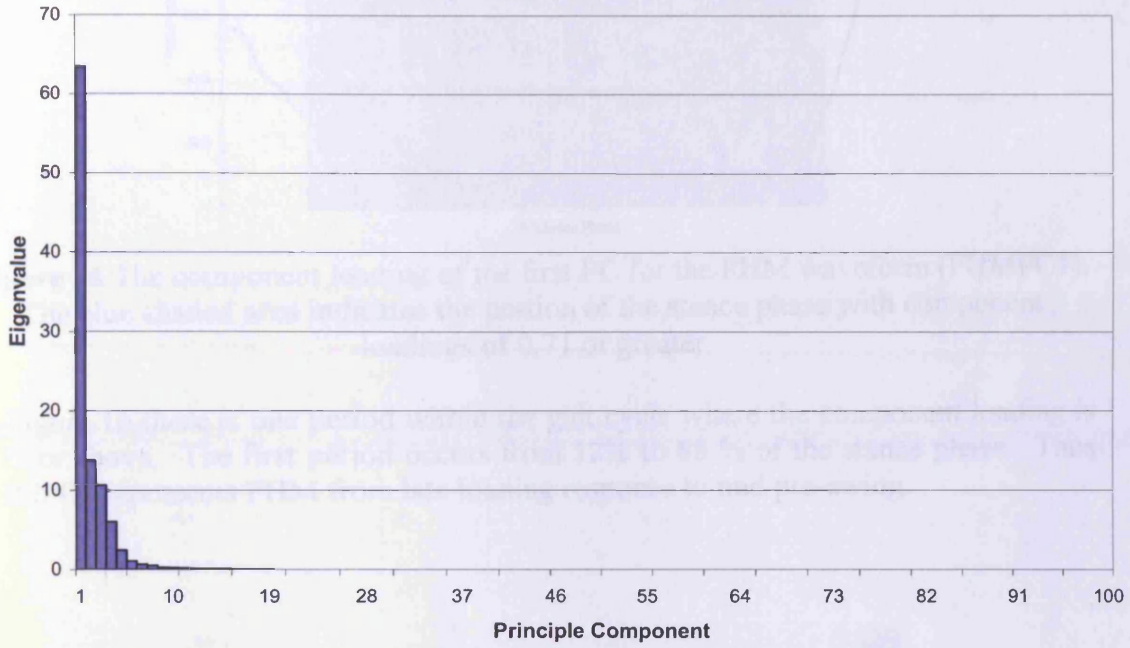

Figure 15 The eigenvalues of the 100 PCs for the FHM waveform

The first 6 PCs explain most of the variation in the original data. After the first few PCs the values of the associated eigenvalues rapidly approach zero. Using Kaiser's rule, six PCs were retained. The eigenvalues of these six PCs are recorded in Table 3.

Table 3 Eigenvalues of the four Frontal Hip Moment Principal Components (FHMPCs) retained using Kaiser's rule

Frontal Hip Moment Principal Component	Eigenvalue
FHMPC1	63.470
FHMPC2	13.772
FHMPC3	10.609
FHMPC4	6.003
FHMPC5	2.464
FHMPC6	1.044

These six PC's account for a combined variance of 97.36%. The six PCs are interpreted by identifying the portions of the cycle with component loadings of 0.71 and above, following Comrey, (1973).

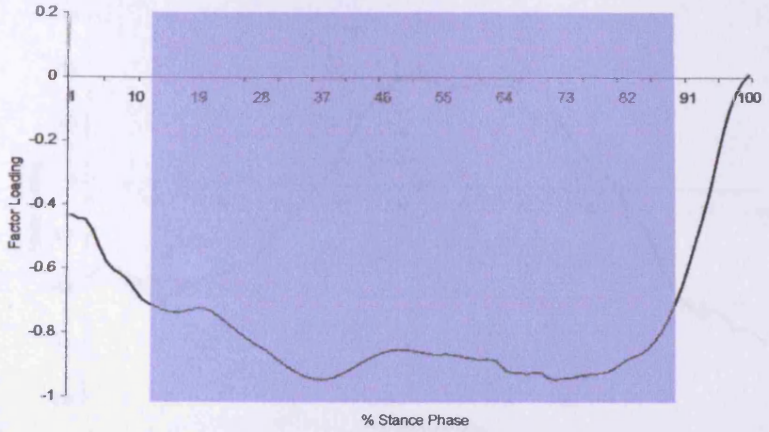

Figure 16 The component loading of the first PC for the FHM waveform (FHMPC1). The blue shaded area indicates the portion of the stance phase with component loadings of 0.71 or greater.

In Figure 16 there is one period within the gait cycle where the component loading is 0.71 or above. The first period occurs from 12% to 88 % of the stance phase. Thus FHMPC1 represents FHM from late loading response to mid pre-swing.

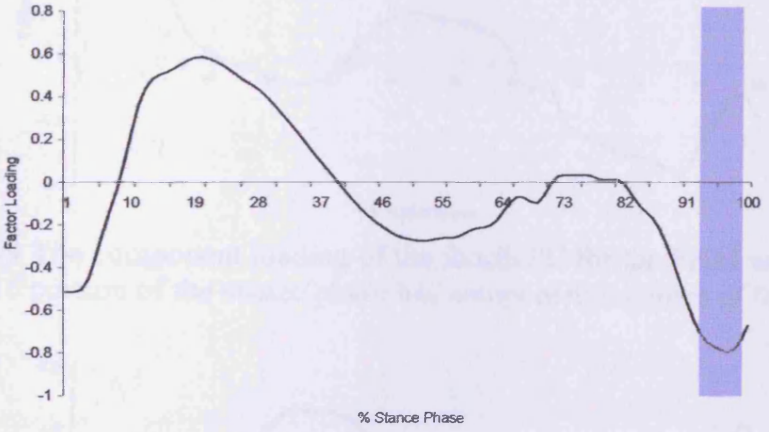

Figure 17 The component loading of the second PC for the FHM waveform (FHMPC2). The blue shaded area indicates the portion of the stance phase with component loadings of 0.71 or greater.

In Figure 17, a single period is highlighted from 94% to 99% of the stance phase where the component loading is 0.71 or greater. Thus FHMPC2 represents the period for late pre-swing phase.

The component loading of the remaining 4 PCs are non-interpretable since no individual portion of the stance phase had loadings equal to or above the required threshold. The first two PCs account for a combined variance of 77.24%.

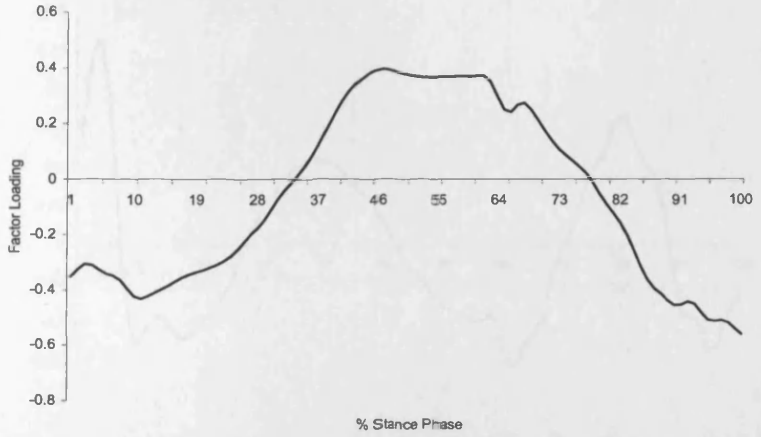

Figure 18 The component loading of the third PC for the FHM waveform (FHMPC3). No portion of the stance phase has component loadings of 0.71 or greater.

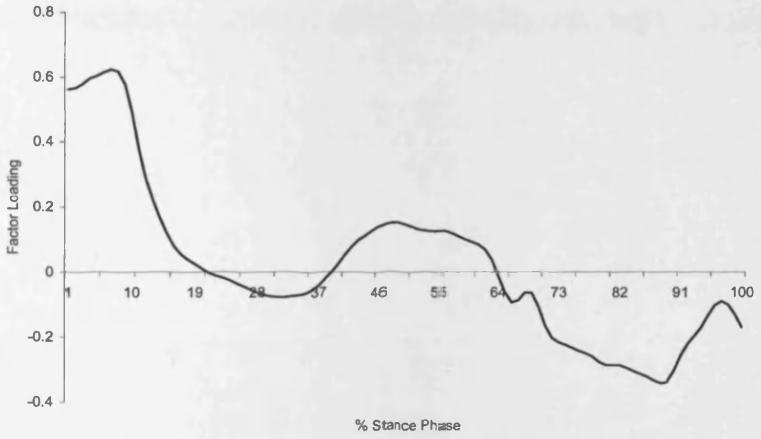

Figure 19 The component loading of the fourth PC for the FHM waveform (FHMPC4). No portion of the stance phase has component loadings of 0.71 or greater.

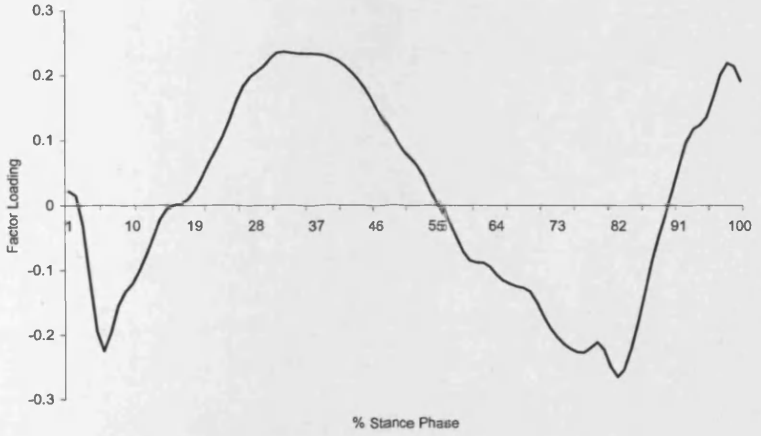

Figure 20 The component loading of the fifth PC for the FHM waveform (FHMPC5). No portion of the stance phase has component loadings of 0.71 or greater.

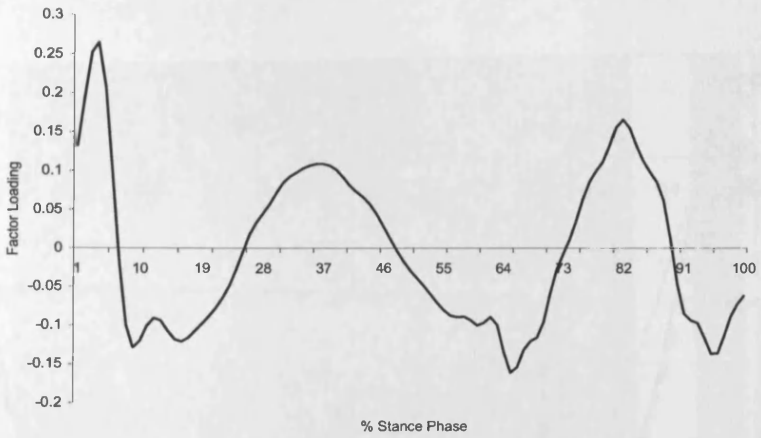

Figure 21 The component loading of the sixth PC for the FHM waveform (FHMPC6). No portion of the stance phase has component loadings of 0.71 or greater.

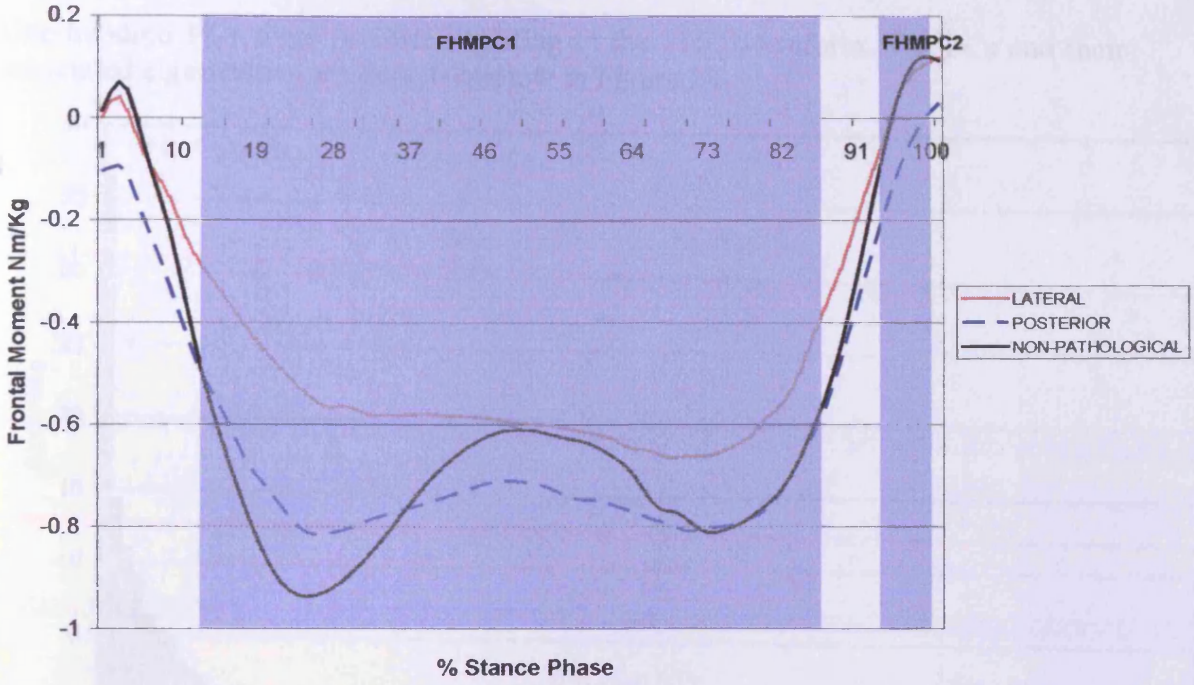

Figure 22 Mean FHM for three cohorts indicating the components of the stance phase described by the Principle Components.

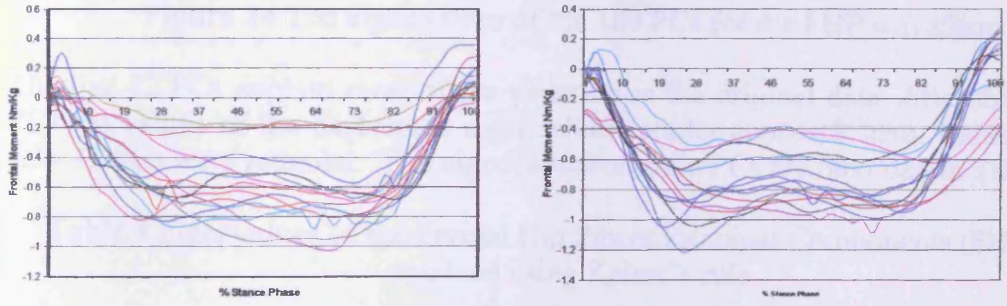

(a)

(b)

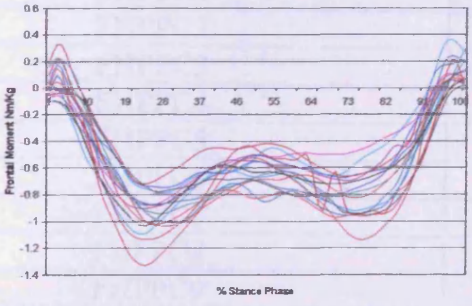

(c)

Figure 23 Variation between subjects in the (a) LA (b) PA and (c) NP cohorts.

Frontal Hip Power (FHP) Results

One hundred PCs were produced relating to the FHP waveform. The PCs and their associated eigenvalues are depicted below in Figure 24.

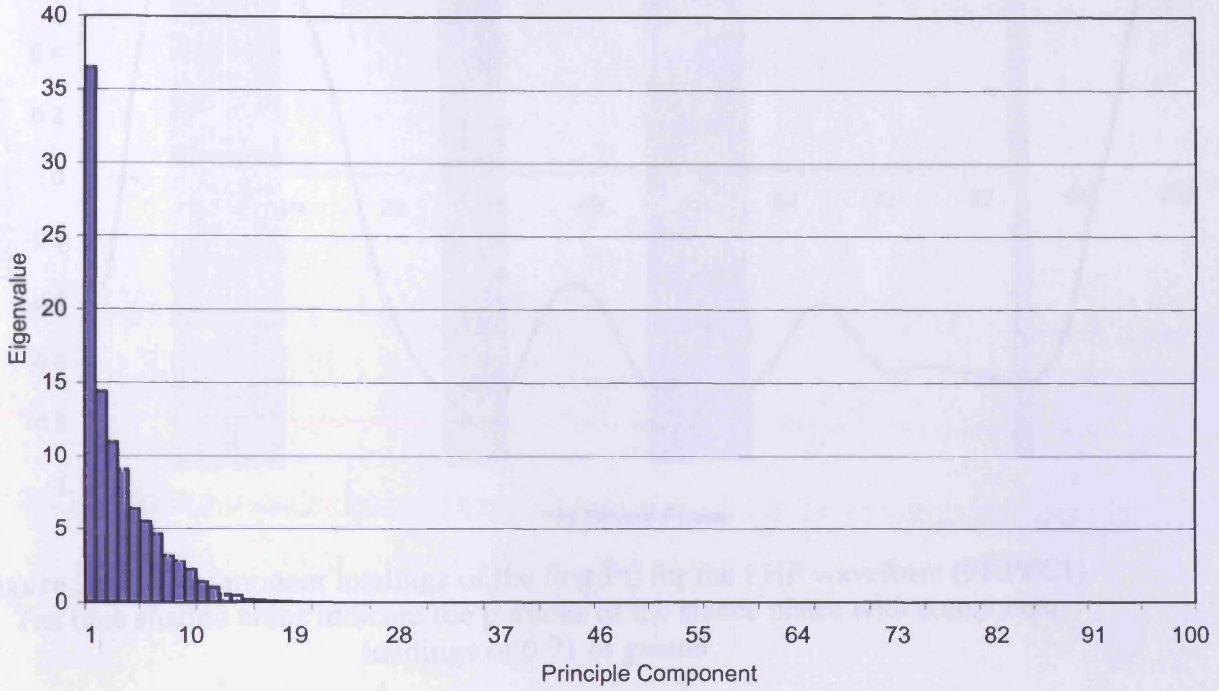

Figure 24 The eigenvalues of the 100 PCs for the FHP waveform

The first 12 PCs explain most of the variation in the original data. After the first few PCs the values of the associated eigenvalues rapidly approach zero. Using Kaiser's rule, 12 PCs were retained. The eigenvalues of these PCs are recorded in Table 4.

Table 4 Eigenvalues of the Frontal Hip Power Principal Components (FHPPCs) retained using Kaiser's rule

Frontal Hip Power Principal Component	Eigenvalue
FHPPC1	36.515
FHPPC2	14.403
FHPPC3	10.941
FHPPC4	9.046
FHPPC5	6.405
FHPPC6	5.507
FHPPC7	4.667
FHPPC8	3.216
FHPPC9	2.822
FHPPC10	2.251
FHPPC11	1.407
FHPPC12	1.0294

These PC's account for a combined variance of 98.21%. The PCs are interpreted by identifying the portions of the cycle with component loadings of 0.71 and above, following Comrey, (1973).

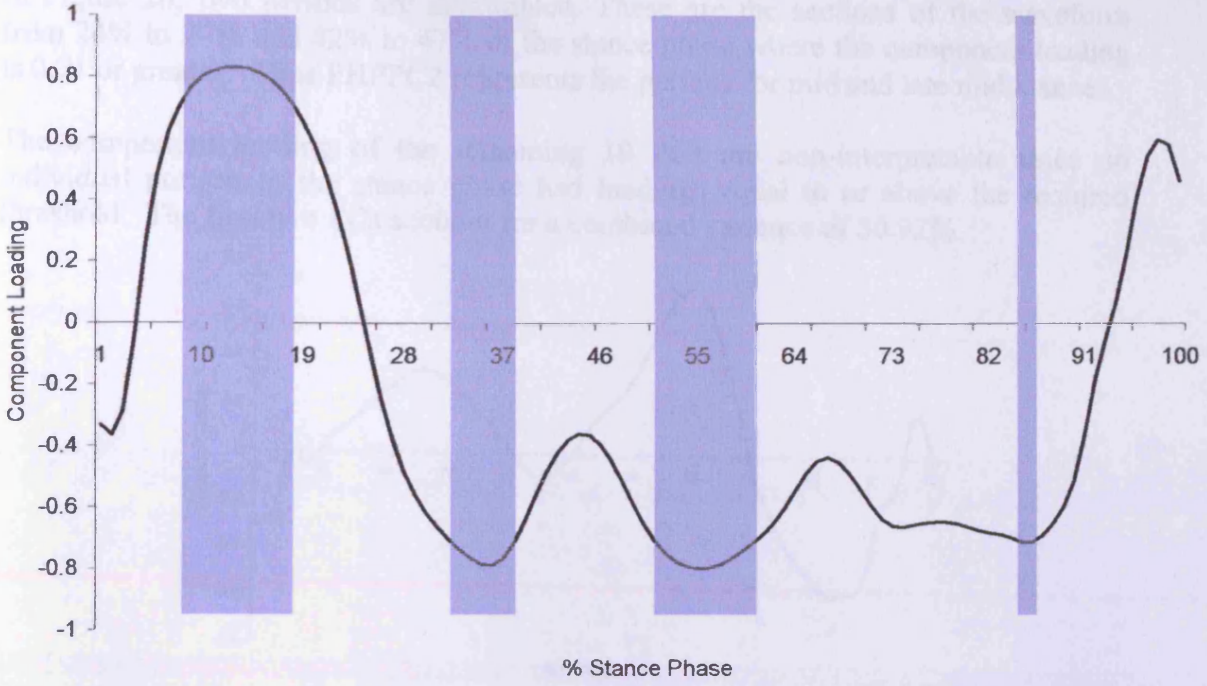

Figure 25 The component loadings of the first PC for the FHP waveform (FHPPC1). The blue shaded areas indicate the portions of the stance phase with component loadings of 0.71 or greater.

In Figure 25 four periods are highlighted, from 9% to18%, 33% to 38%, 52% to 60% and 85% to 86% of the stance phase where the component loading is 0.71 or greater. Thus FHPPC1 represents the periods for mid to early mid stance, mid to late mid stance, mid to late terminal stance and early to mid pre-swing.

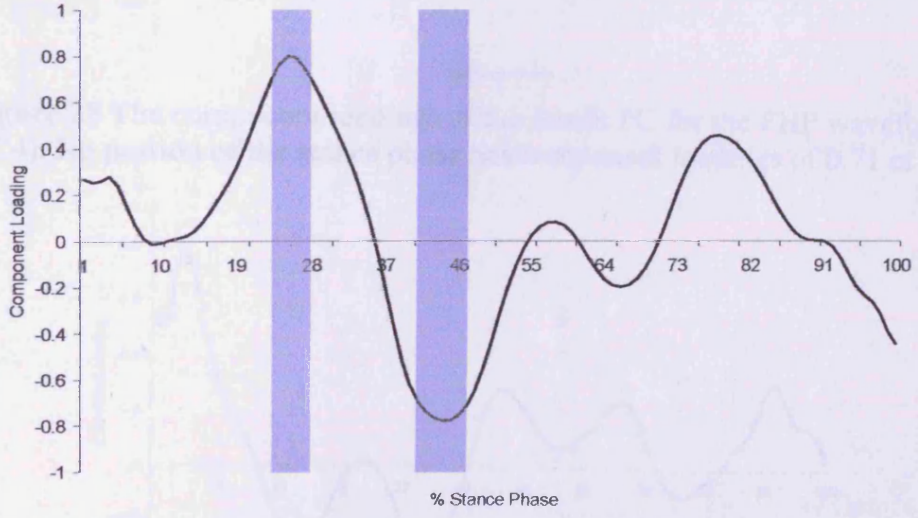

Figure 26 The component loadings of the first PC for the FHP waveform (FHPPC1). The blue shaded areas indicate the portions of the stance phase with component loadings of 0.71 or greater.

In Figure 26, two periods are highlighted. These are the sections of the waveform from 24% to 27% and 42% to 47% of the stance phase where the component loading is 0.71 or greater. Thus FHPPC2 represents the periods for mid and late mid-stance.

The component loading of the remaining 10 PCs are non-interpretable since no individual portion of the stance phase had loadings equal to or above the required threshold. The first two PCs account for a combined variance of 50.92%.

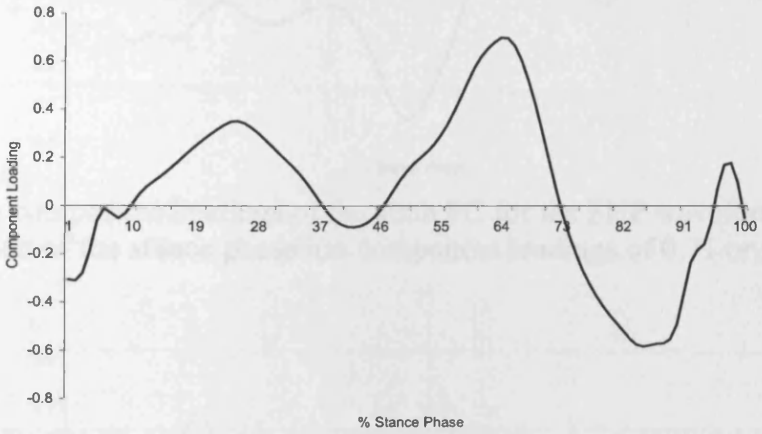

Figure 27 The component loadings of the third PC for the FHP waveform (FHPPC3). No portion of the stance phase has component loadings of 0.71 or greater.

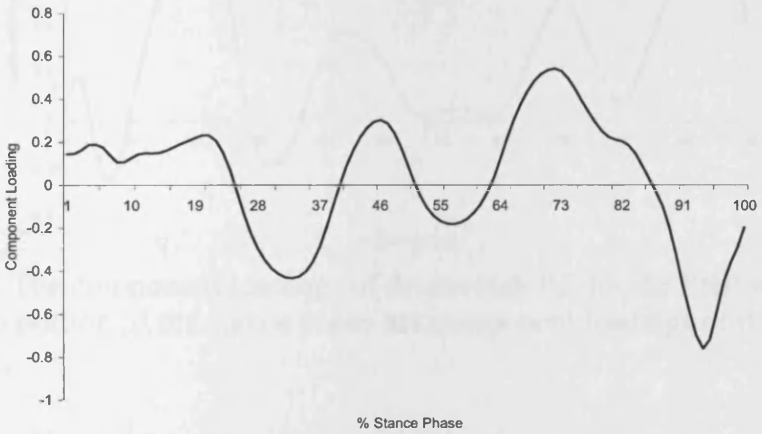

Figure 28 The component loadings of the fourth PC for the FHP waveform (FHPPC4). No portion of the stance phase has component loadings of 0.71 or greater.

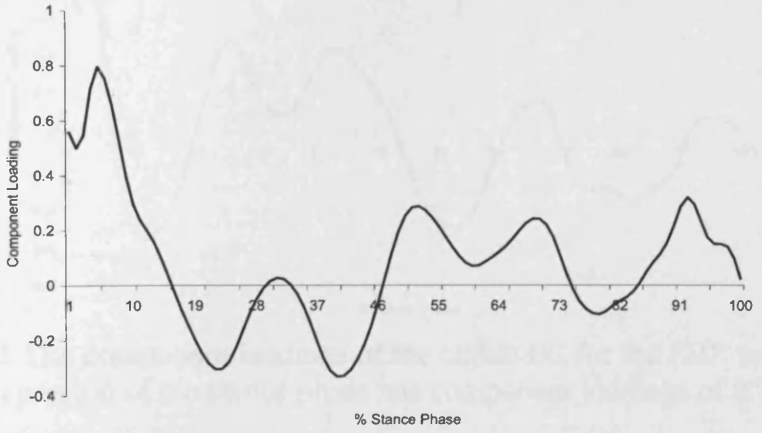

Figure 29 The component loadings of the fifth PC for the FHP waveform (FHPPC5). No portion of the stance phase has component loadings of 0.71 or greater.

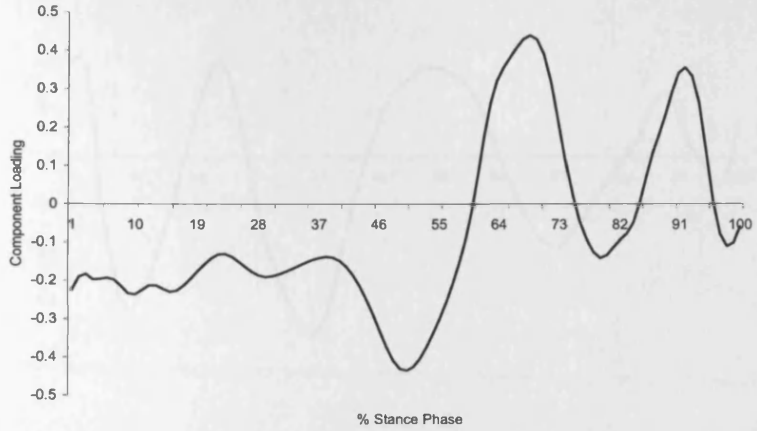

Figure 30 The component loadings of the sixth PC for the FHP waveform (FHPPC6). No portion of the stance phase has component loadings of 0.71 or greater.

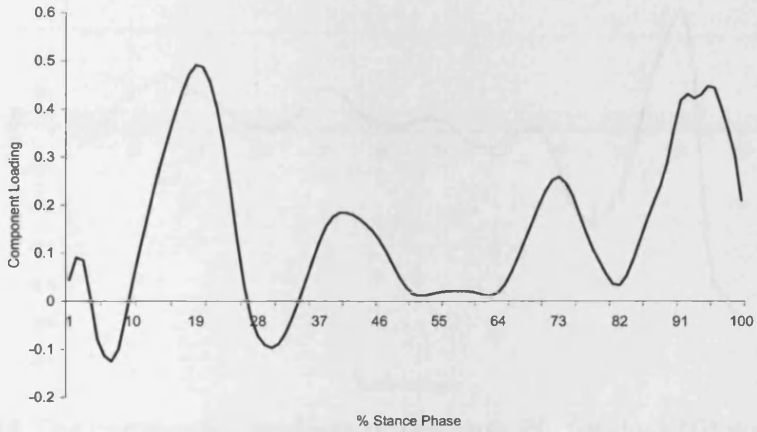

Figure 31 The component loadings of the seventh PC for the FHP waveform (FHPPC7). No portion of the stance phase has component loadings of 0.71 or greater.

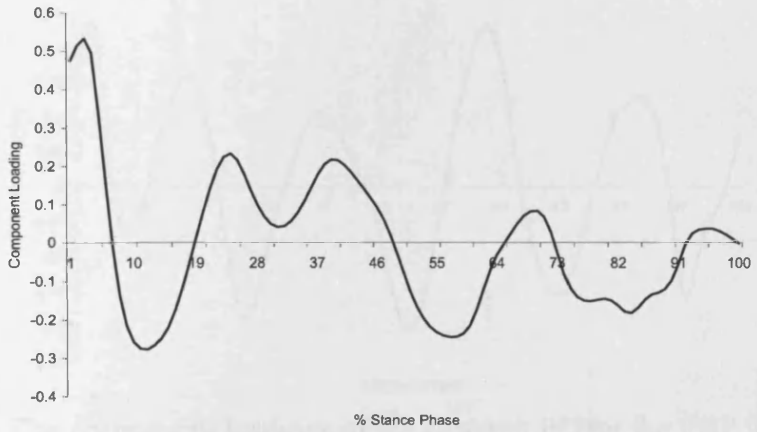

Figure 32 The component loadings of the eighth PC for the FHP waveform (FHPPC8). No portion of the stance phase has component loadings of 0.71 or greater.

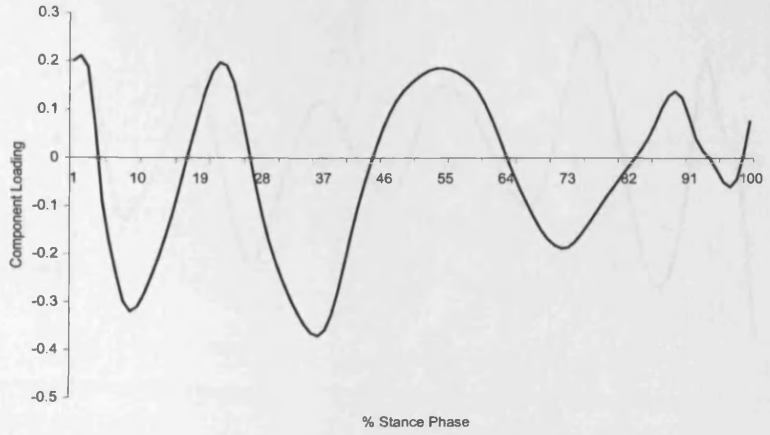

Figure 33 The component loadings of the ninth PC for the FHP waveform (FHPPC9). No portion of the stance phase has component loadings of 0.71 or greater.

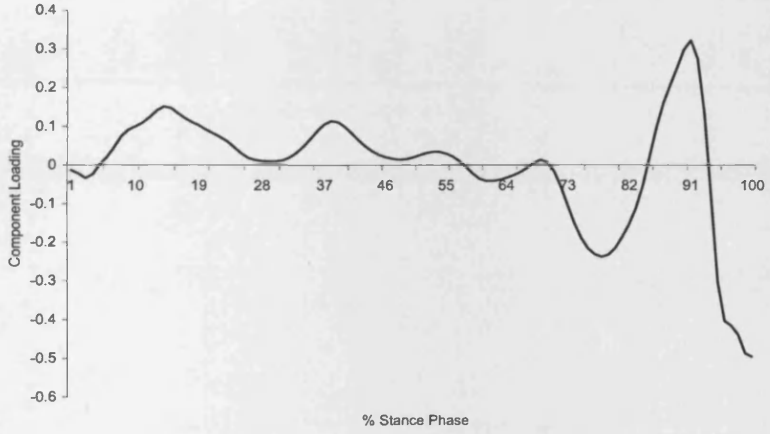

Figure 34 The component loadings of the tenth PC for the FHP waveform (FHPPC10). No portion of the stance phase has component loadings of 0.71 or greater.

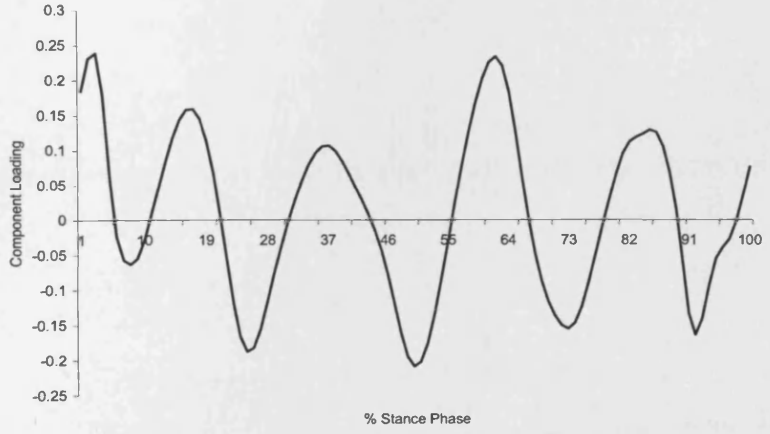

Figure 35 The component loadings of the eleventh PC for the FHP waveform (FHPPC11). No portion of the stance phase has component loadings of 0.71 or greater.

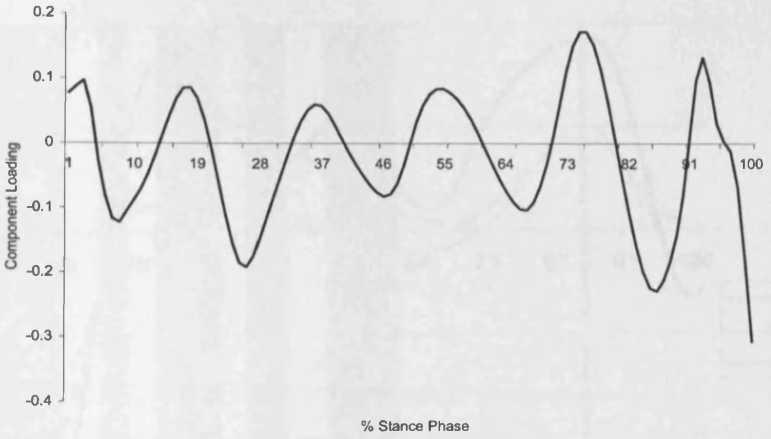

Figure 36 The component loadings of the twelfth PC for the FHP waveform (FHPPC12). No portion of the stance phase has component loadings of 0.71 or greater.

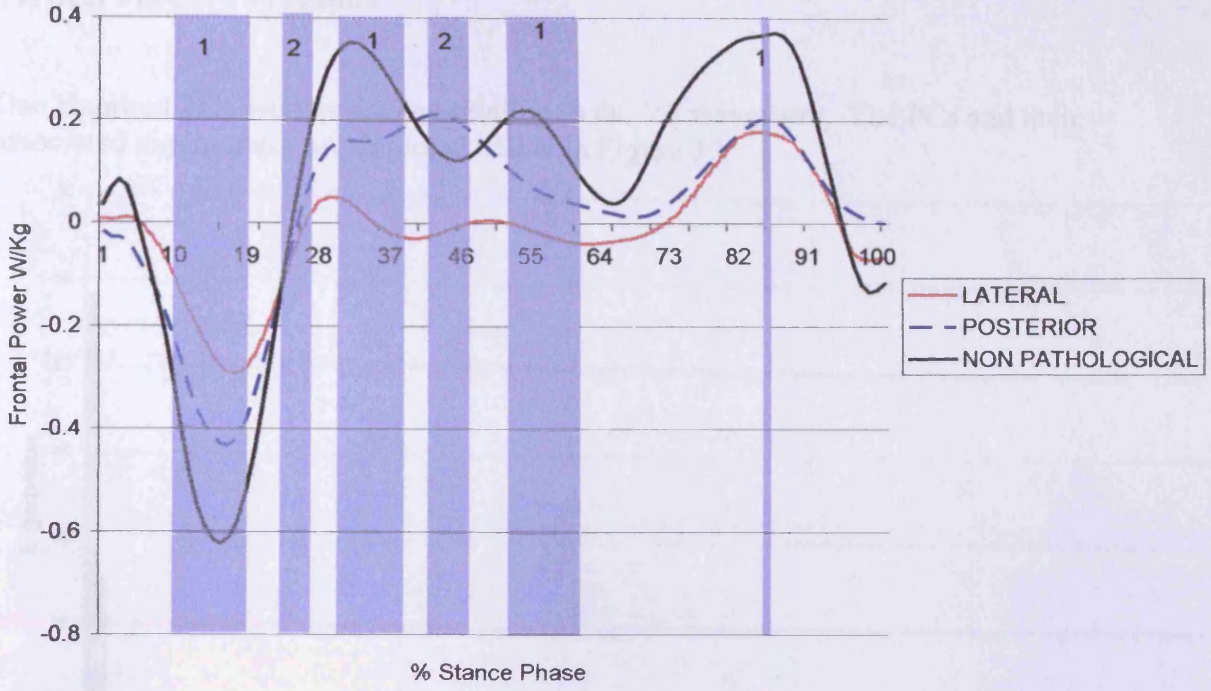

Figure 37 Mean FHP for the LA, PA and NP cohorts indicating the components of the stance phase described by the Principle Components.

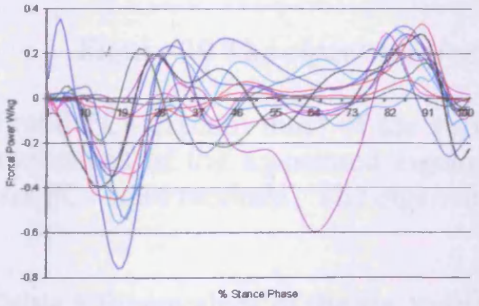

(a)

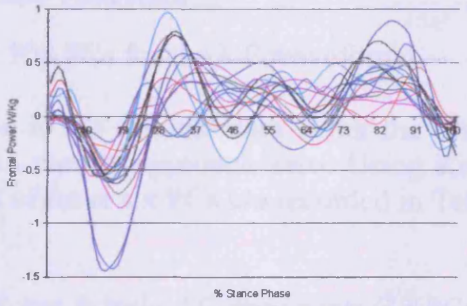

(b)

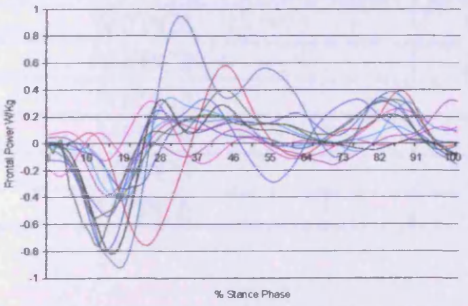

(c)

Figure 38 Variation between subjects in the (a) LA (b) PA and (c) NP cohorts.

Vertical Force (VF) results

One Hundred PCs were produced relating to the VF waveform. The PCs and their associated eigenvalues are depicted below in Figure 39.

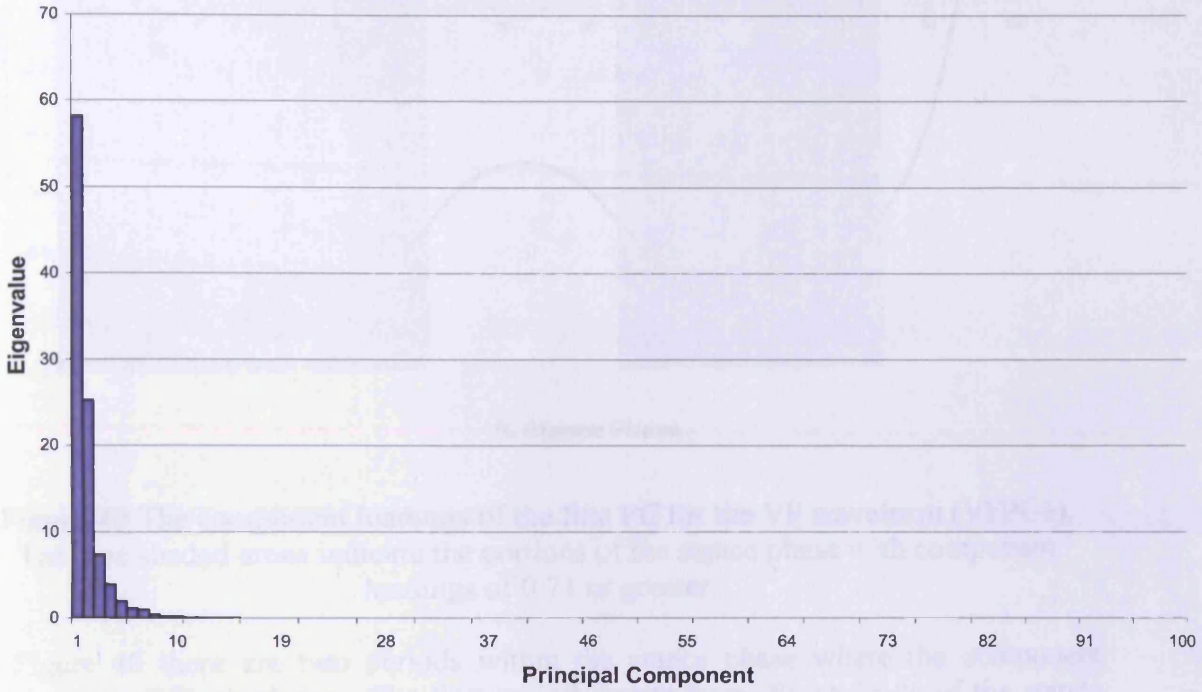

Figure 39 The eigenvalues of the 100 PCs for the VF waveform

The first 6 PCs explain most of the variation in the original data. After the first few PCs the values of the associated eigenvalues rapidly approach zero. Using Kaiser's rule, six PCs were retained. The eigenvalues of these six PCs are recorded in Table 5.

Table 5 Eigenvalues of the six Vertical Force Principal Components (VFPCs) retained using the Kaiser's rule

Vertical Force Principal Component	Eigenvalue
VFPC1	58.222
VFPC2	25.287
VFPC3	7.346
VFPC4	3.922
VFPC5	2.004
VFPC6	1.122

These six PC's account for a combined variance of 97.90%. The PCs are interpreted by identifying the portions of the cycle with component loadings of 0.71 and above, following Comrey, (1973).

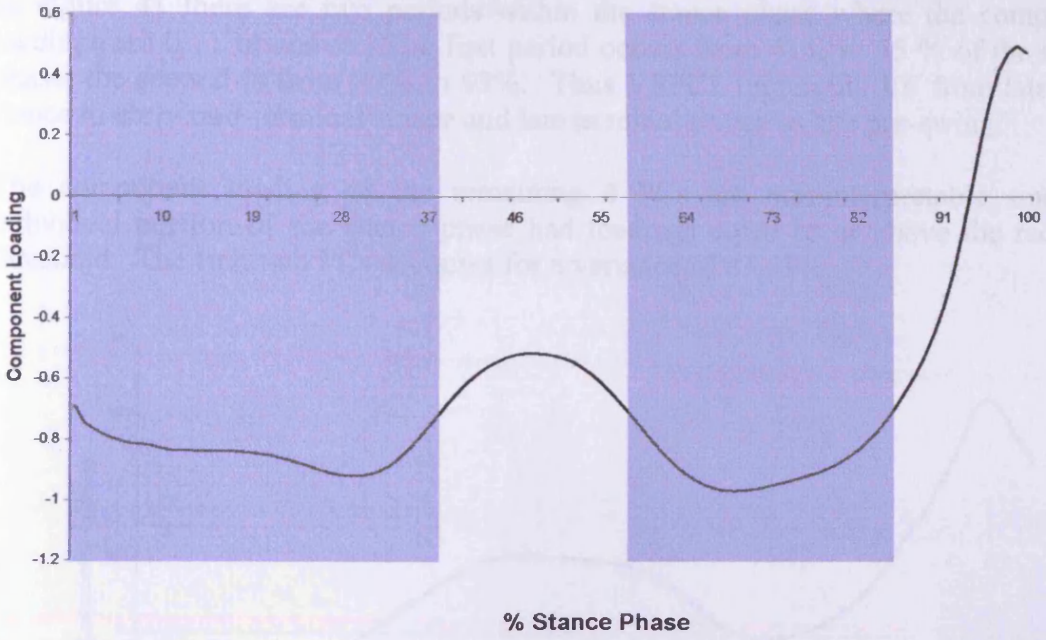

Figure 40 The component loadings of the first PC for the VF waveform (VFPC1). The blue shaded areas indicate the portions of the stance phase with component loadings of 0.71 or greater.

In Figure 40 there are two periods within the stance phase where the component loadings are 0.71 or above. The first period occurs from 2% to 38 % of the stance phase, the second is from 58% to 85%. Thus VFPC1 represents VF from initial contact to mid-stance and mid terminal stance to early pre-swing.

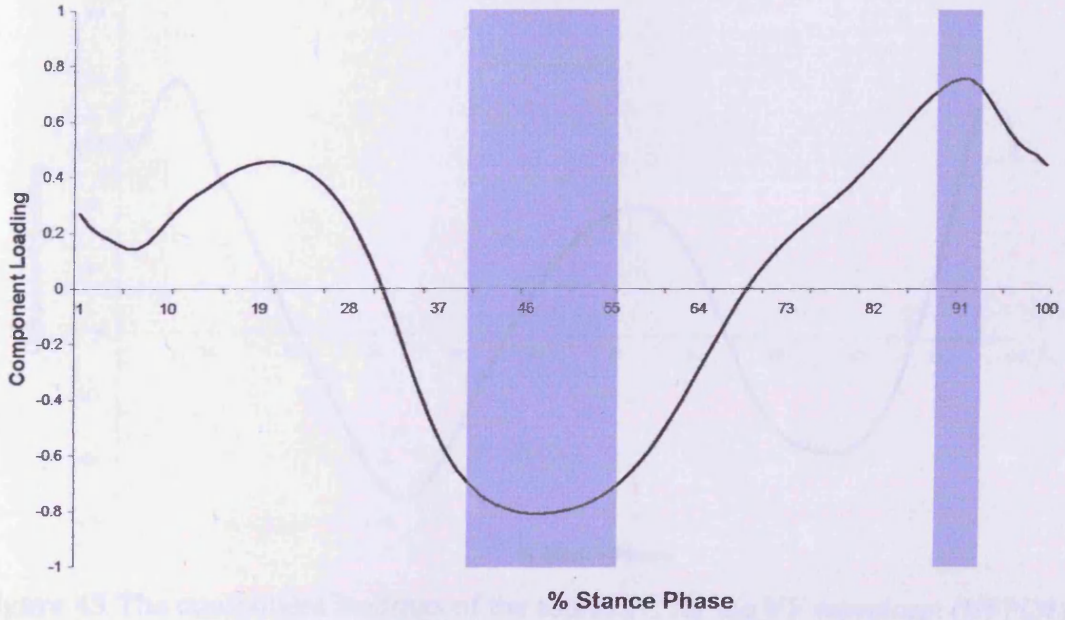

Figure 41 The component loadings of the second PC for the VF waveform (VFPC2). The blue shaded areas indicate the portions of the stance phase with component loadings of 0.71 or greater.

In Figure 41 there are two periods within the stance phase where the component loadings are 0.71 or above. The first period occurs from 41% to 55 % of the stance phase, the second is from 89% to 93%. Thus VFPC2 represents VF from late mid-stance to early mid-terminal stance and late terminal stance to late pre-swing.

The component loading of the remaining 4 PCs are non-interpretable since no individual portion of the stance phase had loadings equal to or above the required threshold. The first two PCs accounts for a variance of 83.51%.

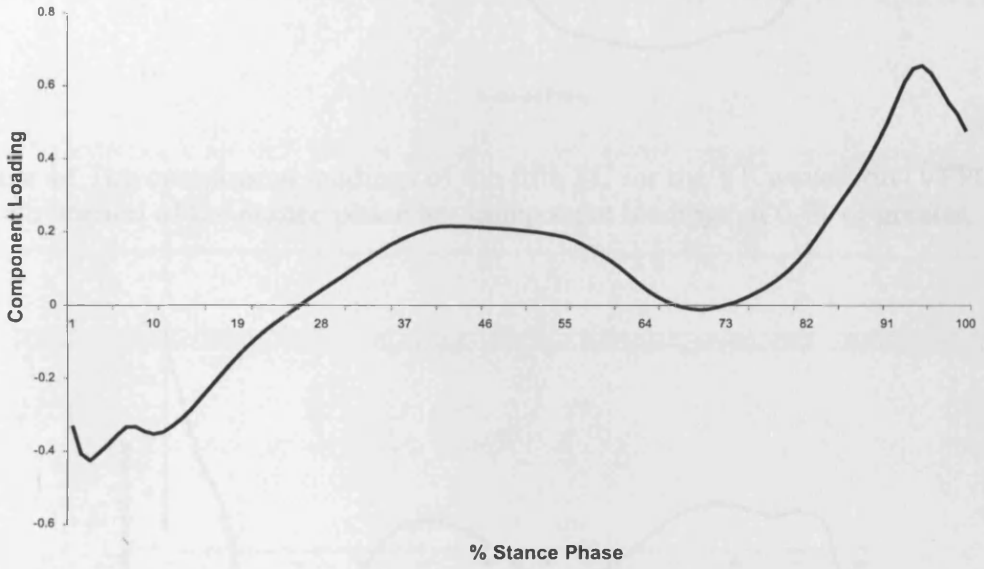

Figure 42 The component loadings of the third PC for the VF waveform (VFPC3). No portion of the stance phase has component loadings of 0.71 or greater.

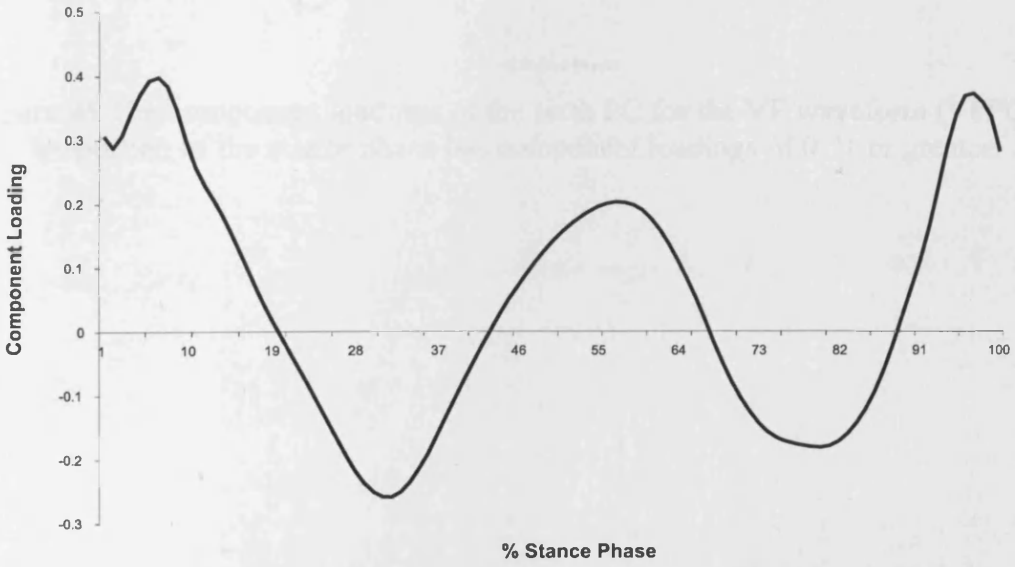

Figure 43 The component loadings of the fourth PC for the VF waveform (VFPC4). No portion of the stance phase has component loadings of 0.71 or greater.

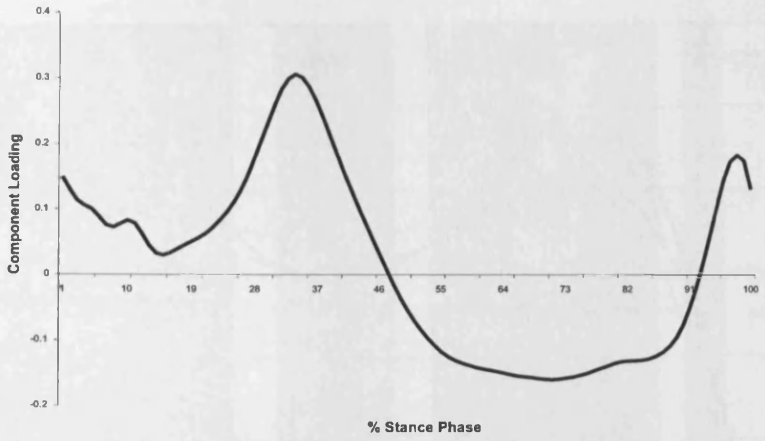

Figure 44 The component loadings of the fifth PC for the VF waveform (VFPC5). No portion of the stance phase has component loadings of 0.71 or greater.

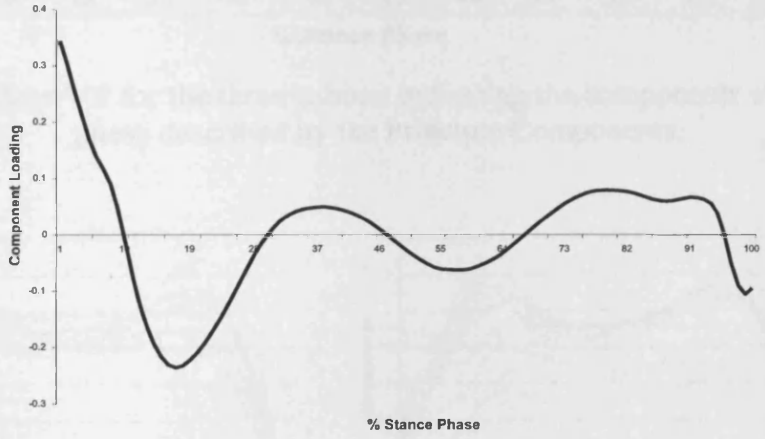

Figure 45 The component loadings of the sixth PC for the VF waveform (VFPC5). No portion of the stance phase has component loadings of 0.71 or greater.

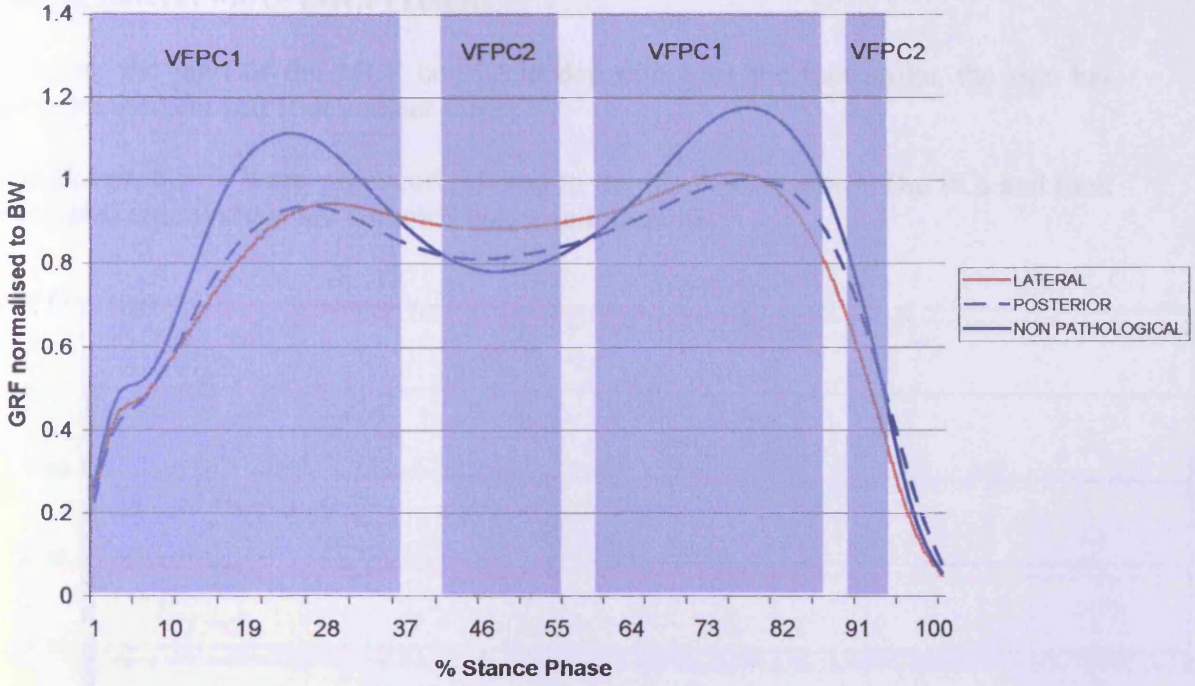

Figure 46 Mean VF for the three cohorts indicating the components of the stance phase described by the Principle Components.

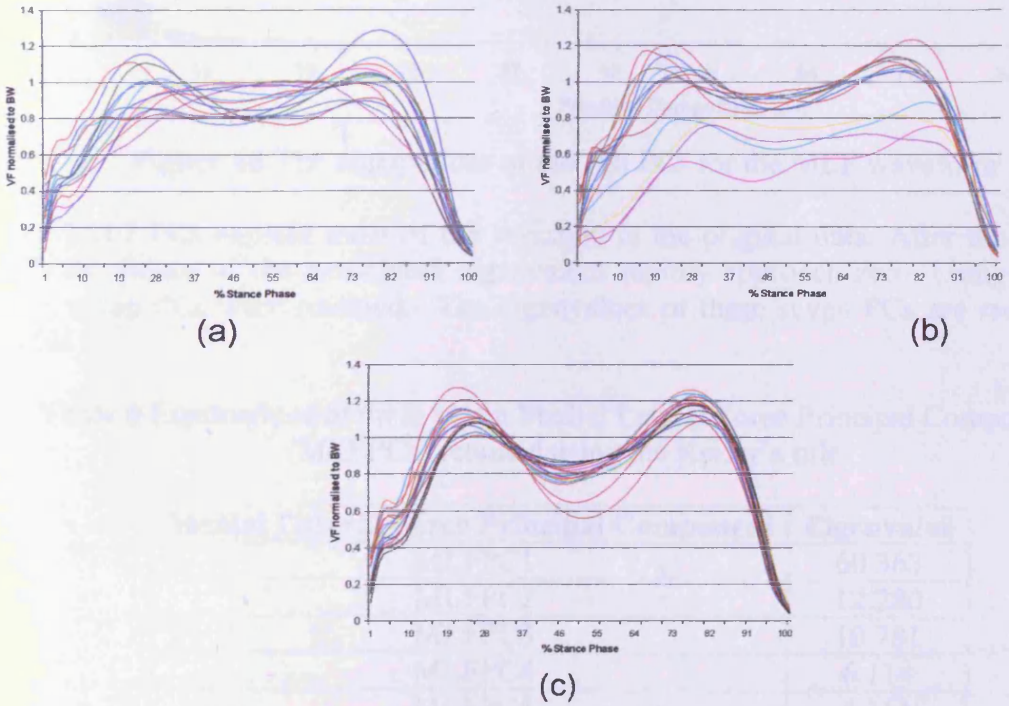

Figure 47 Variation between subjects in the (a) LA (b) PA and (c) NP cohorts.

Medial Lateral Force (MLF) results

To make the sign of the MLF consistent depending on the foot strike, the sign has been changed for left foot contact forces.

One Hundred PCs were produced relating to the MLF waveform. The PCs and their associated eigenvalues are depicted below in Figure 48.

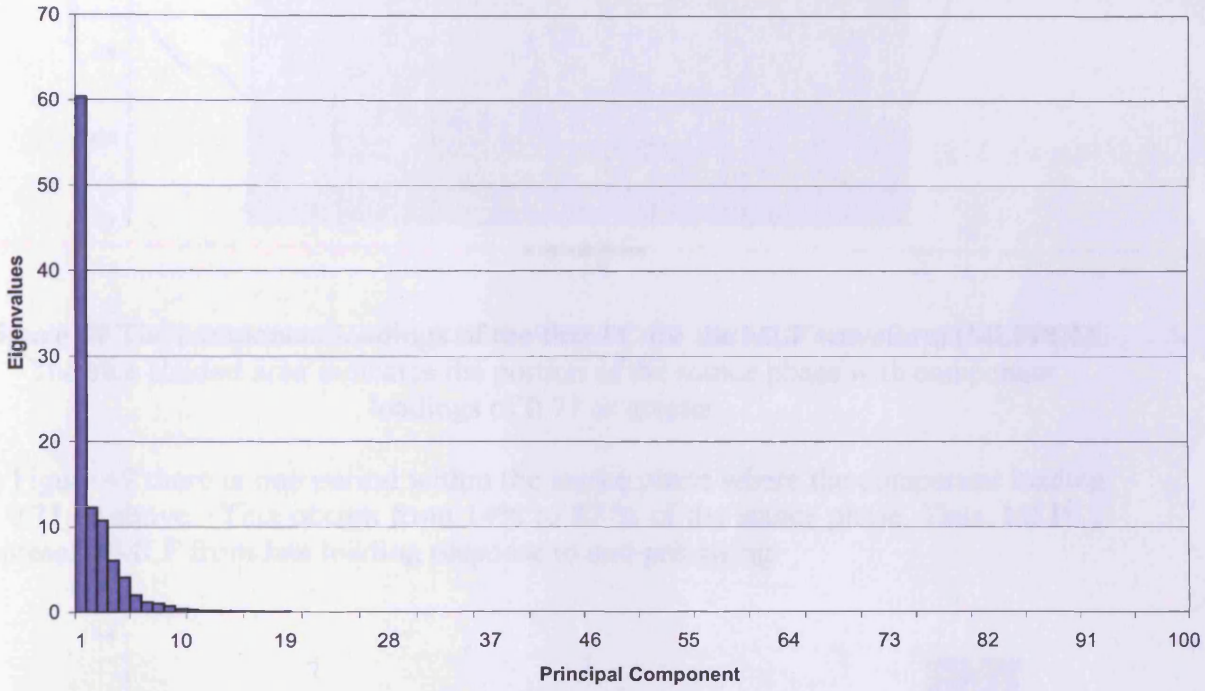

Figure 48 The eigenvalues of the 100 PCs for the MLF waveform

The first 7 PCs explain most of the variation in the original data. After the first few PCs the values of the associated eigenvalues rapidly approach zero. Using Kaiser's rule, seven PCs were retained. The eigenvalues of these seven PCs are recorded in Table 6.

Table 6 Eigenvalues of these seven Medial Lateral Force Principal Components (MLFPCs) retained using the Kaiser's rule

Medial Lateral Force Principal Component	Eigenvalue
MLFPC1	60.363
MLFPC2	12.280
MLFPC3	10.781
MLFPC4	6.114
MLFPC5	4.111
MLFPC6	1.956
MLFPC7	1.153

These seven PC's account for a combined variance of 96.76%. The PCs are interpreted by identifying the portions of the stance phase with component loadings of 0.71 and above, following Comrey, (1973).

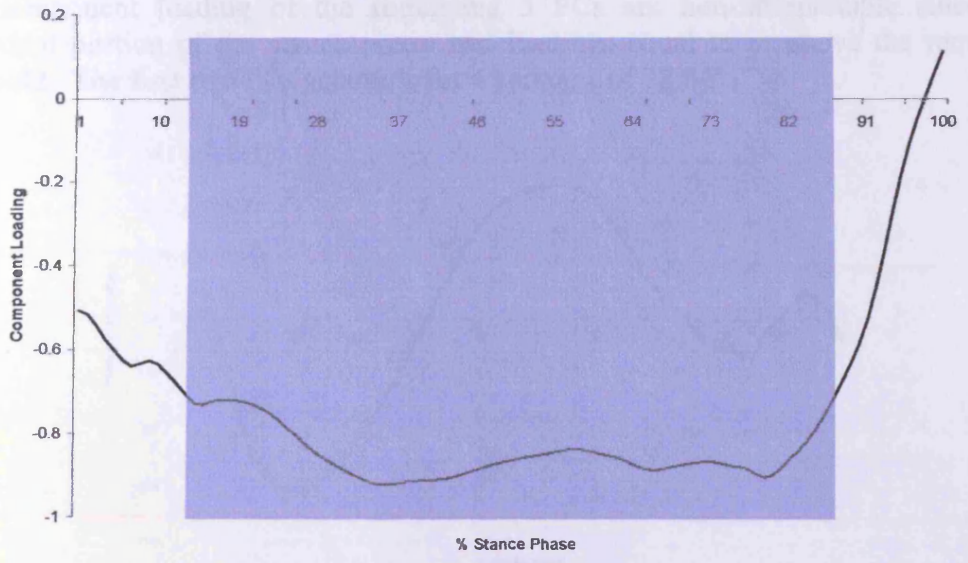

Figure 49 The component loadings of the first PC for the MLF waveform (MLFPC1). The blue shaded area indicates the portion of the stance phase with component loadings of 0.71 or greater.

In Figure 49 there is one period within the stance phase where the component loading is 0.71 or above. This occurs from 14% to 87 % of the stance phase. Thus, MLPC1 represents MLF from late loading response to mid pre-swing.

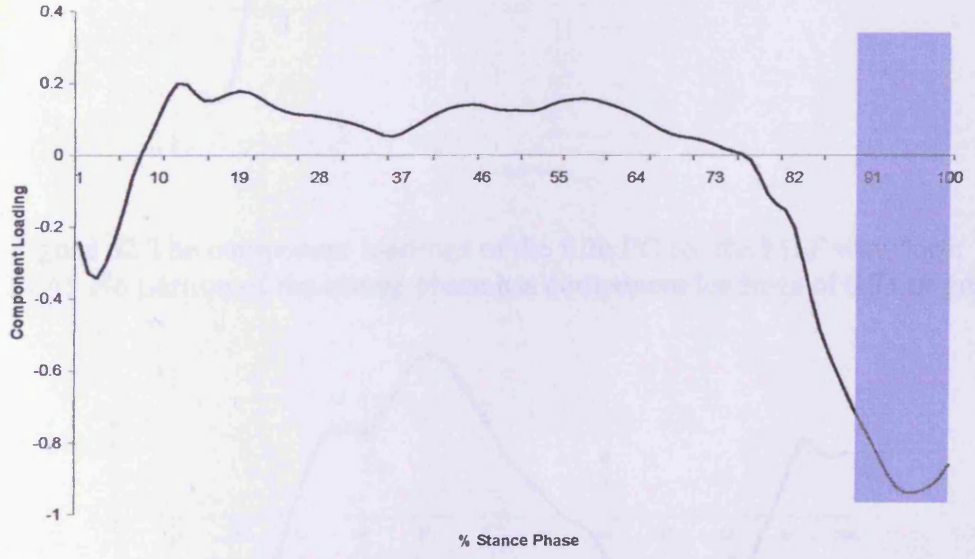

Figure 50 The component loadings of the second PC for the MLF waveform (MLFPC2). The blue shaded area indicates the portions of stance phase with component loadings of 0.71 or greater.

In Figure 50 there is one period within the stance phase where the component loading is 0.71 or above. This occurs from 89% to 100 % of the stance phase. Thus, MLPC2 represents MLF from mid to the end of Pre-Swing.

The component loading of the remaining 5 PCs are non-interpretable since no individual portion of the stance phase had loadings equal to or above the required threshold. The first two PCs accounts for a variance of 72.64%.

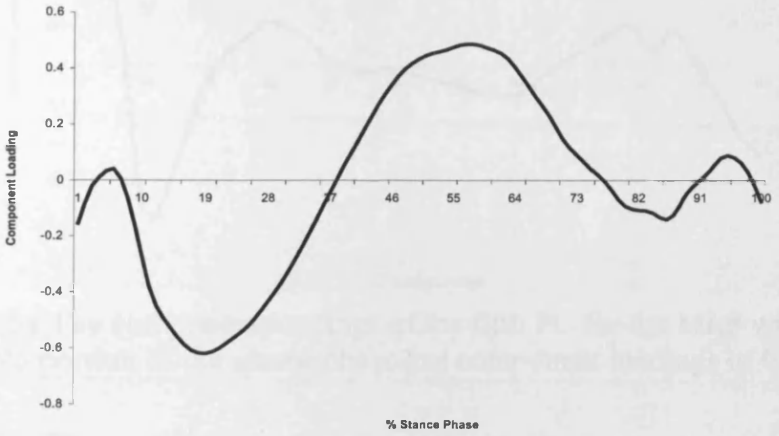

Figure 51 The component loadings of the third PC for the MLF waveform (MLFPC3). No portion of the stance phase has component loadings of 0.71 or greater.

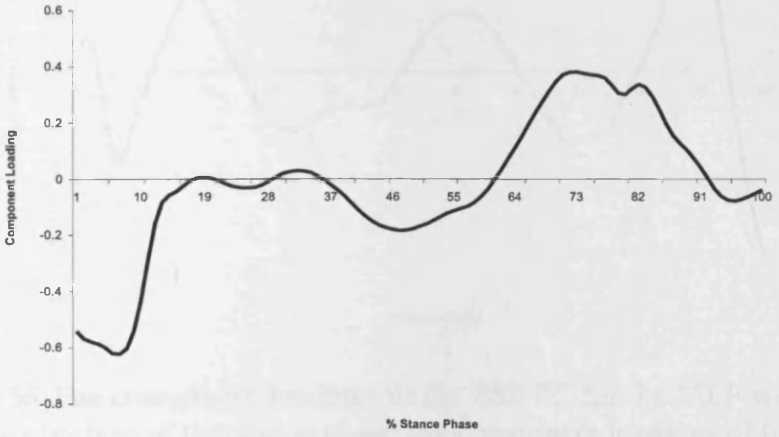

Figure 52 The component loadings of the fifth PC for the MLF waveform (MLFPC4). No portion of the stance phase has component loadings of 0.71 or greater.

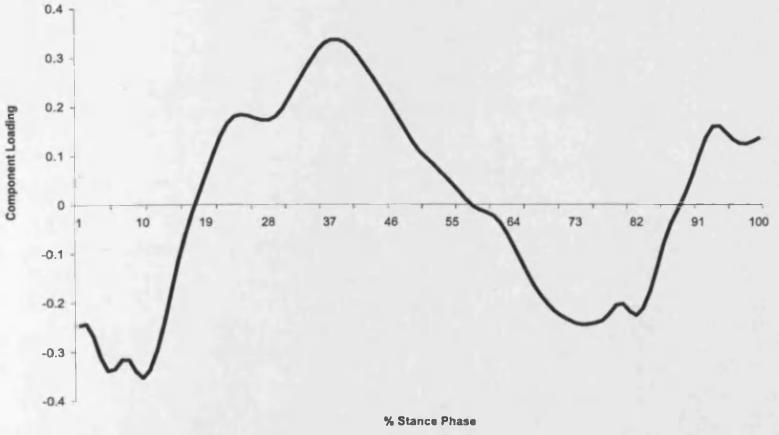

Figure 53 The component loadings of the fifth PC for the MLF waveform (MLFPC5). No portion of the stance phase has component loadings of 0.71 or greater.

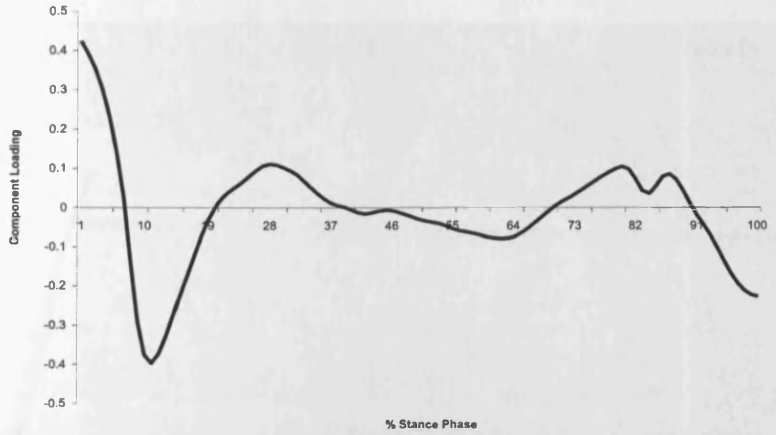

Figure 54 The component loadings of the fifth PC for the MLF waveform (MLFPC6). No portion of the stance phase has component loadings of 0.71 or greater.

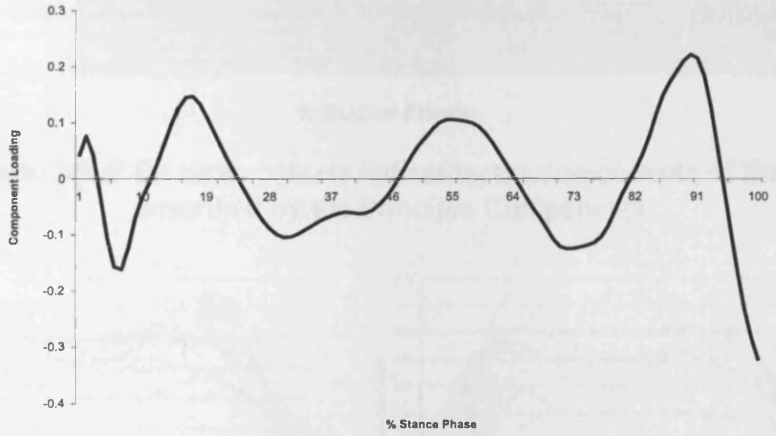

Figure 55 The component loadings of the fifth PC for the MLF waveform (MLFPC7). No portion of the stance phase has component loadings of 0.71 or greater.

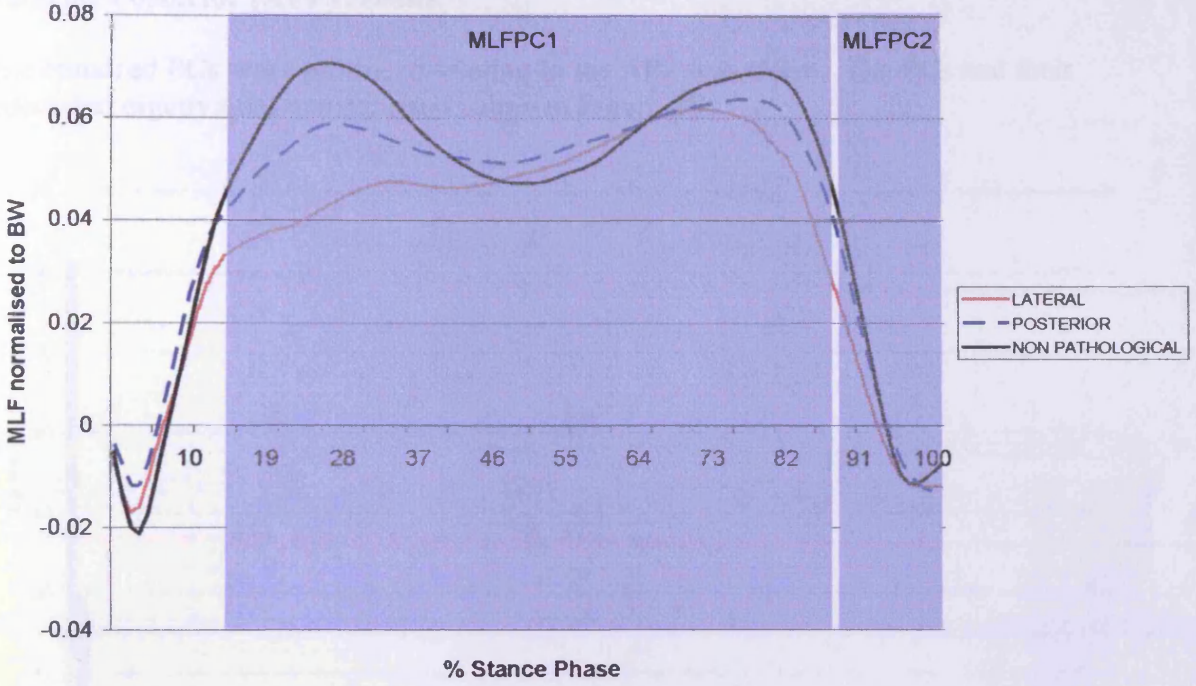

Figure 56 Mean MLF for three cohorts indicating the components of the stance phase described by the Principle Components.

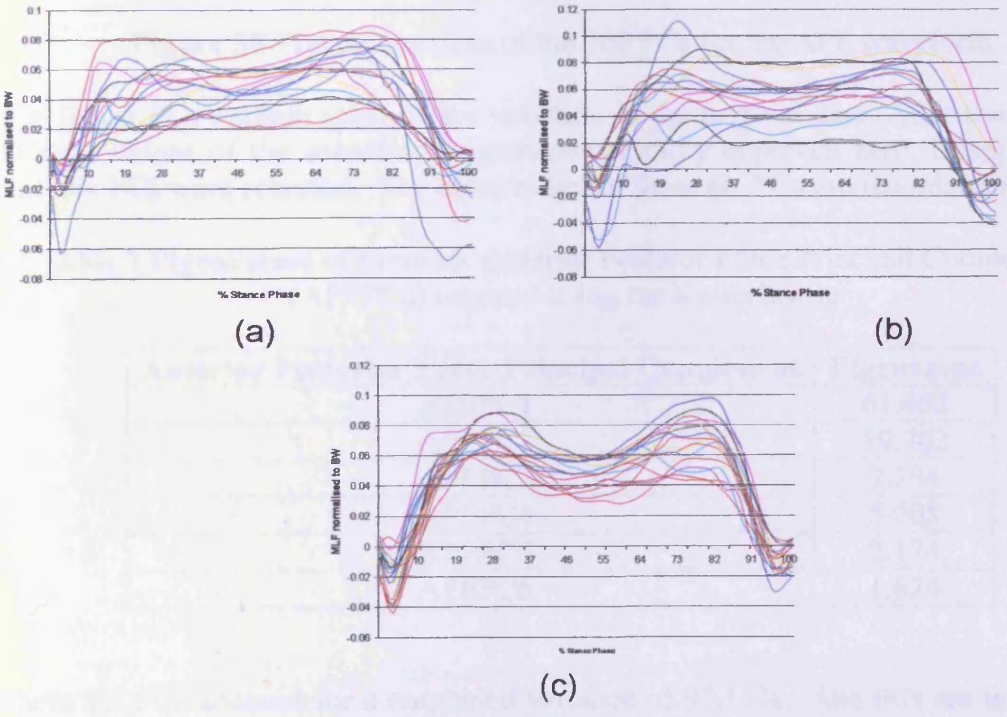

Figure 57 Variation between subjects in the (a) LA (b) PA and (c) NP cohorts.

Anterior Posterior (APF) results

One Hundred PCs were produced relating to the APF waveform. The PCs and their associated eigenvalues are depicted below in Figure 58.

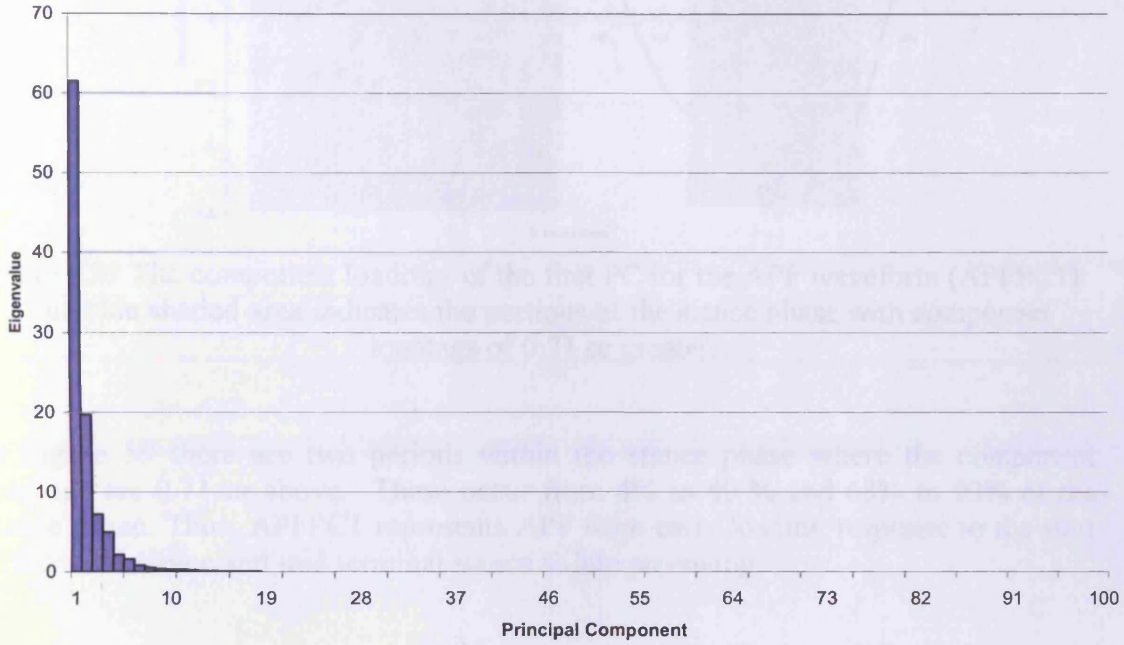

Figure 58 The eigenvalues of the 100 PCs for the APF waveform

The first 6 PCs explain most of the variation in the original data. After the first few PCs the values of the associated eigenvalues rapidly approach zero. Using Kaiser's rule, six PCs were retained. The eigenvalues of these six PCs are recorded in Table 7.

Table 7 Eigenvalues of these six Anterior Posteror Force Principal Components (APFPCs) retained using the Kaiser's rule

Anterior Posterior Force Principal Component	Eigenvalue
APFPC1	61.462
APFPC2	19.702
APFPC3	7.204
APFPC4	5.005
APFPC5	2.174
APFPC6	1.624

These six PCs account for a combined variance of 97.17%. The PCs are interpreted by identifying the portions of the stance phase with component loadings of 0.71 and above, following Comrey, (1973).

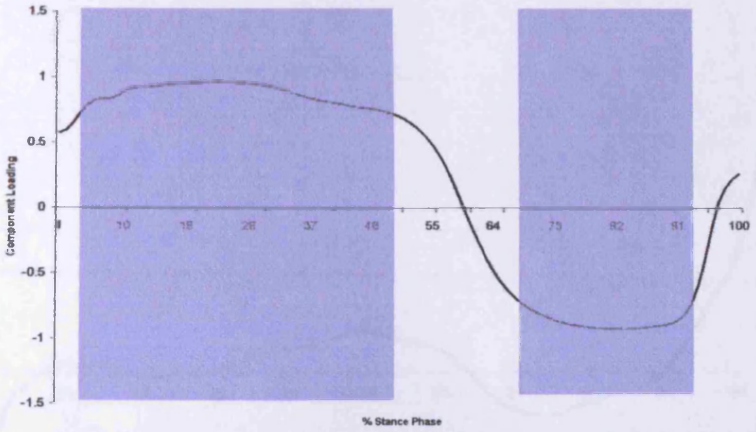

Figure 59 The component loadings of the first PC for the APF waveform (APFPC1). The blue shaded area indicates the portions of the stance phase with component loadings of 0.71 or greater.

In Figure 59 there are two periods within the stance phase where the component loadings are 0.71 or above. These occur from 4% to 49 % and 68% to 93% of the stance phase. Thus, APFPC1 represents APF from early loading response to the start of terminal stance and mid terminal stance to late pre-swing.

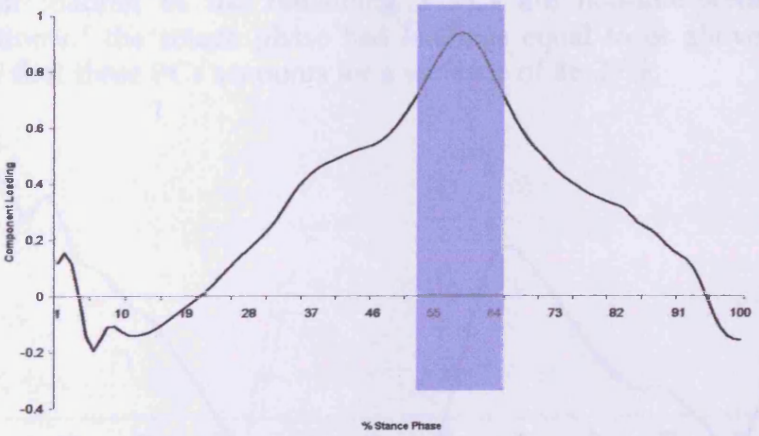

Figure 60 The component loadings of the second PC for the APF waveform (APFPC2). The blue shaded area indicates the portions of the stance phase with component loadings of 0.71 or greater.

In Figure 60 there is one period within the stance phase where the component loading is 0.71 or above. This occurs from 53% to 65% of the stance phase. Thus, APFPC2 represents APF from early terminal stance to mid terminal stance.

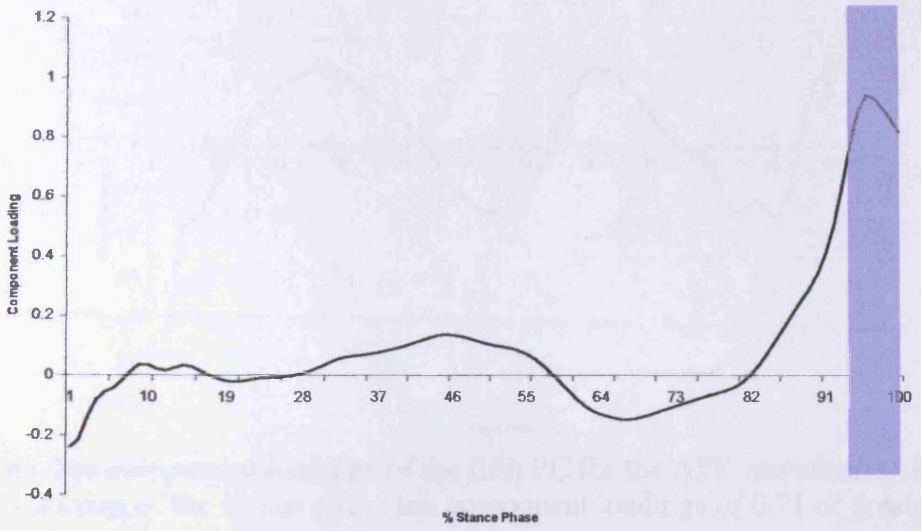

Figure 61 The component loadings of the third PC for the APF waveform (APFPC3). The blue shaded area indicates the portion of the stance phase with component loadings of 0.71 or greater.

In Figure 61 there is one period within the stance phase where the component loading is 0.71 or above. This occurs from 94% to 100% of the stance phase. Thus, APFPC3 represents APF from late pre-swing to the end of the stance phase.

The component loading of the remaining 3 PCs are non-interpretable since no individual portion of the stance phase had loadings equal to or above the required threshold. The first three PCs accounts for a variance of 88.37%.

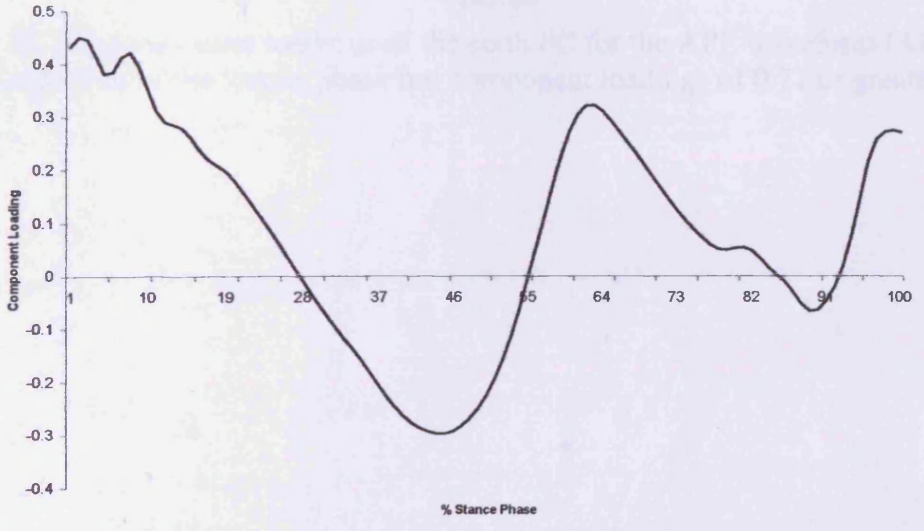

Figure 62 The component loadings of the fourth PC for the APF waveform (APFPC4). No portion of the stance phase has component loadings of 0.71 or greater.

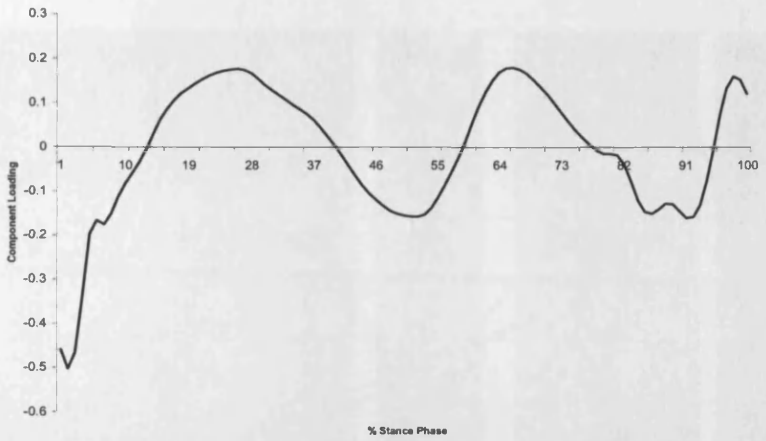

Figure 63 The component loadings of the fifth PC for the APF waveform (APFPC4). No portion of the stance phase has component loadings of 0.71 or greater.

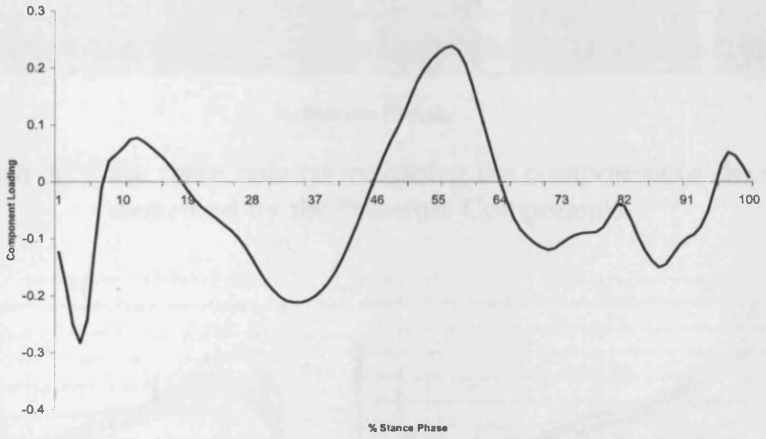

Figure 64 The component loadings of the sixth PC for the APF waveform (APFPC6). No portion of the stance phase has component loadings of 0.71 or greater.

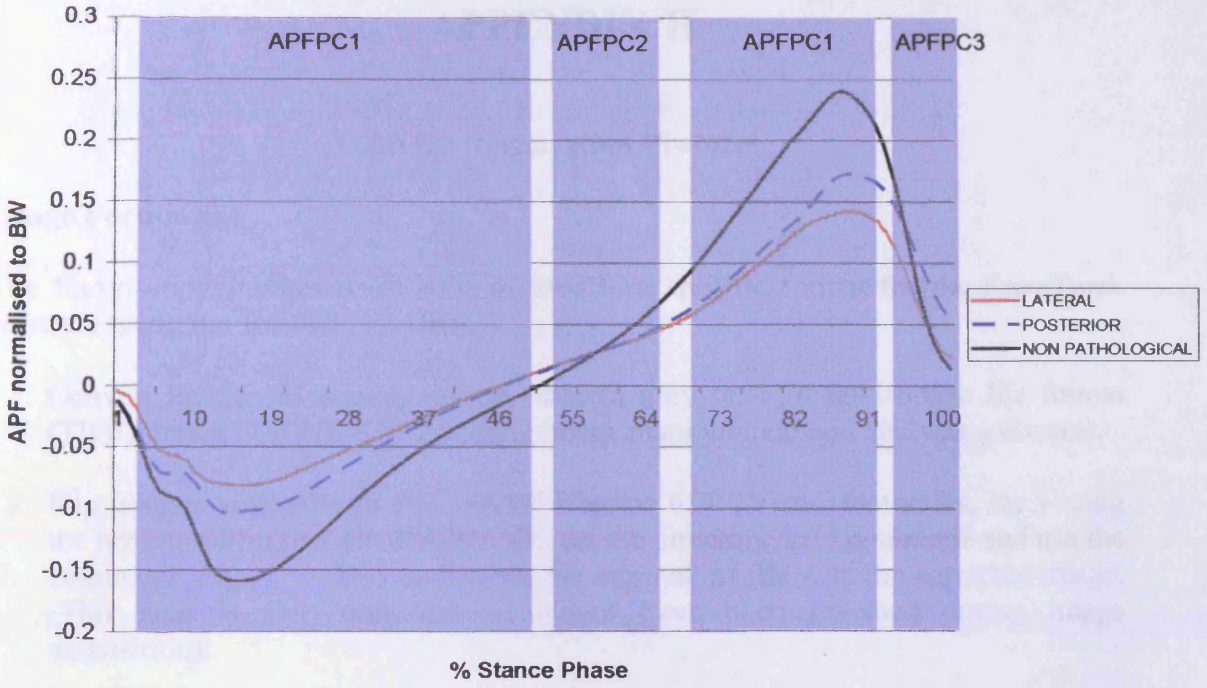

Figure 65 Mean APF for three cohorts indicating the component of the stance phase described by the Principle Components.

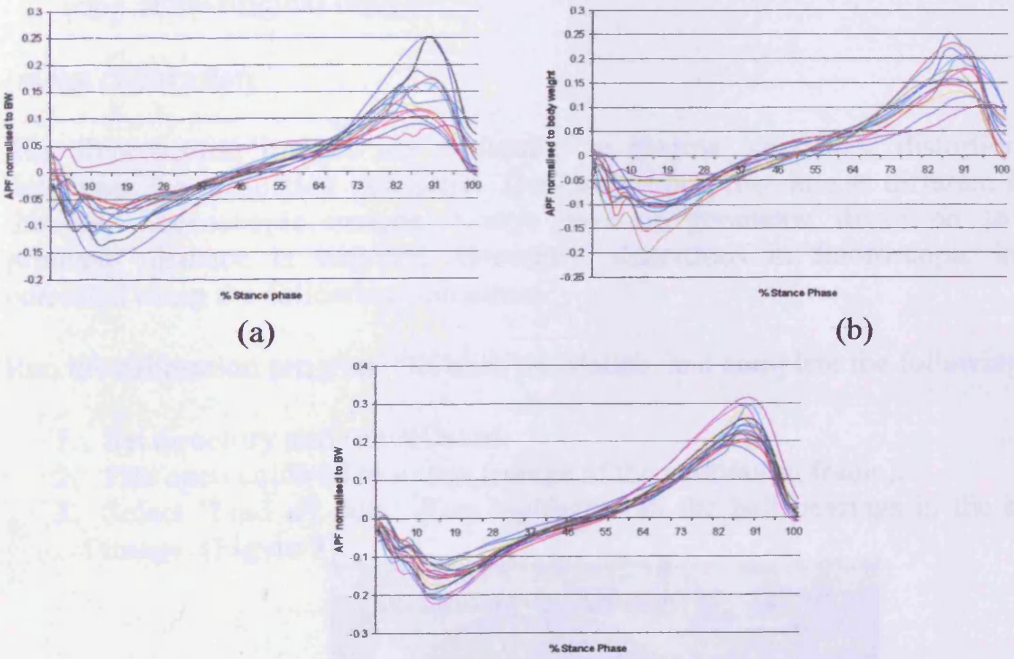

Figure 66 Variation between subjects in the (a) LA (b) PA and (c) NP cohorts.

APPENDIX H

Image Registration Protocol

Image Formatting

The fluoroscopy images must be converted to a specific format for the KneeTrack software using the following 3 steps.

1. Convert images to uncompressed, original grey scale, tagged image file format (TIFF), using OSIRIS 4.07 (medical image manipulation and analysis software).

2. Flip images vertically in PV-WAVE Version 6.20 (Visual Numerics, Inc.) using the program Flip.pro. (In PV-WAVE, set the directory, *cd,' pathname* and use the command: *Flip,'.'*). This overwrites the original .tif file with the corrected image. (This step is only required if images have been reversed during image acquisition).

3. Scale images from 1024x1024 pixels to 512x512 pixels using the program Shrink.pro. (In PV-WAVE, set the directory, *cd,' pathname* and use command: *Shrink,'.'*). This program overwrites the original file, so ensure there is a backup copy of the original image.

Image calibration

The fluoroscopic images are calibrated to remove geometric distortions and to determine the projection geometry. The calibration procedure is different for X-rays than for fluoroscopic images. X-rays have no geometric distortion so only the principal distance is required. Geometric distortions in fluoroscopic images are corrected using the following procedure.

Run the calibration program 'XCal.m' in Matlab, and complete the following steps.

1. Set directory and run XCal.m.
2. File/open calibration image (image of the calibration frame).
3. Select 'Find all dots'. This highlights all the ball bearings in the calibration image, (Figure 1).

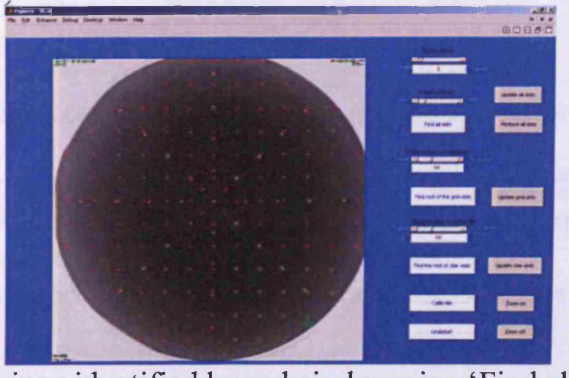

Figure 1 Ball bearings identified by red circles using 'Find all dots' command

4. Change the parameters defining the radius dimensions and image contrast so that all dots are visible.
5. If all dots are not shown, select enhance or imdilate image dots.
6. Add or delete dots by clicking on the image and selecting the a or d key, (a=add, d=delete).
7. Select 'update all dots'.
8. Click on the central grid dot, the dot above it and then the dot to the right of it. Select 'Find rest of grid dots'. Two screens will appear, one showing the grid dots and another with all dots (ball bearings) in the image. Delete superfluous dots.
9. Update grid dots. The position of the ball bearings belonging to the square grid should be visible on a plot, (Figure 2).

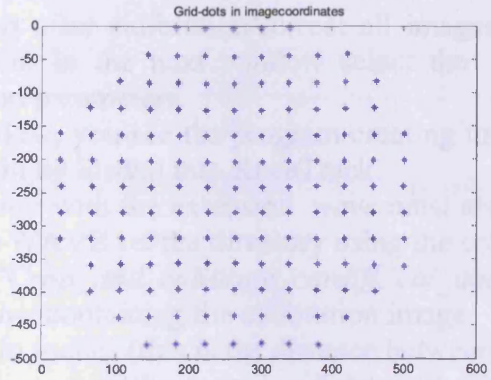

Figure 2 Image coordinates of the square grid on the calibration frame.

10. If any dots forming part of the star were deleted in the above process, click on restore all dots.
11. Click on the dot to the right of the central star dot, the dot to the left of the central star dot and then on the central dot.
12. Update star dots. The position of the ball bearings belonging to the star grid should be visible on a plot, (Figure 3).

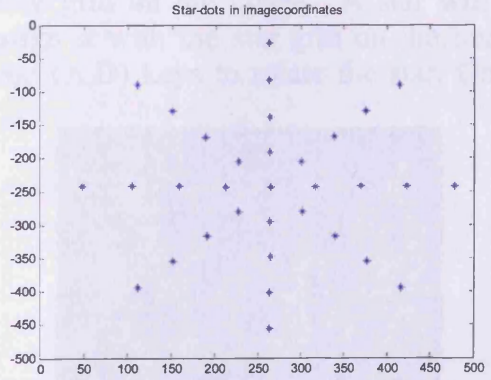

Figure 3 Image coordinates of the star grid on the calibration frame.

13. Click on 'calibrate'. This brings up a window to 'save distortion correction parameters'. Give this a name (e.g. *cal).* It produces a .txt file and *cal.m* file containing the undistortion calibration parameters.
14. Click on the 'undistort' button. This generates the corrected calibration image, (Figure 4).

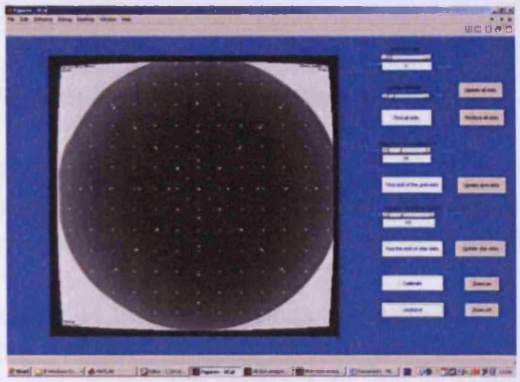

Figure 4 Undistorted image of the calibration frame.

15. Select file/undistort after calibration/correct all images. Open all the images requiring correction. In the next window select the .txt file containing the distortion correction parameters.
16. In the Matlab window, you see the program creating the undist.tif files. These are the files that will be loaded into KneeTrack.
17. A dummy calibration with the extension *.wave* must also be created for use in KneeTrack. In PV-WAVE set the directory using the command *cd,'pathname* . Run the program, *'Crop_and_calibrate_cardiff,'cal_undist.tif','cal_cal.m'.*
18. This opens a window containing the calibration image.
19. Enter image scale in inches (this is the distance between the central grid dot on the far left of the image and the central grid dot on the far right). The scale was 11.811" for the current study.
20. A box will appear on the image. Move the borders to define the grid space. Move the left boarder of the box in line with the furthest central left grid dot using the J and L keys. Move the right boarder of the box in line with the furthest central right grid dot using the J and L keys. Move the boarders in line with the grid dots at the top and bottom of the image using the M and I keys. Press q to quit.
21. This creates a square grid on the image. A star will appear on the image. Move the star to align it with the star grid on the image. Use the (M,I,J,K) keys to translate and (A,D) keys to rotate the star. Once aligned (Figure 5), press q to quit.

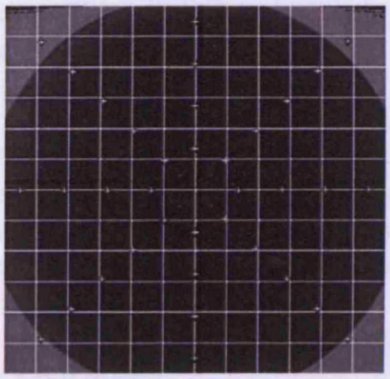

Figure 5 star and square grid aligned with the calibration image.

22. A *.wave* file will be created for use in the KneeTrack program. A *.txt* file is also created, where the fist line provides the Principal distance (P.D) in inches. The P.D in this study was 45.0622".

Implant model preparation

This procedure positions a coordinate system within each model.

1. Convert stl files to ASCII format.
2. Use DOS command prompt to extract all the lines containing vertices. Generate a file containing the coordinates of the vertices making up each implant model.
3. Determine the number of lines of vertices in each file.
4. Modify the scripts entitled 'import_encore_tib' and 'import_3D_femur' to reposition each component with respect to its coordinate system. The axis convention is for the y-axis to point upwards and the z-axis to point medially. The x-axis points anterior for the left knee and posterior for the right knee.
5. For the tibial component, the origin should be positioned at the backside of the polyethylene insert. The distance from the upper rim of the tibial tray to the level where the PE inert sits on the base plate can be measured in Rhinoceros version 4.0.
6. The outline of the tibial plateau is created using the program *connect_the_dots*. The vertices used to produce a picture of contact points is created by manually selecting points on the outline counterclockwise.
7. Save the new models as fem.dat and tib.dat.

Matching procedure in KneeTrack

For matching in KneeTrack, a calibration *.wave* file, *.dat* bone or CAD models and undistorted fluoroscopy images are required. A guide to the matching process is provided below.

Loading files

1. In PV-WAVE set the directory using the command *cd,'pathname.*
2. Type *KneeTrack.*
3. Input the password.
4. A window will open. Select the matching option.
5. Load the calibration *.wave* file.
6. Select *load movies*. Select an image in a sequence and all sequential images will also load.
7. There are 4 views for the image, Raw, ADJ (adjusted image), Edge (performs edge detection) and + (summation of edge and ADJ).
8. Use the low input threshold (li) and high input threshold (hi) sliders to adjust how the edges in the image are detected by the canny edge detector. The aim is to adjust the image to achieve a clear contrast between the implant and bone or the bone and surrounding air and soft tissues. Click on *1* to adjust the current image or *all* to adjust all images in the sequence. Maintain a log of the parameters selected for each image.
9. *Load Fem kin* and *load Tib Kin* opens files that you have previously saved in this workspace.
10. Select *load models,* then the *femoral model* and *tibial model* for matching (these are the tib.dat and fem.dat models).

11. To view the projection of these models on an image click on one of the tape player buttons, as this updates the screen.
12. The centre of the projection is (0,0,0).

Manual matching

13. Match the Femur first. This is because the tibia is symmetric through the midline and two poses will look reasonable. The femur is asymmetric proximally. By matching the femur first, it makes it easier to determine if the solution for the tibia is physiologically possible.
14. Manually match the projected model as closely as possible to the edges in the image. Use the arrow keys to rotate and translate each of the 3D models.
    Caps Lock and an arrow key produces small translations along the x or y-axis.
    CTRL and ← or → arrow keys, rotates the model about the y-axis.
    CTRL and ↑ or ↓ arrow keys, rotates the model about the x-axis.
    Shift and ↑ or ↓ arrow keys, translates the model along the z axis.
    Shift and ← or → arrow keys, rotates the models about the z-axis.
15. Click on pictures button. This shows the medial, lateral, frontal and transverse views of the model.
16. Align the tibia with the femur using the graphs and pictures as a guide. Match the Z translation, Var/Val position and then rotation. Use this information to check that the relative component positions are physiologically possible.

Optimised matching

Use the numerical optimiser to produce the final match.

17. Select  (outline tool) and click on the image. Green points will appear on the outline. Set the border width with the boarder size (BS) slider. The default BS is 10. If the border of the tibia or patella is being identified, reduce the BS to 5. Aim to define an edge with 100-300 pixels. The CP slider changes the number of contour points.
18. Add points if necessary by selecting  and clicking on the image. The new points are heavily weighted during the optimisation. Erase points by selecting  and clicking on the image. Erase points in areas where you are unsure of the implant edge, e.g. where there is cement. (right mouse click to end this tool).
19. Select *automatch*. The size of the increments can be reduced by changing the Xscale, TStp and Fscale settings. The optimisation matches the contours of the projected model to the green points, it does not mean you have the best set of green points selected.

Creating KneeTrack output files

20. Saving the movie produces images of the matching on each image. The models can be visualised as shaded, edges or transparent depending on the settings selected when the movie is saved.
21. Save *fem kin* and *tib kin*. These produce *.man* files. Name the files something unique.

Computing kinematics and contact point data

1. Save all the .man files into 1 file ready for batch processing. The files must end in fem.man and tib.man.
2. Generate .res files in PV-WAVE using:
   cd,'path'
   long_var_names,'.'
3. Produce a batch file in Programmer's File Editor (PFE32) and save it in the same processing folder. The batch file contains 10 lines and defines the patient's name, the location of the femur and tibia and the location of where to save the data for the femur and tibia. The third letter of the batch file must be R or L according to the leg under investigation, e.g. GWR.batch.
4. Create kinematics file in PV-WAVE using the command:
   Batch_kin,'GWR.batch
   This reads an input file to determine the results files to be used for computing joint kinematics.
5. Follow the instructions on the screen.
6. Create joint contacts file using the command.
   Batch_contact,'GWR.batch
   Batch_cor, 'GWR.batch
   This will show a series of contact images, press the return key to move to the next image. In the contact output, thin lines indicate knee extension, thick lines indicate knee flexion. Contacts are defined as the lowest points of the medial and lateral femoral condyles in the tibial coordinate system.
7. View all data for each image using the command:
   Batch_write_text_file,'GWR.batch
8. The data can be interpreted using the descriptions in Table 1.

Table 1 Kinematic descriptions of data in the output file

kinematics	Description
FLX,	Knee Flexion (positive)
ABD,	Knee Abduction (positive)
EXT,	External tibial rotation (positive)
Med A/P,	A/P location of medial femoral condylar contact (Anterior is positive)
Lat A/P,	A/P location of lateral femoral conylar contact (Anterior is positive)
Fem A/P,	Anterior femoral translation is positive
Fem Sup/Inf,	Superior femoral translation is positive
Fem Med/Lat	Medial femoral translation is positive

Translations are computed as the movement of the femoral origin with respect to the tibial coordinate system. Rotations are described by 312 cardan angles.

9. There are several scripts which can be used and adapted depending on the format of the results required. For example, animations of a sequence can be created or the knee pose at the greatest flexion angle can be defined.